

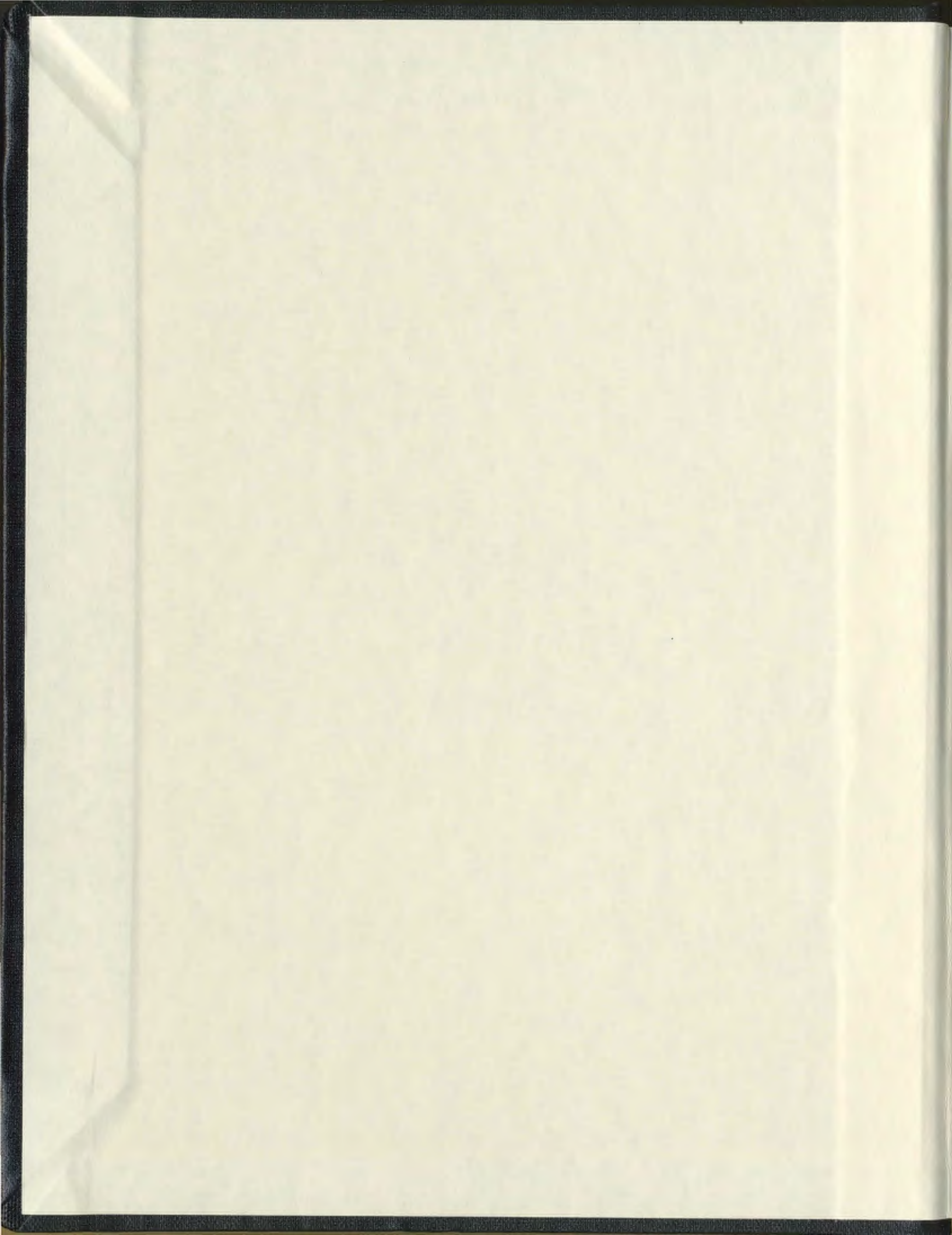
PALEOTECTONIC AND STRUCTURAL SETTING OF THE
WESTERN NOTRE DAME BAY AREA,
NEWFOUNDLAND APPALACHIANS

CENTRE FOR NEWFOUNDLAND STUDIES

**TOTAL OF 10 PAGES ONLY
MAY BE XEROXED**

(Without Author's Permission)

ZBIGNIEW ADAM SZYBINSKI



PALEOTECTONIC AND STRUCTURAL SETTING OF THE WESTERN NOTRE
DAME BAY AREA, NEWFOUNDLAND APPALACHIANS.

BY

ZBIGNIEW ADAM SZYBINSKI

A thesis submitted to the School of Graduate Studies in partial fulfillment of the
requirements for the degree of Doctor of Philosophy

Department of Earth Sciences,
Memorial University of Newfoundland,
St. John's, Newfoundland

1995



National Library
of Canada

Acquisitions and
Bibliographic Services Branch

395, Wellington Street
Ottawa, Ontario
K1A 0N4

Bibliothèque nationale
du Canada

Direction des acquisitions et
des services bibliographiques

395, rue Wellington
Ottawa (Ontario),
K1A 0N4

Author's name reference

Author's name reference

The author has granted an irrevocable non-exclusive licence allowing the National Library of Canada to reproduce, loan, distribute or sell copies of his/her thesis by any means and in any form or format, making this thesis available to interested persons.

L'auteur a accordé une licence irrévocable et non exclusive permettant à la Bibliothèque nationale du Canada de reproduire, prêter, distribuer ou vendre des copies de sa thèse de quelque manière et sous quelque forme que ce soit pour mettre des exemplaires de cette thèse à la disposition des personnes intéressées.

The author retains ownership of the copyright in his/her thesis. Neither the thesis nor substantial extracts from it may be printed or otherwise reproduced without his/her permission.

L'auteur conserve la propriété du droit d'auteur qui protège sa thèse. Ni la thèse ni des extraits substantiels de celle-ci ne doivent être imprimés ou autrement reproduits sans son autorisation.

ISBN 0-612-17653-3

Canada

ABSTRACT

The Appalachian Orogen in Newfoundland records the birth and destruction of the Iapetus Ocean. The Dunnage Zone preserves remnants of the oceanic terranes, and is subdivided into the western (Laurentian) Notre Dame Subzone and the eastern (Gondwanan) Exploits Subzone. This focus of this thesis has been to determine the geologic history of the northernmost part of the Notre Dame Subzone, confined between the Green Bay and Lobster Cove Faults.

The geological history of the western Notre Dame Bay area has been investigated using field, geochemical, geochronological and structural methods. Care was taken to integrate the results obtained from these diverse methods in order to obtain an internally consistent model. As a result of these studies a new stratigraphic order is proposed: a major nappe has been recognized, and the character and tectonic history of one of the oldest intraoceanic sequences in the Notre Dame Subzone of the Newfoundland Appalachians has been determined.

In simple terms, the geological history of the western Notre Dame Bay area can be described as follows: (1) a pre-500 Ma intraoceanic arc/back-arc stage, which involves deposition of the Lushs Bight Group and the lower part of the Western Arm Group (Sugar Loaves Basalt, Skeleton Pond Formation, and Big Hill Basalt), (2) emplacement of the pre-500 Ma sequence on the Laurentian continental margin and intrusion by high-Mg dykes of sanukitoid/bajaite affinities at ~495 Ma, (3) development of a calc-alkalic arc (Cutwell Group and the upper two formations, Welsh Cove and Western Head, of the Western Arm Group) from 485 to ~465 Ma, which is dominantly submarine, but whose chemistry is variably influenced by inputs from continental lithospheric sources, (4) development of a major alpine style fold nappe and its southeasterly directed emplacement (Notre Dame Bay Nappe) in the post-lower Silurian, and (5) post-emplacement structural disruption of the nappe, probably in the post-lower Carboniferous.

ACKNOWLEDGEMENTS

This work was supported by the Geological Survey of Canada and the MDA agreements. Additional support for the study came from the Newfoundland Department of Mines, Memorial University and NSERC grants to my supervisor, Dr. George Jenner. Continuing support for this project also came from Scott Swinden, whose in-depth knowledge of Newfoundland geology was always shared. Scott is also thanked for his becoming a member of the supervisory committee in the last stages of this thesis. Brian Fryer and Peter Cawood were earlier members of this committee, but left for greener pastures before it was completed. I would also like to thank Baxter Kean, Tom Calon and Joseph Hodych for their assistance in the field. Felicity O'Brien and Henry Williams both contributed their paleontological expertise. Late Chris Roddick of the Geological Survey of Canada was instrumental in getting the geochronology data used in this thesis. A number of people assisted me during the course of this study, including Mike Muggerridge, Leonard Mandville, Pat Horan and Darryl Clarke. I would like to thank my Ph.D. student colleagues, namely Bill Davis, Jeroen van Gool, Steve Edwards and Dave van Everdingen, for their encouragement. I would also like to thank my supervisor for his patience.

This project would not have been possible without the support and encouragement of my best friend, Louise Barrette. John Dawson, Robin McGrath, Tomasz Dec and Aphrodite Indares are kindly thanked for all their help, that on many occasions included food and lodging.

TABLE OF CONTENTS

ABSTRACT	ii
ACKNOWLEDGEMENTS	iii
TABLE OF CONTENTS	iv
LIST OF FIGURES	xiii
LIST OF TABLES	xxiii
CHAPTER 1: INTRODUCTION	1 - 1
1.1 Purpose and Scope of Thesis	1 - 1
CHAPTER 2: REGIONAL SETTING OF THE STUDY AREA	2 - 1
2.1 Introduction: The Appalachian Orogen In Newfoundland	2 - 1
2.2 Avalon Zone	2 - 1
2.3 Gander Zone	2 - 2
2.4 Humber Zone	2 - 2
2.5 Dunnage Zone	2 - 2
2.6 Relationships Between The Dunnage And Other Zones	2 - 4
2.7 Overlap Sequences	2 - 6
2.8 Ophiolites And Volcanic-Epiclastic Sequences Of The Notre Dame Subzone	2 - 7
2.8.1 Stage 1: Ca 505 Ma And Older, Upper Cambrian(?) To Middle Tremadoc	2 - 8
2.8.2 Stage 2: Ca 492 To 475 Ma, Middle Tremadoc - Middle Arenig	2 - 8
2.8.3 Stage 3: Ca 484 Ma To 460 Ma, Lower Arenig To Llandeilo/ Caradoc Boundary	2 - 9
2.9 The Western Notre Dame Bay Area	2 - 10
CHAPTER 3: STRATIGRAPHY OF WESTERN NOTRE DAME BAY	3 - 1
3.1 Previous Work And Nomenclature	3 - 1
3.1.1 Lushs Bight Group	3 - 1
3.1.2 Western Arm Group	3 - 2
3.1.3 Catchers Pond Group	3 - 3
3.1.4 Cutwell Group	3 - 3
3.2 Revised Stratigraphy Of The Western Notre Dame Bay	3 - 5
3.2.1 Lushs Bight Group	3 - 7

3 2 1 1 Indian Head Dyke Complex	3 - 7
3 2 1 2 Little Bay Basalt (Formation)	3 - 8
3 2 1 3 Mafic Subvolcanic Rocks	3 - 8
3 2 1 4 Age Constraints On The Lushs Bight Group	3 - 9
3 2 2 Western Arm Group	3 - 9
3 2 2 1 Sugar Loaves Basalt (Formation)	3 - 10
3 2 2 2 Skeleton Pond Formation	3 - 11
Tuff Lithofacies	3 - 12
Flow Lithofacies	3 - 13
Age Constraints	3 - 13
3 2 2 3 Big Hill Basalt (Formation)	3 - 14
3 2 2 4 Isotopic Age Constraints On The Sugar Loaves And Big Hill Basalt, And Skeleton Pond Formation	3 - 14
3 2 2 5 Welsh Cove Formation	3 - 15
3 2 2 5 1 West Water Limestone Bed And Silver Pond Tuff	3 - 17
West Water Limestone Bed	3 - 17
Silver Pond Tuff (Bed)	3 - 17
Age Constraints. Faunal	3 - 18
Age Constraints. Isotopic	3 - 18
3 2 2 6 Western Head Formation	3 - 19
Age Constraints	3 - 20
3 2 2 7 Dolland Quartz Diorite	3 - 20
Age Of The Dolland Quartz Diorite	3 - 21
3 2 2 8 The Colchester-Coopers Cove Pluton	3 - 21
Age Of The Coopers Cove Pluton	3 - 21
3 2 2 9 Brighton Intrusive Complex	3 - 22
Age Of The Brighton Intrusive Complex	3 - 23
3 2 3 Cutwell Group	3 - 23
3 2 3 1 Pigeon Head Formation	3 - 24
Intrusive Member	3 - 25
3 2 3 2 Long Tickle Formation	3 - 25
Tuff Lithofacies	3 - 26
Lapilli Tuff - Tuff Breccia Lithofacies	3 - 27
Flow Lithofacies	3 - 27

Age Constraints	3 - 29
3.2.3.3 Parson's Point Formation	3 - 29
Age Determinations	3 - 31
3.2.3.4 Seal Cove Complex	3 - 31
3.2.3.5 Rocks Intrusive Into The Cutwell Group	3 - 33
Co-Magmatic Intrusive Rocks	3 - 33
Syn- To Post-Kinematic Intrusive Rocks	3 - 33
3.3 Stag Island Formation - Removal From The Cutwell Group	3 - 34
3.3.1 Stag Island Formation	3 - 34
3.3.1.1 Breccia Member	3 - 34
3.3.1.2 Lower Basalt Member	3 - 35
3.3.1.3 Upper Basalt Member	3 - 36
3.3.1.4 Intrusive Member	3 - 36
3.3.1.5 Age	3 - 36
3.3.2 Removal Of The Formation From The Cutwell Group	3 - 36
3.4 Post-Ordovician Overlap Sequences	3 - 37
3.4.1 Springdale Group	3 - 37
3.4.1.1 Red Beds	3 - 38
3.4.2 Red Beds In Kings Point ("Southwest Arm Formation")	3 - 39
3.5 Summary	3 - 40
CHAPTER 4: GEOCHEMISTRY AND PALEOTECTONIC AFFINITIES	4 - 1
4.1 Introduction	4 - 1
4.2 Alteration And Element Mobility	4 - 2
4.3 Nomenclature Of Volcanic Rocks	4 - 6
4.3.1 Lithology	4 - 6
4.3.2 Fractionation	4 - 7
4.3.3 Magma Series	4 - 8
4.3.3.1 Alkalic And Non-Alkalic Series	4 - 9
4.3.3.2 Tholeiitic (TH) and calc-alkalic (CA) series	4 - 10
4.3.3.3 Boninite Series And Other High-Mg Andesites	4 - 12
4.3.3.4 K-Suites	4 - 13
4.3.4 Arc Versus Non-Arc Geochemical Signatures	4 - 13
4.3.4.1 Normalized Multielement Plots	4 - 14
4.3.4.2 Tectonomagmatic Discrimination Diagrams	4 - 15

4.3.4.3 The Nb Anomaly	4 - 17
4.3.5 Summary Of Sources And Processes Contributing To Arc Lavas	4 - 18
4.4 Subdivision And Nomenclature Of Notre Dame Bay Volcanic Rocks	4 - 20
4.4.1 Preliminary Paleotectonic Divisions	4 - 20
4.4.2 Non-arc (NA) and transitional (TR) volcanic rocks - major and trace elements	4 - 22
4.4.2.1 NA Type: high Nb/Th non-arc volcanic rocks	4 - 23
4.4.2.1.1 NA-1 type: E-MORB type tholeiites	4 - 23
4.4.2.1.2 NA-2 type: T-MORB type tholeiites	4 - 23
4.4.2.2 TR type: medium Nb/Th transitional tholeiites	4 - 24
4.4.3 A-type volcanic and volcanoclastic rocks with arc affinities	4 - 25
4.4.3.1 Medium Nb/Th arc rocks	4 - 26
4.4.3.1.1 A-1 type: boninitic rocks	4 - 26
4.4.3.1.2 A-2 type: low-medium-K suites	4 - 26
A-2c(t) subtype: volcanoclastic rocks of arc affinity	4 - 27
A-2f subtype: high-Mg, high-K, calc-alkalic rocks	4 - 28
4.4.3.1.3 A-3 Type: Low-K Tholeiites	4 - 28
4.4.3.1.4 A-4 Type: Low Nb/Th, LREE Enriched Rocks	4 - 28
4.4.4 Geochemistry Of Mafic Subvolcanic Rocks	4 - 29
4.4.4.1 SNA type: subvolcanic non-arc rocks	4 - 29
4.4.4.2 STR Type: subvolcanic transitional rocks	4 - 30
4.4.4.3 SA Type: subvolcanic arc rocks	4 - 30
4.4.4.3.1 SA-1 type: medium Nb/Th, low (La/Yb) _N subvolcanic arc rocks	4 - 30
4.4.4.3.1 SA-2 type: medium Nb/Th, low- to high-K subvolcanic arc rocks	4 - 31
4.4.4.3.2 SA-3 type, low Nb/Th, medium-to high-K subvolcanic arc rocks	4 - 32
4.4.5 Geochemistry of felsic volcanic and subvolcanic rocks (F)	4 - 34
4.4.5.1 Discrimination between felsic volcanic/subvolcanic rocks	4 - 35
4.4.5.2 REE Patterns And Their Aspects	4 - 36
4.4.5.2.1 F-1 Type: Medium-K Felsic Rocks	4 - 36
4.4.5.2.2 F-2 Type: High-K Felsic Rocks	4 - 37

4.4.5.2.3 Post-Kinematic High-K Intrusive Rocks	4 - 37
4.5 Summary	4 - 38
4.5.1 Geochemical Subdivision Of Rocks In The Western Notre Dame Bay Area	4 - 38
4.5.2 NA-type	4 - 39
4.5.3 TR-type	4 - 40
4.5.4 A-type	4 - 41
4.5.5 Geochemistry of mafic subvolcanic rocks	4 - 42
4.5.5.1 SA- subvolcanic arc rocks	4 - 43
4.5.5.1.1 SA-1 medium Nb, Th, low (La/Yb) _N subvolcanic arc rocks	4 - 43
4.5.5.1.2 SA-2 medium Nb, Th, medium to high (La/Yb) _N subvolcanic arc rocks	4 - 43
4.5.6 Felsic Volcanic And Subvolcanic Rocks	4 - 44
CHAPTER 5: CHEMOSTRATIGRAPHY OF THE VOLCANIC ROCKS AND THEIR DETAILED PALEOTECTONIC SETTING	5 - 1
5.1 Introduction	5 - 1
5.2 Geochemical Types Versus Lithostratigraphic Units	5 - 1
5.3 Comparison With Rocks From Modern Settings	5 - 3
5.3.1 Types NA And TR - "Non-Arc" And Transitional Volcanic Rocks	5 - 4
5.3.1.1 The NA-1 Type	5 - 4
5.3.1.2 NA-2 And TR-Type Rocks	5 - 5
5.3.1.2.1 NA-2a	5 - 5
5.3.1.2.2 NA-2b	5 - 7
5.3.1.2.3 NA-2c	5 - 7
5.3.1.2.4 TR-1a	5 - 9
5.3.1.3 Type A - Arc Volcanic And Subvolcanic Rocks	5 - 10
5.3.1.3.1 A-1	5 - 11
5.3.1.3.2 A-2a	5 - 11
5.3.1.3.2 A-2b	5 - 12
5.3.1.3.2 A-2c	5 - 12
5.3.1.3.2 A-2d	5 - 13
5.3.1.3.2 A-2e and A-2e(t)	5 - 13
5.3.1.3.3 A-3	5 - 14

5.3.1.3.4 A-4	5 - 15
5.3.1.4 Subvolcanic High-Mg Andesites	5 - 16
5.3.1.5 Felsic Volcanic And Subvolcanic Rocks	5 - 17
5.4 Sources And Processes Contributing To The Notre Dame Bay Magma	5 - 18
5.4.1 Melting Or Fractional Crystallization?	5 - 19
5.4.2 The Sources	5 - 21
5.4.2.1 The Mantle Wedge	5 - 21
5.4.2.2 Depleted Or Enriched Mantle Source? - The Th/Zr-Nb/Zr Plot	5 - 22
5.4.2.3 Evidence For Mantle Metasomatism - (Th/La) _N -(La/Yb) _N Relationship	5 - 23
5.4.2.4 More Metasomatism - Melt Or Fluid? - Nb Vs. Nb/Th Relationships	5 - 26
5.4.2.5 More Sources - La Vs. La/Nb Relationships	5 - 27
5.4.2.6 Input From The Upper Continental Crust?	5 - 28
5.4.2.6.1 Sm/Nd-Nd Variations	5 - 28
5.4.2.6.2 Nd/Nd* Parameter	5 - 31
5.5 Summary And Conclusions	5 - 32
CHAPTER 6: DEFORMATION HISTORY AND STRUCTURAL GEOMETRY OF THE NOTRE DAME BAY AREA	6 - 1
6.1 Introduction	6 - 1
6.2 Deformation Characteristics Of Lithological Units In The Notre Dame Bay Area	6 - 4
6.2.1 The Little Bay Basalt	6 - 4
6.2.2 The Western Arm Group Basalts	6 - 6
6.2.3 Other Lithologies Of The Western Arm Group	6 - 6
6.2.4 Intrusive Rocks	6 - 7
6.3 Deformation History	6 - 8
6.3.1 D1 Deformation	6 - 8
6.3.2 D2 Deformation	6 - 10
6.3.3 D3 Deformation	6 - 12
6.3.4 D4 Deformation	6 - 13
6.3.5 D5 Deformation	6 - 15
6.4 Structural Geometry	6 - 17
6.4.1 Western Domain	6 - 17

6.4.1.1	Catchers Pond Panel	6 - 18
6.4.1.2	Mistaken Pond Panel	6 - 19
6.4.1.3	Southwest Arm Panel	6 - 20
6.4.1.4	Line Pond Panel	6 - 21
6.4.1.5	Sugar Loaves Panel	6 - 22
6.4.1.6	Little Bay Panel	6 - 23
6.4.1.7	Gull Pond Panel	6 - 24
6.4.2	Eastern Domain	6 - 24
6.4.2.1	Gull Pond Panel	6 - 25
6.4.2.2	Little Bay Panel	6 - 26
6.4.2.3	Mistaken Pond Panel	6 - 28
6.4.2.4	Shag Cliff Panel	6 - 29
6.4.2.5	Nogood Island Panel	6 - 30
6.5	Northern Domain	6 - 32
6.5.1	Long Island Sub-Domain	6 - 32
6.5.1.1	Southern Head Panel	6 - 33
6.5.1.2	Cutwell Arm Panel	6 - 34
6.5.1.3	Aspen Cove Panel	6 - 35
6.5.1.4	Stag Island Panel	6 - 36
6.5.1.5	Little Bay Island Sub-Domain	6 - 37
6.6	The Lobster Cove - Chanceport Fault	6 - 37
6.6.1	Geometry Of The Lobster Cove Fault	6 - 38
6.6.2	Structural Position Of Red Beds	6 - 39
6.6.2.1	The Springdale Area	6 - 39
6.6.2.2	Sunday Cove, Pilley's And Triton Islands	6 - 40
6.6.2.3	Lobster Cove Imbricate Stack	6 - 40
6.6.2.4	Grand Dismal Cove Duplex	6 - 42
6.6.2.5	Intervening Regions	6 - 42
6.6.3	New World Island Area	6 - 43
6.7	Geophysical Constraints	6 - 44
6.8	Constraints On The Ages Of Movement Along The Fault	6 - 45
6.9	Notre Dame Bay Nappe (Ndbn) Definition	6 - 46
6.10	The Green Bay Fault	6 - 47
6.11	Extensional Faults And Thrust Belts - The Case Of The Long Island Tickle Fault	6 - 48

6.11 Summary And Conclusions	6 - 49
CHAPTER 7 - TOWARDS AN INTEGRATED MODEL	7 - 1
7.1 Introduction	7 - 1
7.2 Summary Of Major Results	7 - 1
7.2.1 Stratigraphy	7 - 1
7.2.1.1 The Pre-500 Ma Sequence	7 - 1
7.2.1.2 The 485 - 465 Ma Sequence	7 - 3
7.2.2 Geochemistry	7 - 5
7.2.2.1 Geochemistry Of The Pre-500 Ma Sequence	7 - 5
7.2.2.2 Geochemistry Of The 509 - 488 Ma Dykes	7 - 7
7.2.2.3 Geochemistry Of The 485 - 465 Ma Sequence	7 - 7
7.2.3 Paleotectonic Implications	7 - 8
7.2.3.1 The Pre-500 Ma Sequence	7 - 8
7.2.3.2 The 509 - 488 Ma Dykes	7 - 11
7.2.3.3 The 485 - 465 Ma Sequence	7 - 11
7.2.3.3 Sources For The Notre Dame Bay Magmas	7 - 13
7.2.3 Structure	7 - 14
7.2.3.1 Faults Defining The Boundary Of The Study Area	7 - 15
7.2.3.2 Pre-500 Ma Deformation	7 - 15
7.2.3.3 Pre-Silurian Deformation	7 - 16
7.2.3.3 Notre Dame Bay Nappe	7 - 16
7.2.3.3 Southeasterly Verging Fold And Thrust Belt	7 - 16
7.2.3.4 Post-Emplacement Disruption Of The Notre Dame Bay Nappe	7 - 17
7.3 Geological And Tectonic History Of The Western Notre Dame Bay Area	7 - 18
7.3.1 Pre-500 Ma	7 - 18
7.3.2 First Deformation Event	7 - 20
7.3.3 Intrusion Of High-Mg Dykes	7 - 20
7.3.4 Deposition In The Interval 485-465 Ma	7 - 21
7.3.5 Between 465 Ma And Silurian	7 - 23
7.3.6 Silurian Deposition	7 - 23
7.3.7 Nappe Emplacement	7 - 23
7.3.8 Post-Emplacement Deformation	7 - 24
7.4 Conclusions And Recommendations	7 - 24

REFERENCES	R - 1
APPENDIX A - Faunal list and locations	A - i
APPENDIX B - Geochronology results	B - i
APPENDIX C - Analytical methods	C - i
APPENDIX D - Geochemical results	D - i
APPENDIX E - Structural plots	E - i

LIST OF FIGURES

FIGURE	DESCRIPTION	PAGE
2 1	Tectono-stratigraphic subdivision in Newfoundland	2-12
2 2	Schematic geological map of the Notre Dame Bay area.	2-13
3 1	Distribution of major lithostratigraphic units in the western Notre Dame Bay area	3-43
3 2	Stratigraphic order of units in the western Notre Dame Bay area, Lushs Bight and Western Arm groups	3-44
3 3	Stratigraphic order of units in the western Notre Dame Bay area, Cutwell Group and Stag Formation	3-45
3 4	Legend for lithostratigraphic columns in Figures 3.2 and 3.3.	3-46
3 5	Photo of large pillows and lobes of the Big Hill Basalt.	3-47
3 6	Thin section photo of a typical basalt from the Big Hill Basalt	3-48
3 7	Thin section photo of a "lamprophyric" dyke from the Whalesback Mine area	3-48
3 8	Thin section photo of a pyroxene-phyric dyke from the Whalesback Mine area	3-49
3 9	Thin section photo of a monomictic tuff-breccia from the Welsh Cove Formation	3-49
3 10	Thin section photo of matrix to polymictic lapilli tuff/tuff breccia from the Welsh Cove Formation	3-50
3 11	Thin section photo of a porphyry from Welsh Cove Formation	3-50
3 12	Photo of an outcrop of banded porphyritic tuff.	3-51
3 13	Photo of an outcrop of a mafic tuff and tuff breccia of the Western Head formation	3-51

3.14	Thin section photo of a granular-textured hornblende pyroxenite from the Brighton Intrusive Complex	3-52
3.15	Distribution of major lithostratigraphic units in the western Notre Dame Bay area in view of the present mapping	3-53
3.16	Thin section photo of subophitic and intersertal texture in a diabase cutting tuff breccia of the Pigeon Head Formation	3-54
3.17	Photo of interbedded volcanoclastic sandstone and well laminated volcanoclastic mudstone of the Long Tickle Formation	3-54
3.18	Photo of volcanoclastic sedimentary rocks of the Long Tickle Formation.	3-55
3.19	Photo of the tuff breccia of the Long Tickle Formation	3-55
3.20	Photo of a lobate massive mafic flow overlying the tuff lithofacies of the Long Island Formation	3-56
3.21	Photo of pillowed flows of the Long Tickle Formation	3-56
3.22	Thin section photo of a typical porphyritic andesite of the Long Tickle Formation.	3-57
3.23	Photo of the conodont fauna <i>Periodon aculeatus</i> Hadding from Limestone Island, off the Little Bay Islands' western shore	3-57
3.24	Photo of an andesite-cherty siltstone peperite from the western shore Little Bay Island.	3-57
3.25	Thin section photo of a welded crystal tuff from the Parson's Point Formation.	3-58
3.26	Photo of conodonts <i>Cordylodus? horridus</i> Barnes and Poplawski from limestone breccia, Long Island	3-59
3.27	Photo of a felsic flow of the Seal Cove Complex	3-59
3.28	Photo of a minor felsic dyke of the Seal Cove Complex.	3-60

3 29	Photo of a gabbro sill intruding contact between pillow lavas and breccia of the Stag Formation on League Rock.	3-60
4 1	Legend of abbreviations used in chapters on geochemistry.	4-52
4 2	An outline to divide volcanic rocks of the western Notre Dame Bay area	4-53
4 3	Legend of symbols used in figures of Chapter 4.	4-54
4 4	Diagram highlighting behaviour of SiO ₂ in mafic volcanic rocks of the western Notre Dame Bay area.	4-55
4 5	Diagram indicating divisions of felsic volcanic rocks of the western Notre Dame Bay area.	4-56
4 6	Diagram indicating two broad tectonic settings, in which the mafic volcanic rocks of the western Notre Dame Bay area formed.	4-57
4 7	Diagram of Zr-Ti to indicate origin of the samples from Fig. 4.6.	4-58
4 8	Diagram supporting the division of the Notre Dame Bay area rocks into arc and non-arc types.	4-59
4 9	Diagram indicating the division of samples into arc and non-arc types.	4-60
4 10	Diagram illustrating divisions made within rocks of the Notre Dame Bay area	4-61
4 11	Diagram of extended primitive mantle normalized REE patterns for samples CI-19-24 and NA-1 type	4-62
4 12	Diagram of extended primitive mantle normalized multielement plots of type NA-2	4-63
4 13	Diagram of extended primitive mantle normalized multielement plots of the TR type rocks.	4-64
4 14	Diagram of the multielement patterns for the Lushs Bight Group boninites.	4-65

4.15	Diagram of extended REE patterns for the A-2 type samples	4-65
4.16	Diagram of extended multielement plots of the A-3 type samples	4-67
4.17	Diagram of extended primitive mantle normalized REE patterns for the A-4 type rocks	4-67
4.18	Diagram indicating the predominantly sub-alkalic character of mafic subvolcanic rocks of the western Notre Dame Bay area	4-68
4.19	Diagram indicating two tectonic settings in which the mafic subvolcanic rocks of the western Notre Dame Bay area formed	4-69
4.20	Diagram with samples from Fig. 4-24 plotted to suggest origin of the samples in arc and non-arc tectonic settings.	4-70
4.21	Diagram of subvolcanic rock samples for the western Notre Dame Bay area to indicate origin in arc or non-arc environments.	4-71
4.22	Diagram supporting the division of samples into arc and non-arc types.	4-72
4.23	Diagram illustrating divisions within the subvolcanic rocks and correlations made with the previously recognized different types of mafic volcanic rocks.	4-73
4.24	Diagram of extended primitive mantle-normalized REE plots of the SNA and STR type samples	4-74
4.25	Diagram of multielement primitive mantle-normalized REE patterns of the SA-1 type boninitic dykes.	4-75
4.26	Diagram of extended primitive mantle-normalized REE plots of the SA-2 type.	4-75
4.27	Diagram of extended primitive mantle-normalized REE plots of the SA-3 type.	4-76
4.28	Diagram of discrimination plot for felsic volcanic and subvolcanic rocks of the western Notre Dame Bay area	4-77

4 29	Diagram of Y-Nb for felsic rocks of the western Notre Dame Bay area	4-78
4 30	Diagram of N-Nb/Th for felsic rocks of the western Notre Dame Bay area.	4-79
4 31	Diagram of chondrite normalized REE plots of F-1 and F-2 types of felsic rocks	4-80
4 32	Diagram of extended multielement plots of the F-1 type felsic volcanic and subvolcanic rocks	4-81
4 33	Diagram of extended multielement plots of the F-2 type felsic volcanic and subvolcanic rocks.	4-82
4 34	Diagram of extended multielement plots of the F-3 type post-kinematic intrusive rocks	4-82
5 1	Diagram of geochemical types versus schematic stratigraphic columns of the Lushs Bight/Western Arm groups and the Stag Formation - Cutwell Group	5-35
5 2	Diagram of primitive mantle-normalized extended REE plots of mafic volcanic rocks and tuffs and co-magmatic intrusive rocks.	5-38
5 3	Diagram of primitive mantle-normalized extended REE plots of the NA-1 E-MORB type tholeiites compared to similar rocks from various modern tectonic settings	5-40
5 4	Diagram of extended REE plots of the NA-2 type flows matched with various other lavas and a sills.	5-41
5 5	Diagram of primitive mantle-normalized extended REE plots of the NA-2b and NA-2c rocks and their analogues from modern spreading centers	5-42
5 6	Diagram of primitive mantle-normalized extended REE plots of the FR-1 type volcanic rocks and their modern counterparts.	5-43

5.7	Diagram of primitive mantle-normalized extended patterns of the A type rocks and their modern counterparts	5-44
5.8	Diagram of extended REE plots of the A-2d samples compared to selected rocks from modern settings	5-45
5.9	Diagram of extended multielement plots of the A-2e lavas compared to rocks from present day oceanic and continental arcs	5-46
5.10	Diagram of extended REE profiles of the A-3 type samples and lavas of the Valu Fa Ridge, Lau Basin	5-47
5.11	Diagram of multielement plots of ankaramitic flows of the A-4a subtype and modern analogues	5-47
5.12	Diagram of extended REE plots of samples of the A-4b subtype and a wide range of modern analogues	5-48
5.13	Diagram of extended REE patterns of the SA-2d dykes superimposed upon a pattern of modern high-Mg andesitic rocks	5-49
5.14	Diagram of multielement plots of the F-1 type low-K rhyolites as compared to rocks of modern island arcs	5-50
5.15	Diagram of identification plots for rocks of the western Notre Dame Bay area	5-51
5.16	Diagram of Nb/Zr versus Th/Zr for samples from the western Notre Dame Bay area as compared to present day tectonic settings	5-53
5.17	Diagram illustrating the relationship of Th with respect to REE in the western Notre Dame Bay lavas	5-55
5.18	Diagram of Nb-Nb/Th for compositions of the Notre Dame Bay area.	5-57
5.19	Diagram illustrating two strongly incompatible elements known to have diverse mobility in hydrous fluids	5-58

5 20	Diagram of Nd-Sm/Nd for rocks of the western Notre Dame Bay area of both arc and non-arc affinity	5-60
5 21	Diagram of Nd-Sm/Nd for the high-Mg dykes of the western Notre Dame Bay area	5-62
5 22	Diagram of Sm/Nd versus Nd/Nd* for samples from the western Notre Dame Bay area of both arc and non-arc affinity.	5-63
6 1	Diagram illustrating the three different structural domains in the area of study in western Notre Dame Bay	6-53
6 2	Diagram illustrating the distribution of fault panels within the structural domains of the western Notre Dame Bay area.	6-54
6 3	Thin section photo of "chaotic" chlorite-sericite foliation in dacitic tuff of the Welsh Cove Formation.	6-55
6 4	Thin section photo of mafic pyroxene-phyric tuff of the Skeleton Pond Formation	6-55
6 5	Thin section photo of the S2 "sericite schists" from the western part of the Catchers Pond Panel	6-56
6 6	Thin section photo of the red cherty sediment of the Skeleton Pond Formation.	6-56
6 7	Diagram illustrating the distribution of dykes in the Little Bay Mine area and stereogram plots of poles to both S2 cleavage and dykes.	6-57
6 8	Photo of red chert and intermediate reworked tuff of the Skeleton Pond Formation	6-58
6 9	Photo of a minor hinterland dipping duplex in red chert sediment of the Skeleton Pond Formation	6-58
6 10	Photo of a fragment of a duplex developed in cherty sediment of the Skeleton Pond Formation	6-59

6.11	Photo of strongly carbonitized and mylonitized mafic and ultramafic rocks from Pigeon Island, Long Island	6-60
6.12	Photo of a clast of gabbro surrounded by a mylonitic matrix	6-60
6.13	Photo of southwesterly dipping C5 shear bands cutting across the S2 cleavage and pillow lava of the Lushs Bight Group	6-61
6.14	Thin section photo of domino structures developed in rigid pyroxene phenocrysts in the late D1 dykes of the Whalesback Mine area.	6-62
6.15	Structural sketch of the area west of Springdale	6-63
6.16	Photo of an outcrop of imbricated felsic volcanic rocks of the Welsh Cove Formation.	6-64
6.18	Photo of a D3 minor S-shaped fold-pair	6-66
6.19	Photo of F3 folds that have an appearance of "drag" folds	6-66
6.20	Photo of a probable F3 fold on the southern shore of Lushs Bight	6-67
6.21	Photo of minor F3 Z-shaped folds on Oil Island W of Long Island	6-67
6.22	Photo of low-angle shear planes on Seal Island, NE of Long Island	6-68
6.23	Schematic geological map of the Notre Dame Bay area	6-69
6.24	Photo of a typical cross section of the Lobster Cove Fault	6-70
6.25	Diagram illustrating mylonitic pillow lava along with cherts and tuffs juxtaposed with red sandstones and underlying mafic rocks	6-71
6.26	Diagram illustrating well developed mylonitic S1 foliation within tuffaceous and cherty sediment	6-72
6.27	Diagram of the Lobster Cove Fault in the Grand Dismal Cove area	6-73
6.28	Photo of a reclined F3 syncline in red beds on the Lobster Cove Fault.	6-74

6-29	Bouguer gravity anomaly map for the area from the coast of Notre Dame Bay to the N and NE.	6-75
6-30	Diagram of geological models for gravity and magnetic data across Notre Dame Bay.	6-76
A - i	Location of faunal occurrences	A - v
B - i	$^{40}\text{Ar}/^{39}\text{Ar}$ age spectra for sample 88 - PIG (202).	B - viii
B - ii	$^{40}\text{Ar}/^{39}\text{Ar}$ age spectra for sample 88 - LR - CLT (203)	B - ix
B - iii	$^{40}\text{Ar}/^{39}\text{Ar}$ age spectra for sample 85 - AC - 80 - D233 (207).	B - x
B - iv	$^{40}\text{Ar}/^{39}\text{Ar}$ age spectra for sample RAL - 88 - 1 (208)	B - xi
B - v	$^{40}\text{Ar}/^{39}\text{Ar}$ age spectra for sample 88 - CL16 - 2b (210).	B - xii
B - vi	$^{40}\text{Ar}/^{39}\text{Ar}$ age spectra for sample 88 - LR - INT (211).	B - xiii
B - vii	$^{40}\text{Ar}/^{39}\text{Ar}$ age spectra for sample RAL - 88 - 2.	B - xiv
B - viii	$^{40}\text{Ar}/^{39}\text{Ar}$ age spectra for sample RAL - 88 - 3	B - xv
B - ix	$^{40}\text{Ar}/^{39}\text{Ar}$ age spectra for sample 89 - ASWB - 1 (272)	B - xvi
B - x	$^{40}\text{Ar}/^{39}\text{Ar}$ age spectra for sample 89 - ASWB - 2 (274).	B - xvii
B - xi	$^{40}\text{Ar}/^{39}\text{Ar}$ age spectra for sample 88 - LR - INT (271)	B - xviii
B - xii	$^{40}\text{Ar}/^{39}\text{Ar}$ age spectra for sample 88 - CL - 16 - 2b (273).	B - xix
B - xiii	$^{40}\text{Ar}/^{39}\text{Ar}$ age spectra for sample from Nickey's Nose Tuff, Western Head Formation.	B - xx
B - xiv	$^{40}\text{Ar}/^{39}\text{Ar}$ age spectra for sample WA - 44, Western Head Formation	B - xxi
B - xv	$^{40}\text{Ar}/^{39}\text{Ar}$ age spectra for sample WA - 45, Dolland Head Diorite	B - xxii
B - xvi	$^{206}\text{Pb}/^{238}\text{Pb}$ versus $^{207}\text{Pb}/^{235}\text{U}$ for the Brighton Intrusive Complex Titanites	B - xxiii
B - xvii	Concordia diagram for the Brighton Intrusive Complex	B - xxiv

B - xviii	Concordia diagram for the Catchers Pond Tuff and the Coopers Cove Pluton	B - xxx
E - i	Stereoplot Western Domain Whalesback Mine	E - ii
E - ii	Stereoplot - Western Domain	E - iii
E - iii	Stereoplot - Western Domain	E - iv
E - iv	Stereoplot - Western Domain	E - v
E - v	Stereoplot - Western Domain	E - vi
E - vi	Stereoplot - Western Domain	E - vii
E - vii	Stereoplot - Western Domain	E - viii
E - viii	Stereoplot - Western Domain	E - ix
E - ix	Stereoplot - Eastern Domain	E - x
E - x	Stereoplot - Eastern Domain	E - xi
E - xi	Stereoplot - Eastern Domain	E - xii
E - xii	Stereoplot - Eastern Domain	E - xiii
E - xiii	Stereoplot - Eastern Domain	E - xiv
E - xiv	Stereoplot - Eastern Domain	E - xv
E - xv	Stereoplot - Eastern Domain	E - xvi
E - xvi	Stereoplot - Eastern Domain	E - xvii
E - xvii	Stereoplot - Eastern Domain	E - xviii

LIST OF TABLES

TABLE:	DESCRIPTION	PAGE
4-1	Selected trace and REE ratios for the western Notre Dame Bay volcanic rocks of non-arc and transitional arc/non-arc affinity	4-46
4-2	Summary of tectono-magmatic affinity indicated from various discrimination diagrams for mafic volcanic rocks of non-arc and transitional arc/non-arc affinity	4-47
4-3	Selected trace and REE ratios for the Notre Dame Bay volcanic rocks of arc affinity	4-48
4-4	Summary of tectono-magmatic affinity indicated by various discrimination diagrams for the mafic volcanic rocks of arc affinity	4-49
4-5	Selected trace and REE ratios for the western Notre Dame Bay subvolcanic rocks	4-50
4-6	Summary of tectono-magmatic affinity indicated by various discrimination diagrams for the mafic subvolcanic rocks of the arc, transitional and arc affinities	4-51
B-1	Argon data	B - i
B-2	U/Pb data	B - vii
D-1	Geochemical data - Arc volcanics	D - ii
D-2	Geochemical data - CL and CP samples	D - ix
D-3	Geochemical data - Non-arc volcanics	D - x
D-4	Geochemical data - Transitional volcanics	D - xiii
D-5	Geochemical data - Arc intrusives	D - xv
D-6	Geochemical data - Transitional and non-arc (cp - 92 - 53) intrusives	D - xix
D-7	Geochemical data - Felsic rocks	D - xx

CHAPTER 1: INTRODUCTION

1.1 Purpose And Scope Of Thesis

The early Paleozoic rocks of central Newfoundland have been the subject of interest and controversy since the earliest observations by officers of the Newfoundland Geological Survey (e.g. Murray and Howley, 1881), not only for their widespread metallic mineral deposits (Swinden and Kean, 1988) but also for their potential to tell us much about the early geological and tectonic history of the Appalachian Orogen. Because these rocks represent vestiges of the early Paleozoic oceanic realm commonly referred to as the Iapetus Ocean, their study provides opportunities to understand the geological history of this long-lived and complex ocean and the continental margins which bounded it

During the late Cambrian and early Ordovician, volcanic, subvolcanic and epiclastic rocks presently exposed in western Notre Dame Bay are widely considered to have been generated in a series of island arcs and back-arc basins that fringed the ancient Laurentian continental margin (Williams, H. et al., 1988; Colman-Sadd et al., 1992; Kean et al., 1995). However, the geological and tectonic history of these rocks, and consequently of the continental margin at which they formed, has remained poorly understood. This is in part because

- geological studies in the area have been relatively local rather than regional in focus,
- interpretations have been encumbered with a lithostratigraphic framework that reflects, in many instances, a local rather than regional perspective and is thereby both unnecessarily complex and/or misleading in its assignment of units,
- the structural history of the area has not been understood in sufficient detail to understand the disposition of rock units at map scale; and
- there have been few attempts to integrate modern geochemical and geochronological techniques with regional scale geological mapping

This thesis reports the first comprehensive, integrated geological and geochemical study of volcanic and sub-volcanic rocks in the western part of Notre Dame Bay. The study focuses on rock sequences north of the Lobster Cove Fault and southwest of the Green Bay Fault, which outcrop on the Springdale Peninsula, Little Bay, Pилley's, Triton, and Long

Islands, and a number of intervening smaller islands. It was intended that through a detailed geological and geochemical study of rocks in this area, important new advances could be achieved in understanding the disposition of rock units in the area (both spatially and stratigraphically), their lithostratigraphic framework and depositional history, the tectonic environments in which they formed and the geometry of their present structural disposition. Geological mapping was initially focused in the Catcher's Pond Group southwest of Springdale, where it revealed a more complex stratigraphic and structural history than had previously been envisaged. Mapping was then carried out in rocks assigned to the Western Arm and Cutwell groups to the northeast and east, eventually extending eastward to Triton Island. Contemporary geological mapping in the Lushs Bight Group by the Newfoundland Department of Mines and Energy (Kean et al., 1995) was augmented where necessary by further traversing in this unit, allowing it to be integrated in the evolving stratigraphic and structural framework.

The question of the paleotectonic settings of the rocks and their relative ages were addressed by detailed geochemical studies, and by micropaleontological and $^{40}\text{Ar}/^{39}\text{Ar}$ geochronological studies of the volcanic and subvolcanic rocks. Geochemical sampling accompanied mapping and encompassed all volcanic and subvolcanic rocks as well as some post-tectonic intrusions. The objectives of this work were to aid with stratigraphic interpretations and to permit interpretations of the tectonic environments in which the rocks formed. Coupled with new age information, this work has helped produce a new model for the geological development of this area that is more complete and better constrained than was previously possible.

Following the introduction, Chapter 2 presents a review of the geological setting of central Newfoundland. Particular emphasis is placed on the current understanding of the setting of rocks in western Notre Dame Bay so as to set the stage for the new results of the present study.

Chapter 3 presents a detailed analysis of the lithostratigraphy of the area, based principally on the new geological mapping carried out during the course of this study as well as micropaleontological and geochronological work carried out in conjunction with this study. It has proved possible to correlate in some detail many rock units that were

previously assigned to disparate lithostratigraphic units of uncertain mutual relationship and a revised lithostratigraphy is proposed based on this new understanding. According to the North American Code of Stratigraphic Nomenclature, a thesis is not considered to be the proper venue by which to introduce changes to established stratigraphic nomenclature, because of the theses limited circulation. Therefore, it is customary to distinguish stratigraphic nomenclature by, for instance, using Formation or formation, in reference to formalized and unformalized names of stratigraphic units. Since it is the author's and his co-workers intention to publish the stratigraphic nomenclature introduced in this thesis in referred journal publications, no distinction was made between the formalized and unformalized names by using capitalized or non-capitalized first letters. Care has been taken to clearly discuss and describe the old stratigraphic order, the informal changes made to it and the new proposed stratigraphic order.

Chapters 4 and 5 present the results of the geochemical studies. In Chapter 4, the geochemical characteristics of the volcanic and subvolcanic rocks are described and a classification scheme for all rocks in the western Notre Dame Bay area is developed based on their geochemical characteristics. In Chapter 5, geochemical data are integrated with lithostratigraphy to evaluate the geochemical evolution of rocks in the area. These results are then interpreted in terms of the paleotectonic history of the rocks through comparison with modern environments and petrogenetic considerations concerning the nature of possible source regions for the magmas.

Chapter 6 presents a description of the structural history of the area. Structural data show a complex folding and faulting history in the region and offer a new interpretation of relationship between structures and the disposition of litho- and chemo-stratigraphic units. A major result is the recognition that rocks in the western Notre Dame Bay area are disposed in a recumbent, nappe structure that has been disrupted by later structures.

In Chapter 7, all geological and geochemical data are reviewed and integrated in a model for the tectonic history of the western Notre Dame Bay area. Principal conclusions are reviewed and suggestions for future work are presented.

CHAPTER 2: REGIONAL SETTING OF THE STUDY AREA

2.1 Introduction: The Appalachian Orogen In Newfoundland

Almost three decades ago, Wilson (1966) proposed that the Appalachian - Caledonian orogen records a cycle of ocean development and destruction. The island of Newfoundland lies at the centre of this orogen and provides a complete record of this cycle. Based upon contrasts in structure and stratigraphy of pre-Silurian rocks, the Newfoundland Appalachians have been divided into (from east to west): the Avalon, Gander, Dunnage, and Humber tectono-stratigraphic zones (Fig. 2.1).

The eastern Avalon and Gander zones and the western Humber Zone (Fig. 2.1) represent vestiges of opposing Gondwanan and Laurentian margins, respectively. The Dunnage Zone, forming the internal part of the orogen, is underlain by ophiolitic and volcanic-epiclastic sequences interpreted as fragments of the intervening oceanic realm (e.g. Rodgers and Neale, 1969; Dewey and Bird, 1971; Church and Stevens, 1971; Dean, 1978; Williams, 1979; Kean et al., 1981; Dunning and Chorlton, 1985), commonly referred to as Iapetus Ocean (Harland and Gayer, 1972).

2.2 Avalon Zone

The Avalon Zone (Fig. 2.1) contains Hadrynian clastic and volcanic sequences of Pan-African affinity unconformably overlain by Lower Cambrian to Lower Ordovician sedimentary rocks (Williams, 1979; Strong et al., 1978; King, 1988). Although little deformed and metamorphosed in the eastern part of the zone, Avalonian rocks in the western Avalon Zone and along the south coast of Newfoundland were considerably affected by Paleozoic tectonothermal events (O'Brien et al., 1989). The Avalon Zone is characterized by a variety of magmatic events that took place at about 760 Ma, 680 - 670 Ma, 620 Ma and 580 - 550 Ma (O'Brien et al., 1992) and predate the development of the Appalachian Orogen.

2.3 Gander Zone

The Gander Zone (Fig. 2.1) is characterized by Cambrian and Ordovician, predominantly metasedimentary rocks that display a high degree of deformation and metamorphism. These rocks are thought to represent marine deposits from the eastern margin of Iapetus, and have been widely interpreted as representing the sedimentary wedge derived from Gondwana (Williams, 1979; Colman-Sadd, 1980). The Gander Zone rocks were affected by a major Ordovician deformational event (the Penobscot Orogeny) during which they were structurally overridden by ophiolitic complexes derived from the Dunnage Zone (Dec and Colman-Sadd, 1990; Colman-Sadd et al., 1992).

2.4 Humber Zone

The Humber Zone (Fig. 2.1) represents the ancient North American Laurentian continental margin. Crystalline rocks of the Grenvillian basement are unconformably overlain by latest Precambrian to earliest Cambrian siliciclastic and rift-related volcanic rocks and thence by a Cambro-Ordovician carbonate-dominated sequence developed on a passive continental margin (e.g. Williams, 1979; Williams and Hiscott, 1987). Sedimentary rocks of the zone in Newfoundland were variably affected by Appalachian deformation, although their counterparts overlying the Canadian Shield to the north and west of the Appalachian structural front in Quebec and further south along the orogen, were not

2.5 Dunnage Zone

The Dunnage Zone (Fig. 2.1) is considered to represent remnants of the Iapetus Ocean, which lay between the Laurentian and Gondwanan continents during the early Paleozoic. It is underlain by disrupted and deformed Cambrian to Ordovician ophiolitic complexes, and a complex assemblage of volcanic and volcanoclastic rocks that are variously younger and older than the ophiolitic rocks. Pre-Silurian rocks of the Dunnage Zone are overlain by various Silurian and younger overlap sequences (Fig. 2.1) which record terrestrial volcanism and sedimentation in epi-continental calderas and successor basins, respectively.

The similarity between the volcanic, volcanoclastic and ophiolitic sequences of the central Newfoundland Dunnage Zone and rocks forming in modern volcanic island arcs has been pointed out by many authors in regional syntheses (e.g. Wilson, 1966; Bird and Dewey, 1970; Strong, 1977; Dean, 1978) as well as in more specific study areas (e.g. Cutwell Group: Kean and Strong, 1975; Snooks Arm Group: DeGrace et al., 1976). Geochemical and isotopic studies suggest that both the ophiolites and most if not all of the volcanic/epiclastic sequences were generated in supra-subduction zone environments (Sun and Nesbitt, 1978; Upadhyay and Neale, 1976) and represent a complex assemblage of magmatic arc and marginal basin settings ranging in age from Late Cambrian to Early Ordovician (e.g. Coish et al., 1982; Dunning and Chorlton, 1985; Swinden et al., 1990; Dunning et al., 1991; Jenner et al., 1991).

On the basis of differences in pre-Middle Ordovician regional geology, stratigraphy, fauna, geophysical signatures, and isotopic characteristics, Williams et al. (1988) divided the Dunnage Zone into the Notre Dame and Exploits subzones (Fig. 2.1), which are structurally juxtaposed along a complex fault zone, termed the Red Indian Line (Williams et al., 1988). The major geological difference between the Notre Dame Subzone and the Exploits Subzone is the presence in the latter of a relatively complete post-middle Ordovician, paleontologically dated, succession of Llandeilo to Ashgill black shale, overlain gradationally by sandstone, conglomerate, and melange of Caradoc to late Llandovery age (Dean, 1978; Arnott, McKerrow and Cocks, 1985; Williams, S.H., 1989). This succession is missing from the Notre Dame Subzone. A further difference between the subzones is expressed in contrasts in the affinity of Lower Ordovician fauna. Arenig fauna in the Exploits Subzone are of Gondwanan affinity (e.g. Williams, S.H. et al., 1991); whereas, fauna of similar age in the Notre Dame Subzone are of Laurentian affinity (Nowlan and Thurlow, 1984; O'Brien and Szybinski, 1989; Williams, S.H., 1989). Swinden et al. (1988) and Williams et al. (1988) have noted isotopic contrasts of volcanogenic sulphide deposits on opposing sides of the Red Indian Line. Colman-Sadd et al. (1992) have suggested that these lines of evidence suggest that the Notre Dame Subzone and Exploits Subzones formed in disparate areas of Iapetus, the former near the Laurentian margin and the latter at some outboard position, perhaps in part at the Gondwanan margin.

The first rocks to be accreted to the Laurentian Margin during closing of the Iapetus Ocean were inboard units of the Notre Dame Subzone and their accretion is widely accepted to mark the beginning of the Ordovician Taconian Orogeny. Studies by Neuman (1984) and Colman-Sadd et al. (1992) suggest that the emplacement of Exploits Subzone onto the Gander Zone took place prior to amalgamation of the Notre Dame and Exploits subzones, implying that the pre-Middle Ordovician geological evolution of the Exploits Subzone may have proceeded largely independently from that of the Notre Dame Subzone.

Geochronological studies in recent years (e.g. Dunning and Krogh, 1985; Dunning et al., 1987; Dunning et al., 1991; Jenner et al., 1991) have shown that ophiolitic and volcanoclastic/epiclastic sequences were generated during approximately the same time span (latest Cambrian to Llandeilo) in both subzones. Geochemical studies of volcanic and subvolcanic rocks from a variety of sequences throughout the Dunnage Zone have been interpreted to indicate that ophiolitic and volcanic sequences in both subzones formed in similar tectonic settings (e.g. Jenner and Szybinski, 1987; Swinden, 1988; Jenner et al., 1991; Dunning et al., 1991; Jenner and Swinden, 1993). Taken as a whole, these studies suggest that the Cambro-Ordovician volcanic sequences and associated ophiolites in central Newfoundland evolved in supra-subduction zone environments, which produced similar volcanics in a time-frame similar to that now seen in the southwest Pacific.

2.6 Relationships Between The Dunnage And Other Zones

Boundaries between the Dunnage and both Gander and Humber zones (Fig 2.1) represent boundaries between oceanic and continental realms. The division between the Dunnage and Gander zones was first described in the area north of Gander Lake where it was variously described as a structural boundary (Uzuakpunwa, 1973) or an unconformity (Kennedy and McGonigal, 1972). Although still a matter of some controversy, recent structural studies indicate that the Humber/Dunnage boundary in this area is most likely structural with a long and complex movement history (Goodwin and O'Neill, 1991). Recent work in south-central and southern Newfoundland (e.g. Colman-Sadd and Swinden, 1984; Piasecki, 1988) has shown that the boundary between these zones in this area is also a complex structural boundary, exposed in a number of areas where Dunnage Zone rocks can

be shown to structurally overlie rocks of the Gander Zone. On the basis of reinterpreted published gravity data, Karlstrom (1983) proposed that the Dunnage Zone is allochthonous on the Gander Zone. This and geological evidence in the Mount Cormack area, south-central Newfoundland, led Colman-Sadd and Swinden (1984) to conclude that Gander-type rocks within the Dunnage Zone in this area are exposed in tectonic windows (see also Williams et al., 1988, Colman-Sadd et al., 1992). The minimum age of emplacement of the eastern part of the Dunnage Zone upon the Gander Zone is constrained by the ca. 475 Ma age of the stitching Partridgeberry Hills granite near Coy Pond, and the event has been assigned to the Penobscot Orogeny (Colman-Sadd et al., 1992). Sedimentological linkages were established between the Gander Zone and the eastern part of the Dunnage Zone after the Late Arenig (Colman-Sadd et al., 1992).

The Penobscot Orogeny on the Gondwanan margin was approximately coeval with the Taconian Orogeny on the opposite Laurentian margin of Iapetus, during which rocks of the Notre Dame Subzone were emplaced upon the Humber Zone. The Dunnage - Humber boundary (Fig. 2.1) is represented by the Baie Verte-Brompton Line (BVBL) (Williams and St.-Julien, 1982), a relatively narrow and steep fault zone marked by discontinuous ophiolitic blocks and considered by some workers (e.g. Williams and St.-Julien, 1982) to be the root zone for allochthonous ophiolites (e.g. parts of Hare Bay and Humber Allochthons) emplaced on the Laurentian margin. Ophiolitic and mafic volcanic rocks are common east of the BVBL where they are intruded by the Burlington granodiorite (Silurian, G. Dunning and P. Cawood, pers. comm.). In contrast, west of the BVBL, metamorphosed and deformed clastic rocks of the Humber Zone form the dominant lithology (Williams, 1979).

The BVBL can be traced along the strike extent of the Canadian Appalachians, although locally it is covered by Silurian and younger overlap sequences or overprinted by younger structures (Williams and St.-Julien, 1982). The lineament cannot be detected on seismic profiles, and it appears from seismic evidence not to affect Grenvillian basement, which is interpreted to extend at depth from the Humber Zone eastward for at least 70 km beneath the Dunnage Zone (Keen et al., 1986).

A large klippe termed the Humber Arm Allochthon, derived from the Notre Dame Subzone and the adjacent continental rise and slope, structurally overlies the Humber Zone

(Fig. 2.1) (Williams et al., 1988; Colman-Sadd et al., 1992) Ophiolitic rocks assigned to the Bay of Islands Complex (Fig. 2.1) form one of the structurally highest slices in this allochthon. The emplacement of the Humber Arm Allochthon is widely interpreted as a principal manifestation of the middle Ordovician Taconian Orogeny and its arrival at the Laurentian margin is interpreted to be marked by the first appearance of ophiolitic detritus in fossiliferous late Arenig clastic sediments of the Humber Zone foreland flysch (Williams and Stevens, 1974; Casey and Kidd, 1981; Stevens, 1970; Williams, S.H. and Stevens, 1988). The stratigraphic age is consistent with a $^{40}\text{Ar}/^{39}\text{Ar}$ age of 469 \pm 5 Ma on hornblende from the metamorphic sole of the Bay of Islands Complex (age recalculated with new decay constant from Dallmeyer and Williams, 1975).

2.7 Overlap Sequences

Lower Silurian igneous and sedimentary rocks intruded and were deposited upon the allochthonous Dunnage Zone sequences (Fig. 2.1) following their accretion to the Laurentian margin (e.g. Coyle and Strong, 1987; Whalen, 1989). These rocks are very widespread and the area of exposure of Silurian plutonic and volcanic rocks in central and southern Newfoundland exceeds that of the older oceanic rocks. Silurian volcanic and sedimentary rocks are common in the eastern portion of the Baie Verte Peninsula, and along the west side of White Bay, and they form part of an overlap assemblage that straddles the BVBL (e.g. Coyle and Strong, 1987). Silurian terrestrial volcanic and sedimentary rocks represent the high level expression of a widespread magmatic, metamorphic and deformational event which has been recently widely recognized and termed the Salinic Orogeny (Dunning et al., 1990; O'Brien et al., 1991). In the vicinity of the present study area, Silurian rocks are principally assigned to the Springdale Group and the King's Point Complex.

The Springdale Group is an extensive sequence of subaerial mafic and felsic volcanic rocks, overlain by fluvial sedimentary rocks (red beds). It lies unconformably upon Lower Ordovician volcanic rocks of the Catchers Pond and Robert's Arm Groups (Coyle and Strong, 1987). Volcanic rocks have yielded U-Pb zircon ages from 432 \pm 1 to 425 \pm 3/-3 Ma (Whalen et al., 1987; Coyle, 1990). Geochemical data from rocks of the Topsails

Complex, which is spatially and genetically related to the Springdale Group, indicate that the magmatic activity was apparently tapping sources typical of those commonly associated with subduction zones (e.g. Whalen et al., 1987; Whalen, 1989).

Felsic volcanic and intrusive rocks of the King's Point Complex (Mercer et al., 1985; Kontak and Strong, 1986), are exposed in the eastern part of the Baie Verte Peninsula, separated from the study area by the Green Bay Fault. A U-Pb zircon age of $427 \pm 2/-2$ Ma for a syenitic phase of the intrusion indicates that complex is coeval with the Springdale Group (Coyle, 1990). Further to the north and west on the Baie Verte Peninsula, subaerial volcanic rocks assigned to the Cape St. John Group (Hibbard, 1983) have yielded a U-Pb zircon age of $427 \pm 2/-2$ Ma (Coyle, 1990) and are interpreted to be regionally correlative with the Springdale Group and the King's Point Complex (Coyle and Strong, 1987).

Carboniferous (Alleghenian) orogenic activity is predominantly recognized in the Humber Zone in the development and deformation of post-Late Devonian successor basins (e.g. Knight, 1983). Small outliers of Carboniferous sedimentary rocks are found in the Notre Dame Subzone including a small outcrop which unconformably overlies the Lushs Bight Group at King's Point, but is at least locally fault bounded (Kean and Evans, 1987).

2.8 Ophiolites And Volcanic-Epiclastic Sequences Of The Notre Dame Subzone

The Notre Dame Subzone is underlain by submarine magmatic and sedimentary rocks interpreted to have formed in a series of island arcs and back-arc basins at and near the ancient Laurentian margin. Marine volcanism and sedimentation took place over more than 55 Ma, from the Upper Cambrian to the Middle Ordovician. The sequence of events in the Notre Dame Subzone is currently interpreted on the basis of a number of high precision U-Pb zircon ages (e.g. Dunning and Krogh, 1988) which constrain the magmatic activity in this area to at least two time intervals characterized by the generation of volcanic rocks of island arc affinity and associated epiclastic sediments (ca. 505 Ma and earlier; ca. 482-460 Ma) and an intervening, partially overlapping time interval during which ophiolitic rocks were formed (ca. 492-475 Ma). This series of events is summarized below (U-Pb zircon ages and the time scales of Tucker et al., 1990, and Cooper, 1992, are used):

2.8.1 STAGE 1: CA 505 MA AND OLDER, UPPER CAMBRIAN(?) TO MIDDLE TREMADOC

This time interval is principally represented in the Notre Dame Subzone by the Twillingate Trondhjemite in eastern Notre Dame Bay which has been dated at $507 \pm 3/-2$ Ma (Elliott et al., 1991). Geochemical and geological studies suggest that this intrusion may have formed through partial melting at the base of an island arc (Payne and Strong, 1979). The Twillingate Trondhjemite intrudes mafic pillow lavas of the Sleepy Cove Group, which have geochemical signatures indicative of island arc affinity (H S Swinden, unpublished data), and its age provides a minimum age for this volcanism. In the Humber Arm Allochthon, trondhjemite of the Little Port Complex, widely interpreted to have been derived from the Notre Dame Subzone, has yielded a similar age ($505 \pm 3/-2$; Mattinson, 1975; Jenner et al., 1991) and geochemical studies of the trondhjemite and associated pillow lavas also suggest an island arc affinity (Jenner et al., 1991).

2.8.2 STAGE 2: CA 492 TO 475 MA, MIDDLE TREMADOC - MIDDLE ARENIG

During this time interval, ophiolites were generated in the Notre Dame Subzone. In the western part of the Notre Dame Subzone, ophiolites which are now exposed in and immediately east of the BVBL are considered to be middle Tremadoc, based on a U-Pb zircon age on gabbro from the Betts Cove Complex as $489 \pm 3/-2$ Ma (Dunning and Krogh, 1985). The Bay of Islands Complex in the Humber Arm Allochthon, generally considered to have been derived from the Notre Dame Subzone, has yielded a U-Pb zircon date of $485.7 \pm 1.9/-1.2$ Ma (Dunning and Krogh, 1985). A somewhat younger generation of ophiolitic rocks occurs on the eastern side of the Notre Dame Subzone. The Annieopsquotch Complex has yielded ages of $477.5 \pm 2.6/-2.0$ Ma and $481.4 \pm 4.0/-1.9$ Ma (lower-middle Arenig) (Dunning and Krogh, 1985) and an age of 479 ± 3 Ma on Mansfield Cove Complex trondhjemite (Dunning et al., 1987) provides a minimum age for ophiolitic rocks of the Hall Hill Complex which it intrudes. As previously noted, there is geochemical and/or isotopic evidence in all of these ophiolitic rocks for the involvement of subduction-contaminated mantle sources. This, coupled with the fact that the age of formation of all dated ophiolites is younger than the age of the oldest dated

rocks generated in island arc environments, suggests that the ophiolites represent the back-arc / marginal basin crust rather than Iapetan oceanic crust *sensu stricto* (Sun and Nesbit, 1978, Upadhyay and Neale, 1979; Dunning and Chorlton, 1985; Dunning et al., 1991, Jenner et al., 1991).

The Betts Cove Complex on the eastern edge of the Baie Verte Peninsula (Upadhyay et al., 1971; Upadhyay, 1973) provides a good illustration of the geochemical characteristics of Dunnage Zone ophiolites. Pillow lavas from the extrusive sequence display a wide range of geochemical signatures that includes high-Mg andesites and boninites, tholeiitic basalts of MORB affinity, as well as island arc tholeiites (e.g. Coish et al., 1982; Swinden et al., 1989, G.A. Jenner, unpubl. data). The presence of boninites has been cited as evidence for formation of the Betts Cove Complex in a supra-subduction zone setting (e.g. Sun and Nesbitt, 1978; Coish et al., 1982). The ophiolitic complex is overlain (conformably?) by volcanoclastic rocks interfingered with two units of pillow lava of ocean island affinity (Jenner and Fryer, 1980). Geological information, combined with geochemical signatures of mafic volcanic rocks and Nd isotopic data, suggest that the Betts Cove Complex formed during island-arc rifting; whereas, the overlying Snooks Arm Group represents subsequent volcanism and sedimentation associated with the formation of a back-arc basin.

2.8.3 STAGE 3: CA 484 MA TO 460 MA, LOWER ARENIG TO LLANDEILO/ CARADOC BOUNDARY

During this time interval, a younger generation of island arc(s) rocks was formed that are now exposed mainly in the structurally complex Buchans-Roberts Arm Volcanic Belt along the eastern side of the Notre Dame Subzone (Bostock, 1988; Swinden, 1992; Dec et al., 1994). These rocks are principally distinguished by their ubiquitous calc-alkalic geochemical signatures and the common association with felsic volcanic rocks. The oldest dated rocks are calc-alkalic volcanic rocks of the Cottrell's Cove Group, which have recently yielded a U-Pb zircon age of approximately 484 Ma (Dec et al., 1994). Further to the west and south, felsic volcanic rocks of the Buchans Group and Roberts Arm Group have been dated at $473 \pm 3/-2$ Ma and 473 ± 2 Ma, respectively (Dunning

et al., 1987) Slightly younger felsic rocks of the Cutwell Group yield an age of $469 \pm 5/-3$ Ma (Dunning and Krogh, 1988).

2.9 The Western Notre Dame Bay Area

The focus of this thesis is the geological relationships in the western part of Notre Dame Bay. The area to be considered is bounded to the west and northwest by the Green Bay Fault, to the south by the Lobster Cove Fault, to the east by League Rock and to the north by the ocean. It includes the Springdale Peninsula, Little Bay, Pilley's, Triton and Long Islands, and a number of intervening smaller islands.

The early understanding of the geological character and evolution of the Dunnage Zone was largely based on study of the well exposed coastal sections of the Notre Dame Bay region in central Newfoundland. Interest in the Notre Dame Bay region was fueled in the middle and late 1880's by the discovery of copper deposits in the volcanic rocks, mainly on the Baie Verte and Springdale Peninsulas. In the last quarter of the nineteenth century, the area was a main center for copper production worldwide. The importance of the western Notre Dame area was recognized by the Newfoundland Geological Survey. Early geological work was carried out by A.H. Murray and J.P. Howley (Murray and Howley, 1881; 1918) and continued into first half of twentieth century. Work of particular relevance to the present study was carried out by Espenshade (1937) in the Pilley's Island-Badger Bay area and by MacLean (1947) in the Springdale area. These studies provided the early definition of lithostratigraphic relationships in this area. Since this time, there have been a large number of geological studies within the area. These are detailed and summarized in Chapter 3.

The geological history and setting of the Notre Dame Bay region is complex and reflects many aspects of the tectonostratigraphic development of the Dunnage Zone and its accretion to the Laurentian margin. This region contains structural blocks bounded by a number of major fault zones with potentially long and complicated histories (e.g. Lukes Arm Fault, Green Bay Fault, Lobster Cove Fault, Chanceport Fault) (Espenshade, 1937, MacLean, 1947; Dean and Strong, 1977; Calon and Szybinski, 1988; LaFrance, 1989; Blewett, 1989; Elliott et al., 1990; Cawood and van Gool, 1993).

The geographic distribution of the western Notre Dame Bay area as well as included and adjacent lithostratigraphic units within the Notre Dame Subzone are illustrated in fig. 2.2. The western Notre Dame Bay area is separated from rocks of the Baie Verte Peninsula by the Green Bay Fault and from the Roberts Arm Group by the Lobster Cove Fault.

Prior to this thesis, the stratigraphy in the southwestern part of the western Notre Dame Bay area was described in terms of the following lithostratigraphic units. The Lushs Bight Group, interpreted to be the oldest rocks in the area, consists predominantly of pillowed mafic flows with significant areas of sheeted dykes and minor ultramafic rocks (Kean, 1984, Kean et al., 1995). The Lushs Bight Group is considered to be directly overlain by the Western Arm, Catchers Pond and Cutwell groups to the northwest, southwest, and northeast, respectively. These rocks consist of mafic volcanoclastic rocks interfingered with pillow lava and, to a lesser extent, with felsic pyroclastic rocks (e.g. Dean, 1978, Kean, 1984). Faunal (e.g. Dean, W. 1970; Williams, S.H. 1989), $^{40}\text{Ar}/^{39}\text{Ar}$, and U-Pb zircon ages (Stukas and Reynolds, 1974; Dunning and Krogh, 1989; Ritcey, 1993) indicate that these rocks span the time interval from Lower Tremadoc to Lower Llanvirn (i.e. approx. 40 Ma). Revisions to the currently accepted lithostratigraphy are proposed later in this thesis, to account for new field data. The youngest stratified rocks in the area are a sliver of the Silurian Springdale Group basalt and clastic sediments which structurally overlies rocks of the Catchers Pond Group. Red sedimentary rocks of the Springdale Group are also found along the trace of the Lobster Cove Fault, which forms the southern boundary of the study area. These rocks, form an overlap sequence which provides important evidence as to the movement history of this fault and have considerable bearing on the interpretation of the history of the western Notre Dame Bay area. As well, dykes of Silurian age intruding the latter were documented by Ritcey (1993).

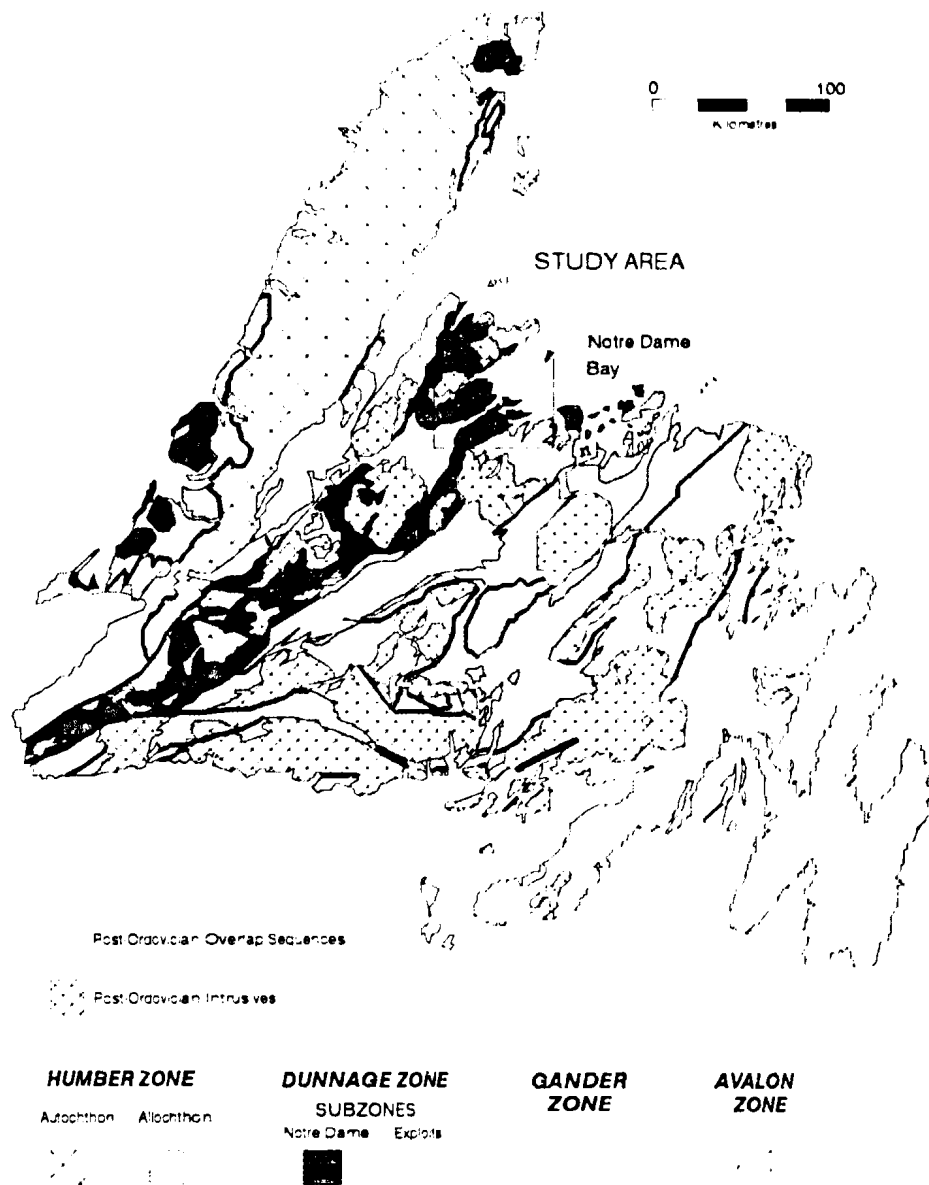


Figure 2.1. Tectono-stratigraphic subdivision in Newfoundland (after Williams, H. et al., 1988).

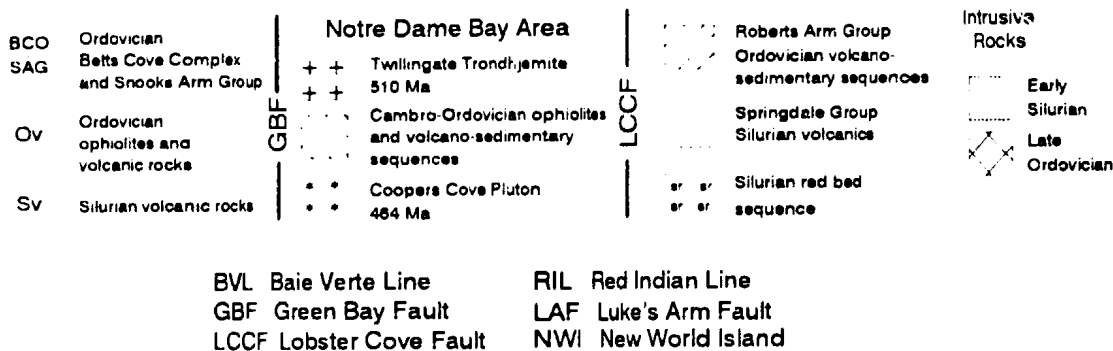
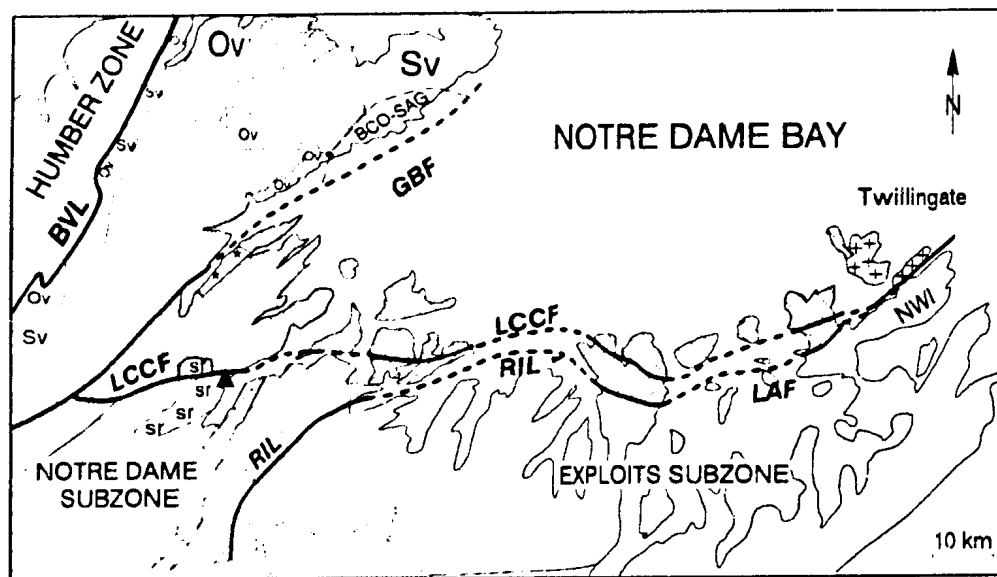


Figure 2.2. Schematic geological map of the Notre Dame Bay area; note that the legend reflects tectonic divisions in the Dunnage Zone.

CHAPTER 3: STRATIGRAPHY OF WESTERN NOTRE DAME BAY

3.1 Previous Work And Nomenclature

The stratigraphic nomenclature in the study area, established prior to this work, recognized four major lithostratigraphic units, the Lushs Bight, Western Arm, Catchers Pond, and Cutwell groups (Fig. 3.1 and Fig. 3.2). The Lushs Bight Group was thought to be the oldest and in either stratigraphic or structural contact with the other three groups (e.g. Williams, 1962; Bird and Dewey, 1970; Marten, 1971a, b). Rocks of the Lushs Bight Group were thought to form the upper part of an incomplete ophiolite (i.e. lacking ultramafics and most of the gabbroic sequences) and to be of oceanic affinity (Smitheringale, 1972; Strong, 1973). The Western Arm, Catchers Pond and Cutwell groups have been interpreted as products of island arc volcanism (Kean, 1973; Kean and Strong, 1975; Strong, 1977; Dean, 1977, 1978), but only the Cutwell Group had sufficient stratigraphic and geochemical data to support this interpretation (Kean, 1973; Kean and Strong, 1975; Strong, 1977). The Western Arm Group lacked any geochemical data and almost nothing in detail was known about the geology of the Catchers Pond Group. More information on previous work and nomenclature within these four units is presented below

3.1.1 LUSHS BIGHT GROUP

The Lushs Bight Group was defined by Espenshade (1937) and named after the type locality in the Lushes (present spelling) Bight area on Long Island. MacLean (1947) correlated the rock units on Springdale Peninsula with the Lushs Bight Group, and divided them into two sections: the lower Little Bay Head Section containing mainly basaltic flows, and the higher Western Arm Section, which also included volcanoclastic and sedimentary rocks. Marten (1971a, b) redefined the group and changed the rank of the Western Arm Section to group, whereas Kean and Strong (1975) included volcanic and volcanoclastic rocks on Long Island in the Cutwell Group. At present the Lushs Group includes only volcanic rocks and sheeted dykes (e.g. Kean and Evans, 1987; Kean et al., 1995), and there are no rocks of the group near Lushes Bight or anywhere on Long Island.

The Lushs Bight Group has been the focus of detailed mapping by a number of workers and descriptions of rock types included in the group are found in Fleming (1970), Marten (1971), Sayeed (1971), DeGrace (1971) and Kean (1983, 1984). The most recent mapping of the Lushs Bight Group (Kean and Evans, 1987a, b) identified two major lithological units; the lowest, exposed unit consists of sheeted dykes, and is overlain by an extensive unit of pillow lavas, lesser pillow breccia and a minor sequence of argillite and jasper. On the basis of subsequent geochemical studies on samples collected during this mapping it was suggested that the Lushs Bight Group formed in a supra - subduction zone environment and records the early stages of island arc evolution (Jenner et al., 1988, Swinden et al., 1989; Jenner et al., 1991; Kean et al., 1995; Jenner et al., in prep.).

The Brighton Complex, interpreted to be in intrusive contact with the Lushs Bight Group (Hussey, 1967), yielded an $^{40}\text{Ar}/^{39}\text{Ar}$ age of 495 +/- 5 Ma (Stukas and Reynolds, 1974), which provided a minimum age of deposition. Thus, the Lushs Bight Group was tentatively assigned an Upper Cambrian - Lower Ordovician age (e.g. Kean, 1984, 1989), although it lacked fossils and/or direct radiometric age determinations

3.1.2 WESTERN ARM GROUP

MacLean (1947) was the first to propose a stratigraphic order in the Western Arm section, which he considered to be the highest unit within the Lushs Bight Group. He divided the section into two basalt pillow-lava formations, the Basal and the Upper, interbedded with the sedimentary and pyroclastic formations, respectively. Marten (1971a, b) changed the status of the section to group, revised the lower boundary of the unit and refined the stratigraphy. He drew the boundary between the Lushs Bight and the Western Arm groups at the base of the first mappable tuff unit in the upper part of the Basal Basalt Pillow-lava Formation, and included the basal pillow lavas (his "black facies") in the Lushs Bight Group. Marten (1971a, b) named the lowest formation within the Western Arm Group the Skeleton Pond Tuff, and suggested that it conformably overlies pillow lava of the "black facies". The Skeleton Pond Tuff consisted of three tuff members interfingering with two flow members, and was overlain by a thick sequence of pillow basalt, the Big Hill Basalt. The Welsh Cove Tuff, a unit composed of felsic

crystal and welded tuffs interbedded with chert, argillite and mafic tuff separated the Big Hill Basalt from the Western Head Agglomerate, a massive coarse, mafic agglomerate forming the top of the group. Sills of diabase, gabbro and a small pluton of quartz diorite (Dolland Arm Head Quartz Diorite of MacLean, 1947) which intruded these units, were interpreted by Marten to be co-magmatic with the volcanism. The Western Arm Group has been correlated with the Snooks Arm Group (Upadhyay, et al., 1971, Marten, 1971b) and the Cutwell Group (Marten, 1971b).

A single specimen of the brachiopod *Discotreta* sp. was reported by MacLean (1947) from shales near the top of the Basal Basalt Pillow-lava Formation (lower part of the Skeleton Pond Tuff of Marten, 1971b). The fossil age was concluded to be "fairly definitely Canadian, probably Late Canadian" (MacLean, 1947), which represents Lower Ordovician (Moore, 1965; Barnes et al., 1981).

3.1.3 CATCHERS POND GROUP

The name "Catchers Pond Group" was introduced, informally, by Bird and Dewey (1970) in their classic paper on the evolution of the Appalachian Orogen. These authors suggested that the Catchers Pond Group overlies the Lushs Bight Group and assigned the group an Arenig age, based upon information from Boucot (1968), who discovered a single bed of fossiliferous limestone within rocks of the group. Trilobites from this limestone bed yielded an Early Ordovician, possibly Arenig age (Dean, 1970, Boucot, 1973). Identification of conodonts from the same locality (Klapper, in Dean, 1970, Bergstrom et al., 1974) supported this age.

Dean (1977, 1978) defined the Catchers Pond Group and included it in the pre-Caradocian "immature island arc" sequences, correlating the group with the Cutwell, Western Arm and Snooks Arm groups, amongst others. He also noted that felsic volcanic rocks are more abundant in this unit than in any of the groups it was correlated with.

3.1.4 CUTWELL GROUP

The Cutwell Group is the most studied unit within western Notre Dame Bay. The Cutwell Group was introduced by Espenshade (1937), who named the volcanic sequence north of the Lobster Cove Fault the "Pilleys Series" and subdivided it into the lower,

mostly pyroclastic Cutwell Group, and overlying it pillow lavas of the Lushs Bight Group. This order was reversed by Williams (1962), who reported fossils of probable lower Middle Ordovician age from limestone breccia associated with volcanic rocks of the Cutwell Group.

The group was formally defined by Kean (1973), who described it as a continuous, south-facing sequence of volcanic and volcanoclastic rocks, comprised, from bottom to top of the:

Stag Island Formation - intrusive breccia, pillow lava and diabase;

Pigeon Head Formation - deep-water chert and turbidite;

Quinton Cove Formation - coarse agglomerate;

Burnt Head Formation - pillow andesite, intermediate pyroclastic rocks, cherty shale and tuff;

Parson's Point Formation - shallow water limestone, greywacke and shale;

Seal Cove Complex - intrusive and extrusive felsic rocks that occur between the upper part of the Burnt Head Formation and the middle part of the Long Tickle Formation, were assigned to this complex; and

Long Tickle Formation - agglomerate, pillowed to massive lava, tuff and thin beds of fossiliferous limestone.

Kean (1984) found that the sequence of pillow lava, tuff breccia, mafic tuff and red argillite rocks previously assigned by Espenshade (1937) to the Lushs Bight Group on Pilley's and Triton Islands were lithologically unlike the typical Lushs Bight Group. He referred to them as "Cutwell Group" type rocks (Kean and Evans, 1987; Kean, 1989).

The stratigraphic order and chemistry of volcanic rocks from this sequence led Kean (1973) to the conclusion that they are of island-arc affinity. In a later paper he interpreted this succession to represent a transition from immature to mature island arc (Kean and Strong, 1975).

The Cutwell Group was tentatively assigned to the Middle Ordovician on the basis of conodont fauna from Little Bay Island (Williams, 1962) and cephalopod fauna from thin beds of limestone along the southern shore of Long Island (Strong and Kean, 1972). A Caradocian age for black shales from the Parson's Point Formation was suggested by

Dean (1977, 1978), based upon graptolite fauna. Following this identification, Dean (1977, 1978) included formations underlying the shale on Long Island in the pre-Caradocian "immature island arc" sequences and formations overlying the shale in post-Caradocian "mature island arc" sequences. The proposed Caradocian age of rock sequences on the island was subsequently shown to be incorrect by conodont fauna from limestone nodules in shale beds on Long and Oil Islands, which gave Llanvirn, probably Lower to Middle Llanvirn ages (Meyer et al., 1988). Dunning and Krogh (1988) obtained an age (U-Pb zircon) of $469 \pm 5/-3$ Ma for a felsic tuff overlying the fossiliferous shale and limestone beds on Oil Island.

3.2 Revised Stratigraphy Of The Western Notre Dame Bay

The most serious problem with the existing stratigraphic framework in the study area is that the structural complexity of the region is considerably greater than any of the previous authors recognized. As will be shown in Chapter 6, the area is located on a large recumbent fold, which was later deformed by extensive fold and thrust systems, likely exposing both limbs of the structure and controlling the present distribution of lithostratigraphic units. Structural modifications, together with lithostratigraphic diachroneity and limited lateral extent of some volcanic facies, complicate stratigraphic analysis within the area. Because of the generally sheared nature of the lithological contacts and the repetition of rock units across many structural discontinuities, contact relationships between various lithostratigraphic units in the Notre Dame Bay area are rarely clear. Failure to recognize these complexities, has in the past, resulted in erroneous correlation of units and a complex stratigraphic nomenclature within the study area, as well as to the south of it, in the Silurian Springdale Group (e.g. Coyle and Strong, 1987; Coyle, 1990).

By combining lithological observations made during this study and previously published reports (Espenshade, 1937; MacLean, 1947; Marten, 1971; and others) with careful documentation of lithostratigraphic contacts and examination of structural relationships between various structural blocks in the area, the following large scale

lithostratigraphic division of units in western Notre Dame Bay and north of the Lobster Cove Fault is proposed (Fig. 3.3 and Fig. 3.4):

- 1) **The Lushs Bight Group**, as defined by Kean and Kean and co-workers (1983, 1984, 1989, 1994), but without the "black facies" of Marten (1971a, b);
- 2) **The Western Arm Group**, modified after Marten (1971a, b), which incorporates in addition rocks previously included in the Catchers Pond Group and the "Cutwell Group" type units on Pilley's and Triton Islands, unconformably overlies the Lushs Bight Group, and
- 3) **The Cutwell Group**, modified after Kean (1973) and Kean and Strong (1975) which is younger and most likely unrelated to either of the above groups, but without the Stag Formation (Kean, 1973).

Identification of three major lithofacies facilitates division of these groups into formations and members. The terminology used herein is adapted from Fisher and Schmincke (1984) and Busby-Spera (1988):

- 1) tuff lithofacies - tuffaceous cherts and shales, fine to sandy textured, reworked tuffs, locally interbedded with pyroclastic, partially welded flows;
- 2) lapilli tuff-tuff breccia lithofacies - a variety of volcanic fragments in a fine to medium grained tuffaceous matrix, interpreted as deposited from debris and pyroclastic flows; and
- 3) primary volcanic (herein called "flow") lithofacies - basaltic to andesitic massive and pillowed flows, pillow breccias, and felsic domes including flows, pyroclastic rocks and minor intrusive phases.

Pyroclastic rocks consist of various volcanic lithic fragments, pumice clasts, glass shards, and pyrogenic crystals. Epiclastic volcanic rocks are formed by weathering and erosion of volcanic rocks, and are referred to as tuffaceous sandstones or siltstones, although the distinction between tuff, reworked tuff and tuffaceous sandstone may be equivocal. The granulometric classification is as follows: tuff is considered to be the lithified equivalent of ash (size <2 mm), lapilli tuff refers to a pyroclastic deposit which contains a visible percentage of lapilli (size 2-64 mm), and tuff breccia contains a visible percentage of bombs or blocks (size >64 mm).

3.2.1 LUSHS BIGHT GROUP

The Lushs Bight Group was recently the subject of a 1:50,000 geological mapping and metallogenic study by Kean, 1983, 1984, 1989; Kean and Evans, 1987a, b; Kean et al., 1995). The area covered by that mapping was covered in this study only by cursory traverses in order to make correlations between widely scattered sections of the Western Arm Group, and to determine the number of deformational events affecting the Lushs Bight Group. This project did not involve re-mapping of the area underlain by the Lushs Bight Group, except for smaller sections, where allocation to the group was questionable (e.g. section south of King's Point). The generalized stratigraphy of the Lushs Bight Group proposed by Kean and co-workers is adopted here, with the following modifications based on the present work.

3.2.1.1 Indian Beach Complex

The name Indian Beach Complex is proposed for the lowest lithostratigraphic unit within the Lushs Bight Group. It is a widespread unit of sheeted dykes and extensive dyke swarms intrusive into pillow lava, generally occurring in fault bounded blocks. The largest outcrop areas of sheeted dykes were only recently recognized in the Indian Head and Little Bay areas of the Springdale Peninsula, and in central and northern Sunday Cove Island by Kean (1983, 1984, 1989), and Kean and Evans (1987a, b). Another large area underlain by sheeted dykes crops out along the northern and northeastern shore of Pilley's Island.

The dykes are typically fine- to coarse-grained diabase. Aphanitic to fine grained mafic dykes are present as well, although generally occurring higher in the pile and immediately below the overlying pillow lavas. The fine grained dykes are on average thinner than the coarse grained diabase dykes that intrude them. The dykes contain altered plagioclase and clinopyroxene arranged in equigranular to intersertal texture. Alteration minerals are dominantly chlorite and epidote, with various amounts of quartz and calcite, both interstitial and in small veins. Minor sulphides (chalcopyrite, pyrite, +/- malachite) are associated with some coarse grained diabase dykes.

3.2.1.2 Little Bay Basalt (Formation)

The rank of formation and the name Little Bay Basalt is recommended here for an extensive, variously altered, intensely folded sequence of pillow lavas and lesser massive flows, which in places directly overlies the Indian Beach Complex. Locally minor amounts of mafic tuff and pillow breccia are interfingered with the pillow lavas.

It is difficult to draw any stratigraphic divisions within this volcanic sequence because of the lack of marker horizons and locally intense deformation. Variolitic and vesicular flows interfinger with non-variolitic and non-vesicular flows, but do not form any extensive horizons. Pillow lavas of the Little Bay Basalt are closely packed, pillow cores are variable epidotized or locally silicified, whereas margins of pillows are strongly chloritized. In general there is relatively little interpillow material, but where present, it consists of milky white, yellowish green or grey chert, fine tuff and isolated hyaloclastite.

Pillow lava of the Little Bay Basalt commonly contains strongly altered plagioclase (up to An₃₄, albite to andesine; Fleming, 1970; Marten, 1971 a, b) and clinopyroxene, although alteration minerals (epidote, chlorite, actinolite, calcite, quartz, titanites) generally obliterate the original mineralogy. Amygdules are filled with epidote, chlorite, and quartz.

3.2.1.3 Mafic Subvolcanic Rocks

Volcanic rocks of the Lushs Bight Group are intruded by numerous sills and sub-concordant dykes of diabase and gabbro, varying in thickness from less than 25 cm to several meters. Chilled margins are visible in places and diabase sills are not easily distinguished from coarser grained massive flows, to which they are petrographically and texturally similar (Fleming, 1970). These intrusive rocks are interpreted to be co-magmatic with the pillow lavas on the basis of comparable geochemistry (Jenner et al., 1988; Jenner et al., in prep; Kean et al., 1995), and the fact that they are affected by the same deformational events.

3.2.1.4 Age Constraints On The Lushs Bight Group

The Lushs Bight Group includes no fossiliferous strata and in general lacks rock types suitable for isotopic age determination. Only minimum ages can be established by $^{40}\text{Ar}/^{39}\text{Ar}$ dating of hornblende-bearing intrusions.

A small circular stock of amphibole gabbro, that is correlated with the Brighton Complex (see 3.2.2.9) by some workers, intrudes sheeted dykes on Pilley's Island and it is itself cut by dykes. Sample 88-PIG was collected from the gabbro for an age determination using the $^{40}\text{Ar}/^{39}\text{Ar}$ method. It records a complex spectrum (see Appendix B for a brief description of the method and figures), with two recognizable plateau: one from approximately 8 to 54% yielding an age of 466 +/- 5 Ma; and the second plateau from 55 to 100%, yielding an age of 483 +/- 6 Ma. The older age is considered to represent the minimum age of intrusion of the gabbro stock into the dyke complex, and the younger age a tectono-thermal event which resulted in resetting of the argon system (see also Chapter 7).

Two hornblende-phyric dykes (see also section 3.2.2.4) that intrude pillow lava of the Little Bay Basalt from the Whalesback mine area were also sampled for dating. Sample WB-1 was collected from a dyke cutting a chloritic shear zone that contains a volcanogenic massive sulphide deposit. It yielded a complex spectrum and a probable age of 484 +/- 4 Ma based on only 24% of the gas). The other sample, WB-2, was taken from a similar looking dyke cutting apparently undeformed flows immediately south of the shear zone, and yielded an age of 493 +/- 5 Ma based on 46% of the gas. It is reasonable to interpret this age (middle Tremadoc?; Coopers, 1992) as an upper age limit on the first deformational event recorded within the Lushs Bight Group. The depositional age of the group must be even older.

3.2.2 WESTERN ARM GROUP

One of the principal results of the present mapping in the Notre Dame Bay area was the recognition that rocks within the Catchers Pond Group as well as the "Cutwell Group" type rocks on Pilley's Island, Triton Island and Halls Bay Head (Kean and Evans, 1987; Kean, 1989) are lithostratigraphically correlative with the Western Arm Group rather than the Cutwell Group (compare Fig. 3.1a with Fig. 3.1b). As a result of this,

some modifications to existing lithostratigraphic nomenclature are proposed. On the basis of priority (North American Stratigraphic Code, 1983), the name Western Arm Group is retained, and its modified stratigraphy and nomenclature are applied to correlative rock units noted above. The rank in the name "Catchers Pond Group" is dropped and the geographic name "Catchers Pond" is used informally in conjunction with the word "section". Hence, the name "Catchers Pond section" of the Western Arm Group applies to the area underlain by rocks formerly included in the Catchers Pond Group, but herein assigned to the Western Arm Group.

Observations from various sections of the Western Arm Group suggest that stratigraphy of the group has to be redefined. The redefined Western Arm Group is well exposed in several geological sections. Proposed changes to the group are detailed below as individual lithostratigraphic units are described. The type section of the original group is in the northern part of Springdale Peninsula, between the Western and Southern Arms of Green Bay (MacLean, 1947; Marten, 1971a, b). The Catchers Pond section is found in the area between Indian Brook to the south, and Catchers Brook and Harry's Brook to the north (Fig. 3.3). The Ovals section, named after three ponds located east of the Springdale-Kings Point road, refers to the area between Catchers Brook and the bottom of Southwest Arm (Fig. 3.3). The Halls Bay Head section of the Western Arm Group occupies the easternmost tip of Springdale Peninsula (MacLean, 1947) and the Pilley's-Triton section the northern part of Pilley's and Triton islands (Fig. 3.3). The Western Arm Group is also well exposed in several smaller areas, referred to as the Harry's Harbour (Peters, 1970; Marten, 1971a, b), Nickey's Nose (Peters, 1970), Eastern Point (Sayeed, 1970) and Fox Neck sections (Fig. 3.3). There are also possible Western Arm Group equivalents on Little Bay Island, Stag Islands, and Long Island.

3.2.2.1 Sugar Loaves Basalt (Formation)

Rocks of the Basal Pillow Formation of MacLean (1947), included by Marten (1971a, b) in the Lushs Bight Group, are petrographically more like the Big Hill Basalt rather than mafic flows elsewhere in the Lushs Bight Group (Marten, 1971a; Fleming, 1970). In addition, these rocks show a pattern of high values in the magnetic vertical gradient (GSC maps C41333G and C41334G), which is very similar to the Big Hill

Basalt. Geochemical data indicate that the unit in question includes some flows that correlate better with rocks of the Western Arm Group, than with rocks of the Lushs Bight Group (see Chapter 6). Therefore, this unit is herein included in the Western Arm Group with the rank of formation. It is informally named the Sugar Loaves Basalt, after two prominent knolls located north of Clam Pond.

The formation consists of a thick sequence of aphanitic to fine grained, locally vesicular, well pillowed basalt and lesser massive flows. Ubiquitous red and green chert forms the interpillow material. Flows are locally interbedded with lenses of chert, with or without laminae of magnetite, and with sparse horizons of pillow breccia and tuff. Dykes and sills of diabase and small stocks of diorite/gabbro intrude the lavas. In the type section, the lower contact of the formation with pillow lavas of the Lushs Bight Group has been interpreted to be gradational (e.g. MacLean, 1947; Marten, 1971a, Kean and Evans, 1987). However, the present mapping shows that basalt in the area of the inferred gradational contact is strongly epidotized and locally intensely sheared, everywhere else the contact appears to be faulted. The character of the contact with the overlying Skeleton Pond Formation is not clear either, being mainly unexposed and presumed to be faulted.

In thin section, the basalt contains clinopyroxene and labradorite (An_{64} , Marten, 1971a) arranged in subophitic to intergranular textures. The main alteration minerals are chlorite, epidote and albite, with chlorite defining a locally-developed cleavage. Plagioclase is commonly zoned and displays albitized margins. The prevalence of chlorite over epidote and the strong magnetic properties distinguish pillow lavas of this unit from pillow lavas in the adjacent Little Bay Formation, in which widespread epidotization has produced a "bleached" appearance in the pillow cores.

The Sugar Loaves Basalt lacks rock types which can be dated directly, and its age remains uncertain.

3.2.2.2 Skeleton Pond Formation

This unit was originally termed the Skeleton Pond Tuff by Marten (1971b). However, the formation is lithologically heterogeneous and includes a significant proportion of mafic flows; it is more appropriately named the Skeleton Pond

Formation The present mapping show the internal stratigraphic order of this formation to be less complex than was previously thought. In the Western Arm section one can clearly discern three tuff members and two flow members (Marten, 1971a, b). However this is not the case in other sections, where the tuff and flow facies commonly interfinger in various combinations, and the number of potential members, their thickness and lithostratigraphic positions vary considerably. Because of this intraformational complexity, the existing lithostratigraphic subdivision is not practical. Instead, the rocks are described in terms of two lithofacies, these being the tuff and the flow members.

The type section of the Skeleton Pond Formation is exposed east and west of the Skeleton Ponds in the Western Arm section. Other major exposures are found on north-central and eastern Pilley's Island, western Triton Island, and Halls Bay Head. As well, a large area immediately north of the Catchers Brook Fault is underlain by tuff, tuff breccia and pillow breccia (DeGrace, 1971) and on the basis of lithological characteristics and geochemistry of overlying pillow lavas is assigned to the Skeleton Pond Formation (cf. Kean and Evans (1987a, b) who placed this area in the Lushs Bight Group).

Tuff Lithofacies

The tuff lithofacies consists of a number of distinctive beds which display contrasting lithological characteristics. The basal beds are predominantly massive, fine- to coarse-grained, aquagene tuff, which possesses a poorly defined compositional layering and local graded bedding. It commonly contains crystal-rich (up to 50%) layers, whereas lapilli size material is rare. Thin laminated pale grey- green chert beds alternate with (or change colour along strike to) red-green and red chert. Dark grey shale and locally magnetite-rich argillite bands are commonly interbedded with the tuff.

The tuff contains broken clinopyroxene and altered plagioclase crystal fragments as well as lithic fragments of basalt. The rock is commonly altered and exhibits patches of chlorite, interstitial albite, minor amounts of quartz and sphene. Small amounts of tremolite/actinolite are present in some thin sections.

The relatively fine-grained tuff is interbedded with and grades into lapilli tuff and tuff breccia ranging from crystal-lithic tuff to pyroclastic breccias. These rocks are predominantly polymictic and the dominant clast size and lithology vary from outcrop to outcrop. The most common clasts in the polymictic breccias are mafic to intermediate volcanic rocks, pillows, mafic tuff and argillite. In places, the argillite clasts have smaller clasts of other rock types attached to them, suggesting they were incorporated prior to lithification. In general, clasts in the lapilli tuff and tuff breccia are poorly sorted, and in places show only crude, normal to reverse grading. The matrix contains a large amount of plagioclase crystals, and mafic and silicic and/or silicified mafic volcanic fragments.

Flow Lithofacies

Massive, locally flow brecciated, to well pillowed mafic flows interfinger with the tuffs. These consist of dark grey to black basalt which is mesoscopically similar to the overlying Big Hill Basalt. Thickness of the flow units ranges from a few to about one hundred meters. Pillows vary in size, locally attaining up to 3m in length. In particular, large pillows and lobes up to several meters long are exposed on the eastern shore of Pilley's Island, in Caplin Cove on Triton Island and Big Triton Island.

The upper contact of the Skeleton Pond Formation with the overlying Big Hill Basalt is not exposed. There is no discernible interleaving of formations, and locally intense, bedding subparallel cleavage is present in tuffs and cherts near the contact with the basalt.

Age Constraints

The brachiopod *Discotreta* sp. reported by MacLean (1947) from within the shale of this unit is the only faunal indicator of its early Ordovician age. The cherty sedimentary rock in the Skeleton Pond Formation commonly contains radiolaria-rich laminae. Several samples collected on Triton Island were examined by Dr. R.J. Stevens, who identified the radiolaria as possibly of Arenig

age (pers. comm., 1989). However samples processed in hydrofluoric acid yielded fauna which were too poorly preserved to allow exact recognition.

3.2.2.3 Big Hill Basalt (Formation)

The Big Hill Basalt consists of a thick sequence of typically magnetic, aphanitic to fine grained, vesicular, well pillowed basalt (Fig. 3.5) and massive flows. Thin beds or lenses of red and green cherts are widespread, and red and green chert commonly occurs in the pillow interstices. Flows are locally interbedded with sparse horizons of pillow breccia and tuff. The Big Hill Basalt is overlain by the Welsh Cove Formation.

In thin section (Fig. 3.6), the basalt contains clinopyroxene and labradorite (An70; Marten, 1971a) arranged in subophitic to porphyritic textures, and local plagioclase euhedra up to 5-6 mm in length and minor amounts of titanite. Secondary minerals include chlorite, epidote and albite; veinlets of prehnite were reported by Marten (1971a).

3.2.2.4 Isotopic Age Constraints On The Sugar Loaves And Big Hill Basalt, And Skeleton Pond Formation

In addition to probable co-magmatic intrusive rocks, the Little Bay Basalt flows and formations of the Western Arm Group up to and including the Big Hill Basalt are intruded by younger post-kinematic dykes, that have been referred to as "lamprophyric" (e.g. Espenshade, 1937; MacLean, 1947; Donahoe, 1968; Fleming, 1970). These are particularly common intrusives into the Lushs Bight Group in the area of the Whalesback and Little Bay mines, where they form swarms that intrude the chloritic shear zones associated with the massive sulphide deposits. Many of these dykes contain large hornblendes (Fig. 3.7) and clinopyroxenes (Fig. 3.8) as well as xenocrysts and/or clustered phenocrystic assemblages, which exceed 50% of the rock. Several dykes contain only large, up to 2 cm in length, euhedral crystals of clinopyroxene, some of which display both oscillatory and sector zoning. Dykes with both hornblende and clinopyroxene are rare, and only one such dyke was observed by author in the Whalesback mine area. A composite "lamprophyric" dyke from the west coast of Halls Bay Head (Donahoe, 1968), consisted of outer zone with hornblende and plagioclase phenocrysts, and an inner zone containing subhedral phenocrysts of augite. The similar

orientation, lack of extensive deformation in all of these dykes (see Chapter 6), and presence of both hornblende and pyroxene crystals in composite dykes, indicates that both types of dykes are most likely related.

Flows of the Big Hill Basalt on Halls Bay Head are intruded by "lamprophyric" dykes similar to those intruding the Lushs Bight Group. They contain crystals of hornblende which are commonly euhedral, often stubby and show a range of crystal forms and sizes (up to 1.5 cm in length). Two hornblende fractions from one dyke (Cl-16-02b) were dated by the $^{40}\text{Ar}/^{39}\text{Ar}$ method, yielding a complex spectra and total fusion ages of 500 +/- 5 Ma and 504 +/- 5 Ma (Appendix B). A plateau based upon 72% of the gas in one fraction yields an age of 499 Ma, while a plateau based on 53% of the gas in the other fraction yields an age of 496 Ma. These ages are comparable within analytical error to the 493 +/- 5 Ma age of a hornblende-phyric dyke intruding pillow lava of the Little Bay Basalt in the Whalesback mine area

3.2.2.5 Welsh Cove Formation

The original name of this unit is changed here from the Welsh Cove Tuff (Marten 1971) to the Welsh Cove Formation, because the unit is lithologically much more heterogeneous than previously thought. The Welsh Cove Formation overlies the Big Hill Basalt, but contact between the two is not exposed in the Western Arm section. The contact is exposed and faulted in the Catchers Pond section, and it seems to be unconformable in the Triton section. The whole stratotype is poorly preserved and obscured by voluminous pyroxene- and plagioclase-phyric diabase sills, which form at least 50% of the section. For this reason, a composite reference section is designated on Triton Island (because of the relatively well exposed contact with the Big Hill Basalt), and in the Catchers Pond section (because of the lithological diversity). In the area northeast and northwest of Springdale, felsic volcanic and volcanoclastic rocks are spatially associated with pillow lavas previously assigned to the Lushs Bight Group (James, 1967; Penney, 1969). These are similar to rocks in the main and supplementary sections and are herein included in the Welsh Cove Formation.

The formation is characterized by massive and brecciated to laminated, locally crystal-rich, felsic tuffs and banded welded tuff. The monomictic felsic tuff-breccias are

recognizable only by observation of weathered surfaces, which reveal the presence of angular fragments of up to 8 cm in diameter. Exposures of ignimbrite commonly reveal a convoluted flow layering, and although the rock is commonly massive, it locally shows a curvilinear to columnar jointing. Most of these rock types are characterized by white to beige chalky weathered surfaces, and a wide variety of a mottled pink, beige, grey-green to pale green colours on fresh surfaces. Locally grey to pale green chert and grey argillites are interbedded with felsic rocks.

In the Triton Island section, sparse felsic and mafic flows, together with cherts and argillites, are present in addition to fine intermediate to felsic, locally ignimbritic tuffs. Well laminated red and green cherts and argillites overlie unconformably the tilted pillow lavas of the Big Hill Basalt, and are interbedded with felsic tuffs. In the Catchers Pond section, the formation is represented by felsic ignimbrites and crystal tuffs, cherts, rare argillites, and sparse felsic lavas. Abundant mafic pillowed flows and tuffs interleave with the felsic rocks of this formation, and are locally strongly silicified and/or epidotized. When unaltered, mafic volcanic rocks are of dark green-grey to blue-grey colour, and fine grained to porphyritic. Beds of polymictic tuff breccia are common, locally with lenses of monomictic breccia consisting of closely packed, altered blocks of felsic volcanic rock in a plagioclase-phyric, andesitic to dacitic matrix (Fig. 3.9). Amongst the various lithic fragments in the matrix there are abundant perlitic glass spherules (Fig. 3.10).

The felsic tuff breccia exposed on Halls Bay Head at Red Fishing Point, is herein correlated with the Welsh Cove Formation. Clasts (bomb size) in this breccia are predominantly of pink plagioclase-phyric felsic rock characterized by trachytic texture. This felsic-breccia grades into a polymictic breccia, containing both clasts of felsic rock and a pyroxene-phyric mafic rock similar to that common in the overlying Western Head Formation.

In thin section, the felsic volcanic rocks consist of dense intergrowths of quartz and plagioclase (now albite), orthoclase, sericite, chlorite and some calcite. Where sheared, they form quartz-sericite schist, with pyrite and limonite present on foliation

planes. Mafic volcanic rocks are microporphyrific, with plagioclase crystal of <0.5mm set in a matrix of altered plagioclase, chlorite, calcite and iron oxides.

3.2.2.5.1 West Water Limestone Bed And Silver Pond Tuff

The Catchers Pond section contains two occurrences of rock types which are not found elsewhere in the Western Arm Group: (1) the West Water Limestone - a fossiliferous limestone; and (2) the Silver Pond Tuff - a felsic tuff. Both rock types form distinctive beds, occupy a stratigraphic position in the upper part of the section, and provide good control on the minimum age of deposition of the formation. Despite contrasting environments of deposition, geological mapping indicates that they represent a similar stratigraphic level in the formation.

West Water Limestone Bed

This is a single, discontinuous bed (up to 40 m thick) of fossiliferous limestone, which is in places recrystallized and partially dolomitized. This bed is exposed in several outcrops east of the passage between West Water and Silver ponds. It can be traced eastwards for a distance of approximately 2.5km.

The limestone bed unconformably overlies the nearby section of mafic flows and reworked tuff breccias, which away from the contact contains felsic ignimbrites and flows typical of the Welsh Cove Formation. The basal part of the limestone bed is massive; whereas, the upper part of the bed is well laminated and contains some lenses of reworked felsic tuff, and lesser amounts of chert and argillite. In outcrop near the northeastern end of West Water a few lenses of dolomitized intra-formational conglomerate are present.

Silver Pond Tuff (Bed)

A bed of predominantly quartz-feldspar-phyric felsic tuff occurs near or at the stratigraphic top of the Welsh Cove formation throughout the Catchers Pond section. The bed is locally associated with quartz-feldspar or feldspar porphyry intrusions. Both tuff and porphyries contain 40 to 80% crystals up to 0.5 cm long in a very fine grained green to brown matrix. Rare lithic clasts are observed in the tuffs in the western part of the section. In places, the tuffs and

subvolcanic porphyry look mesoscopically and microscopically similar, as both consist of crystals of alkali feldspar and quartz, plagioclase, minor chlorite and opaque minerals and accessory zircon in a fine grained siliceous matrix. Quartz is somewhat subordinate to feldspar, both are strained to severely shattered in the tuff but mostly intact in the porphyry. Quartz in the porphyry is commonly embayed (Fig. 3.11). Locally the tuff is characteristically banded, with interleaved rhyolite and dacite (Fig. 3.12).

Age Constraints: Faunal

Several samples collected at random along the West Water Limestone Bed yielded conodont fauna which indicated an Arenig age (Fahreus, pers. comm., 1987). Additional samples were subsequently taken from the base, the center and the top of the bed in one locality (CP-21-21). The extracted conodonts were very small in size, well preserved and with a high Colour Alteration Index (CAI) of 6.5 to 7. The good preservation of the conodonts and their high CAI suggest that the alteration of the limestone bed mainly result from heating to at least 490° C (e.g. Rejabian et al., 1987). The conodont assemblage indicates that the age of the bed ranges from the early Arenig *Prioniodus elegans* Zone near the base of the bed to the middle Arenig *Oepikodus evae* Zone near the top of the bed (O'Brien and Szybinski, 1989).

Age Constraints: Isotopic

A sample of banded porphyritic tuff was collected from locality CP-28-15 (Fig. 3.12) for a U-Pb zircon age determination in order to test the validity of the above interpretation. Three zircon fractions were abraded and analysed. There was no evidence of inheritance in any of the analysed fractions. The data yielded an age of 479.2 +/- 3.6 Ma (Appendix B), early to middle Arenig according to the Cooper's (1992) scale, and are interpreted to represent the primary igneous age. An identical U-Pb zircon age of 480 +/- 3 was recently obtained from felsic tuff in the northwestern part of the Catchers Pond section (Ritcey, 1993).

3.2.2.6 Western Head Formation

The original name of the formation, the Western Head Agglomerate, introduced by Marten (1971b), is changed here to the name Western Head Formation, to avoid using the term "agglomerate" (considered obsolete in Bates and Jackson, 1980). The Western Head Formation is the uppermost unit of the Western Arm Group and is well represented in the type section. Extensive outcrops of rocks assigned to this unit are also present in the Halls Bay Head and Pilley's - Triton sections. On Little Bay Island rocks similar to rocks of the Western Head Formation directly underlie the Cutwell Group.

The Western Head Formation is predominantly made up of a mafic tuff/tuff breccia assemblage (Fig. 3.13). A lens of pillow lava from within the type section was reported by Marten (1971b). On Little Bay Island, pillowed and massive flows grade upwards into autobrecciated flows and ultimately into tuff-breccias very similar to those in the type section. In general, the tuff/tuff breccia assemblage is relatively uniform, poorly graded and sorted, and predominantly clast supported. The rock consist of mafic clasts of various sizes (on average up to 20 cm, but commonly in excess of 0.3 m in diameter) set in a tuffaceous matrix. The clasts are generally subangular to rounded, grey-green, in places strongly porphyritic basalt, akin to that forming the flows and breccias on Little Bay Island. Rare diorite and gabbro clasts were also reported from this unit by Marten (1971b).

Clinopyroxene and plagioclase phenocrysts are present in various proportions, resulting in predominantly pyroxene- or plagioclase-phyric rock types. Euhedral clinopyroxene crystals are up to 3-4 mm in length (locally over 1.5 cm), but plagioclases do not exceed 2mm. Two types of clinopyroxene is recognized microscopically; clasts in the tuff breccia in the Halls Bay Head section contain diopside (Donahoe, 1968), whereas flows and clasts in tuff on Little Bay Island contain augite (O'Brien, 1975). In both locations basalts contain abundant, large size vesicles, indicating an originally high volatile content.

In the area west of Dolland Arm Head, the tuff breccia is locally overlain by a banded tuff characterized by a fine grained, apparently felsic, grey matrix with abundant

hornblende phenocrysts. In the Western Arm and Nickey's Nose sections, this rock forms the uppermost stratigraphic unit, whereas, in the area northeast of Harry's Harbour, it is interleaved with tuff breccia of the Western Head Formation, clasts of which contain considerable amounts of pyroxene.

Age Constraints

Samples of hornblende-phyric tuff from two separate localities (Western Arm and Nickey's Nose sections) yielded hornblende, which was dated by $^{40}\text{Ar}/^{39}\text{Ar}$ (Appendix B). Sample WA-44, tuff from the type section of the Western Arm Group, displays a complex spectrum with two dominant plateaus, one yields an age of 465 +/- 1 Ma based upon 40% of gas, and the other 442 +/- 2 Ma based upon 24% of gas. Sample WA-NN1 (Nickey's Nose section) records a similarly complex spectrum (see Appendix B), with several plateaus, among which the one yielding the oldest age 462 +/- 3 Ma is based upon 21% of gas, and two indicating the youngest ages of 436 +/- 2.5 Ma and 443 +/- 1.8, are based on 24% and 36% of gas, respectively.

3.2.2.7 Dolland Quartz Diorite

A small pluton of predominantly quartz diorite is associated spatially with the Western Head Formation and exposed at Dolland Arm Head. Marten (1971a,b) interpreted it to intrude the tuff and emphasized the similarity of diorite and gabbro clasts present locally in the Western Head Formation to the rock types forming the pluton, suggesting that both of these units may be co-magmatic. However, both Marten (1971a, b) and this author were unable to confirm crosscutting relationships between the pluton and the tuff. The southern, and the only on-land, contact between the diorite and the tuff is faulted and there are no dykes clearly related to the pluton that intrude the tuff. The intrusive relationship between these units is herein considered to be questionable.

Typically, the diorite consists of plagioclase, quartz, hornblende and rare biotite. In the northeastern part of Dolland Arm Head it grades in places into flow-banded dacitic rock, as well as gabbro. Throughout the pluton, diorite exhibits flow-folded igneous layering, accentuated by an interleaving of mesocratic, hornblende-rich diorite

and more leucocratic diorite. Locally, intrusion breccia is exposed containing fragments of diorite, diabase and pyroxenite, immersed in a matrix of leucocratic diorite.

Age Of The Dolland Quartz Diorite

A sample of quartz diorite from Dolland Arm Head contains hornblende, which was used to determine a $^{40}\text{Ar}/^{39}\text{Ar}$ age (Appendix B). Sample WA-45 shows a relatively simple spectrum with a major plateau that yields an age of 477 +/- 4.3 based on 51% of gas, and one smaller plateau indicating an age 482 +/- 2.3 based on 17% of gas.

3.2.2.8 The Colchester-Coopers Cove Pluton

The Colchester-Coopers Cove Pluton is an elliptical, compositionally zoned pluton that intrudes volcanic rocks of the Lushs Bight Group (Sayeed, 1970; Kean et al., 1995) and volcanoclastic rocks of the Western Arm Group. Within the pluton, Sayeed (1970) recognized three broad compositional zones, which from margin to center are diorite, quartz diorite and granodiorite. Although detailed study of the pluton was beyond the scope of this project, cursory mapping revealed that it is in a form of a sill or lens rather than an irregular equidimensional intrusion. The lower contact of the intrusion is strongly sheared, and the whole body incorporated into several horses (thrust sheets) that form a map scale duplex. The granodiorite, in the central part of the exposure, exhibits well developed foliation defined by aligned biotite or chlorite and hornblende. The biotite crystals are bent or broken. The crystals of plagioclase and microcline are not aligned, although microcline (perthitic variety) show evidence for some internal plastic deformation. Quartz is frequently broken into subgrains and displays serrated grain boundaries typical for recrystallized quartz; undulatory extinction is common.

Age Of The Coopers Cove Pluton

The Coopers Cove Pluton was dated using the U-Pb zircon method and yielded an age of 465 +/- 2.5 Ma (Appendix B). This is interpreted to represent the primary igneous age. Three abraded zircon fractions and a duplicate zircon fraction were analysed. There was some evidence of inheritance in this sample, but care was taken not to include any of this materials in the analysed fractions.

3.2.2.9 Brighton Intrusive Complex

Named after the community of Brighton, the Brighton Intrusive Complex is exposed on the Brighton Tickle Islands (several minor islands north of Triton Island) and the northwestern tip of Triton Island. It is spatially associated with the Big Hill Basalt. Magnetic data (EMR, GSC, map 2E/12, 1988) suggest that it is an E-W elongated body broken into several, fault bounded blocks. The exposed part of the complex appears to be the core of the intrusion. The only exposed contact with the Big Hill Basalt observed on the northwestern tip of Triton Island is strongly sheared and lacks evidence for a crosscutting relationship or contact metamorphism (cf. Hussey, 1974).

A small stock of gabbro that intrudes sheeted dykes on Pilley's Island was interpreted by previous workers (Dean, 1978; Kean, 1984) to be part of the Brighton Intrusive Complex and its contact relationships were used to demonstrate the intrusive character of the Brighton Intrusive Complex into the Lushs Bight Group. However, no similar phase is present within the main body of the complex on Brighton and nearby islands, and it cannot be demonstrated that the intrusions are, in fact, related.

Hussey (1974) recognized a number of distinct rock types within the Brighton Intrusive Complex and their identification was confirmed during this study. The dominant exposed lithologies are magnetite-hornblende pyroxenite (Fig. 3.14) and "comb-layered" (Lofgren and Donaldson, 1975) hornblendite. Locally, the pyroxenites exhibit a strong to vague "layering" defined by concentrations of bluish magnetite or zones of hornblende. Pegmatitic patches, larger pods and more extensive bodies of dark green to black hornblendite (+/- minor plagioclase and magnetite) are common throughout the complex and display gradational contacts with the pyroxenite. This implies that both rock types formed within a short period time and possibly represent the same phase in the development of the complex. However, dykes of similar hornblendite and/or hornblende-plagioclase pegmatite of an apparently younger phase cut both pyroxenites and hornblendite. Strongly altered (serpentinized and carbonitized) blocks of ultramafic composition are found throughout the complex.

The youngest intrusive phase cutting the complex appears to be a pale pink diorite (monzodiorite), which forms dykes and plugs of various thickness and orientation. This phase consists predominantly of zoned plagioclase, pyroxene (variably altered to actinolite), little or no quartz, and accessory apatite and zircon. A characteristic feature of these dioritic bodies is an abundance of pyroxene fragments, many of which exhibit a rim of dark green amphibole.

Age Of The Brighton Intrusive Complex

Samples of hornblende from two separate localities and a sample of the youngest phase dioritic dyke were collected in order to determine the time span of intrusion represented by the Brighton Intrusive Complex. Three hornblende fractions from two separate localities from within the Brighton Intrusive Complex were used to determine $^{40}\text{Ar}/^{39}\text{Ar}$ ages and these are presented in Appendix B. Sample RAL-88-1 yielded an age of 475 ± 3 Ma based on 86% of the gas; sample RAL-88-2 yielded an age of 472 ± 3 Ma based on 87% of the gas; and the third hornblende sample, the RAL-88-3, from a separate locality, yielded an age of 475 ± 3 Ma based on 95% of the gas.

Five zircon fractions (4 abraded, 1 unabraded) from the dioritic dyke cutting hornblende pyroxenite in the southwestern part of Cobbler Island yielded a U-Pb age of 478.5 ± 4.5 Ma (see Appendix B).

3.2.3 CUTWELL GROUP

The stratigraphic order interpreted from the present mapping of the Cutwell Group on Long and Little Bay islands differs from that formalized by earlier workers (Kean, 1973; Kean and Strong, 1975; O'Brien, 1975; Dean, 1977, 1978)(Fig. 3.15). The previously-developed stratigraphy does not adequately account for complexity resulting from structural repetition of lithological units and rapid changes in facies. This study found that the Pigeon Head and the Quinton Cove Formations (Kean, 1973) form one continuous sequence that is intruded by a distinct suite of sills and dykes not found elsewhere in the Cutwell Group. Furthermore, close examination of the Long Tickle Formation suggests that it is the lithological equivalent of the Burnt Head Formation and

occupies a similar stratigraphic position. A revised lithostratigraphic division of the Cutwell Group, based on these new observations is presented below.

3.2.3.1 Pigeon Head Formation

The Pigeon Head Formation as defined by Kean (1973) consisted predominantly of tuff lithofacies rocks. Here, it is revised to include the tuff breccia of the Quinton Cove Formation. The most compelling reason for this revision is that both units are intruded by sills and dykes characterized by geochemical signature that differs from that in the other rocks of the Cutwell Group (see Chapters 4 and 5), and implies a different paleotectonic setting. The presence of this intrusive suite within the rocks of the Pigeon Head Formation differentiates this formation from apparently similar rocks in the lower part of Long Tickle Formation.

The revised Pigeon Head Formation is the lowermost unit of the Cutwell Group and is predominantly exposed on Long Island. In general, it is southwest dipping and facing unit, which is particularly well exposed on Pigeon Head, and in the Quinton Cove and Burnt Head areas. The upper contact with the Long Tickle Formation was predominantly faulted where observed during this mapping; however, Kean (1973) considered it to be conformable.

The tuff lithofacies contain a black, in places strongly silicified, cherty shale, interbedded with pale grey silty to sandy textured tuffaceous rocks. Above this are fine grained reworked tuffs with some horizons of siliceous shale and grey tuffaceous sandstones. The tuff lithofacies display a variety of sedimentary features, including rip-ups and load casts. Small, diagenetic limey/siliceous lenses and nodules are common in the shale and siltstone and are commonly associated with euhedral crystals of pyrite.

In thin section, the tuffaceous shale contains rare altered crystals of plagioclase and fragments of altered volcanic rocks. Tuffs predominantly contain variably altered (saussuritized) crystals and crystal fragments of plagioclase, and lesser clinopyroxene. Secondary chlorite, calcite, quartz and euhedral pyrite crystals are present in the shale and the tuff.

The lapilli tuff - tuff breccia lithofacies conformably overlies the tuff lithofacies and consists of a wide spectrum of clasts immersed in a fine grained tuffaceous matrix. Clasts are predominantly plagioclase-phyric, fine grained, mafic volcanic rocks, which are commonly epidotized. Some clasts are characterized by chilled margins and most likely represent bombs. Large rip-up fragments of the underlying tuff lithofacies, up to approximately 1m in length, occur at the base of the unit, and several larger rip-ups (up to ~2.5 x 3.5m) were reported by Kean (1973) from the Seal Island Tickle area.

The matrix of the lapilli tuff - tuff breccia is tuffaceous, generally altered, aphanitic to fine-grained, and characterized by presence of plagioclase crystals and detritus, minor clinopyroxene, and the typical alteration mineral assemblage - chlorite and epidote.

Intrusive Member

A distinctive suite of black aphanitic diabase and fine- to medium-grained gabbro sills and dykes cuts the Pigeon Head Formation, but are not seen to cut other units. The gabbro is most common in the Pigeon Head area; whereas, diabase sills and dykes are confined to the Indian Head and Burnt Head areas. Some of the diabase dykes are plagioclase-phyric and one of the dykes cutting the tuff breccia in Quinton Cove contains up to 20% of plagioclase crystals >2 cm in length. In thin sections the dykes show intergranular to intersertal texture. Both diabase and gabbro contain plagioclase (andesine - ~An 40; Kean, 1973), augite and magnetite (Fig. 3.16). The main alteration minerals are chlorite (defines a locally-developed cleavage in augite), quartz and calcite. Some sills and dykes included in this member contrast geochemically from other co-magmatic intrusive rocks of the Cutwell Group (see Chapters 4 and 5)

3.2.3.2 Long Tickle Formation

The Long Tickle Formation (Kean, 1973) is revised here to encompass rocks previously included in the Burnt Head Formation, and is considered to be stratigraphically higher than the Pigeon Head Formation. The Burnt Head Formation was originally divided into two members: a lower Pyroclastic member and an upper Pillow Andesite member (Kean, 1973). It was found during this mapping that the same

division can be equally well applied to the Long Tickle Formation of Kean (1973). However, these members interleave in numerous combinations, and their thickness' and order vary significantly across Long Island. In view of this intraformational complexity, the Long Tickle Formation is separated into three lithofacies: the Tuff lithofacies; the Lapilli tuff - tuff breccia lithofacies; and the Flow lithofacies. The original name "Pillow Andesite member" of Kean (1973) is changed here to the Flow lithofacies, because massive flows are as common as pillowed flows, particularly in the lower and western part of the unit. Furthermore, while many flows are indeed andesitic, many of them are basaltic.

Tuff Lithofacies

The Tuff lithofacies is made up of locally exposed horizons of a reworked tuff, chert and cherty shale, and together with the Tuff Breccia lithofacies are found throughout the formation. In some outcrops the upper contact with the Tuff Breccia lithofacies is an erosional one, resulting in scouring and channelling of the underlying rocks. The reworked tuff is predominantly grey to green-grey, variably grained and sandy textured. The Tuff lithofacies are similar to rocks of the Pigeon Head Formation, and are well bedded and display a number of sedimentary structures, that include well developed "flame structures" (Fig. 3.17) and rip-ups.

On Southern Head, the Tuff lithofacies interfinger with a felsic pyroclastic flow linked to the overlying felsic dome of the Seal Cove Complex. The pyroclastic flow formed channels within the underlying sediments and contains common rip-up fragments of shale and chert (Fig. 3.18). In this same outcrop area, the well bedded rocks of the Tuff lithofacies are also overlain by autobrecciated massive to pillowed flows of the Long Tickle Formation.

In the area between Milkboy Cove and Aspen Cove, there are several outcrops of tuffaceous, in places bioclastic, limestone interbedded with red argillite and mafic tuff. Similarly, on the west coast of Little Bay Island and its offshore rock, known as Limestone Island, the limestone lenses and limestone

breccia immediately underlying the Seal Cove Complex are associated with beds of red siliceous argillite.

Lapilli Tuff - Tuff Breccia Lithofacies

The Lapilli Tuff - Tuff Breccia lithofacies are made up of extensive horizons of a primary to reworked, predominantly clast supported, lapilli tuff and tuff breccia assemblage. The unit is well exposed in many outcrops along the shores of Wild Bight and Long Island Tickle, and forms a significant part of the inland exposure on Long and Little Bay Islands. It interfingers with the Tuff lithofacies and the massive and pillowed flows of the Flow lithofacies, and it is locally very similar to the tuff breccia assemblage of the Pigeon Head Formation. On Long Island, the thickness of the unit appears to decrease in an easterly direction, although there is an approximately 100m thick section of reworked tuff breccia within the exposed part of the formation at Southern Head (easternmost Long Island).

This unit contains a graded, but poorly sorted, lithologically heterogeneous assemblage of predominantly angular to subangular clasts rarely exceeding 0.3m and immersed in a tuffaceous matrix (Fig. 3.19). The size of volcanic clasts is relatively uniform throughout the unit, but increases rapidly in proximity to Southern Head, reaching, in some cases, over 1m in diameter. Most of the clasts are of mafic flows, fragments or locally whole pillows, as well as sparse rafts of mafic tuff. Three types of mafic volcanic clasts are found within the breccia. One is predominantly plagioclase-phyric, the second is plagioclase-pyroxene-phyric, and the third is aphanitic to fine grained; all have counterparts in the Flow lithofacies. Some of the clasts exhibit well developed chilled margins and clearly represent bombs. In places, there is a significant percentage of felsic volcanic clasts, particularly in the Aspen Cove and Milkboy Cove areas, on the southern shore of Long Island.

Flow Lithofacies

The base of the Flow lithofacies is often marked by fine grained to aphanitic mafic massive flows, which overlie the Tuff and Lapilli Tuff - Tuff Breccia

lithofacies along the shores of Wild Bight (Fig. 3.20). The massive flows are also common on the southwest shore of Long Island, although the lower contact is not exposed. Flow brecciation is locally strong, in particular beneath the felsic dome in the Doolan Folly area, yet broken fragments are closely packed and the matrix is hematitized. Massive flows are up to 3 to 5m thick, aphanitic, vesicular and, in general, grade vertically into pillowed flows or are overlain by one of the pyroclastic members. Some of the massive flows contain large vesicles and amygdules, which are filled with silica and calcite in the eastern part of Long Island, and with large crystals of epidote and hydrogarnet in the western part of the island. Locally (e.g. Gull Cliff area), massive mafic flows interfinger with felsic flows of the Seal Cove Complex.

The pillowed flows are well exposed and very extensive in the eastern part of the island, in particular southeast of Croucher Cove (Fig. 3.21). They are predominantly plagioclase-phyric, and only a few pyroxene-phyric or aphanitic pillowed flows are present. Vesicles are present in most of the pillows, principally confined to the outer zone. However, in a few isolated pyroxene-phyric flows vesicles form several distinctive concentric rings. Interstices between pillows are normally filled with white to greenish chert and locally with jasper.

Microscopically, the massive flows contain plagioclase microlites in a partly crystalline, but mostly opaque matrix. Although flows appear to be relatively fresh in outcrop, in thin section they display extensive chloritization and epidotization, and secondary Fe-oxides. The pillowed lavas consist of plagioclase phenocrysts set in a matrix of plagioclase microlites and an assemblage of secondary chlorite, epidote, opaque minerals and calcite (Fig. 3.22). Plagioclase rarely exhibits zoning and is moderately to strongly saussuritized. The pillowed flows rarely contain a variable amount of relatively unaltered clinopyroxene phenocrysts, predominant with respect to the plagioclase, and set in fine grained, much altered matrix of clinopyroxene, plagioclase, secondary chlorite, epidote, calcite and iron oxides.

Age Constraints

An assemblage of graptolites was collected by Dr. H. Williams, in conjunction with the author, from the highest horizon (siliceous shale) in the Tuff lithofacies on Southern Head. The fauna is indicative of the late Arenig *I. v. maximus* Zone (Williams, S.H., 1989, 1992), and corresponds to approximately 473 Ma on the Cooper's (1992) time scale.

A conodont fauna from blocks in a limestone debris flow on Limestone Island is believed to represent the boundary of the *Microzarcodina flabellum parva* Zone/ *Eoplacognathus? variabilis* Zone (late Arenig, Tucker et al., 1990) (O'Brien and Szybinski, 1988, 1989). The uppermost horizon of the Tuff - Tuff Breccia assemblage included in the formation underlies conformably(?) limestone breccia of the Parsons Point Formation near the bottom of Cutwell Arm. A collection of limestone clasts from the Tuff - Tuff Breccia unit contains a conodont fauna characteristic of numerous zones, the youngest of which is from the upper part of the *E. suecicus* Zone (O'Brien and Szybinski, 1988, 1989), and indicates the early Llanvirn age (Tucker et al., 1990).

The conodonts extracted from limestone blocks on Limestone Island were relatively well preserved and with very high CAI of 8 (Fig. 3.23). The good preservation of the conodonts and their high CAI implies that the alteration of the limestone breccia is mostly due to an increase in temperature to at least 600°C (Epstain et al., 1977, Rejabian et al., 1987). Much lower CAI values of 4 to 4.5 were displayed by the conodonts from limestone breccia on Long Island, which suggests that they have been heated to only 300°C.

3.2.3.3 Parson's Point Formation

The Parson's Point Formation contains interbedded welded mafic tuff, greywacke, shale, limestone and limestone breccia. An extensive layer of andesite and dacite - siliceous siltstone peperite is also present (Fig. 3.24), and is well exposed along the Lushes Bight-Beaumont road and on the western shore of Little Bay Island. As a result of the relatively low competency of these rocks, it has been locally intensely deformed,

which resulted in complex intraformational stacking of shale beds, and repetitions by thrust-related folding. It is difficult to determine the extent of the formation, since it is preserved in a form of a large lens, interfingering with both the underlying Long Tickle Formation and the overlying Seal Cove Complex. The lower contact is interpreted to be transitional, since mafic tuffs and lapilli tuff - tuff breccias of the underlying Long Tickle Formation locally contain sparse to widespread clasts of limestone. The Parson's Point Formation interfingers with and is conformably overlain by felsic pyroclastic rocks of the Seal Cove Complex, that are well exposed north and east of Lushes Bight.

The greywacke contains predominantly plagioclase, lesser volcanic rock fragments, some magnetite, minor quartz and limestone. Limestone-rich laminae in the greywacke are interbedded with more siliceous laminae which stand out because of differential weathering. Limey fossiliferous and cherty black shale and lenses of minor limestone debris flows are interbedded with the greywacke. Interbedded throughout the formation is an assemblage of welded/non-welded mafic tuff (Fig. 3.25). It is characterized by distinctive pale green (epidotized) very thin (up to 6cm) beds of welded plagioclase-phyric tuff with flattened, wispy pumice (Fig. 3.25), interbedded with similarly thin beds of plagioclase-phyric non-welded mafic tuff with angular pumice fragments.

In the Lushes Bight area the unit contains several limestone debris flows with an average clast size from 5 to 30 cm in diameter, but with several larger blocks. The breccia is clast supported, with a muddy carbonate or plagioclase-rich tuffaceous matrix. A sequence of limestone debris flows separated by horizons of bedded clastic limestone is exposed in and south of two quarries on the southern side of the road between Lushes Bight and Beaumont. The limestone debris flows cut through underlying shale, greywacke and mafic to felsic tuffs, and appear to be preserved in a small paleo-canyon or gully. The essentially monomictic limestone breccia is underlain by a more polymictic type, which contains some clasts of felsic and mafic volcanic rocks, siltstone, and limestone in a plagioclase - phyric tuffaceous matrix. The amount of limestone clasts decreases towards the east. Further east of the quarries only a

slightly disrupted interbedded siltstone/mafic tuff sequence is present. The western contact of the limestone debris flow with the underlying rocks is sharp.

Age Determinations

A broad microfauna of inarticulate brachiopods is found in association with the conodonts in blocks of the limestone breccia. The breccia also contains a rich fauna of sponges, cephalopods (goniatites), crinoid ossicles and possible algae (F.C.H. O'Brien, pers. com:n.). Conodont fauna from limestone clasts and graptolite fauna from the shale have been collected from several localities within the Cutwell Group. The conodont fauna from various limestone debris flows reveals a significant diversity in age (O'Brien and Szybinski, 1988, 1989). On Long Island, the main body of the fauna from the lower horizon of the limestone breccia is from the top of the *E. ? variabilis* Zone and from the lower part of the *E. suecicus* Zone (Fig. 3.26), uppermost Arenig to early Llanvirn on the Tucker et al. (1990) time scale. The upper horizon of the limestone breccia yields a younger fauna, representing the upper part of the *E. suecicus* Zone and the *P. serrus* Zone, a time span from the early/middle Llanvirn to the late Llanvirn, and possibly to the base of the Llandeilo according to Tucker et al (1990).

The graptolites assemblage obtained from the Parson's Point Formation shale in the quarry east of Lushes Bight indicates a "late Arenig age at earliest", but most likely an early Llanvirn age for the shale (Williams, S.H., 1989, 1990). A rich, cosmopolitan graptolite fauna was found and interpreted to be of open-ocean type (Williams, S.H., 1989, 1992) and to be different from that of the Southern Head area. The remains of the same assemblage of fauna was found in three different localities in the Lushes Bight area (southern shore of Lushes Bight, and south of it in two localities along the loose surface road) and in two localities on the west coast of the island (Flint Islands area).

3.2.3.4 Seal Cove Complex

The major outcrop of the Seal Cove Complex forms a triangle-shaped area defined by Lushes Bight, Flint Islands and the southwestern end of Cutwell Arm

Another large area underlain by felsic volcanic rocks included in this unit is present in the eastern part of the Long Island between Southern Head and Windsor Lookout. Several smaller exposures of the complex are found on Oil Islands, on the west shore of Long Island south of Lushes Bight and in the south-central part of the Long Island.

Felsic volcanic rocks forming the complex vary from rare flows to plagioclase-phyric tuffs and common tuff breccias. Only locally the tuffs exhibit some poor bedding or compositional banding, and it is difficult in places to distinguish between the tuffs and co-magmatic intrusive phases of the complex, especially in the northern part of the main outcrop, where all phases are covered by Fe-oxide staining. Felsic rocks are usually light green to buff in colour, but where sulphide mineralization is present (e.g. Doolan Folly area, Oil Island), they display a yellow to rusty stain.

The Doolan Folly area in the easternmost part of Long Island is underlain by columnar jointed, flow banded felsic rock, overlying mafic pillow lavas, tuff breccia and hematitic tuff. Flows and monomictic felsic tuff breccia are present immediately overlying the mafic rocks or hematitic mafic tuff (Fig. 3.27). Locally, the flow banding is folded and has the appearance of "soft sediment" deformation, i.e. folds are highly non-cylindrical and lack cleavage of any kind. The felsic rock is predominantly massive, yet in places flow brecciation is present. A smaller fragment of this felsic body is exposed on Southern Head, where it overlies a breccia made up of felsic clasts and rip-up fragments of argillite and shale. The felsic body on Southern Head is very similar to the main body of felsic rock, and was interpreted to form a feeder to the larger body, interpreted as a partly emergent cryptodome (Muggridge, 1989). Several smaller dykes associated with that dome intrude the underlying sedimentary rocks of the Long Tickle Formation (Fig. 3.28). A large, map-scale block of felsic tuff and intrusive phases of the Complex is also found on the southern shore of Long Island, east of Milkboy Cove.

The extrusive rocks are commonly silicified, sericitized and locally carbonitized, and it is not possible to determine the original mineral assemblage (Kean, 1973; Muggridge, 1989).

3.2.3.5 Rocks Intrusive Into The Cutwell Group

The Cutwell Group is intruded by a variety of dykes, sills, plugs and small plutons which range from diabase and gabbro to quartz-feldspar porphyry and granite. Some types of intrusive rocks (such as the Intrusive member of the Pigeon Head Formation) are associated with particular units. Majority of rocks intrusive into the Cutwell Group are co-magmatic, however some larger granodioritic bodies and dykes are post-kinematic with respect to main deformational events (see Chapter 6)

Co-Magmatic Intrusive Rocks

Various types of mafic dyke cut the Long Tickle Formation, and texturally resemble the pillowed and massive flows of the Cutwell Group. Several of the dykes can be traced into and are clearly conduits feeding the flows. Some of the dykes are plagioclase- or pyroxene-phyric; however most are aphanitic- to fine-grained, similar to massive flows of the Long Tickle Formation. Microscopically, the porphyritic dykes contain altered plagioclase (epidote, albite, calcite and sericite), lesser chloritized augite, and accessory magnetite. The aphanitic ones are mainly cryptocrystalline.

Several small stocks of gabbro and diabase dykes may predate or be coeval with the mafic dykes. On Indian Island in the Wild Bight area, there is a small gabbro pluton and several plugs intruding silicified pillow lava. Both these rock types are cut by an extensive suite of diabase dykes which form locally up to 40% of the outcrop.

Syn- To Post-Kinematic Intrusive Rocks

A large suite of felsic, aphanitic to porphyritic dykes, sills and minor stocks intrude deformed rocks of the Cutwell Group. These rocks are common in central and northern parts of Long and Little Bay Islands, particularly in rocks of the Seal Cove Complex and around the elongate area of granite outcrop north of the major exposure of the Seal Cove Complex, between North China Head and Billy Tool Cove.

The porphyries are mostly plagioclase-phyric, often plagioclase - quartz - phyric with a pale grey-green aphanitic matrix. They may contain variable

amounts of biotite and rare hornblende. In thin sections they exhibit inequigranular porphyritic texture, with perfectly euhedral and zoned altered plagioclase crystals, and slightly rounded and resorbed quartz phenocrysts. Biotite is commonly altered to chlorite, as is accessory hornblende.

Associated with the porphyry dykes are small bodies of granodiorite. These intrusions are mineralogically similar to the porphyry dykes and are not cut by the aphanitic dykes (cf. Kean, 1973). The largest post-kinematic intrusive body is found in the very southwestern part of Long Island and is named the Long Island Pluton. It contains xenoliths of strongly altered (hornblende, actinolite, chlorite) mafic rock which consists of hornblende (replacing pyroxene), lesser plagioclase and magnetite.

3.3 Stag Island Formation - Removal From The Cutwell Group

This formation was originally defined and included in the Cutwell Group by Kean (1973). It is exposed on the Stag Islands (north of Long Island), on Seal Island (northeast of Long Island) and on League Rock, an islet east of Long Island. Several offshore rocks, formed of pillow basalt, between Stag Islands and Long Island were also included by Kean (1973) in this formation. A few exposures of rocks correlated with various parts of the formation were found during this study on the southeastern shore of the Little Bay Island and Copper Island (an islet south of Little Bay Island). Contacts between the Stag Island Formation and other Cutwell Group rocks are offshore and not exposed, except on Little Bay Island, where they are in fault contact. Kean (1973) recognized an internal division to the Stag Island Formation, consisting of the Breccia, two Basalt and Intrusive members.

While the description and internal division of Kean (1973) are valid, new evidence obtained during this study suggest that the Stag Formation cannot be considered part of the Cutwell Group. Details are given below.

3.3.1 STAG ISLAND FORMATION

3.3.1.1 Breccia Member

The Breccia Member consists of a poorly bedded and poorly-sorted breccia - conglomerate sequence. Lesser, but locally extensive, tongues of green to rusty black,

flow brecciated, pillowed basalt interfingers with and grades into the breccia. Fractured single pillows also occur within the breccia. The majority of the clasts in the breccia are of intrusive affinity, predominantly gabbro, diabase, and lesser amounts of hornblende-plagioclase pegmatite and trondhjemite. Small quantities of devitrified glassy pillow margins, sparse limestone, shale and blocks of massive sulphides are also present. In general, clasts are angular to subangular on Stag Islands; however, on League Rock the breccia is interbedded with horizons of pebbly conglomerate and sandstone characterized by well rounded grains. The size of the clasts varies from close to 1.5 m to sand, yet much larger blocks of gabbro were reported by Kean (1973) from the northern part of Stag Islands. Overall, the unit fines upward and the top is marked by a horizon of coarse arkosic sandstone and strongly sheared shale. The sandstone contains a abundant broken plagioclase crystals in addition to lithic fragments similar to those found in the breccia. The sandstone and the shale are conformably overlain by and locally structurally intermingled with the Lower Basalt Member.

3.3.1.2 Lower Basalt Member

The Lower Basalt Member consists of pale grey-green, strongly fractured and brecciated, consistently glassy to aphanitic pillows and local horizons of pillow breccia. Locally there are some porphyritic plagioclase-phyric glassy flows. The pillows of this member look unlike any other pillows observed in the study area. There is a significant range of pillow sizes within the pillows; pillows buds 10-15 cm in diameter occur next to those 1.0-1.5 m in length. Interstices are commonly filled with fine grained calcite and locally with hyaloclastite. Microscopically, the porphyritic pillows contain plagioclase, pyroxene and minor olivine crystals in a devitrified matrix. The alteration mineral assemblage includes chlorite, epidote, albite and calcite.

A bed of shale, lenses of limestone and minor mafic tuff are interbedded with the pillows on Seal Island. The shale and intervening limestone are the locus of locally intense deformation and form zones of tectonic melange (see Chapter 6 for details). Several samples from the limestone lenses were processed for microfauna, but no fossils were found. Rare fine grained mafic dykes cut the Lower Basalt Member.

3.3.1.3 Upper Basalt Member

The Upper Basalt Member is exposed on several offshore rocks between Stag Islands and Long Island. It is represented by closely packed, fine grained, dark green pillow lavas, which are fractured and autobrecciated and display "bread crust" texture. Interstices between the pillows are typically filled with jasper, and in places with fine plagioclase-phyric tuff. In thin sections volcanic rocks consist of plagioclase +/- clinopyroxene microphenocrysts in a fine grained matrix of similar composition. Although, in general, less altered than basalts of the Upper Member, these basalts display an assemblage of chlorite, epidote, and calcite.

3.3.1.4 Intrusive Member

Irregular sills and dykes of diabase and gabbro intrude the Breccia Member (Fig. 3.29). These represent a multiphase intrusive event with at least two generations of gabbroic intrusions and an intervening diabase phase. Diabase dykes and plugs are texturally and chemically similar to brecciated pillow lava flows found within the Breccia Member, and most likely represent feeder dykes.

3.3.1.5 Age

The shale horizon within the Breccia member was searched unsuccessfully for remnants of graptolites. A sample of hornblende gabbro (CI-LR-01a) intruding the contact between the breccia and pillow lava of the Breccia Member on League Rock (Fig. 3.29) was collected for a $^{40}\text{Ar}/^{39}\text{Ar}$ age determination. It yielded a well defined plateau corresponding to an age of 506 +/- 5 Ma (representing 97% of all the gas; Appendix B). This places a minimum age of late Cambrian/early Ordovician (van Eysinga, 1983) or early Tremadoc (Cooper, 1992) on the Breccia Member.

3.3.2 REMOVAL OF THE FORMATION FROM THE CUTWELL GROUP

The lithology of the Stag Island Formation differs considerably from that of other units in the Cutwell Group. It is lithologically more comparable to rock units of the Lushs Bight and the Western Arm Groups. The mafic clasts found within the Breccia Member appear to be similar to lithologies in the Lushs Bight Group sheeted dykes and sills. Trondhjemite clasts are particularly common in the breccia on League Rock, but trondhjemite is not present elsewhere within the study area. However, a large exposure

of trondhjemite, with a similar age, is found on South Twillingate Island. This locality is north of the Lobster Cove - Chanceport Fault and within the Notre Dame Sub-zone (Williams et al., 1988). Pillow lavas of the Upper Member are very similar in their texture, colour and ubiquitous red jasper in the interstices - to lavas of the Western Arm Group. Geochemical data further corroborate correlation of parts of this formation with the Western Arm Group (Upper Member), but also indicate a possible correlation with the Lushs Bight Group (Breccia Member and Intrusive Suite)(see Chapter 6)

In conclusion, the age of at least the Breccia Member and geochemical data on a variety of mafic rocks support removal of this formation from the Cutwell Group, and it is considered here as an independent unit.

3.4 Post-Ordovician Overlap Sequences

The Lower Ordovician pillow lavas and pyroclastic rocks are overlain unconformably by volcanic and sedimentary rocks of the Lower Silurian Springdale Group (e.g. Maclean, 1947; Kalliokoski, 1953; Neal and Nash, 1963, McGonigal, 1970; Coyle and Strong, 1986a, b), and by a small sliver of red beds in the Kings Point area. Brief descriptions of both units are presented below.

3.4.1 SPRINGDALE GROUP

The Springdale Group has been mapped in detail by Coyle and Strong (1986a,b) and Coyle (1990). These authors presented a comprehensive description of lithological units in the group, which is made up of (up proposed stratigraphic order): 1) welded lithic-crystal tuff; 2) mesobreccias and red sandstones; 3) andesitic to dacitic flows; 4) crystal-lithic and lapilli ash-flow tuffs; 5) basaltic flows; 6) silicic ash-flow tuffs, 7) dacitic to rhyolitic ash-flow tuff, breccias, and domes; 8) rhyolitic-vitric ash-flow tuffs and breccias; 9) clastic sedimentary rocks - red beds; and 10) crystal-lithic tuff. This volcanic-sedimentary assemblage was interpreted to be indicative of a large epicontinental collapse caldera (Coyle and Strong, 1986; Coyle, 1990). The U-Pb zircon ages presented by various workers indicated that the group evolved from 432.4 ± 1.7 - 1.4 Ma to 425 ± 3 Ma (Chandler et al., 1987; Whalen et al., 1987; Coyle, 1990).

During this study, mapping was extended into the northern part of the Springdale Group in order to clarify the contact relationships along the Lobster Cove Fault and to determine the amount and order of post-Ordovician deformational events. In the course of the mapping it was established that stratigraphy of the Springdale Group is in reality much simpler than that proposed by Coyle and Strong (1986a,b) and Coyle (1990). These workers did not recognize that rocks of the group were deformed by two major deformational events, of opposing polarity, which were responsible for repetition of lithostratigraphic units. It seems that there are three major lithostratigraphic units within the group, namely: a mafic basaltic-andesitic unit; a felsic unit; and red beds. The red beds are the youngest one and all may not be part of the Springdale Group (see Chapter 6). Much of the complex stratigraphic scheme worked out for the Springdale Group (Coyle and Strong, 1986 a,b ; Coyle, 1990) was based on presumed vertical variations; whereas, it appears that lateral variations in lithology, complicated by deformation are the primary cause of the variation. .

3.4.1.1 Red Beds

Volcanic and volcanoclastic rocks of Silurian age in the Springdale area, thought to be erupted in a large epicontinental-type caldera (Coyle and Strong, 1987; Coyle, 1990), are overlain by red beds. Wessel (1975), who studied the red bed sequence in the Springdale area in detail, interpreted the sandstone and conglomerate to have been deposited in a large regional downwarp; whereas, Coyle (1990) considered red beds to represent "caldera fill". Although a complete undisturbed section is nowhere exposed, red beds in the central part of the Springdale Group reach a thickness in excess of several hundred meters, and thin rapidly towards the edges of the group. Red beds in the thickest exposures consist of (not necessarily in stratigraphic order): coarse polymictic conglomerates, locally with boulders up to 0.8-1 m in diameter; conglomerates and sandstones with layers of mud-chip intraformational breccia; and sandy siltstones, in places with caliche. This association, locally repeated within the section, is observed in most outcrops, although the basal conglomerate is not always present and in places, sandstone immediately overlies volcanic rocks of the Springdale Group.

There is a significant variation in clast size, roundness of clasts and lithology between outcrops within the basal conglomerate. A rather atypical, clast-supported talus breccia is present on Triton Island which consists of angular fragments of red argillite and jasper, variously altered basalts, and clasts of diabase in a sparse fine to coarse sandy matrix. However, in many locations, the conglomerates are matrix supported, containing well rounded cobbles and boulders of rhyolite, andesite, basalt, argillitic chert and locally abundant granodiorite to granite. Most clasts are rock types typically found in the Springdale Group. However, some of them (in particular red chert, diabase and gabbro) appear to be derived from the Roberts Arm or/and Lushs Bight/Western Arm groups.

3.4.2 RED BEDS IN KINGS POINT (= SOUTHWEST ARM FORMATION ?)

At the bottom of Southwest Arm, an approximately 1.2 km thick sequence of clastic sedimentary rocks is exposed in a northeast plunging syncline. The rocks consist of red arkosic conglomerate and sandstone, that grade into green-grey and red siltstone, the latter of which contains several beds of dirty white to pale gray limestone. Presence of the limestone (silty micrite), combined with lack of sedimentary structures in the conglomerate-siltstone assemblage, was taken by Wessel (1975) as an evidence for deposition of these rocks in shallow-marine conditions.

The age of this unit and its correlation with the Springdale Group has been a matter of considerable controversy. It was originally included in the Springdale Group by MacLean (1947), whose correlation was later tentatively accepted by Neale and Nash (1963) on the basis of a paleomagnetic study carried out by R.F. Black in 1961. Wessel (1975), who studied the red beds of the Springdale Group and in King's Point in detail, accepted the correlation as well, although he provided evidence that the two units formed in different environments (i.e. fluvial vs. marine, respectively). Thus, it is very likely these two have very little in common. Marten (1971b) reassigned the Kings Point beds to the Carboniferous. This interpretation was accepted by Kean et al (1981). This author favours the younger age for this sequence of clastic rocks, because unlike red beds overlying volcanic rocks of the Springdale Group, the red beds in the King's Point

area display strong similarity to poorly consolidated red beds of the Carboniferous age in the Humber Zone, and show evidence of only one major deformation.

The limestone is sparsely fossiliferous (contains strongly recrystallized brachiopods) and Wessel (1975) reported the presence of ostracodes, although these were not identified. Samples from five limestone beds were collected by this author and processed for microfossils by F. C. H. O'Brien, but none were found.

3.5 Summary

The present mapping resulted in several major and minor changes to the previously established stratigraphy of the western Notre Dame Bay area. One of the main outcomes of this study is the recognition that pillow lavas, tuff/tuff breccias and cherty sedimentary rocks on Pilley's Island, Triton Island and Halls Bay Head, previously thought to be related to the Cutwell Group (Kean and Evans, 1987; Kean, 1989), are correlative with the Western Arm Group. Rocks of the Catchers Pond Group, which includes both mafic and felsic flows and tuffs, and rocks in the area immediately northwest of Springdale, have also been assigned to the Western Arm Group. The redefined Western Arm Group is thus exposed in several geological sections which include:

- the type section in the northern part of Springdale Peninsula as defined by MacLean (1947) and Marten (1971a, b);
- the Catchers Pond section located north of Indian Brook;
- the Ovals section in the area between Catchers Brook and the bottom of Southwest Arm;
- the Halls Bay Head in the easternmost tip of Springdale Peninsula; and
- the Pilley's-Triton section in the northern part of Pilley's and Triton islands.

Rocks of the Western Arm Group are in addition exposed in several smaller outcrop areas, which are named here the Harry's Harbour, Nickey's Nose, Eastern Point and Fox Neck sections. Possible Western Arm Group equivalents are exposed on Stag Islands, Long Island and Little Bay Island.

Within the Western Arm Group, the rocks of the Basal Pillow Formation of MacLean (1947) are reinstated as the Sugar Loaves Basalt. This unit had been stripped from the

Western Arm Group and included in the Lushs Bight Group by Marten (1971a, b). Flows of the Sugar Loaves Basalt are petrographically very similar to lavas of the Western Arm Group (in particular to those of the Big Hill Basalt), and show high values of the magnetic vertical gradient the same as the Big Hill Basalt. The restored unit also displays geochemical similarities to rocks of the Western Arm Group (see Chapter 6).

Another result of this mapping is the identification (together with Kean and Jenner) of a suite of ~500 Ma old dykes that cut the Little Bay Basalt flows and formations of the Western Arm Group up to and including the Big Hill Basalt. These dykes, referred to in the past as "lamprophyric", are locally characterized by large hornblende and clinopyroxene phenocrysts and/or phenocrystic clusters, which exceed 50% of the rock. The dykes are particularly common near or intruding the D₁ shear zones within the Lushs Bight Group pillowed flows.

The stratigraphic order interpreted from the present mapping of the Cutwell Group on Long and Little Bay islands also differs from that formalized by earlier workers (Kean, 1973; Kean and Strong, 1975). In this study the Pigeon Head Formation (shale, chert, siltstone and sandstone and tuff breccia) include the Quinton Cove Formation (tuff/tuff breccia), as both formations were found to form one continuous sequence that is intruded by a distinct suite of sills and dykes not found elsewhere in the Cutwell Group. The geology of the Long Tickle Formation (mainly massive and lesser pillowed flows, tuff/tuff breccia) suggests that it is the lithological equivalent of the Burnt Head Formation (mainly pillowed and lesser massive flows, tuff/tuff breccia, shale and chert) and occupies a similar stratigraphic position. Here, rocks of the latter unit are included in the Long Tickle Formation.

During this mapping, the Stag Formation (breccia containing blocks of diabase, gabbro and trondhjemite; pillow lava; dykes and minor diabase and gabbro intrusions) was recognized in two more areas away from the type section. One area of outcrop is on the southeastern shore of the Little Bay Island and Copper Island (an islet south of Little Bay Island), the other is on League Rock, an islet east of Long Island. Hornblende gabbro intruding the contact between the breccia and pillow lava of the formation on League Rock was dated using the $^{40}\text{Ar}/^{39}\text{Ar}$ method and yielded an age of ~506 Ma (early Tremadoc of

Cooper, 1992) Based on lithology and age, the Stag Island Formation is more comparable to rock units of the Lushs Bight and the Western Arm groups, rather than with the Cutwell Group. Additional support for this correlation is also available from the geochemical data (Chapter 4). Thus, the Stag Formation is removed from the Cutwell Group, and it is considered here as an independent unit.

In conclusion, the presence of the ~500 Ma old dykes cutting only part of the stratigraphic succession, isotopic dating of zircons and hornblendes in tuffs and intrusive rocks, as well as faunal age constraints resulted in redefinition of the stratigraphy in western Notre Dame Bay, and, in particular, recognition of two main sequences of rocks. The first of these sequences is older than 500 Ma, and consists of the Lushs Bight Group, Stag Formation, and the Sugar Loaves Basalt, Skeleton Pond Formation and Big Hill Basalt (i.e. the lower and middle part of the Western Arm Group). The second sequence spans the time interval from ~485 to ~465 Ma, and consists of the Welsh Cove and Western Head Formations (i.e. the upper part of the Western Arm Group) and the Cutwell Group.

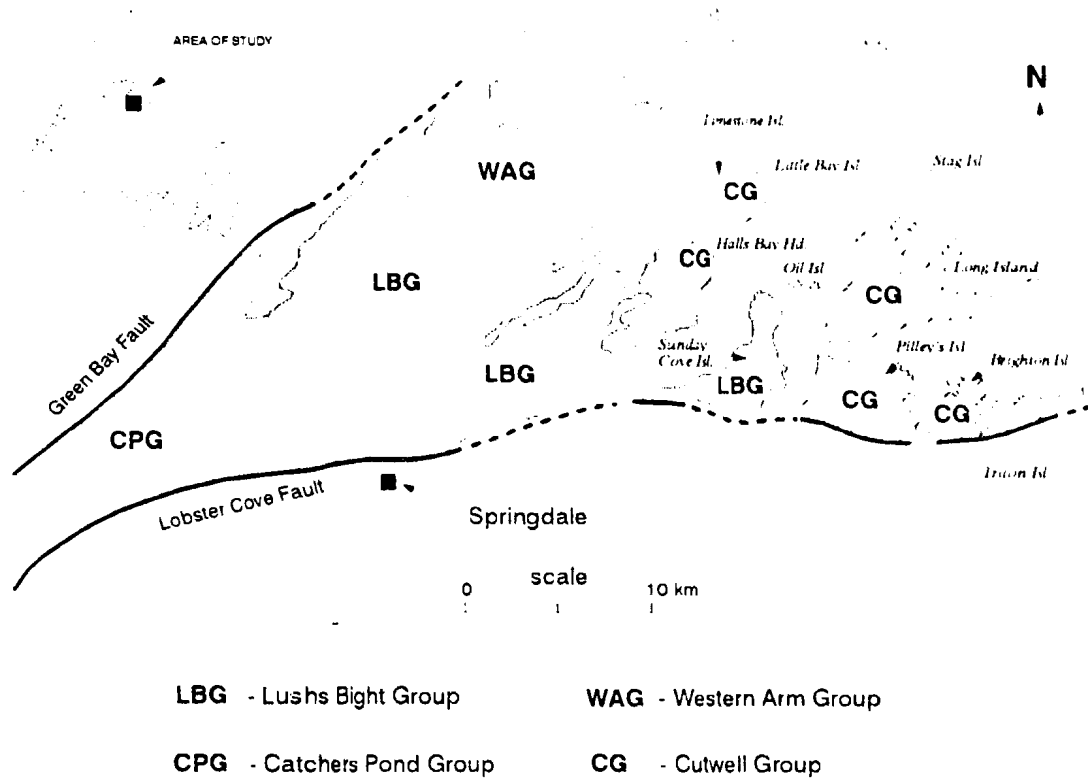


Figure 3.1. Distribution of major lithostratigraphic units in the western Notre Dame Bay area according to previously established stratigraphic order (simplified after Kean et al., 1981; and Kean and Evans, 1987a, b).

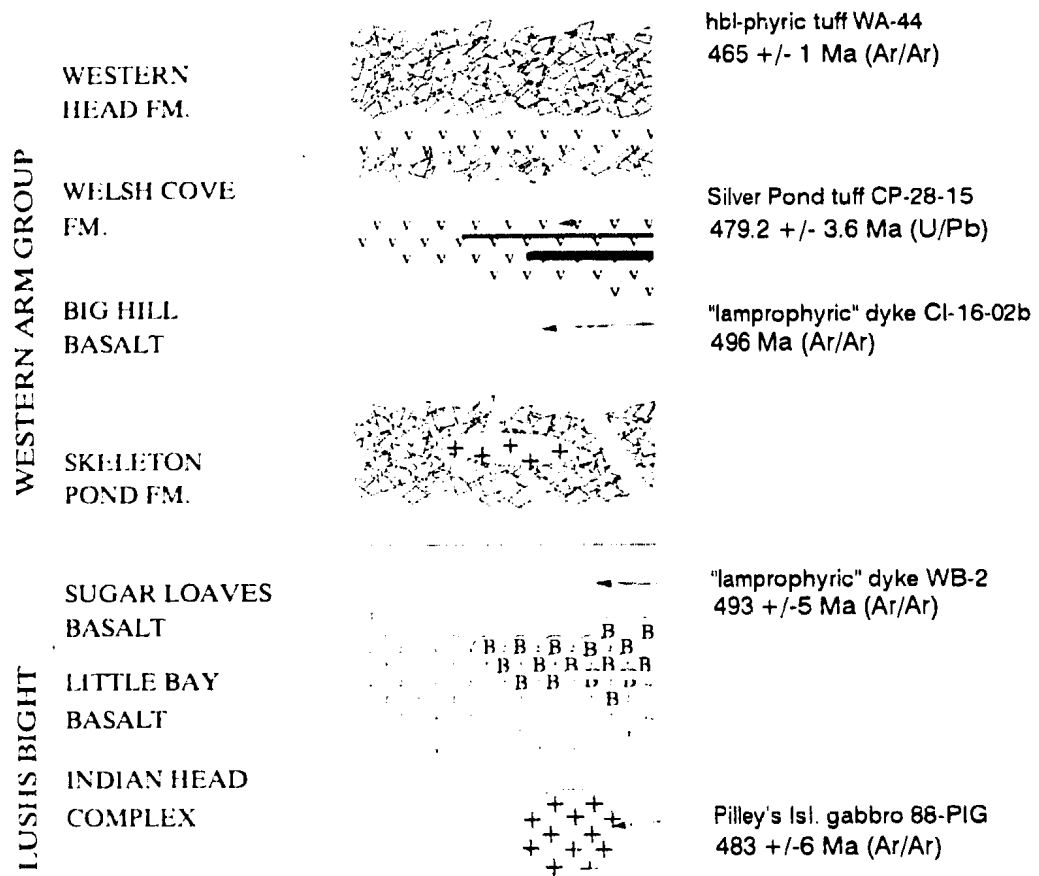


Figure 3.2. Stratigraphic order of units in the western Notre Dame Bay area revised in view of the present mapping; the Lushs Bight and Western Arm Groups. Isotopic ages referred to in the chapter are shown on the right side of the column

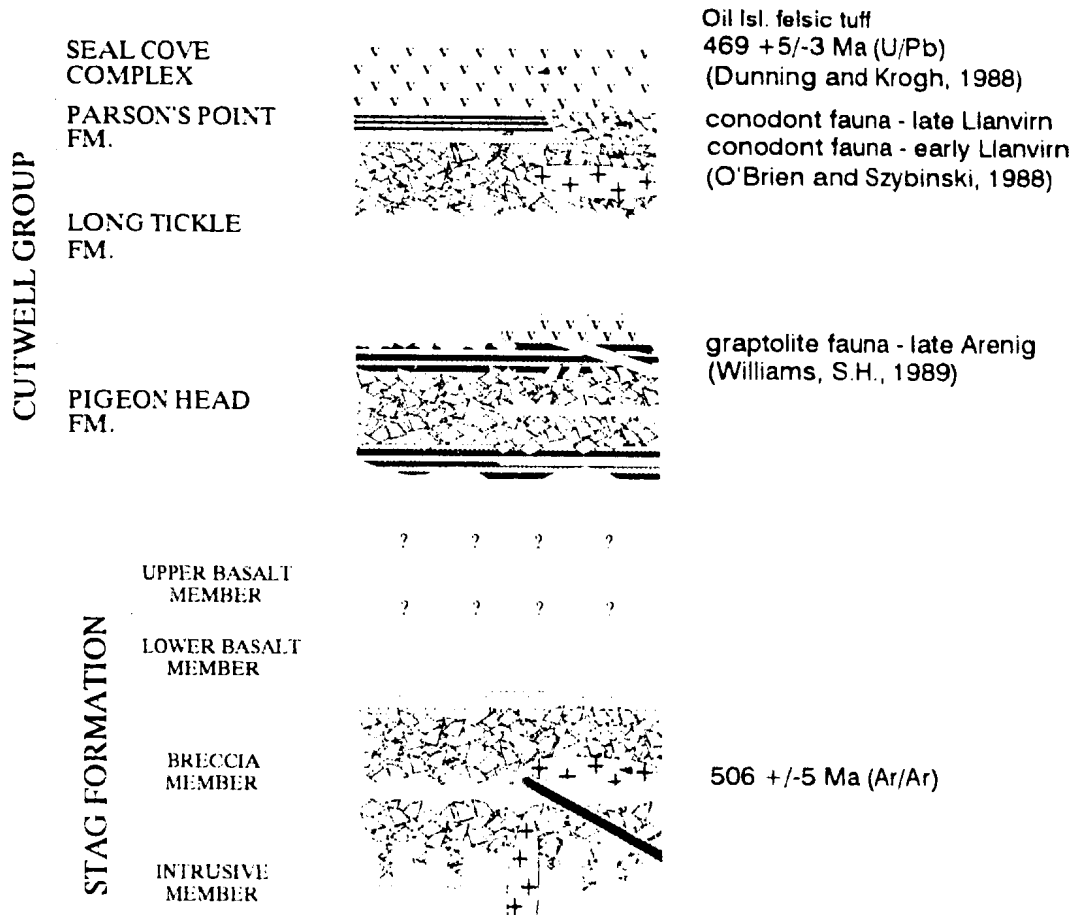


Figure 3.3. Stratigraphic order of units in the western Notre Dame Bay area revised in view of the present mapping; the Stag Formation and the Cutwell Group Isotopic ages referred to in the chapter are shown on the right side of the column

LEGEND

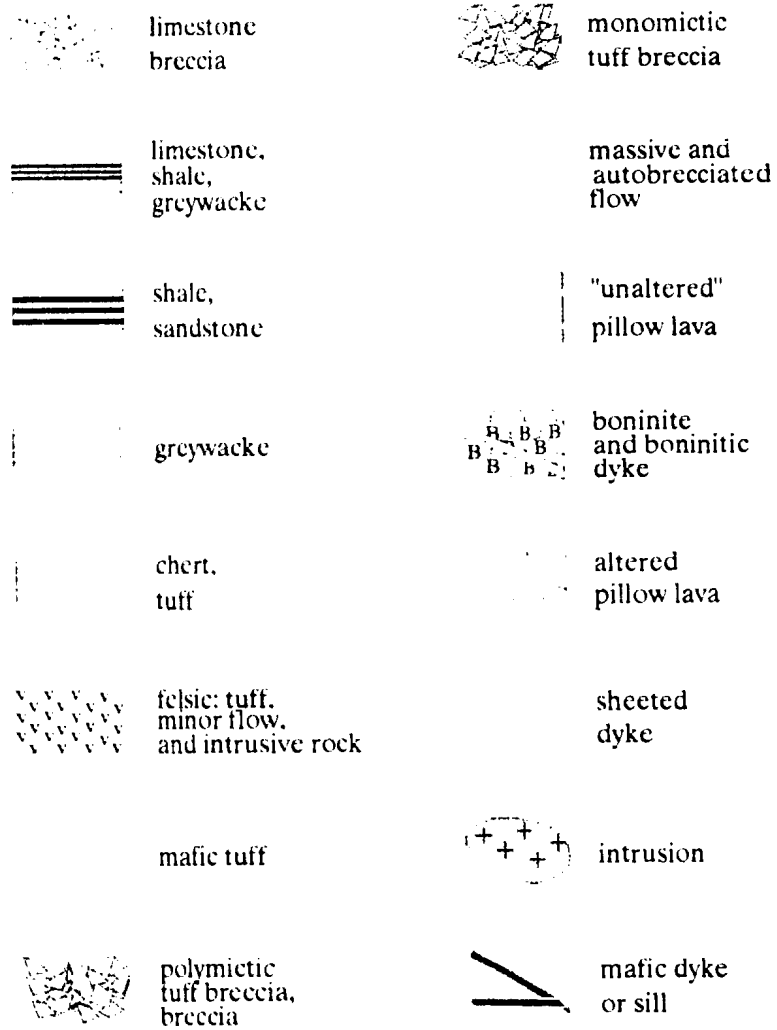


Figure 3.4. Legend for lithostratigraphic columns in Figures 3.2. and 3.3.

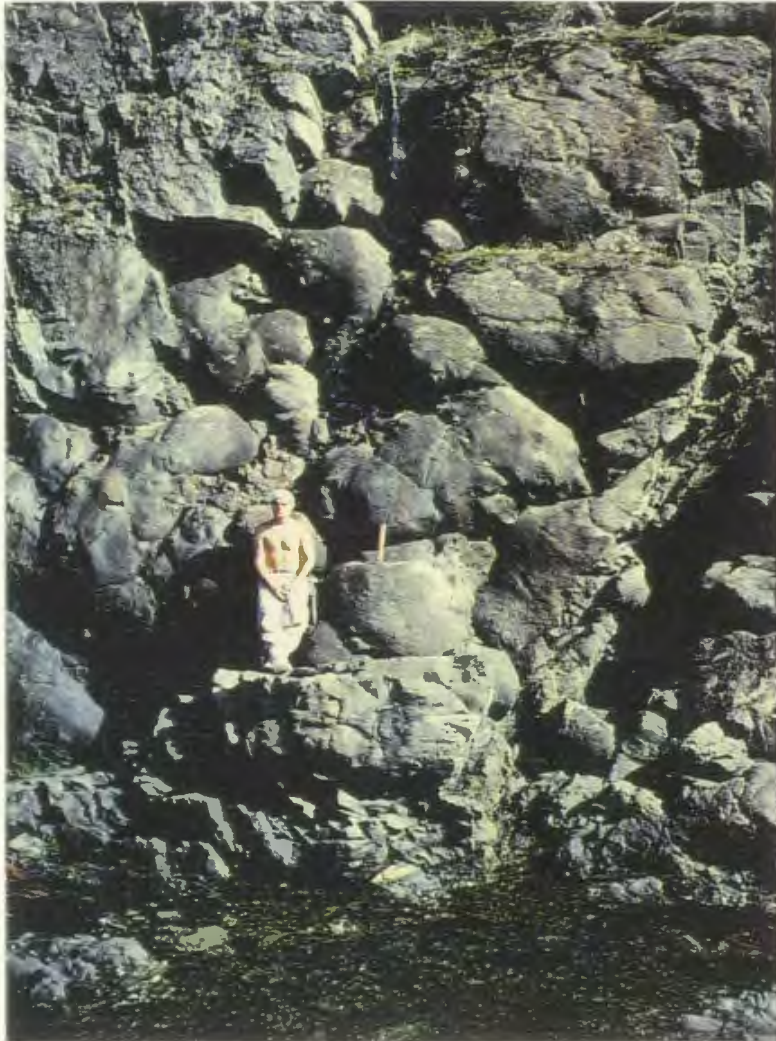


Figure 3.5. Large pillows and lobes of the Big Hill Basalt on the western shore of Big Triton Island. L. Mandville for scale.

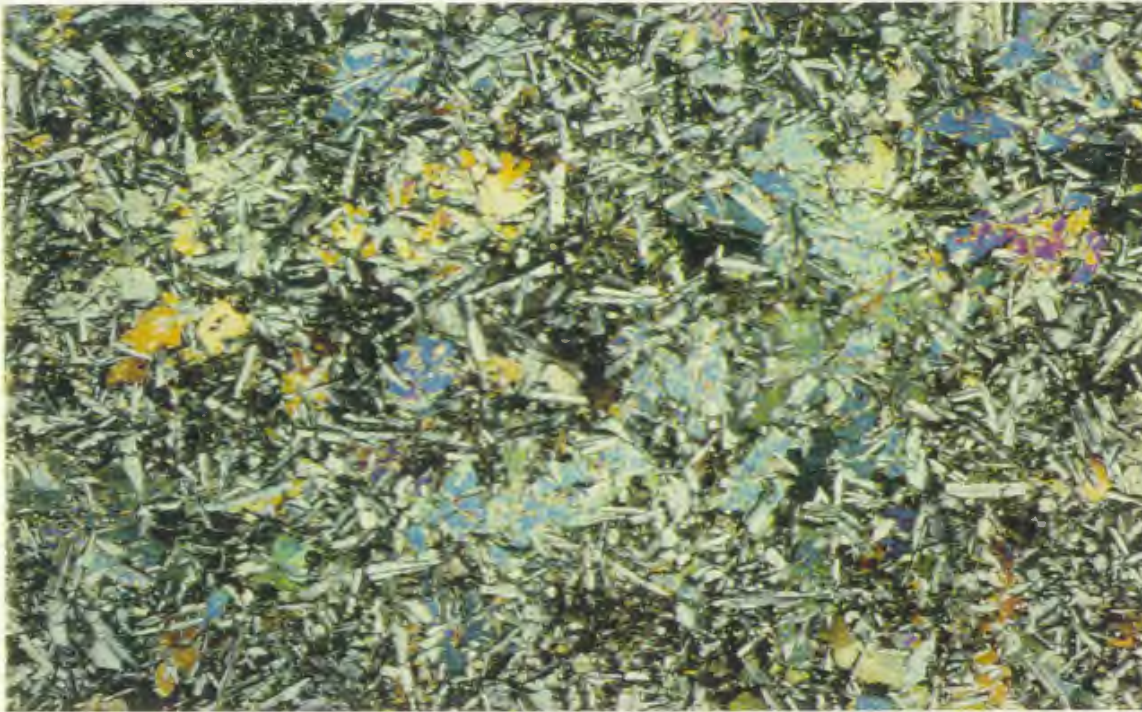


Figure 3.6. Thin section of a typical basalt from the Big Hill Basalt. It is characterized by the intersertal and subophitic texture which consists of plagioclase crystals partly enclosed by and partly penetrating beyond clinopyroxenes. Minute opaque magnetite is also present; magnification (X) 12.2, cross polarized light (XPL).

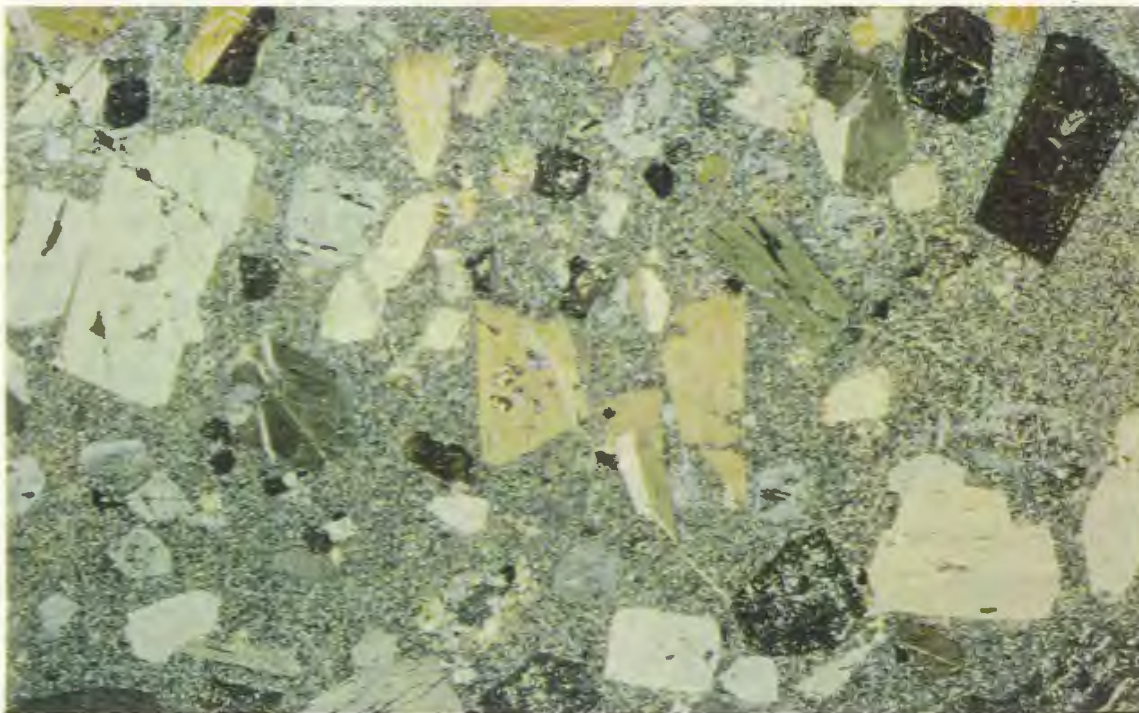


Figure 3.7. Thin section of a "lamprophyric" dyke from the Whalesback Mine area. The rock is characterized by porphyritic texture with relatively large euhedral hornblende phenocrysts (black, white, pale yellow, greenish grey colours) in a fine-grained matrix; X 6.8, XPL.

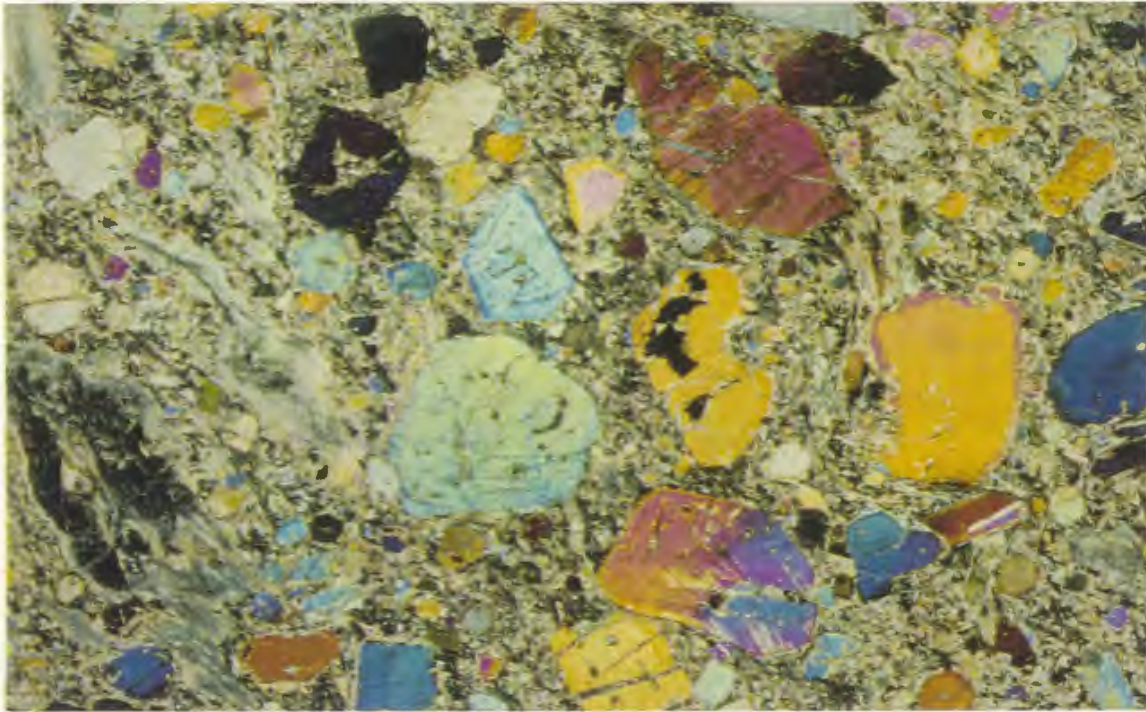


Figure 3.8. Thin section of a pyroxene-phyric dyke from the Whalesback Mine area. A few generations of clinopyroxene (large subhedral phenocrysts, euhedral microphenocrysts and minute groundmass crystals) are present in sheared and altered (chlorite, sericite) matrix. Note oscillatory twinning (e.g. bottom of the photo) and marginal zoning (centre and at the right of the field of view) in clinopyroxenes; X 3.8, XPL.



Figure 3.9. Monomictic tuff-breccia from the Welsh Cove Formation consisting of angular rhyolite clasts in a matrix of predominantly plagioclase crystals, lesser quartz crystals, and lithic fragments.

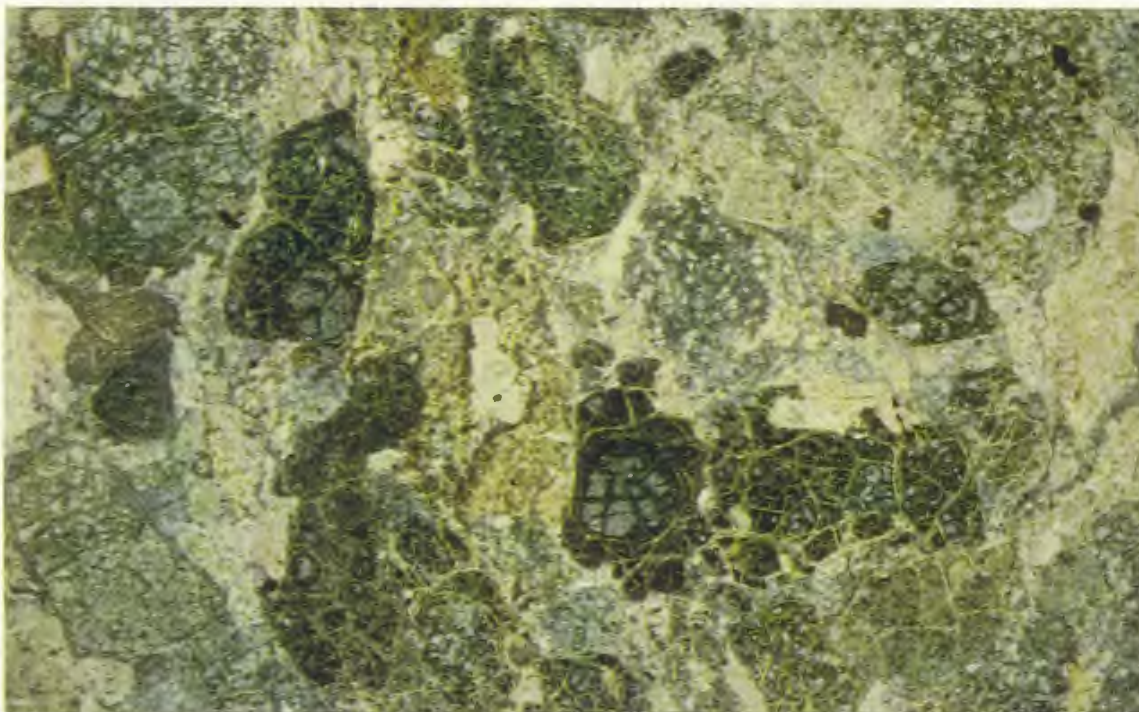


Figure 3.10. Thin section of matrix to polymictic lapilli tuff/tuff-breccia from the Welsh Cove Formation, Catchers Pond section. Among lithic detritus present in the groundmass, there is a significant number of devitrified glass fragments characterized by spherical fractures - perlitic cracks; X 9.9, XPL.

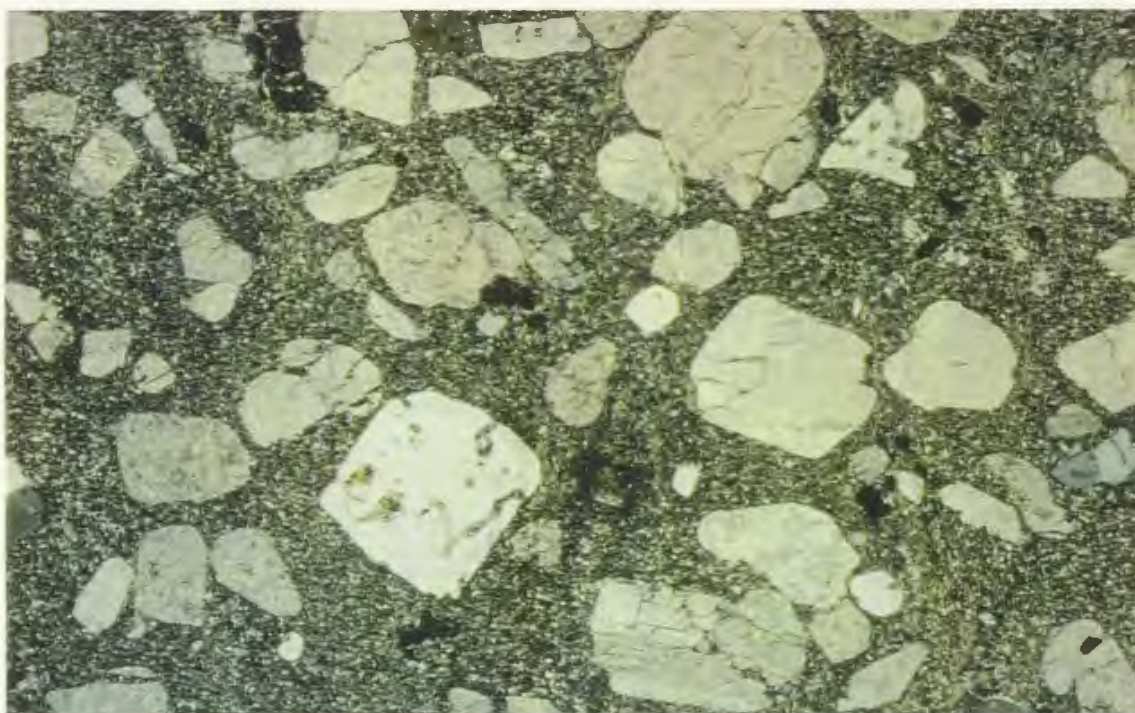


Figure 3.11. A porphyry containing phenocrysts of alkali-rich feldspar, lesser plagioclase and quartz in a fine grained groundmass. Some opaque iron oxide crystals are also present; Welsh Cove Formation, Catchers Pond section; X 8.4, XPL.



Figure 3.12. An outcrop of banded porphyritic tuff (locality CP-28-15) with interbedded rhyolite (light coloured bands) and dacite (darker bands). Three zircon fractions from this tuff yielded an age of 479.2 ± 3.6 Ma, early to middle Arenig according to the Cooper (1992) scale, interpreted to represent the primary igneous age.



Figure 3.13. An outcrop of a mafic tuff and tuff breccia of the Western Head Formation on the eastern shore of Pilley's Island. This photo shows coarse volcanic breccia grading into lapilli tuff, and eventually tuff. The field of view is about 5m.

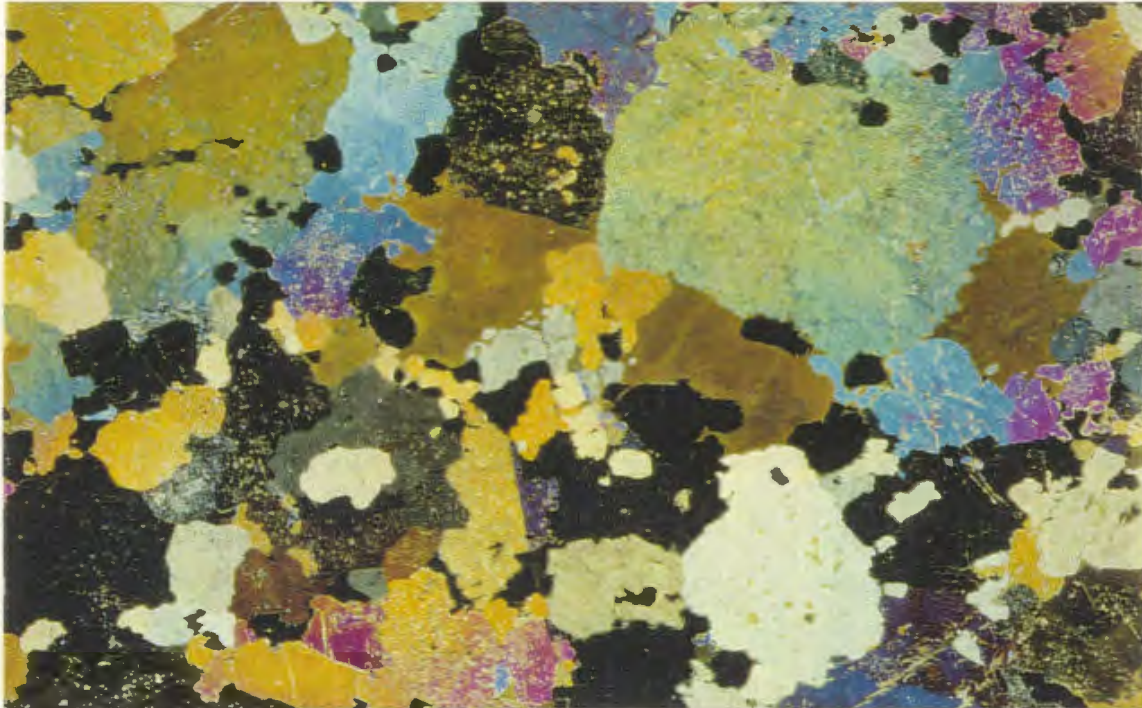


Figure 3.14. Granular-textured hornblende pyroxenite from the Brighton Intrusive Complex. The opaque mineral is magnetite. The large crystal of clinopyroxene in the upper right of the photo and another crystal in the upper left show irregular extinction, indicating that the clinopyroxenes are strained; X 6.2; XPL.

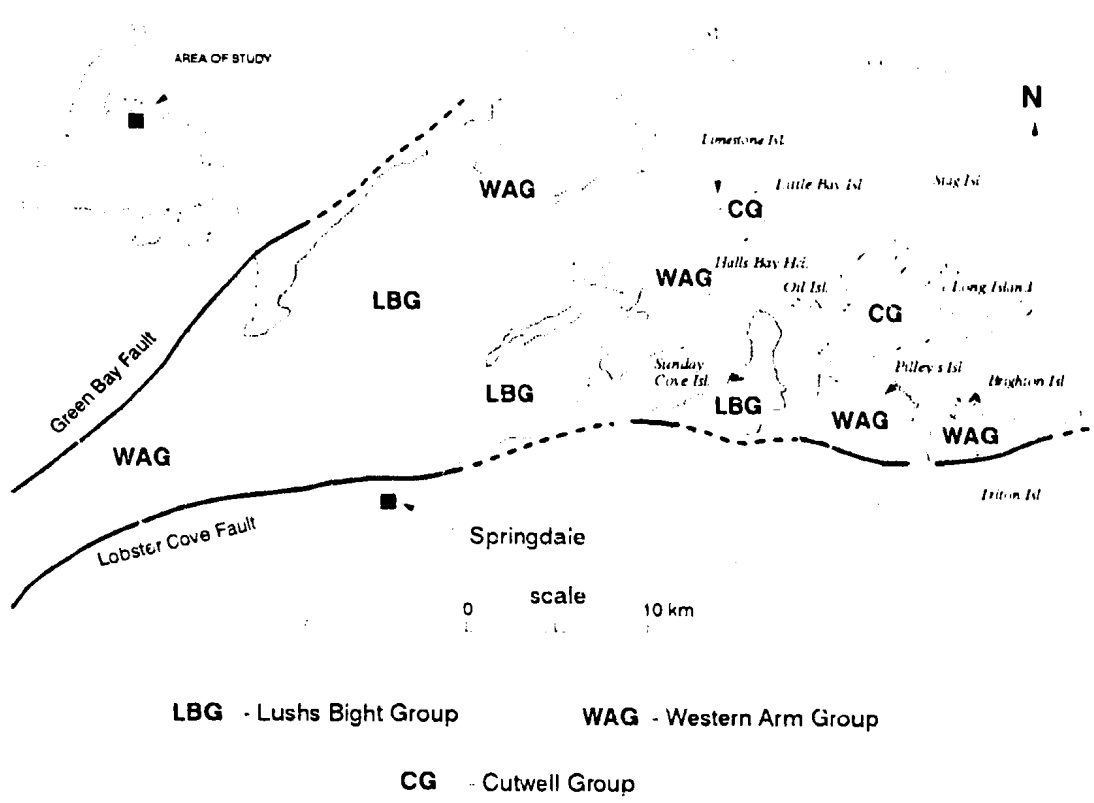


Figure 3.15. Distribution of major lithostratigraphic units in the western Notre Dame Bay area in view of the present mapping.



Figure 3.16. Subophitic and intersertal texture in a diabase dyke cutting tuff breccia of the Pigeon Head Formation, Long Island. This diabase consists of plagioclase crystals embedded in or partially enclosed by clinopyroxene in a subophitic manner. Some opaque magnetite crystals are scattered throughout the rock. Note close textural and mineralogical similarity of this diabase to the Big Hill Basalt sample; X 12.2, XPL.



Figure 3.17. Interbedded volcaniclastic sandstone and well laminated volcaniclastic mudstone of the Long Tickle Formation tuff lithofacies, the Southern Head area. Stratification of the mudstone is mainly planar, but "flame structures" occur locally.

Figure 3.18. (Right) Volcaniclastic sediments of the Long Tickle Formation channelled by the felsic pyroclastic flow of the Seal Cove Complex, which has ripped-up fragments of shale and chert, Southern Head, Long Island. The scale is about 15cm long.



Figure 3.19. (Below) The tuff breccia of the Long Tickle Formation, southern shore of Long Island. It is characterized by angular to subangular clasts of mafic volcanic rocks surrounded by the lapilli tuff matrix. Note mafic flow dipping gently to the right (above the hammer); hammer 35cm for scale.





Figure 3.20. Lobate massive mafic flow overlying the tuff lithofacies of the Long Tickle Formation, Bread and Cheese Cliff, Wild Bight, northeastern shore of Long Island; hammer 35cm long for scale.



Figure 3.21. Pillowed flows of the Long Tickle Formation interfingered with bedded tuff, west of Southern Head, Long Island. The field of view is about 25m.

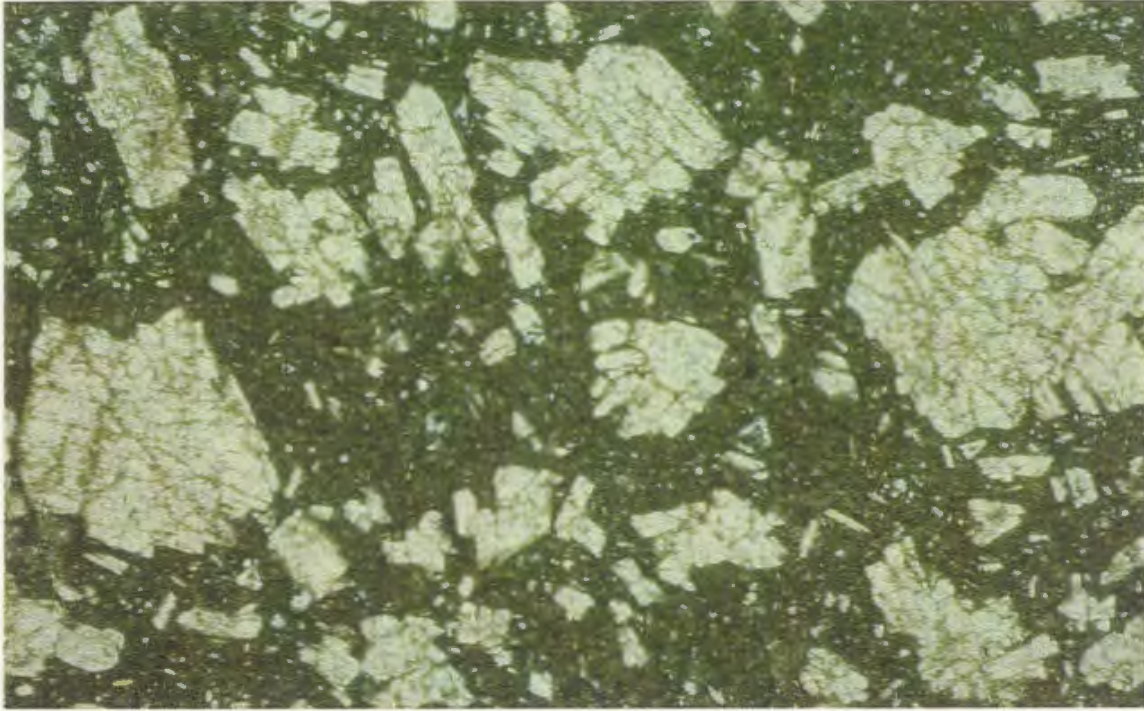


Figure 3.22. Typical porphyritic andesite of the Long Tickle Formation. The phenocrysts and microphenocrysts are plagioclase in a microcrystalline groundmass consisting of plagioclase microlites, secondary chlorite and epidote; X 11.0, XPL.



Figure 3.23. The conodont fauna *Periodon aculeatus* Hadding from Limestone Island, off the Little Bay Island western shore. Conodonts are believed to represent the boundary of the *Microzarcodina flabellum parva* Zone/*Eoplacognathus? variabilis* Zone (late Arenig; Tucker et al., 1990). Colour Alteration Index (CAI) of 8. (photo courtesy of F.H.C. O'Brien).



Figure 3.24. Andesite-cherty siltstone peperite from the western shore of Little Bay Island. The photo shows a zone of intricate mixing between feldspar - phyric andesite and siltstone, with patches and wispy blobs of andesite within siltstone.

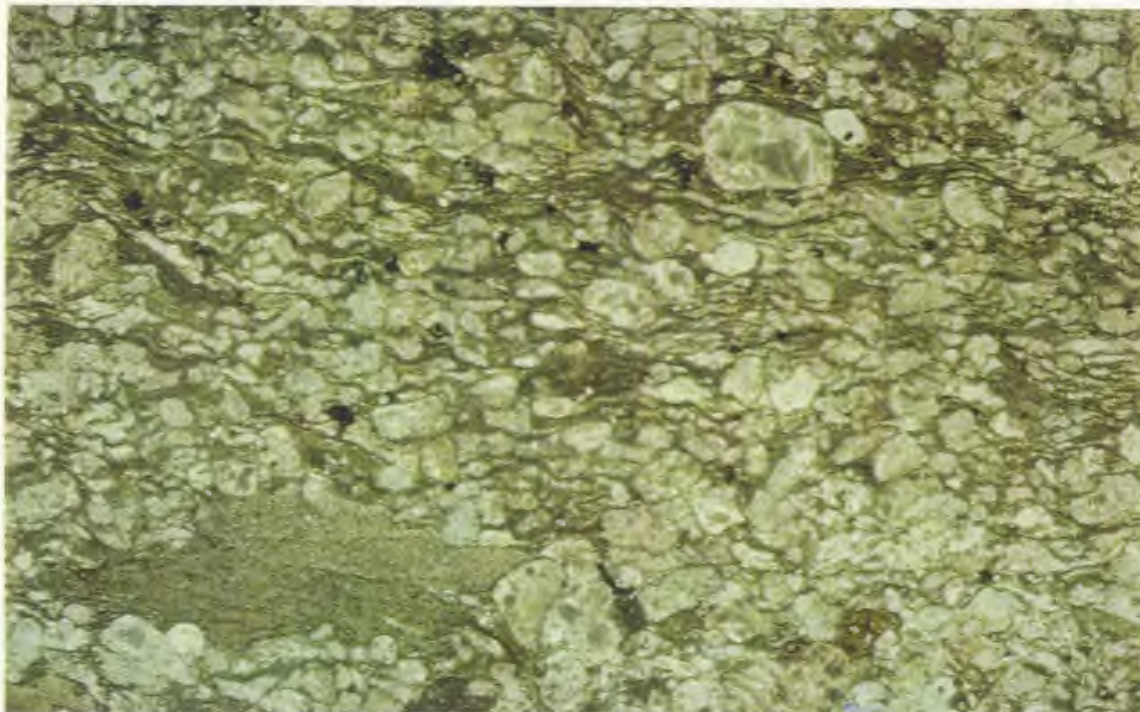


Figure 3.25. Thin section of welded crystal tuff from the Parson's Point Formation, characterized by eutaxitic texture and plagioclase crystals embedded in flattened pumice fragments and a fine ash matrix. The upper part of the photo captures a transition zone to nonwelded tuff, whereas a pumice fragment which is only partially flattened is present in the upper right corner; X 7.6, XPL.



Figure 3.26. Conodonts *Cordylodus? horridus* Barnes and Poplawski, from limestone breccia (quarries south of the Lushes Bight-Beaumont road), Long Island. The fauna is from the lower part of the *E. suecicus* Zone (uppermost Arenig to early Llanvirn; Tucker et al., 1990). The conodonts display a relatively low CAI of 4. (photo courtesy of F.H.C. O'Brien).



Figure 3.27. Felsic Flow of the Seal Cove Complex overlying hematitic tuff in the Doolan Folly area, eastern Long Island. The white scale is about 15cm long.



Figure 3.28. (Top) A minor felsic dyke of the Seal Cove Complex intrudes cherty tuffaceous sediment of the Long Tickle Formation on Southern Head, Long Island. The white scale is about 15cm long.

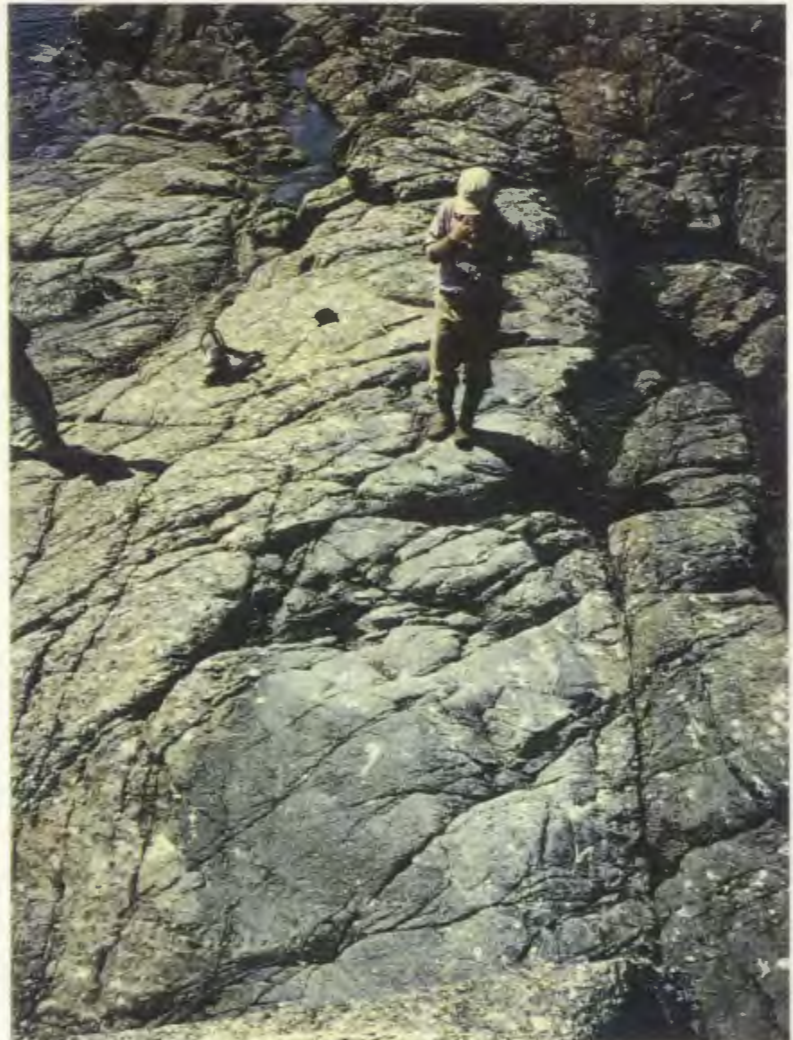


Figure 3.29. (Right) Gabbro sill (centre of the photo) intruding contact between pillow lavas (right) and breccia (left) of the Stag Formation on League Rock. For scale, S. Swinden contemplating the field relationship. Hornblende from this gabbro dated by the $^{40}\text{Ar}/^{39}\text{Ar}$ method yielded an age of 506 +/- 5 Ma (early Tremadoc; Cooper, 1992).

CHAPTER 4: GEOCHEMISTRY AND PALEOTECTONIC AFFINITIES

4.1 Introduction

This chapter presents the results of a detailed geochemical sampling of volcanic and subvolcanic rocks within the western Notre Dame Bay area. Previous studies (Kean, 1973; Kean and Strong, 1975; Strong, 1977; Jenner et al., 1988; Swinden et al., 1989) used field and, most importantly, geochemical evidence to suggest that rocks in the Notre Dame Bay area had formed in both arc and non-arc tectonic settings. However, the meaning of this mixture of tectonic environments, as indicated by geochemical signatures, is unclear: does it reflect poorly designed tectonomagmatic discrimination diagrams, alteration, analytical uncertainty, or is it of primary petrogenetic and tectonic significance? The primary aim of this chapter is to present and evaluate the geochemical data, ascertain their reliability and petrogenetic significance, and use them to subdivide the samples (data) into types that can be interpreted in terms of their stratigraphic and paleotectonic significance.

Considerable caution must be exercised in interpretation of paleotectonic environments from geochemical data alone. However, geochemical data in combination with lithological and stratigraphic information can provide reliable interpretations. During the course of this study, it became clear that the geochemical types recognized using geochemical data correspond only in a general way with the lithostratigraphic framework presented in the previous chapter. Therefore, in this chapter subdivisions of volcanic, volcanoclastic and subvolcanic rocks reflect only their geochemical characteristics. Names of geographically distinct sections and lithostratigraphic units are locally referred to, indicating from which units the samples were collected. Chemostratigraphy and its relationship to the established lithostratigraphy, and comparison with modern analogs, are examined in Chapter 5.

The terms N-MORB, E-MORB and OIB, with or without the prefix "typical", are used extensively in this chapter and refer, respectively, to trace element geochemical signatures of normal and enriched mid-ocean ridge and ocean island basalts from Sun and McDonough (1989). Similarly, references are made to the geochemical signature of average continental crust (UCC) of Taylor and McLennan (1985) and average amphibolite facies gneiss (AFG)

of Weaver and Tarney (1981). Values for these important geochemical reference compositions are listed in Appendix D

For a legend spelling out these and other abbreviations (text, tables and figures) used in this and the next chapters see Figure 4.1. Analytical methods are described in Appendix C, and complete major and trace element analyses for samples used in this study are listed in Appendix D. To clarify the systematics used in classifying and subdividing the volcanic rocks in this study a summary flow chart is given in Figure 4.2, and the symbols used to define the groups throughout the chapter are given in Figure 4.3.

4.2 Alteration And Element Mobility

Prior to presenting the geochemical results, it is important to consider the effects of secondary processes on the absolute and relative concentrations of elements in the analyzed rocks. There is a substantial amount of literature dealing with the effects of the mobility of elements in volcanic rocks during hydrothermal alteration, carbonatization and metamorphism (e.g. Thompson, 1973; Stauffer et al., 1975; Coish, 1977; Hellman et al., 1979; Hynes, 1980; Murphy and Hynes, 1986; Sturchio et al., 1986; Biennu et al., 1990; Bau, 1991; Marsh, 1991; Price et al., 1991). When dealing with ancient volcanic rocks, it is important to consider that these rocks may have been altered more than once in a variety of different environments -- reflecting the range of geological and tectonic events to which they may have been subjected.

In pillow lavas and massive volcanic flows, seafloor alteration can occur by weathering and/or by interaction with hydrothermal fluids; both tend to occur primarily along pillow margins and in fractures. Substantial dispersion of major elements in ancient volcanic rocks resulting from these processes has been documented by many authors (e.g. Stauffer et al., 1975; Coish, 1977; De Wit et al., 1987). Element abundances may differ by as much as 50% between pillow cores and rims (e.g. Thompson, 1973; Ludden and Thompson, 1979; Biennu et al., 1990). It has also been shown that element mobility effects can be particularly drastic in sheared and intensely hydrothermally altered rocks. During the course of these studies it was likewise found that several key trace or minor elements (e.g. K, Rb, Ba, Sr), which are widely used in characterization of volcanic rocks erupted in present day

settings, are easily mobilized. This is particularly true in mafic volcanic rocks that have undergone greenschist facies alteration and metamorphism.

Several studies have shown that some trace elements (Ti, P, Zr, Hf, Nb, Ta, Cr, Ni, V, Y) appear to be immobile during normal seafloor alteration and these elements have been used to establish tectonic and petrogenetic discrimination diagrams (e.g. Wood et al., 1979; Pearce and Norry, 1979; Shervais, 1982). In addition to these elements, the rare earth elements (REE) are commonly used in classification of both contemporary and ancient rocks, under the presumption that they remain immobile during metamorphism. In contrast to this widely held opinion, the mobility of some of these trace and rare earth elements during seawater alteration has been documented in altered basaltic glasses and crystalline basalts. For example, in a study of altered MORB glasses (Bienvenu et al., 1990) the immobility of Nb, Ta, Zr, Hf, Ti, and Ce was confirmed, but it was shown that some REE and Y can be depleted and Th enriched. Examination of seawater alteration effects on MORB by Verma (1992) showed that: the REE (notably light-REE) are mobile and increase in crystalline basalts (but decrease during palagonitization of glasses); Th remains almost constant in crystalline samples; and contrary to the findings of Bienvenu et al. (1990), Th actually decreases considerably in palagonitized MORB glasses. A recent study by Bau (1991) concluded that the low REE content in alteration fluids suggests that hydrothermal or metamorphic alteration of the REE patterns should not be significant, unless the water/rock ratio is $\gg 10^2$ - 10^3 . It is important to note that dehydration experiments carried out at 12 kbar and 850°C by Tatsumi et al. (1986) also demonstrated almost absolute immobility of Nb.

Addition of Mg, prominent dispersion of some of the trace elements (Ti, P, Zr, Nb and Y) and addition of REE was shown to take place in rocks which experienced glaucophane schist, blueschist to greenschist facies metamorphism involving the presence of high CO_2 levels in the fluid phase (Hynes, 1980; Murphy and Hynes, 1986; Vocke et al., 1987). Apparently, while REE are mobile in such environment, Th stays practically immobile (Vocke et al., 1987), although it can be increasingly mobile under higher P-T conditions (Sorensen and Grossman, 1989). Additional mobility of REE was documented

in various regions during low-temperature weathering and hydrous burial metamorphism (Hellman et al., 1979; Ludden and Thompson, 1979; Marsh, 1991; Price et al., 1991)

Extreme continental weathering of volcanic rocks may be accompanied by progressive mobilization and net removal from the weathered samples of Si, Mg, Ca, Na, K, Rb, Sr, Ba and V; whereas Cr, Y and REE show drastic variations and redistribution (Marsh, 1991; Price et al., 1991). Mobility of these elements during weathering appears to be a function of the ionic radius and charge, groundwater parameters, and the secondary mineral assemblages developed (Marsh, 1991; Price et al., 1991). Several elements, most notably Fe, Ti, Al, Zr, Hf, Sc and Ni, are immobile and their proportions are preserved, and ratios between these elements are not fractionated (Marsh, 1991).

While it is clear that evidence for mobility of REE and Ti, P, Zr, Hf, Nb, Ta, Cr, Ni, V and Y does exist, the cases in which it has been documented primarily involve intense hydrothermal activity (i.e. high water/rock ratio), metamorphism or weathering, and/or glasses, rather than crystalline rocks. Every precaution was taken during the study to collect samples from fresh, crystalline pillow cores, or from the centers of massive flows and dykes/sills, that showed the least evidence of a hydrothermal overprint. Samples were collected well away from the stratigraphic contact with Silurian and Carboniferous volcanic and sedimentary rocks, as these areas were most likely subjected to continental type weathering. This approach and subsequent petrographic assessment of the freshness of the rocks allowed to exclude, prior to analysis, samples in which effects of alteration were particularly evident. The following assessment of element mobility based upon available literature and experience of workers familiar with alteration systematics of volcanic rocks in Newfoundland Appalachians (Coish, 1977; Coish et al., 1982; Jenner and Szybinski, 1987; Swinden, 1987; Swinden et al., ; 1990; Jenner, 1991; Dunning et al., 1991; Jenner and Swinden, 1993; Kean et al., 1995) has been adopted in interpreting the geochemical data acquired during this study:

- Si, Ca, Na and low field strength elements (LFSE) - K, Rb, Ba, Sr are considered to be mobile under hydrothermal alteration and greenschist facies conditions;
- Mg and total Fe are mobile, but to a lesser extent and may not be significantly mobile during sub-seafloor metamorphism at low water/rock ratios. The

degree of Mg and Fe mobility is of concern, since the FeO^*/MgO (FeO^* being total iron) ratio and the Mg# (molecular proportion $100 \text{ MgO}/[\text{MgO} + \text{FeO}]$) are commonly used as indicators of fractionation. It appears that at low water/rock ratio and under greenschist conditions, the original ratio of these elements may be preserved in pillow interiors (Swinden, 1987) and can be used to indicate the relative degree of fractionation of the rock; and

- Al, transition metals Cr, Ni, V, high field strength elements (HFSE) Ti, P, Nb, Zr, Y, the low field strength element (LFSE) Th, and rare earth elements (REE) are considered to be essentially immobile during greenschist facies seafloor alteration under lower water/rock ratio, but may be mobile at higher water/rock ratios, under higher grade metamorphic conditions or during any-grade of metamorphism involving a CO_2 -rich fluid phase (Dunning et al., 1991)

In active geothermal systems and under conditions of low grade metamorphism, felsic volcanic rocks experience a similar redistribution of elements to that exhibited by their mafic counterparts (e.g. Pearce et al., 1984; Sturchio et al., 1986). Si, Mg, K, Na and the low field strength elements (Rb, Ba and Sr) are particularly mobile and their concentration in altered rocks may not reflect magmatic abundances (Arth, 1979; Sturchio et al., 1986). In particular Na, Ca, Sr and Ba are associated with zeolites in altered samples, whereas Mg, K and Rb are associated with clays. Chloritization may result in removal of K and Rb, whereas sericitization reflects addition of these elements to the rock (e.g. Swinden, 1987). Samples of silicic rocks were collected from outcrops which did not show strong hydrothermal alteration. Further petrographic identification of alteration in specimens (quartz veining, sericitization, chloritization, etc.) was used to screen out any strongly altered samples.

4.3 Nomenclature Of Volcanic Rocks

There are a number of considerations that bear on the nomenclature or name given to a volcanic rock based on its geochemical signature. For example, some of the criteria that need to be established are: lithology (e.g., basalt, rhyolite), degree of fractionation (e.g. primitive, parental or highly fractionated); magma series (e.g., calc-alkalic, tholeiitic), tectonic affinity (e.g. arc, non-arc, transitional); and the equivalent arc rock series based on K-content (through the use of immobile elements). Before presenting and discussing the geochemistry of rocks in the western Notre Dame Bay, the concerns regarding nomenclature and the approach taken in this study are briefly reviewed.

4.3.1 LITHOLOGY

One geochemical convention for subdivision or naming volcanic rocks involves the use of weight percent SiO_2 , for example: basalt <52% SiO_2 , low silica andesite - 52-56% SiO_2 ; high silica andesite - 56-62% SiO_2 ; dacite - 62- 66%, rhyolite >66% SiO_2 (based on volatile-free recalculated analyses) (e.g. Winchester and Floyd, 1977, Gill, 1981, LeMaitre, 1989). This method is not as useful or as preferred as the total alkalis versus silica method (LeMaitre, 1989); however, the alkali elements are particularly susceptible to alteration effects. Abundant evidence also suggests silica mobility during alteration, resulting in either addition or subtraction of SiO_2 , and this mobility of SiO_2 poses a problem in applying the simple silica-based nomenclature. However, a cross check based on immobile incompatible element ratios can be applied and guidelines on the reliability of using silica as first-order tool in naming the rocks established. This approach has proven useful in other geochemical studies in Dunnage Zone rocks (e.g. Jenner et al., 1991).

A set of the samples from the western Notre Dame Bay area, consisting of non-fragmental, non-quartz phyric and apparently mafic rocks is plotted on the Nb/Y-Zr/TiO₂ and Zr/TiO₂-SiO₂ diagrams of Winchester and Floyd (1977) (Fig. 4.4). On the first of these diagrams (Fig. 4.4A) the majority of samples form a cluster within the basalt /andesite field. On the second diagram (Fig. 4.4B), the data form a vertical trend within a relatively narrow range of Zr/TiO₂ ratios, and with the majority of samples still falling into the basalt and andesite fields. However, several samples plot within the

rhyodacite/dacite field and 3 samples (2 inverted and 1 upright filled triangles) plot well in the upper part of the andesite field. These results indicate that while silica redistribution may have taken place, only in a few samples has there been sufficient addition of silica to cause the rock type to be misclassified.

Felsic rocks plotted on these diagrams are shown in (Fig. 4.5). There are two major types of felsic rocks in the western Notre Dame Bay area in terms of their silica content: dacite/rhyodacite with silica in range 65-73% and rhyolite with silica in the range 75-79% (Fig. 4.5B). The low silica type represents mostly felsic rocks of the Cutwell Group whereas, the high silica type comprises chiefly samples from the Catchers Pond section of the Western Arm Group. On the Nb/Y-Zr/TiO₂ diagram (Winchester and Floyd, 1977) the two groups overlap and fall predominantly in the rhyodacite/dacite field, implying addition of SiO₂ to at least some felsic rocks from the Catchers Pond section.

In this study, the division between mafic and felsic volcanic rocks was made at approximately 63-65 weight % SiO₂ and reflects a small but apparent SiO₂ "gap" between high-silica andesites and spatially associated - dacites in the western Notre Dame Bay area. This gap corresponds to a silica value adopted by Winchester and Floyd (1977) as the boundary between the andesite and rhyodacite/dacite fields (Figs. 4.4 and 4.5). In general, it appears that the silica values approximate the original SiO₂ concentrations, and provide a good first approximation to the name of the rock. Thus, the silica-based conventional nomenclature has been used in this study, although it has been corrected where necessary, by the one based upon immobile incompatible element ratios.

4.3.2 FRACTIONATION

The term "fractionation" is applied to the process by which various derivative lavas evolve from a parental magma (e.g. Cox et al., 1979, Best, 1982). Synonymous with the term "fractionation", and often used by petrologists, is the term "differentiation". There are a number of different mechanisms by which the parental magma can fractionate, including crystal-liquid fractionation processes (fractional crystallization and partial melting) which dominate the evolution of igneous rocks, progressive contamination and

assimilation of country rock, and mixing of magmas. There is a need to arrange geochemical data from volcanic rocks in an order, which will reflect chemical evolution from the potentially "parental" compositions towards more evolved "daughter" compositions. To do so, one needs to use some sort of indicator(s) of that chemical evolution: these are called fractionation indices. Authors working with fresh, unaltered rocks commonly use SiO_2 or MgO as indices. Both of those indices have their drawbacks, as SiO_2 is not particularly sensitive in the early stages of crystallization, and it is affected by alteration and metamorphism; whereas, the MgO index is not sensitive to the crystallization of plagioclase, and it may be affected by alteration (Cox et al., 1979). More reliable and useful are indices based upon various combinations of iron and magnesium ratios (e.g. Miyashiro, 1974), such as Mg\# (molecular proportion $100 \text{MgO}/[\text{MgO}+\text{FeO}^*]$) and the FeO^*/MgO ratio (FeO^* being total iron), although, these also may fail when crystallization of ferromagnesian phases is accompanied by extensive magnetite precipitation. Despite those limitations, both the Mg\# and FeO^*/MgO are commonly used as fractionation indices in ancient rocks and they are used for this purpose in this thesis.

4.3.3 MAGMA SERIES

Magma series (also known as associations or trends, e.g. McBirney, 1984) were originally defined on the basis of changes in differentiation trends within rock suites from single centers and spatially associated volcanoes (e.g. Kuno, 1960; Miyashiro, 1974). However, as Miyashiro (1974), Gill (1981), and Takahashi (1986) have pointed out, during the history of a single volcano different parental magmas may coexist, and impede attempts to identify distinct series. Rocks from a given igneous center may include rocks tapping various sources and represent more than one series, these can be referred to as a suite (e.g. McBirney, 1984). It should be noted, that there is no indication, other than close spatial association, that lavas in the western Notre Dame Bay area defining any particular geochemical trend were actually erupted from the same volcanic center and/or are co-magmatic.

Three distinct arc magma series - tholeiitic (TII), calc-alkalic (CA) and alkalic are recognized (e.g. Kuno, 1960; MacDonald and Katsura, 1964; Irvine and Barager, 1971,

Miyashiro, 1974, 1978), and the concept of these series or trends is very important for present models of arc volcanism. Their recognition potentially has important paleotectonic implications, for example, some workers have documented a systematic positive correlation between the ratio of CA/TH volcanism and crustal thickness of the arc (e.g. Miyashiro, 1974, Coulon and Thorpe, 1981; Takahashi, 1986; Plank and Langmuir, 1988; Miller et al., 1992).

4.3.3.1 Alkalic And Non-Alkalic Series

The first step in assigning volcanic rocks to a magma series is to determine whether they are alkalic or non-alkalic and, if non-alkalic, to further distinguish between tholeiitic and the calc-alkalic series. In fresh rocks, the distinction between alkalic and non-alkalic series is relatively straightforward, based upon alkali contents and silica versus alkali ratios (e.g. MacDonald and Katsura, 1964; Irvine and Barager, 1971; Middlemost, 1975; LeMaitre, 1989). A different approach and nomenclature, proposed with respect to silica-undersaturated lavas by Green (1969) is based upon the presence of normative nepheline and hypersthene. Neither of the above methods is appropriate in altered rocks because of the probability of alkali element and silica mobility.

In order to differentiate between alkalic and sub-alkalic series in altered rocks, Floyd and Winchester (1976, 1977) devised several diagrams that use the HFSE, P_2O_5 , and SiO_2 contents (Zr/P_2O_5 -Nb/Y, Zr/P_2O_5 - TiO_2 , Nb/Y-Zr/ TiO_2 and Zr/TiO_2 - SiO_2). However, with the exception of Y, the HFSE elements employed by Floyd and Winchester (1976, 1977) are precisely those which in subduction-related volcanic rocks, are considered to be depleted relative to oceanic basalts. This raises the possibility of misidentification of alkalic versus non-alkalic series using the HFSE, and indeed these diagrams fail to reveal alkalic affinities of at least some alkalic volcanic suites erupted in subduction related environments including Grenada (Thirlwall and Graham, 1984), rifted arcs in the Marianas (Bloomer et al., 1989; Lin et al., 1989) and Fiji (Gill and Whelan, 1989) and a continent-continent collision zone in Eastern Anatolia (Pearce et al., 1990). Only part of the suite from Grenada exhibits an alkalic affinity, the greater part of the volcanic suite from Anatolia plots as non-alkalic, and shoshonitic basalts from Fiji and alkalic basalts from Grenada plot as non-alkalic on all

four diagrams. Data from the Marianas shoshonites (Bloomer et al., 1989; Lin et al., 1989), which lack Nb data, plot as non-alkalic on both (Zr/P_2O_5 - TiO_2 and Zr/TiO_2 - SiO_2) diagrams. Therefore, it is possible that the "alkalic" character of ancient subduction related volcanic suites investigated here may be misidentified using these diagrams

4.3.3.2 Tholeiitic (TH) And Calc-Alkalic (CA) Series

Further division of sub(non)-alkalic magma series into tholeiitic and calc-alkalic series, for rocks from present day settings, is customarily made on the AFM ($A=Na_2O_3+K_2O$; $F=FeO+Fe_2O_3$; $M=MgO$) diagram of Irvine and Barager (1971), and on the $FeO^*/MgO-SiO_2$ diagram of Miyashiro (1974). Grove and Baker (1984) used normative olivine-clinopyroxene-quartz and olivine-plagioclase-quartz projections to illustrate differences between TH and CA trends. Clearly, alkali element and silica mobility make these approaches inappropriate for altered volcanic rocks. However, CA and TH series can be identified using immobile elements. Miyashiro (1974) and Miyashiro and Shido (1975) have shown that in typical TH series volcanic rocks, the FeO^* , TiO_2 and V contents increase and then decrease with advancing fractional crystallization; whereas, in typical CA series, the FeO^* , TiO_2 and V contents decrease continuously. Based on this observation, two diagrams - the TiO_2 - and FeO^*-FeO^*/MgO (Miyashiro, 1974; Miyashiro and Shido, 1975) - are used to define TH and CA suites within rocks of the western Notre Dame Bay area. While these diagrams provide a useful guide to identifying TH and CA suites in the western Notre Dame Bay area, they are not in themselves necessarily definitive. There are a range of processes put forward in the literature to explain the origin of TH and CA rocks, and identification of the series is hampered by ubiquitous transitional rocks. The following brief discussion highlights the present uncertainty in the origin of these two different suites. A wide range of processes has been proposed to explain the origin, evolution and differences between the tholeiitic and calc-alkalic series (Kuno, 1960; Masuda and Aoki, 1979; Gill, 1981; Kay et al., 1982; Myers et al., 1985; Miller et al., 1992). Authors of several recent studies of volcanic rocks and mafic/ultramafic inclusions from the Aleutian and Lesser Antilles island arcs argued on petrochemical grounds, that tholeiitic and calc-alkalic trends are the result of low-pressure versus high-pressure

crystal fractionation and mixing (e.g. Cawthorn et al., 1973; Arculus and Wills, 1980; Perfit and Gust, 1981; Conrad and Kay, 1984; Nye and Reid, 1986). Others (e.g. Plank and Langmuir, 1988, Miller et al., 1992), suggest that low pressure crystal fractionation and mixing trends are superimposed upon fundamental differences in the major element chemistry established by different melting processes in the mantle, which are responsible for the generation of the tholeiitic and calc-alkalic parents.

The significance of amphibole fractionation in the development of the calc-alkalic trend has been argued over the years by many petrologists (e.g. Cawthorn and O'Hara, 1976; Anderson, 1980; Green, 1982; Foden and Green, 1992). Field and geochemical data were presented emphasizing importance of hornblende in the evolution of calc-alkalic magmas in the Aleutian arc (Perfit et al., 1980b; Conrad and Kay, 1984; Kay and Kay, 1985; Romick et al., 1992), the Lesser Antilles arc (e.g. Cawthorn et al. 1973; Arculus and Wills 1980), the Surda arc (e.g. Foden, 1983), and volcanic rocks from other arcs (e.g. Grove and Donnelly-Nolan, 1986).

Grove and Baker (1984) proposed that the development of contrasting tholeiitic and calc-alkalic trends is controlled by the proportions of olivine, plagioclase and pyroxene that crystallize from the basaltic parental melt. In the case of the calc-alkalic trend, this mineral assemblage begins the differentiation history and it is followed by further crystallization of amphibole, as a result of reaction of olivine, plagioclase and augite with the liquid (Helz, 1973; Grove and Donnelly-Nolan, 1986). Grove and Baker (1984) noted that more evolved tholeiites and transitional calc-alkalic magmas may both be derived from a tholeiitic parent, and recognized that although pressure controls the proportions of fractionating olivine, clinopyroxene and pigeonite, water is the factor which most influences phase chemistry.

Experimental and theoretical investigations by P.B. Kelemen and co-workers (Kelemen, 1990; Kelemen et al., 1990a, b) suggest that interaction between strongly depleted peridotite and magnesian olivine tholeiite produces liquids which possess the major and trace-element characteristics of the calc-alkalic trend. Field evidence for such reaction between hot basaltic magma and ultramafic/mafic rocks at the

mantle/crust boundary has been presented by several workers (Conrad and Kay, 1984, Takahashi, 1986).

4.3.3.3 Boninite Series And Other High-Mg Andesites

A distinct, non-alkalic magma type, termed boninitic, has been recognized in subduction-related environments (e.g. Cameron et al., 1979; Jenner, 1981; Tatsumi and Ishizaka, 1981; Hickey and Frey, 1982; Bloomer and Hawkins, 1987; Beccaluva and Serri, 1988; Falloon and Crawford, 1991), as well as, in ancient ophiolitic complexes (e.g. Coish et al., 1982; Swinden et al., 1989; Pedersen and Hertogen, 1990; Brown and Jenner, 1991; Kean et al., 1995). Boninites are characterized by high (andesitic) SiO₂ and MgO contents, strong depletion of Ti and other HFSE, enrichment of Zr and Hf relative to the REE and other HFSE, overall depletion in the MREE and HREE, and a LREE enrichment that gives rise to a concave-upward REE pattern. These characteristics are interpreted to be the result of melting of a refractory mantle source upon which there was superimposed a metasomatic enrichment event (Nesbitt and Sun, 1978; Jenner, 1981, Hickey and Frey, 1982). It is suggested that the concave-upward REE pattern results from an amphibole imprint on the component that metasomatizes the mantle source (Pearce et al., 1992).

Less common than boninite is another type of high-Mg andesite, referred to locally as sanukitoids (Tatsumi and Ishizaka, 1981) or bajaites (or bajaite series) (Saunders et al., 1987). These andesites are characterized by high MgO, Cr, Ni, and have abundances of HFSE, LFSE and REE that are more typical of island arc andesites than boninites. They appear to represent hydrous partial melting of relatively undepleted mantle sources and are found in island arc settings that are characterized by an input of hot asthenospheric material associated with: subduction of a spreading ridge (Saunders et al., 1987; Tatsumi and Maruyama, 1989) and/or formation of a slab-window (Rogers and Saunders, 1989; Hole et al., 1991); active continental rifting (Lühr et al., 1989), and possibly with the initiation of normal back arc spreading (Tatsumi and Maruyama, 1989).

4.3.3.4 K-Suites

A different method of dividing mafic volcanic rocks was introduced by Gill (1981), who defined three suites within volcanic rocks on the basis of the contents of K_2O and the K-type elements (Rb, Cs, Ba and Sr), and named them low-K, medium-K and high-K suites. The K-suites are known to include members of both tholeiitic and calc-alkalic series; but it has been shown that the low-K series is composed primarily of tholeiites, and the medium-K series more often consists of calc-alkalic rocks (e.g. Gill, 1981; Ewart, 1982; Wilson, 1989; Hess, 1989).

As K_2O and related trace elements are highly mobile in ancient volcanic rocks, the distinction between the different K-suites in these rocks can be made using the slope of normalized REE patterns (Gill, 1981). In general, rocks of low-K suites have negative or flat patterns and the lowest REE concentrations among any volcanic rocks. Medium-K suites have moderately positive REE patterns, and high-K suites have steep positive patterns. Light REE contents and the slope of their patterns increase steadily from low to high-K suites, whereas heavy REE patterns remain constant or change little. Swinden (1987) quantified this division based upon $(La/Yb)_N$ (chondrite normalized) values and proposed that the $(La/Yb)_N$ of low-K suites is <1.5 ; medium-K suites is 1 to 5 and of high-K suites is >5 . A similar but less specific breakdown was proposed by Coulon and Thorpe (1981), who combined several characteristics of island-arc tholeiitic and calc-alkalic series and showed that the La/Yb ratio = 3.5 ($(La/Yb)_N=2.5$) forms in general a divide between these two associations.

4.3.4 ARC VERSUS NON-ARC GEOCHEMICAL SIGNATURES

Of primary concern in this study is to ascertain if the igneous rocks sampled have an arc or non-arc geochemical signature. Geochemical signature is defined as combinations of element concentrations and/or ratios, which are characteristic of the magmas. In general, geochemists use incompatible trace element contents, since these more accurately reflect the source material and/or the processes that affected that source material during generation of the magma. Incompatible trace elements are also less likely to be fractionated from each other during magma evolution. However, the compatibility of an element can be affected by the mineral phases crystallizing during fractionation or

by residual minerals in the source, and due care must be given to this possibility. Geochemists generally illustrate geochemical signatures on multielement diagrams, either by defining empirical fields based on modern day examples, or by plotting them normalized relative to a hypothetical source composition or reference rock type. Such diagrams have allowed geochemists to identify geochemical signatures peculiar to or characteristic of certain plate tectonic settings. The origin of these signatures is not always clearly understood.

4.3.4.1 Normalized Multielement Plots

The trace element and REE data are commonly presented in a graphical form normalized to element abundances in chondrites or the "primitive mantle" (e.g. Wood et al., 1979; Sun et al., 1979; Thompson et al., 1983; Briquet et al., 1984; Sun and McDonough, 1989). In such diagrams the REE elements are commonly presented in order of increasing ionic radii. In diagrams that combine the REE and other trace element groups, the element order reflects incompatibility, but the detailed arrangement of elements in such diagrams can vary somewhat depending on how the behavior of an element has been predicted. For mafic to intermediate igneous rocks, the arrangement reflects decreasing incompatibility (or increasing value of bulk D) of the elements from left to right in a spinel lherzolite peridotite mineral assemblage. Order has also been based on the depletion pattern in N-MORB and the systematics of concentration ratios in E-MORB and OIB (e.g. Sun, 1980; Thompson et al., 1983, 1984; Sun and McDonough, 1989). Since the Earth is not chondritic with respect to some of the elements used on these diagrams (i.e. Rb, U, Pb), model primitive mantle (PM) abundances are the preferred normalizing values (Hofmann, 1988; Sun and McDonough, 1989). Primitive mantle is conceptually a hypothetical bulk silicate Earth, before any differentiation occurs.

As an alternative to normalizing relative to primitive mantle, it is common to normalize to an average N-MORB composition. The ordering of elements on N-MORB normalized plots is generally the same as for primitive mantle-normalized plots, although authors are freer to reorganize the elements in order to illustrate some process (e.g. Pearce 1983, McCulloch and Gamble, 1991).

It is commonly accepted by petrologists that several sources contribute to arc magmas. The magmas are most likely generated in the mantle wedge above the subduction zone, thought to be composed of refractory or depleted MORB mantle, which is variably enriched by fluids originating from subducted altered oceanic crust and sediment. On their ascent, the magmas may be contaminated by a silicic component derived from thickened arc or continental crust (Pearce, 1983; Hole et al., 1984; Tatsumi et al., 1986; Arculus and Powell, 1986; Davidson et al., 1987; Ellam and Hawkesworth 1988; Hildreth and Moorbath, 1988). Some authors also propose, mostly on the basis of isotopic data, that enriched E-MORB and OIB sources also contribute to arc magmas (e.g. Stern, 1981; Morris and Hart, 1983, Lin et al., 1990; Kostopoulos and Murton, 1993), although the basis of such proposals is questioned (Perfit and Kay, 1986)

Many primitive mantle and N-MORB normalized multielement plots include elements that are easily affected by alteration (i.e. Rb, Cs, Ba, Pb, K, Sr). In this study, a restricted set of elements (immobile) is used to construct the normalized multielement plots, and Th is the only LFSE included.

4.3.4.2. Tectonomagmatic Discrimination Diagrams

Geochemical studies of rocks formed in known/recent tectonic environments has led to the recognition of geochemical characteristics that are typical, but not necessarily unique, for rocks formed in these environments. Some of these signatures or characteristics have been illustrated using selected major, minor and trace elements ratios, leading to the creation of a number of tectonomagmatic discrimination diagrams that are used to interpret the tectonic setting of volcanic rocks. Some of these diagrams employ elements that are mobile during alteration and metamorphic processes, and therefore can not be used for altered ancient rocks. Even diagrams involving immobile elements should not be used indiscriminately, since their ability to distinguish different environments may be limited by the fact that they do not compensate for complex processes which modify magmas (Duncan, 1987; Arculus, 1987; Wang and Glover, 1992).

Despite these limitations, tectonomagmatic discrimination diagrams have been found to be helpful in a preliminary assessment of tectonic setting of early Paleozoic rocks in the Appalachians and Caledonides (e.g. Jenner and Fryer, 1980, Grenne, 1987, Swinden, 1987; Dostal, 1989; Leat and Thorpe, 1989; Paktunc, 1990; Dunning et al., 1991; Jenner et al., 1991). In particular two plots, the Ti-V (Shervais, 1982) and the Zr-Ti (Pearce and Cann 1973) have been found to be effective preliminary discriminants between arc and non-arc settings. The Zr/Y-Zr plot (Pearce and Norry, 1979, Pearce, 1983) can be applied to mafic volcanic rocks already identified as having non-arc or volcanic arc character, to distinguish between MORB and WPB, and between oceanic and continental arcs, respectively. The $\text{MnO} \cdot 10\text{-I}_2\text{O}_5 / 10\text{-TiO}_2$ diagram of Mullen (1983), the $\text{Zr}/4\text{-Nb} \cdot 2\text{-Y}$ diagram of Meshede (1986), and the $\text{Zr-Ti}/100\text{-Y} \cdot 3$ of Pearce and Cann (1973) may also be employed to further strengthen the divisions. Most of these tectonic discriminants have been used in evaluating the data for the western Notre Dame Bay area (see Tables 4.1 to 4.6). However, the results are illustrated only on the Ti-Zr and Ti-V plots, which were found to be the simplest and most effective diagrams.

There is some degree of agreement amongst various authors that basalts erupted from mid-ocean spreading centers may be distinguished from basalts formed in an arc setting by their Nb/Th ratio. Such separation can be accomplished using the Th-Hf-Ta diagram of Wood (1980) and the Th/Yb versus Ta/Yb diagram of Pearce (1982) and these are used to further determine different environments of eruption of western Notre Dame Bay area volcanic rocks. Zr/36 and Nb/17.5 values are used in Wood's (1980) diagram instead of Hf and Ta, respectively, and Nb/17.5 is used instead of Ta in Pearce's diagram (36 and 17.5 represent chondritic/primitive mantle values of Zr/Hf and Nb/Ta ratios from Sun and McDonough, 1989). The primitive mantle Nb/Th ratio has recently proved to be a sufficient primary discriminant of rocks erupted in ancient arc and non-arc environments of the Newfoundland Appalachians (e.g. Swinden et al., 1989, 1990; Jenner et al., 1991). All of the above diagrams are applicable strictly to mafic volcanic rocks, but the Th- Zr/36- Nb/17.5 ternary diagram of Wood (1980) is used, as well, to determine the volcanic setting of the felsic rocks.

4.3.4.3 The Nb Anomaly

One of the most notable geochemical features of volcanic rocks erupted in an arc setting is their characteristically low abundance of Nb(Ta) relative to Th and the LREE (e.g. Wood et al, 1979; Saunders et al., 1980a; Gill, 1981; Pearce, 1983; Briquet et al., 1984; Arculus and Powell, 1986). This feature of arc lavas is reflected on normalized multielement plots in the form of a negative Nb(Ta) anomaly with respect to Th and La and it is referred to as an "arc" or "supra-subduction zone" signature. Since it was first identified, the presence of this geochemical signature has been widely recognized and confirmed in rocks from various modern arcs, although its origin is a subject of continuing discussion (e.g. Pearce, 1983; Arculus, 1987; McCulloch and Gamble, 1990; Saunders et al., 1991). It is important to realize, however, that the Nb anomaly is not unique to magmas generated in the arc regions. Rocks with this and other characteristics of arc lavas (e.g. overall depletion in HFSE and enrichment in LFSE and LREE) are found commonly within continental flood basalts, where the signatures likely result from a contamination of asthenospheric melts by upper continental crust (e.g. Lightfoot and Hawkesworth, 1988; Saunders et al., 1992). Similarly, some lavas erupted in collision zones and derived from lithosphere carrying the subduction signature from pre-collision subduction events may also display characteristics of arc rocks (Pearce et al., 1990).

A number of studies have noted the resemblance between basalts formed in back-arc basins and mid-ocean spreading ridges, though emphasizing at the same time numerous differences in relative HFSE depletion, LFSE and LREE enrichment (e.g. Gill, 1976; Saunders and Tarney, 1979 and 1984; Hawkins and Melchior, 1985; Sinton and Fryer, 1987). More recent geochemical data from back-arc spreading ridges of Mariana Trough and Lau Basin have shown a strong Nb underabundance in erupted rocks and various LREE enrichment, which produced normalized multielement patterns similar to those of arc rocks (e.g. Jenner et al., 1987; Hawkins et al., 1990; Stern et al., 1990; Vallier et al., 1991). Addition of a minor, but significant, "arc-source" derived component to the back-arc basin mantle source is confirmed by the isotopic

characteristics of samples from the Lau Basin and Mariana Trough spreading ridges (Jenner et al., 1987; Hawkins et al., 1990).

The presence of the "arc signature" in rocks erupted both in arc and back-arc settings emphasizes the need for high quality Th, Nb(Ta) and REE data in analyzing ancient volcanic rocks. It is particularly important in evaluation of rocks formed in the ancient back-arc environment, some of which if structurally displaced from rocks displaying arc affinities, would be classified as non-arc depleted MORB, on the basis of V, Ti, Zr and Y ratios (Jenner et al., 1991; Vallier et al., 1991).

4.3.5 SUMMARY OF SOURCES AND PROCESSES CONTRIBUTING TO ARC

LAVAS

Ultimately, the origin of the arc geochemical signature illustrated by normalized multielement plots and tectonic discrimination diagrams reflects the variety of processes occurring in the supra-subduction zone environment. Although processes involved in the generation of arc magmas are still very controversial, it is now widely accepted that there are three potential source regions which contribute to the arc magmas: 1) variably depleted to variably enriched (?) MORB-like mantle located in the wedge above subducting slab; 2) subducted oceanic crust (altered MORB) with or without sediment, which provides material to the mantle wedge via mass transfer involving fluid phases and/or melts; and 3) arc or continental crust (e.g. Pearce, 1983, Arculus and Powell, 1986; Ewart and Hawkesworth, 1987; Crawford et al., 1987; Ellam and Hawkesworth, 1988). The mantle wedge is envisaged to be the major source of HFSE in subduction related magmas, whereas subducted oceanic and continental crust (as sediment) are responsible for a large proportion of LFSE. The sediment component is characterized by moderately high LFSE/HFSE ratios, and slightly elevated Zr/Y with respect to MORB, whereas the slab derived fluid phase is characterized by high LFSE/LREE and high LFSE/HFSE ratios. The latter component is responsible for LFSE enrichment with respect to the HFSE and LREE in subduction related lavas. Ellam and Hawkesworth (1988) stressed that although decreasing degree of melting can fractionate LREE with respect to higher degree melts, it can not produce relative HFSE depletion

Some authors (e.g. Morris and Hart, 1983; Gill, 1984) proposed that the mantle wedge has OIB characteristics, and that geochemical input from the subducted oceanic crust and overlying sediment may be minimal. To account for the depletion in HFSE with respect to LFSE and LREE typically found in arc lavas, they arbitrarily suggested the presence of residual Ti-rich phase(s). However, Green and Pearson (1986) and Ryerson and Watson (1987) have shown that stabilizing a Ti-rich phase in the source region of arc magmas is unlikely.

Emphasizing the importance of the sediment component, it had been suggested that the presence of negative Ce anomalies in some volcanic arc rocks must be inherited from pelagic sediment added to regions of magma generation (Hole et al., 1984). This idea was challenged by Ben Othman et al. (1989), who believed that this property of arc lavas instead reflects fractionation of LFSE from REE as a result of slab dehydration and metasomatism. Sediment subduction and involvement in the generation of arc magmas has been positively demonstrated by beryllium isotopes and B-Be systematics in volcanic arc rocks (e.g. Brown et al., 1982; Tera et al., 1986; Morris et al., 1990).

Experimental studies (Tatsumi et al. 1986) supported earlier observations that components added from the subducted slab into the mantle wedge do not affect the abundances and ratios of HFSE in the wedge. Thus, it has been proposed that HFSE ratios reflect the composition of the unmetasomatized (MORB-like) mantle wedge (Pearce, 1983; Ellam et al., 1988; Edwards et al., 1991) and plots utilizing these elements are used to evaluate the sources, other than the mantle wedge, that have contributed elements to arc magmas.

An important question is the depth at which melting takes place in the mantle beneath the arc. The REE may give some clues with respect to the depth of melting, since the distribution of these elements between melt and solid is strongly controlled by phases which are affected by pressure. Initial (low degree) melts derived by partial melting of garnet peridotite are characterized by strong enrichment in LREE and equally pronounced depletion of the HREE (Shimizu and Arculus, 1975; Hanson, 1980). Increasing degree of partial melting of garnet lherzolite tends to flatten REE patterns making them difficult to distinguish from spinel lherzolite melts of similar degree (e.g.

Lin et al., 1989). Yet, a low degree partial melt of spinel peridotite, although similarly enriched in LREE, can be distinguished from a partial melt of garnet lherzolite by its flatter HREE pattern (Lin et al., 1989). Low pressure melts of basaltic source materials leaving amphibolite residue are characterized by strongly depleted MREE and concave upwards REE patterns (Gromet and Silver, 1987).

4.4 Subdivision And Nomenclature Of Notre Dame Bay Volcanic Rocks

A representative suite of mafic and felsic volcanic and subvolcanic rocks from the western Notre Dame Bay area were analyzed for major and trace elements. On the basis of initial results a smaller set of samples was chosen for further analysis of selected HFSE, Th and REE.

Subdivision of rocks from the study area was undertaken in several stages with initial emphasis on paleotectonic subdivisions, and then focusing on specific incompatible element ratios and normalized multielement patterns. As other workers have found when working with ancient altered rocks, the use of major and trace element data may provide only limited information on the tectonic environment in which rocks formed. Better and more reliable information was found using a combination of REE and HFSE data. Therefore, emphasis in this presentation of geochemical data is on samples for which a whole set of information is available. The overall approach to interpreting the data is schematically outlined in Figure 4.2; a legend of symbols used in subsequent figures is presented in Figure 4.3.

4.4.1 PRELIMINARY PALEOTECTONIC DIVISIONS

The complex geochemistry of rocks in the western Notre Dame Bay area is reflected in the wide range in abundances of Ti, Zr and V and in ratios of immobile elements illustrated by the Ti-V and Zr-Ti diagrams (Figs 4.6, 4.7). These diagrams indicate that the rocks were erupted in at least two distinct tectonic settings. On the Ti-V diagram (Fig. 4.6), one set of samples (solid squares and diamonds) has a relatively broad range of Ti and V abundances and Ti/V ratios between 20-50, similar to that expected in MORB. The same set of samples plots within the OIB field and beyond (towards OIB compositions) on the Zr-Ti diagram (Fig. 4.7), which supports their

non-arc oceanic affinity. In contrast to this MORB type, samples marked by circles and triangles (both open and filled), as well as open diamonds and asterix's, plot mainly in the arc field on the Ti-V plot (Fig. 4.6). On the Zr-Ti diagram this second set of samples plots as calc-alkalic basalts (CAB) and low-K tholeiites (LKT), with some samples (open circles) extending into the OFB field. These geochemical relationships are consistent with, although not definitive of, an arc tectonic setting.

To test the validity of dividing the Notre Dame Bay rocks into arc and non-arc types based on Ti-V-Zr, the next step was to determine if samples in these sets have developed the more definitive arc geochemical signature, i.e. the Nb depletion with respect to Th and La. On the Th-Zr-Nb diagram of Wood (1980) (Fig. 4.8), samples marked as triangles and circles that already revealed an island arc affinity on the basis of the Ti-V and Ti-Zr variations, demonstrate a strong enrichment in Th relative to Nb, and plot within the CA and TH arc field, respectively. Samples marked as squares display relatively high Nb/Th ratios and plot within fields of MORB and OIB. Compared to the non-arc oceanic array, represented by typical N-, E-MORB and OIB, nearly all of the western Notre Dame Bay area samples demonstrating OFB affinity are shifted slightly in the direction of the arc field. The samples also plot in the non-arc field on the Th/Nb-Nb/Yb diagram of Pearce (1983) (Fig. 4.9). The division line, $Nb/Th=8.5$, in this diagram coincides with the chondritic and primitive mantle Nb/Th value (Sun and McDonough, 1989) and works well as a discriminant between arc and non-arc lavas. This property of the primitive mantle Nb/Th ratio was originally recognized by Swinden et al. (1989) and Jenner et al. (1991), who used the primitive mantle of Hofmann (1988; Nb/Th = 7.4) as a reference line dividing arc and non arc rocks on their Y-Nb/Th plot.

Samples, marked as filled "diamonds", plot in the OFB field on the Ti-V and Ti-Zr diagrams, but have lower Nb/Th ratios than ocean floor volcanics and plot outside the OFB field and within the island arc field on the Th-Zr-Nb and Nb/Yb-Th/Yb diagram (Fig. 4.8 and 4.9). This type appears to possess geochemical signatures which are transitional between arc and non-arc. This is consistent with the evidence noted above that most of the non-arc rocks in the western Notre Dame Bay area are slightly shifted away from the usual OFB field, and suggests the potential for a continuum in mixing

relationships. This, in any case, justifies utmost caution in assigning tectonic settings for these non-arc rocks.

To illustrate these variations in geochemical signatures an additional plot involving Nb/Th and (La/Yb)_N was devised (Fig. 4.10). The rationale for using (La/Yb)_N was that this ratio is a good indicator of relative LREE enrichment and indicates affinity with different K-suites. The Nb/Th ratio on this plot (Fig. 4.10) separates the rocks into three sets, one with the ratio >8.5, a second with the ratio between 8.5 and 1, and a third with the ratio <1. The explanation of the division line, Nb/Th = 8.5, was given above in the description of the Nb/Yb-Th/Yb diagram of Pearce (1983). Using the (La/Yb)_N - Nb/Th diagram, the western Notre Dame Bay area volcanic rocks can be divided into three major types displaying diverse tectonic affinities (Fig. 4.10).

- **NA-type:** non-arc volcanic rocks that include samples identified as having oceanic affinity on most of tectonic discrimination diagrams,
- **TR-type:** rocks transitional in geochemical characteristics between rocks erupted in non-arc and arc settings;
- **A-type:** arc volcanic rocks encompassing samples of clearly defined arc affinity. Within this type, a number of sub-groups of rocks have been recognized based on combinations of element ratios. In particular, the (La/Yb)_N has been used to divide the samples into low-, medium- and high-K equivalents

Average trace element ratios for each type are presented in Table 4.1 and 4.3, and paleotectonic affinities, as derived from tectonomagmatic discrimination diagrams, are summarized in Tables 4.2 and 4.4. A complete discussion of the divisions and rationale used can be found in the following detailed descriptions

4.4.2 NON-ARC (NA) AND TRANSITIONAL (TR) VOLCANIC ROCKS - MAJOR AND TRACE ELEMENTS

These types consist predominantly of basaltic lavas (~ 75%) (Fig. 4.4). The majority are characterized by Mg# between 57 and 63, and TiO₂ ranging from about 1.2 to 2.5%. Ti increases with increasing FeO*/MgO ratio suggesting a tholeiitic character (Miyashiro, 1974; Miyashiro and Shido, 1975). Samples defined as transitional have somewhat lower TiO₂ at given FeO*/MgO ratio than do non-arc samples

4.4.2.1 NA Type High Nb/Th Non-Arc Volcanic Rocks

The NA rocks are predominantly sub-alkalic (Fig. 4.4) and the elevated Zr/Y >3 of most NA samples suggests a within plate affinity. The Nb/Th and La/Nb ratio values (Table 4.1) are used here to divide the NA rocks into two major geochemical types of distinct magmatic affinity. Type NA-1 consists of samples which have Nb/Th and La/Nb ratios near those of the average E-type MORB. Type NA-2 differs from the former in having lower Nb/Th >8 and <13 and higher La/Nb ratios. The NA-2 type is further divided into four subtypes on the basis of the REE plots and incompatible element ratios (Table 4.1).

4.4.2.1.1 NA-1 type: E-MORB type tholeiites

Type NA-1 rocks are found in the Lower Basalt member of the Stag Formation. There are only four samples and these have Mg# between 45 and 60. Compared to rocks of the NA-2 type, NA-1 rocks have: higher Nb/Th; lower Zr/Nb, Zr/Y, Ti/Y and La/Nb. Sample Cl-19-24 shows an incompatible element pattern transitional between typical N-MORB and E-MORB (Table 4.1 and Fig. 4.11A). Incompatible element ratios and extended REE patterns of most NA-1 samples match closely the ratios and pattern of a "typical" E-MORB (Table 4.1 and Fig. 4.11B).

4.4.2.1.2 NA-2 type: T-MORB type tholeiites

This type includes samples from the Big Hill Basalt in the Western Arm, Pilley's Island and Triton Island sections of the Western Arm Group. Samples CP-01-08, CP-22-14 and CP-33-19 included in this geochemical type were collected in the Catchers Pond section of the Western Arm Group.

Type NA-2 rocks are divided into three subtypes. Incompatible element ratios in Table 4.1 allow closer comparison between lavas included in the NA-2 and basalts from non-subduction settings (Sun and McDonough, 1989). The ratios show an increase in the value of the Ti/V and La/Yb ratios and associated decrease in the Zr/Nb ratio between NA-2a and NA-2c subtypes (Table 4.1). The Ti/Y ratios of all samples in the type are higher than that of typical E-MORB, and the Zr/Y ratios of subtypes NA-2b through -2c are higher than

that of E-MORB. The La/Yb ratios of the type increase from near N-MORB in the NA-2a samples to higher than E-MORB in the NA-2c subtype.

The division into subtypes reflects a gradual increase in the degree of LREE and MREE enrichment indicated on the primitive mantle (PM) normalized extended REE patterns (Fig. 4.12). REE profiles of average N-MORB and E-MORB are plotted on these diagrams for comparison. The general trend is from patterns of NA-2a (Fig. 4.12A) rocks, that are subparallel to N-MORB, to patterns with positive slope in the NA-2c (Fig. 4.12C) subtype samples. NA-2a samples (Fig. 4.12A) display a range of REE abundances and patterns that overlap with average E-MORB, except for Ce, La, Nb and Th, which are lower and rather similar to N-MORB. NA-2b samples (Fig. 4.12B) have higher REE and trace element concentrations than E-MORB for most elements, but in particular Zr, Ti, Y and MREE.

One sample, CP-22-14, has not been matched with any of these subgroups. An extended REE diagram of the sample (Fig. 4.12D) reveals a basic similarity to average E-MORB between La and Yb, but a relative depletion in Nb and Th.

4.4.2.2 TR Type: Medium Nb/Th Transitional Tholeiites

This type consists predominantly of samples from the Big Hill Basalt and the Skeleton Pond Formation. One sample, CI-16-01, is a flow, which was collected in the area immediately south of the MacLean Fault (Halls Bay), apparently from within the section included in the Little Bay Basalt. The major geochemical characteristics of the TR-type rocks are an enrichment in Th and LREE relative to Nb and HREE when compared to the NA-type counterparts. This relationship is particularly obvious on the $(La/Yb)_N$ -Nb/Th plot (Fig. 4.10), on which at given $(La/Yb)_N$, rocks of the TR type have consistently lower Nb/Th values. This is also true with respect to samples defined as of arc affinity, which always have lower Nb/Th values than the TR-type samples at the same $(La/Yb)_N$ ratio. Consideration of the degree of Th and LREE enrichment allows further division of the TR-type rocks into two subtypes, and recognition of three samples that are not clearly affiliated with any of these subtypes.

Incompatible element ratios are not notably different from those of the NA samples (Table 4.1), with exception of Nb/Th, which is less than 8.5. Ti/V ratios are typical of N- and E-MORB, whereas Ti/Zr, Zr/Y and Ti/Y are intermediate between those of E-MORB and OIB. The LREE and MREE abundances are slightly higher in the TR-1a subtype than in the typical E-MORB (Fig. 4.13B), and are somewhat transitional towards that of OIB in the TR-1b subtype (Fig. 4.13C). In general, samples of the TR-1a and -1b subtypes display close similarity to rocks of non-arc affinity included in the NA-2b (Fig. 4.12B) and -2c subtypes, respectively (Fig. 4.12C).

Sample CI-16-01 is similar to, and plots near on most diagrams, the NA-2a subtype samples. It has an incompatible element pattern subparallel to N-MORB (Fig. 4.13A), but slightly depleted in Yb, La, and Nb, and enriched in Th. Two samples, CI-01-14 and CI-16-08a are clearly not a part of either subtype. Sample CI-01-14 has LREE abundances similar to OIB (Fig. 4.13D) but displays a distinct negative Nb anomaly. Sample CI-16-08a has a REE pattern very similar to CI-01-14, but characterized by lower concentrations of REE (particularly LREE and HREE), Nb and Th.

4.4.3 A-TYPE: VOLCANIC AND VOLCANICLASTIC ROCKS WITH ARC AFFINITIES

Samples with an arc affinity produce scattered trend(s) on all the bivariate diagrams involving the fractionation index FeO^*/MgO . Therefore, the arc suite was divided into types on the basis of trace element ratios (Table 4.3) and normalized multielement patterns. Volcanic and volcanoclastic rocks of arc affinity were grouped using the degree of Th and La enrichment with respect to Nb: first based on Nb/Th ratio >1 and La/Nb ratio <3 ; secondly, with Nb/Th ratio <1 and La/Nb ratio >7 . Additional subtypes were recognized using the (La/Yb)_N ratio as an indicator of original K content (see Fig. 4.10 and Table 4.3). Average trace element and REE ratios are presented in the Table 4.3, whilst paleotectonic affinities, as interpreted from tectonomagmatic discrimination diagrams, are summarized in Table 4.4.

4.4.3.1 Medium Nb/Th Arc Rocks

4.4.3.1.1 A-1 type: boninitic rocks

Type A-1 contains three samples collected from two outcrop areas of the Lushs Bight Group that are in structural contact with the Western Arm Group southwest of Western Arm and on the west coast of Pilley's Island. The fourth sample (CP-24-20) was taken from the Catchers Pond section of the Western Arm Group. All samples are characterized by very low incompatible element abundances and have concave-upward normalized REE patterns. Normalized plots reveal enriched Th with respect to La, and distinctively positive Zr with respect to Nd and Sm (Fig. 4.14). Three of these samples are closely related petrogenetically, and the fourth sample, CP-24-20, differs somewhat in having a less concave pattern and a positive Ti anomaly with respect to Gd and Dy. Data for CP-24-20 were not included in the average for the type (Table 4.3).

4.4.3.1.2 A-2 type: low-medium-K suites

The A-2 type of samples can be further subdivided on the basis of geochemical characteristics into five subtypes (Table 4.3). The division of type A-2 rocks into five subtypes reflects variations in the strength of the arc signature, a systematic increase in the slope of REE patterns and the degree of incompatible element enrichment as indicated on normalized multielement plots (Fig. 4.15). The general trend is from strongly LREE depleted patterns of A-2a rocks (Fig. 4.15A) to almost flat, N-MORB parallel patterns of the A-2c (Fig. 4.15C) and slightly positive LREE slope in patterns of the A-2d (Fig. 4.15D) and A-2e (Fig. 4.15E) subtypes. The A-2b extended REE patterns (Fig. 4.15B) are similar to and overlap with those of the previously recognized IAT (island arc tholeiites) type lavas of the Lushs Bight Group (Swinden et al., 1989; Jenner et al., 1991; Kean et al., 1995). On average, decreasing Mg#, increasing Zr/Y, Ti/Y, Ti/V, and a decrease in Ti/Zr accompany the change from A-2a to A-2e subtypes (Table 4.3). This reflects the presence of a relatively well defined linear trend formed within (La/Yb)_N-Nb/Th space by the A-2 type samples.

Samples assigned to subtypes A-2a and A-2b represent mafic flows of the Little Bay Basalt. Those of the A-2c geochemical subtype were collected within the Skeleton Pond Formation, and the Upper Basalt and the Breccia members of the Stag Formation. The A-2d subtype includes flows in the Skeleton Pond Formation in Western Arm and the Pillar's Island and Triton Island sections of the Western Arm Group. One sample in A-2d subtype, CP-24-10, was collected in the Catchers Pond section of the Western Arm Group. However the Catchers Pond section supplied all samples included in the A-2e subtype.

Most of the Type A-2 rocks are defined as low-K tholeiites, with the exception of the A-2e subtype, which on the basis of the $(La/Yb)_N$ ratio (≈ 2.3) is a medium-K suite, and the A-2e(t) and A-2f subtypes (see below). Two samples included in the A-2a subtype are strongly LREE depleted and plot as tholeiitic on the Th-Zr-Nb (Wood, 1980), Nb/Yb-Th/Yb (Pearce, 1983) and most other diagrams (Table 4.4). The A-2b and -2c subtypes are defined as tholeiitic arc rocks, although the Ti/Zr, Zr/Y, Ti/Y and La/Yb ratios of the A-2c subtype resemble closely those of the average N-MORB (Sun and McDonough, 1989) (see Table 4.3). The A-2d and A-2e subtypes, even though tholeiitic according to Miyashiro's and Mullen's classification, plot as transitional TH/CA and calc-alkalic, respectively, on the Th-Zr-Nb plot of Wood (1980) (Fig.4.8) and Nb/Yb-Th/Yb plot of Pearce (1983) (Fig.4.9). The A-2e subtype is highly heterogeneous in terms of incompatible element ratios, which reflects variable underabundance in Zr and Ti with respect to the REE's in some of the samples. For this reason, samples form a significant scatter on discrimination diagrams employing those elements.

A-2e(t) subtype: volcanoclastic rocks of arc affinity

The A-2e(t) type consists of four samples of pyroxene- and hornblende-phyric tuffs collected from within Western Arm Group. These were analyzed because of their mineralogic and textural similarity to, and the possibility of matching them with, the "lamprophyric" dykes that intrude lavas

of the Lushs Bight and Western Arm Groups. The tuffs are plotted on all diagrams using open triangles and show chemical characteristics similar to samples included in the A-2e subtype (e.g. Figs. 4.6, 4.7, 4.8). Their incompatible element ratios (Table 4.3) and multielement normalized patterns (Fig. 4.15F) also show marked similarity to those of the A-2e subtype (Table 4.3; Fig. 4.15E).

A-2f subtype: high-Mg, high-K, calc-alkalic rocks

This subtype contains three samples from the Western Arm Group: one (CI-11-11) is from a massive mafic flow (or sill) from the thin wedge of rocks assigned to the Welsh Cove Formation on Triton Island, and two are from clasts (bombs) in the Western Head Formation tuffs on Pilley's Island and Halls Bay Head. The A-2f subtype samples have a relatively high Mg# (62-52) and together with the A-2a and -2b are among the most primitive rocks in the A-2 type. (La/Yb)_N ratios range from 4.3 to 6.1 (av. 5.1; Table 4.3, Fig. 4.15G) and indicate that A-2f samples are medium- to high-K.

4.4.3.1.3 A-3 type: low-K tholeiites

Two pillowed flows from the Stag Formation Breccia Member form the A-3 type. Although, their (La/Yb)_N (=0.9) and Zr/Y (=2) ratios are within the range of the values of the A-2 type rocks, their Nb/Th (=0.7) and La/Nb (=7.1) ratios are very similar to those of the A-4 type. Their multielement patterns (Fig. 4.16) differ from those of the A-2 type samples (Fig. 4.15) in having a much stronger arc geochemical signature (high Th, low Nb). The two A-3 samples also display minor depletion in Zr relative to REE (Fig. 4.16). They are classified as low-K tholeiites on most discrimination diagrams.

4.4.3.1.4 A-4 type: low Nb/Th, LREE enriched rocks

This low Nb/Th type encompasses exclusively mafic volcanic rocks of the Cutwell Group. Rocks of type A-4 can be divided into two geochemical subtypes on the basis of their relative LREE enrichment as illustrated on normalized multielement plots (Fig. 4.17), and ratios of more incompatible to less incompatible elements (e.g. Zr/Y, Ti/Y, Ti/V; Table 4.3). The A-4a basalts

have a relatively high Mg# (60-53), Ni (19-92) and Cr (86-214) concentrations and are the most primitive rocks of the A-4 type samples. Volcanic rocks of the A-4 type are characterized by well developed negative Nb anomalies and LREE enrichment (Fig. 4.17). $(La/Yb)_N$ ratios range from 2.0 to 5.3 (Fig. 4.10) and indicate that A-4a and A-4b are medium- to high-K.

4.4.4 GEOCHEMISTRY OF MAFIC SUBVOLCANIC ROCKS

Based on field relationships, mafic subvolcanic rocks (dykes, sills, minor plutons) and the volcanic units that they intrude were interpreted to be genetically related (Chapter 3). This interpretation is investigated here by comparing the geochemistry of the mafic intrusive rocks with the volcanic rocks.

The subvolcanic rocks of the western Notre Dame Bay area are predominantly non-alkalic based on their low Nb/Y ratios (Fig. 4.18A; Floyd and Winchester, 1976, 1977). Average trace element and REE ratios are presented in the Table 4.5, whilst paleotectonic affinities, as interpreted from tectonomagmatic discrimination diagrams, are summarized in Table 4.6. Incompatible element ratios (Table 4.5), discrimination diagrams (Table 4.6; Figs. 4.19 - 4.22) and normalized multielement plots permit subdivision of the mafic subvolcanic rocks into two major types, with one anomalous sample. This division is reflected as well on the $(La/Yb)_N$ -Nb/Th plot (Fig. 4.23), on which groups of subvolcanic rocks can be compared to previously established geochemical groups of volcanic rocks. One sample which plots above the Nb/Th=8.5 line is of non-arc MORB affinity. The second type includes rocks with arc and transitional arc affinities. A third type includes samples of predominantly arc affinity. Increasing $(La/Yb)_N$ further subdivides the samples into different K-suites. The acronyms SNA (subvolcanic non-arc rocks), STR (subvolcanic transitional rocks, and SA (subvolcanic arc rocks) are used to simplify discussion of the data.

4.4.4.1 SNA Type: Subvolcanic Non-Arc Rocks

The SNA type contains only one sample (CP-92-53) of a dyke, that cuts rocks assigned to the Welsh Cove Formation in the Catchers Pond section of the Western Arm Group. This sample consistently plots in OFB or MORB fields on most diagrams, but also as WPB (Table 4.8), reflecting high concentrations of Ti, Zr, V and Nb in the

dyke. The Nb/Th ratio = 9.5 of this sample clearly indicates its non-arc nature (Fig 4.23).

A multielement normalized pattern of this rock (Fig. 4.24A) shows close resemblance to the NA-2c&d subtypes (Fig. 4.12) and an overall similarity to typical E-MORB. Similar incompatible element ratios (Table 4.7 and 4.2) also indicate an affinity with NA-2d, although the slightly anomalous Ti concentration in SNA affects ratios using this element (Table 4.7).

4.4.4.2 STR Type: Subvolcanic Transitional Rocks

The STR type contains samples of sills and dykes intruding the Pigeon Head Formation on Long Island and the Skeleton Pond Formation. The identifying characteristics of the STR-type rocks are relatively low Nb with respect to Th (Nb/Th <8.5) and LREE. Incompatible element ratios do not differ significantly from those of the TR samples (Tables 4.2 and 4.5). Nb/Th-(La/Yb)_N relationships were used to divide the STR-type rocks into two subtypes, STR-1 and STR-2. This division is also reflected in normalized multielement plots (Fig. 4.24C, D).

Two samples, CI-04-08 (Fig. 4.24B) and CI-01-14a (Fig. 4.24E), are not included in these subgroups. CI-04-08 sample is similar to rocks of the STR-1, but differs somewhat in the REE (lower (La/Yb)_N ratio). CI-01-14 is a strongly alkalic dyke (Fig 4.18A), with (La/Yb)_N=14. Its multielement plot exhibits a slight Nb depletion and Th enrichment relative to the LREE.

4.4.4.3 SA Type: Subvolcanic Arc Rocks

Similarly to the division of mafic volcanic rocks of arc affinity, subvolcanic rocks of arc affinity presented in this section are also divided based upon the amplitude of the "arc signature". The Nb/Th and La/Nb ratios separate the rocks into two types, one with the Nb/Th ratio between 1 and 8.5, and the La/Nb ratio <4, and the second with the Nb/Th ratio <1 and the La/Nb ratio >5 (Table 4.7). Variations in the (La/Yb)_N ratio permit both of types to be subdivided into several subtypes (Table 4.7).

4.4.4.3.1 SA-1 type: medium Nb/Th, low (La/Yb)_N subvolcanic arc rocks

The SA-1 subtype contains samples of two dykes cutting boninitic flows of the A-1 subtype in the Western Arm area. They are almost identical to the

boninitic flows they cut, having very low incompatible element abundances and concave-upward normalized REE patterns (Fig. 4.14 and 4.25). Multielement normalized plots show strong enrichment in Th with respect to La and positive Zr anomalies with respect to Nd and Sm (Fig. 4.25).

4.4.4.3.1 SA-2 type: medium Nb/Th, low- to high-K subvolcanic arc rocks

The SA-2a subtype contains two samples from the northern shore of Pilley's Island. One, CI-01-01, is from a dyke in the Indian Beach Complex, and the second, CI-06-06a, is from the Pilley's Island gabbro stock, that intrudes the sheeted dykes. Both display slightly LREE depleted patterns with negative Nb anomalies (Fig. 4.26A), similar to the A-2a and -2b type flows (Fig. 4.15) and to the low-Ti (LOTI) type flows and IAT dykes from the Lushs Bight Group identified by Swinden et al. (1989) and Jenner et al. (1991). In addition to these dykes, subtype SA-2a includes a gabbro clast, CI-19-27, from the Stag Formation Breccia Member. It has a similar multielement pattern and very low element abundances like the A-2a subtype samples (Fig. 4.15).

The SA-2b subtype consists of a dyke sample from the Indian Beach Complex on Pilley's Island, and of a sample (CI-19-27a) from a diabase plug intruding the Stag Formation Breccia Member on Stag Island. Neither sample has an exact match within the volcanic rocks, but both are very similar to samples of the A-3 subtype (see Fig. 4.26B and 4.16), albeit with a somewhat weaker arc signature (higher Nb/Th). SA-2b normalized patterns (Fig. 4.26B) display the characteristic negative Ti with respect to REE, not present in patterns of the A-3 type (Fig. 4.16), and lesser enrichment in LREE and Th than in the latter type. This and some differences in Zr and Y abundances in relation to the A-3 samples resulted in rather different element ratios (Tables 4.5, 4.3).

CI-LR-1a is from a gabbro sill intruding the Stag Formation Breccia Member on League Rock, which has been isotopically dated (see Chapter 3). It is presented separately, because it does not correspond geochemically to any of subvolcanic groups. This sample is strongly depleted in incompatible elements with abundances near those of primitive mantle (Fig. 4.26C).

Two dykes form the SA-2c subtype. These dykes intrude pillow lavas (Big Hill Basalt on Halls Bay Head and Pilley's Island) and one of them, CI-16-02b, was dated (Chapter 3). The normalized incompatible element plots of rocks from this type show similarities with flows from the A-2d subtype (Fig. 4.15D and 4.26D, Tables 4.3, 4.5). There is a minor difference between the subtypes in Nb/Th and $(La/Yb)_N$ ratios due to the relatively lower La and Th in the SA-2c.

The SA-2d subtype encloses samples of dykes intrusive predominantly into the Little Bay and Big Hill Basalt Formations. Their Nb/Th (1.7) and La/Nb (3.5) ratios are within the range of the SA-2 type, but every other ratio differs significantly in value from other subtypes in this type. Samples in this subtype are characterized by relatively high Mg number (=68) similar to that of the Lushs Bight Group boninites (subtype SA-1). Their high $(La/Yb)_N$ values (~10) and Th-La variation defines them as members of the high-K series, and they plot within the calc alkalic field on several discrimination diagrams (Table 4.6). Affinity to within plate volcanism is implied by Zr-Ti-Y and Zr-Nb-Y diagrams (Table 4.6). Samples of this subtype form a well defined cluster within the continental arc field on the Zr-Zr/Y (Table 4.6) and Nb/Yb-Th/Yb diagrams of Pearce (1983) (Fig. 4.22). Primitive mantle-normalized patterns of the SA-2d subtype (Fig. 4.26E) are characterized by depleted HREE, higher Nb and significantly elevated LREE and Th. One of the samples in the subgroup, WB-1, has notably lower $(La/Yb)_N$ (6) than other samples in this subtype (av. $(La/Yb)_N=14$), and it also has the lowest Mg# (59 versus av. 68). This sample, dated isotopically (see Chapter 3), appears to be transitional between the SA-2d subtype and the SA-3a subtype described below.

4.4.4.3.2 SA-3 type, low Nb/Th, medium-to high-K subvolcanic arc rocks

This type of subvolcanic intrusive rock (Fig. 4.27) is comprised predominantly of samples from the Cutwell Group, but it includes, as well, dykes intruding pillow lavas of the Lushs Bight Group. All samples in this type display a very pronounced negative Nb anomaly and a considerable enrichment

in LREE with respect to HREE (Fig. 4.27). On the basis of the $(La/Yb)_N$ ratio (Table 4.7; Fig. 4.27) rocks of the SA-3 type are defined as belonging to medium- to high-K suites.

Most SA-3 samples overlap geochemically with the A-4 type (Fig. 4.17 and 4.27), although some samples exhibit higher $(La/Yb)_N$ ratios and plot outside the field defined by their volcanic counterparts. The SA-3 type is divided into five subtypes, and one anomalous sample (CI-19-20b/1), using incompatible element ratios (Table 4.7) and normalized multielement plots (Fig. 4.27). The Zr/Y, Ti/V and $(La/Yb)_N$ ratios within the SA-2 type (Table 4.7) show a general increase from the SA-3a to the SA-3e subtype and the CI-19-20b/1. This trend is associated with a decrease in the value of the Ti/Zr ratio (Table 4.7).

SA-3a includes three samples of dykes intruding the Little Bay basalt, one dyke sample (CP-33-21a) cutting the Big Hill Basalt in the Catchers Pond section, and one dyke (CI-19-20c) intruding the Stag Formation Breccia Member. The calc alkalic affinity of the SA-3a is suggested by most discrimination diagrams (Table 4.6). The $(La/Yb)_N$ (3.4) in these samples categorizes them as members of a medium-K suite. Dykes of the SA-3a subtype are associated spatially with dykes of the SA-2d and SA-2c subtypes, and although $(La/Yb)_N$ ratios differ between these subtypes (10, 3.4, and 1.7 respectively), there is overlap in the patterns of the SA-3a and sample WB-1 of the SA-2d subtype (Fig. 4.27A and 4.26E, respectively). Unlike the SA-2d, the SA-3a feature pronounced negative anomalies in Zr relative to other incompatible elements (Fig. 4.27A). On the $(La/Yb)_N$ -Nb/Th plot (Fig. 4.23), the SA-3a subtype overlays with the A-4a subtype (Fig. 4.10) of volcanic rocks and their respective incompatible element ratios are reasonably close (tables 4.4 and 4.7), although trace element ratios in the latter subtype are affected by the lack of or a much smaller Zr anomaly.

The SA-3a subtype overlaps on the $(La/Yb)_N$ -Nb/Th plot (Fig. 4.23) with samples of two other subgroups, the SA-3b and SA-3c, all of which are from

the Cutwell Group. Both these later subtypes are members of a medium-K suite (Table 4.7), but their affinities to a magma series are not clear. They have lower Mg# and higher incompatible element abundances than SA-3a. Normalized plots of all three subtypes are generally similar (Fig. 4.27). Samples of the SA-3b and -3c subtypes plot within the oceanic arc field on the Nb/Yb-Th/Yb diagram (Fig. 4.22), but the average Zr/Y ratio (≈ 4) of the SA-3b subtype samples places them within the continental arc field on Zr-Zr/Y plot (Table 4.5, 4.6).

The two samples making up the SA-3d subgroup, also of the Cutwell Group, have a higher (La/Yb)_N ratio (6) than the SA-3a to -3c subtypes and are part of a high-K suite. According to most discrimination diagrams these are calc-alkalic (Table 4.6). In terms of incompatible element concentrations, the SA-3d samples are similar to those of the SA-3c subgroup, but their normalized plots (Fig. 4.27D) are marked by more negative Ti anomalies and little or no depletion in Zr. The Zr/Y ratio (≈ 5) and position on the Zr-Zr/Y plot implies formation within a continental arc (Table 4.5, 4.6).

The SA-3e subtype contains two samples, with the CI-LIP-1 representing the Long Island Pluton. They are part of a high-K suite ((La/Yb)_N = 7.5) and on the Nb/Yb-Th/Yb diagram (Fig. 4.22) they plot on the boundary between calc-alkalic and shoshonitic rocks. The high Zr/Y ratio in the Zr-Zr/Y (Pearce, 1983) (Table 4.6) plot implies that these rocks were formed in the continental arc environment, an affinity also suggested by the Nb/Yb-Th/Yb diagram (Pearce, 1983) (Fig. 4.22).

4.4.5 GEOCHEMISTRY OF FELSIC VOLCANIC AND SUBVOLCANIC ROCKS (F)

Silicic volcanic rocks are found in several areas of the western Notre Dame Bay area interstratified with mafic volcanic rocks of arc and transitional (arc/non-arc) affinities. A particularly large outcrop of felsic volcanic rocks is present in the Catchers Pond section of the Western Arm Group and felsic tuffs are found in the stratotype section of the group, dissected by numerous diabase sills. There are widespread occurrences of felsic tuffs in the vicinity of Springdale town, a narrow interval of felsic

tuffs and flows along the Lobster Cove Fault on Triton Island, and lenses of silicic volcanic rocks throughout the Cutwell Group on Long and Little Bay Islands. Several felsic post-kinematic dykes and plutons are plotted together with felsic volcanic and subvolcanic rocks for comparison, but their geochemical characteristics are described in the end of the section

4.4.5.1 Discrimination Between Felsic Volcanic/Subvolcanic Rocks

A few attempts were made in the past to develop methods to geochemically "fingerprint" and discriminate between leucocratic rocks formed in various tectonic settings. The Th-Zr-Nb diagram of Wood (1980) is the only one, that can be applied to both mafic and felsic volcanic rocks, and when applied to the set of felsic volcanic/subvolcanic rocks of the western Notre Dame Bay area, it implies a calc alkalic arc affinity for all of the samples (Fig. 4.28). The arc affinity is also indicated by the Y-Nb diagram of Pearce et al. (1984) (Fig. 4.29) on which all samples of the set plot within the volcanic arc granites / syn - collision granites (VAG/syn-COLG) field.

The (La/Yb)_N-Nb/Th plot was used in previous sections to separate rocks with various amplitudes of "arc signature" and with affinities to different K-suites. It can also be usefully applied to felsic volcanic and subvolcanic rocks of the western Notre Dame Bay area. There are two broad groups of samples present (Fig. 4.30). One type consists predominantly of the Welsh Cove Formation felsic tuffs and is characterized by lower (La/Yb)_N ratios (~1.6-4.5) and higher Nb/Th ratios (~0.3-2.1), that classify the type as of medium-K suite. The other type is mostly the Cutwell Group felsites characterized by higher (La/Yb)_N (7.2-12.3) and lower Nb/Th (<1) ratios, thus belonging to the high-K suite. Following these differences, felsic volcanic rocks of the western Notre Dame Bay area are divided into two types: the F-1 type, the low abundance type, and the F-2, the high abundance type. Three samples, one of diorite from the Brighton Intrusive Complex and two of diorite from the Coopers Cove/Colchester pluton, although of high-K suite, do not conform to the latter type. The post-kinematic intrusive rocks (crosses) form yet another high-K type.

4.4.5.2 Ree Patterns And Their Aspects

Most of the felsic rocks are characterized by concave-upward REE patterns (Fig. 4.31) reflecting apparent depletion in MREE with a minimum at Dy-Er. The REE plots (Fig. 4.31) further support divisions made between two types of felsic volcanic and subvolcanic (pre-kinematic) rocks. The F-1 type is characterized by flatter concave-upward REE patterns, with less enrichment in LREE than the steeper, more "spoon"-like patterns of the F-2 type. Most of the REE plots display minor negative Eu anomalies. The extended versions of REE plots (Fig. 4.32) generally have well defined negative Ti anomalies.

4.4.5.2.1 F-1 type: medium-K felsic rocks

The F-1 samples, collected predominantly from the Welsh Cove formation of the Western Arm Group, are with exception of one sample (JLB-9) from the Catchers Pond section. Sample JLB-9 is from the area northwest of Springdale. The F-1 type is divided into three subtypes and one anomalous sample. Two high Nb/Th rhyolites are combined in the F-1a subtype, whereas the set of medium-K rhyolites is included in the F-1b and -1c subtypes.

The extended patterns of the F-1a subtype are characterized by almost flat HREE segments, and relatively enriched MREE and LREE with positive slope (Fig. 4.32a). The pattern displayed by sample CP-20-07j is characterized by a positive Zr anomaly, which combined with a negative Ti anomaly is typical of some trondhjemites (e.g. the Little Port Complex, Jenner et al., 1991).

The samples included in the F-1b and 1c subtypes are characterized by slightly varying REE patterns (Fig. 4.32B, C), and different (La/Yb)_N and Nb/Th ratios. Differences between the F-1b and F-1c type extended REE patterns include elevated Zr and Y with respect to the REE and a more pronounced negative Ti anomaly in the former. Sample CP-05-05 is somewhat similar in element abundances and an overall shape of the pattern to that of the F-1c subtype, except for a pronounced positive Zr anomaly.

4.4.5.2.2 F-2 type: high-K felsic rocks

All but two (CP-09-06 and CI-11-09) samples of the F-2 type are felsic volcanic rocks (tuffs, flows and feeder dykes) from the Cutwell Group. CP-09-06 is a tuff collected in the Catchers Pond section and CI-11-09 is from the Triton Island section of the Western Arm Group. Extended multielement patterns of felsites assigned to the F-2a subtype (Fig. 4.33A) are similar to those of the F-1c, but are more enriched in LREE and Th. All samples are characterized by strong negative Nb and Ti anomalies.

Several other samples included in the F-2 type are not included within the F-2a subtype and are shown on separate diagrams. Two of them (CI-24-03/2, CI-19-11a) have extended REE patterns somewhat similar to those of the F-2a samples, but have higher (La/Yb)_N values (Fig. 4.33B, C). Three more samples, CC-90/2 and 3324 (the latter from Kean et al., 1995) of the Coopers Cove/Colchester Pluton, and CL-BR-7 of the Brighton intrusion, are included in the high-K type. Samples CC-90/2 and 3324 (Fig. 4.33D) of the Coopers Cove/Colchester sill dioritic phase show overall similarity in its extended REE pattern to those of the F-2a subtype samples (Fig. 4.33A). Sample CI-BR-7 of the Brighton Complex dioritic phase differs considerably from other rocks of the high-K type. The CI-BR-7 falls into the alkalic basalt field on the Nb/Y-Zr/TiO₂ diagram of Winchester and Floyd (1977) (Fig. 4.5) and is characterized by a relatively strong depletion in HREE, which makes the extended REE pattern (Fig. 4.33E) somewhat similar to those of post-kinematic high-K intrusive rocks (see below).

4.4.5.2.3 Post-kinematic high-K intrusive rocks

A third type of felsic rocks, the post-kinematic dykes and plutons, combines samples of two dykes and a minor pluton from Long Island and a sample of a larger intrusion on Little Bay Island, all intruding the Cutwell Group. All these rocks are classified as rhyodacites on the Zr/TiO₂-SiO₂ diagram (Winchester and Floyd, 1977) (Fig. 4.5), but on the Nb/Y-Zr/TiO₂,

diagram (Winchester and Floyd, 1977) (Fig. 4.5) they straddle the boundary between andesites and dacites.

All samples in the F-3 type are of arc affinity. Their position within the Th-Zr-Nb diagram of Wood (1980) indicates calc alkalic arc affinity (Fig. 4.28). Arc affinity is also suggested by the Y-Nb diagram (Pearce et. al, 1984) (Fig. 4.29) on which these intrusive rocks plot within the VAG/syn-COLG (volcanic arc granites / syn - collision granites) field, and are characterized by low Y and Nb abundances.

On the (La/Yb)_N-Nb/Th diagram (Fig. 4.30) all samples plot near the cluster formed by the F-2 type samples, but on average exhibit slightly higher (La/Yb)_N ratios (~11.5-16.3). The F-3 type extended REE patterns (Fig. 4.34) are relatively smooth and characterized by strongly depleted HREE and relatively enriched LREE.

4.5 Summary

4.5.1 GEOCHEMICAL SUBDIVISION OF ROCKS IN THE WESTERN NOTRE DAME BAY AREA

The mafic and felsic volcanic and subvolcanic rocks of the western Notre Dame Bay area are geochemically heterogeneous, as reflected in a wide range of trace element (e.g., Ti, Zr and V) abundances and ratios e.g., Zr/Ti and Ti/V). Tectonomagmatic discrimination diagrams employing these elements allow an initial broad subdivision of the rocks into two types with contrasting tectonic affinities. The first includes samples that have Ti/V ratio between 20-50, and plot within OFB field on both Ti-V and Zr-Ti diagrams; these diagrams suggest a non-arc tectonic affinity for these rocks. The second is characterized by Ti/V values of mainly <20; these diagrams indicate an island arc affinity for these rocks.

The validity of the division into arc and non-arc types was tested using the more definitive arc geochemical signature, i.e. the Nb depletion with respect to Th and La. The Th-Zr-Nb and Nb/Yb-Th/Yb diagrams (Wood, 1980; Pearce, 1983, respectively), both employing Nb/Th, were used for that purpose. Samples that had already revealed

an island arc affinity on the basis of the Ti-V-Zr variations, demonstrate a strong enrichment in Th relative to Nb, and on both diagrams plot within the TH and CA arc field. However, on the Th-Zr-Nb diagram, nearly all samples of non-arc affinity display a slight shift away from the oceanic mantle array in the direction of the arc field, and a number of those apparently non-arc samples plot within the arc field on both this and the Th/Nb-Nb/Yb diagrams. This suggests the presence of a third type of rocks, with geochemical signatures transitional between rocks from arc and non-arc settings. These transitional rocks are characterized by Ti/V and Ti/Zr ratios typical of ocean floor volcanic rocks, but lower Nb/Th ratios characteristic of rocks from arc environments.

Variations in geochemical signatures of all three types are clearly displayed in Nb/Th and (La/Yb)_N space, where the (La/Yb)_N ratio is an indicator of relative LREE enrichment and affinity with different K-suites, and the Nb/Th ratio = 8.5 representing the chondritic and primitive mantle Nb/Th value (Sun and McDonough, 1989), provides a good discriminant between arc and non-arc lavas (Swinden et al., 1989; Jenner et al., 1991). The Nb/Th and (La/Yb)_N diagram, together with the above described characteristics, indicates that the western Notre Dame Bay area volcanic rocks are divisible into three major types, herein termed NA, TR and A types, displaying diverse tectonic affinities.

4.5.2 NA-TYPE

The NA type comprises non-arc volcanic rocks, i.e. those identified as having oceanic (OFB) affinity on most tectonic discrimination diagrams. They are predominantly sub-alkalic and the elevated Zr/Y (>3) of most NA samples suggests a within plate affinity. They are characterized by extended REE patterns similar to oceanic basalts (N-MORB to E-MORB range). NA type rocks are found within the Sugar Loaves, Skeleton Pond, Big Hill Basalt formations of the Western Arm Group and in the Stag Formation.

The NA type rocks can be divided on the basis of Nb/Th and La/Yb ratios into two major sub-types of distinct magmatic affinity:

- Type NA-1 consists of samples which have Nb/Th and La/Nb ratios and extended REE patterns matching closely these of average E-MORB.

- Type NA-2 has lower Nb/Th (>8 and <13) and higher La/Nb ratios. The NA-2 type is further divided into four subtypes, what reflects gradual increase. Samples of this Type display substantial variation in the degree of LREE and MREE enrichment indicated on the primitive mantle-normalized extended REE patterns, from substantially LREE-depleted to moderately LREE-enriched and this forms the basis for a further 4-fold subdivision. The four NA-2 subtypes display geochemical characteristics ranging from those typical of N-MORB to E-MORB.

4.5.3. TR-TYPE

The TR type is sub-alkalic and consists of rocks with geochemical characteristics transitional between rocks typical of non-arc and arc settings. They are characterized by normalized extended REE patterns that show a weak to moderate enrichment in Th with respect to their non-arc counterparts. Effectively, this means they record the development of a slight negative Nb anomaly (arc signature) in rocks that otherwise have dominantly non-arc geochemical characteristics. This is consistent with the observation that on the diagrams applying Nb and Th, even non-arc rocks from the western Notre Dame Bay area are slightly shifted away from the mantle array, and suggests the potential for a continuum in mixing relationships. TR type rocks are apparently interbedded with rocks of non-arc affinity and are, in general, found in the same lithostratigraphic units. The presence of this transitional type of rocks suggests that, in the setting in which these rocks erupted, arc and non-arc magma sources coexisted.

The defining geochemical characteristic of the TR-type rocks is an enrichment in Th and LREE relative to Nb and HREE when compared to the NA-type counterparts. Application of the degree of Th and LREE enrichment allows division of the TR-type rocks into two subtypes, as well as recognition of three individual samples that are not clearly affiliated with any of these subtypes. The LREE and MREE abundances are slightly higher in the TR-1a subtype than in the typical E-MORB, and are somewhat transitional towards that of OIB in the TR-1b subtype. In general, samples of the TR-1a and -1b subtype display close similarity to rocks of non-arc affinity included in the NA-2b and -2c subtype.

4.5.4. A-TYPE

The A-type volcanic rocks are sub alkalic and consist of samples with a clearly-defined island arc affinity. Rocks with island arc geochemical signatures typically display enriched LREE and Th with respect to Nb, giving them pronounced "negative" Nb anomalies - a widely accepted geochemical signature of the island-arc environment. Rocks with these characteristics are generally found within the Lushs Bight Group, the Stag Formation and the Skeleton Pond, Welsh Cove, and Western Head Formations of the Western Arm Group. Rocks of arc affinity are also prevalent in the Cutwell Group.

Volcanic and volcanoclastic rocks of arc affinity can be subdivided using the degree of Th and La enrichment with respect to Nb. A first order division is into rocks with Nb/Th ratio >1 and La/Nb ratio <3 , and rocks with Nb/Th ratio <1 and La/Nb ratio >7 . Further subdivision reflects affinity to different K-series using the $(La/Yb)_N$ ratio as an indicator.

The A-1 type, containing three samples collected within the Lushs Bight Group and one from the Catchers Pond section of the Western Arm Group, is characterized by very low incompatible element abundances and has concave-upward normalized REE patterns, characterized by enriched Th with respect to La, and distinctively positive Zr with respect to Nd and Sm. These characteristics are characteristic of boninites.

The A-2 type is highly heterogeneous and can be subdivided into five subtypes reflecting variations in the strength of the arc signature and a systematic increase of the slope of REE patterns. The trend is from strongly LREE depleted patterns of subtype A-2a rocks to almost flat, N-MORB parallel patterns of subtype A-2c and slightly positive LREE slope in patterns of subtypes A-2d and A-2e. Decreasing Mg#, increasing Zr/Y, Ti/Y, Ti/V, and a decrease in Ti/Zr accompany the change from A-2a to A-2e subtypes. In general, all rocks of the A-2 type are defined as low-K tholeiites, with the exception of A-2e subtype, which is a medium-K suite.

Samples assigned to subtypes A-2a and A-2b represent mafic flows of the Little Bay Basalt and those of subtype A-2c the Skeleton Pond Formation, and the Upper Basalt and the Breccia members of the Stag Formation. The A-2d subtype includes samples of volcanic flows from the Skeleton Pond Formation in the Western Arm,

Pilley's Island and Triton Island sections of the Western Arm Group. One sample in subtype A-2d, CP-24-10, was collected in the Catchers Pond section of the Western Arm Group. The Catchers Pond section supplied all samples included in the A-2e subtype. The A-2e(t) subtype consists of four samples of pyroxene- and hornblende-phyric tuffs collected from within Western Arm Group. The tuffs have incompatible element ratios and multielement normalized patterns that show marked similarity to those of the A-2e subtype.

Subtype A-2f comprises high-Mg, high-K, calc-alkalic rocks. With a relatively high Mg# (62-52), these are among the most primitive rocks in the A-2 type. Their $(La/Yb)_N$ ratios indicate that they are medium- to high-K.

The A-3 type consists two pillowed flows from the Stag Formation Breccia Member. Their $(La/Yb)_N$ and Zr/Y ratios are within the range of the values of the A-2 type rocks, but the Nb/Th and La/Nb ratios (the strength of the arc signature) are stronger, similar to those of the A-4 type. Their multielement patterns also display a stronger arc geochemical signature (high Th, low Nb). These rocks are classified as low-K tholeiites.

Type A-4 rocks are low Nb/Th, LREE enriched rocks. They encompass exclusively mafic volcanic rocks of the Cutwell Group. Rocks of the A-4 type can be divided into two subtypes on the basis of their relative LREE enrichment reflected on normalized multielement plots, and ratios of more incompatible elements. The A-4a basalts have a relatively high Mg# (60-53), Ni (19-92) and Cr (86-214) values and are the most primitive rocks of the A-4 type samples. Volcanic rocks of the A-4 type are characterized by well developed negative Nb anomalies and LREE enrichment, and their $(La/Yb)_N$ ratios indicate that A-4 are medium-K.

4.5.5. GEOCHEMISTRY OF MAFIC SUBVOLCANIC ROCKS

The subvolcanic rocks of the Notre Dame Bay area are predominantly of non-alkalic character based on their low Nb/Y ratios. On the $(La/Yb)_N$ -Nb/Th plot, one sample plots above the Nb/Th=8.5 line and is of non-arc MORB affinity. The second type includes rocks with transitional arc/non-arc affinities (STR). A third type includes samples of predominantly arc affinity (SA). Increasing $(La/Yb)_N$ further subdivides the

samples into different K-suites. All have analogues in the volcanic rocks of the western Notre Dame Bay area suggesting that the observed dykes are genetically related to the flows.

The STR type contains samples of sills and dykes intruding the Pigeon Head Formation on Long Island and the Skeleton Pond Formation. The identifying characteristics of the STR-type rocks are relatively low Nb with respect to Th ($Nb/Th < 8.5$) and LREE. Incompatible element ratios are similar to those of the TR samples. $Nb/Th-(La/Yb)_N$ relationships were used to divide the STR-type rocks into two subtypes, STR-1 and STR-2. This division is also reflected in normalized multielement plots. In addition this type contains two samples, CI-04-08 and CI-01-14a. CI-04-08 sample is similar to rocks of the STR-1 but differs in the lower $(La/Yb)_N$ ratio. CI-01-14 is a strongly alkalic dyke, with $(La/Yb)_N=14$.

4.5.5.1 SA: Subvolcanic Arc Rocks

The division of subvolcanic rocks of arc affinity is also based upon the amplitude of the "arc signature". The Nb/Th and La/Nb ratios separate the rocks into two types, one with the Nb/Th ratio between 1 and 8.5, and the La/Nb ratio < 4 , and the second with the Nb/Th ratio < 1 and the La/Nb ratio > 5 . Variations in the $(La/Yb)_N$ ratio permit both types to be subdivided into several subtypes.

4.5.5.1.1 SA-1: medium Nb/Th, low $(La/Yb)_N$ subvolcanic arc rocks

The SA-1 subtype contains samples of two dykes cutting boninitic flows of the A-1 subtype in the Western Arm area, and almost identical to the boninitic flows they cut, having very low incompatible element abundances and concave-upward normalized REE patterns. Multielement normalized plots show strong enrichment in Th with respect to La and positive Zr anomalies with respect to Nd and Sm.

4.5.5.1.2 SA-2: medium Nb/Th, medium to high $(La/Yb)_N$ subvolcanic arc rocks

The SA-2a subtype contains two samples from the Indian Head sheeted dyke complex, including one of gabbro stock, that intrudes the sheeted dykes. Both display slightly LREE depleted patterns with negative Nb anomalies, and

are similar to the A-2a and -2b type flows and to the IAT flows and dykes from the Lushs Bight Group (Swinden et al., 1989; Jenner et al., 1991).

The SA-2b subtype consists of a dyke sample from the Indian Head sheeted dyke complex on Pilleys Island, and of a similar sample (CI-19-27a) from a diabase plug intruding the Stag Formation Breccia Member.

Sample CI-LR-1a of a gabbro sill intruding the Stag Formation Breccia Member on League Rock, is strongly depleted in incompatible elements with abundances near those of primitive mantle.

Another two dykes form the SA-2c subtype. These dykes intrude pillow lavas (Big Hill Basalt on Halls Bay Head and Pilleys Island) and one of them, CI-16-02b, was dated. These dykes are characterized by relatively flat extended REE patterns with noticeable negative Zr anomalies.

The SA-2d subtype encloses samples of dykes intrusive predominantly into the Little Bay and Big Hill Basalt Formations. Although their Nb/Th and La/Nb ratios are within the range of the SA-2 type, every other ratio differs significantly in value from other subtypes in this type. Samples in this subtype are characterized by relatively high Mg number (68) and high (La/Yb)_N values (~10) and Th-La variation defines them as members of the high-K series. Affinity to within plate volcanism is implied by Zr-Ti-Y and Zr-Nb-Y diagrams.

They also show affinity to the continental arc (Zr-Zr/Y and Nb/Yb-Th/Yb diagrams of Pearce, 1983). primitive mantle-normalized patterns of the SA-2d subtype are characterized by depleted HREE, higher Nb and significantly elevated LREE and Th.

4.5.6 FELSIC VOLCANIC AND SUBVOLCANIC ROCKS

Silicic volcanic rocks are found in the Catchers Pond section of the Western Arm Group, in the vicinity of Springdale town, on Triton Island, and throughout the Cutwell Group on Long and Little Bay Islands. Application of the Th-Zr-Nb diagram indicates a calc alkalic arc affinity for all of the samples consistent with relationships on the Y-Nb diagram.

The $(La/Yb)_N$ -Nb/Th plot discriminates two broad groups of samples. One, termed F1 and consisting predominantly of the Welsh Cove Formation felsic tuffs, is characterized by lower $(La/Yb)_N$ ratios (~1.6-4.5) and higher Nb/Th ratios (~0.3-2.1), that classify the type as of medium-K suite. The other, termed F2 consisting mostly of Cutwell Group felsites, is characterized by higher $(La/Yb)_N$ (7.2-12.3) and lower Nb/Th (<1) ratios, and apparently belongs to the high-K suite. Most of the felsic rocks are characterized by concave-upward REE patterns reflecting apparent depletion in MREE with a minimum at Dy-Er. The former type is characterized by flatter concave-upward REE patterns, with less enrichment in LREE than the steeper patterns of the latter.

A third type of felsic rocks, F3, the post-kinematic dykes and plutons, combines samples of two dykes and a minor pluton from Long Island and a sample of a larger intrusion on Little Bay Island, all intruding the Cutwell Group. All these rocks are of arc affinity. On the $(La/Yb)_N$ -Nb/Th diagram, they plot near the F-2 type samples, but on average exhibit slightly higher $(La/Yb)_N$ ratios (~11.5-16.3). The F-3 type extended REE patterns (Fig. 4.34) are relatively smooth and characterized by strongly depleted HREE and relatively enriched LREE.

Table 4.1. Selected trace and rare earth element ratios for the western Notre Dame Bay area volcanic rocks of non-arc and transitional arc/non-arc affinity. N-MORB, E-MORB and OIB data from Sun and McDonough (1989), except for Ti/V from Shervais (1982).

TYPE - \blacktriangleright SUB- TYPE - \blacktriangleright RATIO \downarrow	N-MORB	NA-1		NA-2				TR					E-MORB	OIB
		CL-19-24	NA-1a	NA-2a	NA-2b	NA-2c	CP-22-14	CL-16-01	TR-1a	TR-1b	CL-16-06	CL-01-14		
MG #	-	41	54	53	43	52	55	43	58	48	83	37	-	-
Ti/Zr	103	66	92	82	74	87	115	114	76	74	60	75	82	61
Zr/Nb	32	24	11	42	29	19	26	55	30	20	18	12	9	6
Zr/Y	3	4	3	4	4	4	3	2	4	4	5	4	3	6
Ti/Y	271	248	262	315	304	348	310	279	314	270	288	280	273	593
Ti/V	20-50	31	23	29	32	31	28	24	27	32	28	26	20-50	>50
Nb/Th	19	16	14	12	10	11	15	8	6	4.5	7	5	14	12
La/Nb	1.1	0.8	0.9	1.7	1.4	1.3	2.3	1.7	1.7	1.6	1.4	1.9	0.8	0.8
(La/Sm)N	0.7	0.9	1.4	0.8	1.0	1.3	1.3	0.6	1.1	1.6	1.7	2.5	1.6	2.5
(La/Yb)N	0.6	1.2	1.8	1.2	1.6	2.5	1.7	0.6	1.7	2.6	3.4	4.5	1.9	12.2

Table 4.2. Table summarizing tectono-magmatic affinity indicated from various discrimination diagrams for the mafic volcanic rocks of non-arc and transitional arc/non-arc affinity.

TYPE/SUBTYPE	TECTONO-MAGMATIC DISCRIMINANTS									
	Ti/1000 - V	Th - La	Nb - La	Th - Zr - Nb	Nb/Yb - Th/Yb	Zr - Zr/N	MnOx10 - P2O5x10 - TiO2	Zr - Ti	Zr - Ti/100 - Yx3	Zr/4 - Nb/2 - Y
CI-19-24	ofb	e-morb	e-morb	n-morb	morb	wpb	oit	wpb	ofb/cab	n-morb/vab
NA-1A	ofb	e-morb	e-morb	e-morb	morb	morb/lab	morb/lat	ofb/kt	ofb	n-p-morb
NA-2A	ofb	n-/e-morb	n-morb	n-morb	morb	morb/wp	morb/lat	ofb	ofb/cab/wp	n-morb/vab/wpt
NA-2b	ofb	n-/e-morb	n-morb	n-morb	arc/morb	wpb	morb/oa	ofb	ofb/cab	n-morb/vab/wpt
NA-2c	ofb	n-/e-morb	n-morb	n-morb/e-morb	morb/arc	wpb	morb/oa/oit	ofb	ofb/wp	vab/wpt
CP-22-14	ofb	n-morb	-	n-morb	morb	morb	lat	wpb	kt/ofb	n-morb/vab
CI-16-01	ofb	-	n-morb	prn th arc	arc	morb/lab	lat	ofb	ofb/kt	n-morb/vab
TR-1A	cfb	e-morb	n-morb	prn th arc	th arc	wpb	morb/lat	ofb	ofb/cab	n-morb/vab/wpt
TR-1B	ofb	med-K	n-morb	th/ca arc	ca arc	wpb	morb/oit	ofb	cab/ofb	n-morb/vab/wpt
CL-16-08a	ofb	e-morb	n-morb	tr	ca arc	wpb	morb	wpb	cab	vab/wpt
CL-01-14	ofb	e-morb	-	ca arc	ca arc	wpb	oa	wpb	ofb/cab	p-morb

Table 4.3. Selected trace and rare earth element ratios for the Notre Dame Bay volcanic rocks of arc affinity. N-MORB, E-MORB and OIB data from Sun and McDonough (1989), except for Ti/V from Shervais (1982).

TYPE SUB- TYPE RATIO ↓	N-MORB	A-1			A-2				A-3	A-4		E-MORB	OIB	
		A-2a	A-2b	A-2c	A-2d	A-2e	A-2e(f)	A-2f		A-4a	A-4b			
MG #	-	65	60	58	48	43	45	-	58	48	56	40	-	-
Ti/Zr	103	40	147	119	111	105	85	113	79	156	100	71	82	61
Zr/Nb	32	20	39	61	66	28	26	16	23	103	66	51	9	6
Zr/Y	3	5	1	2	2.5	3	4	2	4.5	2	3	3	3	6
Ti/Y	271	195	195	215	264	304	308	248	343	284	281	219	273	593
Ti/V	20-50	3	9	14	17	18	15	16	13	15	13	18	20-50	>50
Nb/Th	19	2.5	2.9	5.4	5	4.1	2.3	2.1	1.3	0.7	0.6	0.4	14	12
La/Nb	1.1	1.7	1.8	2	2	1.7	2.5	2.4	3.7	7.1	7.3	9	0.8	0.8
(La/Sm)N	0.7	3.0	0.6	0.5	0.6	1.0	1.6	1.7	2.3	0.9	1.8	2.3	1.6	2.5
(La/Yb)N	0.6	1.9	0.3	0.4	0.6	1.3	2.3	2.1	5.1	0.9	2.3	4.1	1.9	12.2

Table 4.4. Table summarizing tectono-magmatic affinity indicated by various discrimination diagrams for the mafic volcanic rocks of arc affinity.

TYPE/SUBTYPE	TECTONO-MAGMATIC DISCRIMINANTS									
	Ti/1000 - V	Th - La	Nb - La	Th - Zr - Nb	Nb/Yb - Th/Yb	Zr - Zr/N	MnOx10 - P2O5x10 -TiO2	Zr - Ti	Zr - Ti/100 - Yx3	Zr/4 - NbX2 - Y
A-1	arc	low-K	low-K	ca arc	oc/cont ca arc	-	-	-	cab	wpt/vab
A-2a	arc	low-K	low-K	prim th arc	oc th arc	oc arc?	cab	cab/ikt	-	vab/ n-morb
A-2b	arc	low-K	low-K	prim th arc	oc th arc	oc arc	iat	ikt/ofb	ikt/ofb	vab/ n-morb
A-2c	arc	low-K	low-K	prim th arc	oc th arc	oc arc	iat	ikt/ofb	ikt/ofb	vab/ n-morb
A-2d	arc	low-K	low-/ med-K	th/ca arc	th/ca oc arc	oc/cont arc	iat/ morb	ikt/ofb	ikt/ofb	vab/ n-morb
A-2e	arc	low-/ med-K	med-K	ca arc	oc/cont ca arc	oc/cont arc	iat	ikt/cab/ ofb	ikt/ofb/ cab/wpb	vab/ n-morb
A-2e(t)	arc	low-/ med-K	low-/ med-K	ca arc	oc/cont ca arc	oc/cont arc	cab	ikt/ofb	ikt/ofb	vab/ n-morb
A-2f	arc	med-/ high-K	med-K	ca arc	cont ca arc	cont arc	iat/ cab	ikt/cab/ ofb	wpb/cab	vab/wpt
A-3	arc	low-K	low-K	ca arc	oc th arc	oc arc	iat/ cab	cab/ikt	ikt	vab/ n-morb
A-4a	arc	low-K	low-K	ca arc	oc ca arc	oc/cont arc	cab/ iat	ikt/cab	ikt/ofb	vab/ n-morb
A-4b	arc	med-/ high-K	med-/ high-K	ca arc	oc ca arc	oc arc	iat/cab	ikt/cab	cab/ofb	vab/ n-morb

Table 4.5 Selected trace and rare earth element ratios for the western Notre Dame Bay area subvolcanic rocks. N-MORB, E-MORB and OIB data from Sun and McDonough (1989), except for Ti/V from Shervais (1982).

TYPE SUB- TYPE RATIO ↓	N-MORB	SNA				SA-1	SA-2					SA-3					E-MORB	OIB	
		CF-92-S3	CL-04-08	STR-1	STR-2		CL-01-14a	SA-2a	SA-2b	CL-1#	SA-2c	SA-2d	SA-3a	SA-3b	SA-3c	SA-3d			SA-3e
MG #	-	55	47	52	53	51	68	52	57	72	47	68	64	36	43	46	61	-	-
Ti/Zr	103	101	71	90	82	32	45	114	72	61	78	45	136	90	66	25	32	82	61
Zr/Nb	32	22	29	16	24	16	21	79	81	49	29	19	28	48	43	38	58	9	6
Zr/Y	3	6	4	4.5	6	15	5	2	2.5	3	3.5	7	2.5	4	3	5	10	3	6
Ti/Y	271	567	279	400	493	468	220	243	184	207	266	326	290	319	216	125	330	273	593
Ti/V	20-50	42	23	36	37	84	3	12	10	8	14	32	9.5	16	17	26	33	20-50	>50
Nb/Th	19	9.5	6.2	5.9	2.1	2.7	2.7	2.8	1.4	4.1	3.1	1.7	0.8	0.6	0.5	0.4	0.6	14	12
La/Nb	1.1	1.8	1.8	1.5	2.5	1.8	1.3	2.9	4.1	2.0	2.3	3.5	6.6	6.4	7.9	6.6	5.2	0.8	0.8
(La/Sm)N	0.7	1.7	0.9	1.7	2.1	3.2	2.1	0.7	0.9	0.8	1.4	3.1	2.1	2.2	2.4	3.0	2.9	1.6	2.5
(La/Yb)N	0.6	3.3	1.7	3.1	4.6	13.6	1.4	0.5	0.8	0.9	1.7	10	3.4	3.8	4.4	6.2	7.5	1.9	12.2

Table 4.6. Table summarizing tectono-magmatic affinity indicated by various discrimination diagrams for the mafic subvolcanic rocks of the non-arc, transitional, and arc affinities.

TYPE/SUBTYPE	TECTONO-MAGMATIC DISCRIMINANTS									
	Ti/1000 - V	Th - La	Nb - La	Th - Zr - Nb	Nb/Yb - Th/Yb	Zr - Zr/Y	MnO - P2O5 - TiO2	Zr - Ti	Zr - Ti/100 - Y*3	Zr/4 - Nb*2 - Y
CP-92-53	morb/oib	n-morb	n-morb	n-morb	e-morb	wpb	-	ofb	wpb	wpt/vab
CL-04-08	morb	e-morb	n-morb	th arc	th oc arc	wpb	lat	ofb	ofb/cab	n-morb
STR-1	morb	e-morb	n-morb	ca arc	ca cont arc	wpb/morb	morb/oia	ofb	wpb	wpt/vab
STR-2	morb	med-/high-K	high-K	ca arc	ca cont arc	wpb	ofb	ofb	wpb	wpt/vab
CL-01-14a	-	high-K	-	ca arc	sh cont arc	off wpb	-	outside ofb/cab	outside wpb/cab	outside wpa
SA-1a	arc	low-K	low-K/n-morb	ca arc	oc/cont ca arc	cont arc	cab	depl	cab	wpt/wpa
SA-2a	arc	low-K	low-K	th arc	th oc arc	oc arc	lat	lkt/ofb	lkt/ofb	vab/n-morb
SA-2b	arc	low-K	low-K	th/ca arc	th oc arc	oc arc	cab	lkt/ofb	ofb/cab	vab/n-morb
CL-LR-1a	arc	low-K/n-morb	low-K/n-morb	th arc	th oc arc	oc/cont arc	-	depl	ofb/cab	vab/n-morb
SA-2c	arc	low-K	low-/med-K	ca arc	ca oc arc	oc/cont arc	cab	cab/lkt	ofb/cab	vab/n-morb
SA-2d	arc/morb	med-/high-K	med-/high-K	ca arc	ca oc arc	cont arc	cab	cab	cab/wpb	wpt/vab
SA-3a	arc	low-/med-K	low-/med-K	ca arc	ca oc arc	oc arc	cab?	lkt/cab	lkt	vab/n-morb
SA-3b	arc/ofb	med-K	med-K	ca arc	ca oc arc	cont arc	cab/lat	lkt/ofb	ofb	vab/n-morb
SA-3c	arc	med-/high-K	med-/high-K	ca arc	ca oc arc	oc/cont arc	morb?	cab/lkt	ofb/cab	vab/n-morb
SA-3d	arc	high-K	high-K	ca arc	?	cont arc	-	cab	cab	vab/wpt
SA-3e	arc	med-/high-K	med-K	ca arc	ca/sh cont arc	cont arc	-	cab	outside cab/wpb	off wpt

Abbreviations:

AFG (afg) - amphibolite facies gneiss
 AB - alkali basalt
 Alk-Bas - alkali basalt
 Bas - basanite
 Bsn - basanite
 CA - calc alkalic
 CA-Arc - calc-alkalic island arc
 CAB - calc-alkalic basalt
 E-MORB - enriched mid-ocean ridge basalt
 FeO* - total iron
 HFSE - high field strength elements
 HREE - heavy rare earth elements
 LFSE - low field strength elements
 LKT - low-K tholeiites
 LREE - light rare earth elements
 Mg# - molecular proportion $100 \text{ MgO}/(\text{MgO} + \text{FeO})$
 MREE - middle rare earth elements
 Neph - nephelinite
 Nph - nephelinite
 N-MORB - normal mid-ocean ridge basalt
 OIB - ocean island basalt
 OFB - ocean floor basalts
 ORG - ocean ridge granites
 PAWMS - Pacific authigenic weighted mean sediment
 PM - primitive mantle
 REE - rare earth elements
 SA - subvolcanic arc (rock)
 SHO - shoshonite
 SNA - subvolcanic non-arc (rock)
 STR - subvolcanic transitional (rock)
 Sub-AB - sub-alkalic basalt
 TH-Arc - tholeiitic arc
 TH - tholeiitic
 T-MORB - transitional mid-ocean ridge basalt
 Trach - trachyte
 TrAn - trachy-andesite
 TR - transitional (arc/non-arc rock)
 UCC (ucc) - upper continental crust
 VAG+Syn-COLG - volcanic arc + syn-collision granites
 WPB - within-plate basalts
 WPG - within-plate granites

Figure 4.1. Legend of abbreviations used in chapters on geochemistry (4 and 5).

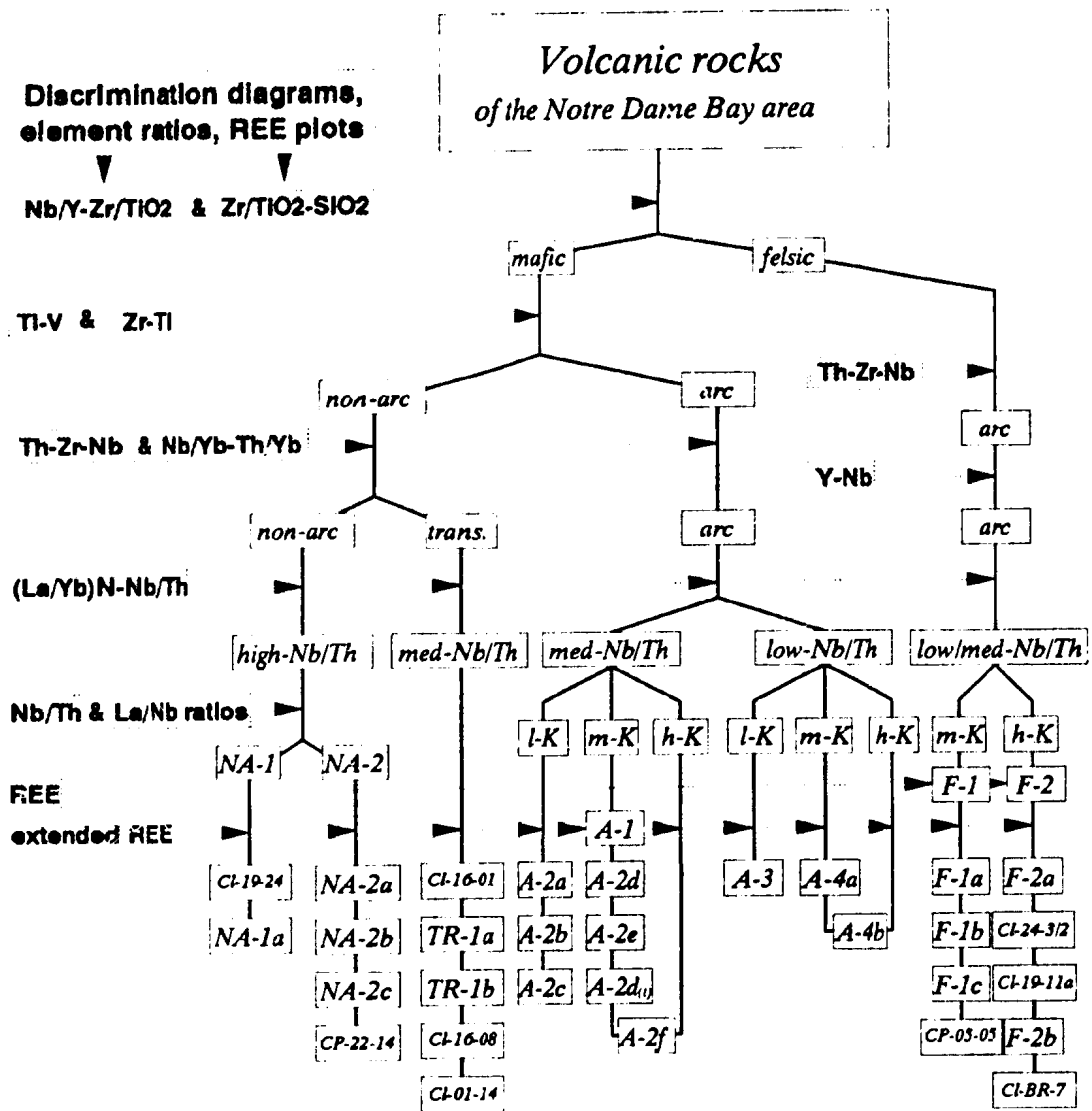


Figure 4.2. A schematic outline of the step by step approach used to divide volcanic rocks of the western Notre Dame Bay area on the basis of geochemical data. Abbreviations: Trans. - transitional; med. - medium; l - low; m - medium.

Legend of symbols

MAFIC VOLCANIC ROCKS

NON-ARC

- NA-1, NA-2

TRANSITIONAL

- ◆ TR-1a, TR-1b

ARC

- ▲ A-1
- A-2a, A-2b, A-2c
- A-2d
- ▲ A-2e
- △ A-2e(t)
- ▽ A-2f
- A-3
- ▼ A-4a
- ▼ A-4b

FELSIC VOLCANIC AND SUBVOLCANIC ROCKS (ARC)

- F-1
- F-2
- ◇ CP-09-06
- ◀ 90-2CC, 1543324
- ★ CL-BR-07

POST-KINEMATIC INTRUSIVE ROCKS

- + F-3

MAFIC SUBVOLCANIC ROCKS

NON-ARC

- SNA

TRANSITIONAL

- ◆ STR-1, STR-2

ARC

- SA-1
- SA-2a, SA-2b
- ◇ CI-19-27
- ▲ SA-2c
- △ SA-2d
- ▽ SA-3a
- ▼ SA-3b, SA-3c, SA-3d, SA-3e

Figure 4.3. Legend of symbols used in subsequent figures in this chapter.

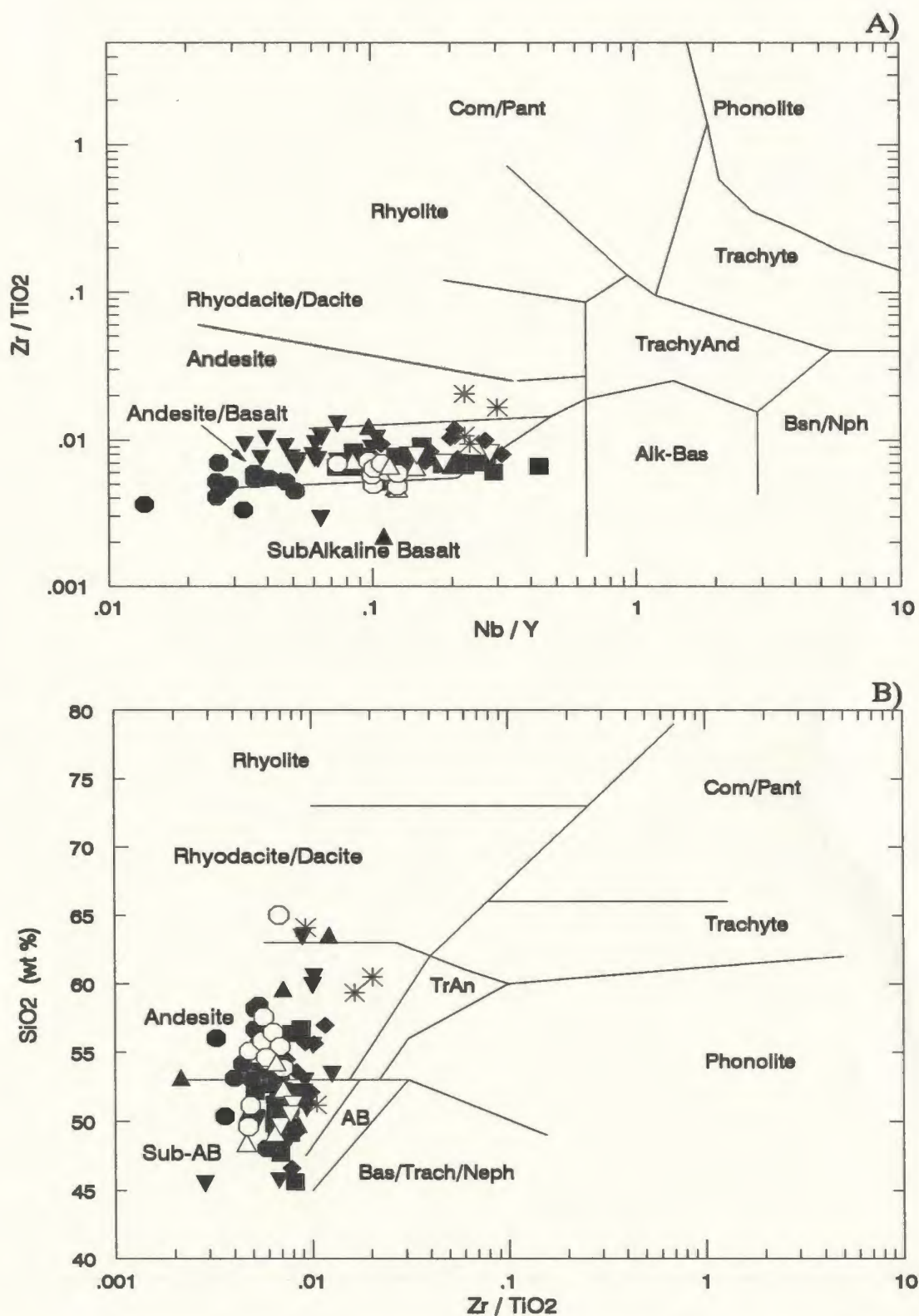


Figure 4.4. The Nb/Y-Zr/TiO₂ (4.4 A) and Zr/TiO₂-SiO₂ (4.4 B) diagrams (Winchester and Floyd, 1977) highlighting the behavior of SiO₂ in mafic volcanic rocks of the western Notre Dame Bay area. Abbreviations: bas - basanite; trach - nephelinite; TrAn - trachyandesite; sub-AB - subalkaline basalt; com/pant - comendite/pantellerite; AB - alkaline basalt.

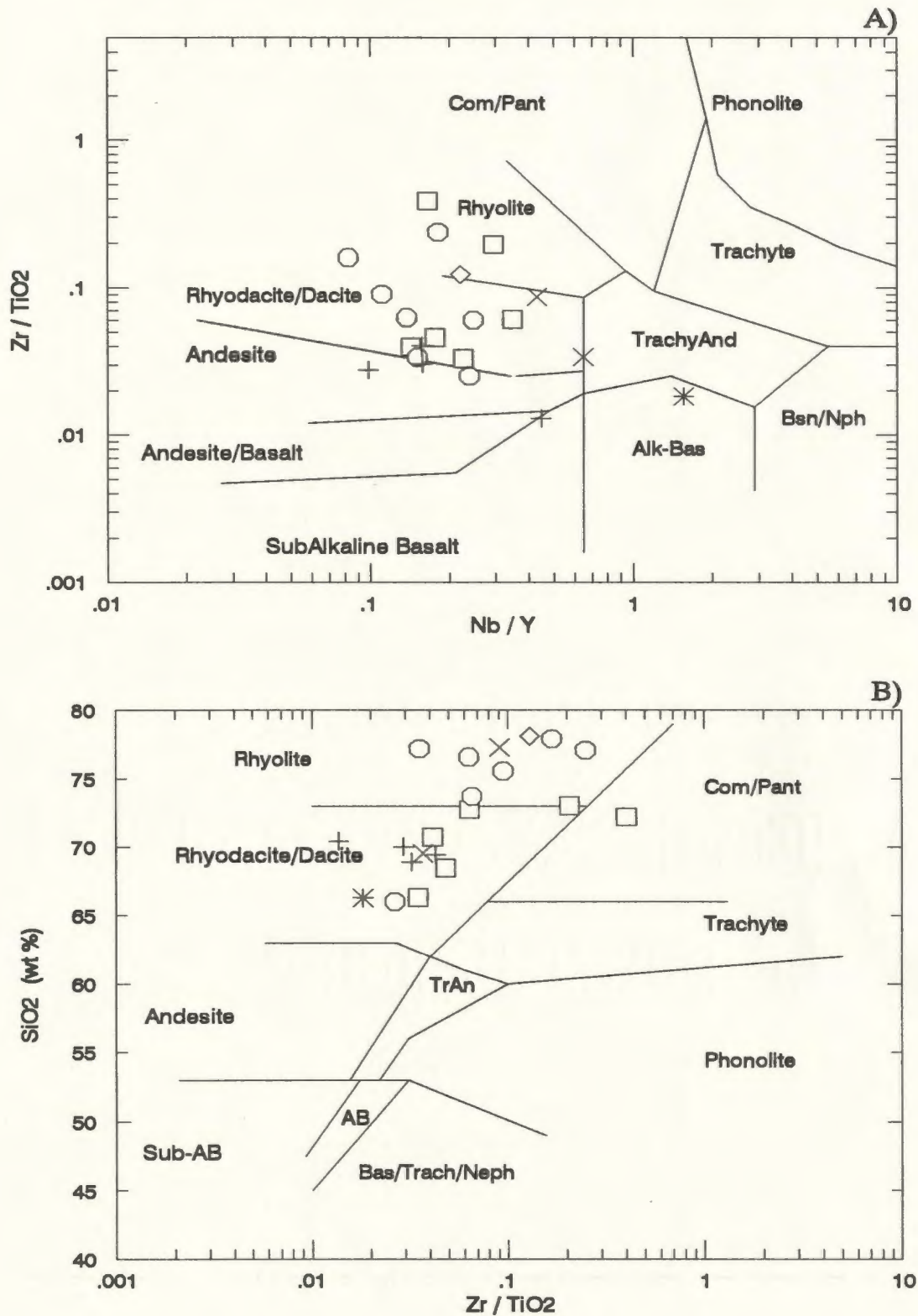


Figure 4.5. The Nb/Y-Zr/TiO₂ (4.5 A) and Zr/TiO₂-SiO₂ (4.5 B) diagrams (Winchester and Floyd, 1977) indicating divisions of felsic volcanic rocks of the western Notre Dame Bay area. See Figure 4.4 for definition of abbreviations.

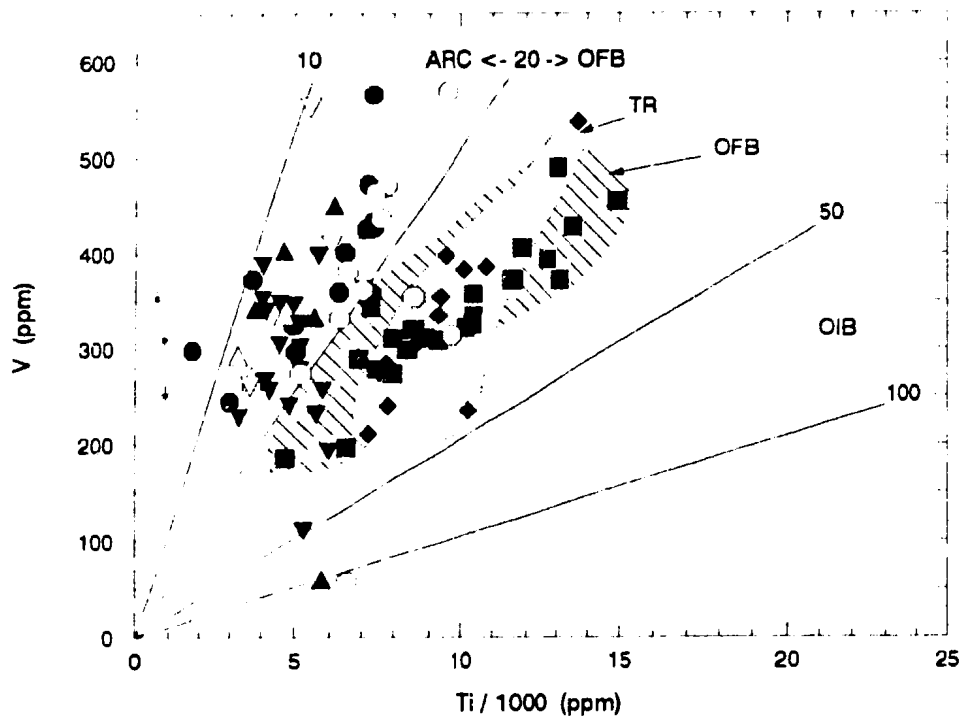


Figure 4.6. The Ti/1000 - V diagram of Shervais (1982) indicating two broad tectonic settings, in which the mafic volcanic rocks of the western Notre Dame Bay area formed. Outlined within the MORB field are two types of samples, one of which (filled squares) is of non-arc (NA) affinity, whereas the other (filled diamonds) is later shown to be transitional (TR) between non-arc and arc rocks. OFB - ocean floor basalt; OIB - ocean island basalt.

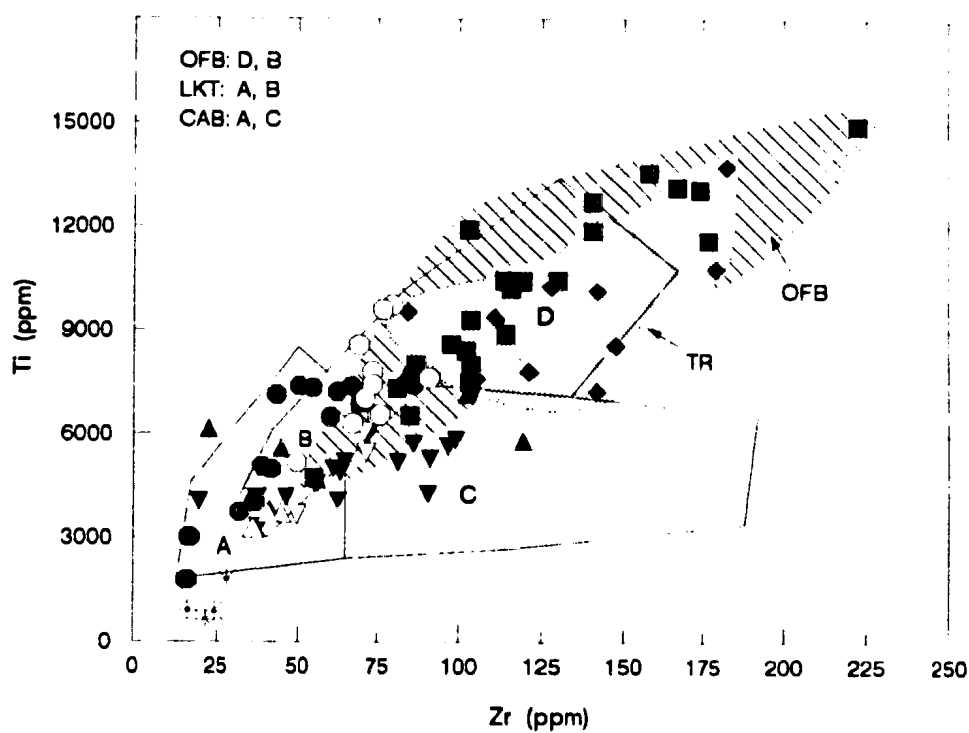


Figure 4.7. The Zr-Ti diagram of Pearce and Cann(1973). The set of samples used in the Fig. 4.6 plots here within fields that indicate origin of the samples in two broad tectonic settings, arc and non-arc. Note that both the NA and TR samples plot mostly within the OFB fields; however some samples (open circles) previously displaying an arc affinity, plot in this diagram in the OFB field. OFB - ocean floor basalt; LKT - low-K tholeiite; CAB - calc-alkaline basalt.

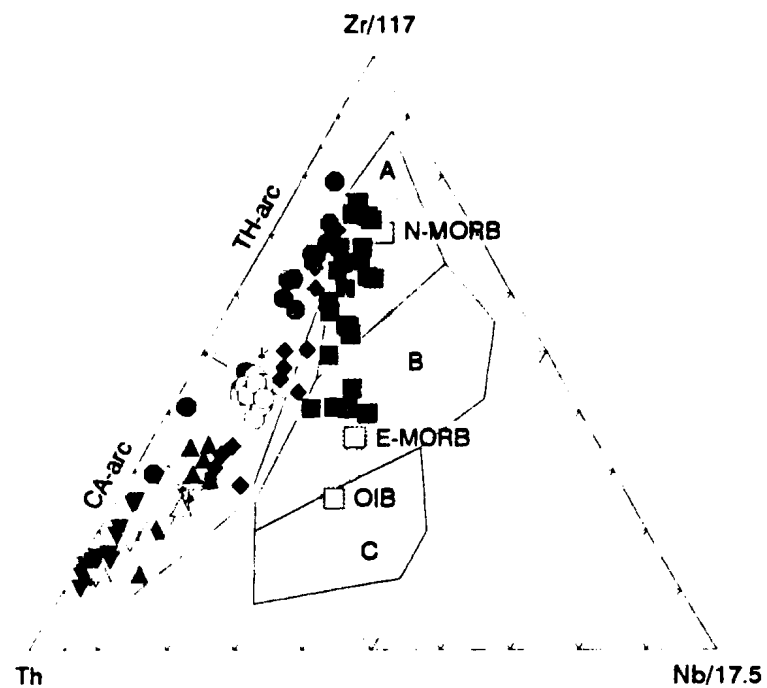


Figure 4.8. The Th-Zr-Nb diagram (from Wood,1980) supporting the division of the Notre Dame Bay area rocks into arc and non-arc types. This diagram indicates also an existence within the samples of a third type (filled diamonds), that on previous diagrams demonstrated an affinity to a non-arc setting; whereas, on this diagram they plot within the arc field.

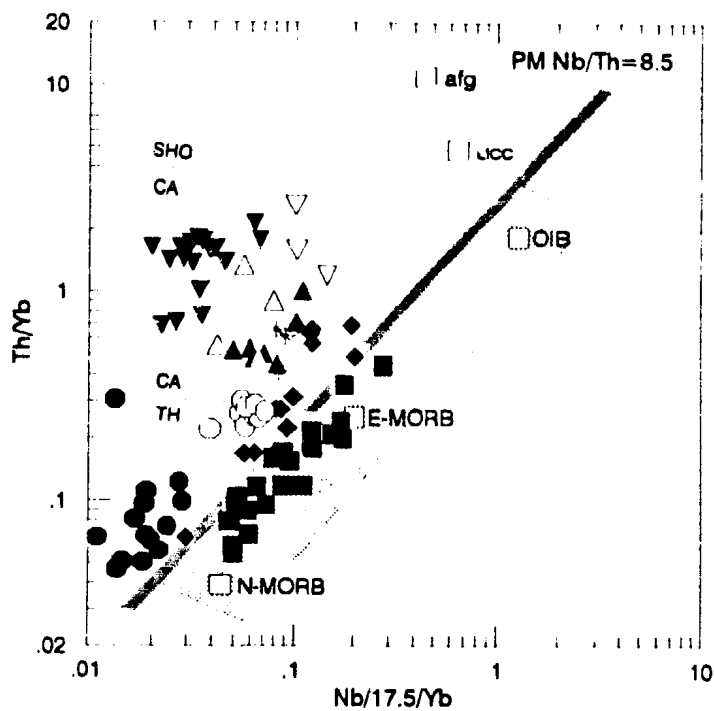


Figure 4.9. The Nb/Yb-Th/Yb diagram of Pearce(1983) provides, as well, division of the samples into the arc and non-arc types confirming the transitional character of samples marked as filled diamonds.

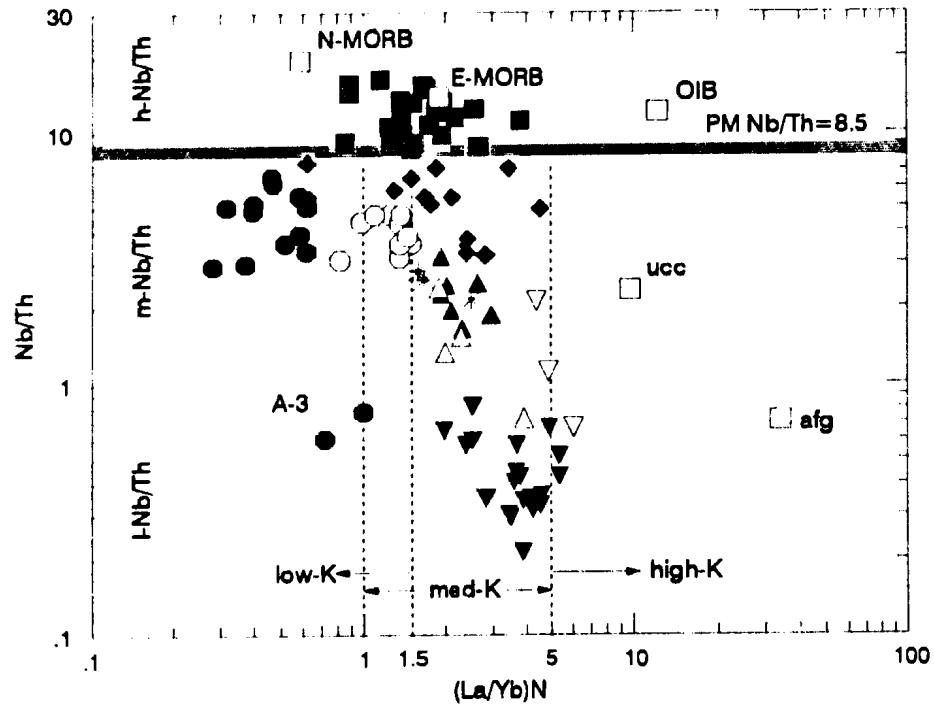


Figure 4.10. The $(La/Yb)_N$ -Nb/Th diagram illustrating divisions made within the rocks of the Notre Dame Bay area. A major division is made into a high-Nb/Th non-arc(NA) and a lower Nb/Th arc(A) rocks along the line representing primitive mantle Nb/Th ratio = 8.5 (Sun and McDonough, 1989). An additional division into medium- and low-Nb/Th rocks is also shown. The low-, medium- and high-K separations for the arc rocks are from Swinden, 1987.

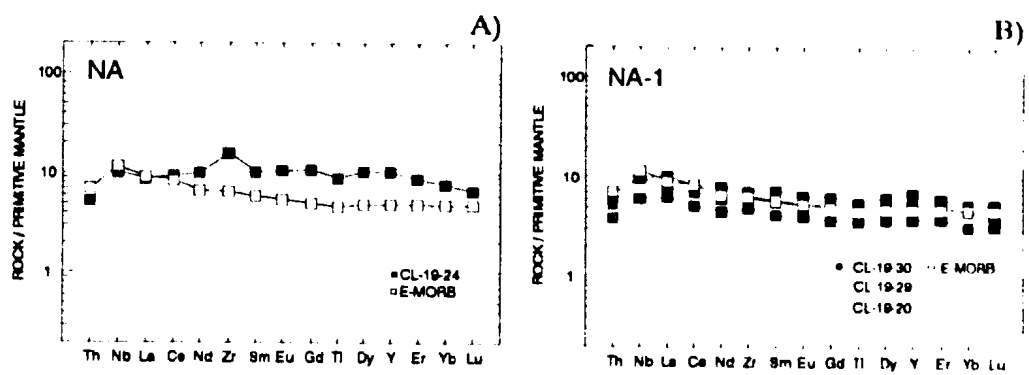


Figure 4.11. Extended, primitive mantle normalized REE patterns of: A) the CL-19-24 sample; and B) the NA-1 type samples. A pattern of typical E-MORB is shown for comparison. In this and following figures, N-MORB, E-MORB and OIB values are from Sun and McDonough(1989). Normalizing values for primitive mantle from Sun and McDonough(1989).

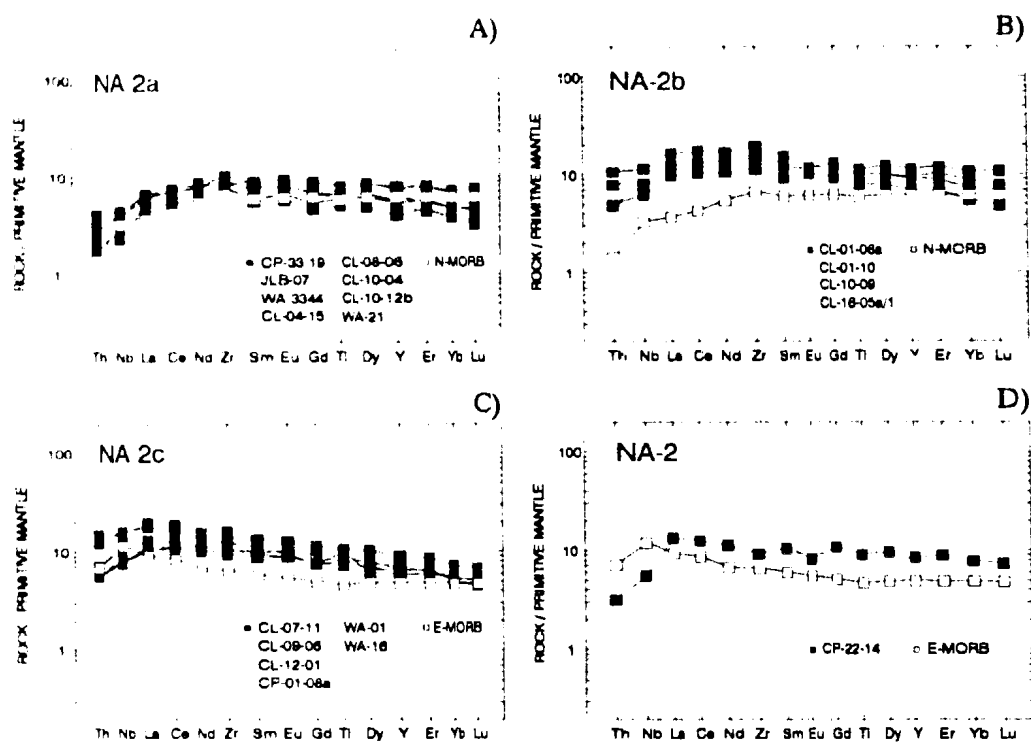


Figure 4.12. Extended, primitive mantle-normalized multi-element plots of the type NA-2 samples: A) samples included in the NA-2a subtype; B) samples of the NA-2b subtype; C) samples of the NA-2c subtype; D) sample CP-22-14. N-MORB and E-MORB are shown for comparison. Note the significant enrichment in MREE with respect to E-MORB in both the NA-2b and NA-2c subtypes.

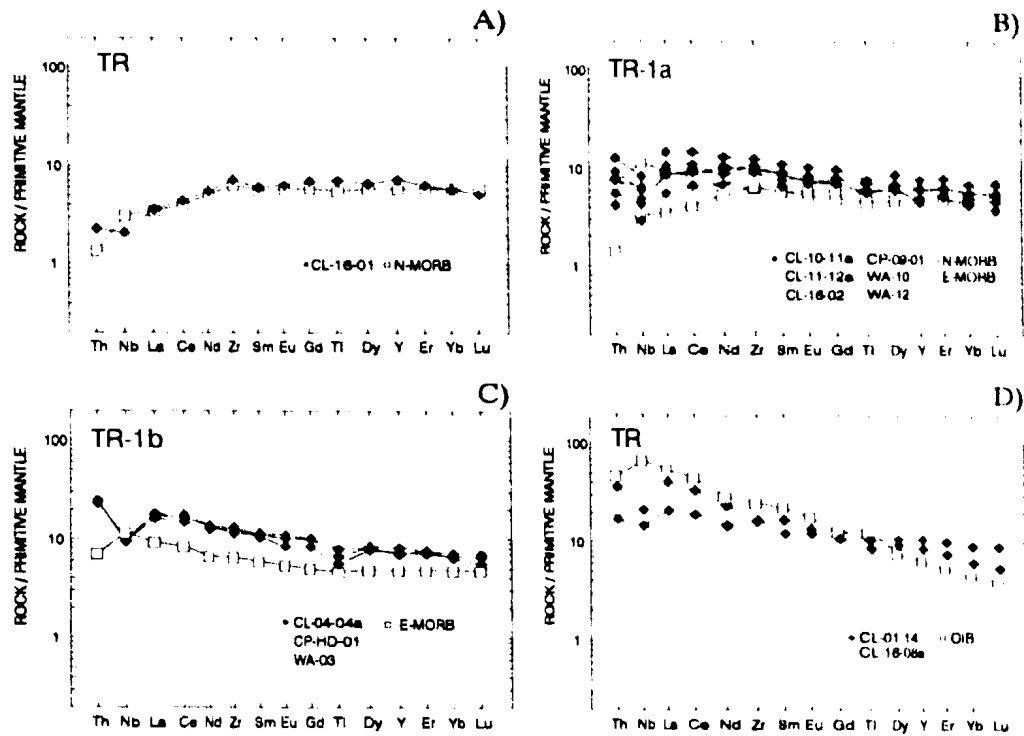


Figure 4.13. Extended, primitive mantle-normalized multi-element plots of the TR type rocks: A) sample CL-16-01; B) the TR-1a subtype samples; C) the TR-1b subtype samples; and D) samples CL-16-08a and CL-01-14.

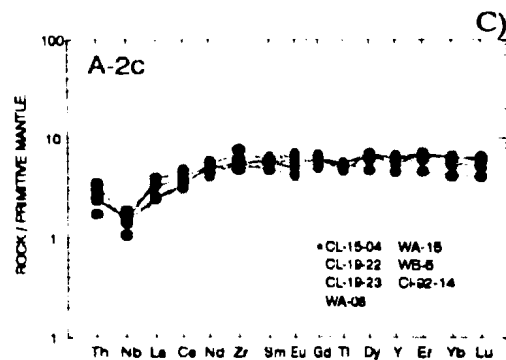
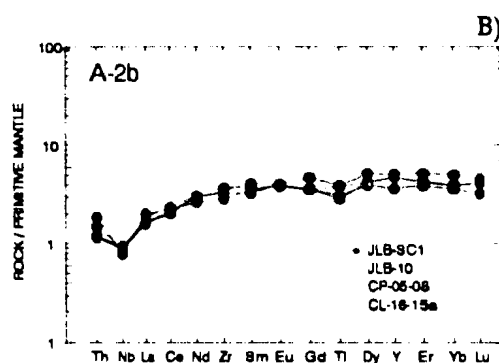
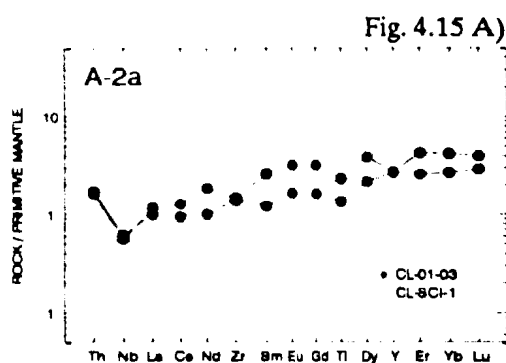
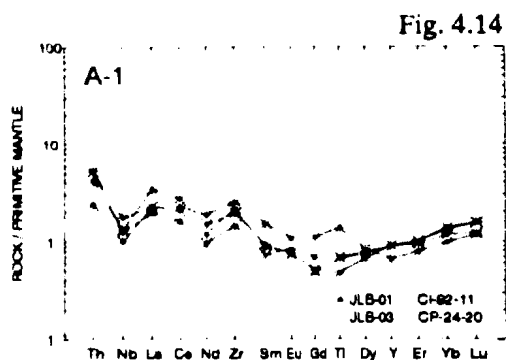


Figure 4.14. Multi-element patterns for the Lushes Bight Group boninites of the A-1 type.

Figure 4.15. Extended REE patterns for the A-2 type samples: A) strongly depleted tholeiites of the A-2a subtype; B) depleted tholeiites of the A-2b subtype; C) island arc tholeiites of the A-2c subtype, that in general are similar to samples of the A-2b subtype, but differ in having slightly higher Ti abundances and Mg#.

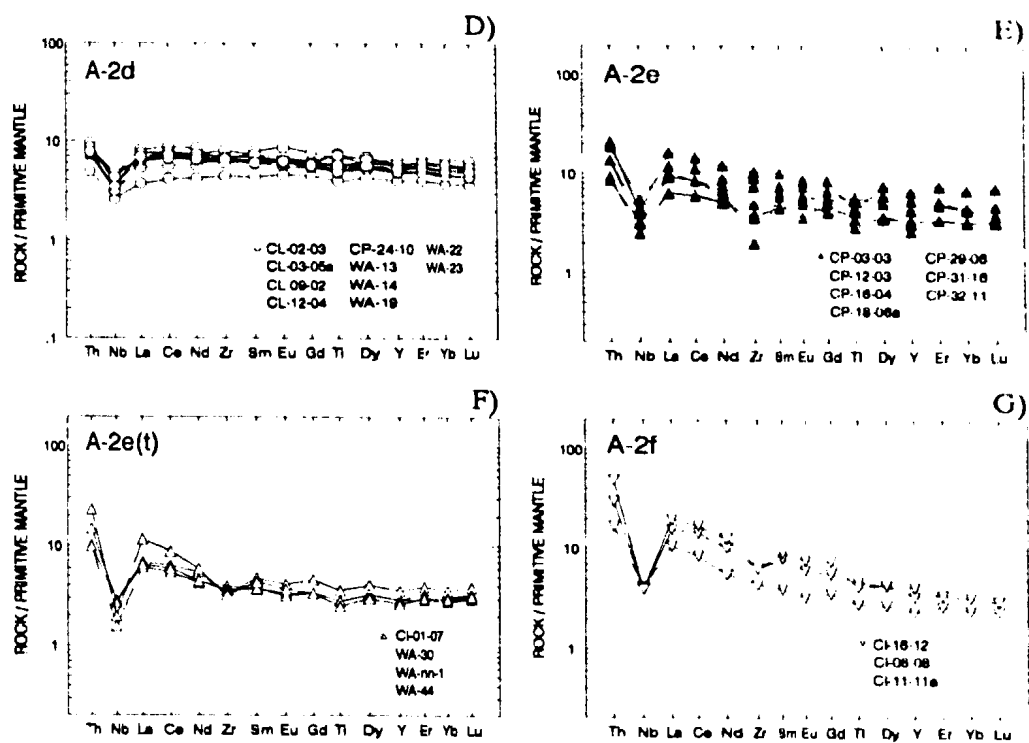


Figure 4.15. (continued) D) tholeiites of the A-2d subtype; E) rocks of the A-2e subtype; F) the A-2e (t) subtype mafic tuffs displaying close affinity to the A-2e subtype mafic flows; and G) samples of high-Mg, high-K rocks (two bombs and mafic flow or sill) combined in the A-2f subtype.

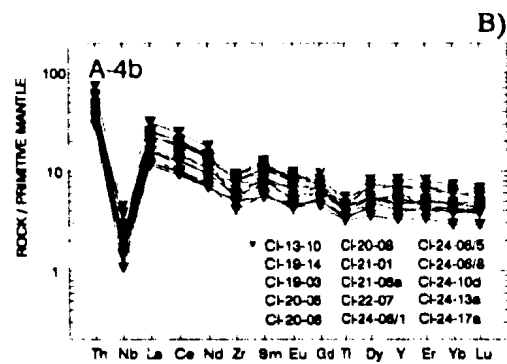
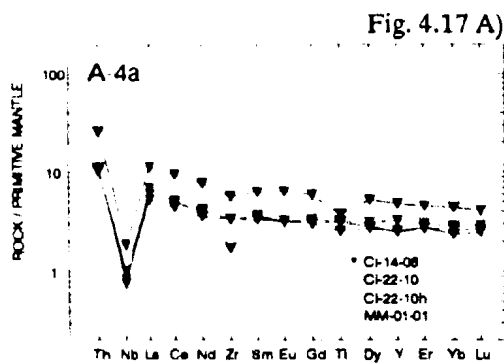
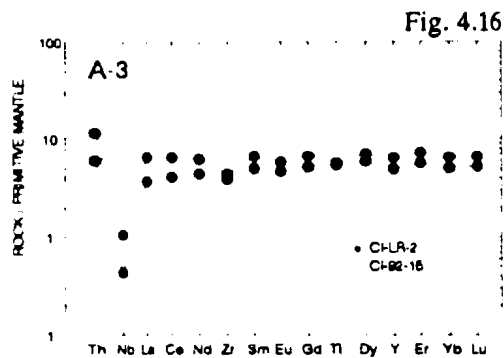


Figure 4.16. Extended multielement plots of the A-3 type samples. Note the characteristically strong arc signature (relative depletion in Nb) with respect to the A-2 type rocks.

Figure 4.17. Primitive mantle normalized extended REE patterns for the A-4 type rocks: A) high-Mg basalts of the A-4a subtype; and B) samples of the A-4b subtype.

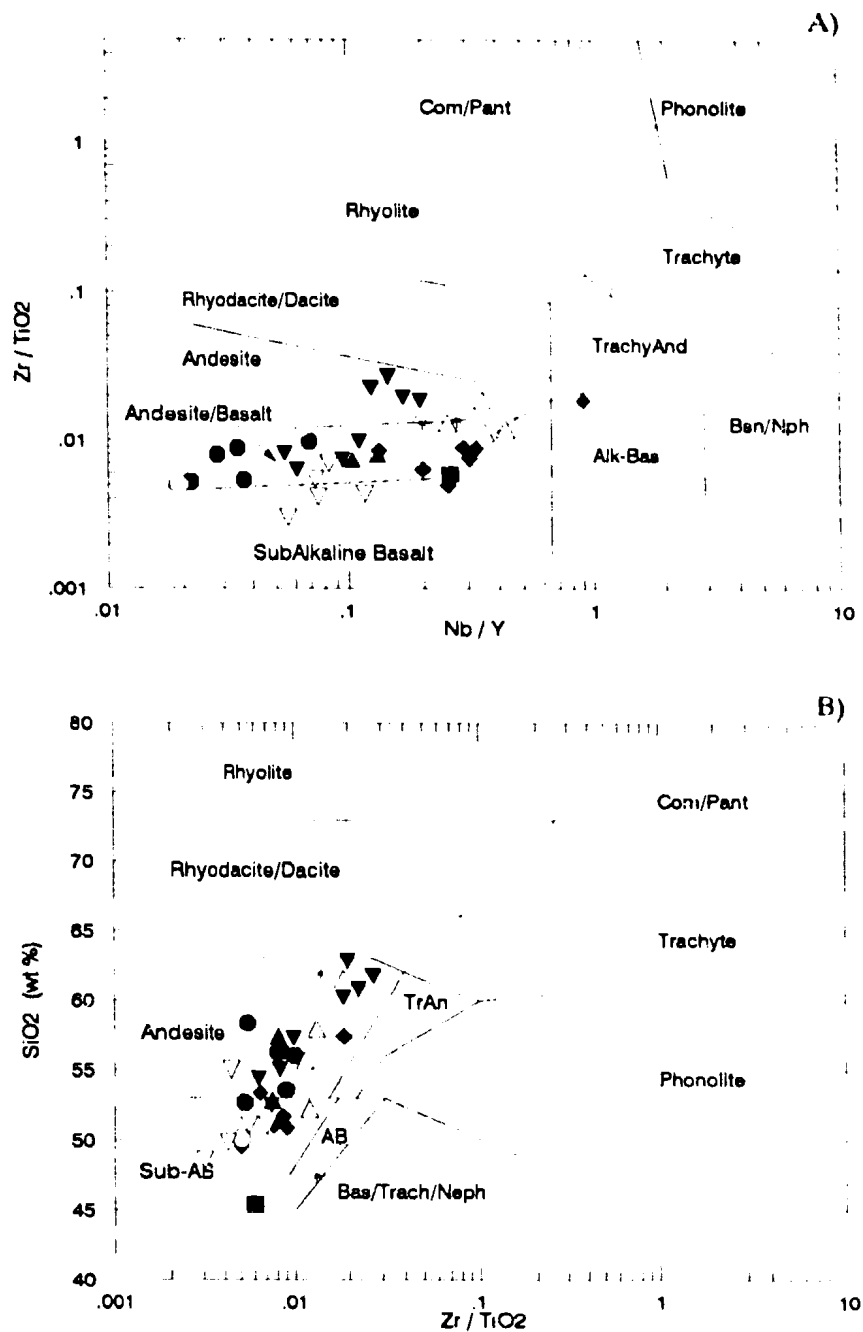


Figure 4.18. The Nb/Y-Zr/TiO₂ (4.18A) and Zr/TiO₂-SiO₂ (4.28B) diagrams (Winchester and Floyd, 1977) indicating the predominantly sub-alkalic character of mafic subvolcanic rocks of the western Notre Dame Bay area. The only sample showing a strong alkalic character is CI-01-14a.

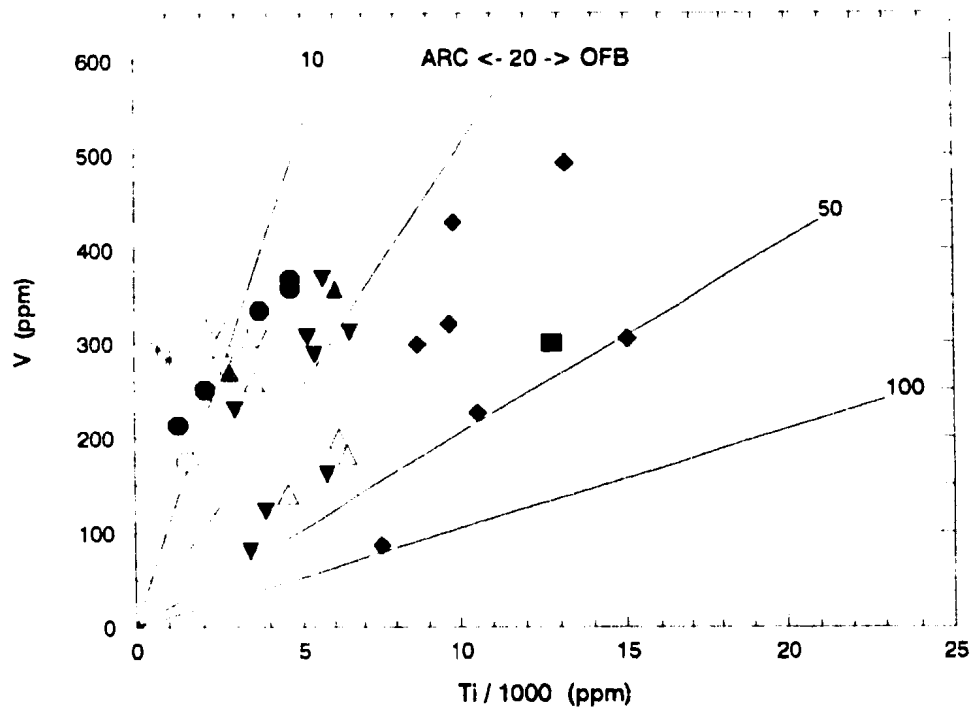


Figure 4.19. The Ti/1000 - V diagram of Shervais(1982) indicating two tectonic settings, an arc and non-arc, in which the mafic subvolcanic rocks of the western Notre Dame Bay area formed. OFB - ocean floor basalt.

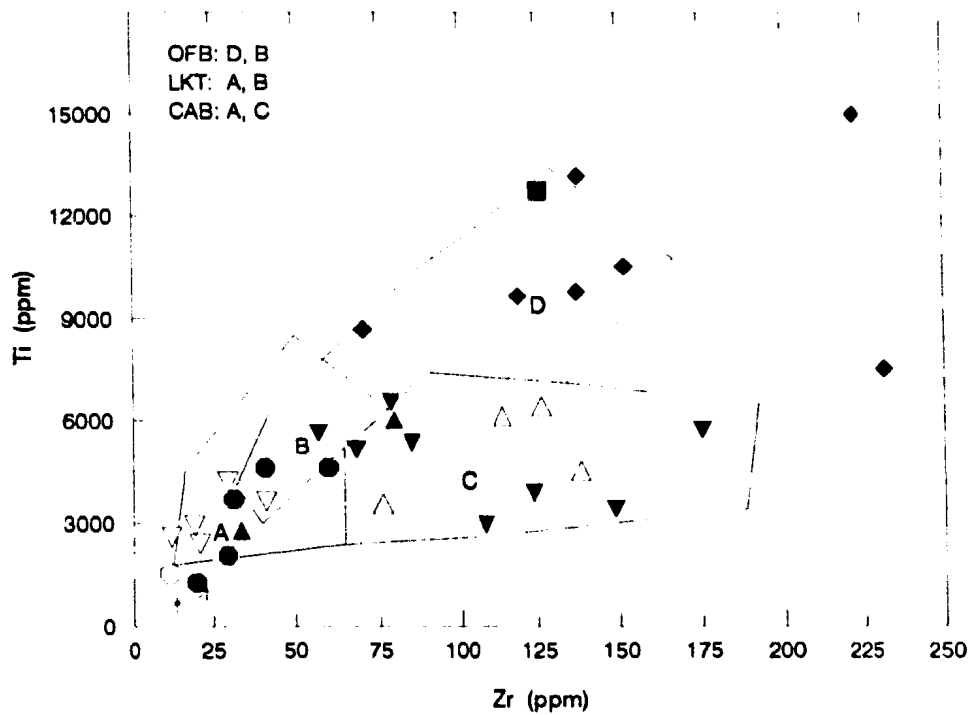


Figure 4.20. The Zr-Ti diagram of Pearce and Cann(1973). The same set of samples used in Fig. 4.24 plots here, as well, within fields that suggest origin of the samples in arc and non-arc tectonic settings. OFB - ocean floor basalt; LKT - low-K tholeiite; CAB - calc-alkalic basalt.

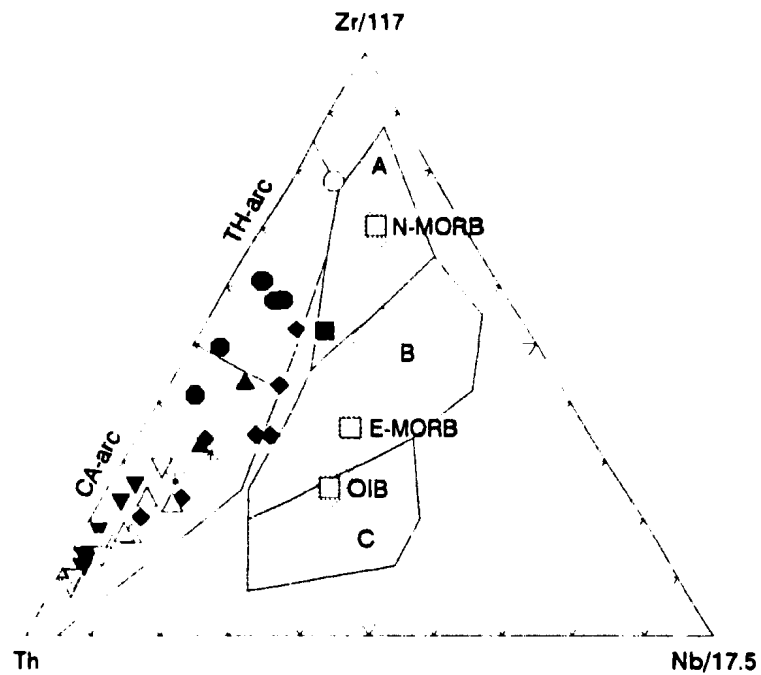


Figure 4.21. The Th-Zr-Nb diagram (from Wood,1988) for the western Notre Dame Bay area subvolcanic rocks. Rocks plot in two fields indicating origin in arc and non-arc environments, respectively. On this diagram, samples marked as filled diamonds and previously (Fig.4.19 and 4.20) presumed to be of oceanic affinity, plot within the arc field.

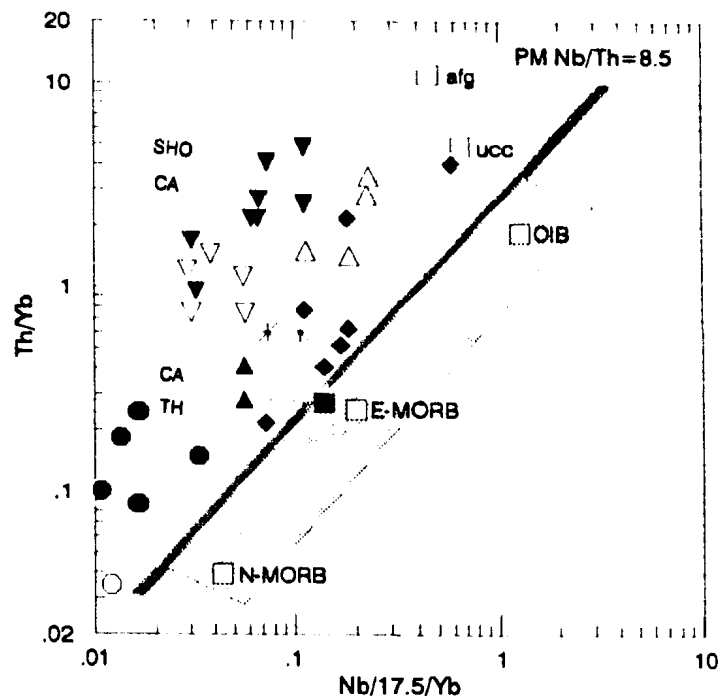


Figure 4.22. The Nb/Yb-Th/Yb diagram of Pearce(1983) supports the division of the samples into arc and non-arc types, and confirms the transitional character of samples marked as filled diamonds, which plot away from the mantle array and above the primitive mantle Nb/Th = 8.5.

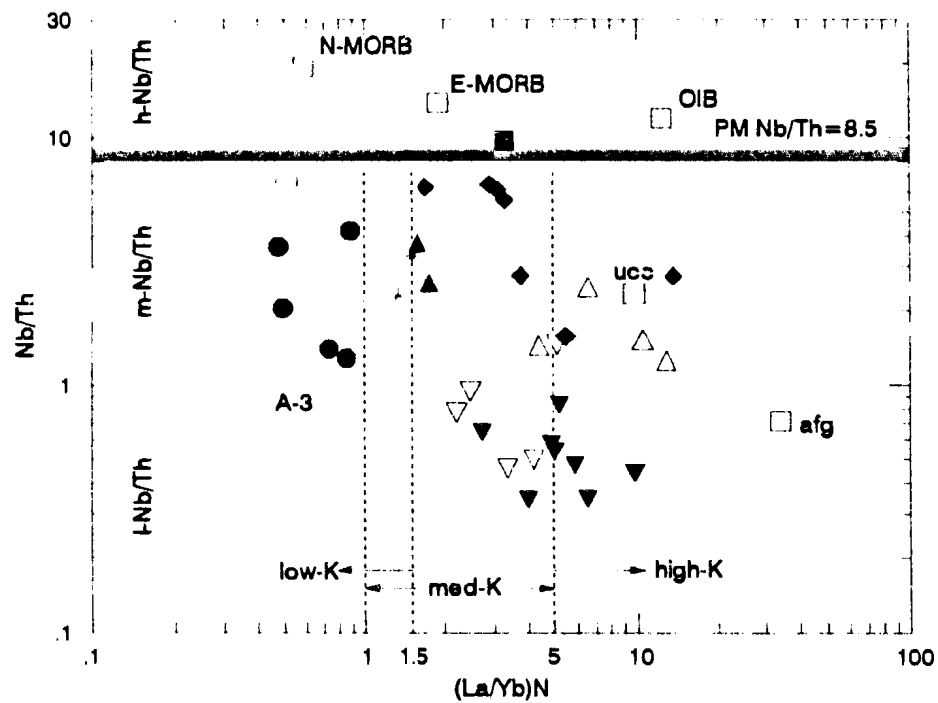


Figure 4.23. The $(La/Yb)_N$ -Nb/Th diagram illustrating divisions within the subvolcanic rocks, and correlations made with the previously recognized, different types of mafic volcanic rocks (Fig.4.10 and shaded outlines in this figure) of the western Notre Dame Bay area. A major division is made into arc (A) and non-arc (NA) rocks along the line representing primitive mantle Nb/Th ratio = 8.5 (Sun and McDonough, 1989). Additional divisions into low-, medium- and high-K arc rocks are from Swinden, 1987.

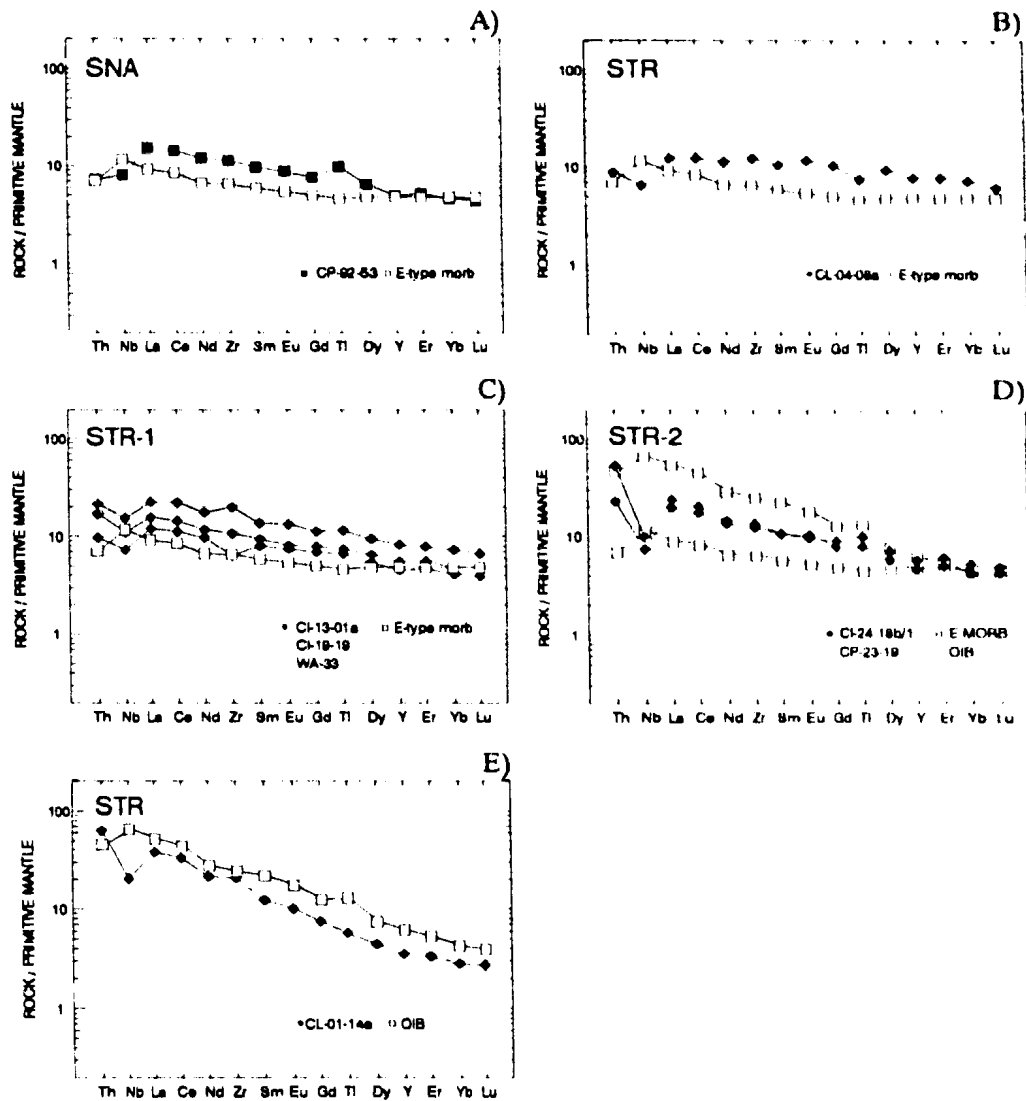


Figure 4.24. Extended primitive mantle-normalized REE plots of the SNA and STR type samples: A) sample CP-92-53 - a dyke from the Catchers Pond section of the Western Arm Group, included in the SNA type; B) sample CL-04-08a - stock or sill included in the STR type; C) samples combined in the STR-1 subtype; D) samples included in the STR-2 subtype; E) sample of an anomalous dyke CL-01-14a, that intrudes similarly atypical pillowcd flow CL-01-14 (Fig. 4.13 D).

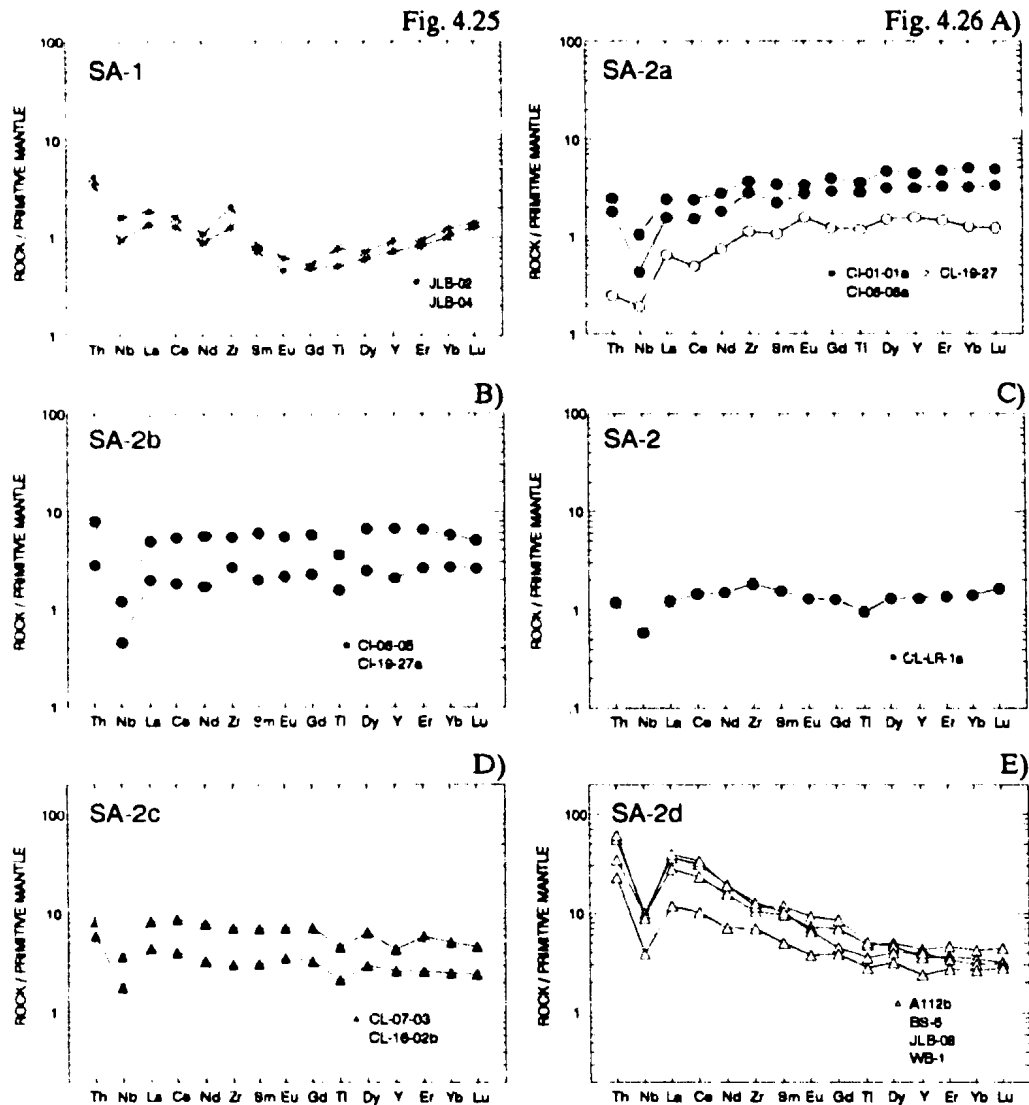


Figure 4.25. Multi-element primitive mantle-normalized REE patterns of the SA-1 type boninitic dykes.

Figure 4.26. Extended primitive mantle-normalized REE plots of the SA-2 type: A) depleted tholeiites of the SA-2a subtype, sample CI-19-27 is a gabbro clast from the Stag Formation, Breccia Member; B) tholeiites of the SA-2b subtype; C) sample CI-LR-1a of a gabbro intruding the Stag Formation, Breccia Member on League Rock; D) samples of the SA-2c subgroup; E) high-Mg dykes of the SA-2d subgroup.

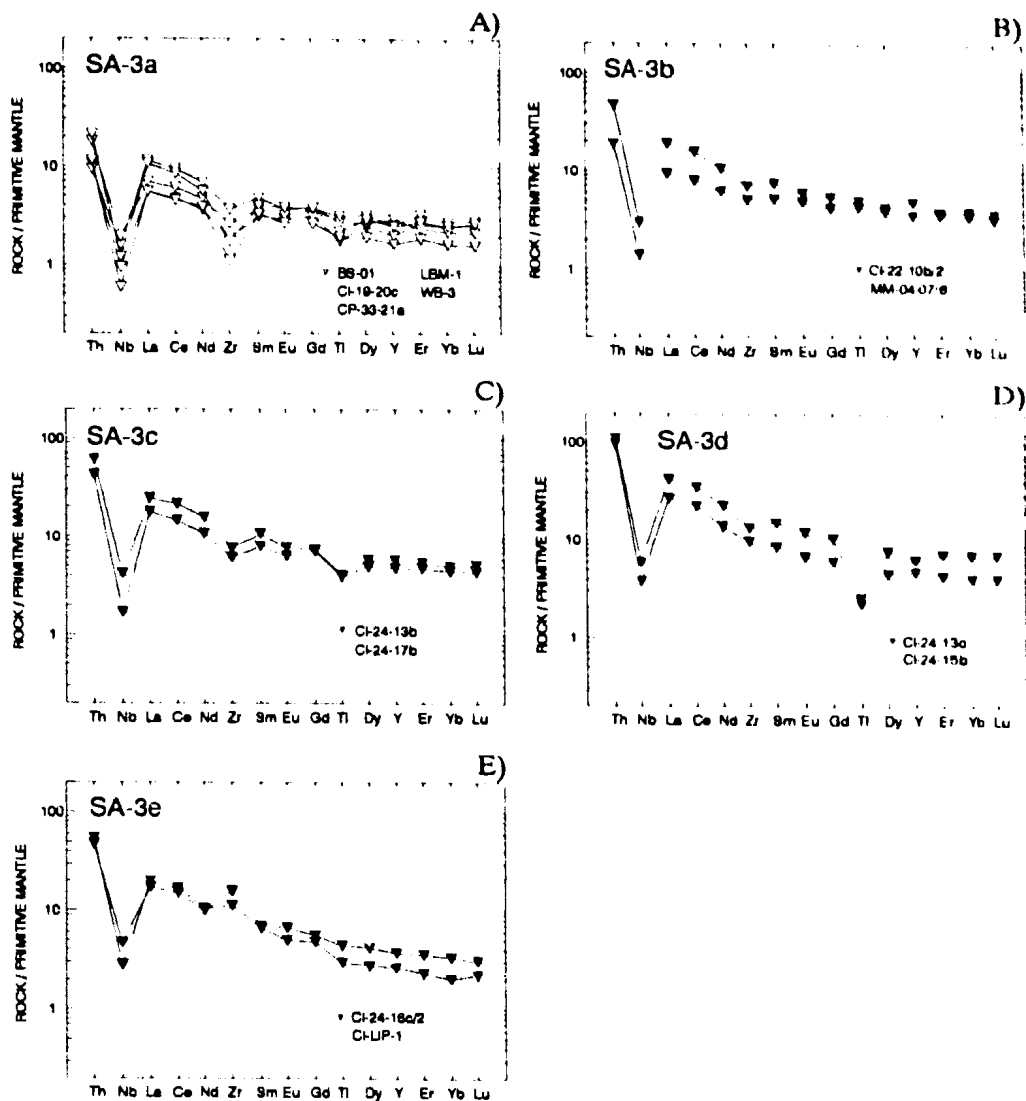


Figure 4.27. Extended primitive mantle-normalized REE plots of the SA-3 type: A) high-Mg dykes of the SA-3a subtype; B) dykes of the SA-3b subtype; C) dykes of the SA-3c subtype; D) dykes of the SA-3d subtype; E) intrusive rocks of the SA-3e subtype.

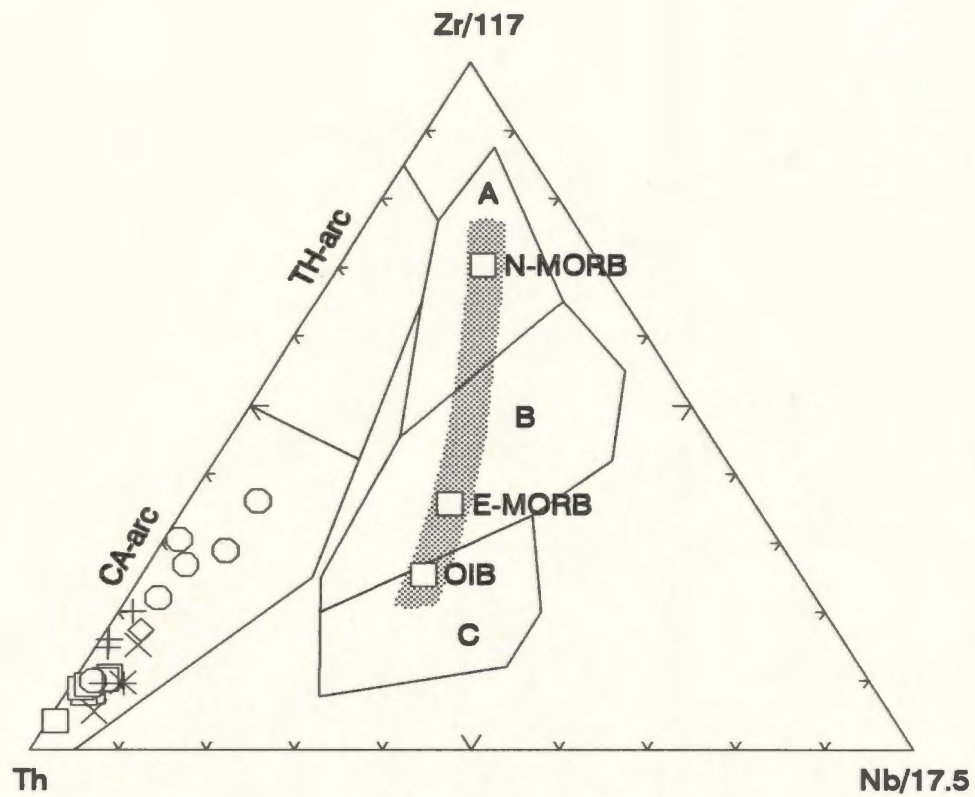


Figure 4.28. The Th-Zr-Nb discrimination plot (Wood,1980) for felsic volcanic and subvolcanic rocks of the western Notre Dame Bay area. Note that all samples plot within the calc-alkalic field.

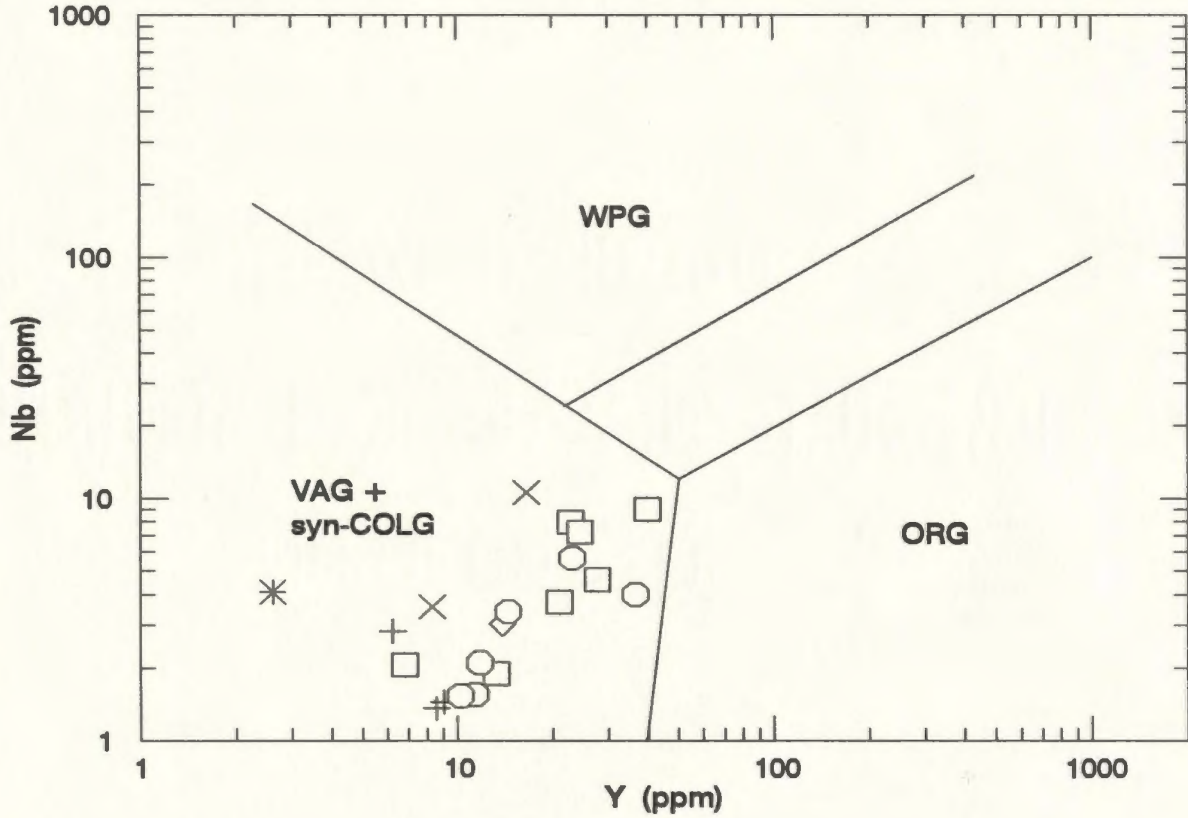


Figure 4.29. The Y-Nb diagram (Pearce et al., 1984) for felsic rocks of the western Notre Dame Bay area. This plot supports the affinity for all the studied felsic rocks with volcanic arc rocks.

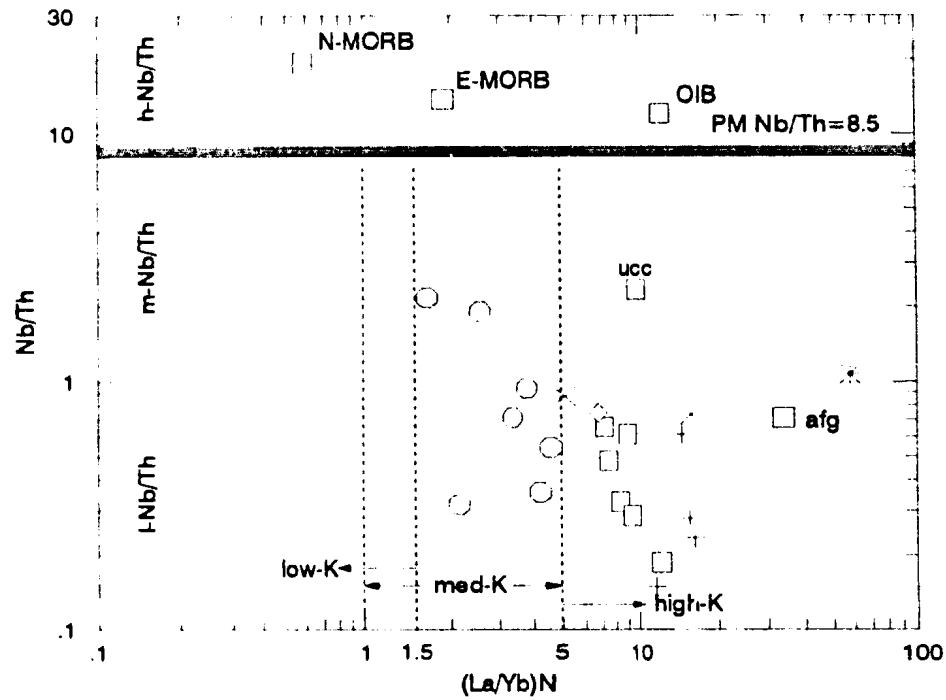


Figure 4.30. The $(La/Yb)_N$ -Nb/Th plot for felsic rocks of the western Notre Dame Bay area. Felsic rocks are clearly divisible into two main types: low-K and high-K. The low-K type consists of rocks from the Catchers Pond section of the Western Arm Group; whereas, the high-K type is dominated by the Cutwell Group felsic rocks. Two samples, CP-09-06 and CP-11-09, from the Welsh Cove Formation of the Western Arm Group plot with the high-K type samples. The post-kinematic dykes (crosses), the Brighton Complex diorite (asterisk) and the Coopers Cove/Colchester pluton samples (X) form the other high-K type samples.

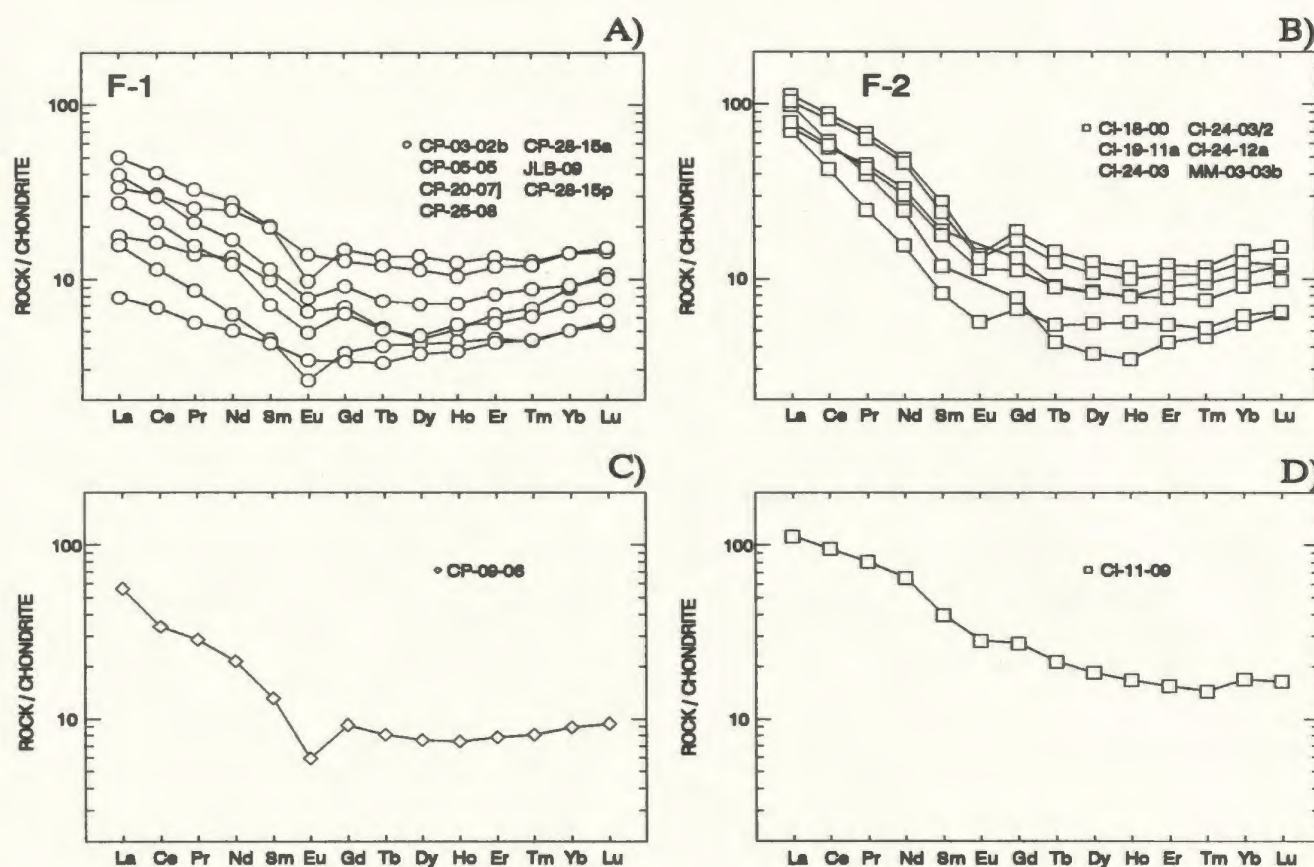


Figure 4.31. Chondrite normalized (Sun, 1982) REE plots of A) the F-1; and F-2 types of felsic rocks. Samples CP-09-06 and CI-11-09, of the Welsh Cove Formation, are characterized by REE patterns (C and D, respectively) broadly similar to that of the F-2 type samples.

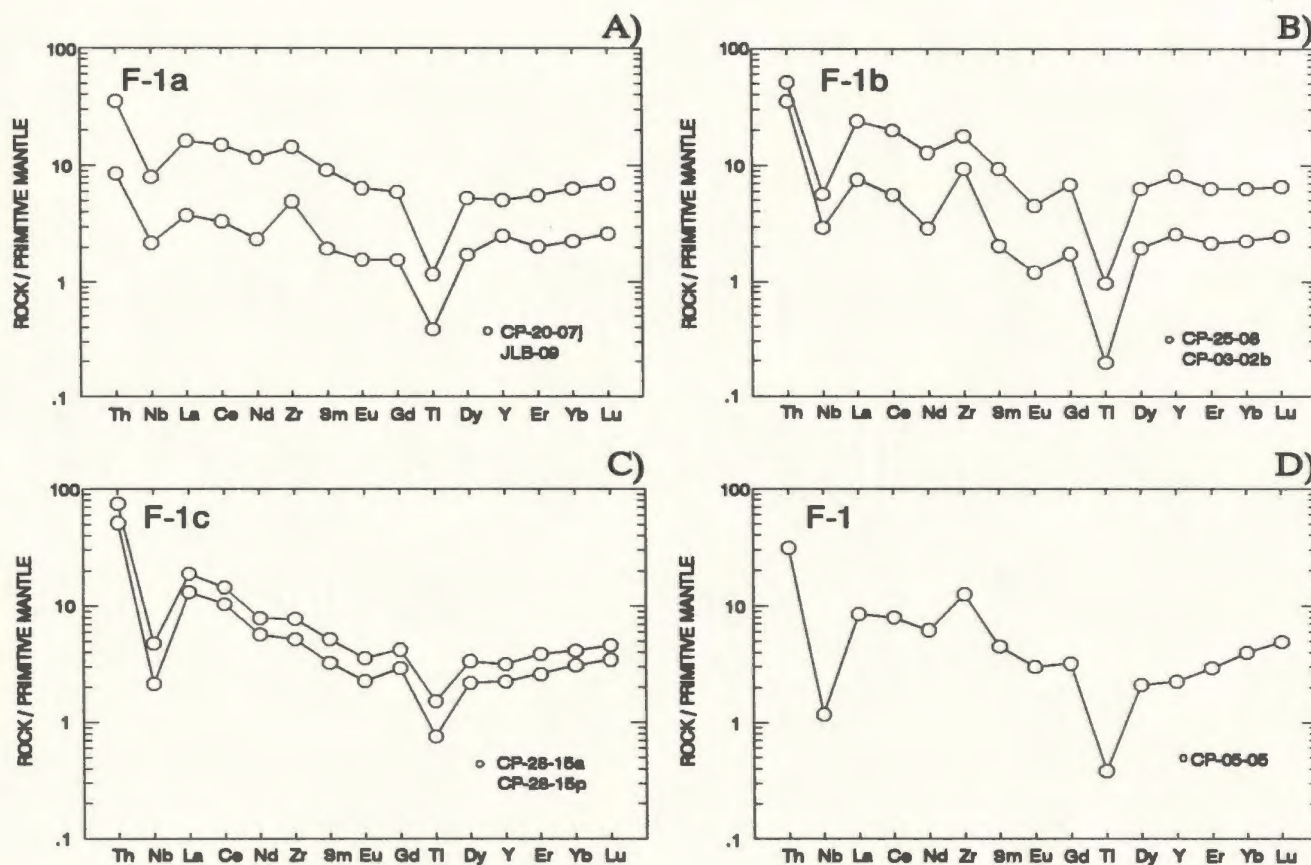


Figure 4.32. Extended multi-element plots of the F-1 type felsic volcanic and subvolcanic rocks: A) the F-1a subtype felsic rocks; B) the F-1b subtype felsic rocks; C) the F-1c subtype felsic rocks; and D) sample CP-05-05.

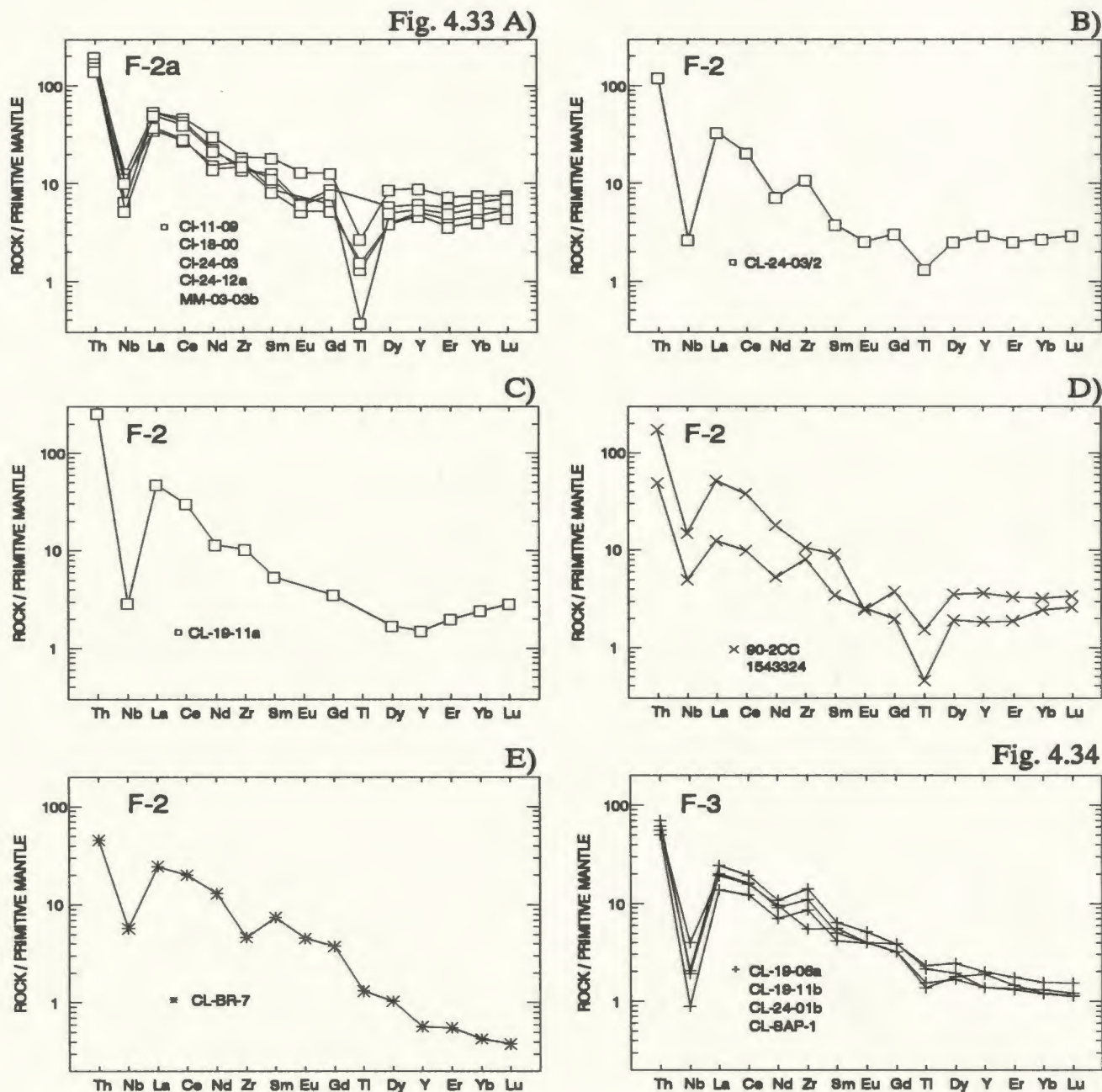


Figure 4.33. Extended multielement plots of the F-2 type felsic volcanic and subvolcanic rocks: A) the F-2a subtype felsic rocks; B) sample Cl-24-3/2; C) sample Cl-19-11a; D) sample CC-90/2 of the Coopers Cove diorite and sample 3324 of the Colchester diorite (the 3324 from Kean et al., 1994); and E) sample Cl-BR-7 of the Brighton Complex diorite.

Figure 4.34. Extended multielement plots of the F-3 type post-kinematic intrusive rocks.

CHAPTER 5: CHEMOSTRATIGRAPHY OF THE VOLCANIC ROCKS AND THEIR DETAILED PALEOTECTONIC SETTING

5.1 Introduction

The geochemical data presented in Chapter 4 indicate that rocks in the western Notre Dame Bay area were formed in both arc and non-arc environments. Close examination of the geochemistry also indicated the presence of rocks with "mixed" geochemical signatures, i.e. rocks transitional between arc and non-arc. Evidently, rocks in western Notre Dame Bay were formed in a range of tectonic settings. In order to interpret the tectonic settings from the geochemistry, it is first necessary to determine the relationship between lithostratigraphy and geochemical signatures in the area of study. Therefore, the first part of this chapter focuses on the correlation between geochemical rock types depicted in Chapter 4, and lithostratigraphic units presented in Chapter 3. Following this, present day tectonic settings are reviewed to find the best analogues for the western Notre Dame Bay area. Comparison with modern tectonic settings forms the basis for interpreting the various alternative tectonic environments in which these rocks may have been formed.

According to some of the tectonomagmatic discrimination diagrams used in Chapter 4, many of the NA-type rocks of the Western Arm Group are classified as "within plate", an affinity that is difficult to reconcile with the arc setting inferred for the spatially and temporally associated A-type rocks. Additionally, there are indications from some tectonomagmatic diagrams that some of the arc rocks may have been generated in a continental arc, rather than in an intra-oceanic setting. In order to resolve these issues, the comparison between geochemical aspects of the western Notre Dame Bay rocks and modern counterparts is followed by an attempt to explain specific characteristics of sources contributing to the western Notre Dame Bay lavas.

5.2 Geochemical Types Versus Lithostratigraphic Units

Figures 5.1a and 5.1b present schematic stratigraphic columns of the Lushs Bight / Western Arm groups, and the Stag Formation / Cutwell Group, respectively. Geochemical types of volcanic rocks as identified in Chapter 4 are shown on the left side of the column;

whereas, geochemical types of subvolcanic rocks are indicated on the right side of the column. The companion figure (Fig. 5.2) shows extended REE plots of volcanic rocks, tuffs and co-magmatic intrusive rocks, bracketed by stratigraphic divisions. Several observations can be made from these figures with respect to systematic changes in geochemical signature with stratigraphic position. Perhaps most striking is the trend of gradually increasing LREE with respect to HREE with increasing stratigraphic height. A second obvious feature is the presence of a well-defined arc signature only at the bottom and the top of the column (Fig. 5.2A), while the central part reveals interleaving of lavas with diverse tectono-magmatic signatures. Briefly, for each major lithostratigraphic unit, the other important observations are:

- 1) the Lushs Bight Group (Fig. 5.2A) - is dominated by strongly depleted and refractory arc lavas of the A-1 (boninitic) and A-2 (island arc tholeiite) types. Compared to the other units studied here, it appears to be relatively homogeneous; however, the more detailed sampling of this group by Kean et al. (1994) recognized somewhat more complexity with the island arc tholeiite suite. The A-1 type (boninites) is cut by dykes of the SA-1 type (also boninites). The relationship between the A-1 and A-2 groups is unclear; however, Kean et al. (1994) report that an A-2 type dyke cuts an A-1 lava.
- 2) the Cutwell Group (Fig. 5.2B)- is dominated by the LREE enriched arc lavas of the A-4 type and intruded by similar rocks of the SA-3 type. The STR-1 sills of the lower Pigeon Head Formation are the only type of igneous rock in this group that lacks a strongly developed negative Nb anomaly or island arc geochemical signature. The age of these sills has not been established by age dating; however, as documented in Chapter 3, they would appear to be of Ordovician age. The Pigeon Head Formation on Long Island is intruded by sills and dykes that are geochemically identical to those in the Welsh Cove Formation, Western Arm Group.
- 3) the Western Arm Group (Fig. 5.2A)- contains rocks that belong to NA, TR and A geochemical types. The NA and TR type flows interfinger in the Big Hill Basalt; whereas, in the overlying Welsh Cove Formation, felsic tuffs with arc

affinity are intruded by sills with transitional-type chemistry and dykes with non-arc type chemistry.

4) the Stag Formation (Fig.5.2B)- this unit is comprised dominantly of arc and non-arc lavas, cut by dykes with similar chemistry. The arc lavas are flat to slightly LREE - depleted island arc tholeiites. The non-arc lavas are E-MORB type lavas, unlike any other non-arc volcanic rocks in the area. The arc dykes with LREE-enrichment that cut this formation are the 493-498 Ma high-Mg dykes (type SA-3A).

(5) The distribution of geochemical types between the Lushs Bight and Western Arm Groups (Fig.5.2A) additionally suggests that, at least across the defined contacts, there is no definitive change in the chemistry of pillow lavas. Lavas with geochemical features similar to Lushs Bight Group flows are found as high-up as the Skeleton Pond Formation in the Western Arm Group. In the Stag Formation, such lavas are found within the Breccia Member and Upper Basalt Member, separated by E-MORB-type flows. Note that the cross-cutting of the Stag Formation by the high-Mg dykes further strengthens the comparison with the Lushs Bight and lower Western Arm Group. Taken altogether the geochemical evolution of these groups supports a very gradational or transitional change between the tectonic setting in the Lushs Bight and Western Arm groups and suggests that the Stag Formation represents a combination of these two lithostratigraphic units.

5.3 Comparison With Rocks From Modern Settings

Geochemical data presented in Chapter 4 and the preliminary screening of these using standard tectono-magmatic diagrams do not in themselves lead to a detailed interpretation of the tectonic environment(s) of the western Notre Dame Bay rocks. The "within plate" affinity of the NA-type rocks implied by some of these diagrams, is at odds with the setting invoked for the A-type rocks. The continental arc affinity for some arc samples does not fit well with field observations either. In addition, the complex association of geochemical types within some lithostratigraphic units shows clearly that the chemostratigraphy in the

study area is not straightforward. The chemostratigraphic order preserved in the Western Arm Group (i.e. from bottom to top, NA-, A-, NA- and TR-, and A-type rocks again) is not easily interpreted in terms of a simple tectonic history. Neither is the apparent coexistence of flows with diverse non-arc and arc signatures within a single lithostratigraphic unit that does not show any evidence of major structural complication (i.e. Stag Formation or Cutwell Group).

In order to allow for the possibility that lavas with particular geochemical characteristics may have erupted in more than one tectonic environment, the rocks of the western Notre Dame Bay area are briefly compared to the widest range of volcanic lavas with equivalent geochemical features, regardless of tectonic setting. The order in which the rocks are described is the same as in Chapter 4, i.e. rocks of non-arc affinity and transitional rocks are discussed first, followed by those of arc affinity.

5.3.1 TYPES NA AND TR - "NON-ARC" AND TRANSITIONAL VOLCANIC ROCKS

Samples displaying a geochemical signature with non-arc and transitional affinities are geochemically similar to a wide range of volcanic rocks erupted at mid-ocean ridges (e.g. Schilling et al., 1983; Jenner and Hertogen, 1986), rifts and aseismic ridges associated with mantle plumes (e.g. Humphris et al., 1985), hot spots/ocean islands and in some marginal basins (e.g. Jenner et al., 1987; Hawkins et al., 1990).

5.3.1.1 The NA-1 Type

The NA-1 E-MORB type tholeiites are characterized by chemical features similar to those of volcanic rocks erupted from the "anomalous" ridge segments at numerous locations along the Mid-Atlantic Ridge (MAR) (e.g. Schilling et al., 1983; Humphris et al., 1985). In particular the NA-1 samples closely resemble lavas from the MAR segment between 44° and 47°N, both in terms of major element chemistry and REE patterns (Fig. 5.3A).

Lavas akin to E-MORB have also been identified in many back-arc basins. For example, sills and lava flows cored at ODP sites 794 and 797 in the Japan Basin (Allan and Gorton, 1992), are very similar to the NA-1 samples in terms of REE patterns and other geochemical characteristics (Fig. 5.3B). The Japan Sea lavas display only a minor

positive Th inflection reflecting perhaps their poorly developed, subduction-related signature (Kaneoka, 1990; Allan and Gorton, 1992; Pouclet and Bellon, 1992). REE patterns of the NA-1 samples also closely resemble samples dredged from spreading axes of the Scotia Sea Rise (Hawkesworth et al., 1977; Saunders and Tarney, 1979), Mariana Trough (e.g. Hawkins and Melchior, 1985; Sinton and Fryer, 1987; Hawkins et al., 1990; Stern et al., 1990), and Ogasawara Trough (Ikeda and Yuasa, 1989; Fryer et al., 1990; Hochstaedter et al., 1990a,b). The Scotia Sea Rise lavas differ, however, from the NA-1 flows in having significantly higher La/Nb ratios = 1.0-2.2, probably indicating the presence of a negative Nb anomaly. Many of the Mariana and Ogasawara Trough samples show a pronounced Nb depletion associated with LFSE and LREE enrichment (Fig. 5.3C), both interpreted to result from addition of a subduction or arc component to the otherwise MORB-like source (Hawkins and Melchior, 1985; Hawkins et al., 1990; Hochstaedter et al., 1990b).

The NA-1 samples display considerable similarity in incompatible element ratios and REE patterns to "intra-plate oceanic" or "hot-spot"-like flows of Esmeralda Bank, a submarine volcano on the edge of the Mariana Arc and Mariana Trough (Stern and Bibee, 1984). The NA-1 rocks are, as well, comparable to tholeiites of Mauna Loa (Fig. 5.3D), an ocean island volcano (Basaltic Volcanism Study Project, 1981).

5.3.1.2 NA-2 And TR-Type Rocks

The NA-2 type flows have particularly good analogues amongst flows erupted from "anomalous" segments of ridges associated presently and in the past with mantle plumes/hot spots.

5.3.1.2.1 NA-2 a

A close match for the NA-2a subgroup rocks and their TR kin, CI-16-01, is found among samples dredged from the MAR segment between 47° and 52°N (Fig. 5.4A), a plume segment located south of the Charlie-Gibbs Fracture Zone (Schilling et al., 1983). Another good analogue for the NA-2a flows are lavas from the southern segment of MAR between 32°S and 46°S (Fig. 5.4B), an area under the influence of the Tristan da Cunha mantle plume (Humphris et al., 1985). The NA-2a samples have FeO*/MgO ratios slightly higher than MAR

rocks (1.5-1.7 vs. 0.9-1.5, respectively) and exhibit slightly elevated V and Zr/Y ratios, as well as somewhat lower P_2O_5 and Sm/Nd ratios with respect to those from the MAR.

Two localities associated with mantle plumes on the Pacific floor provide more analogues for the NA-2a lavas, the spreading center located near the Galapagos hot-spot (Fig. 5.4C) (Schilling et al., 1982) and the Tamayo Fracture Zone (Fig. 5.4D)- transform fault displacing the East Pacific Rise (EPR) near the mouth of Gulf of California (Saunders et al., 1982; Bender et al., 1984). Both have erupted lavas with REE patterns and chemical characteristics similar to those of the NA-2a type rocks, although minor differences between these were noted. The NA-2a rocks are characterized by slightly higher Al_2O_3 content (at given MgO), and partly lower FeO^* , Ti and Zr abundances.

Extended REE patterns and most other chemical aspects of the NA-2a samples closely resemble the lower sill unit from ODP hole #794 in the Yamato Basin, Sea of Japan (Fig. 5.4E) (Allan and Gorton, 1992; Pouclet and Bellon, 1992). The Japan Sea is a marginal basin formed by crustal thinning and rifting of a continental volcanic arc (proto-Japan arc) in the mid-Tertiary (Tamaki et al., 1990; Tamaki et al., 1992), and the Yamato Basin in the southern part of the Sea is founded on extended continental crust. Genesis of the Yamato Basin tholeiites, classified as back-arc basin basalts (Pouclet and Bellon, 1992), is attributed to contributions from two mantle sources: a) depleted mantle (depleted N-MORB source); and b) enriched mantle (OIB-type source). Isotopic and geochemical data reveal only a minor addition of crustal (Kaneoka, 1990) or subduction (Allan and Gorton, 1992; Pouclet and Bellon, 1992) component to the resulting magmas, reflected in a slight Th inflection on extended primitive mantle-normalized REE plots (Fig. 5.4E).

There are few reported lavas in modern intraoceanic back-arc basins similar to the NA-2a flows. Although, many lavas erupted at spreading centres in the Mariana-Izu and Tonga back-arc basins have REE patterns very similar to the NA-2a (Fig. 5.4F), they also exhibit distinctive differences in terms of their

major and trace element chemistry, including well-defined negative Nb anomalies, enrichment in Th, the relatively low HFSE - features that are characteristic of island arc tholeiites rather, than MORB (Jenner et al., 1987; Hochstaedter et al., 1990b; Vallier et al., 1991).

5.3.1.2.2 NA-2b

The NA-2b rocks also have adequate analogues at present day spreading centres. Two such centres have erupted lavas particularly similar to the NA-2b samples, the spreading center of the Galapagos Platform (Fig.5.5A) that is associated with a mantle plume (Schilling et al., 1982), and the spreading ridge in the Guaymas Basin (Fig.5.5B), Gulf of California (Saunders et al., 1982; Sawlan, 1991), although the NA-2b samples are somewhat more fractionated than their modern equivalents. Authors working on these regions have provided various explanations for the relatively high La/Yb ratios in the lavas. Schilling et al. (1982) concluded that the Galapagos hotspot is enriched in H₂O and LFSE, and that the enrichment in volatiles would lower the melting point of the mantle and broaden the depth range of partial melting, resulting in tapping of a variably metasomatized upper mantle. The mantle underlying the Guaymas Basin and the central part of the Gulf of California is also thought to be metasomatized and contain a minor sub-continental (calc-alkalic) component inherited from prolonged arc volcanism in that region (Saunders et al., 1982; Sawlan, 1991). This has resulted in the eruption of transitional rift tholeiites with La/Yb and Zr/Ti ratios, and contents of low field strength elements (e.g Ba, Sr) that are higher than, for example, those from the mouth of the Gulf of California or East Pacific Rise, where there is no history of arc volcanism.

5.3.1.2.3 NA-2c

Volcanic rocks with REE patterns and trace element chemistry similar to the NA-2c subtype have been found among basalts erupted from spreading centres in the Yamato Basin (Fig.5.5C), Sea of Japan, and in Hawaii (Fig.5.5D). This type of rock is thought to have a major input from an asthenospheric source (Nohda et al., 1988; Tatsumi et al., 1989; Basaltic Volcanism Study Project,

1981). A group of sills enriched in incompatible elements from Yamato Basin seems to be a particularly good match for the NA-2c samples on the basis of the shape of extended REE patterns (Fig.5.5C) and trace element ratios, although the NA-2c samples are more fractionated than their Yamato equivalents and possess somewhat higher abundances of HFSE. These sills, cored in ODP holes #794 and #797, intrude sediments on both sides of the Yamato spreading center (Yamato Basin) (Allan and Gorton, 1992; Pouclet and Bellon, 1992), and although found to be broadly similar to rocks from other marginal basins (Allan and Gorton, 1992), are linked by Pouclet and Bellon (1992) to "continental initial rifting".

The Hawaii samples from Mauna Loa (Basaltic Volcanism Study Project, 1981), which display extended REE plots broadly similar to those of the NA-2c samples (Fig.5.5D), are considered to be typical ocean island tholeiites generated during the main shield-building stage (e.g. Clague, 1987), and to represent uncontaminated partial melts of the plume source (e.g. Wilson, 1989). The NA-2c samples have similar trace element ratios to these Hawaii analogues, but higher concentrations of Cr and Nb, and lower concentrations of the HREE.

Lavas with some NA-2c type chemical signatures are found in settings other than oceanic spreading centres. For example, Palaeocene volcanic plateau lavas of Skye, part of the British Tertiary Igneous Province (Thompson and Morrison, 1988) formed during the opening of the North Atlantic Ocean, reveal similar chemical characteristics to the NA-2c samples (Fig.5.5E). Skye magmas are interpreted to have been derived from an asthenospheric source, and were variably contaminated by overlying lithosphere during ascent (e.g. Thirlwall and Jones, 1983; Thompson and Morrison, 1988). REE patterns and trace element ratios of the NA-2c samples overlap with the least-contaminated Skye lavas, but they have somewhat higher HREE abundances and lower Nb than comparable lavas from Skye.

The TR-1 type volcanic rocks have REE patterns that are almost identical to their non-arc counterparts (NA-2b and NA-2c types). For most aspects of the TR-type samples, as was the case for the NA-type rocks, the best geochemical analogues are basalts erupted in rift environments, both intraoceanic such as Galapagos (Schilling et al., 1982), and intracontinental such as the Guaymas Basin (Saunders et al., 1982). However, the TR-type samples typically exhibit more pronounced negative Nb and positive Th anomalies compared to NA-type rocks, and this appears to preclude an origin at intraoceanic spreading ridges or ocean islands. Marginal basin environments are considered to be the most likely setting of their formation.

5.3.1.2.4 TR-1a

The closest analogues from modern back-arc basins for the TR-1a samples, in terms of extended REE patterns, Sm/Nd ratios and Nb abundances, are found in the Ogasawara Trough (Fig.5.6A), a nascent back-arc behind the Izu-Ogasawara arc (Ikeda and Yuasa, 1989; Hochstaedter et al., 1990a&b). The Ogasawara Trough rocks are characterized by REE patterns that show affinity to E-MORB, but their relatively low Ti/V, Nb, Ti and Zr are characteristic of island arc tholeiites. The Izu-Ogasawara back-arc lavas are thought to result from variable mixing of E-type MORB, which may be generated at rift initiation, and depleted IAT magmas (Ikeda and Yuasa, 1989, Hochstaedter et al., 1990a,b). One of the simplistic scenarios for mixing is envisaged by Ikeda and Yuasa (1989): (1) the depleted IAT magma, that supplies the active arc, is derived from depleted mantle and slab-derived components; (2) the rising mantle diapir brings about back-arc extension, induces melting and formation of the E-type MORB melt, and obstructs upward penetration of the IAT magma; (3) both depleted IAT and E-MORB magmas mix prior to eruption.

Lavas erupted on the Valu Fa spreading ridge (Lau Basin) are somewhat similar to the TR-1a samples and Izu-Ogasawara back-arc lavas, but less LREE-enriched. They exhibit distinctive differences with respect to MORB in their major and trace element chemistry, including well-defined negative Nb

anomalies and enrichment in Th. These characteristics of the Valu Fa lavas have been explained by mixing of depleted mantle with either a small amount of sediment and fluid derived from subducted slab or with older arc lithosphere (Jenner et al., 1987; Vallier et al., 1991). Some workers have described a similar Nb anomaly in the Mariana Trough lavas (Fig.5.6B). Hawkins et al. (1990) proposed that these lavas represent variable mixing of a Mariana island-arc source mantle with a MORB-source mantle whereas Sinton and Fryer (1985) suggested metasomatism of the back-arc mantle source by partial melts of altered crust and/or subducted sediments, and by fluid transport.

The TR-1b flows are strikingly similar in their extended REE patterns and other geochemical characteristics, although they exhibit somewhat lower Ti and V contents, to sills from ODP hole #797 on the floor of the Yamato Basin (Fig.5.6C). The TR-1b subtype flows are also comparable in terms of their multi-element plots and many ratios to lavas associated with mantle plumes and contaminated by continental crust such as Skye (Fig.5.6D) (Thompson and Morrison, 1988) and Deccan (Fig.5.6F) (Mahoney, 1988; Lightfoot et al., 1990). The only evidently alkalic sample in the TR group, CI-01-14, is markedly similar in its extended REE pattern to the international standard BCR-1 (Fig.5.6F), representing the Columbia River flood basalts.

In summary, the NA-type lavas show a strong affinity to MOR basalts, and specifically to those erupted from "anomalous" segments of spreading ridges. Many of these rocks also display a close similarity to the products of within plate volcanism. However, their TR counterparts have better analogues in flows from back-arc basins, particularly those in an incipient or immature stage of evolution (e.g. Ogasawara Trough, Mariana Trough, Lau Basin), as well as in flows from young and more mature marginal basins (e.g. Gulf of California and Japan Sea, respectively). The TR-type samples also show a close geochemical similarity to magmas associated with mantle plumes that underwent crustal contamination during ascent, such as those from Deccan and Skye.

5.3.1.3 Type A - Arc Volcanic And Subvolcanic Rocks

5.3.1.3.1 A-1

The A-1 type rocks reveal REE patterns that are typical of boninites. Boninites are unusual high-Mg rocks, usually of Tertiary age and found in several western Pacific island areas/islands such as the Bonin Islands, Papua New Guinea, New Caledonia, the Mariana Trench, the Tonga ridge (e.g. Kuroda et al., 1978; Jenner, 1981; Hickey and Frey, 1982; Bloomer and Hawkins, 1987; Falloon and Crawford, 1991; Murton et al., 1992; Pearce et al., 1992). Boninites are thought to be associated exclusively with intraoceanic arc settings and their genesis has generally considered been linked to the onset of subduction (e.g. Hickey and Frey, 1982; Beccaluva and Serri, 1987; Bloomer and Hawkins, 1987; Pearce et al., 1992). However, more recent studies emphasize the fact that magmas with boninitic affinities have been found at various stages of arc evolution (e.g. the Izu-Bonin forearc; Murton et al., 1992), and rocks with some geochemical features of boninites have been recovered from actively spreading back-arc basins (e.g. the Lau Basin, Falloon et al., 1992). In terms of geochemical characteristics, the best analogues to the A-1 samples are boninites from the type locality, in the Bonin Islands (Fig. 5.7A) (e.g. Hickey and Frey, 1982; Murton et al., 1992; Pearce et al., 1992), which have characteristic features such as very low abundances of MREE, HREE, and most HFSE, and a positive Zr anomaly. The enrichment in Th, LREE and Zr with respect to other REE and HFSE is widely interpreted to reflect the addition of a subduction-related component to a very refractory source region. The somewhat peculiar enrichment in Zr and its fractionation from other HFSE, Nd and Sm, is not seen in other arc-related rocks. It has recently been suggested that the concave-upward shape of the boninite REE pattern reflects the role of amphibole during fractionation (Murton et al., 1992; Pearce et al., 1992).

5.3.1.3.2 A-2a

It is particularly difficult to find good modern analogues for the strongly depleted samples in the A-2a subtype. This may reflect the fact that strongly depleted volcanic rocks are commonly associated with the early stages of arc evolution, the record of which is generally buried in the volcanic pile or incorporated into arc crust (e.g. Stern et al., 1989). Nevertheless, a few occurrences of such rocks have been reported from a number of localities. Rare earth element profiles of the A-2a samples show close similarities with two strongly depleted rocks from the East Halmahera Ophiolite (Eastern Indonesia) (Fig. 5.7B) described by Ballantyne (1991) and referred to as "boninites". Although not boninites *sensu stricto*, they do reveal some similarities to low-Ca boninites of Crawford et al. (1989). The A-2a subtype rocks display some resemblance to REE profiles of boninites from DSDP site 458 (Hickey and Frey, 1982), but differ in most of the HFSE ratios. They are similar to strongly depleted arc tholeiites recovered from the trench wall at the intersection between the Mariana and Yap trenches (Crawford et al., 1986).

5.3.1.3.2 A-2b

Similarly, very few modern volcanic edifices have yielded lavas matching those of the A-2b samples. One area is from the Kermadec island arc, where REE patterns of some lavas are similar to the A-2b samples (Fig. 5.7C) (Ewart and Hawkesworth, 1987), although the Kermadec samples display relatively pronounced LREE enrichment with respect to the A-2b. A variably depleted MORB-like source in the mantle wedge of the Kermadec islands was postulated by Ewart and Hawkesworth (1987).

5.3.1.3.2 A-2c

Flows geochemically similar to the A-2c subgroup samples are rarely found in modern island arcs, but similar rocks do occur in the Mariana (Fig. 5.7D) (Bloomer et al., 1989; Lin et al., 1989) and Tonga (Fig. 5.7E) (Ewart and Hawkesworth, 1987; Falloon et al., 1987) island arcs. Two of the Tonga samples were dredged from the trench wall, and the Mariana samples are from the older, southern part of the arc. In both arcs, this type of flow is interpreted

to be associated with an early stage of arc evolution. There is a relatively good overlap of REE patterns between the A-2c samples and those from both modern arcs.

5.3.1.3.2 A-2d

Volcanic rocks with REE and chemical characteristics of the A-2d subtype are somewhat more common in modern arc settings. Selected samples from Ata Island (Fig. 5.8A) (Tongan arc; Vallier et al., 1985, 1991), Fiji (Gill, 1987) and the Scotia arc (Hawkesworth et al., 1977) have REE patterns that parallel and/or overlap with those of the A-2d subtype, although the A-2d samples have higher Ti and Zr/Ti ratios than Ata and Scotia's rocks, and are matched in terms of those elements only by samples from Fiji. IAT-like basalts recovered from back-arc spreading centres of the Tonga (Fig. 5.8B), Izu-Ogasawara (Fig. 5.8C) and Mariana (Fig. 5.8D) back-arc basins (Jenner et al., 1987; Ikeda and Yuasa, 1989; Fryer et al., 1990; Hochstaedter et al., 1990a, b; Vallier et al., 1991) form much better analogues to the A-2d lavas. The similarity of these back-arc basalts to IAT is variously interpreted to result from mixing of E-type MORB and depleted IAT magmas (Ikeda and Yuasa, 1989; Hochstaedter et al., 1990a, b), by mixing of depleted mantle with the slab derived fluid, or by contamination of mantle derived melts with older arc lithosphere (Jenner et al., 1987; Vallier et al., 1991).

5.3.1.3.2 A-2e and A-2e(t)

Flows with chemical features similar to the A-2e and A-2e(t) rocks are present, and locally common, in the oceanic island arcs of Fiji (e.g. Gill, 1987; Gill and Whelan, 1989) and the Marianas (Hole et al., 1984; Bloomer et al., 1989; Lin et al., 1989). Shoshonitic to calc-alkalic flows from Fiji that display extended REE patterns similar to the A-2e and A-2e(t) rocks (Fig. 5.9A) are linked to volcanic activity arising from rifting of the Vitiaz arc (Gill and Whelan, 1989). The Fiji flows differ from the A-2e lavas and A-2e(t) tuffs only in having higher P_2O_5 abundances and in slightly lower Zr and Ti concentrations.

Flows from the central part of the Mariana arc show a very good correspondence of extended REE patterns (Fig.5.9B), including HFSE, with those of the A-2e subtype. These lavas are interpreted to have been derived from a relatively depleted mantle that was enriched by alkali-rich hydrous fluids, underwent melting within the stability field of spinel lherzolite, and then underwent various amounts of low pressure fractionation (Lin et al., 1989; Bloomer et al., 1989; Woodhead, 1989). The lavas compared here with the A-2e and A-2e(t) rocks are typical of the mature central part of the arc and are not like the enriched shoshonitic rocks of the northern, submarine part of the arc (Lin et al., 1990).

REE patterns of the A-2e and A-2e(t) samples are also rather similar to lavas erupted from volcanoes in the southern volcanic zone of the Andes (Fig.5.9C) (Hickey et al., 1986). In particular, the A-2e and A-2e(t) rocks display a similarity to basaltic lavas from volcanoes located on thinner continental crust from 38°-41° S. Geochemical characteristics of the Andean lavas are often explained by variable mixing of two components, one of which is derived from subducted crust (thought to be characterized by high ratios of Th and alkaline earth elements to REE and HFSE) and the other from enriched mantle similar to OIB source or subcontinental lithosphere (Hickey et al., 1986). However, an important contribution to the genesis of these magmas may also be from mid- and upper-crustal melts and intracrustal coexistent assimilation and fractional crystallization (AFC; De Paolo, 1981) (Hildreth and Moorbath, 1988). According to Hildreth and Moorbath (1988) the role of the crust is reflected in the rise of Th and Ce/Yb with the thickness of crust; whereas, the increase in the Ce/Yb ratio probably results from suppression of HREE by garnet (Hildreth and Moorbath, 1988).

5.3.1.3.3 A-3

REE profiles and most chemical features of the A-3 group samples are reminiscent of lavas from the Tonga and Kermadec arcs (Falloon et al., 1987; Ewart and Hawkesworth, 1987). They are also somewhat like lavas of the Valu

Fa Ridge, Lau Basin, in which a well defined Nb anomaly indicates the presence of a slab-derived component in the back-arc basin mantle source (Jenner et al., 1987; Vallier et al., 1991). REE patterns of the A-3 samples are subparallel to those of the Valu Fa Ridge samples (Fig.5.10), although they are less fractionated than their modern counterparts and differ from them in the lower Ti, Zr and Zr/Y, and higher V.

5.3.1.3.4 A-4

Ankaramitic flows included in the A-4a subtype have only a few modern analogues in little fractionated, medium- to high-Mg lavas, that are considered to represent parental or primitive magmas, and are rarely exposed in island arcs. Ankaramites from Western Epi, Vanuatu (Fig.5.11A) (Barsdell and Perry, 1990), the ID1 picrite from Okmok Volcano, Aleutians (Fig.5.11B) (Nye and Reid, 1986), and the parental magma compositions calculated for the picrites of New Georgia (Solomon Islands; Ramsay et al., 1984) are particularly good analogues for the A-4a samples in terms of REE patterns. The A-4a ankaramites are more fractionated than most of these counterparts, but have similar Ti and Zr contents, and generally slightly higher Zr/Y ratios than their analogues.

Samples of the A-4b subtype have a wide range of modern analogues, that are associated with both intraoceanic and continental arc settings. Volcanic rocks comparable to the A-4b samples have been recognized amongst flows of the Rechesnoi Volcano, Aleutians (Fig.5.12A) (Miller et al., 1992), Sunda arc (Fig.5.12B) (Stolz et al., 1990) and the Southern Volcanic Zone of the Chilean Andes (Fig.5.12C) (Hickey et al., 1986; Ferguson, et al., 1992). Despite the similarity of their REE patterns, each of these rock sets represents a different magma series. Basalts of the Rechesnoi Volcano form a calc-alkalic trend whereas selected samples of the Sunda suite contain both tholeiitic and calc-alkalic volcanics and the fairly uniform suite of Andean flows possesses characteristics transitional between tholeiitic and calc-alkalic rocks. Samples of the A-4b subtype show a reasonably good match of REE patterns to all three

modern suites. However, they are more fractionated and have higher FeO^*/MgO than rocks from Andes and Aleutians (1.7-2.7 vs. 0.8-1.8, respectively) suites. The A-4b rocks show good agreement in Zr/Ti ratios with Andean samples, similar Zr/Y ratios to Sunda rocks, and the lowest Ti/V values in comparison to all those counterparts.

Other good analogues for the A-4b samples are shoshonitic, rift related lavas of Fiji (Gill and Whelan, 1989), mildly shoshonitic lavas from the northern Mariana arc (Fig. 5.12D) (Bloomer et al., 1989; Lin et al., 1989). The shoshonitic lavas of the northern Mariana arc are thought to be derived from a source which is similar to that of OIB (Lin et al., 1989). All these volcanic suits display a reasonably good fit of REE patterns with those of the A-4b type samples, and an overlap of Zr/Ti, Zr/Y ratios, and to a degree Ti/V ratios.

The A-4b type lavas resemble the wide range of ankaramites, alkali basalts and basanitoids from the islands of Grenada (Fig. 5.12E) and Martinique, Lesser Antilles (Shimizu and Arculus, 1975; Thirlwall and Graham, 1984; Davidson, 1986), displaying a good conformity of REE patterns, and similar Zr/Ti, Zr/Y and Ti/V ratios and element contents, although the A-4b rocks are relatively strongly fractionated and have higher FeO^*/MgO ratios. Samples of the Martinique and Grenada suites are interpreted to be derived from magmas that assimilated continentally-derived sediment (Thirlwall and Graham, 1984; Davidson, 1986).

There is also a good similarity in geochemical signatures between the A-4b samples and flows of the Bushe Formation in Deccan (Fig. 5.12F), which are interpreted to be strongly contaminated by upper continental crust (Mahoney, 1988; Lightfoot et al., 1990). Although geological relationships show that this is clearly not a viable analogue for the A-4b rocks, the geochemical similarity to contaminated flood basalts is pointed out here to emphasize the possibility of input from similar sources and/or processes in generating magmas parental to the A-4b type rocks.

5.3.1.4 Subvolcanic High-Mg Andesites

The majority of subvolcanic rocks of the western Notre Dame Bay area are geochemically similar to their volcanic counterparts (see chapter 4), and suggest the same modern analogues. However, among these subvolcanic rocks there are a significant number of unusual high-Mg dykes, assigned to the SA-2c, SA-2d and SA-3a types. Similar dykes were described by Kean et al. (1994) who noted that they post-date the main eruptive events in the Lushs Bight Group. Some of these dykes are characterized by concave-upward, boninitic-like REE patterns. Samples of the SA-2d type match some rare modern high-Mg andesitic rocks termed "bajaites", the sporadic occurrence of which (Baja California, S.Chile, Aleutians) is linked to the termination of subduction resulting from a ridge-trench collision (e.g. Saunders et al., 1987, Rogers and Saunders, 1989). Rogers and Saunders (1989) speculated that an extensional crustal regime may be necessary to allow the high-Mg magmas to rise to the surface while retaining their primitive character. REE and extended REE patterns of the SA-2d type dykes display a particularly good correspondence with some samples from the Baja California region (Fig.5.13A) (e.g. Saunders et al., 1987; Rogers and Saunders, 1989), and show, as well, a good analogy in various trace element ratios and FeO^*/MgO . On the other hand, dykes of the SA-3a type display a relatively close similarity to a particular class of modern high-Mg andesites named sanukitoids (Fig.5.13B) (considered to represent primary andesitic magmas), that occur in southwest Japan (e.g. Tatsumi and Ishizaka, 1982). Tatsumi and Maruyama (1989) observed that sanukitoids are generated in tectonic settings similar to that of boninite formation, i.e. near the trench and during the subduction of a hot and young lithosphere. These authors pointed out that the short-lived high-Mg magmatism apparently occurred immediately after initial back-arc opening.

Rogers and Saunders (1989) did not view the high-Mg magmas as primary

5.3.1.5 Felsic Volcanic And Subvolcanic Rocks

Felsic rocks of the western Notre Dame Bay area display well defined concave-upward REE patterns. The multi-element plots of the F-1 type low-K rhyolites are characterized by almost flat HREE segments, and a positive slope in the enriched MREE and LREE. The patterns are similar to those of felsic rocks from modern island

arcs such as the tonalite - trondhjemite Tholo suite of Fiji and rhyolites from the Bismarck Arc (Gill and Stork, 1979; Smith and Johnson, 1981). Figures 5.14A and 5.14B illustrate normalized F-1 type patterns compared with the field of low- to medium-K rhyolites from New Britain (Smith and Johnson, 1981) and low-K trondhjemites from Fiji (Gill and Stork, 1979). Ewart (1979) pointed out a correlation between the chemistry of felsic eruptives and their tectonic setting and concluded that low-K orogenic rhyolites are presently found primarily within intraoceanic island arcs (S.W. Pacific, Tonga-Kermadec), but also in regions underlain by young or subcontinental type crust (e.g. Taiwan, Japan). An almost perfect match for the F-2 type felsic rocks is found among high-K rhyolites from New Britain (Fig.5.14C) (Smith and Johnson, 1981).

Dacitic and rhyolitic tephra with somewhat concave REE patterns similar to those of the F-1 and F-2 types samples are present in the central Aleutians (Romick et al., 1992). REE profiles within the suite of Aleutian volcanic rocks are interpreted to show a clear indication of amphibole involvement in their genesis; yet only some of them contain hornblende phenocrysts whereas many contain exclusively pyroxene phenocrysts. This has led some authors to conclude that these rocks evolve in a complicated (open) system in which the hornblende-phyric rocks erupted from a magma that rapidly migrated through the upper crust; whereas, pyroxene-phyric tephra were derived from magmas that experienced a prolonged residence in the crust, during which hornblende was replaced by pyroxene.

5.4 Sources And Processes Contributing To The Notre Dame Bay Magmas

The presence of more siliceous, andesitic to rhyolitic rocks in addition to A-type basalts, in the Western Arm Group favours its interpretation as an ancient arc environment, and excludes settings of magmatism such as intra-oceanic rifts and ocean islands, even though some NA-type rocks show a strong similarity to rocks formed in the latter settings.

Volcanic rocks of the western Notre Dame Bay area with geochemical signatures indicating an arc setting, display geochemical similarities to two types of arcs, intraoceanic and continental. The "intraoceanic" affinity of many of the western Notre Dame Bay area

arc samples is in good agreement with widespread field evidence for subaqueous deposition of the volcanic rocks. There is no compelling field evidence for any subaerial volcanism in the western Notre Dame Bay area. In an intraoceanic arc this would not be surprising, since intraoceanic volcanoes are consistently affected by erosion, which removes not only the central, but also most of the proximal and part of the distal, facies before they are buried in the stratigraphic column (e.g. Francis, 1983). However the lack of a subaerial component in a continental setting is difficult to explain, and in order to be credible, the interpretation of the continental arc affinity of some samples needs to be demonstrated in a more satisfying manner, and then convincingly explained.

For over a decade some petrologists (e.g. Arculus and Johnson, 1981; Gill, 1981, Pearce, 1983; Arculus and Powell, 1986; Ellam and Hawkesworth, 1988; Hawkesworth et al. 1991; McCulloch and Gamble, 1991) have advocated that arc magmas show evidence for contributions from several sources, that include: the mantle wedge; subducted oceanic crust and sediment; fluids derived from the subducted lithosphere; and the possibility of input from assimilated continental crust and continentally-derived sediment (see also Chapter 4).

Although the geochemical results of Chapter 4 show that the broad environment in which the western Notre Dame Bay rocks were formed is an arc environment, an important question is: Was it an intraoceanic or continental arc? To answer this question, it is critical to try to identify all potential sources contributing to the western Notre Dame Bay lavas. Recognition of these sources may help to additionally constrain and more accurately interpret the tectonic settings of volcanic rocks in this area.

5.4.1 MELTING OR FRACTIONAL CRYSTALLIZATION?

Geochemical effects of fractional crystallization may be difficult to distinguish from effects resulting from variable degrees of melting of a homogeneous source. Various diagrams have been presented in the literature that illustrate the qualitative behaviour of trace elements during these processes (e.g. Pearce and Flower, 1977; Pankhurst, 1977, Minster and Allegre, 1978; O'Hara and Mathews, 1981). Use of these types of diagrams can help identify processes involved in the petrogenesis of the western Notre Dame Bay magmas.

The LaN versus (La/Yb)_N, LaN versus (La/Sm)_N, and to a degree the Sm/Nd-Nd, variations reflect differences in the shape and slope of REE patterns and are employed here to analyze the processes leading to the observed geochemical variation in the various magmatic types recognized within the western Notre Dame Bay rocks. On the LaN-(La/Yb)_N plot, partial melts of different sources, such as spinel lherzolite and garnet lherzolite, define linear trends with very different slopes (e.g. Pankhurst, 1977; Allegre and Minster, 1978; Lin et al., 1989). The horizontal trend is predicted for steady-state products of a periodically replenished magma chamber (PRMC; e.g. O'Hara and Mathews, 1981; Langmuir, 1989).

On the LaN-(La/Yb)_N and LaN-(La/Sm)_N process identification plots (Allegre and Minster, 1978; Minster and Allegre, 1978), the majority of geochemical types recognized within the western Notre Dame Bay rocks form relatively scattered trends (Fig. 5.15), none of which is readily interpreted as simply varying degrees of melting of a homogeneous source as illustrated by the modelled trends. However, even these scattered trends have one common feature, a general positive correlation between (La/Yb)_N and LaN (less so in the NA-type rocks). This increase in LREE with respect to HREE may indicate that varying degrees of melting of one heterogeneous or several sources may be, amongst other processes, involved in the formation of magmas from which these rocks were derived. In the case of the NA-type rocks, a dominant control by fractional crystallization, on the evolution of these magmas, is suggested by the approximately subhorizontal trend.

On the companion plot, the LaN-(La/Sm)_N, an oblique trend in the western Notre Dame Bay area rocks suggestive of control by partial melting processes is less apparent, and most of the A-4b subtype trend is subparallel to the fractional crystallisation trend. It appears that both melting and fractionation may have exerted some control on the evolution of the western Notre Dame Bay lavas (and tuffs). It is also possible that other, more complex processes affected them as well.

Incompatible elements are used to determine sources supplying material to the lavas from the western Notre Dame Bay area. Extensive low pressure fractionation may work

to conceal geochemical signatures of source regions, but it should not affect the highly incompatible elements.

5.4.2 THE SOURCES

5.4.2.1 The Mantle Wedge

Arc related magmas are generally considered to be generated in the mantle wedge above a subduction zone. The mantle wedge is thought to be composed of refractory or depleted N-MORB mantle (Jenner, 1981; Pearce, 1983; Arculus and Powell, 1986; Ellam and Hawkesworth 1988;), although some authors argue on the basis of isotopic data, that more enriched E-MORB and OIB sources are present and contribute to arc magmas (e.g. Stern, 1981; Morris and Hart, 1983; Stern et al., 1991).

As Ellam and Hawkesworth (1988) simply stated, the observed fractionation between LFSE and HFSE and the distinctive trace element geochemistry of subduction related basalts, cannot readily be generated by melting processes in equilibrium with common mantle phases. For that reason most widely accepted arc petrogenetic models involve the mantle wedge being metasomatized by LFSE-rich fluids originating from the subducting oceanic lithospheric plate. A number of researchers believe that the mantle beneath arcs may be metasomatized in a manner similar to mantle beneath the continents (e.g. Foley and Wheller, 1990). Many of the mantle-derived peridotite xenoliths found in lavas associated with magmatism within continental plates, and less commonly in the arc environment, contain veins of LFSE-rich hydrous amphibole and/or phlogopite (e.g. Lloyd et al., 1985; Tatsumi et al., 1986; Defant et al., 1991; O'Reilly et al., 1991); thus attesting to mantle metasomatism by a fluid phase. The presence of phlogopite in the mantle wedge is thought to reflect addition of a siliceous hydrous fluid phase or siliceous melts added from a subducting slab to an otherwise strongly depleted mantle. The fluid phase is inferred to originate from the breakdown of hydrous phases (amphibole) in the altered MORB, and to be LFSE-enriched and HFSE-depleted (Hole et al., 1984; Tatsumi et al., 1986; Ryerson and Watson, 1987). There is also evidence that Nb, Ta and Ti depletion in arc magmas may be related to such a fluid phase since at least some ultramafic mantle xenoliths display depletion in these elements (Shimizu, 1987; Defant et al., 1991). However, some mineral phases in

metasomatized spinel lherzolites show enrichment in particular trace elements. For example apatite tends to strongly concentrate Th and high levels of REE, whereas amphibole and mica have a strong affinity for Nb and Ta (O'Reilly et al., 1991).

The relative enrichment in LREE and constant or decreasing HREE can be explained by fractionation of an assemblage in which hornblende or garnet is a major constituent. Hornblende fractionation is a very effective suppressant of HREE (e.g. Gromet and Silver, 1987), but to be effective and not to leave petrographic evidence, hornblende fractionation must occur during deep - crustal processes (Hildreth and Moorbath, 1988). Alternatively, a similar effect can be obtained by interaction with wall rocks containing these phases. As pointed by Hildreth and Moorbath (1988), interaction of primitive basalts with hornblende-rich lower-crustal rocks, by assimilation and/or reaction with the wall-rock or by mixing with silicic partial melts of the latter, will result in suppression of HREE.

The crust beneath the Cambro-Ordovician "arc(s)" that produced the western Notre Dame Bay rocks was clearly very rich in gabbroic-tonalitic intrusions as evidenced by extensive hornblende-bearing intrusive clasts in the Stag Formation breccia. These indicate that even at a relatively early stage (pre-506 Ma; see Chapter 3) of the western Notre Dame Bay arc(s) evolution, a significant amount of water was most likely transported into the mantle in a form of a fluid phase from subducted crust, and subsequently by mantle-generated basaltic magma into lower crust (e.g. Takahashi, 1986; Hildreth and Moorbath, 1988).

5.4.2.2 Depleted Or Enriched Mantle Source? - The Th/Zr-Nb/Zr Plot

In light of the view that more enriched E-MORB and OIB sources may contribute to arc magmas (e.g. Stern, 1981; Morris and Hart, 1983; Stern et al., 1991) (instead of a dominant role for depleted or refractory N-MORB mantle), an important question is: Do the western Notre Dame Bay magmas reflect only a depleted mantle source, or did an enriched mantle end-member contribute to their petrogenesis as well? The Nb/Zr ratio is a potentially effective tool in evaluating this question (e.g. Pearce and Norry, 1979; Edwards et al., 1991; Pearce et al., 1992) whereas the Th/Zr ratio is sensitive to addition of continental crust.

The Nb/Zr against Th/Zr diagram is presented in Figure 5.16, with samples from several present day tectonic settings Figure 5.16B, D (for reference), and the western Notre Dame Bay area samples plotted in Figure 5.16A (arc affinity), C (non-arc and transitional affinity). The western Notre Dame Bay samples of non-arc affinity exhibit a marked increase in Nb/Zr at almost constant Th/Zr relative to N-MORB. The TR samples plot in a similar fashion, but show a minor shift away from the trend defined by the NA-type samples and mantle array (typical N-MORB and E-MORB) and several samples on the higher Nb/Zr end of the trend also have higher Th/Zr.

The A-2d lavas form a short trend parallel to the mantle array, but removed towards slightly higher Th/Zr. A cluster of the A-2e and A-2c(t) samples is clearly separated from the array of the NA rocks. A few samples included in these subgroups have both ratios elevated due to low Zr values (see Chapter 4). An entirely opposite behaviour is revealed by the group A-4 samples, which show an irregular trend marked by an increase in Th/Zr in a relatively narrow range of Nb/Zr values.

The Th/Zr-Nb/Zr plot suggests that an enriched mantle component was indeed present in the NA and TR magma sources. The enriched mantle might have contributed to the source of the A-2E lavas, but such input, if any, may have been partially obliterated by contamination by upper continental crust, as it is documented for the Deccan lavas in Figure 5.16D. If there was any input from the enriched mantle into the source region of the A-4 type lavas, then evidence of it has been wiped out by a contribution from other sources and/or processes, which shall be identified below.

5.4.2.3 Evidence For Mantle Metasomatism - (Th/La)_N-(La/Yb)_N Relationship

More information with respect to the nature of source(s) supplying arc magmas can be obtained from the LFSE/LREE relationship, as LFSE behaviour is independent of fractionation, at least under lower pressure conditions (e.g. Kay, 1984). A high Ba/La ratio is characteristic of modern island arc volcanic rocks, and is interpreted to reflect the high Ba/La of fluid phases derived from dehydration of subducting slab (e.g. Davidson, 1986; Lin et al., 1989; Defant et al., 1991). A number of authors (e.g. Saunders et al., 1980; Hole et al., 1984; Tatsumi et al., 1986) have presented arguments for mantle source metasomatism by a LFSE-rich, REE-depleted, possibly siliceous fluid

phase which may represent the dehydration product of the subducting slab. Tatsumi et al. (1986) have shown that Nb is most likely not soluble, and that Ti and Zr would have exceedingly low concentrations in the fluid phase. Other characteristics of such a fluid phase may include enrichment in Si and Al (Schneider and Eggler, 1986).

Ryerson and Watson (1987) calculated that up to 87% of the Th in the sources of island arc magmas may be metasomatically introduced, and anticipated even more extreme addition of Cs, Rb and Ba. Th is also, besides Rb, the element with the strongest affinity for the continental crust (Allegre and Lewin, 1989), and, in particular, for the upper crust (Taylor and McLennan, 1981). Amongst the LFSE, Th is the only element which appears to resist postmagmatic alteration.

The relationship of Th with respect to REE in the western Notre Dame Bay lavas is illustrated on the $(Th/La)_N$ versus $(La/Yb)_N$ plot. Three major trajectories reflecting processes that are expected to influence behaviour of Th and the REE in the arc environment are shown schematically in Figure 5.17A and C. The horizontal trajectory parallel to the E-MORB - OIB segment of the mantle array illustrates a decreasing degree of partial melting; the diagonal trajectory connects MORB sources with the continental crust field (defined by the upper Archaean crust, McLennan, 1992; upper continental crust, McLennan, 1992), and the third, vertical trajectory represents metasomatism by a fluid with an extremely high $(Th/La)_N$ ratio and low $(La/Yb)_N$ ratio.

On the $(Th/La)_N$ - $(La/Yb)_N$ diagram, the western Notre Dame Bay samples with an arc affinity plot along a diffuse diagonal trend that extends from above the origin towards upper right corner of the diagram. This trend is at high angle to the mantle array and approximately along the mixing line between N-MORB and the composition representing average upper continental crust.

Samples in some geochemical subtypes of mafic volcanic rocks form well defined linear trends approximately normal to the main trend and display a relatively wide range of $(La/Yb)_N$ ratios. It seems unlikely that these trends are formed in response to fractional crystallization of some phase, but this interpretation relies heavily upon presently available K_d values. The only phases which have K_d 's suitable to impose

these trends are plagioclase and apatite (e.g. Irving and Frey, 1984). An unacceptably high degree of plagioclase fractionation would be required to produce such trends and this hypothesis is rejected here on the basis of geochemical (lack of corresponding large negative Eu anomalies) and petrographic (most of the flows retain plagioclase) evidence. Apatite fractionation from lavas of the western Notre Dame Bay area is also considered to be unlikely as P_2O_5 does not reach the suitable saturation level in mafic lavas (Green and Watson, 1982); moreover, apatite tends to strongly concentrate Th (O'Rielly et al., 1991).

The distribution of the data in the linear trends perpendicular to the mantle-crust "mixing" line and extending towards high $(La/Yb)_N$ values implies that Th is derived from, and its behaviour may be controlled by, a different source than La (and by default the remainder of the LREE) and Yb. Such a source enriched in Th and depleted in REE is clearly different from that expected from the upper continental crust and MORB. According to the presently accepted ideas, the only source that fits these conditions is the slab component. The composition of a potential dehydration product of subducted altered oceanic crust was calculated by Hole et al. (1984) and shown to be enriched in Th and other LFSE, and strongly depleted in REE. It appears that such a component (liquid or melt) would be appropriate in modifying potential mantle source regions for the western Notre Dame Bay area magmas. Perhaps the most convincing argument is the fact that the Lushs Bight Group boninites also form a well defined trend towards the high Th/La ratio as evinced on Figure 5.17B.

The $(Th/La)_N - (La/Yb)_N$ plot indicates that there may be three distinct sources that contributed directly or indirectly to the western Notre Dame Bay area lavas. The Th-poor, low $(La/Yb)_N$ source is represented by depleted N-MORB mantle source. It is likely that such depleted mantle was metasomatized by a similarly REE-poor, but Th-rich fluid phase, similar to the one envisaged by Hole et al. (1984), resulting in formation of a composite source. The second source has MORB characteristics and displays a range from T-MORB to strongly enriched E-MORB, but it is clearly distinct from the OIB source. The third source, characterized by high $(Th/La)_N$ and high

(La/Yb)_N, may be the upper continental crust or a sediment derived from the continental crust

5.4.2.4 More Metasomatism: Melt Or Fluid? - Nb Vs. Nb/Th Relationships

There is strong evidence, based upon the behaviour in (Th/La)_N-(La/Yb)_N space of some of the western Notre Dame Bay samples, that a metasomatizing fluid(s) rich in Th was one of the principal agents modifying the mantle. However, there is little agreement in the literature as to the character of those metasomatizing agents. Some favour melts over a metasomatic fluid phase as agents of mantle enrichment (e.g. Brophy and Marsh, 1986). Ryerson and Watson (1987) estimated that melts derived from dehydrated subducted slab will have Nb/Th values similar to that of the mantle wedge (and MORB), but low degree hydrous partial melts of the slab will exhibit a reduced Nb/Th ratio, because of enhanced TiO₂ solubility (rutile is thought to withhold Nb in the source). They modelled hybridization of the mantle source with a rutile-bearing MORB quartz eclogite, similar to the one proposed by Brophy and Marsh (1986), and graphic results of that modelling are applied here to the western Notre Dame Bay lavas on the Nb-Nb/Th diagram.

In Figure 5.18 the compositions of the Notre Dame Bay area lavas are compared to the calculated lines representing mixing of the MORB-depleted mantle with slab-derived melt for two different fractions (0.05 and 0.2; Ryerson and Watson, 1987). The mixing lines indicate that the Nb/Th ratio is controlled by the slab-derived melt and that this control decreases with increasing degree of melting of the slab. Although some of the western Notre Dame Bay samples plot within the field defined by these mixing lines, they are arranged in several trends that are at high angles to the calculated mixing lines and emphasize the generally positive correlation between Nb and Nb/Th in the western Notre Dame Bay arc lavas.

If Nb/Th systematics are closely similar to that of Nb/U, as suggested by Ryerson and Watson (1987), then the interpretation of Vukadinovic and Nicholls (1989) may shed some light on what type of a medium metasomatized the mantle source to the western Notre Dame Bay rocks. These authors proposed that behaviour such as that observed in Figure 5.18 results from the decreased ability of metasomatizing fluids to

affect the Nb/U ratio in the mantle with high abundances of Nb and U. This behaviour of the western Notre Dame Bay rocks of arc affinity is identical to that observed by Vukadinovic and Nicholls (1989) in Nb-Nb/U space for Indonesian island arc basalts, and indicates that the Nb/Th ratio in the western Notre Dame Bay rocks is dominated by a slab-derived, high-Th hydrous fluid rather than melt.

5.4.2.5 More Sources - La Vs. La/Nb Relationships

Further deductions about the sources contributing to the western Notre Dame Bay area magmas can be made from the diagram involving two strongly incompatible elements known to have diverse mobility in hydrous fluids, such as La and Nb (e.g. Tatsumi et al. 1986). In the La vs. La/Nb diagram (Fig. 5.19), melts derived from a depleted source should have La/Nb ratios and La content approaching those of the source, particularly with increasing degree of partial melting. Less partial melting of this same source will yield higher La abundances and a relatively low La/Nb ratio; mixing with mantle melts such as E-MORB or OIB would produce a similar effect. The same depleted source modified by hydrous fluids or melts originated from subducted slab would most likely have elevated La/Nb ratios, but not particularly elevated La (e.g. Tatsumi, 1986; Hole et al., 1984).

On the La vs. La/Nb diagram (Fig. 5.19), the mantle array (N-MORB to OIB) forms a trend in which La/Nb decreases slightly with increasing La. The non-arc, transitional, and some arc samples (of the A-2e and A-2c(t) subtypes) form trends subparallel to this array. Trends formed by samples in the A-2c and -2d subgroups are inclined to the mantle array, with the La/Nb ratios increasing with increasing La. The A-4 samples do not form a well-defined trend, but plot in a scattered cluster characterized by high La/Nb ratios and La values approaching those of the continental crust (AFG).

If the assumptions made at the beginning of this sub-section are right, then it may be concluded from Figure 5.19 that at least four different sources contributed to various magmatic types within the western Notre Dame Bay area flows. Distribution of the western Notre Dame Bay area samples on the La-La/Nb plot implies a contribution from: 1) a strongly depleted, N-MORB-like source; 2) a MORB source within the

range of normal to strongly enriched; 3) input from hydrous fluids reflected in the range of the La/Nb values at a more or less fixed La; and 4) upper continental crust and/or PAWMS-type sediment (PAWMS = Pacific authigenic weighted mean sediment; Hole et al., 1984), with La and La/Nb characteristics similar or even higher than average Lewisian amphibolite facies gneiss - AFG (Weaver and Tarney (1981).

5.4.2.6 Input From The Upper Continental Crust?

It comes as no surprise that the arc depleted mantle, enriched mantle, and fluids derived from the subducted plate are the major sources of the western Notre Dame Bay magmas. However, discrimination diagrams used in the Chapter 4 (Table 4.4) implied that some of the lavas may have formed in a continental arc setting. This affinity appears to contradict the field observations, i.e. there is a general lack of evidence for subaerial volcanism, continentally-derived sediment, or presence of older crustal rocks. However, one fraction of zircons from the 469 \pm 5/-3 Ma felsic tuff on Oil Island (Dunning and Krogh, 1988) contained inclusions of inherited zircon with an Archaean upper intercept age of 2965 Ma (Dr. G. Dunning, pers. comm.). Various diagrams based upon ratios of incompatible elements reveal some evidence for an upper crustal component in the western Notre Dame Bay lavas.

Average continental crust is strongly enriched in LREE and other incompatible elements (e.g. Taylor and McLennan, 1985). In general HFSE occur in higher concentrations in continental-margin arcs than in intraoceanic equivalents (Gill, 1981). Some authors (e.g. Hildreth and Moorbath, 1988) imply that there are large crustal HFSE contributions to continental arc magmas and the higher HFSE abundances result from intracrustal processes rather, than from the subduction component. Pearce (1983) has shown that the Zr/Y ratio is, in general, higher in lavas generated at continental margins than in intraoceanic island arcs. This observation gets some support from Nd isotopic data, which display, in general, a negative correlation with increasing Zr/Y; both features have been interpreted as resulting from crustal contamination (e.g. Thirlwall and Graham, 1984; Hickey et al., 1986) although others (e.g. Ellam and Hawkesworth, 1988) attributed them to a subducted sediment contribution.

5.4.2.6.1 *Sm-Nd-Nd variations*

Figure 5.20 illustrates variations between Sm and Nd, elements that are most likely immobile or insignificantly mobile (Tatsumi et al., 1986; Watson and Zindler, 1987) during dehydration of subducted altered oceanic crust. Therefore, their respective fractionation in volcanic rocks should reflect input from other sources and/or processes. Most common mineral phases in island arc lavas have relatively low distribution coefficients for both Nd and Sm (e.g. Irving and Frey, 1984); thus their relative concentrations should not change greatly with varying degree of melting or fractionation. This makes the Sm/Nd-Nd plot (Davidson, 1986) particularly sensitive to amphibole fractionation, as amphibole is the only common mineral phase which is able to fractionate Nd from Sm (compilation of Kd's from various sources by G.A. Jenner, 1984; Irving and Frey, 1984). Several model curves shown schematically on the diagram illustrate the effects of fractionating hornblende, plagioclase, two poly-mineralic assemblages (one including hornblende), and 50% bulk mixing of crust for parental arc compositions. One more curve representing 50% addition of crust and 50% fractionation is shown for a parental N-MORB-like composition (all modelled by Davidson, 1986). The model curves clearly indicate that contamination by crust may affect Nd concentrations and Sm/Nd ratios much more effectively than any fractionating assemblage. The reliability of these curves is tested using different suites of rocks from various tectonic settings (fig. 5.20B, D).

It is apparent from the Sm/Nd-Nd plot that several sources and processes, including fractional crystallization, but also crustal assimilation, contribute to the western Notre Dame Bay area lavas. The mafic lavas group in several clusters that conform to the previously established geochemical types (Chapter 4). These form a relatively broad trend between Sm/Nd values of 0.15 and 0.5, and Nd contents ~0-25 ppm. The trend begins with the A-2a to A-2c samples at Nd and Sm/Nd values characteristic of a strongly depleted MORB-like source, and ends with the most evolved flows of the A-4 group at Sm/Nd ratios

intermediate between the mantle array and the UCC and Nd values near those of the UCC. Most of the felsic samples are shifted from the mafic trend towards lower Sm/Nd ratios, an observation that is in an agreement with depletion of the middle to heavy REE and characteristic of hornblende fractionation. However, hornblende fractionation does not account for the wide range of Nd concentrations observed within the suite of felsic rocks (see trends defined by the Alcutian tephra before and after removal of hornblende; Romick et al, 1992), which form a double trend ending up (one sample exceeding it) at the Sm/Nd-Nd values of the UCC and AFG. This provides quite convincing evidence for contamination of parental magmas by an upper crustal component. The presence of two discrete linear trends within the wider trend of felsic rocks and their shift away from mafic compositions additionally illustrates importance of not only contamination by the crust, but also of amphibole fractionation.

On the Sm/Nd-Nd plot, samples of the A-2d (and some of the A-2c) subgroup are shifted across the mantle array into the MORB field, and plot along the model curve showing assimilation of upper crustal material by the N-MORB liquid. This is consistent with the previously noted position of these samples on various discrimination diagrams, on which they commonly straddle the boundary between oceanic and arc rocks (Table 4.5, chapter 4). On the other hand, most of the western Notre Dame Bay area rocks with non-arc and transitional affinities are confined to the MORB field on the Sm/Nd-Nd plot. The transitional and NA-2d samples are displaced towards the mantle array and slightly higher Sm/Nd ratios from the remainder of the NA samples. Since both the TR and NA-2d rocks display a noticeable LREE and Th enrichment with respect to HFSE (in particular with respect to Nb) and HREE, it is conceivable that their displacement away from the other NA samples is caused by assimilation of a minor amount of crustal material. This possibility will be examined in some detail in following sections.

Figure 5.21 illustrates variations between Sm and Nd for high-Mg dykes. Similarly to felsic rocks of the western Notre Dame Bay area, the high-Mg

dykes define two distinct linear trends, one of which (mainly SA-2d and SA-3a) samples is shifted away from the mantle array towards continental crust compositions and provides a strong indication of contamination of magmas parental to the dykes by an upper crustal component.

5.4.2.6.2 *Nd/Nd** parameter

Thirlwall (1982) and Thirlwall and Graham (1984) introduced the parameter Nd/Nd^* , that represents the ratio of measured Nd to the Nd value calculated by a log-linear interpolation between La and Gd on the chondrite normalized REE pattern. This parameter indicates curvature and steepening of the REE pattern. Nd/Nd^* was shown to be an effective indicator of crustal contamination, reflecting addition of a component with a concave-upward LREE pattern to a magma generated in a source with MORB-like characteristics (Thirlwall and Graham, 1984). However, as La and Ce abundances may be controlled to some degree by metasomatism (e.g. Tatsumi et al., 1986), the Nd/Nd^* calculated by the above method may also reflect the combined results of crustal contamination and mantle metasomatism by the La enriched fluids. For this reason, the factor Nd^* is here measured by log-linear interpolation between Pr and Sm using the formula

$$Nd/Nd^* = NdN / [(PrN)(SmN)]^{1/2}$$

On the Sm/Nd versus Nd/Nd^* diagram (Fig.5.22), samples from the western Notre Dame Bay area form a fairly continuous trend that shows a gradual increase in Nd/Nd^* with the decreasing Sm/Nd . The order in which samples are arranged in the Sm/Nd - Nd/Nd^* space conforms generally to the division into types and subtypes made in chapter 4. Subgroups A-2a to A-2c display the lowest values of Nd/Nd^* in the range 0.85-1.05, with most samples <1.00 and the mantle array. Other western Notre Dame Bay rocks of arc affinity range between Nd/Nd^* values of 0.97 and 1.12, and plot predominantly above $Nd/Nd^* = 1.00$. Felsic rocks of F-1 and F-2 types have Nd/Nd^* values in the range 1.00 to 1.17 and approach the composition of UCC. Surprisingly, many of the NA rocks have relatively high Nd/Nd^* values (0.97-1.12), and there is

substantial overlap between the NA, TR, and the A-2d and A-2e samples in both the Nd/Nd* and Sm/Nd ratios.

Nevertheless, consistent with many of the diagrams presented above, the Sm/Nd vs. Nd/Nd* plot implies that addition of upper crustal material to magmas generated in various mantle sources might have had a significant impact on the final composition of some western Notre Dame Bay area lavas.

5.5 Summary And Conclusions

The emphasis in this chapter has been on a detailed interpretation of the paleoenvironments in which rocks of the western Notre Dame Bay area were formed and the sources from which they were derived. The geochemical signatures of types defined in Chapter 4 were compared to the lithostratigraphy and to geochemical results from rocks of moderately to well-defined modern tectonic settings.

Integration of geochemical data with lithostratigraphy shows consistencies in the magmatic evolution of the western Notre Dame Bay magmatic rocks. Within the pre-500 Ma sequence, rocks in the stratigraphically-lowest position (The Lushs Bight Group), exhibit geochemical signatures of boninites and low-Ti arc tholeiites. The arc tholeiites persist into the basal units of the overlying Western Arm Group before giving way to a succession dominated by NA and TR rocks. Comparison with modern environments reveals good analogues for all the pre-500 Ma geochemical types in the western Notre Dame Bay area in modern island arcs, intraoceanic back-arc and/or near continent marginal basins. The presence of boninites in the Lushs Bight Group may record the initiation of subduction in this Late Cambrian island arc, whereas the arc tholeiites probably represent primitive phases of arc magmatism, such as presently occur in the Kermadec arc. The presence of non-arc and transitional lavas higher in the pre-500 Ma sequence interbedded in the lower part with IAT-type lavas has analogues in modern back-arc (e.g. Lau Basin, Mariana and Ogasawara Throughs), whereas chemically the NA and TR type lavas of the western Notre Dame Bay are more like those from marginal basins (e.g. particularly Sea of Japan and Gulf of California Lau Basin). Thus, the back-arc basin is believed to be the most likely environment for these rocks. The lower part of the pre-500 Ma sequence (the Lushs Bight

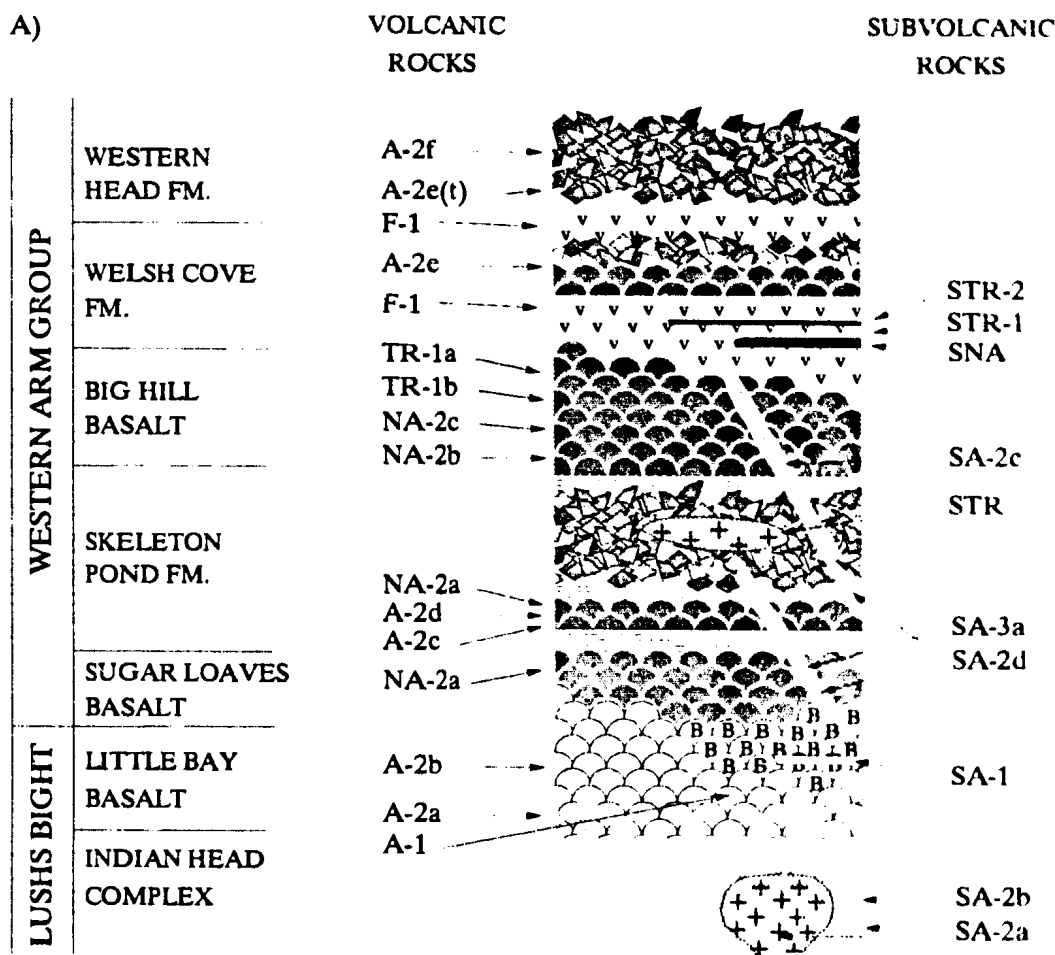
Group), then would appear to be best interpreted as recording the establishment of a primitive island arc followed by a gradual transition to a back-arc basin. If the simplest scenario is assumed, then the only setting in which non-arc, arc and transitional flows can be generated and be present in the stratigraphic order recorded within the Western Arm Group is the frontal-arc margin of a back-arc basin. It is exactly the part of the arc/back-arc environment that is predicted to be preferentially preserved in ancient assemblages (Busby-Spera, 1988).

The ca 496 Ma high Mg dykes are of considerable interest as they help constrain the environments of magmatism between the two volcanic episodes. They cut all rocks of the pre-500 Ma volcanic sequence and are one of the principal geological features that constrain the age of these rocks. Geochemical data indicate that they are subduction-related and comparison with modern environments reveals an affinity with sanukitoids and bajaites, which erupt in modern settings characterised by the presence of continental crust. This indicates that at the time these rocks were intruded, magma sources typical of continental crust were available at depth below the pre-500 Ma assemblage.

The younger volcanic sequence, represented by the upper part of the Western Arm Group and the Cutwell Group, is dominantly of island arc origin. Modern analogues for mafic and felsic volcanic rocks are present in island arcs, both those that are intraoceanic and those which are built upon continental crust. This sequence appears to represent renewed arc volcanism in the western Notre Dame Bay area approximately 20 Ma after the cessation of activity in the older arc sequence.

A detailed consideration of possible sources for the western Notre Dame Bay magmas, using various combinations of trace elements that behave in diverse manners during different petrogenetic processes, permits an interpretation of the nature of the magma sources, some insight into the petrogenetic processes that formed the magmas, and helps further constrain the environments in which the magmatism occurred. This analysis suggests that at least four types of sources can be identified as having contributed to western Notre Dame Bay magmatic rocks: 1) normal depleted mantle like that commonly invoked as the source for N-MORB - type lavas; 2) somewhat enriched mantle like that commonly invoked for the formation of T-MORB, E-MORB and OIB lavas; 3) a metasomatic source

that is believed to originate on the subducting slab; and 4) continental crust. The influence of these various sources varies considerably from one magma type to another. N-MORB and E-MORB sources dominate in the NA and TR types; the latter is also influenced by a metasomatic, slab-derived source, which is interpreted to cause the characteristic Th inflection in these rocks. The influence of continental crust is not clearly evident in most rocks in the western Notre Dame Bay area. However, there is geochemical evidence in both mafic and felsic lavas of the 485-465 Ma sequence that continental crust was involved in their petrogenesis and that hornblende fractionation played a major role in their petrogenesis. This raises the possibility that this younger arc was based upon continental lithosphere.



not to scale!

Figure 5.1. Geochemical types versus schematic stratigraphic columns of the Lushes Bight / Western Arm groups (Fig.5.1A), and the Stag Formation / Cutwell Group (Fig.5.1B). Geochemical types of volcanic rocks are shown on the left side of the column, whereas, geochemical types of subvolcanic rocks are indicated on the right side of the column.

The Lushes Bight Group (Fig.5.1A) is dominated by strongly depleted and refractory arc lavas of the A-1 (boninitic) and A-2 (island arc tholeiite) types. The Western Arm Group contains rocks that belong to NA, TR and A geochemical types. The NA and TR types flow interfinger in the Big Hill Basalt, whereas, in the overlying Welsh Cove Formation, felsic tuffs with an arc affinity are intruded by sills with transitional-type chemistry and dykes with non-arc type chemistry.

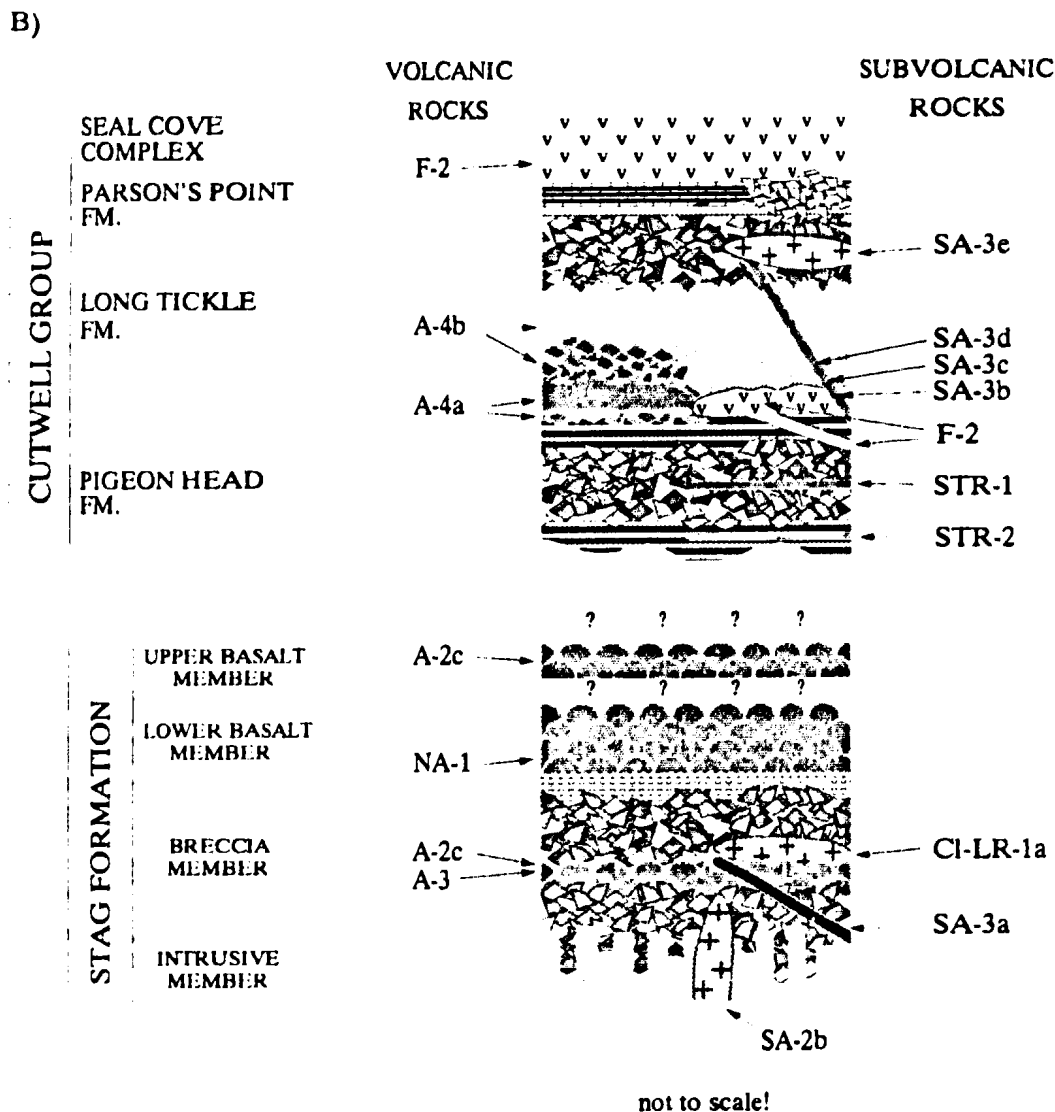


Figure 5.1. (continued). The Stag Formation (Fig.5.1B) is comprised of the arc lavas (flat to slightly LREE - depleted island arc tholeiites) and non-arc lavas (E-MORB). The high-Mg dyke (type SA-3A) cuts this formation. The Cutwell Group is dominated by the LREE enriched arc lavas of the A-4 type and intruded by similar rocks of the SA-3 type. The STR-1 and STR-2 sills intruding the lower Pigeon Head Formation, are geochemically identical to those in the Welsh Cove Formation, Western Arm Group.

LEGEND



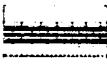

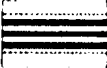

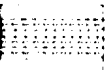
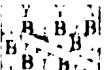

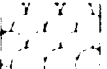






	limestone breccia		monomictic tuff breccia
	limestone, shale, greywacke		massive and autobrecciated flow
	shale, sandstone		"unaltered" pillow lava
	greywacke		boninite and boninitic dyke
	chert, tuff		altered pillow lava
	felsic: tuff, minor flow, and intrusive rock		sheeted dyke
	mafic tuff		intrusion
	polymictic tuff breccia, breccia		mafic dyke or sill

Figure 5.1.(continued) Legend for lithostratigraphic columns in Figure 5.1.

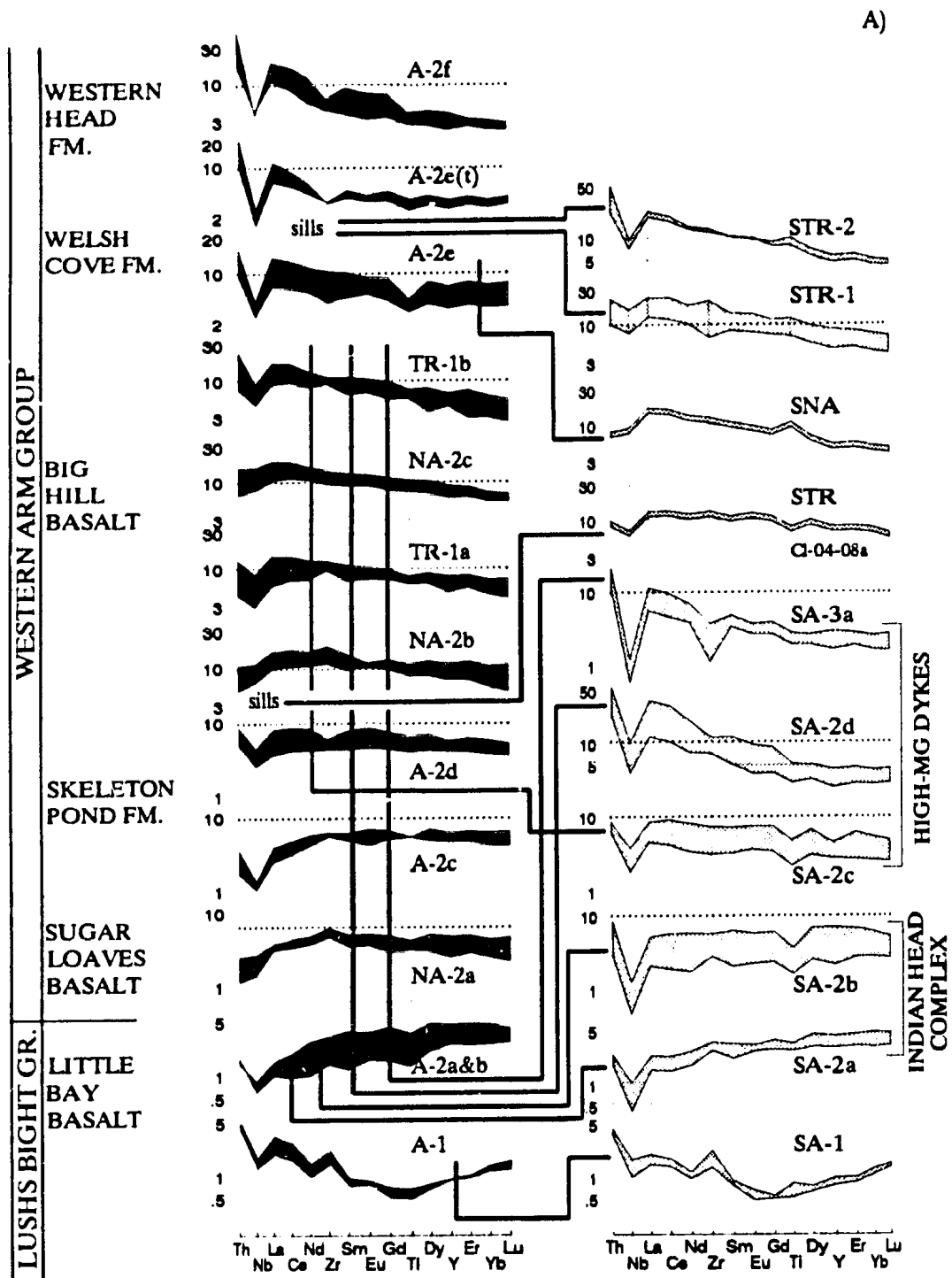


Figure 5.2. Primitive mantle-normalized extended REE plots of mafic volcanic rocks and tuffs (on the left), and co-magmatic intrusive rocks (on the right), bracketed by stratigraphic divisions of the Lushs Bight / Western Arm groups (Fig.5.2A), and the Stag Formation / Cutwell Group (Fig.5.2B).

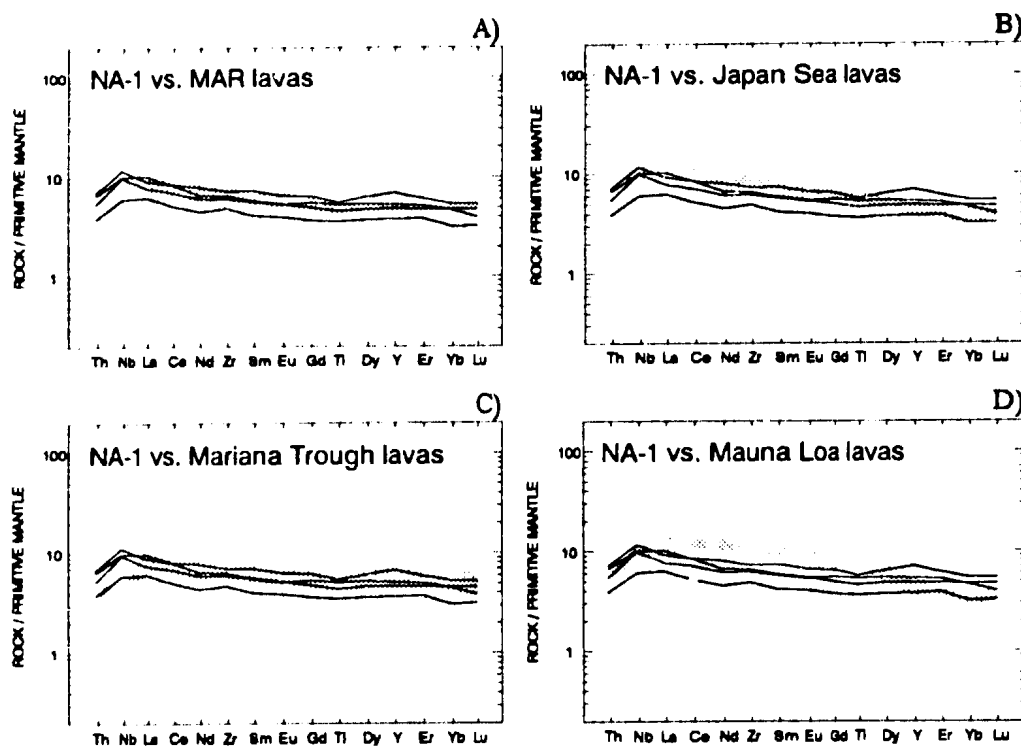


Figure 5.3. Primitive mantle-normalized extended REE plots of the NA-1 E-MORB type tholeiites (lines) compared to similar rocks (shaded) from various modern tectonic settings: A) volcanic rocks erupted from the "anomalous" Mid-Atlantic Ridge (MAR) segment between 44 degrees and 47 degrees N (Schilling et al., 1983); B) sills cored at ODP sites 794 and 797 in the Japan Basin (Allan and Gorton, 1992); C) Mariana Trough lavas (Hawkins et al., 1990); D) tholeiites of Mauna Loa, an ocean island volcano (Basaltic Volcanism Study Project, 1981).

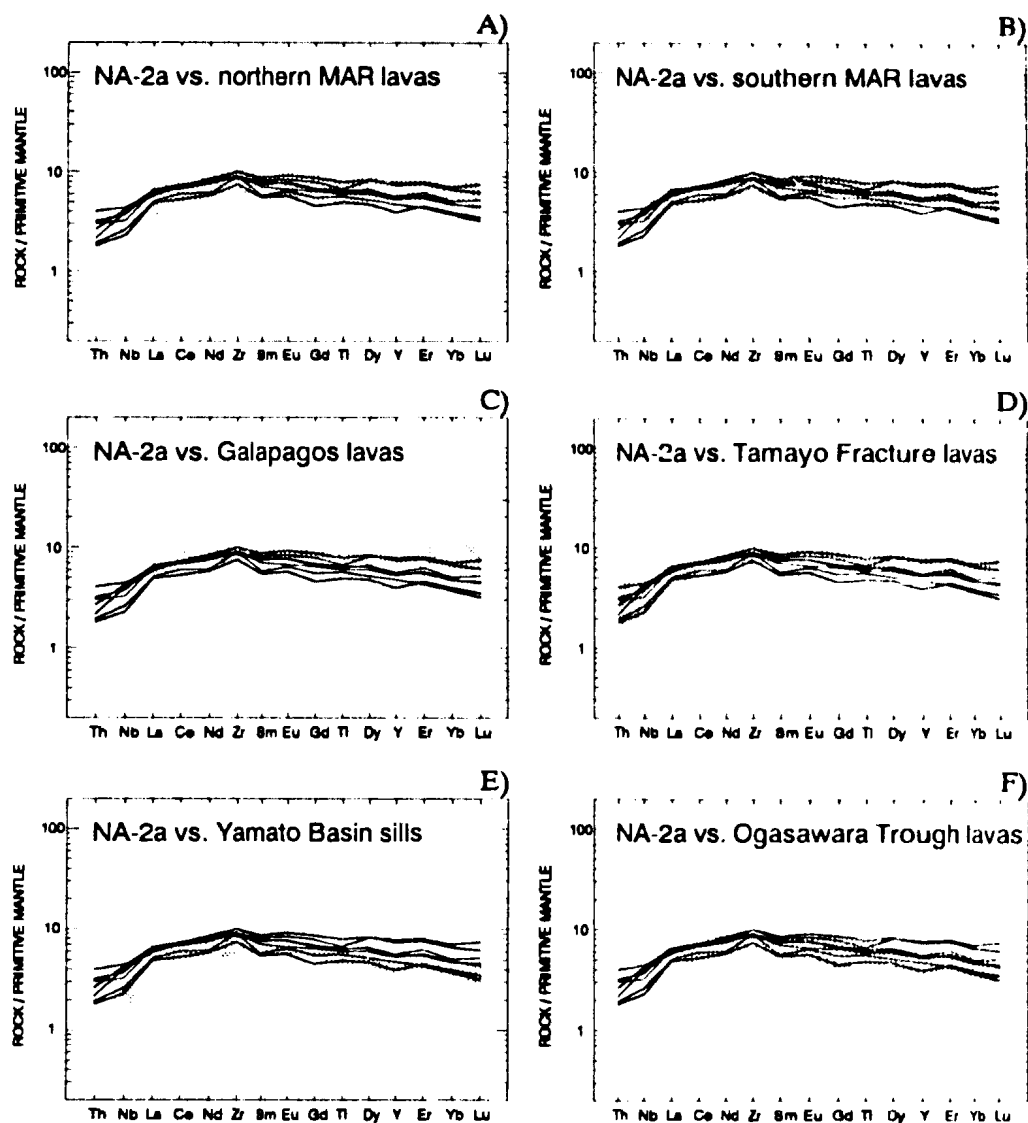


Figure 5.4. Extended REE plots (primitive mantle-normalized) of the NA-2 type flows (lines) matched with (shaded): A) samples from the MAR plume segment located south of the Charlie-Gibbs Fracture Zone (Schilling et al., 1983); B) lavas from the southern MAR segment under the influence of the Tristan da Cunha mantle plume (Humphris et al., 1985); C) flows from the Galapagos spreading center (Schilling et al., 1982); D) lavas from the Tamayo Fracture Zone - transform fault displacing the East Pacific Rise (Saunders et al., 1982); E) samples from the lower sill unit of the Yamato Basin, Sea of Japan (ODP hole #794; Allan and Gorton, 1992); and F) flows from the spreading center behind the Izu-Ogasawara arc (Hochstaedter et al., 1990b).

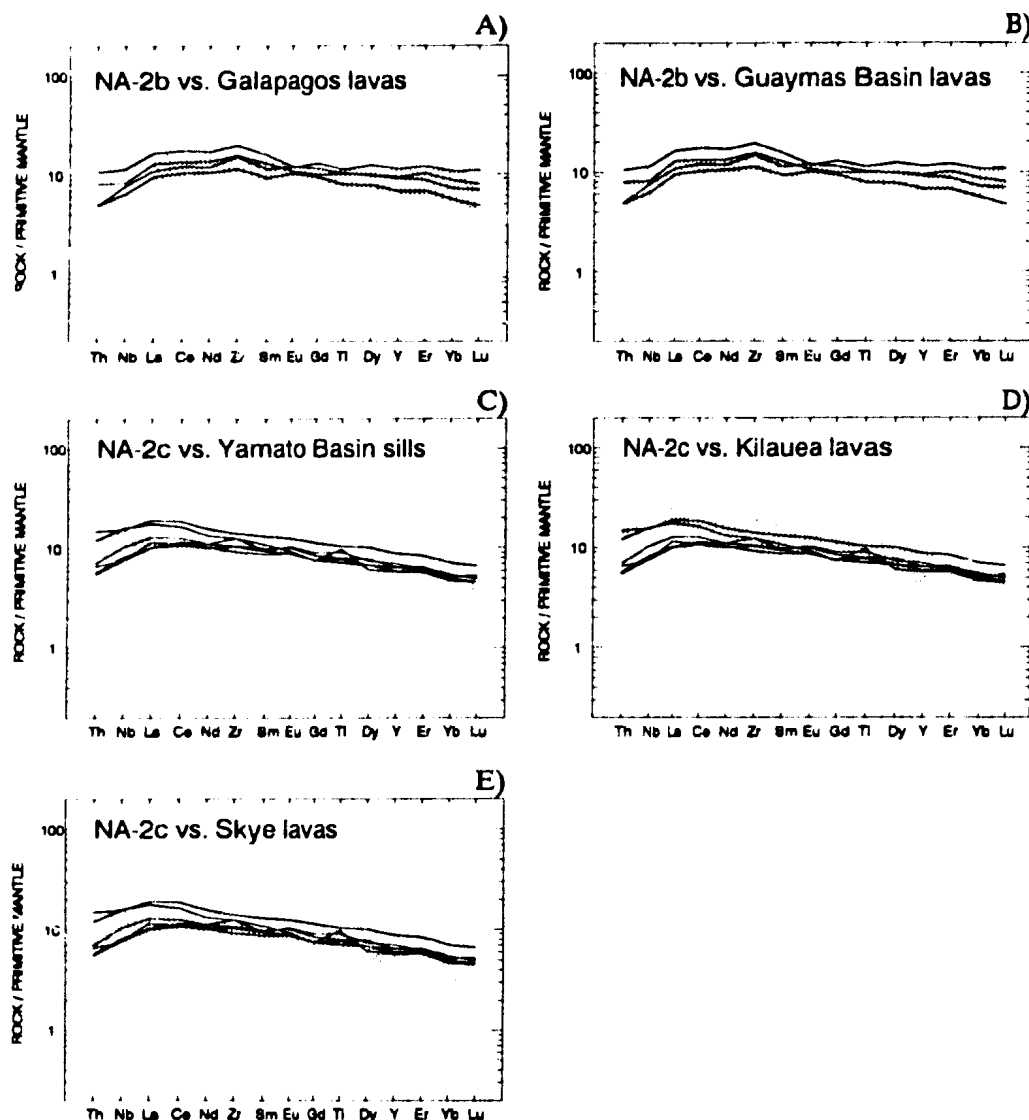


Figure 5.5 Primitive mantle-normalized extended REE plots of the NA-2b and NA-2c rocks (lines) and their analogues (shaded) from modern spreading centers: A) the NA-2b samples and lavas erupted from the spreading center associated with the Galapagos mantle plume (Schilling et al., 1982); B) the NA-2b samples and flows of the Guaymas Basin spreading ridge, Gulf of California (Sawlan, 1991); C) the NA-2c flows and sills, cored in ODP holes #794 and #797, from the Yamato spreading center (Yamato Basin) (Allan and Gorton, 1992; Pouclet and Bellon, 1992); D) the NA-2c samples and the Hawaii samples from Kilauea (Basaltic Volcanism Study Project, 1981); E) the NA-2c subtype rocks and the least crust-contaminated volcanic plateau lavas of Skye, British Tertiary Igneous Province (Thompson and Morrison, 1988).

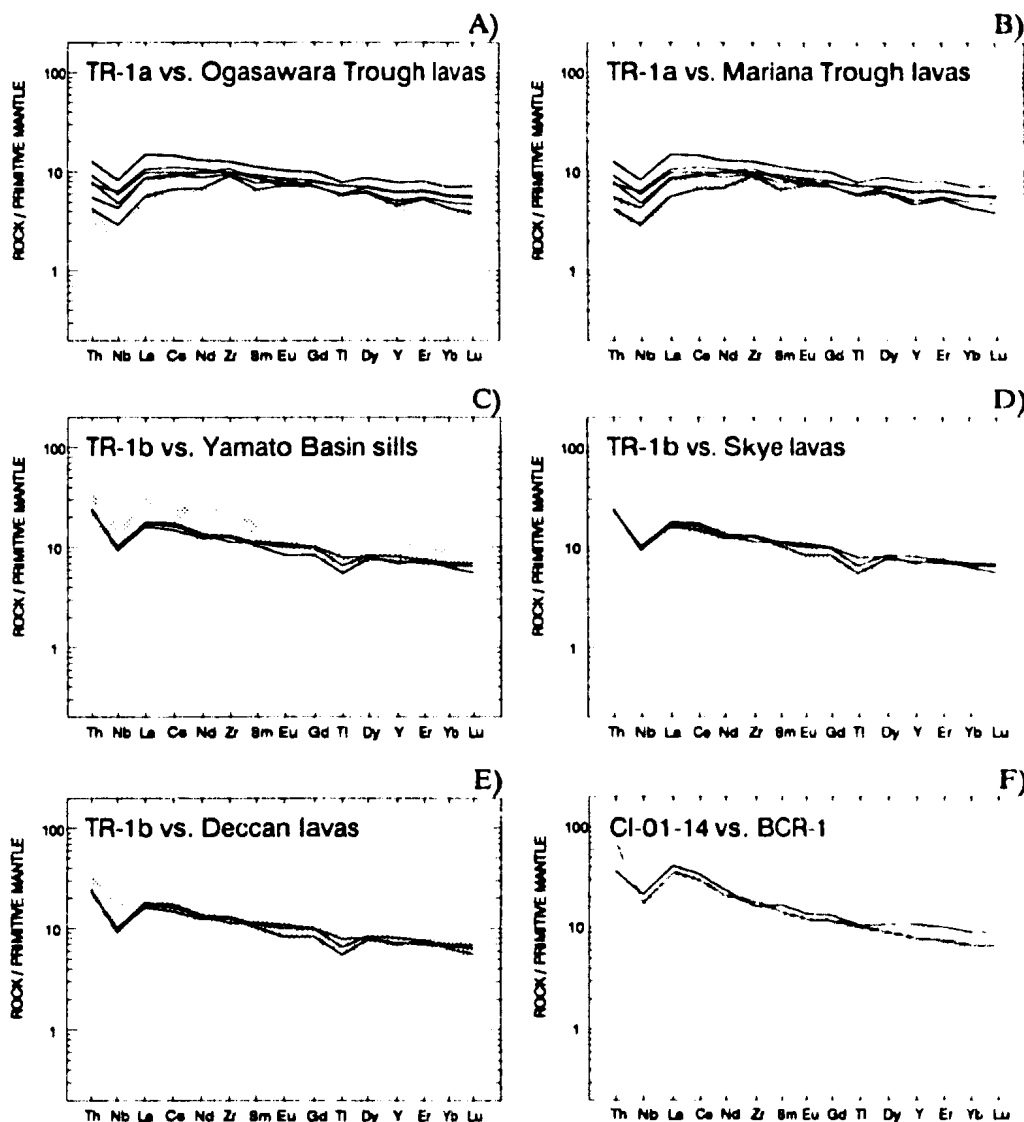


Figure 5.6. Extended, primitive mantle normalized, REE plots of the TR-1 type volcanic rocks (lines) and their modern counterparts (shaded): A) the TR-1a rocks of the Ogasawara Trough lavas, thought to be generated at rift initiation (Ikeda and Yuasa, 1989; Hochstaedter et al., 1990a,b); B) the TR-1a samples and the Mariana Trough lavas (Hawkins et al., 1990); C) the TR-1b flows and sills from ODP hole #797 on the floor of the Yamato Basin (Allan and Gorton, 1992; Pouclet and Bellon, 1992); the TR-1b subtype flows and D) contaminated by continental crust lavas from Skye (Thompson and Morrison, 1988); and E) Deccan (Mahoney, 1988; Lightfoot et al., 1990); F) CI-01-14 sample (TR type) and the markedly similar international standard BCR-1 (Columbia River flood basalt) (Jenner et al., 1990).

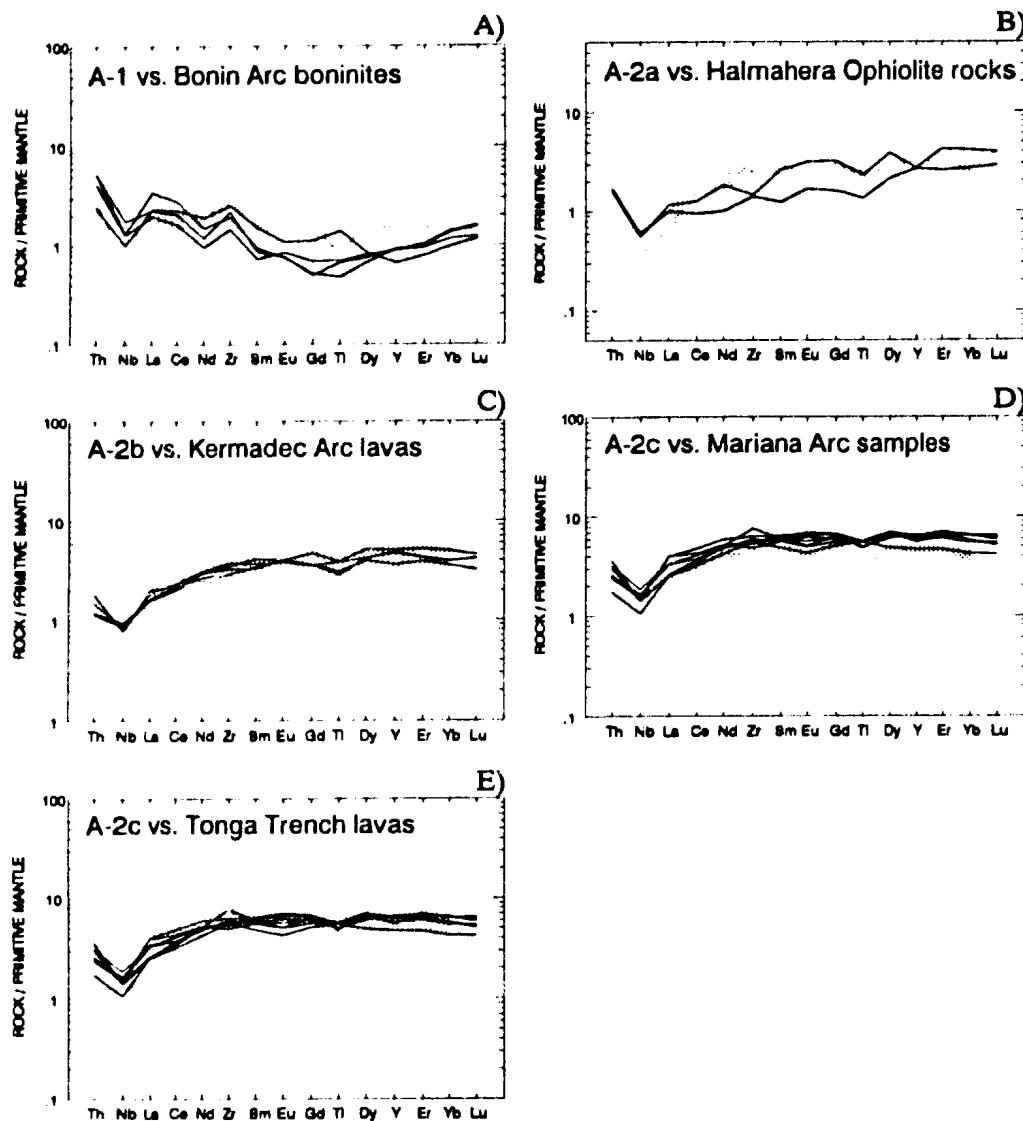


Figure 5.7. Primitive mantle normalized, extended patterns of the A type rocks (lines) and their modern counterparts (shaded): A) the A-1 type boninites and boninites from the type locality, Bonin Islands (Pearce et al., 1992); B) samples of the A-2a subtype and strongly depleted rocks from the East Halmahera Ophiolite, Eastern Indonesia (Ballantyne, 1991); C) the A-2b samples and lavas from the Kermadec arc (Ewart and Hawkesworth, 1987); D) the A-2c rocks and geochemically similar lavas from the older, southern part of the Mariana arc (Lin et al., 1989); and E) rocks dredged from the Tonga trench wall (Falloon et al., 1987). In both latter arcs, this type of flow is interpreted to be associated with an early stage of arc evolution.

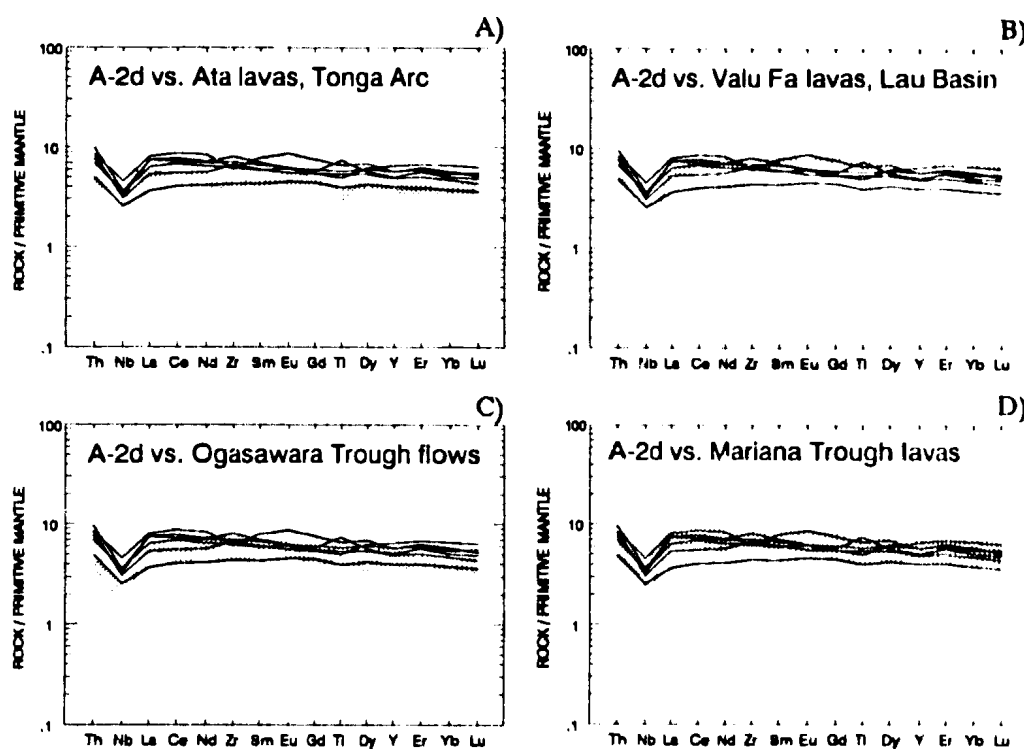


Figure 5.8. Extended REE plots of the A-2d samples (lines) compared to selected rocks from modern settings (shaded): A) samples from Ata Island (Tongan arc; Vallier et al., 1985, 1991); B) IAT-like lavas from Valu Fa ridge, Lau Basin (Jenner et al., 1987; Vallier et al., 1991); C) IAT-like flows from the Ogasawara Trough (Hochstaedter et al., 1990a,b); and D) IAT-like basalts from back-arc spreading center of the Mariana (Fryer et al., 1990). The similarity of these back-arc basalts to IAT is variously interpreted to result from mixing of E-type MORB and depleted IAT magmas (Ikeda and Yuasa, 1989; Hochstaedter et al., 1990a,b), by mixing of depleted mantle with the slab-derived fluid, or by contamination of mantle derived melts with older arc lithosphere (Jenner et al., 1987; Vallier et al., 1991).

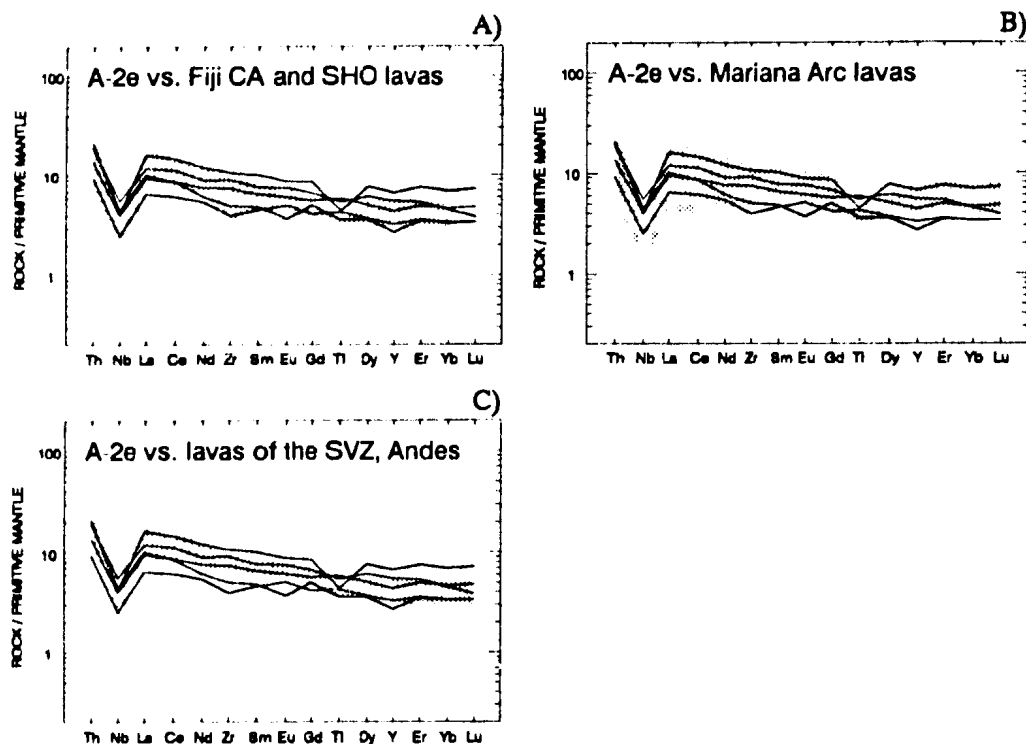


Figure 5.9. Extended multielement plots (normalized to primitive mantle) of the A-2e lavas (lines) compared to rocks from present day oceanic and continental arcs (shaded): A) mildly shoshonitic to calc-alkalic flows from Fiji linked to volcanic activity arising from rifting of the old (Vitiav) arc (Gill and Whelan, 1989); B) rocks typical of the mature central part of the Marianas (Hole et al., 1984) interpreted to have been derived from a relatively depleted mantle that was enriched by alkali-rich hydrous fluids (e.g. Lin et al., 1989); and C) lavas erupted from volcanoes in the southern volcanic zone (SVZ) of the Andes (Hickey et al., 1986), located on a relatively thin continental crust. The Andean magmas are thought to result from variable mixing of components derived from subducted crust and from enriched, OIB-like mantle source (Hickey et al., 1986), overprinted by intracrustal assimilation and fractional crystallisation (Hildreth and Moorbath, 1988).

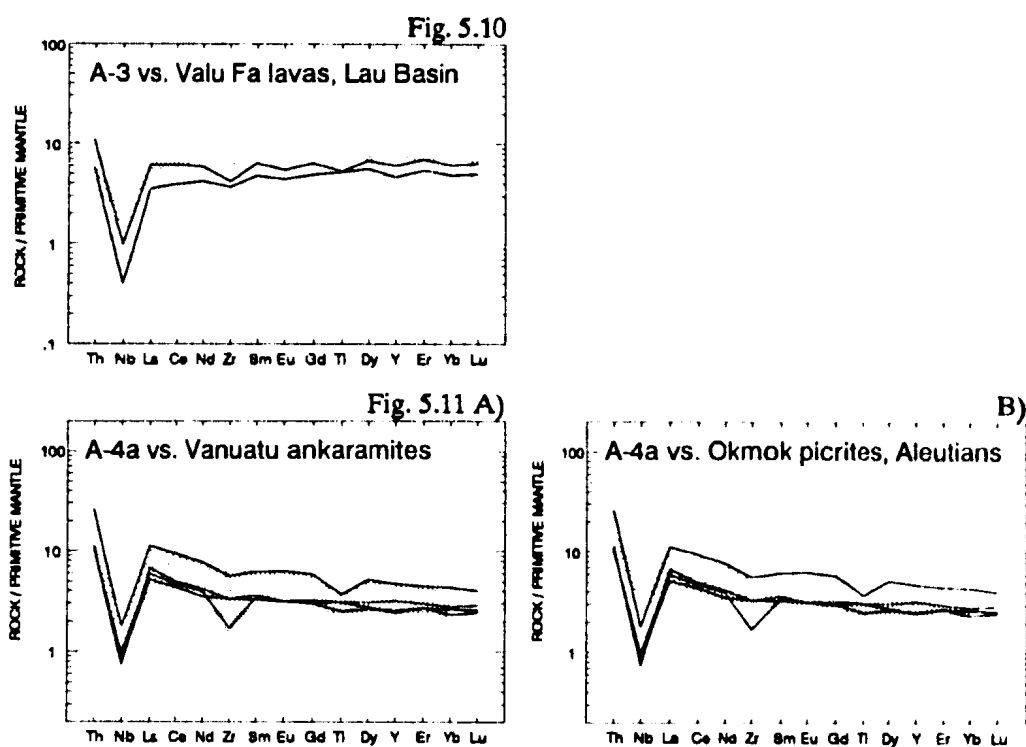


Figure 5.10. Extended REE profiles of the A-3 type samples (lines) and lavas of the Valu Fa Ridge, Lau Basin, in which a well defined Nb anomaly indicates the presence of a slab-derived component in the back-arc basin mantle source (Jenner et al., 1987; Vallier et al., 1991).

Figure 5.11. Multi-element plots of ankaramitic flows of the A-4a subtype (lines) and modern analogues (shaded): A) ankaramites from Western Epi, Vanuatu (Bardsell and Berry, 1990), considered to represent parental or primitive magmas; and B) the ID1 and associated picrites from Okmok Volcano, Aleutians (Nye and Reid, 1986), thought to represent parental magma composition.

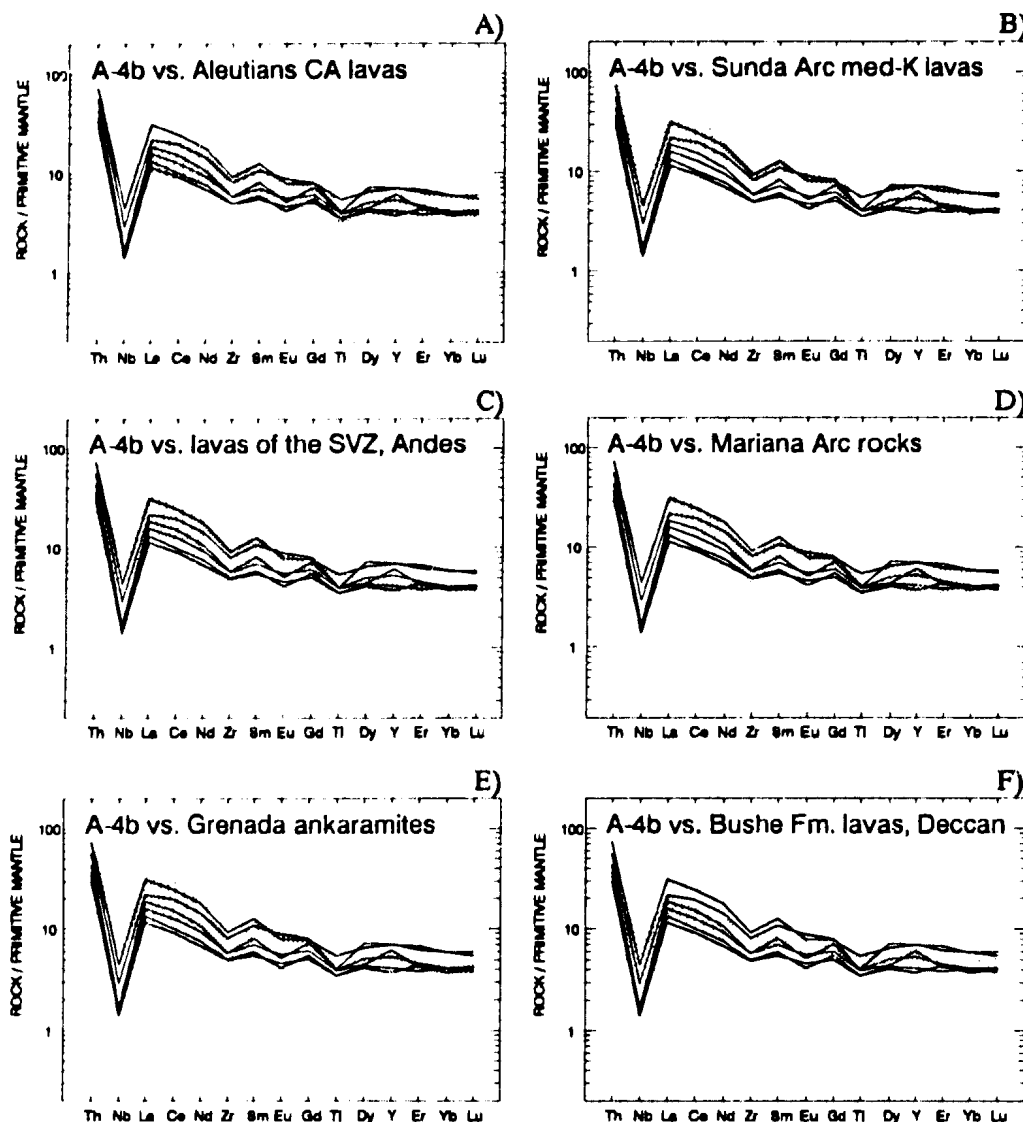


Figure 5.12. Extended REE plots of samples of the A-4b subtype (lines) and a wide range of modern analogues (shaded), associated with intraoceanic and continental arc settings: A) CA rocks of the Rechesnoi Volcano, Aleutians (Miller et al., 1992); B) medium-K, TH and CA lavas from the Sunda arc (Stolz et al., 1990); C) transitional TH and CA rocks from the Southern Volcanic Zone of the Chilean Andes (Ferguson, 1992); D) mildly shoshonitic lavas from the northern Mariana arc (Lin et al., 1989); E) ankaramites from the island of Grenada, Lesser Antilles (Thirlwall and Graham, 1984), interpreted to be derived from magmas that assimilated continentally-derived sediment; and F) strongly contaminated by upper continental crust flows of the Bushe Formation, Deccan (Mahoney, 1988; Lightfoot et al., 1990).

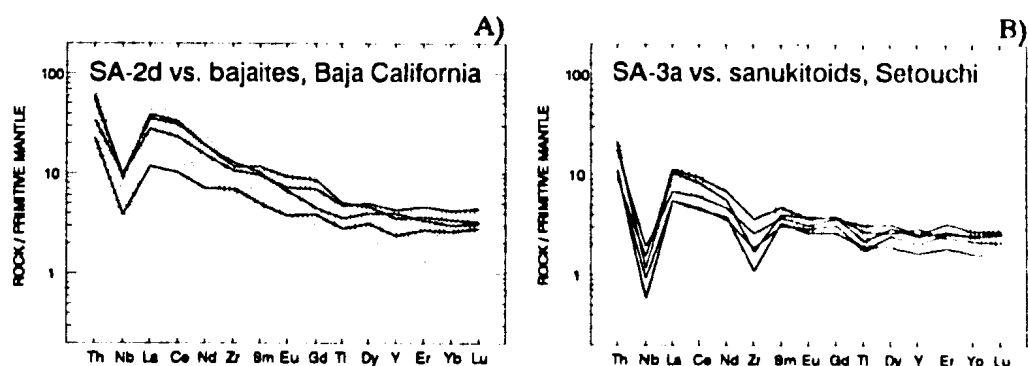


Figure 5.13. Extended REE patterns of the SA-2d dykes (lines) superimposed upon pattern (shaded) of modern high-Mg andesitic rocks termed "bajaites" (A), the sporadic occurrence of which (Baja California, S.Chile, Aleutians) is linked to the termination of subduction resulting from a ridge-trench collision (e.g. Saunders et al., 1987; Rogers and Saunders, 1989). The SA-3a dykes (lines) display a relatively close similarity to another suite of modern high-Mg andesites named sanukitoids (considered to represent primary andesitic magmas), that occur in southwest Japan (e.g. Tatsumi and Ishizaka, 1982).

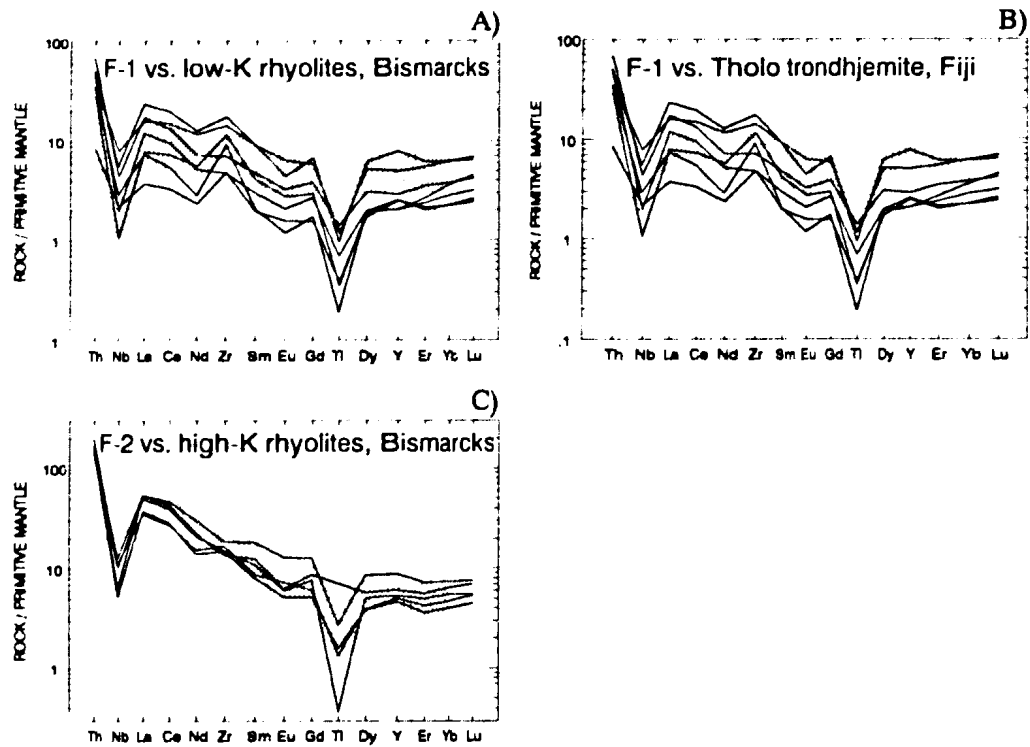


Figure 5.14. The multi-element plots of the F-1 type low-K rhyolites are similar to those of felsic rocks from modern island arcs, e.g. rhyolites from the Bismarck Arc (A) (Smith and Johnson, 1981), and the tonalite-trondhjemite Tholo suite of Fiji (B) (Gill and Stork, 1979). Figure 5.14C illustrates normalized F-2 type patterns compared with the field of high-K rhyolites from New Britain, Bismarck Arc (Smith and Johnson, 1981).

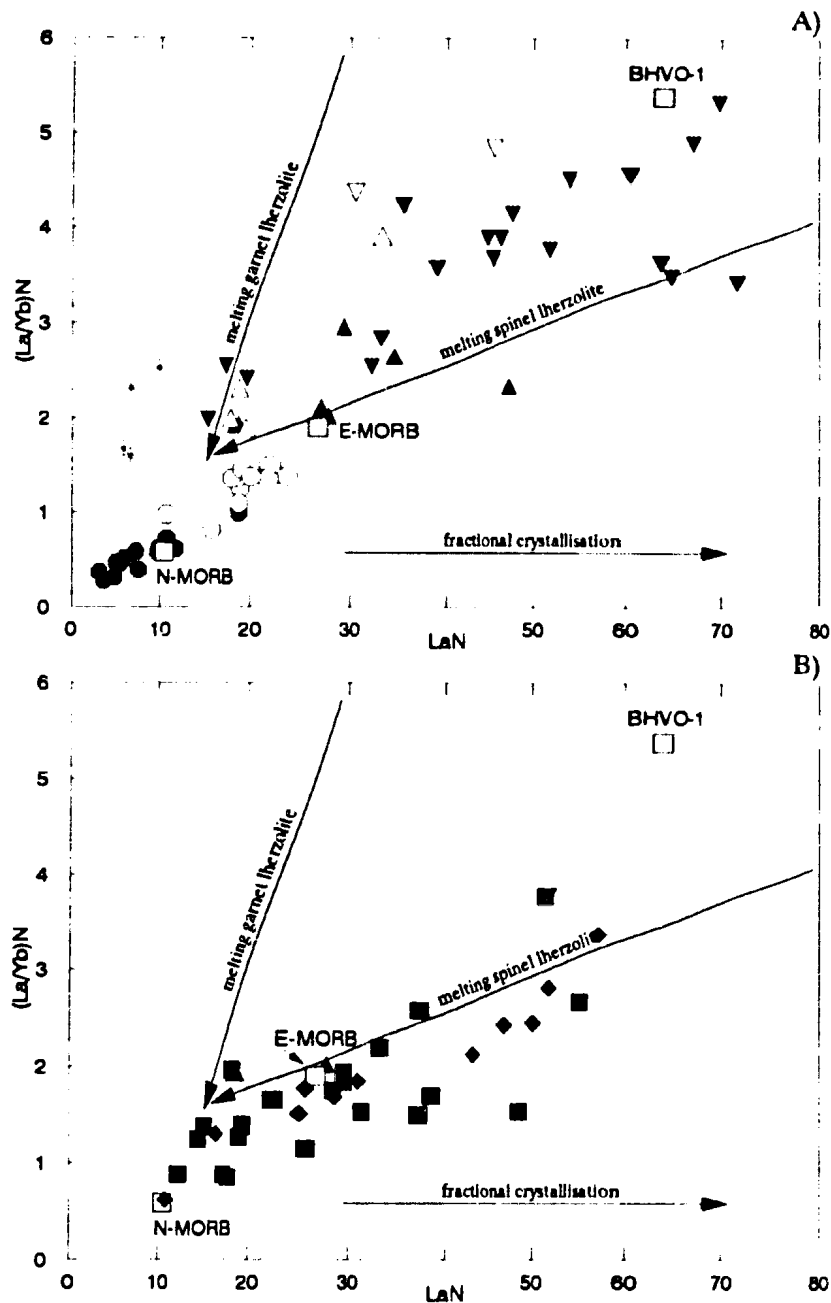


Figure 5.15. The LaN versus $(La/Yb)N$ and LaN versus $(La/Sm)N$ process identification plots (Allegre and Minster, 1978; Minster and Allegre, 1978) for the rocks of the western Notre Dame Bay area. Linear trends defined by partial melts of different sources (spinel and garnet lherzolites; e.g. Pankhurst, 1977; Allegre and Minster, 1978; Lin et al., 1989), and the fractional crystallisation trend (e.g. O'Hara and Mathews, 1981; Langmuir, 1989) are shown for reference.

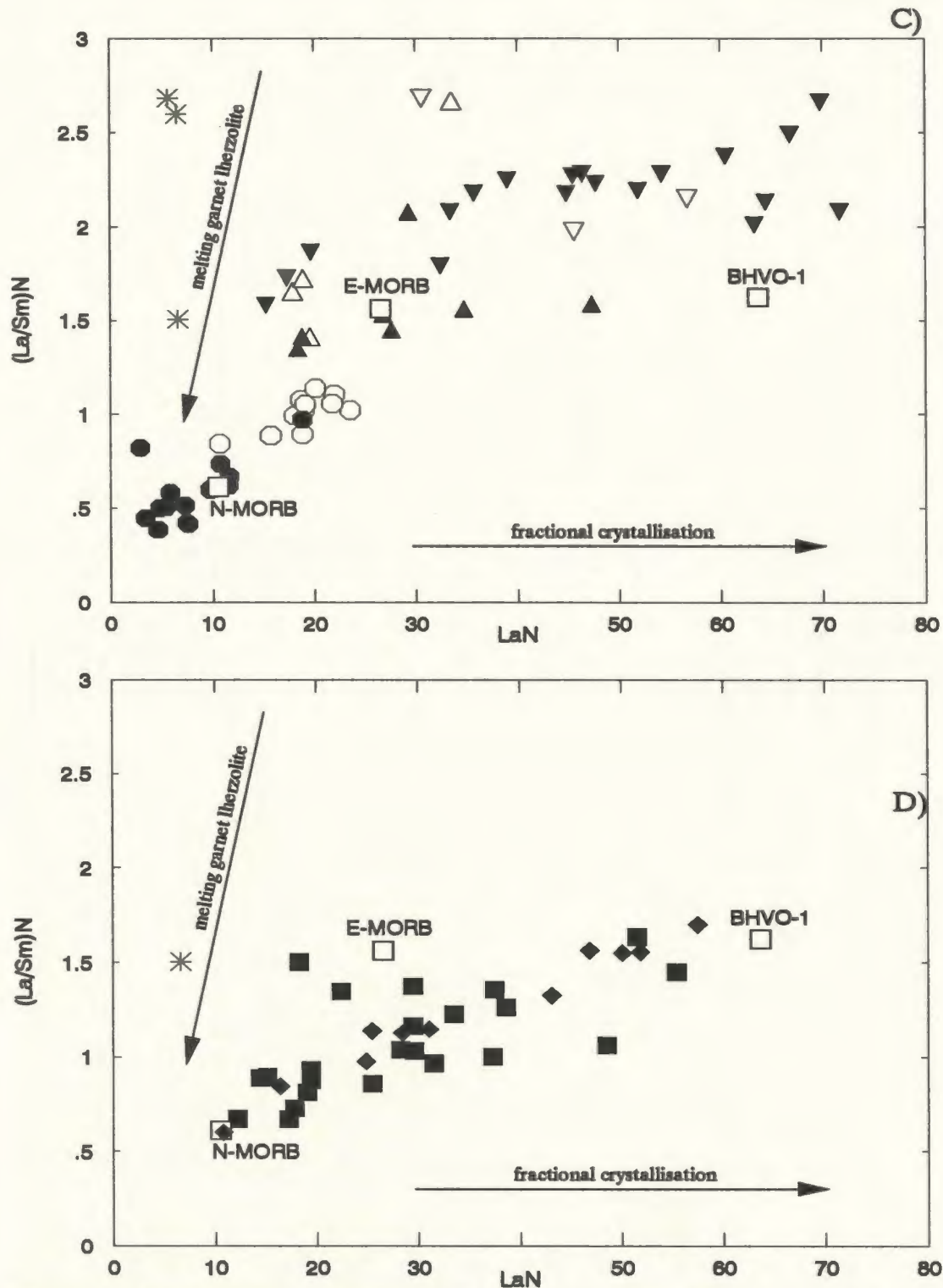


Figure 5.15. (continued) On these plots, a general positive correlation between $(La/Yb)_N$ and La_N indicates that varying degrees of melting of one heterogeneous or several sources may be, amongst other processes, involved in the formation of magmas from which these rocks were derived. A dominant control by fractional crystallisation is suggested by the subhorizontal trend of some of the NA-type rocks. A subparallel trend of the A-4 type on the La_N - $(La/Sm)_N$, is also suggestive of the fractional crystallisation trend.

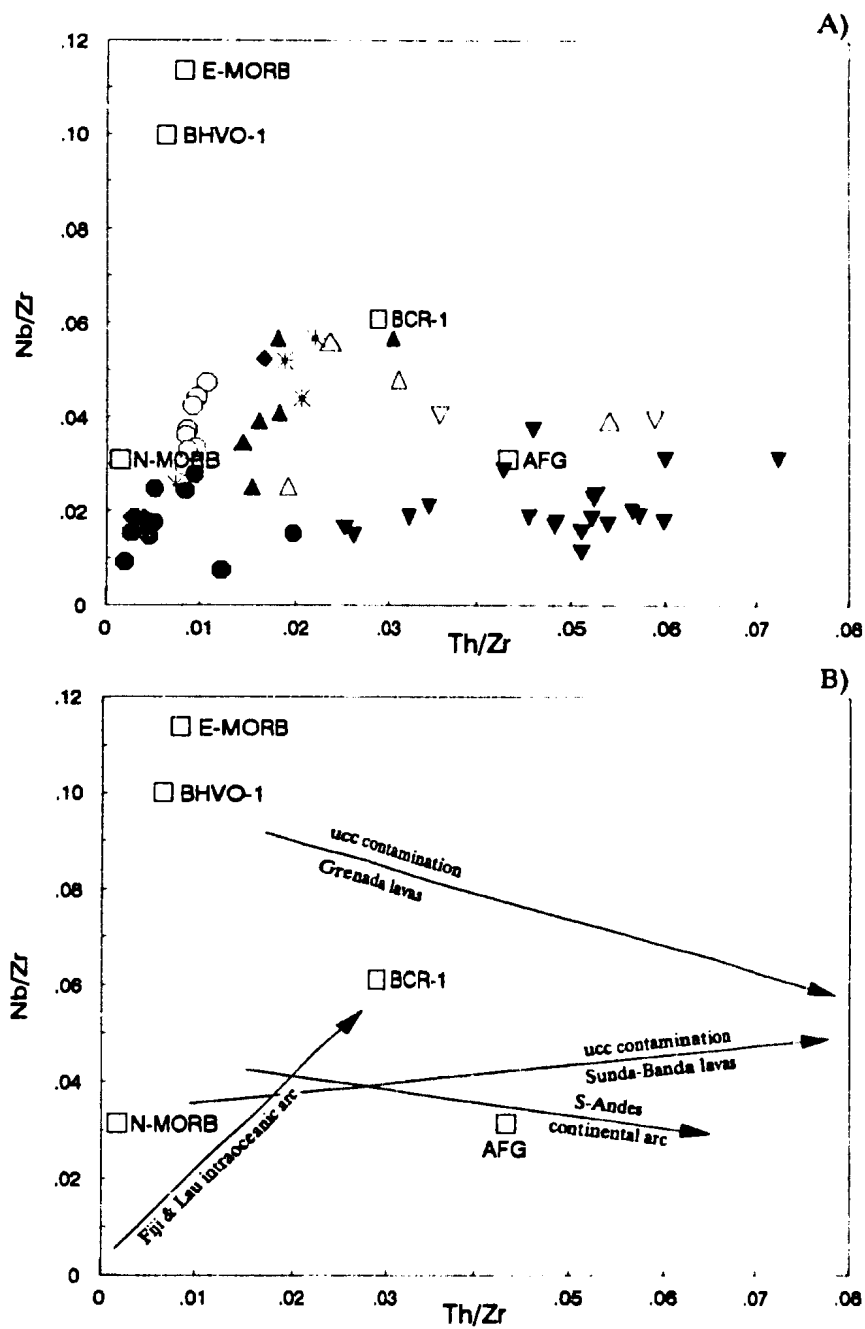


Figure 5.16. The Nb/Zr vs. Th/Zr diagram for: A) and C) samples from the western Notre Dame Bay area; and B) and D) samples (represented by trends) from several present day tectonic settings (for reference).

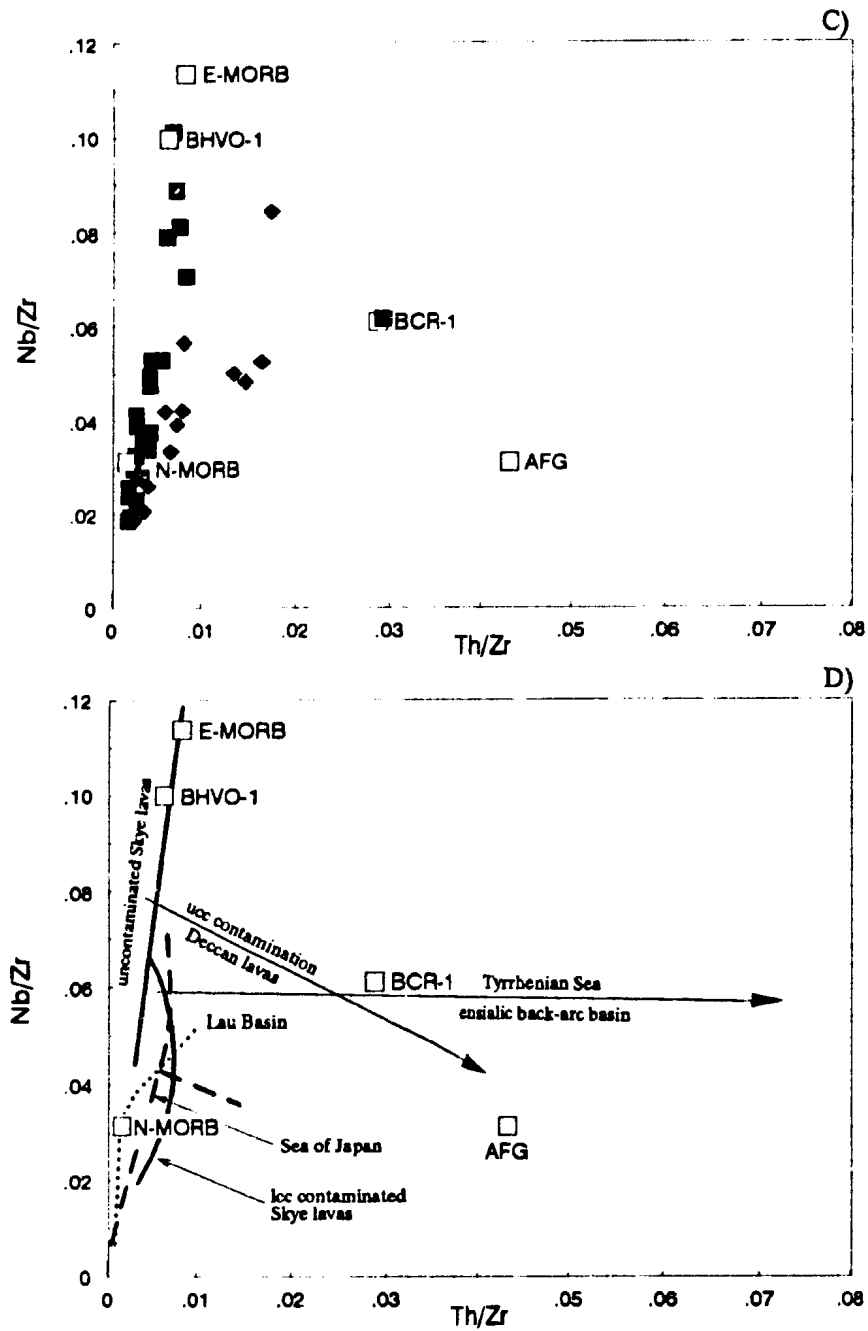


Figure 5.16. (continued) The Th/Zr-Nb/Zr plot suggests that an enriched mantle enriched mantle component was present in the NA and TR magma sources. Evidence of any input from the enriched mantle into the source region of the A type lavas may have been partially obliterated by contamination by upper continental crust, as it is documented for the Deccan lavas (Fig. D).

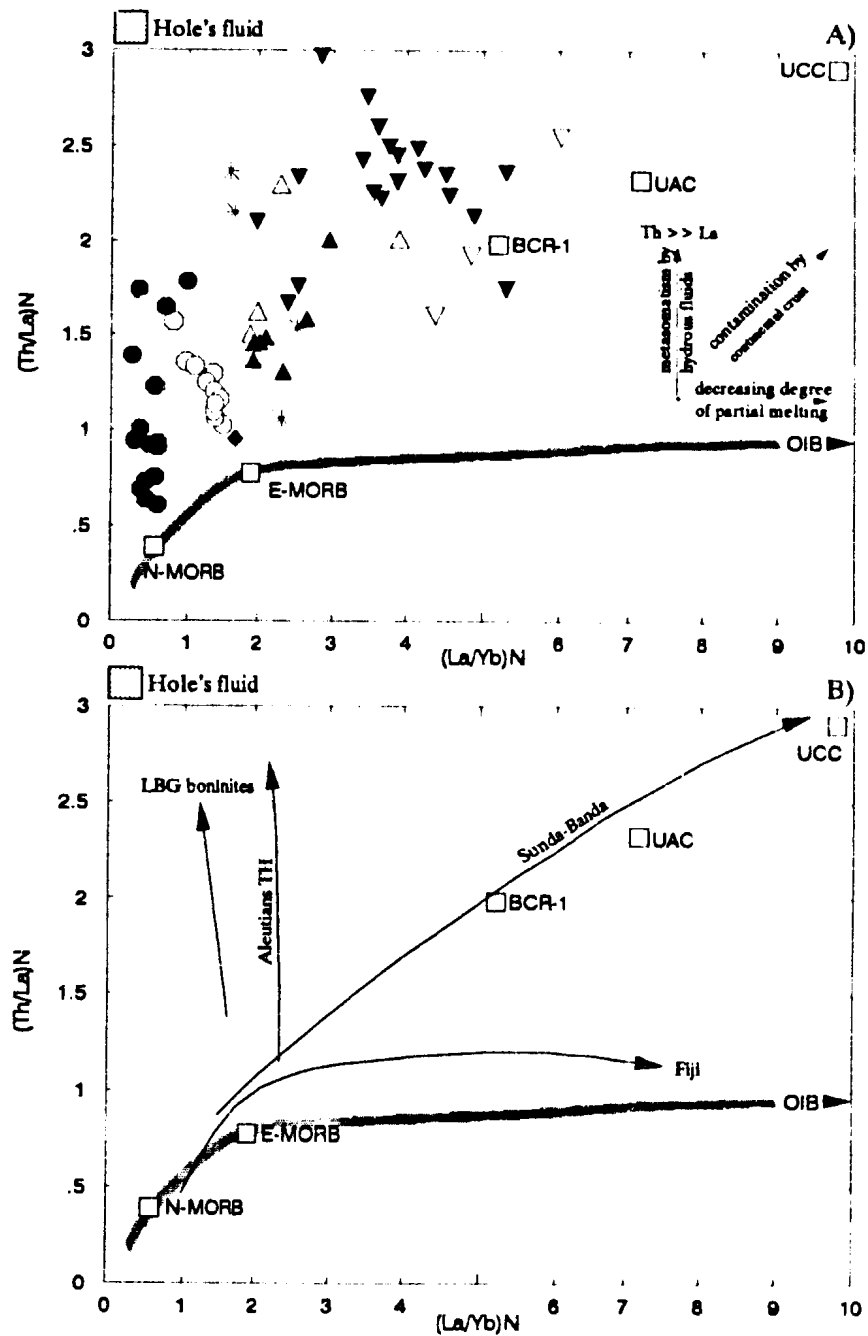


Figure 5.17. The $(Th/La)_N$ versus $(La/Yb)_N$ plot illustrates the relationship of Th with respect to REE in the western Notre Dame Bay lavas in Figure 5.17A&C. Three major trajectories reflecting processes that are expected to influence behavior of Th and the REE in the arc environment are also shown schematically in Figure 5.17A&C. Figures B and D show trends defined by samples from several tectonic settings.

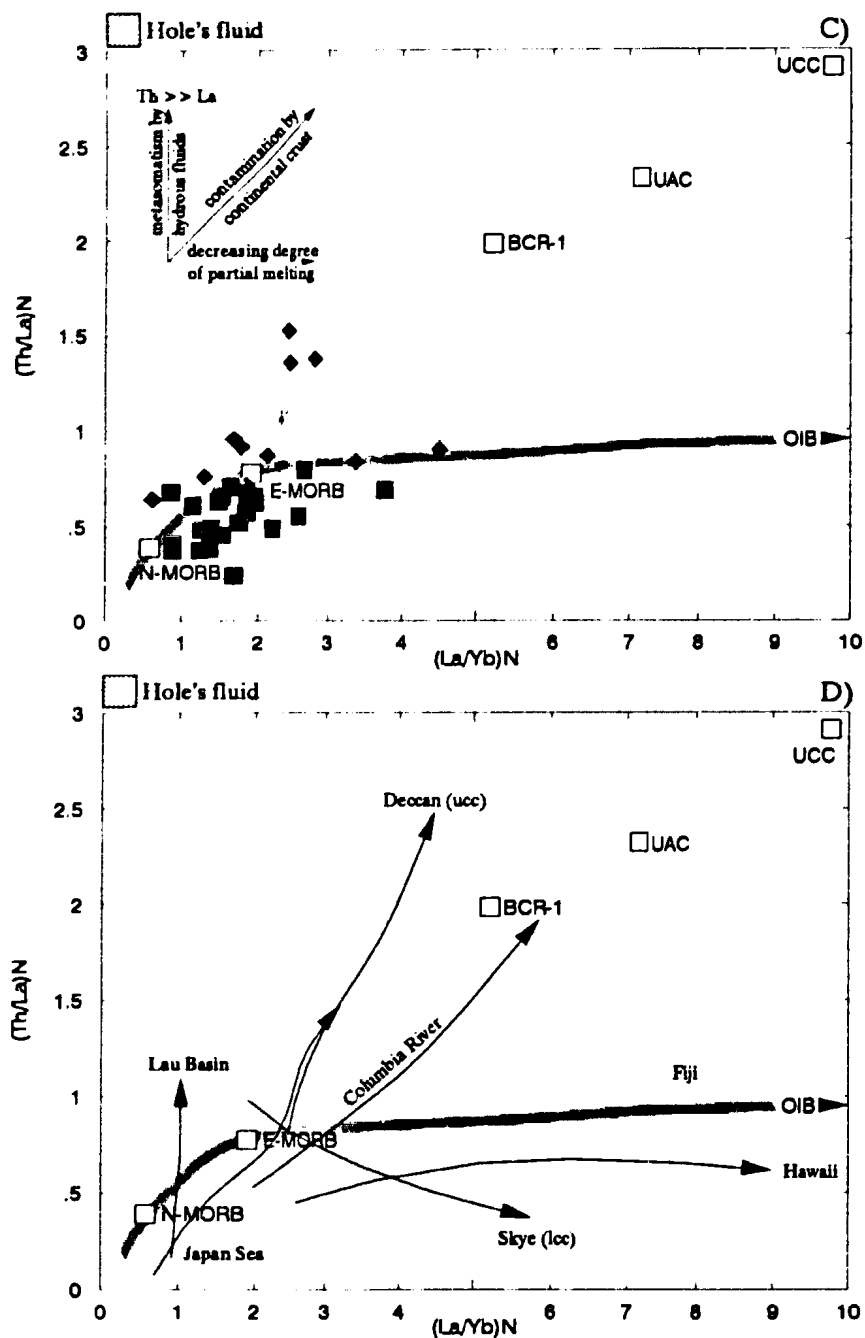


Figure 5.17. (continued). As the $(Th/La)_N$ - $(La/Yb)_N$ plot indicates, there may be three various sources that contributed directly or indirectly to the western Notre Dame Bay area lavas: a) a depleted N-MORB mantle source, metasomatized by a REE-poor, Th-rich fluid phase, similar to the one envisaged by Hole et al. (1984); b) T-MORB to strongly enriched E-MORB source; c) the third possible source may be the upper continental crust.

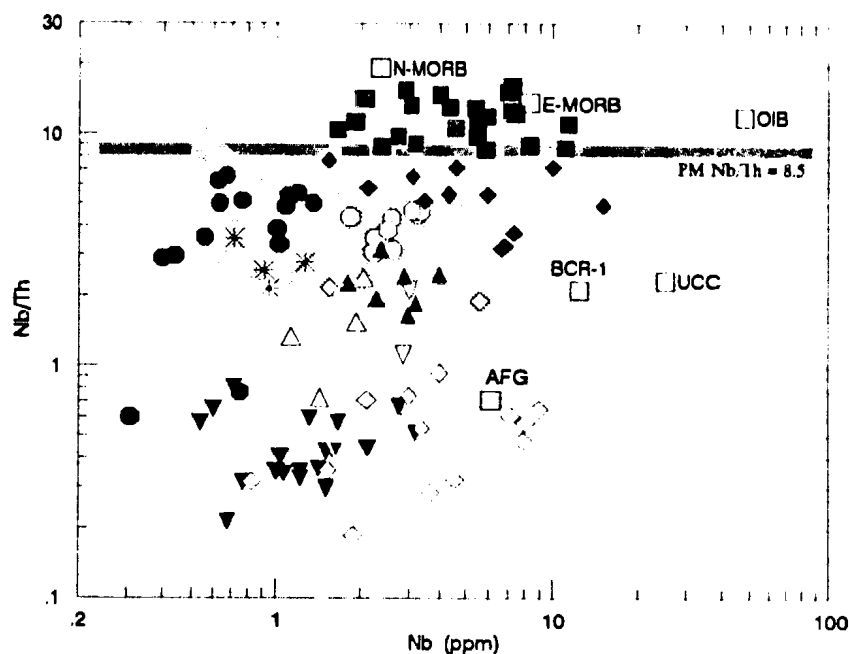


Figure 5.18. The Nb-Nb/Th diagram for compositions of the Notre Dame Bay area lavas. The shaded field reflects modelled hybridization of the mantle source with a rutile-bearing MORB quartz eclogite and is constrained by two lines representing different melt fractions (0.05 and 0.2; Ryerson and Watson, 1987). Although some of the western Notre Dame Bay samples plot within the field defined by these mixing lines, they are arranged in several trends that are at high angles to the calculated mixing lines and emphasize the generally positive correlation between Nb and Nb/Th in the western Notre Dame Bay arc lavas.

It is thought that such behavior results from the decreased ability of metasomatizing fluids to affect the Nb/Th ratio in the mantle with high abundances of Nb and Th (Vukadinovic and Nicholls, 1989). This behavior of the western Notre Dame Bay rocks of arc affinity indicates that the Nb/Th ratio in these rocks is dominated by a slab-derived, high-Th hydrous fluid rather than melt.

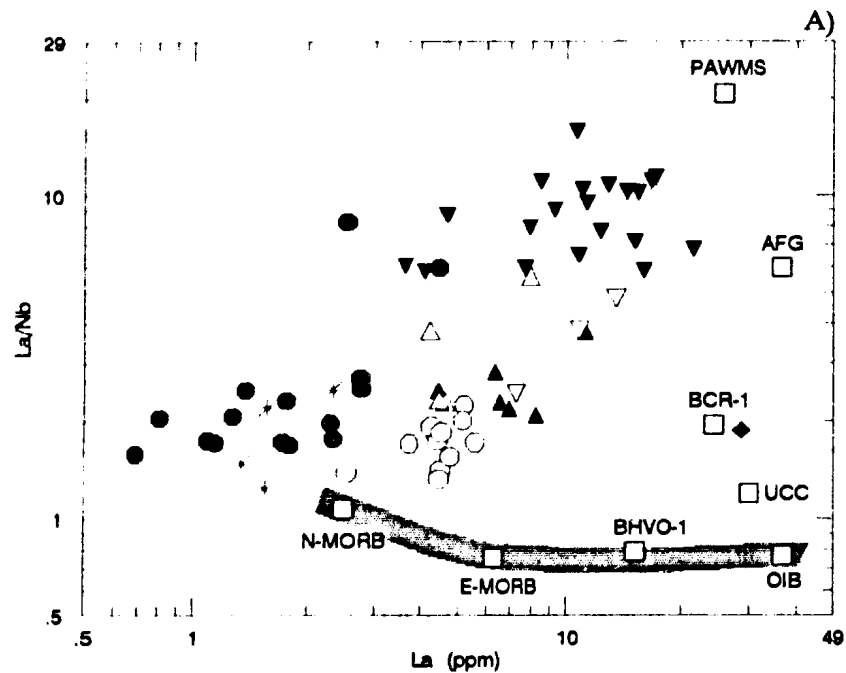


Figure 5.19. The La vs. La/Nb diagram involves two strongly incompatible elements known to have diverse mobility in hydrous fluids (Tatsumi et al., 1986). In the La vs. La/Nb diagram, melts derived from a depleted source should have La/Nb ratios and La content approaching those of the source, particularly with increasing degree of partial melting. Less partial melting of this same source will yield higher La abundances and a relatively low La/Nb ratio; mixing with mantle melts such as E-MORB or OIB would produce a similar effect. The same depleted source modified by hydrous fluids or melts originating from a subducted slab would most likely have elevated La/Nb ratios, but not particularly elevated La (e.g. Tatsumi, 1986; Hole et al., 1984).

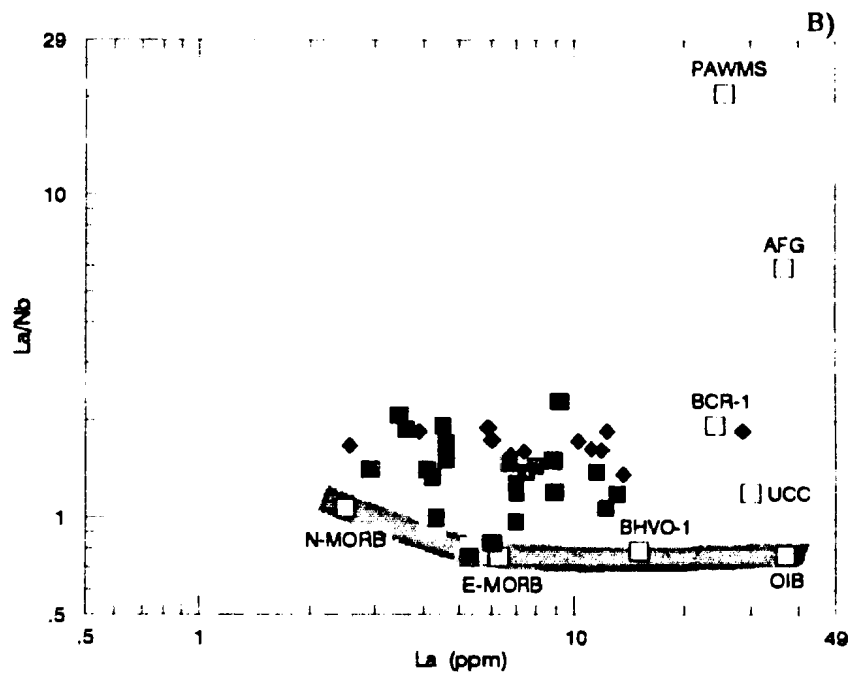


Figure 5.19. (continued) Distribution of the western Notre Dame Bay area samples on the La-La/Nb plot implies a contribution from: 1) a strongly depleted, N-MORB-like source; 2) a MORB source within the range of normal to strongly enriched; 3) input from hydrous fluids reflected in the range of the La/Nb values at a more or less fixed La; and 4) upper continental crust and/or PAWMS-type sediment, with La and La/Nb characteristics similar or even higher than average Lewisian AFG (Weaver and Tarney, 1981).

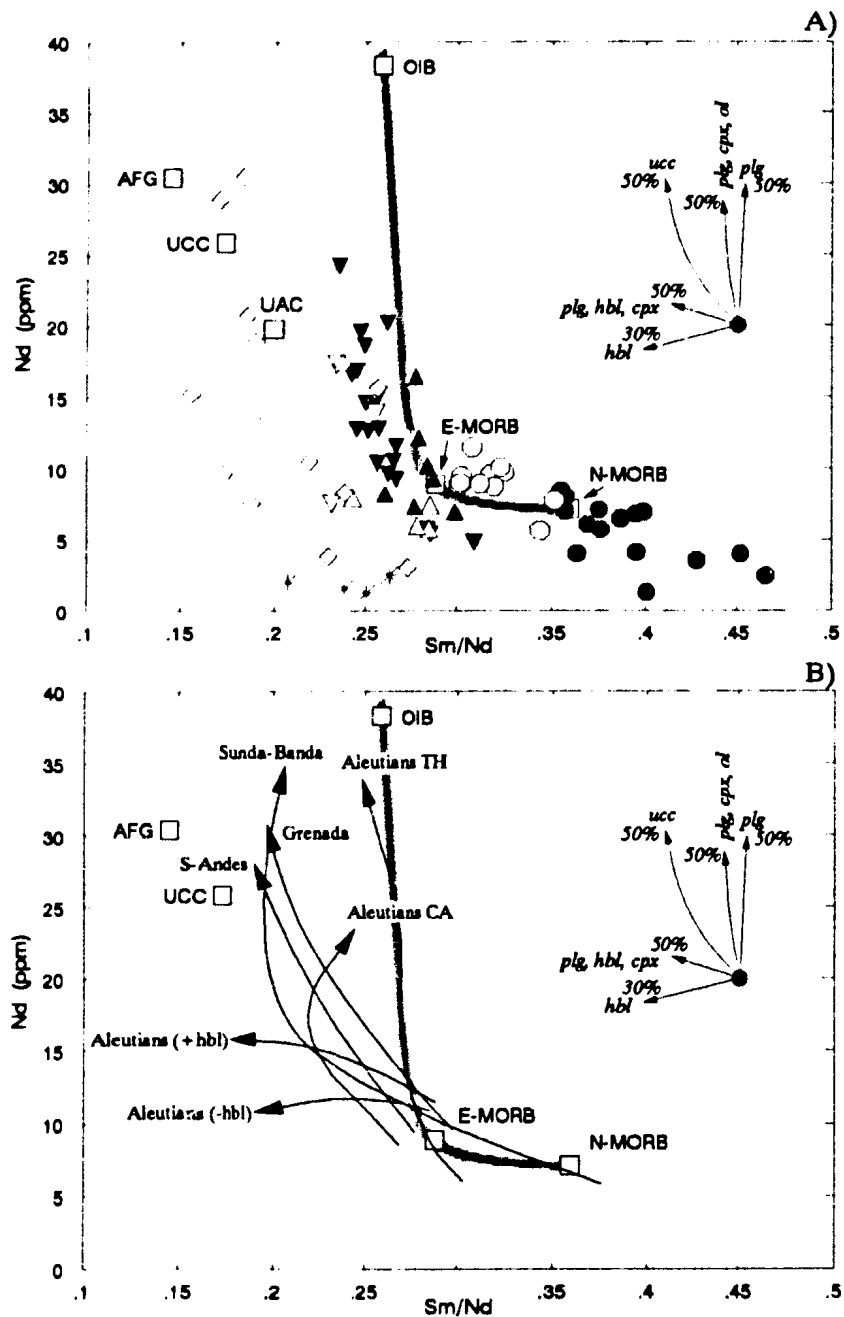


Figure 5.20. The Sm/Nd plot (Davidson, 1986) for rocks of the western Notre Dame Bay area of an arc affinity (A), and non-arc and transitional affinity (C). Curves shown schematically on the diagram illustrate the effects of fractional crystallization and crustal assimilation on arc rocks (A, B). Open diamonds in A represent combined felsic rocks of the F-1 and F-2 types. A curve representing 50% addition of crust to a parental N-MORB-like composition is also shown (C, D).

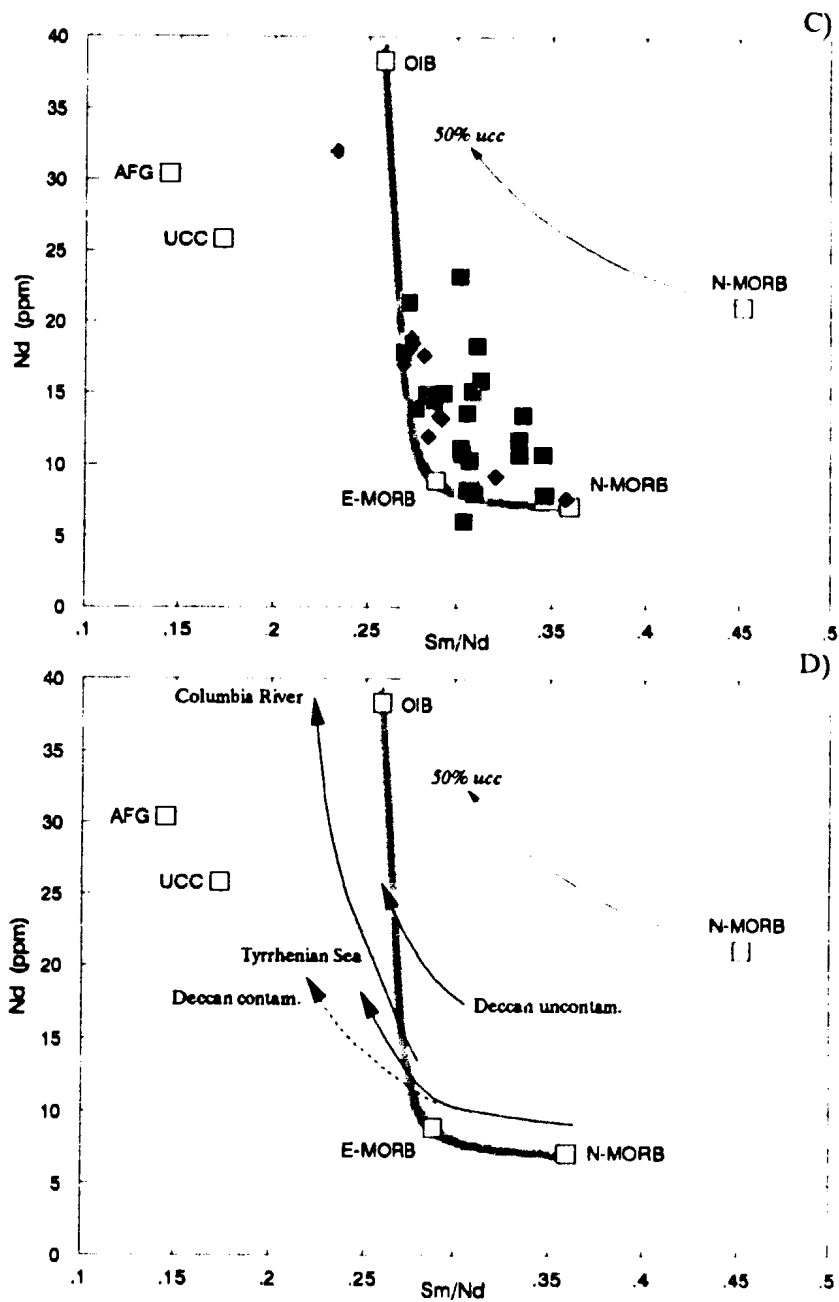


Figure 5.20. (continued) The model curves clearly indicate that contamination by crust may affect Nd concentrations and Sm/Nd ratios much more effectively than any fractionating assemblage. The reliability of these curves is tested using different suites of rocks from various tectonic settings (B, D). It is apparent from the Sm/Nd-Nd plot that sources and processes contributing to the western Notre Dame Bay area lavas include, among others, crustal assimilation.

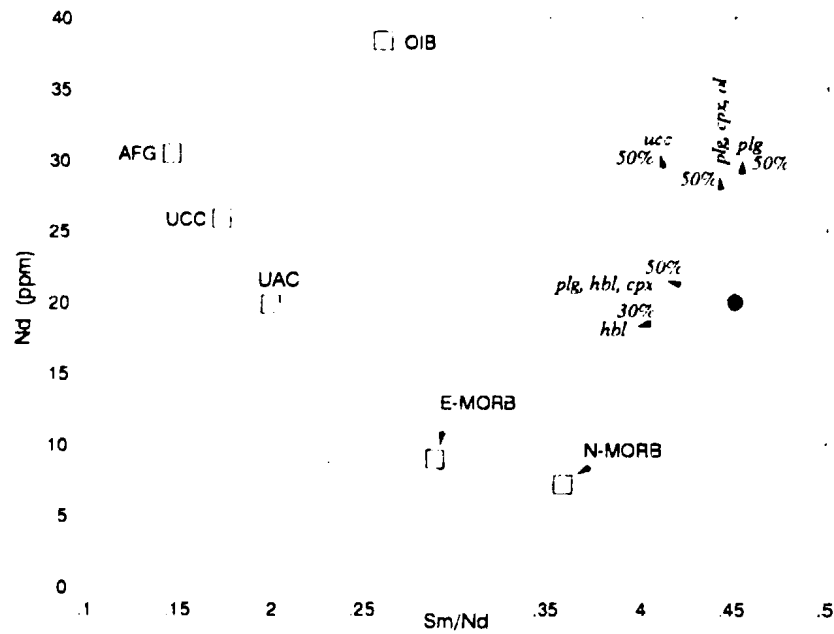


Figure 5.21. The Sm/Nd plot (Davidson, 1986) for the high-Mg dykes of the western Notre Dame Bay area (data from this study and Kean et al., 1994). The distribution of data may reflect a possibly strong effect of crustal contamination on final geochemical composition of the dykes.

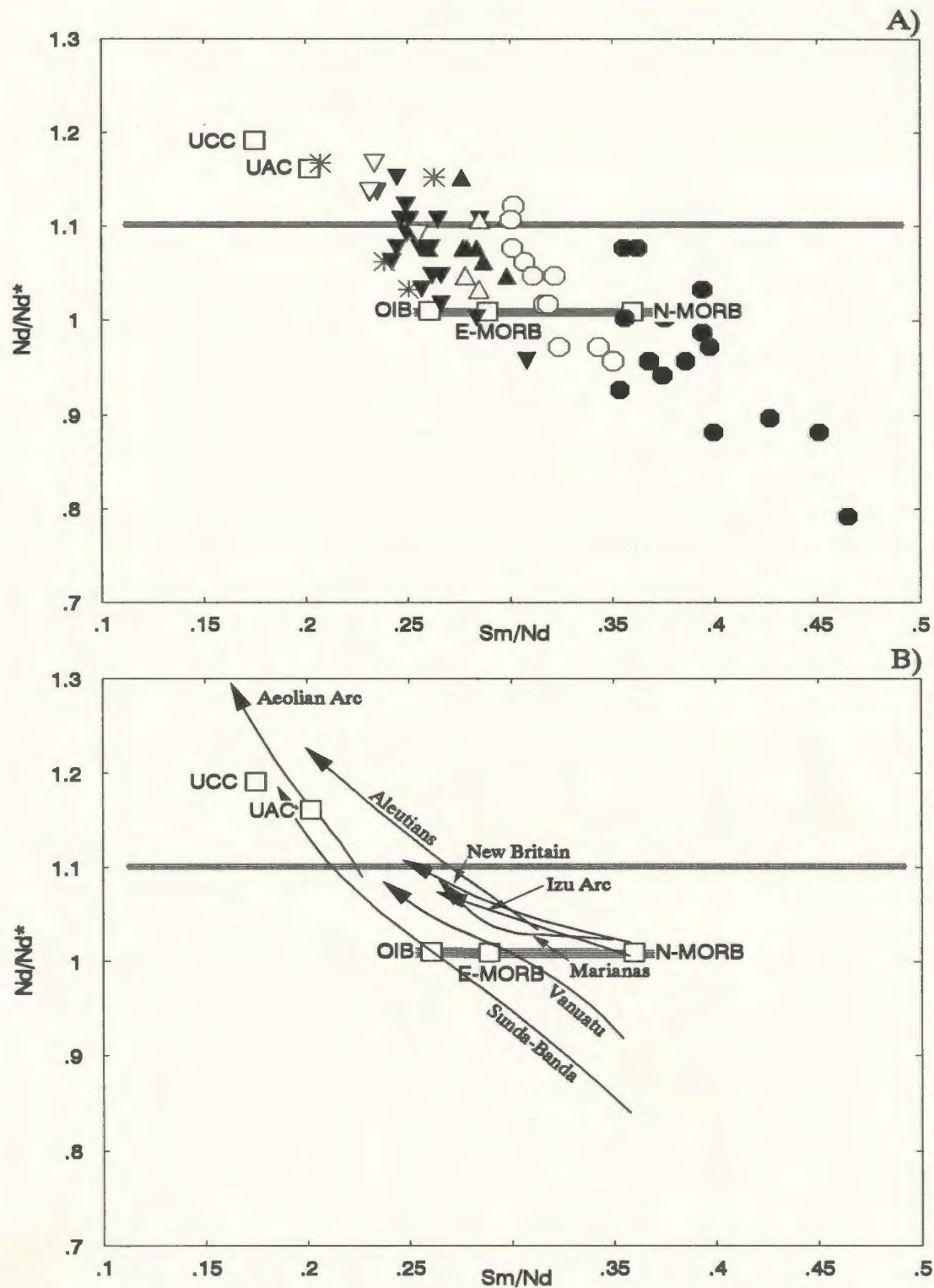


Figure 5.22. The Sm/Nd versus Nd/Nd* diagram for samples from the western Notre Dame Bay area of an arc affinity (A), and non-arc and transitional affinity (C). The parameter Nd/Nd* (Nd measured/Nd calculated from a log-linear interpolation between Pr and Sm) is an effective indicator of crustal contamination, and the Sm/Nd vs. Nd/Nd* plot indicates that addition of crustal component to magmas generated in mantle sources had a strong impact on the final composition of many western Notre Dame Bay area lavas, including some of the NA and TR rocks.

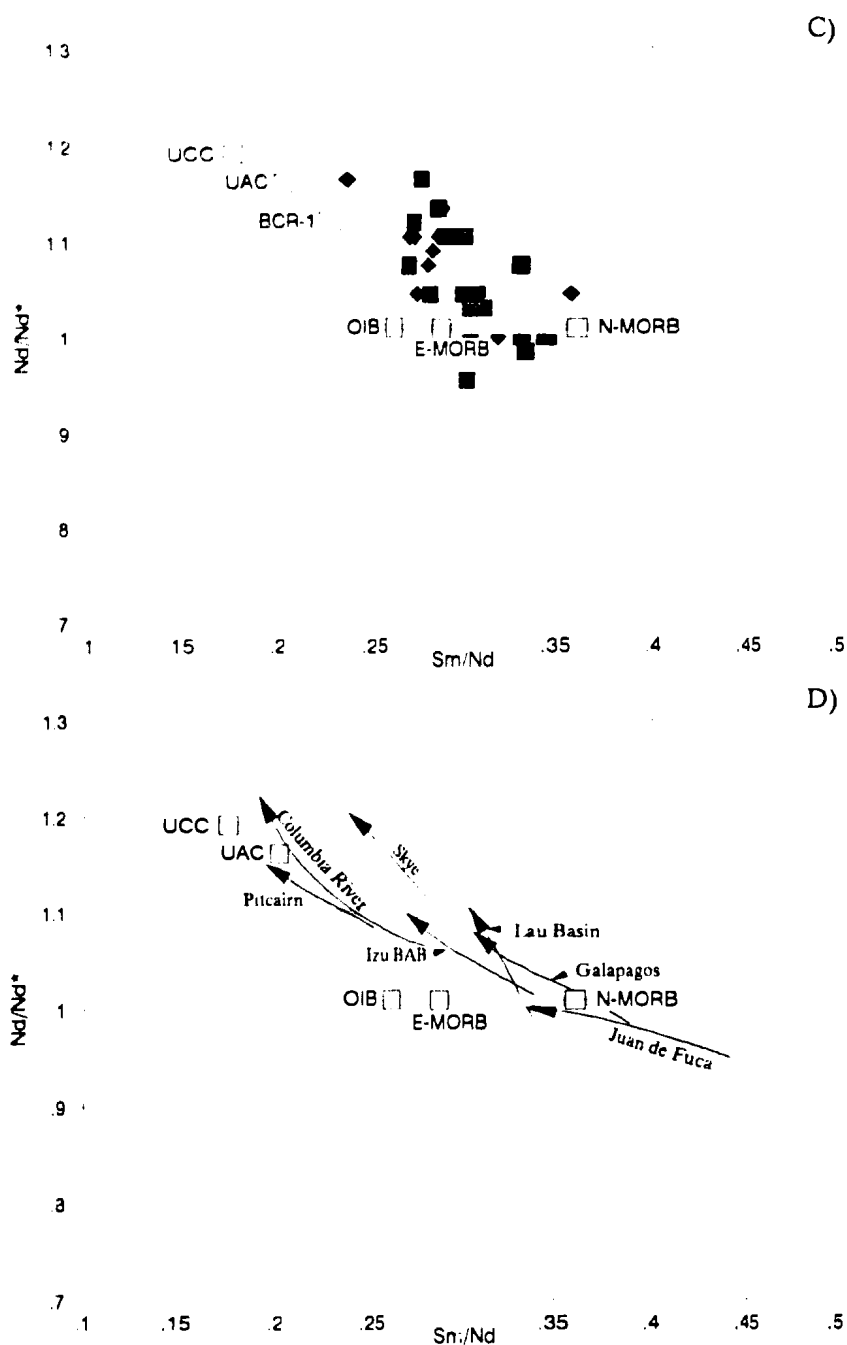


Figure 5.22. (continued). Trends defined by samples from several present day tectonic settings (B, D) suggest that the $Nd/Nd^* = 1.1$ represents an upper limit of the Nd/Nd^* values for the intraoceanic island arcs and back-arc basins. Lavas from arcs evolved upon continental crust (e.g. Sunda-Banda, Aeolian arc), and from mantle plumes contaminated by continental crust (e.g. Skye), display higher Nd/Nd^* values. Similar division may emerge between the HIMU-type and EM-type ocean island basalts (e.g. Galapagos and Pitcairn, respectively).

CHAPTER 6: DEFORMATION HISTORY AND STRUCTURAL GEOMETRY OF THE NOTRE DAME BAY AREA

6.1 Introduction

This chapter is a presentation of structural data and a review of the deformation in the western part of the Notre Dame Bay area. The deformation characteristics, phases of deformation, and structural geometry are documented, and the structure is described and discussed in terms of the thrust tectonics that dominate this part of the Dunnage Zone (e.g. Thurlow, 1981; Thurlow and Swanson, 1987; Calon and Green, 1987; Pope et al., 1990). These data demonstrate that the area of study represents a part of a southeasterly verging, polydeformed, alpine-style nappe.

No detailed account of the deformation history and macroscopic structural geometry of the area has previously been presented. Some smaller structural entities within the Notre Dame Bay area (Western Arm section and Long Island, respectively) have previously been interpreted to represent north dipping homoclines (Marten, 1971; Kean, 1973). Other workers recognized the polyphase deformation in the area (Donahoe, 1968; DeGrace, 1971; Kennedy and DeGrace, 1971; Sayeed, 1970), but because these studies were restricted to relatively small areas, compared to that covered by the present study, the authors were unable to demonstrate a link between identified deformational events and the present distribution of lithostratigraphic units.

The structural observations for this study were carried out at mesoscopic and macroscopic scale. This work was predominantly aimed at defining the structural geometry of the Western Arm and Cutwell Groups, i.e. units with relatively good stratigraphic control. Additional observations were undertaken within the rocks of the Lushs Bight Group, to aid in correlating deformational events recognized in various sections of the Western Arm Group, and to better understand the regional structure. Nonetheless, unravelling of even the general structural history of the latter group is difficult because of the lack of distinct lithological horizons and the diverse behaviour of pillowed lavas during deformation.

Structural data collected during the course of this study have been augmented by data from MacLean (1947), Donohoe (1968), Sayeed (1970), Fleming (1970), Marten (1971), DeGrace (1971), and Kean and Evans (1987). The collected and compiled data are plotted on equal-area projection and lower hemisphere stereo plots. Orientations of planar and linear structural elements used in this thesis are presented in form of: dip=>dip direction (azimuth) (e.g. 30=>180). Structural orientation data are generally compiled for relatively large areas, that encompass many geological structures that vary considerably in style and size. This has resulted in some cases in poorly defined, locally nondescript clusters on some stereograms.

The structural geometry of the western Notre Dame Bay area is complex and the lithostratigraphic units are disposed in at least two regional fold and thrust belts. In the western part of the study area, these belts are of opposing polarity; however in the eastern part of the area, their polarity is crosscutting. Consideration of the orientation data for whole area, coupled with regional geological observations, suggests that the area can be divided into three structural domains (which internally are relatively homogenous); herein termed the: Western; Eastern; and Northern domains (Fig. 6.1). Each of the domains consists of a number of rectangular, laterally discontinuous blocks surrounded by moderately to steeply dipping, brittle to ductile shear zones. These blocks, some of which were referred to as sections in Chapters 3 and 4, are referred to here as fault panels (Fig. 6.2). The structure of the Western Domain is controlled by a northeasterly-trending and southeasterly-verging polydeformed fold and thrust belt. The Eastern Domain is generally characterized by a northerly verging, polydeformed, fold and thrust belt. The Western and Eastern Domains are separated, at least along part of their mutual contact, by the previously unrecognized Halls Bay Fault. The Northern Domain is similar in style to the Eastern Domain, but is separated from it by the prominent Long Island Tickle Fault. There is geological and geophysical evidence that the Northern Domain may be a block, exposed in a horst, related to the Buchans-Roberts Arm Volcanic Belt. This possibility is explored in some detail later in this chapter.

Most of the structures observed and interpreted in the field are folds or thrusts and high-angle reverse faults. Several generations of structures were observed, but not all can

be correlated on a regional scale. At least five events were identified in the deformational history of the Notre Dame Bay area on the basis of structural and geological observations, and timing of some of those events is constrained by stratigraphic evidence and the $^{40}\text{Ar}/^{39}\text{Ar}$ dating. These events are presented briefly below and described in more detail later in the chapter.

The D1 event is a non-penetrative deformational event which is reflected in the formation of chloritic shear zones with a strongly mylonitic foliation, that are normally developed within pillow lavas of the Lushs Bight Group. Some of these shear zones are closely associated with sulphide deposits (e.g. MacLean, 1947; Fleming, 1970; Kennedy and DeGrace, 1972; Kean et al., 1995). The ~500 My old, hornblende- and pyroxene-phyric dykes, although they intrude rocks of both the Lushs Bight and Western Arm Groups, are particularly numerous within or near the D1 shear zones where they locally form swarms. No D1 folds have been identified.

The D2 deformation is a regionally penetrative event that produced closed to tight major upright folds and an associated axial planar cleavage. The D2 folding and associated cleavage does not affect the dyke swarms intruding the D1 shear zones in the Little Bay and Whalesback mine areas. However, the Coopers Cove pluton, which has been dated as 465 +/- 2.5 Ma (see Chapter 3), displays a well developed foliation that parallels the S2 cleavage in the volcanic/volcaniclastic country rocks; for that reason the D2 event is considered to be coeval with or younger than this magmatic event.

The D3 deformation is a major regional event manifested in the emplacement of an alpine-style nappe consisting of the Cambrian-Ordovician rocks of the Lushs Bight and Western Arm Groups, upon the Lower Silurian Springdale Group and the underlying Roberts Arm Group. This event is interpreted to have closely followed deposition of the post-Lower Silurian red beds that overlie both the Springdale and Robert's Arm Groups. The red bed unit, which marks the sole thrust fault to the nappe (the Lobster Cove Fault), is interpreted to be dynamically related to the nappe, having been deposited in the foreland basin formed in front of the advancing nappe. It is thought that many of the large NE trending folds both within the nappe and underlying rocks of the Springdale Group, as well as most of the major, NE striking and southeasterly verging thrust faults were generated

during this event. The D3 deformation is, to a large degree, responsible for the present distribution of lithostratigraphic and structural units within the western Notre Dame Bay area. The event may have taken place in two, sequential phases; the first phase having been responsible principally for nappe emplacement; and the second phase having involved imbrication and further deformation of the nappe and its footwall rocks.

The D4 deformation is expressed only in the Eastern and Northern Domains. It is reflected in an apparent rotation of the Lobster Cove Fault, and by folding and thrusting in rock units north and south of the fault. This deformation seems to be associated with generation of a large regional, northerly plunging antiform, the hinge zone of which is located in the southern part of the Halls Bay Head Peninsula.

The D5 deformation represents the second major regional event, and resulted in north-northwest directed high-angle thrusting and creation of a number of foreland propagating duplexes of various size (e.g. in the Western Arm section). This event involves rocks of the red bed unit of the probable Lower Carboniferous age.

6.2 Deformation Characteristics Of Lithological Units In The Notre Dame Bay Area

One of the main problems with establishing a definitive lithostratigraphic framework for the western part of the Notre Dame Bay area stems from the locally intense and strongly heterogeneous brittle and plastic deformation that has affected the volcanic sequence. Strain has been partitioned heterogeneously between the locally isotropic to highly anisotropic pillow lavas, the interbedded mafic tuff facies, and the overlying, isotropic to partially anisotropic felsic tuffs, and cherty sedimentary rocks. Felsic tuffs and flows responded mostly by brittle fracturing, but locally (e.g. in the Catchers Pond section) form a spectrum of final lithological products that vary from brecciated felsic protolith to a mylonite represented by quartz sericite schist. A whole range of structures can be seen in pillow lavas and mafic tuffs resulting from the brittle fracturing, as well as from a higher degree of penetrative strain.

6.2.1 THE LITTLE BAY BASALT

This unit is disposed in typically large, lozenge-like blocks surrounded by anastomosing high strain zones, clearly visible in plan view on aerial photos and radar

images. Within these blocks, pillows are steeply dipping to vertical indicating that they occur on the steep limbs of tight to isoclinal folds. The fold limbs are commonly strongly sheared and pillow tops can not be determined.

The pillowed flows of this unit were particularly susceptible to deformation and exhibit a wide spectrum of mylonitic foliations in various stages of development. The pillow margins are invariably less competent than the cores, reflecting contrasts in the prevailing alteration minerals, i.e. chlorite (on the margins) vs. epidote (in the cores). Typically, deformed pillows of the Little Bay Basalt show pear-shaped, thickened selvage tails formed of material transposed from pillow margins, and indicative of a heterogeneous strain history (e.g. Borradaile and Poulsen, 1981). In many locations, previously homogeneously strained pillows have been overprinted by mesoscopic shear bands, with tails of the deformed pillows rotated towards the direction of movement. This type of deformation is typically associated with shear zones and is well exposed in the Little Bay mine area, on Fox Neck, on the west coast of Pilleys Island and in the hanging wall of the MacLean Fault on the Halls Bay Head peninsula.

The cleavage within the basalt is defined by an alignment of actinolite and chlorite, and undulating traces of fine grained sphene. Phenocrysts of altered, euhedral to subhedral plagioclase are commonly strained, broken or bent. In more schistose mafic volcanic rocks plagioclase crystals are rotated towards the foliation (see also: Fleming, 1970; Marten, 1971a). Commonly, clots and veins of epidote are either crosscut and deformed or augened by cleavage.

The angular relationships between the orientation of pillows and cleavage is generally very difficult to determine, and is impossible to discern in tightly to isoclinally folded lavas in which pillows are strongly deformed and rotated towards schistosity. Even in less-deformed parts of structural blocks, pillowed flows pose a similar problem, showing the effects of non-coaxially accumulated strain that makes them useless for way-up and bedding determinations.

Pillows which experienced intense homogenous plastic deformation are strongly flattened into "pancake" shapes. In zones of particularly high strain, pillow shapes can no longer be discerned, and the pillow lavas exhibit a compositional layering in the form of

"ribbon" mylonites. This fabric is parallel to foliation and is defined by laminae of alteration minerals, predominantly epidote and chlorite, which were derived from transposed epidotized pillow cores and chloritized pillow margins, respectively. Zones of such ribbon mylonites are commonly found within deformed flows of the Little Bay Basalt. Particularly good examples were observed in the hanging wall of the MacLean Thrust on the east coast of Halls Bay Head, and on west coast of Pilley's Island.

6.2.2 THE WESTERN ARM GROUP BASALTS

In contrast to pillow lavas of the Lushs Bight Group, most pillowed and massive basalts in the Western Arm Group are unstrained or possess only a weakly-developed foliation. Where present, the foliation is defined by thin bands of segregated chlorite and actinolite, and augens of pyroxene crystals and rare blebs of epidote. This suggests that the regional deformation, that produced the cleavage post-dates alteration but may have been coeval with metamorphism.

Locally strong flattening and folding of pillows was observed in the Catchers Pond section of the Western Arm Group where, close to the Green Bay Fault, the pillowed basalt displays a very heterogeneous deformation. In intensely deformed flows, the pillowed protolith has been obliterated and mafic volcanic rocks form mylonites, similar to those observed in deformed pillows of the Little Bay Basalt. The transition from almost undeformed pillows to mylonite occurs within a very short distance, i.e. a few meters (see also Dube et al., 1992).

6.2.3 OTHER LITHOLOGIES OF THE WESTERN ARM GROUP

In the Western Arm Group, the pillowed and massive basalts are interbedded with mafic tuffs, felsic tuffs, minor felsic flows, cherts and argillites. Mafic and intermediate tuffs are predominantly isotropic and respond to deformation mostly by brittle fracturing, or locally by development of chaotic incipient chlorite-sericite foliation with variably fractured phenocrysts (Fig. 6.3). In zones of higher strain associated with faults, e.g. the MacLean Fault, the tuffs display well developed chlorite-sericite foliation, which wraps around rotated phenocrysts (Fig. 6.4). Rhyolitic tuffs, minor flows and felsic subvolcanic intrusive bodies are highly isotropic and developed mostly brittle fractures in response to deformation. Yet, in zones of higher strain such as the northwestern part of

the Catchers Pond section, these rocks contain a strong mylonitic foliation confined to belts of quartz-sericite schist which wrap around larger boudins of less deformed felsic volcanic rocks. It can be shown that partitioning of strain in felsic rocks is controlled locally by original facies changes. Zones of "sericite schists" display a well developed differentiation into quartz-rich laminae, divided by thin mica-rich films, and common trails of opaque minerals parallel to the S2 microlithons (Fig. 6.5). Quartz-filled tension gashes and quartz veins associated with sericite shear zones attest to the importance of pressure solution as a mechanism of deformation.

Red and green cherty sedimentary rock, that is characteristic of the Skeleton Pond Formation deformed in a brittle fashion. However, in many places it shows evidence of a strong penetrative strain, expressed by transposition of bedding into cleavage and the formation of intrafolial and rootless folds typical of well developed transposition fabrics. This type of fabric is commonly found in cherty beds along the Lobster Cove Fault zone on Sunday Cove, Pilley's and Triton Islands (Fig. 6.6), but also within the hinges and limbs of isoclinal regional folds.

6.2.4 INTRUSIVE ROCKS

Most of the rocks that intrude volcanic and volcanoclastic rocks in the area of study do not show any well developed fabric. The deformation observed is usually brittle, resulting in boudinage of dykes (e.g. in the Whalesback mine area) and fracturing of the larger intrusive bodies. Locally, strong brecciation was observed in plutons adjacent to faults (e.g. southern contact of the Brighton Complex). In other bodies, megafoliation is well developed (e.g. dioritic body on the western shore of Pilley's Island).

Unlike many other plutonic bodies, the Coopers Cove and Colchester units exhibit a well-developed foliation defined by 25-30% aligned biotite or chlorite and hornblende. The biotite crystals are bent or broken, but the plagioclase and microcline crystals are not aligned; although, microcline (perthitic variety) shows evidence for some internal plastic deformation. Quartz is typically broken into subgrains and displays serrated grain boundaries and the undulatory extinction typical of recrystallized quartz. Pyroxene, where present, forms augens within the chlorite (Sayeed, 1970). The fabric

(biotite alignment) conforms to the crystal plastic strain type of Hutton (1987), i.e. the deformation affected the pluton after full crystallisation, yet with enough heat preserved in the system to allow at least partial plastic deformation.

6.3 Deformation History

On the basis of the field observations and consideration of the available orientation data, it is feasible to divide the deformation history of the western Notre Dame Bay area into five distinct phases. All five of these phases are related to contractional events; three of them, D2, D3 and D5, were regionally penetrative, reflected in folding and faulting, as well as in the development of related planar/linear features. These three events are primarily responsible for the present distribution of lithostratigraphic units, and for the overall structural grain in the Notre Dame Bay area.

Only a few structural elements in the area of study can be unequivocally ascribed to a major extensional event, and most extensional structures (e.g. shear bands, minor listric faults, extensional reactivation of some thrust faults) can be readily incorporated into otherwise contractional events. Two aspects of the geological makeup of the Notre Dame Bay area are thought to provide evidence of extensional phases in the history of the area. One of them is the presence of widespread Silurian magmatism (Whalen, 1986, 1989; Coyle and Strong, 1987; Coyle, 1990), and the other is the existence of a small red bed unit in the King's Point area, that is interpreted to be of Carboniferous age (Kean and Evans, 1987a, b). However, there is little evidence in the area that these two potentially extensional events have significantly influenced the structural evolution of the western Notre Dame Bay area.

6.3.1 D1 DEFORMATION

The D1 deformation is reflected in the presence of "chlorite schist zones" in the Lushs Bight Group, some of which are hosts to the sulphide mineralization (e.g. Fleming, 1971; Kennedy and DeGrace, 1972; Kean and Evans, 1989). Kennedy and DeGrace (1972) interpreted these zones to be early structures resulting from the imposition of a regional penetrative foliation on an earlier inhomogeneous fabric. Two of the chlorite schist zones were studied in some detail during this study, one in the Whalesback Mine area, and the other in the Little Bay Mine. Each of the zones was the

focus of several deformational events. The S1/S2 foliation is developed heterogeneously and varies from a truly mylonitic fabric within high strain chloritic shear zones, to a weakly developed schistosity affecting only pillow margins barely a few meters away from the zones.

In the Little Bay Mine, the shear zone contains layers of pyrite (+/-quartz) interlayered with chloritic schist. The pyrite/quartz layers are in places strongly boudinaged, forming subvertical elongate lozenges. The boudins are most commonly of the "pull-apart" type, indicating that they are related to a subhorizontal stretching. The boudins are characterized by wing-like appendages (visible in perpendicular cross sections), the shape of which indicates development in a dextral strike-slip regime (e.g. Hanmer and Passchier, 1991). The "wings" in some of boudins are also deformed by shear bands that additionally support development of these boudins in dextral strike-slip. The intervening chlorite schist is folded around subhorizontal axes parallel to the shear zone; whereas, flattened pillow lavas that surround the zone are cut by the steeply south dipping, mesoscopic shear bands. Evidently, original subhorizontal stretching and formation of boudins was related to a different event, than that which produced subhorizontal folds in chloritic schist and southerly-dipping shear bands in the pillow lava, both of which indicate northwest-directed, high angle reverse faulting.

Volcanic and subvolcanic rocks of the Lushs Bight and Western Arm Groups are typically intruded by pyroxene- and amphibole-plagioclase-phyric dykes. The dykes intrude only the lower part of the Western Arm Group, including the Big Hill Basalt, and dykes have not been observed in the Welsh Cove and Western Head formations. The dykes are especially common within or near D1 chloritic shear zones, and this is particularly evident in the Little Bay and Whalesback mines. A dyke from the latter area was isotopically dated at 493 +/-5 Ma (see Chapter 3). The D1 shear zones are intruded by dykes, mostly en-echelon but locally conjugate (?) to the main trend (Fig. 6.7 and Appendix E, Fig. E-i). The mean orientation of the predominantly en-echelon dykes in the Little Bay mine area is 89.5=>288 (Fig. 6.7), which suggests extension in the direction ~108-288°. In the Whalesback mine area, dykes form two en-echelon sets intruding at 88.5=>128 and at 89=>003 (Appendix E, Fig. E-i). The dykes account for a

cumulative E-W extension of approximately 3-4% in the immediate area of the Little Bay Mine "glory hole" (Fig. 6.7)

Only the first set of dykes cuts the Whalesback shear zone, and it is significant that this particular set of dykes forms a relatively large scatter on the stereogram; whereas, the E-W trending dykes form a relatively tight cluster (Appendix E, Fig. E-i). The majority of the dykes are planar, but some exhibit buckling interpreted to be related to anticlockwise rotation and reflected in the scatter of data on the stereogram. Together with a slight bend at their terminations, this supports the strong possibility of a late-kinematic emplacement. Moreover, several dykes studied in the Whalesback and Little Bay mines show evidence for a slight sinistral slip along their margins, which is reflected in a minor "drag" folding of the foliation at the dyke margins.

6.3.2 D2 DEFORMATION

The D2 event produced the earliest, regionally recognizable deformation in the western Notre Dame Bay area. It is manifested on a large scale, by predominantly NE- to NNE-trending tight to isoclinal folds. A large bulk D2 shortening strain resulting from tight to isoclinal folding is reflected in transposition of bedding into parallelism with the S2 fabric (e.g. in volcanoclastic rocks and cherts of the Western Arm Group). The D2 deformation resulted in a heterogeneously developed S2 foliation, that post-dates greenschist facies metamorphism. The S2 foliation varies in style from a weakly developed axial planar cleavage visible only in the chloritized margins of pillows, to a truly mylonitic fabric in "chloritic" shear zones - zones of high strain. Commonly, aggregates and veins of epidote are crosscut and deformed by cleavage, or surrounded by cleavage which augens around clots of epidote. This suggests that alteration affecting the Little Bay Basalt is older than the first penetrative deformation (see also Marten, 1971a).

A locally well developed mineral stretching lineation with consistently steep plunges is observed on the S2 cleavage planes, particularly in the Lushs Bight Group pillow lavas, but also in rocks of the Western Arm Group in the northwestern part of the Catchers Pond section. In the western part of the study area, this lineation plunges vertically to steeply NNW. Although data are very limited in the eastern part of the area,

the relationship between S2 and L2 appear to be very similar. Most likely both the S2 and an associated L2 lineation resulted from the same event, controlled by a simple shear deformational event with the initial (prior to steepening by the D5 event) azimuth of the stretching direction indicating the shear direction.

F2 folds range in scale and their wavelength varies from tens to hundreds of meters, but they have not been observed at outcrop scale. The character of these predominantly macroscopic F2 folds can be deduced in outcrops by inspection of the relationship between bedding and cleavage, which permits the identification of normal and overturned limbs. Locally, where bedding has been transposed into the cleavage, folds have been delineated by following contacts between different lithological units rather than by relying on angular relationships between bedding and cleavage. This approach combined with sparse evidence for the overturning of stratified units, confirmed the previously inferred presence of an overturned limb in the area south of King's Point (MacLean, 1947; DeGrace, 1971). Regional considerations, including interpolation of field observations within larger fault panels, indicate that most of the Western Domain of the study area is located on the lower, overturned limb of a gently inclined to possibly recumbent (if the roll-back resulting from D5 thrusting is taken under consideration), east-facing and east-closing fold. The macroscopic parasitic folds are predominantly tight to perhaps isoclinal, and display well developed axial planar cleavage. The folds are approaching class two of fold profiles (similar style), with variably attenuated limbs, and poorly recognizable to non-existent hinges (considered to be faulted off by Kean et al., 1995). This type of "hingeless" folds resulted from the transposition of bedding into the S2 foliation and is especially common within the Lushs Bight Group pillowed flows.

The absolute age of the D2 event is not known, but at least one line of evidence suggests that the Colchester and Coopers Cove pluton, dated at 465 +/- 2.5, is late to immediately post-kinematic with respect to D2. Foliation within the pluton parallels that of the volcanic/subvolcanic host rock and it is considered to be the S2. Locally in the marginal dioritic zone of the pluton, well foliated mafic xenoliths are present in which the fabric parallels the S2, although the fabric in the diorite is less evolved than in xenoliths.

The central zone of the Colchester pluton consisting of granophyric granodiorite, contains only a minor amount of schistose inclusions, but the host rock shows only the cataclastic texture. Sayeed (1970) reported a strongly cataclastic contact in the Colchester pluton, between marginal diorite and quartz monzonite, with the zone of cataclasis having been intruded by swarms of felsic dykes. The well-developed fabric in the marginal zone of both plutons (hornblende, biotite and chlorite alignment) conforms to the crystal plastic strain type of Hutton (1987), i.e. deformation affected the granodiorite after full crystallisation, although with enough heat preserved in the system to allow at least partial plastic deformation.

6.3.3 D3 DEFORMATION

The D3 deformation is to a large degree responsible for the present distribution of lithostratigraphic and structural units within the Notre Dame Bay area. The D3 deformation is characterized by the emplacement of a previously assembled, regional scale, F2 recumbent fold (i.e. alpine style fold nappe; e.g. Ramsay, 1981; McClay, 1991) upon rocks of the Roberts Arm Group and the overlying volcanic and sedimentary rocks of the Springdale Group. Folds associated with this event are northeast-trending and asymmetric in the hangingwall (i.e. within the nappe itself), but mostly concentric in the footwall (i.e. Springdale Group rocks).

The further imbrication of the nappe and incorporation into a southeasterly verging fold and thrust belt also probably occurred during the D3 event, but may represent a separate, latter phase of deformation. The fragmentation of the nappe and the formation of a large scale east-southeast verging imbricate fan was associated with a development of hangingwall antiforms (exposing younger rocks) and footwall synforms (in which the lower parts of the stratigraphy are now preserved). Sparsely developed S3 axial planar cleavage is generally very difficult to distinguish from S2, especially within the Lushs Bight Group. However, along the Catchers Brook Fault, the S3 foliation is locally present in rocks of the Western Arm Group where it dips WNW and cuts across the S2 cleavage. The dip of the S3 foliation may be up to 30° shallower than that of S2 fabric away from D3 high strain zones such as the Davis Pond Fault. Along the Davis Pond Fault it is impossible distinguish between the S2 and S3 foliations, perhaps because

S2 is transposed into the S3 cleavage. The S3 planes, similarly to S2, contain in places a well defined down-dip mineral stretching lineation, which also plunges at a more shallow angle than its L2 equivalent.

Several D3 folds in the Western Domain differ in trend and plunge from the general regional trend and plunge of D3 folds. Those are described below in sections dealing with with structures within the individual fault panels.

The style of the D3 deformation differs from D2 in the development of numerous brittle-plastic shear zones (of which the Davis Pond Fault is good example) and associated, dominantly brittle, imbricate thrust systems (Boyer and Elliot, 1982) in the Ordovician hangingwall rocks and in the Silurian footwall rocks. A foreland dipping duplex south of the Catchers Brook Fault involving rocks of the Springdale Group is one of the best examples of the latter structural style.

Within the Eastern Domain, evidence for the D3 deformation is difficult to see as it is largely overprinted by the D4 deformation. The existence of the D3 event can be convincingly demonstrated only within the Lobster Cove Fault shear zone (see section on the fault below), away from which structures thought to be related to D3 are rare (Fig 6.8).

6.3.4 D4 DEFORMATION

The D4 deformation affected primarily the eastern part of the study area. This event was a non-penetrative contraction approximately parallel to the trend of the D3 fold and thrust system in the western part of the area. It is reflected best in folding and rotation of the sole thrust to the nappe, the Lobster Cove Fault, which is subhorizontal in the Springdale area, nearly north-dipping and vertical on Sunday Cove Island, and overturned and south dipping on Pilley's Island and Triton Island. The deformation produced folds with approximately NW-SE trending, SE plunging axes, and was associated with an intense imbrication of the part of the nappe included in the Eastern Domain, which resulted in formation of a NE verging fold and thrust belt. Similar, but less intense, deformation has been recognized in the Northern Domain.

No penetrative cleavage is associated with the D4 event. Locally in zones of high strain associated with the southwesterly dipping thrusts, a new cleavage was developed,

that on average is slightly shallower than, but similar in strike to, pre-existing, rotated S2/3(?) The imbrication is particularly intense in cherts and mafic tuffs of the Skeleton Pond formation, and these commonly form macroscopic to mesoscopic duplexes (Figs. 6.9 and 6.10), which are enclosed by larger scale imbricate systems developed in overlying and underlying pillow lavas of the Western Arm Group.

The F4 folds plunge approximately towards the east, but their axes and D4 thrusts "wrap" around the outcrop of the Brighton Complex, having a SE azimuth on Pilley's Island, an ESE azimuth in western Triton Island, and an ENE azimuth in eastern Triton Island. This shape of the D4 fold and thrust belt indicates that the Brighton Complex was not imbricated and/or incorporated into the belt, but instead formed a rigid obstacle for the propagating belt. This indented shape of the belt is in contrast to the straight outline of the southern shore of Long Island, that is separated from Pilley's and Triton Islands by the Long Island Tickle Fault. Pigeon Island, an islet off the Long Island's southern shore, consists of altered gabbro and serpentinite blocks in a carbonitized, strongly sheared matrix, which is characterized by an omnipresent C-S mylonitic fabric (Fig. 6.11). Orientation of sympathetic shear fractures in several gabbro blocks implies sinistral strike-slip (Fig. 6.12); whereas, the C-S mylonites reveal oblique thrusting in a NE direction.

In the Northern Domain, the D4 deformation is reflected by the presence of a large scale regional fold, anticline-syncline pair, with a gently southeasterly-plunging and trending axis. In this area, deformation produced an axial planar cleavage, confined to zones of higher strain that are typically localized in narrow hinges and on steep to locally overturned limbs of tight folds in the Wild Bight area. In places in the Wild Bight area, bedding of the Pigeon Head Formation rocks is transposed into the cleavage. Everywhere in the Northern Domain, the D4 event is associated with north-directed folding and thrusting on smaller scale.

The impact of the D4 event in the Western Domain is unknown; no structures comparable to the north-verging fold and thrust belt in the Eastern Domain have been recognized in the west.

6.3.5 D5 DEFORMATION

The D5 deformation produced a northwest verging, NE-SW trending fold and thrust belt, that is predominantly manifested by variably sized folds in the Eastern and Northern Domains, but mainly by high-angle reverse faults in the Western Domain. The D5 folds form a wide variety of styles, and exhibit major differences in their shapes, interlimb angles and profile geometry. Bedding, and to some extent pre-existing cleavage, still have a strong mechanical control on folding, but at this stage major differences are controlled mainly by the shape of early fold profiles (e.g. Watkinson, 1981).

The F5 fold system forms a well defined pattern on a regional scale and produces a relatively complex fold interference pattern, which varies from the "crescent and mushroom" (type 2), to more complex "double zigzag" (type 3) patterns (Ramsay, 1967). The simple "dome and basin" (type 1) pattern is less common and mostly observed in the Northern Domain, probably because of the fact that well developed early F2 folds in the Western and Eastern domains were mainly isoclinal. This is consistent with the observations of Skjernaas (1975), who noted, that the type 1 interference pattern forms only when early folds are open, and it disappears when early folds are isoclinal (see also Watkinson, 1981).

A large, NE-SW trending and SW plunging regional F5 anticline dominates the southern part of Long Island and forms a large domal culmination off-shore within Wild Bight, as a result of interference with an early NW-SE trending fold. Parasitic D5 folds were observed in several exposures along the shore of Wild Bight, but it was not possible to follow any of them for any distance, because of the complexity of interference pattern, and the dense system of high angle reverse faults associated with those folds. The F5 faults are slightly overturned towards the northwest; whereas, the associated axial planar cleavage and high angle reverse faults dip steeply towards the SE. There, the resulting interference pattern is of type 1 and the dominant fold trend changes from panel to panel. The overall large scale interference pattern for whole island is 1(→2)

The structural geometry on both Pilley's and Triton Islands is controlled by a similar fold and thrust system, which also involves the Lobster Cove Fault. Red beds, as

well as the Robert's Arm Group to the south of the fault (see section on the fault), are aligned with the fold. It is not clear which fold system is dominant on Triton Island, since the F5 fold and thrust system is approximately co-axial with F4 in the eastern part of the island and since one amplifies the other, the interference pattern cannot be clearly distinguished. In the western part of Triton Island and on Pilley's Island, the F5 fold system overprints the F4 with an angular relationship and the resulting interference pattern is of type 2(=>1). Sunday Cove Island displays a large scale 1=>2 interference pattern between the F4 and F5 fold systems; whereas, on Halls Bay Head, the interference pattern is present, but the F4 dominates and controls the pattern.

In the Western Domain, the D5 deformational event is predominantly reflected in northwest-directed high angle reverse faulting, which includes reactivation of some of the suitably-oriented D3 thrust planes. Locally developed, southwesterly dipping shear bands present in pillow lavas of the Lushs Bight Group (Fig. 6.13) are thought to be related to this event. The late D1 dykes in the Whalesback area are also affected by northwest directed high angle reverse faulting, which is here attributed to D5. Some dykes exhibit discrete deformation in the form of an anastomosing chloritic/sericitic fabric surrounding competent phenocrysts of pyroxene, which produced domino structures in response to shearing (Fig. 6.14a and b). Shear fracturing of these competent pyroxene phenocrysts suggests that the dykes were affected by post-emplacement, northwest-directed, high angle reverse faulting.

The main structures in the Western Domain thought to be formed during the D5 event, are hinterland-dipping duplexes, such as that within units of the Western Arm Group in the Western Arm area. This structure apparently developed by the collapse of a footwall to the Mistaken Pond Panel, which during this event was moved in the NNW direction. More importantly, the Mistaken Pond Panel is thrust partially over the Southwest Arm Panel in the King's Point area, where that panel is covered by red beds of the probable Carboniferous age (e.g. Kean and Evans, 1987). As a result of the thrusting, red beds are folded and possibly provide the lower bracket for the age of the D5 event.

6.4 Structural Geometry

The structural geometry of the Notre Dame Bay area is complex. Orientation data for the study area as a whole suggest that it can be considered in terms of three internally, fairly homogenous, structural domains: Western, Eastern and Northern (Fig. 6.1). Each of the domains consists of a number of rectangular, laterally discontinuous fault-bounded panels, surrounded by moderately- to steeply-dipping, brittle to ductile shear zones. The nearly down-dip elongation lineation in the S2 foliation plane and associated kinematic indicators, together with stratigraphic evidence attests to the contractional nature of the shear zones and indicates that they are thrust faults. The structures repeat parts of the stratigraphy; however, it is rarely possible to apply stratigraphic criteria to the evaluation of main structural features in the area because of overprinting by younger folding and thrusting events. This results in problems in establishing the number of events, assigning various structures to particular events, and determining the age relationship between the events

6.4.1 WESTERN DOMAIN

The Western Domain is bounded to the west by the Green Bay Fault, which occupies a deep, northeasterly trending valley filled in part by the waters of Southwest Arm. This domain comprises at least three major thrust sheets, which are incorporated into a southeasterly verging fold and thrust belt. The domain can be subdivided into several large fault panels (Fig. 6.2), which evolved mainly during the D2, D3 and D5 events, and are separated by major thrust faults, many of which show evidence of multiple reactivation. Subsidiary thrusts divide the panels into smaller horses to form secondary imbricate fans or duplexes, that are refolded by subsequent deformations. Thus, some of the fault panels are further subdivided to reflect this complexity. The Western Domain displays many structural similarities to fold and thrust belts within the Buchans-Roberts Arm Belt (Thurlow and Swanson, 1987; Calon and Green, 1987; Pope and Calon, 1990).

The major listric panels separating thrust faults in the eastern part of the Western Domain clearly merge in the area west of Springdale and along Indian Brook. This indicates that in this part of the domain, rocks are incorporated into a southeasterly

vergent large scale imbricate fan, in which thrust faults occurring as brittle/ductile shear zones dip steeply to the northwest. Those main thrust faults seem have originated in main F3 footwall synforms and were formed parallel to the F3 fold axial surfaces.

6.4.1.1 Catchers Pond Panel

The Catchers Pond Panel comprises the southwestern-most section of the Western Arm Group rocks in the Notre Dame Bay area. It is bounded to the northwest by the Green Bay Fault, and to the south by the Lobster Cove Fault (Fig. 6.2). The eastern boundary of the panel is much more complicated. The northern segment of this boundary is formed by the Catchers Brook Fault, the north to northeasterly dipping, folded floor thrust to the Mistaken Pond Panel (see below). In the footwall of the Catchers Brook Fault, both felsic rocks of the Western Arm Group and the Springdale Group are imbricated and assembled into a SE verging, foreland-dipping duplex (Figs 6.15 and 6.16). The N-S trending southern segment of the boundary between Ordovician and Silurian rocks strikes at nearly right angle to, and eventually disappears beneath or joins, the Catchers Brook Fault. This fault is dipping easterly and is interpreted to form the sole thrust to the above mentioned foreland-dipping duplex involving rocks of the Western Arm Group, the Silurian Springdale Group and younger red beds (Fig. 6.15). Horses within the duplex involving Silurian rocks are further folded into a syncline with an axis trending 41-100; the northern limb of this syncline swings into a trend parallel to the Catchers Brook Fault.

The main structure of the panel is thought to be dominated by a large, southwesterly plunging, D2 antiform. In numerous outcrops in the southeastern part of the panel, bedding dips are steeper than cleavage and this, in combination with the upward-facing of rock units and the overall SW plunge of the structure (Appendix E, Fig. E-ii) indicates an antiformal syncline. This D2 antiformal syncline is divided into two smaller antiforms by a relatively tight and narrow D3 synformal anticline - the same structure which refolds the Mistaken Pond Panel (see below). As a result, the overall profile of the fold is of M-type. The southeastern antiform is overturned slightly to the southeast, and is additionally refolded. The distribution of bedding and the S2 cleavage orientation data on the stereogram indicates that both are refolded about very steep

axes (Appendix E, Fig. E-ii). As a result of this folding, the northeastern segment of the antiform changes the direction, swings into the E-W trend and follows the Catchers Brook Fault towards the east. A type 3 macroscopic interference pattern (Ramsay, 1967) has formed where the latter fold overprints the pre-existing F2 fold system characterized by tight to isoclinal folds overturned towards the SE.

6.4.1.2 Mistaken Pond Panel

The Mistaken Pond Panel is located southeast of King's Point and is bounded by the Davis Pond - Deer Pond Fault in the east, the Southern Arm - South Brook fault in the northwest, and the Catchers Brook Fault in the south (Fig. 6.2). The Mistaken Pond Panel is thrust over the Catchers Pond Panel along the Catchers Brook - Harry's Brook Fault. In addition to the main panel, it probably includes an isolated slice (i.e. klippe) that overlies the Catchers Pond Panel to the north, as well as even larger klippe(n) preserved on the western slope of the valley occupied by the Green Bay Fault, northeast of Rattling Brook.

MacLean (1947) and DeGrace (1971) found that rocks south of King's Point which are included in this panel form the lower limb of a "southerly" overturned anticline; that finding was verified during this study. The Western Arm Group rocks exposed in the southwestern part of the panel display an S2 cleavage which is commonly more shallow than bedding, indicating that they are a regionally downward-facing sequence on an overturned limb of a southeasterly-closing recumbent anticline. The central and northern part of the panel is underlain by the deformed pillowed flows of the Little Bay Basalt, therefore the stratigraphic and structural criteria cannot be used in the analysis of greater part of the panel.

Two other panels, the Little Bay Panel and Gull Pond Panel, adjacent to the Mistaken Pond Panel in the east, are thought to contain more fragments of this same lower limb of the overturned anticline.

In the western part of the panel, the swing in bedding and S2 cleavage orientations defines a large scale synform south of King's Point. On a stereogram, S0 and the S2 cleavage define a partial girdle, indicating that the synform has an axis with a plunge of $53 \Rightarrow 38$ and $46 \Rightarrow 36$, respectively; whereas, the fold system in the entire

panel is characterized by a mean axis $54 \Rightarrow 049$ (Appendix E, Fig. E-iv). The distribution of data shows that the D3 folds are fairly cylindrical, especially when the isoclinal/overtaken character of F2 is taken into consideration.

The two faults, that cut a SE verging, foreland dipping duplex, involving rocks of the Springdale and Western Arm Groups in the footwall of the Mistaken Pond Panel, do not cut across the Mistaken Pond Panel, but appear to generate in it a D3 anticline-syncline pair. Those faults are interpreted to be blind thrusts, because they do not emerge in the Mistaken Pond Panel, but are compensated by D3 folding and cleavage development.

6.4.1.3 Southwest Arm Panel

The Southwest Arm Panel is bounded in the west by the West Brook - Nickey's Nose Cove Fault, along which it is overthrust in the northwest direction by the Line Pond Panel. The Southwest Arm Panel is characterized by the presence of two distinct sections, separated by a fault of indeterminate kinematic history, the southeastern termination of which is overlain by the Line Pond Panel (see below).

The southern section, here referred to as the Coopers Cove-Colchester section, consists of a complex, northwest verging duplex, horses of which incorporate fragments of the Coopers Cove and Colchester plutons, their host rocks, and undivided volcanic rocks of the Lushs Bight and Western Arm groups. The S2 cleavage data from volcanic and volcanoclastic rocks hosting the Coopers Cove pluton plot around the margin the stereogram (Appendix E, Fig.E-iv) indicating the presence of a refolded fold. A similar distribution was previously identified from a much larger data base on stereograms presented by Sayeed (1970). The S2 data for the Coopers Cove pluton itself define a girdle and the probable axis of an F3 fold trending $70 \Rightarrow 012$ (Appendix E, Fig.E-iv). However, a number of observed S2/S3 intersection lineations plunge at various angles towards the west and are not compatible with that axis. The S2 data from the Colchester pluton area define a girdle and an axis of $78 \Rightarrow 122$ (Appendix E, Fig.E-iv). Such a large discrepancy in the orientation of constructed fold axes from this relatively small area is interpreted to be related to intense refolding of the F2 folds by F3 folds and /or to the imbrication of thrust sheet(s) containing both plutons.

The very southwestern end of the Coopers Cove-Colchester section is overlain unconformably by red sandstone and conglomerate and sparse limestone beds of presumed Lower Carboniferous age. The sedimentary succession occupies a minor syncline, which is mainly under the waters of Southwest Arm; however, there is sufficient exposure to determine that red beds are overridden in the northwesterly direction by the Mistaken Pond Panel and folded at the fault contact with that panel producing an F5 fold. Numerous minor folds are found within the silty laminae in that succession which have an appearance of ripplemarks but a well-developed axial cleavage and are thought to be related to the D5 event. Axes of these minor folds with a mean $\phi = 27 \Rightarrow 214$ coincide with an axis $\phi = 26 \Rightarrow 224$ constructed from the strongly clustered bedding data (Appendix E, Fig. E-v).

The northern section, here termed the Jackson's Cove section, is composite and contains at least two thrust sheets. The lower thrust sheet contains rocks of the Western Arm Group that are upright and exposed in Shilly Cove, Eastern Point and Nickey's Nose around the edges of the Jackson's Cove section. The upper thrust sheet contains rocks of the Lushs Bight Group. The Jackson's Cove section is dominated by a southerly plunging syncline that is parallel to the regional NE trend and swings and plunges towards the west (see also Sayeed, 1970), folded around a subvertical axis. The swing in the trend of the fold is spatially associated with and parallel to the faulted contact between the Jackson's Cove and Coopers Cove-Colchester blocks, similar to relationships observed in the Catchers Brook antiform.

6.4.1.4 Line Pond Panel

The Line Pond Panel is a narrow NE-SW trending block bounded by the West Brook Fault in the west and Southwest Brook fault in the east. The latter divides this panel from the Sugar Loaves Panel (see below). Rocks of the panel are thrust upon the Southwest Arm Panel. The Line Pond Panel is dominated by the Lushs Bight pillow lavas, both tholeiites and boninites, which are most likely overturned and overlie structurally cherts and pillow lavas of the Western Arm Group. The whole sequence is folded by a synform-antiform pair, with rocks of the Western Arm Group exposed in a core of the antiform in the bottom of Western Arm.

6 4 1.5 Sugar Loaves Panel

The Sugar Loaves Panel is bounded by the Southwest Brook fault to the west and the Southern Arm - South Brook Fault to the east. The Harry's Harbour section, located on the western side of Western Arm, is also included in this panel. The Sugar Loaves Panel differs from all other panels in the Western Domain, in that it exhibits upward-facing volcanic units which, combined with the recorded bedding/cleavage relationship (cleavage always steeper than bedding), indicate an upper, normal limb of the southeasterly closing regional anticline. Of all panels in the Western Domain, the Sugar Loaves Panel displays most convincingly the presence of two major fold- and thrust-producing events. It comprises a large, southeasterly verging D2(3?) syncline - anticline pair with an axial planar cleavage, overprinted by a northwesterly verging D5 imbricate fan. The imbricate fan is clearly formed in the footwall of the Middle Arm Fault, and it is here interpreted to include a long and narrow block bounded by the Middle Arm and Southern Arm faults (c.f. Marten, 1971a, b). This suggestion is based upon the fact that in this block, as in the rest of the Sugar Loaves Panel but unlike the rest of the Western Domain, the rocks are upward-facing.

It is not clear whether the southeasterly verging fold belt in the Sugar Loaves Panel is related to the D2 or D3 event, since there appears to be only one generation of cleavage. Measurements of bedding and cleavage planes define the northeasterly plunging axis for the fold system (Appendix E, Fig.E-vi). The S0/S2(3?) intersection lineations generally plot around the axis $41 \Rightarrow 046$ (Appendix E, Fig.E-vi), although in the Harry's Harbour section, the orientation of the axis defined by the intersection lineations, is $52 \Rightarrow 087$ (Appendix E, Fig.E-vii). This suggests that the Harry's Harbour section has undergone some rotation with respect to the Western Arm section, possibly along a fault in Western Arm which separates them. A few minor folds associated with a poorly developed cleavage and plunging to the NW were mapped in the Harry's Harbour Section, but their timing with respect to the other generation of folds and the associated cleavage is unknown.

6.4.1.6 Little Bay Panel

The Little Bay Panel is separated from the Mistaken Pond Panel by linked segments of several faults that include the Davis Pond, Deer Pond and the Southern Arm Faults. In the east it is bounded by the Little Bay Arm and Gull Pond Faults, which separate it from the Gull Pond Panel. The Little Bay Panel incorporates predominantly sheeted dykes and pillow lavas of the Lushs Bight Group, locally with variable but substantial amounts (>25%) of diabase dykes and sills. In the very southern part of the Little Bay Panel there is an outcrop of felsic tuffs and possible flows tentatively included in the Western Arm Group. The overall structure of the panel is interpreted to be an imbricated synformal anticline, with the sheeted dykes in the core of the synform and pillowed flows on the margins of the panel. Felsic volcanic rocks and minor mafic tuffs are exposed at southern termination of the panel near the Lobster Cove Fault. S2 and S3 cleavage orientations for the panel plot on a stereogram in the form of a scattered cluster (Appendix E, Fig. E-viii).

In the north, the Little Bay Panel is divided into three smaller blocks, that are flanked symmetrically by two larger, northeasterly trending faults subparallel to the boundaries of the panel. Between these and the two panel bounding faults, smaller steeply southeasterly dipping to vertical en-echelon faults define a series of lensoid horses. Such geometry (Fig. 6.17) is typical of strike-slip duplexes formed by duplexing on straights (Woodcock and Fischer, 1986). Assuming that the panel is correctly interpreted as facing downwards, the apparent sense of movement deduced from the fault pattern and from the fact that sheeted dykes are preserved in central horses of the duplexes rather than in marginal ones, is dextral strike slip (Fig. 6.17) with an extensional geometry of the duplexes. Alternatively, since most field evidence indicates that the structures have a contractional character, this may be a contractional duplex formed in a sinistral strike-slip regime.

Observations along the Davis Pond Faults and faults in the Whalesback and Little Bay mine areas provide evidence of a multiple deformational history which includes sinistral and dextral strike-slip and down-dip displacement.

6.4.1.7 Gull Pond Panel

The Gull Pond Panel occupies a large area between the Little Bay Arm and Gull Pond faults in the west, and the Lobster Cove and Halls Bay faults in the east. Because only southern and the very northern terminations of the panel were covered with traverses during this study, the internal geological relationships are relatively poorly understood. The northeastern segment of the Gull Pond Fault divides the panel into two areas, but not enough is known about the structure of the panel to justify any further division. The southwestern part of the panel is underlain by folded and refolded rocks of the Lushs Bight and Western Arm Groups, but central and northeastern areas are underlain predominantly by pillowed flows of the Lushs Bight Group. cursory observations in the southern part of the panel suggest that this is most likely an overturned sequence similar to other panels in the Western Domain. Although bedding tops have not been convincingly established, the overall lithostratigraphic order implies a younging direction of the volcanic sequence towards the Lobster Cove Fault. felsic volcanic tuffs, strongly magnetic mafic flows, and mafic tuff-breccia, all characteristic of the Western Arm Group, are typically found lower in the sequence in fault contact with red beds along most of the fault exposure in the Western Domain. The strongly altered pillowed flows and the associated lavas with sills and dykes characteristic of the Lushs Bight Group are higher in the volcanic pile and crop out consistently away from the fault (see also below, section on the Lobster Cove Fault).

6.4.2 EASTERN DOMAIN

The Eastern Domain covers the area from Fox Neck in the northwest to Triton Island in the east, and includes Halls Bay Head on the Springdale Peninsula, and most of Sunday Cove and Pilley's Islands. The Eastern Domain is not easily divisible into fault panels because of the lack of continuous exposure and the fact that islands in the east (Pilley's and Triton Islands) are topped by a higher thrust sheet(s) and progressively younger lithostratigraphic units. Yet, many of the Eastern Domain panels can be linked to its "parent" panel in the Western Domain on the basis of its lithostratigraphic and structural position with respect to other panels.

The major structural difference between the Western and Eastern domains is the direction in which the regional planar elements strike and dip. The Western Domain is characterized by the NE striking foliation(s) and faults (see above), and by generally steep (frequently NW) to vertical dips; whereas, the Eastern Domain exhibits a regional structural grain ranging from SE in the west to ENE in the east, with mainly southerly dips of foliations and faults. The change in fabric orientations forms part of a structure referred to by Church (1965) as the Notre Dame Orocline.

This structural transition from the Western to Eastern Domain is best evinced in the Halls Bay Head area in the very eastern part of the Springdale Peninsula, and in the Fox Neck area. On Halls Bay Head it is reflected in the swing of the NE striking foliations and faults characteristic of the Western Domain, towards generally SE regional trend in this part of the Eastern Domain.

Fox Neck is a very narrow, northeast trending cape east of Beachside. Here, the contact between the Western and Eastern Domains is displayed by a very abrupt change from the typically NE trend of structural elements in the Western Domain to the SE direction of planar elements in Eastern Domain. The Eastern Domain here appears to overlie the Western Domain, which dips southeasterly beneath the former.

Most of the observations and structural measurements referred to below, are from these two areas. Sunday Cove Island was covered only by a few brief traverses, and although observations made allowed the recognition of a few fault panels similar to those present in the Halls Bay Head and Fox Neck areas, the detailed structural geometry of the Sunday Cove sub-domain is not well understood.

The Pilley's and Triton Islands differ considerably from the remainder of the Eastern Domain. The clear continuity of the panels observed between the Fox Neck, Halls Bay Head and Sunday Cove Island areas is absent and correlations between fault panels on the Pilley's and Triton Islands and those to the west is less obvious. Only two panels are designated within the Pilley's and Triton Islands

6.4.2.1 Gull Pond Panel

The Gull Pond Panel, southern-most in the Halls Bay Head and Sunday Cove Island areas, is underlain by pillow lavas of the Lushs Bight Group, with some minor

argillite, chert and mafic tuff, and bounded by the Saltwater Pond Fault to the northwest, the Ward Harbour Fault (MacLean, 1947; Donohoe, 1968) to the northeast and the Lobster Cove Fault to the south.

The Gull Pond Panel is the only panel in the Eastern Domain, which in the Halls Bay Head area, clearly displays a swing in the orientation of planar fabrics from those typical of the Western Domain, to those typical of the Eastern Domain. The hinge region of the fold is delineated by changes in trends of bedding, S2 cleavage and regional faults, and to the south by folding of the Lobster Cove Fault. Using bedding data from red bed exposures along the Lobster Cove Fault on both limbs of this fold (one north of Springdale, and the other on Sunday Cove Island), a regional axis of approximately 70-→355 has been constructed.

Unlike the Lobster Cove Fault, the Ward Harbour Fault, which divides the Gull Pond and Little Bay Panels in the Halls Bay Head area and on Sunday Cove Island, strikes northwesterly and dips northeasterly. In the China Head area (northwestern shore of Sunday Cove island), a splay of the Ward Harbour Fault brings a horse of the Little Bay Panel (sheeted dykes with screens of pillow lava) on the top of the Gull Pond Panel. Since little is known about the kinematics of the Ward Harbour Fault, this is the most convincing indication that this fault is a thrust.

6.4.2.2 Little Bay Panel

The lithostratigraphic assemblage of the Little Bay Panel (pillow lavas and sheeted dykes of the Lushs Bight Group), the probability that its strata are overturned, and its structural position between other panels in the Eastern Domain, is consistent with this panel being the counterpart of the Little Bay Panel in the Western Domain.

The Little Bay Panel is bounded by the Ward Harbour Fault in the southwest and the Woodford Cove Fault in the northeast. The Woodford Cove Fault dips southwesterly and separates the Little Bay Panel from the Mistaken Pond Panel. Here it is proposed that this fault represents the refolded Ward Harbour Fault, a sole thrust to the Little Bay Panel. Both bounding faults are considered to represent the same folded thrust fault which is the sole thrust to the panel.

In several outcrops in the northwestern part of the domain, well preserved pillow lavas display both upright and overturned tops within a distance of a few hundred meters, indicating that the F2 folds are tight to isoclinal and overturned to the northeast (see also Donohoe, 1968). Within the panel, both the penetrative S2 cleavage and the bedding determined from the nesting of pillows dip towards SW. However the cleavage commonly dips more shallowly than bedding (Appendix E, Fig E-ix). This implies that the panel is underlain by an overturned, downward-facing sequence and is consistent with the presence of pillow lavas in cores of at least two larger antiforms within the panel; whereas, sheeted dykes in the area are generally interpreted to occupy the cores of synforms.

On stereograms, the pillow orientations define a relatively tight cluster with two poorly developed maxima. The best fit girdle defines an axis 68-→258. However, it is not clear what this represents, and most likely it is a "composite" axis. The F2 fold axes and S0/S2 intersection lineations plunge both northwesterly and southeasterly as a result of refolding by the younger generation of F5 folds defining a great circle on the stereoplot (Appendix E, Fig.E-ix). The F5 fold axes, which in this situation are also expected to form a great circle on the stereoplot (e.g. Mulchrone, 1991), instead form a cluster that is slightly scattered around 40-→200. This implies that the F5 folds may be of larger amplitude and wavelength than the F2 folds and such geometry may have resulted in a biased collection of data in the field which could have had the effect of excluding the effects of the smaller F2 folding.

The Little Bay Panel on Sunday Cove Island, occupies the central part of the island, and in addition to sheeted dykes and pillow lavas of the Lushs Bight Group, it comprises a diorite intrusion (Wellmans Cove Pluton; Kean and Evans, 1987). No facing direction was directly established for sheeted dykes and pillow lava. Only the northerly dip of pillows in several outcrops in southeastern part of the panel on Sunday Cove Island implies that they may underlie the dykes, and allows for the possibility that the Little Bay Panel in this area also contains an overturned sequence, similar to that in the Halls Bay Head area and the Western Domain.

A probable equivalent of the Little Bay Panel is exposed in the northernmost part of Pilley's Island and Brighton Tickle Islands. It contains mainly sheeted dykes and lesser pillow lavas of the Lushs Bight Group, and possibly the Brighton Complex. In at least two localities, most notably at Red Cliff Point (Pilley's Island), sheeted dykes overlie a strongly schistose mafic tuff. The characteristic rock assemblage suggests the correlation of this panel with the Little Bay Panel, although here the sequence is facing right way-up.

6.4.2.3 Mistaken Pond Panel

The Mistaken Pond Panel is a narrow, elongated panel, parallel to and southwest of the MacLean Fault that consists entirely of Lushs Bight Group pillow lavas, which are progressively more flattened towards the northeast. Kinematic indicators within the shear zone of the MacLean Fault reveal, that the fault is clearly associated with the northeast-directed thrusting. The pillow lava of the Lushs Bight Group, which is exposed in the hanging wall of the fault, displays outcrop-scale shear bands (C planes) which rotate the generally steeper S2 cleavage (pillow-flattening) into alignment with the C planes and towards direction of movement (i.e. NE). Both S2 and C planes contain a downdip mineral stretching lineation.

Pillow lavas within this panel are deformed similarly to rocks of the Little Bay Panel, and the combined bedding data for both panels plotted on a stereogram define a girdle with axis $60 \Rightarrow 274$ (Appendix E, Fig.E-ix). Both the orientation of pillows and the S2 cleavage within the Mistaken Pond Panel dip towards SW, but the cleavage dip is steeper than that of the bedding, again similar to the Little Bay Panel.

On Sunday Cove Island, the Mistaken Pond Panel occupies a large area immediately east of the Little Bay Panel, and is underlain predominantly by pillow lavas of the Lushs Bight Group, locally with swarms of dykes. Minor outcrop of mafic tuff of the Western Arm Group is confined to the Jerry Harbour/Jerry Head area in the eastern part of the panel. Outcrops of sheeted dykes with pillow screens are exposed in several places within and along the margins of the panel. A larger exposure of sheeted dykes is present in the northern part of the Mistaken Pond Panel, where it overlies predominantly pillow lava and pillow breccia of the Lushs Bight Group, but also limited

outcrop of the Western Arm Group rocks. These slivers of sheeted dykes are here considered to be klippen related to the Little Bay Panel.

The fault separating the Mistaken Pond Panel from the Little Bay Panel on Sunday Cove Island has previously been correlated with the MacLean Fault (e.g. Donohoe, 1968). Here, it is concluded that it is instead a segment of the Woodford Cove Fault.

6.4.2.4 Shag Cliff Panel

The northeastern-most panel in the Fox Neck, Halls Bay Head and Sunday Cove Island areas is named the Shag Cliff Panel. It is underlain by argillite, chert, mafic tuff and tuff breccia characteristic of the Skeleton Pond Formation, pillow lava of the Big Hill Basalt, and tuff breccia of the Western Head Formation. The Welsh Cove Formation is poorly represented by a few scattered outcrops of predominantly felsic tuff breccia. Rocks in this panel are increasingly more deformed towards the fault contact with pillow lavas of the Mistaken Pond Panel, and are folded into several syncline-anticline pairs, the F2 fold geometry of which is more open than in the Little Bay Panel. In general, rocks in the panel are upward facing, except on the northerly overturned limbs of open to tight folds where they are downward facing. This relationship is particularly well exposed in the area immediately adjacent to the MacLean Thrust and in the Shag Cliff syncline, where rock units are overturned towards the NE. In the footwall of the MacLean Thrust, argillites, shales and tuffs display discrete shear planes that are approximately parallel to the S0 and cut the S2. Locally an internal imbrication and folding within the shear bounded blocks is present, perhaps indicating extension related to the collapse of the initial thrust.

On Fox Neck, volcanoclastic and sedimentary rocks of the Shag Cliff Panel are clearly overturned towards the NE and face downwards. Both, the bedding and S2 cleavage are dipping towards the SW, with S2 at a lower angle than S0 (Appendix E, Fig E-x). In combination with the downward facing of these rocks, this indicates that in the Fox Neck area, the Shag Cliff Panel is located on an overturned limb of a southwesterly closing syncline. Treated separately, the S0 and S2 measurements define southeasterly plunging fold axes at $62 \Rightarrow 218$ and $33 \Rightarrow 211$, respectively (Appendix E,

Fig E-x). The fold axis obtained from the distribution of bedding data coincides with axes of minor F5(?) folds, which lie on the great circle defined by S0 and S2 (Appendix E, Fig.?). This behaviour implies that the F2 folds are considerably larger than F5 folds in this area.

In the Halls Bay Head area, the S2 cleavage is poorly developed and refolded by subsequent deformational events. It is clear from the field observations and aerial photographs that there are at least three and perhaps more generations of structures recorded in rocks of this panel. Apart from the F2 folds, there are folds generated between NW trending and SW dipping faults that parallel the MacLean Thrust. The F3 and F5 folds that are dominant in the Little Bay Panel, are here perhaps of similar or even smaller size than F2, as they do not affect distribution of bedding and cleavage measurements to the same degree. Although displaying some scatter, both the S0 and S2 orientations define similar great circles on the stereogram (Appendix E, Fig E-xi), each with two maxima, and define the fold axis at $\sim 30 \rightarrow 274$. Whereas this fold axis is most likely composite, it is perhaps dominated by that of early F2 folds. Both, reverse and normal movement took place on discrete faults parallel to axial planes of the F2 folds as observed in the Shag Cliff syncline.

6.4.2.5 Nogood Island Panel

Most of the Pilley's and Triton islands is underlain by rocks of the Skeleton Pond Formation, Big Hill Basalt, Welsh Cove and Western Head formations, and named here the Nogood Island Panel. Pillow lava of the Lushs Bight Group are exposed in the cores of two minor antiforms south of Langdons Cove on Pilley's Island. In the southern part of the panel, facing directions, where determinable, are consistently normal, or in the case of strongly imbricated cherts and tuffs of the Skeleton Pond Formation on Triton Island, vertical to slightly overturned and facing north to northeast. In several outcrops in the northern part of the panel on Pilley's Island, younging directions indicate that the rocks are downward facing and a lack of convincing way-up indicators elsewhere suggests the possibility that this part of the panel is dominated by isoclinal to tight folds overturned towards north, such as is observed on the outcrop scale. Only two outcrops with clearly overturned tops were

mapped on Triton Island, one being pillow lavas of the Big Hill Basalt near a fault contact with the Brighton Complex, and the other tuff breccia of the Skeleton Pond Formation in Great Triton Harbour.

The panel is intensely faulted internally, forming a northwesterly verging, hinterland dipping, D5 imbricate stack. Small scale folds associated with the imbrication overprint pre-existing larger scale, NW trending folds that are associated with the previous (D4) event of northeast directed thrusting. The resulting complex fold interference pattern controls the present structure of the panel. Bedding and cleavage data show significant scatter, and although they tell very little about the orientation of younger, smaller folds, they indicate older dominant fold orientations in the panel. The composite axis of the older larger folds as determined from widely scattered bedding measurements is $\sim 58 \Rightarrow 144$ (Appendix E, Fig.E-xii). Axes of the folds determined in the field or constructed by measuring bedding orientations on opposite limbs or bedding/cleavage intersections, display a wide scatter, and azimuths of only several of those match the azimuth of the axis obtained from the stereogram, most display a more shallow plunge (Appendix E, Fig.E-xii).

It is difficult to discriminate between different generations of cleavage in rocks on Pilleys Island, because they are rarely well developed. Truly overprinting cleavages were seen only in one outcrop. The combined cleavage data from Pilleys Island (Appendix E, Fig.E-xii) form several clusters, and although cleavage orientations in various clusters are thought to be associated with different structural blocks within the panel, such associations are ambiguous. The girdle calculated from the overall distribution of cleavage data on the stereogram has an axis $57 \Rightarrow 248$, the azimuth of which corresponds roughly to the trend of the NW-directed thrusts.

On Triton Island, the more open F2(?) folds are folded and wrap around the outcrop of the Brighton Complex. In the northwestern Triton Island, scattered bedding defines a girdle with an axis of $21 \Rightarrow 103$ (Appendix E, Fig.E-xiii), which does not differ much from average $16 \Rightarrow 112$, calculated from field measurements of axes to existing folds and S0/S2 intersection lineations. A different fold orientation, $61 \Rightarrow 167$, is obtained from the distribution of the S2 cleavage; whereas, the F2 axes show evidence

of refolding around an axis of 35-→221. This is thought to represent axes of younger generation folds, some of which are present in the northeastern part of Pilley's Island, but not reflected in insufficient field data. In eastern Triton Island, the fold axis obtained from distribution of bedding (Appendix E, Fig.E-xiv) is 11-→075 and it coincides much better with the orientation 24-→068 obtained from the S2 distribution. Both of these values are also fairly similar to a mean of fold axes and S0/S2 intersection lineations collected in the field (Appendix E, Fig.E-xiv).

6.5 Northern Domain

The name Northern Domain refers to the area north of the Long Island Tickle Fault, which includes Long and Little Bay Islands, each considered as a sub-domain, and several encircling islets. The Stag Formation rocks may form part of a separate thrust sheet, originally unrelated to this domain, but because they are spatially associated and structurally interleaved with the units of the Northern Domain, they are here considered as part of it.

6.5.1 LONG ISLAND SUB-DOMAIN

The Long Island sub-domain contains a large scale, D5(?) southwest to west plunging anticline-syncline pair in the southern part of the island, and a southwestern limb with a possible hinge area of another anticline in the northern part. The sub-domain is divided into four fault panels: the Southern Head Panel, the Cutwell Arm Panel, the Aspen Cove Panel and the Stag Island Panel. Two faults form the boundaries of these panels on Long Island. The Milkboy Cove fault trends northwesterly from Milkboy Cove on the southern shore of Long Island, and separates the Southern Head Panel in the southeastern part of the island from the Aspen Cove Panel in the southwestern part of the island. The Black Head fault, trends WNW from Wild Bight and separates the Southern Head and Aspen Cove panels from the Cutwell Arm Panel in the northern part of the island. The contact between the Cutwell Arm Panel and the Stag Island Panel is offshore and presumed to be a thrust (see section on the Stag Island Panel).

6.5.1.1 Southern Head Panel

The northeastern edge of the Southern Head Panel, the southern shore of Wild Bight, has a semicircular shape, and is marked by a discontinuous outcrop of the Tuff lithofacies of the Long Tickle Formation. Rocks of the other lithofacies partially follow this pattern.

Between the Southern Head area and Gull Cliff, rocks of the Tuff lithofacies are exposed in the cores of successive parasitic(?) anticlines. These anticlines (and synclines) have typically domal (and basinal) shapes, indicating that the panel is polydeformed. The field measurements of fold axes in this panel show both southwesterly and northeasterly plunges (Appendix E, Fig. E-xv). On the stereogram, bedding data form a scattered girdle, which corresponds to an axis of 20-→240, and roughly to the majority of the fold axes measured in the field (Appendix E, Fig. E-xv). The bedding girdle is dominated by two well defined maxima, which are interpreted to represent opposite limbs of the macroscopic F5 anticlines. The distribution of bedding data on the stereogram is characterized by the presence of two well developed maxima, indicating that most of folds have straight limbs and narrow, rounded hinges, with some folds approaching a chevron style.

Cleavage orientations are less revealing and produce a broad cluster with a mean cleavage orientation of 73⇒180. Many of the cleavage data clearly are not consistent with the fold axis defined by the bedding girdle, and possibly are related to a different set of folds, that is most likely oblique to the major fold system. Bedding/cleavage intersection lineations also form two scattered clusters (Appendix E, Fig. E-xv), from which only a few lineations correspond to measured fold axes, and most plunge towards WNW and ESE. Therefore, the presence of at least two discrete fold systems in the Southern Head Panel is indicated by structural data. The distribution of the bedding data suggest that the WNW-ESE trending generation of folds has a minor effect on bedding, and is much larger than the NE-SW trending folds.

Both systems of folds are associated with thrust faults. In the case of the NE-SW trending belt, thrusts have this same orientation and are directed northwesterly, whereas, the WNW-ESE trending fold system is related to northeasterly directed

thrusting. The latter generation of folds and thrust faults is folded by the NE-SW trending folds and cut by associated thrusts, indicating that the WNW-ESE trending fold and thrust belt is the older one.

Several geometrical properties indicate that the NE-SW trending folds which dominate the panel are verging northwesterly. These include: 1) an affiliation of these folds with northwest directed high angle reverse faults; 2) the generally moderate southerly dip of the axial plane cleavage; and 3) the slightly steeper northwestern limbs of parasitic folds. The vergence and asymmetry of the WNW-ESE trending folds is much more problematic and little can be inferred about those folds. Only one mesoscopic fold evidently associated with this generation of folds was observed in the Southern Head panel (Fig. 6.18). Several minor folds thought to be related to this deformational event were seen within bedded tuffaceous sedimentary rocks interbedded with mafic flows; they are overturned and verging northeasterly (Fig. 6.19) and have appearance of "drag" folds. It is possible that these folds are also related to the same event which produced the previously described fold, but clearly are modified by simple shear acting parallel to limbs of the fold.

6.5.1.2 Cutwell Arm Panel

The Cutwell Arm Panel displays similar structural characteristics to the Southern Head Panel and is dominated by the SW plunging folds. Both poles to the bedding planes and hinges of minor folds measured in the field define very similar axes of $\sim 33 \Rightarrow 246$ (Appendix E, Fig E-xvi), which is close to the mean $20 \Rightarrow 240$ axis of the dominant fold generation in the Southern Head domain. The moderately SW dipping cleavage suggests partly inclined axial planes and defines a girdle with an axis of $52 \Rightarrow 204$ that is different from that inferred from the bedding distribution. Although there is no evidence from those data for another folding event in the panel, field observations reveal thrusting in the Burnt Head area that is not compatible with the southwest trending folds. There, intraformational imbrication was observed within tuffaceous sandstones and cherts interbedded with massive mafic flows which took place along minor thrust faults with orientations varying from $45 \Rightarrow 185$ to $35 \Rightarrow 275$.

The nearly downdip lineation present on the fault planes indicates generally northeast directed movement on the faults.

The distribution of bedding orientations on the stereogram suggests that the style of the SW trending folds differs from that of the Southern Head domain folds. Data are spread more evenly on the stereogram and there is a lack of obvious maxima, implying folds with broader, more rounded hinges than those of the Southern Head Domain.

6.5.1.3 Aspen Cove Panel

The Aspen Cove Panel differs structurally from the previous two panels in the orientation of the dominant fold generation. The fold axes shown in the stereogram (Appendix E., Fig.E-xvii) were collected mostly in the northern part of the panel and almost exclusively within rocks of the Parson's Point Formation. Yet, they correspond relatively well to fold axis orientations inferred from the distribution of bedding and cleavage data (Appendix E, Fig.E-xvii) and are believed to be representative of fold orientation in the rest of the panel. Two populations of fold axes are recorded on the stereogram, one plunging northwesterly and the other southeasterly, both are thought to belong to one generation refolded by a subsequent deformational event.

Many mesoscopic structural features associated with northeast thrusting and folding are preserved in shale and the interbedded limestone breccia, bedded limestone and greywacke of the Parson's Point Formation. Most of those are minor thrusts and duplexes, and associated folds. Folds preserved in the bedded limestone vary; some, e.g. on the southern shore of Lushs Bight, are non-cylindrical, with poorly developed or absent cleavage (Fig. 6.20), and an overall appearance suggesting pre-lithification deformation; others, e.g. in bedded limestones and shales on Oil Island (Fig. 6.21), are cylindrical to mildly non-cylindrical and display well developed axial-planar cleavage - clearly the result of post-lithification deformation. Within the sheared contact between limestones/shales and the overlying felsic tuff on Oil Island, there are several minor folds which also resemble "slump" folds in their highly chaotic appearance, but locally display a fairly well developed cleavage. However, the presence of cleavage does not exclude the possibility that these structures are the result of shearing of unconsolidated to partially consolidated material (e.g. Agar, 1988). Both types of folds are

approximately co-planar, but they are not (at present) co-axial. The non-cylindrical folds on the southern shore of Lushs Bight and Oil Island are moderately inclined and overturned towards the northeast, and are plunging southeast. Folds of the second type on Oil Island are also moderately inclined and slightly overturned towards the NE, but are plunging in a northwesterly direction.

6.5.1.4 Stag Island Panel

The Stag Island Panel is characterized in general by a poorly developed cleavage in its pillow lavas and breccia, and by the presence of fractures and fracture cleavage. The panel includes several dispersed islets (one, League Rock, is more than 10km SW of the Stag Islands), and because of the outcrop discontinuity and fairly competent rock types, it does not provide much structural information. Yet, there are indications from the bedding facing directions that the panel may represent the hinge zone of a major regional fold (see also Kean, 1973) with a subhorizontal axis ($05 \Rightarrow 156$), suggested by the distribution of bedding data on the stereogram. Of two fold hinges measured in the field, one ($03 \Rightarrow 140$) coincides fairly closely with the constructed axis; whereas, the other plunges steeply in the opposite direction.

The SE-trending folds may be associated with and related to the easterly directed thrusting, evidence for which was found on Seal Island. The southwestern part of Seal Island is underlain by moderately SW dipping and upward-facing pillow lavas but in the northeastern part, across a high angle reverse fault, pillow lavas are overturned. In the western and southern part of the island, where thin beds of shale and limestone are present between typically pillowed flows, sedimentary rocks and adjoining pillow lavas form zones of a foliated melange that contains blocks of limestone and lesser pillow fragments enclosed in the shaly matrix (Fig. 6.22). The melange displays steep, SW-dipping, intensely developed foliation that is cut by low-angle, westerly to southwesterly dipping minor thrust faults (Fig. 6.22) with grooves and slickensides indicating ENE directed transport. The orientation of thrust planes and the direction of transport is similar to that in the northeastern part of the Cutwell Arm Panel (see above).

6.5.1.5 Little Bay Island Sub-Domain

The Little Bay Island subdomain includes Little Bay Island and several islets located between it and Halls Bay Head. The lithostratigraphic units represented within this sub-domain include the Cutwell Group and the Stag Formation. There are not enough bedding and cleavage data to accurately define various fault panels within the sub-domain, but the lithostratigraphic differences and locally important faults indicate that this sub-domain is divisible into three fault panels that are named: the Northern Head Panel, the Southern Harbour Panel, and the Copper Island Panel.

The Northern Head Panel occupies the very northern part of the Little Bay Island and is divided from the Southern Harbour Panel by the North Harbour Fault, the kinematics of which is unknown. In the southeastern part of Little Bay Island, rocks of the Copper Island Panel (Stag Formation), are emplaced structurally upon rocks of the Southern Harbour Panel (Cutwell Group) along the south-southeasterly dipping Marshall Beach Thrust. The Southern Harbour Panel is located on westerly dipping limb of an anticline with a hinge to the east of the island.

6.6 The Lobster Cove - Chanceport Fault

The NE-SW to E-W trending Lobster Cove Fault was first recognized on Pилley's Island by Espenshade (1937), who traced it from near Springdale to the eastern end of Triton Island. In the Pилley's Island area, Espenshade (1937) concluded that volcanic rocks of the Roberts Arm Group and the red sandstones that overlie them were disposed in an overturned anticline which is thrust northwards. He interpreted the Lobster Cove Fault as a north-directed thrust with an element of strike-slip displacement. MacLean (1947) traced the Lobster Cove Fault for a further 15 kilometres southwest from Springdale. In outcrop west of Springdale, he found schistose rocks of the Lushs Bight Group thrust upon rocks of the Springdale Group, and on this evidence considered the fault to be a south-directed thrust. Wessel (1975), working in the Springdale area, suggested that the present juxtaposition of rock units across the fault was the result of dextral strike-slip movement.

Several workers have proposed the correlation of the Lobster Cove Fault with other large faults in Notre Dame Bay. MacLean (1947) suggested that the Lobster Cove Fault

was related to the Lukes Arm Fault (Fig.6.23). Horne and Helwig (1969) also argued that the Lobster Cove and Lukes Arm faults together constitute the major fault system in the Notre Dame Bay area. Dean and Strong (1977) were the first to correlate the Lobster Cove Fault with the Chanceport Fault (Fig. 6.23), and suggested that the Lobster Cove - Chanceport Fault represents a south-directed thrust, folded during in the mid-Paleozoic.

6.6.1 GEOMETRY OF THE LOBSTER COVE FAULT

The geometry and orientation of the Lobster Cove Fault change along its strike. On Sunday Cove Island, the short exposed fragment of the Lobster Cove Fault trends approximately E-W and is slightly convex to the north. Towards the east on Pilley's Island and Triton Island, the Lobster Cove Fault maintains an overall E-W trend, but it is convex to the south. Between Sunday Cove and Triton islands the fault shows an apparent dextral offset. In the Springdale area to the southwest, the trend of the fault is towards the southwest, bringing rocks of the Lushs Bight and Western Arm Groups over the red bed sequence and volcanic rocks of the Springdale Group (e.g. MacLean, 1947; Jenner and Szybinski, 1987; Coyle and Strong, 1987).

In the area between Springdale and Triton Island, the Lobster Cove Fault juxtaposes rocks of the Lushs Bight and Western Arm groups to the north with the Roberts Arm and Springdale groups to the south. Deformation within the Roberts Arm Group has produced predominantly northeasterly-trending and southeasterly-verging fold and thrust belts (Thurlow and Swanson, 1987; Bostock, 1988; Pope et al., 1990). Rocks of the Lushs Bight and Western Arm groups also form thrust and fold belts, geometry and orientation which are similar but characterized by more brittle deformation.

The red bed sequence overlying the Roberts Arm Group immediately south of the Lobster Cove Fault is the youngest stratigraphic unit affected by movements along the fault. On Sunday Cove, Pilley's and Triton Islands, the strike of the Lobster Cove Fault is nearly parallel to bedding in the vertical to overturned and north-younging red bed sequence. The fault appears also to be parallel to the trend of volcanic and sedimentary rocks in the Robert's Arm Group. In most outcrops, the generally more deformed rocks of the Lushs Bight and Western Arm Groups face into the Lobster Cove Fault.

The Lobster Cove Fault zone is characterized by a series of imbricate structures in the region of Sunday, Pilley's and Triton islands, and by an imbricate thrust stack in the Springdale area. Deformation within the fault zone involved the red bed sequence, the Silurian and Ordovician volcanic rocks, and the fault itself. The major E-W trending segment of the fault zone and adjoining rock units are steeply dipping, so that in current orientation the duplexes appear as contractional structures formed in a dextral strike-slip fault system.

6.6.2 STRUCTURAL POSITION OF RED BEDS

6.6.2.1 The Springdale Area

Previous workers have suggested that the Springdale Group is simply deformed in a single, open northeast-plunging syncline (e.g. Kaliokoski, 1953; Wessel, 1975; Coyle and Strong, 1987). However, deformation structures in the red bed sequence and the underlying volcanic rocks of the Springdale Group indicate that these units are imbricated and deformed into a southeasterly-verging thrust belt related to overthrusting along the Lobster Cove Fault by a hanging wall consisting of rocks of the Lushs Bight and Western Arm groups, .

As the fault crosses Halls Bay, a major change in its trend is observed from E-W (as seen on Sunday Cove Island) to an overall NE-SW trend (as seen between Springdale and the Green Bay Fault). Near Springdale, the fault swings from an overall northeast trend to a west-northwest trend along the short section of the fault immediately west of town (Fig. 6.15). This change in the trend of the fault results from D4 folding, and in the Springdale area the fault is exposed on both limbs of a regional, northerly plunging D4 syncline. This syncline provides two cross-sections of the Lobster Cove fault zone, which are at an angle one to the other. The redbed sequence follows the surface expression of the fault around this bend and dips north to northwesterly. Younging directions within the red bed sequence (and locally the Springdale Group) in vicinity of the fault suggest that the rocks are generally overturned and locally tightly folded, although no fold hinges were observed. The zone of overturned to steeply dipping red sandstones and Springdale Group rocks ends

southwest of Springdale, where strata are also folded, but upward-facing and dip northwest to southeast.

6.6.2.2 Sunday Cove, Pilley's And Triton Islands

In contrast to the east-southeasterly thrusting of the Lushs Bight and Western Arm groups over the Springdale Group/red bed sequence in the west, movement on the Lobster Cove Fault on Sunday Cove, Pilley's and Triton islands is apparently dextral strike-slip. The trace of the fault is marked by a steeply dipping to overturned red bed sequence facing into the fault. The maximum thickness of the red bed sequence in this area (<200m) is significantly less than in the Springdale area.

The contact between red bed sequence and the underlying rocks of the Roberts Arm Group on Pilley's and Triton islands is an angular unconformity. The general trend of tuffs and pillow lavas in the Robert's Arm Group appears to be parallel to the strike of bedding in the red beds, but the dip of the sandstones and conglomerates diverges everywhere from the Robert's Arm Group rocks by 20°-70° (see also Bostock, 1988). Bostock (1988) has pointed out that this implies widespread, probably pre-lower Silurian, deformation within the Buchans-Robert's Arm Volcanic Belt.

Red beds along the Lobster Cove Fault, together with the Ordovician rocks of the Robert's Arm Group and locally volcanic rocks of the Lushs Bight Group, are affected by at least two or possibly three phases of deformation in post-lower Silurian times. The earliest of these events corresponds with the southeast-directed thrusting in the Springdale region. It has a heterogeneous, variable character and is expressed by ductile deformation north of the Lobster Cove Fault on Sunday Cove, Pilley's and Triton islands and rather brittle to locally ductile deformation in red beds (and the Robert's Arm Group rocks) south of the fault.

Two map scale duplexes along the Lobster Cove Fault, documented below, are ascribed to this event.

6.6.2.3 Lobster Cove Imbricate Stack

The first of these duplexes is located in Lobster Cove on Sunday Cove Island. Strongly flattened and sheared pillow lava and mylonites of the Lushs Bight Group, with a thin cover of Skeleton Pond Formation cherts and tuffs, north of the Lobster

Cove Fault are juxtaposed with red sandstones and underlying Ordovician mafic rocks of the Roberts Arm Group south of the fault (Fig. 6.25). The red bed sequence consists of red, massive, cross-laminated, coarse sandstones which locally contain bright red shale rip-up clasts. These are underlain by almost undeformed rocks of the Robert's Arm Group. Rocks on both sides of the fault are steeply dipping and facing the fault, being predominantly overturned in the Robert's Arm Group.

Rocks along the southern margin of the Lobster Cove Fault at this locality form an imbricate stack consisting of the red bed sequence and rocks of the Roberts Arm Group arranged in northeast- to northwest-trending domino-type horses. These are bounded by high-angle brittle, conjugate faults. Several of these horses contain red beds in their northern parts. The thickness of preserved red bed sections within consecutive horses decreases generally westwards, where they are truncated by the Lobster Cove Fault. Deformation features within the red bed sequence including east-verging and north-plunging asymmetric folds and "drag" folds on faulted contacts between horses are attributed to this event of duplex formation. These kinematic indicators suggest that the Lushs Bight Group rocks to the north of the fault has moved east with respect to the Roberts Arm block to the south.

Other kinematic indicators in the red bed sequence show that the sequence has also been affected during a later deformational event. The red beds are deformed into west-verging kink folds with broken, north-northeasterly plunging hinges (brittle fractures parallel to axial planes). Locally, the kinks overprint the previously formed drag folds. The sense of movement derived from these late brittle structures implies movement of the northern block to the west, the opposite sense to the earlier deformation associated with duplex formation.

Well developed mylonitic S1 foliation is present within cherty sedimentary rocks on Sunday Cove Island, in the area immediately north of the Lobster Cove Fault. There, a strongly flattened and altered pillow lava and overlying mylonitized sequence of tuffaceous and cherty protolith is exposed. The mylonites exhibit a well-developed stretching lineation. The mylonitic foliation is also cut and crenulated by discrete shear

bands. Two generations of post-mylonitic, intrafolial folds are present as well (Fig 6.26).

6.6.2.4 Grand Dismal Cove Duplex

The second duplex is located at the eastern end of Triton Island in the Grand Dismal Cove area. There the Lobster Cove Fault is offset approximately 1.3 km along a northeasterly trending, sinistral strike-slip fault (Fig 6.27, inset). East of the offset, units juxtaposed along the Lobster Cove Fault are intensively and complexly deformed into the Grand Dismal Cove duplex. The duplex involves repetition of the red bed sequence, volcanic rocks of the Roberts Arm Group, and cherty to tuffaceous sedimentary rocks of the Lushs Bight block, as well as the Lobster Cove Fault itself

The duplex contains two horses consisting, from south to north, of pillow lava of the Roberts Arm Group; unconformably overlying conglomerate and sandstone of the red bed sequence; the Lobster Cove Fault zone; and mafic tuff and cherty sedimentary rocks of the Lushs Bight Group (Figs 6.24 and 6.27). The whole section south of the fault is overturned and dips steeply south-southeast. Well-developed folds in the red bed sequence are reclined, verge northeasterly and plunge southeasterly (Fig 6.28). Smaller mesoscopic east-verging, south-plunging folds are present in the Lushs Bight block rocks in the southern horse. These are similar in style, vergence and plunge to folds in the red bed sequence. The overall sense of movement on the Lobster Cove Fault, as deduced from kinematic indicators in this area is dextral. Two faults with apparent minor dextral offset cut the northern horse at a high-angle to the Lobster Cove Fault.

In this same area, rocks of the Welsh Cove Formation north of the Lobster Cove Fault are deformed in highly non-cylindrical folds, possibly of the "sheath" type. This type of fold is typically found in simple shear zones characterized by a high strain

6.6.2.5 Intervening Regions

There is almost continuous outcrop of the red bed sequence along the Lobster Cove Fault on Sunday Cove, Pilley's and Triton islands between the Lobster Cove and Grand Dismal Cove areas.

In northern areas, kinematic indicators consistently point to two deformational events similar to those observed at Lobster Cove and Grand Dismal Cove. The first, based on the presence of tight to isoclinal Z folds (e.g. Fig. 6.28), involved eastward movement of the rocks north of the Lobster Cove Fault, with respect to the Roberts Arm Group rocks south of the fault. It was followed by brittle deformation producing westerly-verging broken kinks. During this event the northern block moved west with respect to the block south of the fault.

6.6.3 NEW WORLD ISLAND AREA

East of Triton Island the trace of Lobster Cove Fault lies under the waters of Notre Dame Bay. It comes on shore again on the Fortune Harbour Peninsula, where it is named the Chanceport Fault. The Chanceport Fault is traced east towards New World Island where it eventually merges with the Luke's Arm fault, the eastern most segment of the Red Indian Line. The Chanceport and Luke's Arm Fault divides the New World Island area into three structural blocks (cf. Williams, H. et al., 1988). The Roberts Arm Group equivalent in this area is narrow and wedge shaped, and thins structurally towards the east, finally being truncated between the converging Luke's Arm and Chanceport faults.

North of the Chanceport Fault, the Notre Dame Bay block consists of late Cambrian pillow lavas of the Sleepy Cove and Moreton's Harbour groups intruded by the Twillingate trondhjemite, dated (U/Pb zircon) as $507 \pm 3/-2$ Ma (Elliot et al., 1991). Immediately northwest of the Chanceport Fault this pluton is cut by a high grade (amphibolite) mylonitic shear zone, which parallels the fault for the last several kilometres of its exposure on land (Williams, H., 1976; Stander, 1984). Kinematic indicators show that this is a thrust zone, in which rocks to the north moved up with respect to those south.

Williams, P. et al. (1988) and Elliot et al. (1991) have shown that the structural evolution of the Chanceport Fault and related splays on New World Island record both dextral and sinistral movement. Initial deformation involved ductile, dextral, transcurrent movement and may have involved hundreds(?) of kilometres of displacement on the Chanceport Fault. This event predates intrusion of the Loon Bay igneous suite, which

has an age of 408 ± 2 Ma (Elliot et al., 1991). Folds associated with this event have variable plunge but display a consistent z-asymmetry when viewed down or to the northeast. Subsequent movement on the Chanceport Fault involved brittle, sinistral movement and post-dated the Loon Bay suite. The ordering and character of events involving initial dextral and later sinistral movement is similar to that described above from western Notre Dame Bay.

Virtually nothing is known about the kinematics of the Chanceport Fault on the Moretons Harbour Peninsula. A recent study in the Fortune Harbour area of central Notre Dame Bay has shown the Chanceport Fault to be a northeast(?) directed thrust with only a small displacement (O'Brien, 1991). Most recent field observations along the fault and new geochemical data from rocks on either side of the fault are at odds with the present interpretation of the Chanceport Fault as a major structural element (Dee and Swinden, 1994).

6.7 Geophysical Constraints

There are geophysical data available that can be integrated with the field observations providing further constraints on the shape and extent of the Lobster Cove - Chanceport Fault. Figure 6.29 presents a detailed Bouguer gravity anomaly map of the Notre Dame Bay and offshore region (modified from Howarth and Miller, 1982). The gravity anomaly map, as well as corresponding magnetic field data (Geological Survey of Canada magnetic Map 1709A), reveals an elliptical area with Bouguer anomaly higher than 30 mGal confined to the shores of Notre Dame Bay. The 30 mGal contour coincides relatively well with the trace of the Lobster Cove - Chanceport Fault and is bounded to the south by fairly flat values in the 20 mGal range. This area trends approximately northeast and the gravity anomaly is most intense on the edges of the structure. Modelling of gravity and magnetic data on a series of transects across Notre Dame Bay was carried out by Howarth and Miller (1982) and Miller (1990) and are reproduced on Figure 6.30. The data show that internal peaks and troughs within the overall region of the gravity high can be modelled as a series of imbricate thrust sheets of mafic rocks floored by ultramafic rocks. The modelling suggests that the thrust sheets dip into the centre of Notre Dame Bay from either side

forming an overall synformal structure and that there is a deepening of the thrust stack northward away from the Lobster Cove - Chanceport fault to a depth of around 25 km (Fig. 6 30). The correspondence of the southern boundary of the Notre Dame Bay gravity high with the Lobster Cove - Chanceport Fault, as well as the geophysical modelling implying internal imbrication of the region over the gravity high, suggests that the elliptical gravity pattern bounded by the 30 mGal contour corresponds with the offshore extent of the Notre Dame block.

The western boundary of the elliptical gravity high in Green Bay appears to correspond with the Green Bay Fault, a major splay of the Cabot Fault system. The gravity high locally extends west of the trace of the fault, coinciding with the surface exposure of the Betts Cove ophiolite along the eastern side of the Baie Verte Peninsula. It is uncertain if the Betts Cove ophiolite represents a displaced fragment of the Notre Dame block or if it just has a similar geophysical signature because of its similar mafic and ultramafic lithologies.

The eastern boundary of the Notre Dame block is believed to be marked by the pronounced northeast-trending gravity gradient extending offshore from the along-strike extension of the Chanceport-Luke's Arm Fault system. Gravity data do not clearly define the northern limit of the block.

6.8 Constraints On The Ages Of Movement Along The Fault

The precise age of displacements along the Lobster Cove-Chanceport Fault is not known. It appears that easterly movement of the Lushs Bight block immediately post-dated deposition of red beds as there is little evidence of post-depositional erosion of this unit. The red beds which overlie the Springdale Group are lithologically similar to and have been commonly correlated with alluvial and deltaic red beds of the Botwood Group in the Exploits subzone. The Botwood Group red bed sequence is underlain by shallow marine strata which contain a Late Llandovery to Early Wenlock fauna (Eastler, 1969; Berry and Boucot, 1970; O'Brien, 1991). However, relations between the marine and the terrestrial sediments of the Botwood Group are not clear, and in a detailed sedimentological study, Wessel (1975) suggested that the Springdale basin and the Botwood basin were filled

separately. U-Pb zircon ages of $429 \pm 6/-5$ Ma and 425 ± 3 Ma on felsic tuff of the Springdale Group underlying these red beds establishes a Llandovery/Wenlock age for the upper part of the Springdale Group (Chandler et al., 1987; Coyle, 1990, respectively).

A ductile dextral movement on the Chanceport Fault and the Red Indian Line in the New World Island area post-dates mafic dykes intruding the Twillingate pluton, but predates intrusion of the Late Silurian Loon Bay igneous suite. Metamorphosed (blue-green amphibole, albite/oligoclase and strain-polygonized quartz) mafic dykes cutting the main body of the Twillingate trondhjemite were dated by $^{40}\text{Ar}/^{39}\text{Ar}$ as 438-443 Ma (Williams et al., 1976). An undeformed felsic dyke of the Loon Bay igneous suite which cuts folds related to this deformation in rocks south of the Red Indian Line has been dated by U-Pb zircon at 408 ± 2 Ma and similar dyke from the locality north of the Chanceport Fault yielded an age of $409 \pm$ Ma (Elliot et al., 1991). This places an upper limit on the age of this event. The younger, brittle sinistral event associated with the Chanceport Fault and Red Indian Line zone overprints previous ductile dextral deformation and post-dates the Loon Bay suite (Williams, P. et al., 1988; Elliot et al., 1991).

Therefore, available data bracket the age of emplacement of the Notre Dame Bay nappe between the minimum age of the base of the red bed sequence (approximately 425 Ma) and the age of emplacement of the Loon Bay suite (~ 408 Ma).

6.9 Notre Dame Bay Nappe (NDBN): Definition

Rocks north of the Lobster Cove - Chanceport Fault (Lushs Bight and Western Arm groups), referred to as the Notre Dame Bay Nappe, form a relatively coherent stratigraphic and structural block of early Paleozoic intra-oceanic volcanic, subvolcanic and related volcanoclastic rocks, which were thrust over adjacent units (Roberts Arm and Springdale groups) of the Notre Dame subzone. Relationships which provide evidence of the thrust emplacement of the Notre Dame Bay nappe are best preserved in the Springdale area. The emplacement of the Notre Dame Bay Nappe over the Silurian rocks of the Springdale Group and the apparent younging of rocks on either side towards the fault on Sunday Cove, Pilley's and Triton Islands implies that the rocks within the nappe were overturned during and as a result of nappe emplacement. It is postulated that rocks exposed in the Notre

Dame Bay Nappe represent an overturned limb of a recumbent fold, i.e. a nappe in the "alpine" sense. The southern and eastern boundaries of the nappe are formed by the Lobster Cove Fault and its along strike eastern extension, the Chanceport Fault. The steep dips along the fault in this region are a result of late-stage deformation overprinting an original flat-lying to shallow-dipping thrust. The western boundary of the nappe, coincides, at least in part, with the Green Bay Fault; whereas, the northern boundary lies off-shore and is not exposed. Details of the boundaries and character of the nappe, constraints on the mechanism and timing of juxtaposition of the nappe with the remainder of the zone, and a discussion of the implications of this hypotheses for the regional tectonic evolution of the zone are given below.

6.10 The Green Bay Fault

The Green Bay fault is an important structure of regional extent within the Notre Dame Subzone in which it forms the western boundary of the study area. The surface trace of the Green Bay Fault trends southwestward from the study area, and connects with the Cabot/ Long Range Fault system, a major fault system extending from White Bay through the Carboniferous Deer Lake Basin to the area north of Cape Ray in the southwestern part of Newfoundland. The Green Bay Fault, along with other prominent fault systems in northwestern Newfoundland, including the Baie Verte-Brompton Line and the Doucer's Valley Fault Complex, is considered to be a splay of the Cabot Fault System..

In the study area the Green Bay Fault is, in general, poorly exposed (Jenner and Szybinski, 1987; Dubé et al., 1992), and its kinematic history is, therefore, poorly constrained. There are no direct structural observations that permit an interpretation of the movement history and previous interpretations have relied on correlation of geological units interpreted to have been displaced by it. The earliest movement on this fault may be coeval with disruption and/or emplacement of the pre-500 Ma sequence upon the continental margin of Laurentia. The Green Bay Fault juxtaposes felsic volcanic and intrusive rocks of the King's Point Complex (Mercer et al., 1985; Kontak and Strong, 1986) northwest of the fault and the Southwest Arm of Green Bay with Cambrian/Ordovician units to the southeast of it. Geochemical data and U-Pb zircon dating indicate that the Silurian Springdale Group

and its associated intrusive rocks are regionally correlative with the Cape St. John Group and Cape Brule Porphyry exposed approximately 50 km to the north on the Baie Verte Peninsula, and most likely are parts of the same large caldera (Coyle and Strong, 1987, Coyle, 1990). Paleogeographic reconstructions of Coyle and Strong (1986, 1987) bring these two units next to the Springdale Group, and at the same time place the Betts Cove Complex (ophiolites) and Snooks Arm Group (volcanic-volcaniclastic sequence) adjacent to the Lush's Bight and Western Arm Groups. Approximately 50 km of dextral movement on the Green Bay Fault during or after the major Silurian magmatic episode is suggested by these authors. The latest established movement on this fault took place during or in the post-Carboniferous (Hibbard, 1983). Although the sense of latest movement is not constrained by direct structural observations, post Lower Carboniferous movement on related faults (D5) involved thrusting towards the north-northwest, and this implies that coeval movement on the Green Bay Fault was oblique sinistral.

6.11 Extensional Faults And Thrust Belts - The Case Of The Long Island Tickle Fault

There are some indications that late normal, extensional faults, that were probably related to the collapse of the orogen (?), indirectly influenced the development of the D4 and D5 thrust belts in the Eastern Domain. The steep orientation of the Long Island Tickle Fault and its oblique orientation with respect to the direction of thrusting imply that it may represent an inverted extensional fault. A mass of rocks behind that fault, represented by Long and Little Bay Islands, formed the buttress. The steep attitude of this fault would inhibit an orthogonal convergence and reactivation of the fault would not be mechanically possible.

It is suggested, that the development of the D4 fold and thrust belt was accelerated by the presence to the north of the Lobster Cove Fault, of a horst or half-horst emerged along a high angle listric fault - represented now by the Long Island Tickle Fault. The Long Island Tickle Fault formed a buttress, too steep and too high to be a suitable ramp for the D4 thrust and fold belt propagating from the south. When the belt reached a buttress, the thrust propagation was restrained and the thrust stack started to fold and to imbricate. In this case thrust sheets simply piled in front of the horst along the Long Island Tickle Fault.

The D4 event was probably accommodated on Long Island by a formation of footwall shortcut faults, which probably led to the formation of D4 thrusts and folds in the Long Island subdomain. In the Halls Bay Head area, secondary thrust faults in the footwall cut into the Cutwell Group and Stag Formation rocks resulting in a footwall thrust stack.

An additional barrier was possibly formed by the Brighton Complex. The indented shape of the fold and thrust belt on Pilley's and Triton Islands is in contrast with the straight outline of southern shore of Long Island, that is separated from Pilley's and Triton Islands by the Long Island Tickle Fault. Pigeon Island, a rock off Long Island's southern shore, probably represents a fragment of the Brighton Complex, pushed against the wall of the high angle Long Island Tickle Fault. The rock on Pigeon Island consists of altered gabbro and serpentinite blocks immersed in a carbonitized, strongly sheared matrix, which is characterized by an omnipresent C-S mylonitic fabric. An orientation of sympathetic shear fractures in the several gabbro blocks implies sinistral strike-slip in present position (Fig. 6.12); whereas, the C-S mylonites reveal oblique thrusting in the NE direction. Although there are no indications with respect to relative timing of these two movements, it is assumed that rigid blocks preserved the memory of an older event (sinistral strike-slip?); whereas, the C-S fabric in the mylonitized matrix indicates the latter event.

6.11 Summary And Conclusions

Field relationships suggest that at least five major deformational events affected the Notre Dame Bay area. The first event (D1) is associated with non-penetrative deformation reflected in formation of chloritic shear zones within pillow lavas of the Lushs Bight Group. The shear zones display a strongly mylonitic foliation, and several are associated with sulphide deposits (Fleming, 1970; Kennedy and DeGrace, 1972; Kean et al., 1995). The ~500 My old, hornblende- and pyroxene-phyric dykes intrude rocks of the Lushs Bight and Western Arm groups, are particularly abundant within or near the D1 shear zones, and are post-tectonic with respect to D1. No D1 folds have been identified.

The second event (D2) is a regionally penetrative event that produced closed to tight major upright folds and an associated axial planar cleavage which can be recognized throughout the Notre Dame Subzone (e.g. Calon and Green, 1987; Pope et al., 1990). The

Coopers Cove pluton displays a well developed S2 foliation, and its U-Pb (zircon) age of 465 +/- 2.5 Ma provides a maximum age for the D2 deformation. To the south of the Lobster Cove - Chanceport Fault, this event predates deposition of the Springdale Group and red beds.

The third deformational event (D3) is a major regional event manifested by the emplacement of an alpine style nappe consisting of the Cambrian-Ordovician rocks (Lushs Bight and Western Arm Groups) upon the Lower Silurian Springdale Group and the underlying Lower Ordovician Robert's Arm Group. Sedimentary red beds of post-Lower Silurian age that overlie both the Springdale and Robert's Arm groups, mark the sole thrust fault (the Lobster Cove Fault) to the nappe throughout the study area, and are interpreted to be dynamically related to the nappe, having been deposited in the foreland basin forming in front of the advancing nappe. A large scale imbrication took place during this event, both within the nappe and underlying rocks of the Springdale Group, and most of the major, NE striking and southeasterly verging thrust faults were generated at this time. The D3 deformation is primarily responsible for the present distribution of lithostratigraphic and structural units within the Notre Dame Bay area.

The effects of the D4 deformation are mainly visible in the Eastern and Northern Domains. It is reflected in an apparent rotation of the Lobster Cove Fault, and folding and thrusting in rock units north and south of the fault. This deformation seems to be associated with a generation of a large regional, northerly plunging antiform, that has a hinge zone located in the southern part of the Halls Bay Head Peninsula, and a similar northerly plunging syncline with the hinge zone in the Springdale area.

The D5 deformation represents the second major regional event, which resulted in north-northwest directed high-angle thrusting and creation of several foreland propagating duplexes of various size (e.g. in the Western Arm section). This event involves rocks of red bed unit and is probably of Lower Carboniferous age.

Structural and stratigraphic relations observed along the Lobster Cove - Chanceport fault indicate a multi-stage movement history of initial eastward emplacement of the Notre Dame Nappe during the mid-Silurian(?), followed by post-emplacement, smaller-scale movement to the west, and then late stage steepening of structures and rock units in the

region. Deformation associated with the nappe emplacement resulted in widespread disruption of the hanging-wall of the Lobster Cove - Chanceport Fault. The Ordovician igneous and sedimentary rocks of the Notre Dame Bay Nappe next to the fault on Sunday Cove, Pilley's and Triton islands are steeply dipping and face the fault and the red bed sequence. The emplacement of the Notre Dame Bay Nappe over the rocks of the Springdale Group and the apparent younging of rocks in both units towards the fault implies that the hanging-wall thrust sequence forms part of a regional-scale recumbent fold, i.e. it is an "alpine" style nappe. The footwall sequence was also deformed and locally, in the Springdale area, the red bed sequence is overturned. East of Springdale, deformation in the footwall decreases and the nappe overlies a sequence of red beds and Ordovician rocks of the Roberts Arm Group. The strong spatial association of the red bed sequence with the Lobster Cove - Chanceport fault suggests that the red beds are dynamically related to the nappe and they are interpreted to have been deposited in a foreland basin which was eventually overridden by the nappe. Age constraints implying a post-425 Ma age for the red bed sequence and pre-408 Ma for nappe emplacement are consistent with this model, but are as yet insufficient to firmly establish a temporal link between the two events. As the nappe moved progressively eastward, the basin migrated with it and red beds are found as far east as New World Island. Away from the Springdale basin, the red bed sequence occurs in a relatively condensed section.

The root zone for the nappe emplacement is not known; however, there are at least two possibilities. One is that the Green Bay Fault rather, than the Baie Verte Line, was the root zone for the Notre Dame nappe during Early Silurian compression. The major, NE-SW trending Green Bay Fault forms the western limit to the Notre Dame nappe, and in general thrusts in both Dunnage Zone and Humber zone are verging away from this fault. This fault also bisects the western Dunnage Zone and truncates the southern part of the Baie Verte Line. The latter has traditionally been mapped as the boundary between the Dunnage Zone, the ancient continental margin of North America (Humber Zone) and the root zone for ophiolite emplacement. Occurrences of ophiolitic fragments between the Baie Verte Line and the Green Bay Fault are common and they are intruded by the Silurian Burlington Granodiorite.

The presence of the Notre Dame Bay Nappe has significant implications for the definition and distribution of the Notre Dame Subzone (Williams, H. et al., 1988). The nappe emplacement records a distinctive geologic event in the evolution of the Dunnage Zone and requires reappraisal of current tectonostratigraphic divisions, which should not only reflect lateral, but also vertical zonation to address the presence of a nappe pile with subhorizontal rather than vertical boundaries. The Notre Dame Bay Nappe may be defined as an additional Dunnage subzone, and then the Notre Dame Subzone must be redefined, or alternatively, the Notre Dame Subzone composed of different nappes, such as the Notre Dame Bay Nappe and Buchans-Roberts Arm Volcanic Belt, can be treated as one of nappe complexes within the Dunnage allochthon, similarly to the nomenclature used presently in the Scandinavian Caledonides.

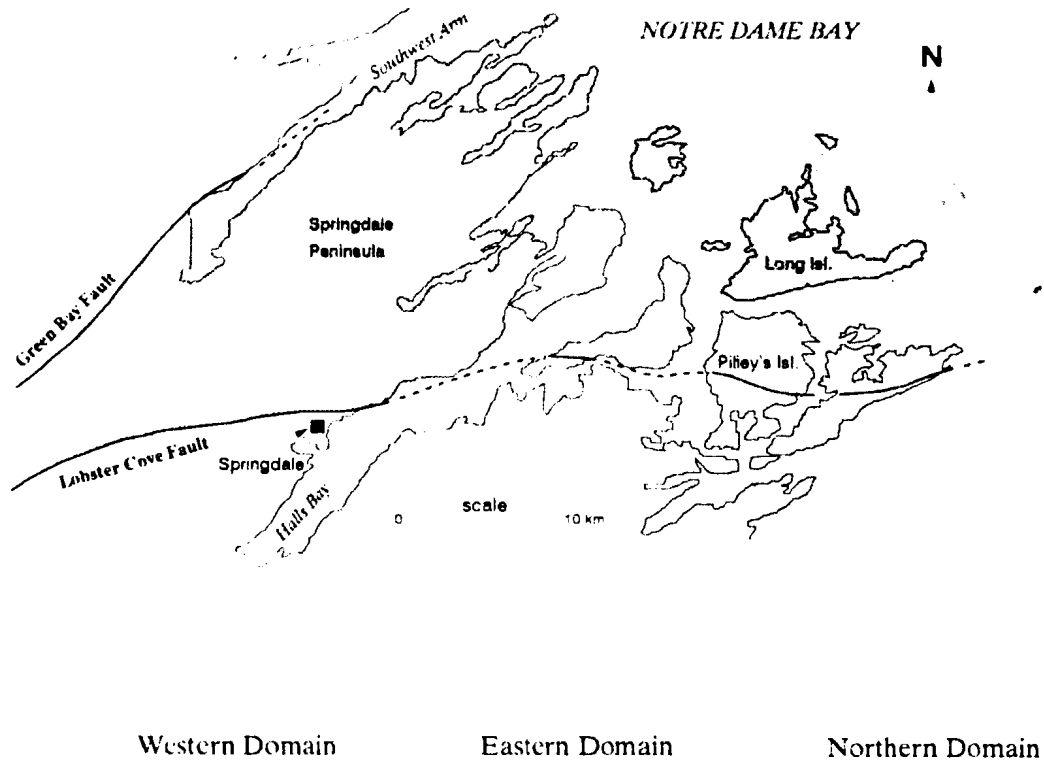
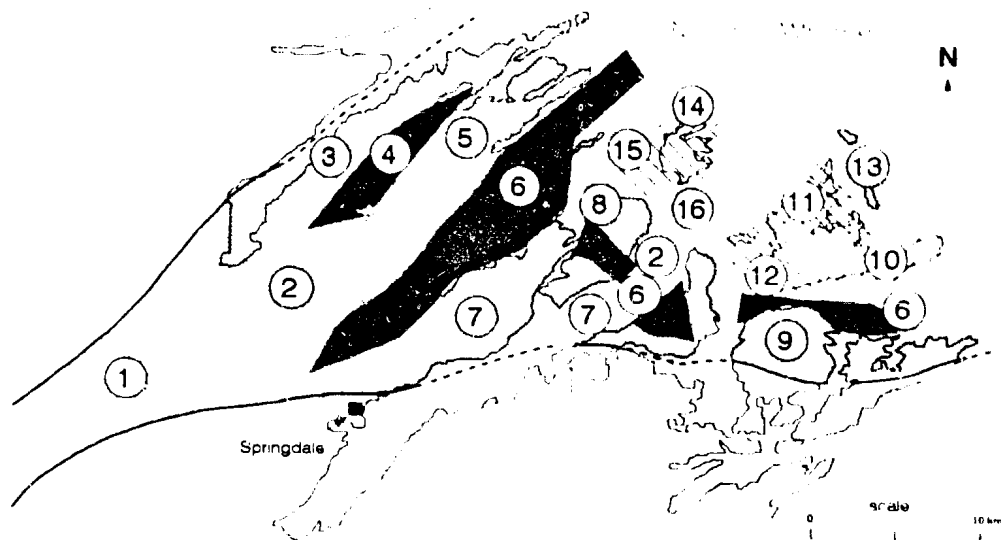


Figure 6.1. An outline of the three different structural domains in the area of study in the western Notre Dame Bay.



- | | | | |
|---|---------------|---|------------------|
| ① | Catchers Pond | ⑨ | Nogood Island |
| ② | Mistaken Pond | ⑩ | Southern Head |
| ③ | Southwest Arm | ⑪ | Cutwell Arm |
| ④ | Line Pond | ⑫ | Aspen Cove |
| ⑤ | Sugar Loaves | ⑬ | Stag Island |
| ⑥ | Little Bay | ⑭ | Northern Head |
| ⑦ | Gull Pond | ⑮ | Southern Harbour |
| ⑧ | Shag Cliff | ⑯ | Copper Island |

Figure 6.2. Distribution of fault panels within the structural domains of the western Notre Dame Bay.

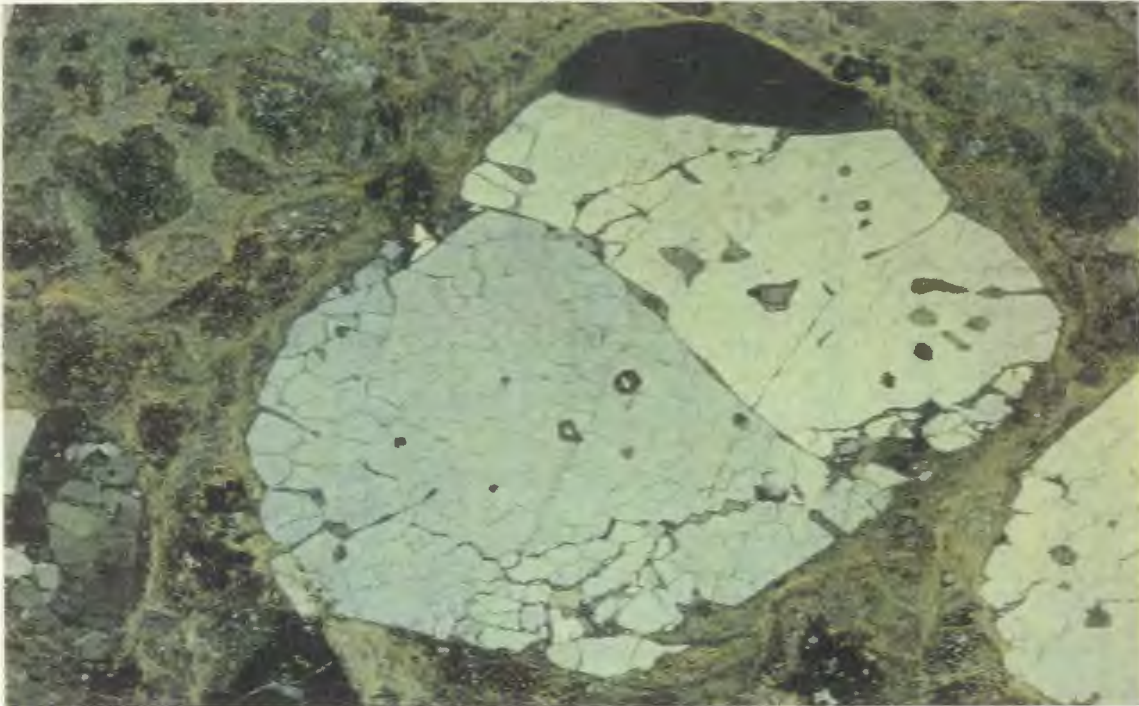


Figure 6.3. "Chaotic" chlorite-sericite foliation in dacitic tuff of the Welsh Cove Formation (Catchers Pond Panel). The S₂ wraps around quartz phenocryst and lithic fragments. Note the "honeycomb" pattern of fracturing in the quartz phenocrysts; X 8.4, XPL.



Figure 6.4. Mafic pyroxene-phyric tuff of the Skeleton Pond Formation displays well developed S₂ cleavage. Pyroxene phenocrysts reveal tails derived from the phenocrysts by grain size reduction, and deflected by rotation of phenocrysts; X 7.6, XPL.



Figure 6.5. The S2 "sericite schists" (western part of the Catchers Pond Panel) displaying well developed differentiation into quartz-rich laminae, separated by thin mica-rich films, and trails of opaque minerals parallel to the microlithons. The S2 fabric was folded probably during strike-slip movement on the Green Bay Fault. X 7.6, XPL.



Figure 6.6. Red cherty sediment of the Skeleton Pond Formation (the Lobster Cove Fault zone, Triton Island) shows evidence of a strong penetrative strain, expressed by transposition of bedding into cleavage and the formation of intrafolial and rootless folds; X 6.8, XPL.

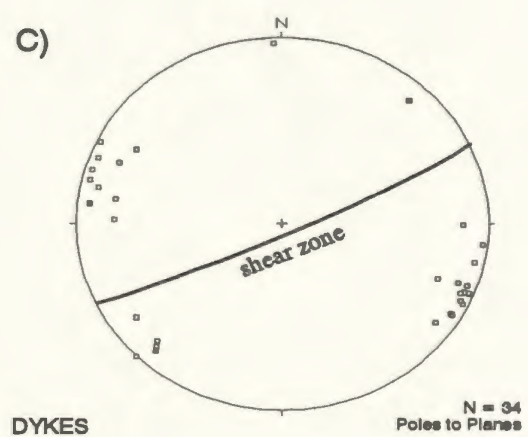
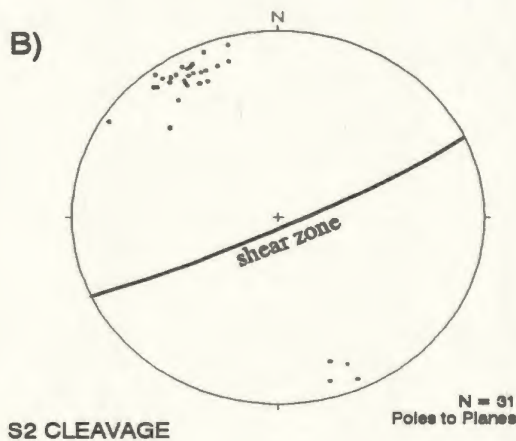
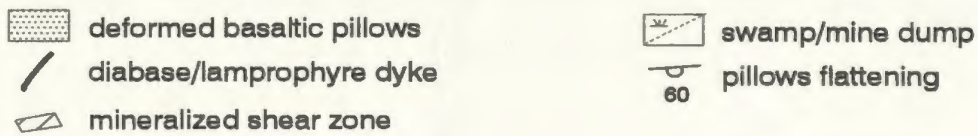
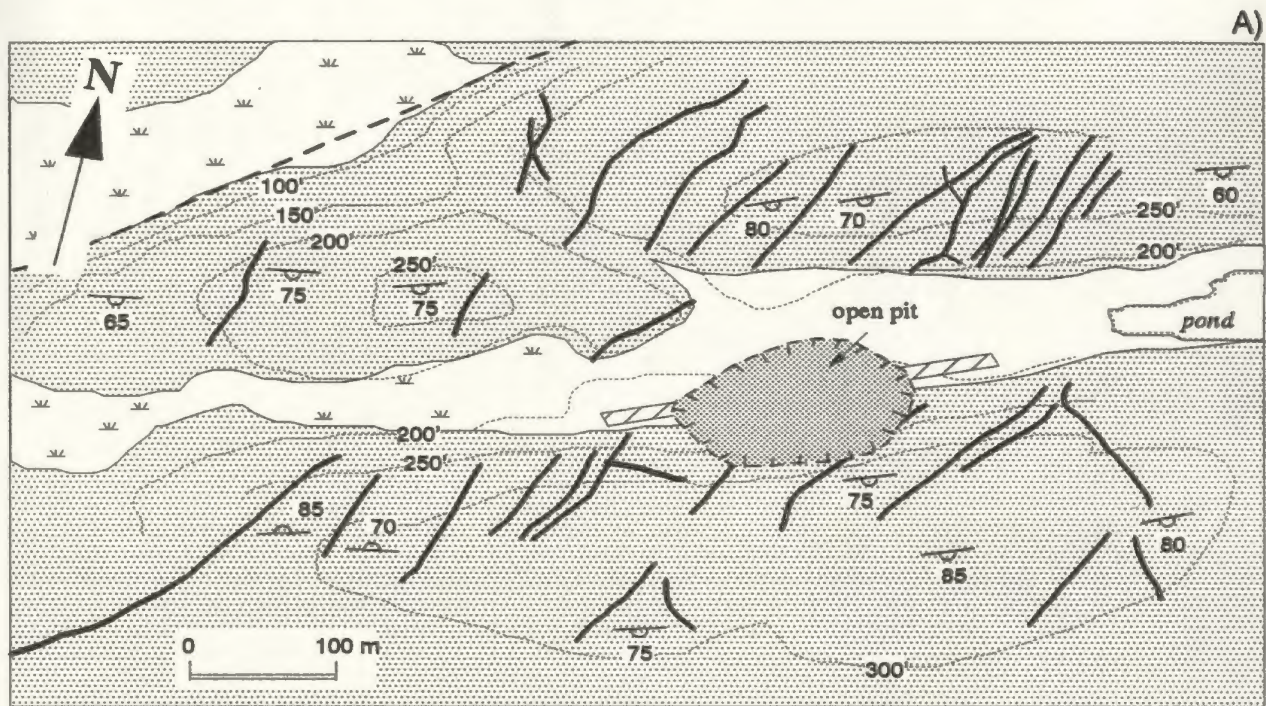


Figure 6.7. A) Distribution of "lamprophyric" and diabase dykes in the Little Bay Mine area (modified from MacLean, 1947); B) stereogram of poles to S2 cleavage in the immediate area of the mine; C) stereogram of poles to dykes.



Figure 6.8. Red chert and intermediate reworked tuff of the Skeleton Pond Formation (Triton Island) with the S_3 fracture cleavage and small scale thrusts and folds thought to be related to nappe emplacement.



Figure 6.9. Minor hinterland dipping duplex in red chert sediment of the Skeleton Pond Formation (western Triton Island).



Figure 6.10. A fragment of a duplex (probably antiformal stack) developed in cherty sediment of the Skeleton Pond Formation (eastern Triton Island).

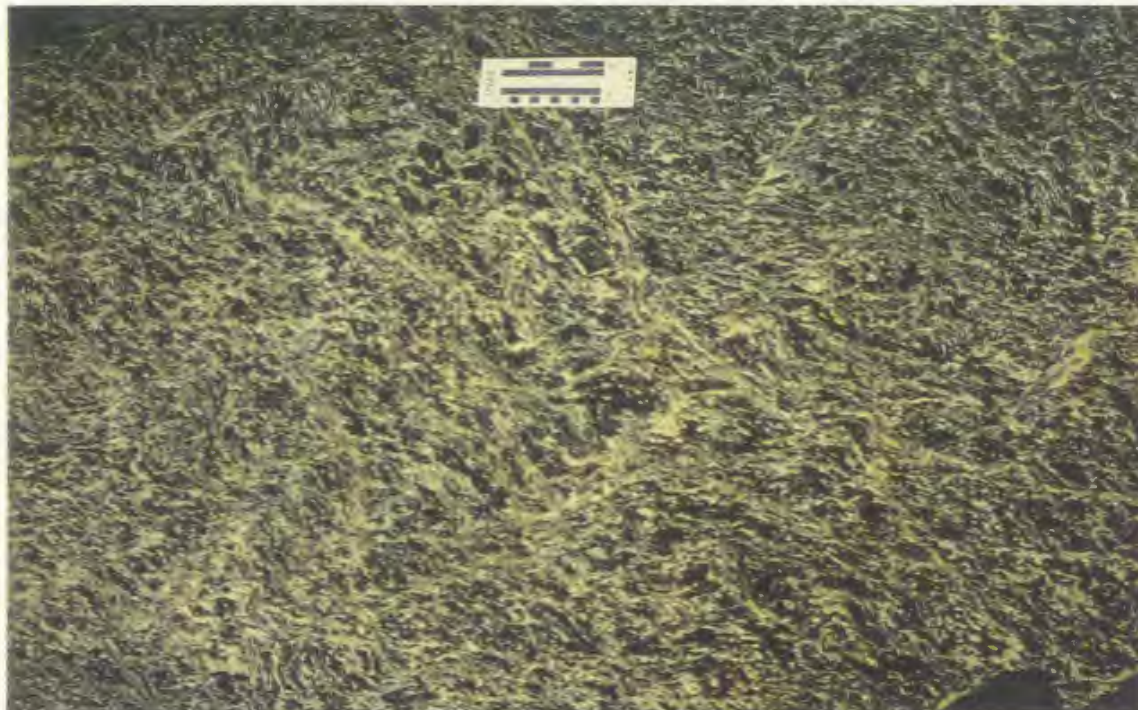


Figure 6.11. Strongly carbonitized and mylonitized mafic and ultramafic rocks from Pigeon Island (southern shore of Long Island). The ubiquitous C-S mylonitic fabric indicates oblique thrusting in the NE direction.

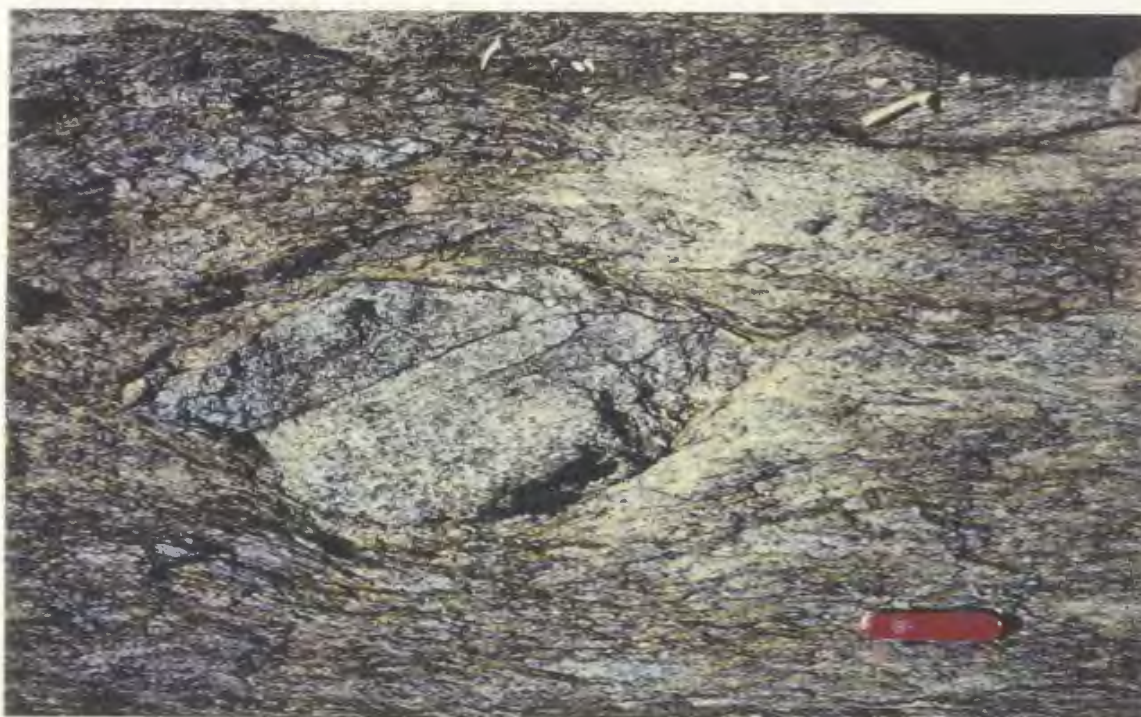


Figure 6.12. A clast of gabbro surrounded by mylonitic matrix like that in Fig. 6.11. The orientation of shear fractures within the clast and a slip direction implies sinistral strike slip.

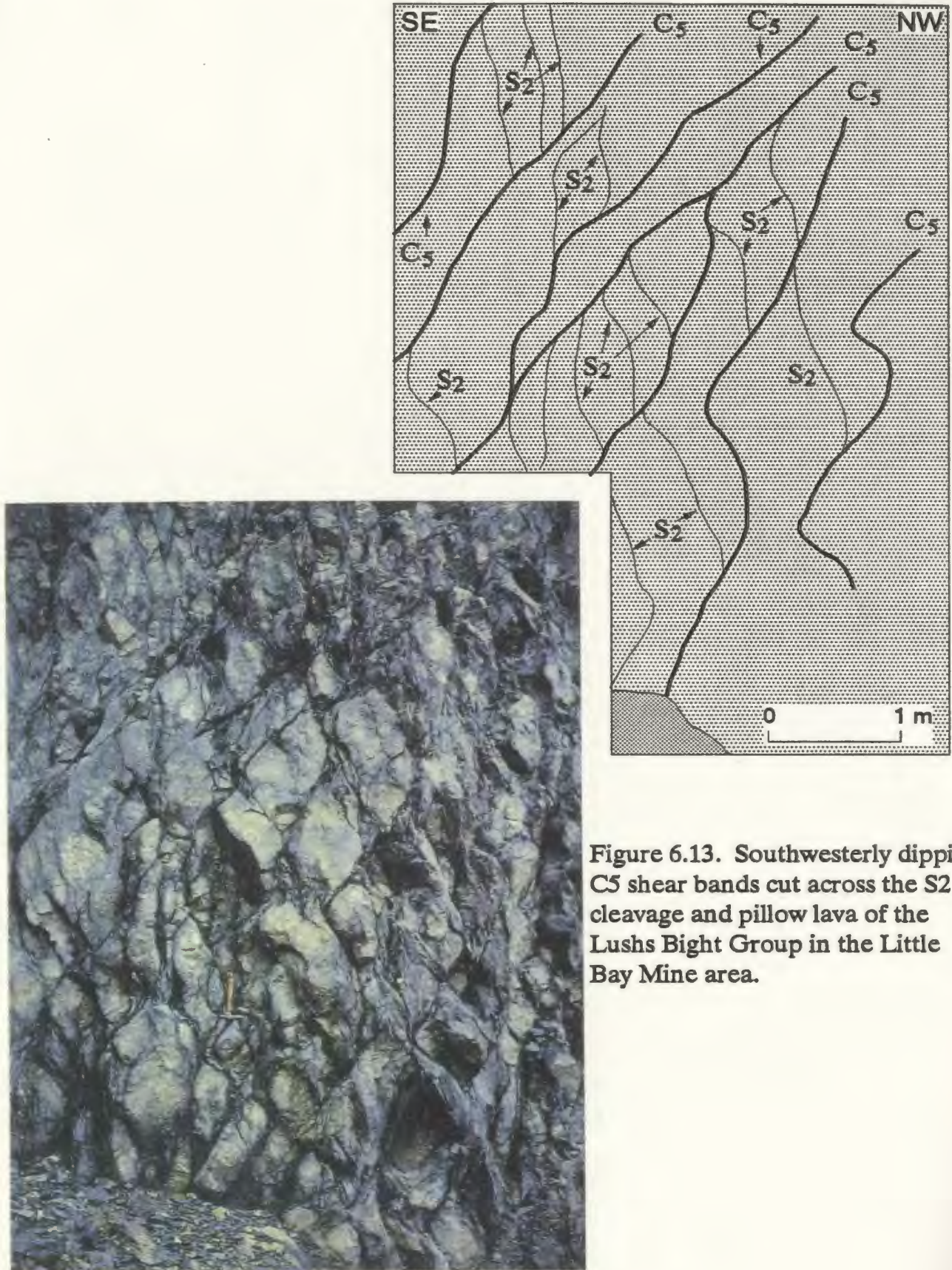
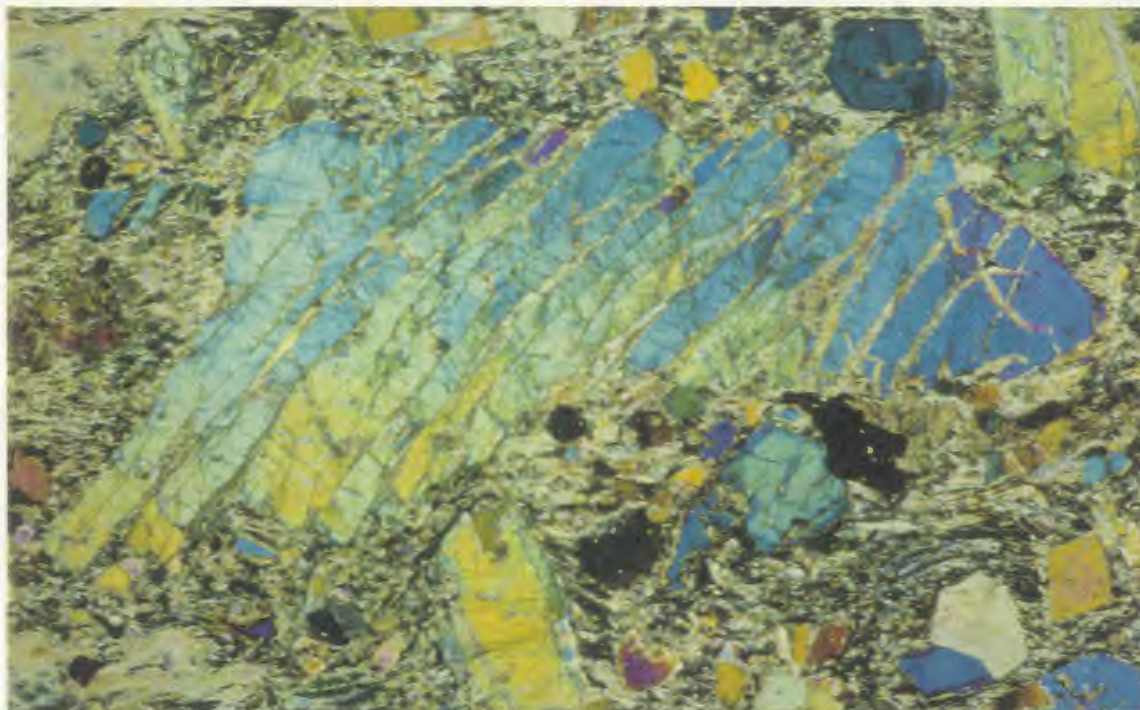


Figure 6.13. Southwesterly dipping C5 shear bands cut across the S2 cleavage and pillow lava of the Lushs Bight Group in the Little Bay Mine area.

A)



B)

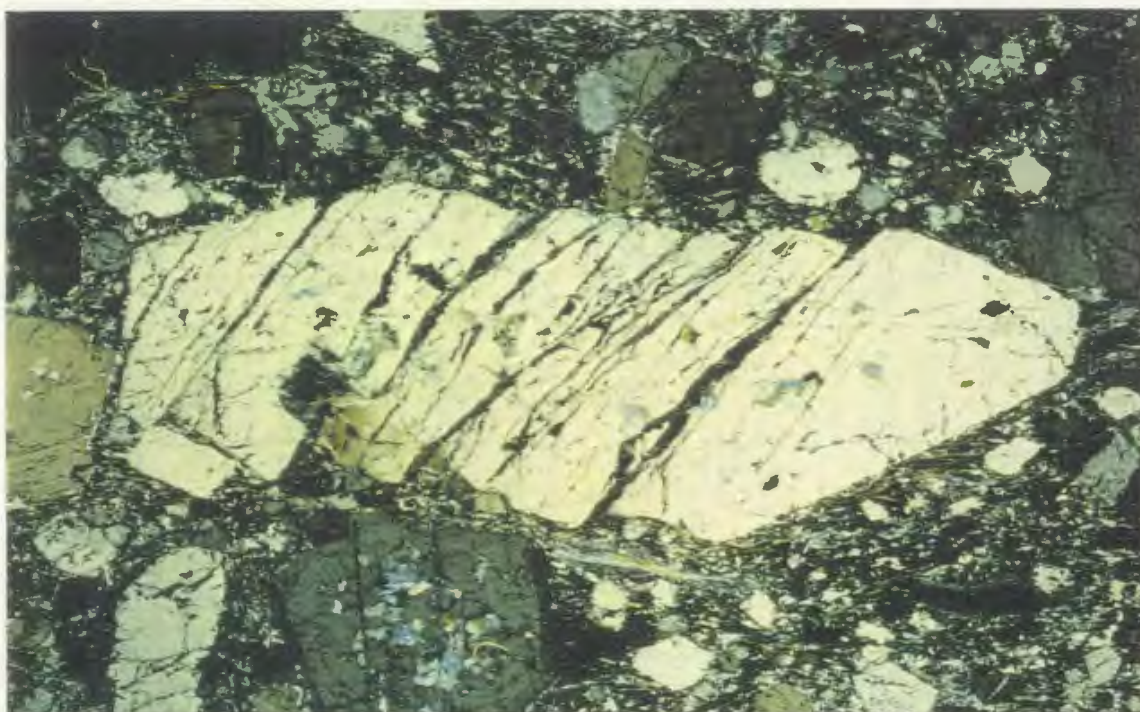


Figure 6.14 A, B. Domino structures developed in rigid pyroxene phenocrysts in the late D1 dykes in the Whalesback Mine area. The matrix also exhibits discrete deformation in the form of an anastomosing chloritic/sericitic fabric surrounding pyroxene phenocrysts. Dykes are deformed by northwest directed high shear bands and minor faults, thought to be related to the D5 deformational event.

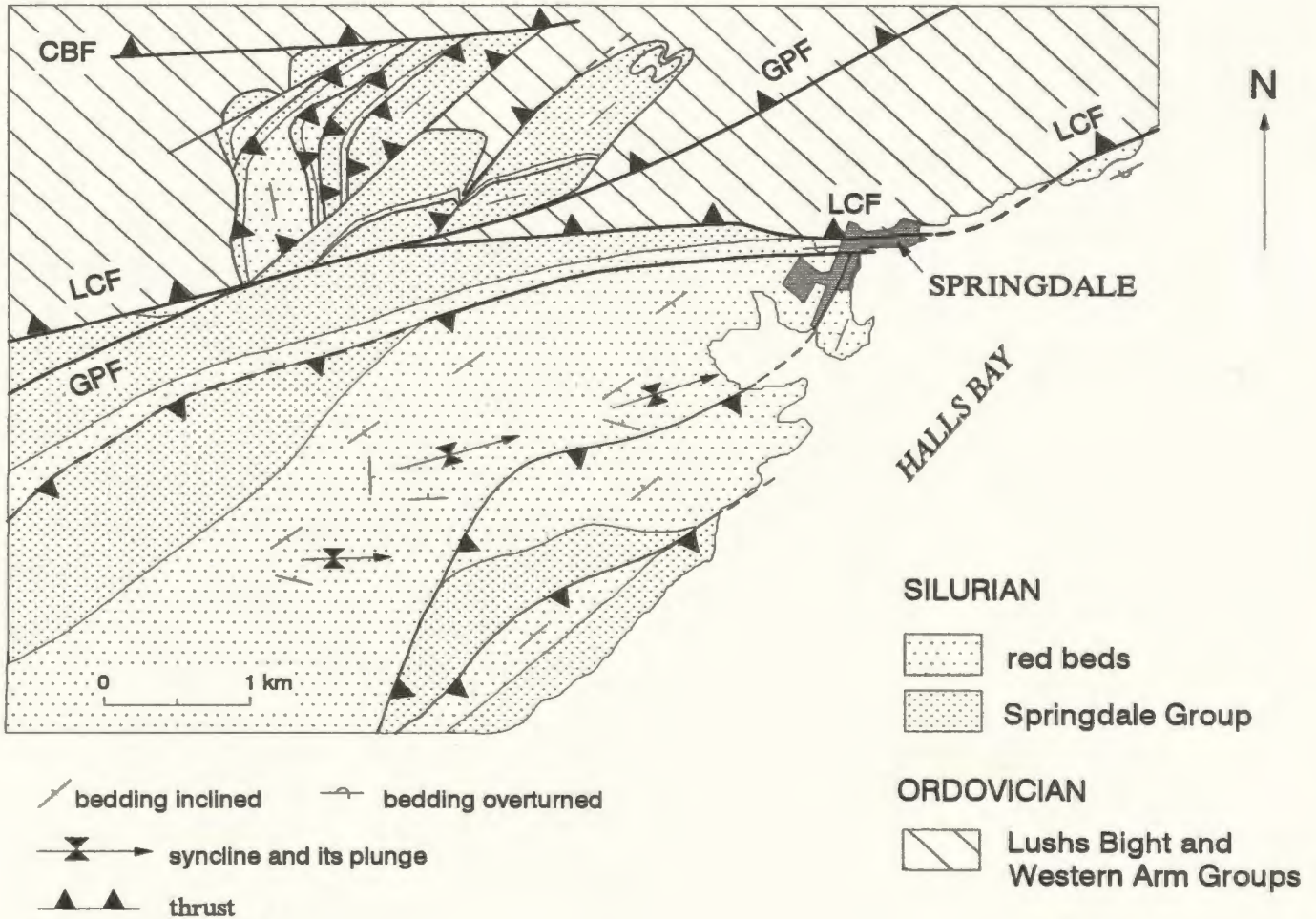


Figure 6.15. Structural sketch of the area west of Springdale depicting relationships between various panels of the Western Domain and the Silurian rocks of the Springdale Group and red beds; CBF - Catchers Brook Fault; LCF - Lobster Cove Fault; GPF - Gull Pond Fault.



Figure 6.16. Outcrop of imbricated felsic volcanic rocks of the Welsh Cove Formation along the road linking the Trans-Canada Highway with the community of King's Point. This is a part of a larger foreland dipping duplex which predominantly involves rocks of the Springdale Group; the field of view is about 20m wide.

Pagination Error

Text Complete

Erreur de pagination

Le texte est complet

National Library of Canada

Canadian Theses Service

Bibliothèque nationale du Canada

Service des thèses canadiennes



Figure 6.18. A D3 minor S-shaped fold-pair with an anticlockwise sense of asymmetry, developed on the normal fold-limb between a major antiform lying up-dip to the left (NW), and a major synform lying down-dip to the right (SE). The Southern Head area, eastern Long Island, looking east. The scale is 15cm high.



Figure 6.19. F3 folds that have an appearance of "drag" folds and are characterized by notably long normal limbs and short overturned limbs. Probably formed originally by buckling, and subsequently modified by simple shear acting parallel to bedding. The Southern Head area, eastern Long Island, looking southeast. The scale is 15cm high.

Figure 6.20. (Right) The probable F3 fold in limestone on southern shore of Lushs Bight, Long Island. This fold has an overall appearance of pre-lithification deformation, is non-cylindrical and lacks a well developed cleavage. It may have resulted from refolding of an original soft-sediment structure. Looking east. The hammer is 35cm long.



Figure 6.21. (Bottom) Minor F₃ Z-shaped folds with a clockwise sense of asymmetry, developed in bedded limestone and limey shale on Oil Island, west coast of Long Island. The fold geometry implies a major syncline to the left, and an anticline to the right. Looking northwest. M. Muggridge for scale.





Figure 6.22. Low-angle shear planes (thrusts) developed in intensely foliated melange on Seal Island, northeast of Long Island. Orientation of shear planes and cleavage is consistent with northeast-directed movement. The melange consists of blocks of strongly fractured limestone and mafic flows surrounded by shaly matrix. Looking northwest. The scale is 15cm high.

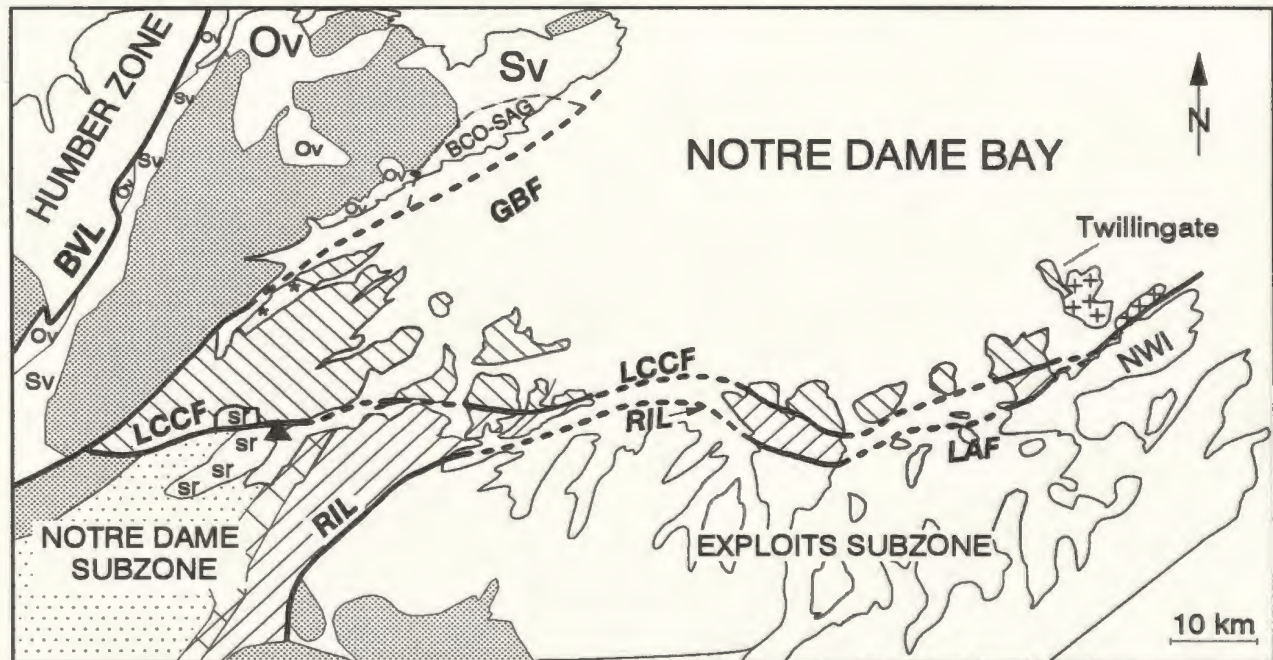


Figure 6.23. Schematic geological map of the Notre Dame Bay area; note that the legend reflects tectonic divisions in the Dunnage Zone.



Figure 6.24. A typical cross section of the Lobster Cove Fault in the Grand Dismal Cove area, western Triton Island. Looking west. Lithological units exposed in the outcrop are (from left to right): conglomerate and sandstone of the red bed unit; mafic (green) tuff of the Western Arm Group that is mylonitic on the contact with red sandstone, but only weakly schistose away from it; and on the extreme right, pillow lava of the Western Arm Group. L. Mandville for scale.

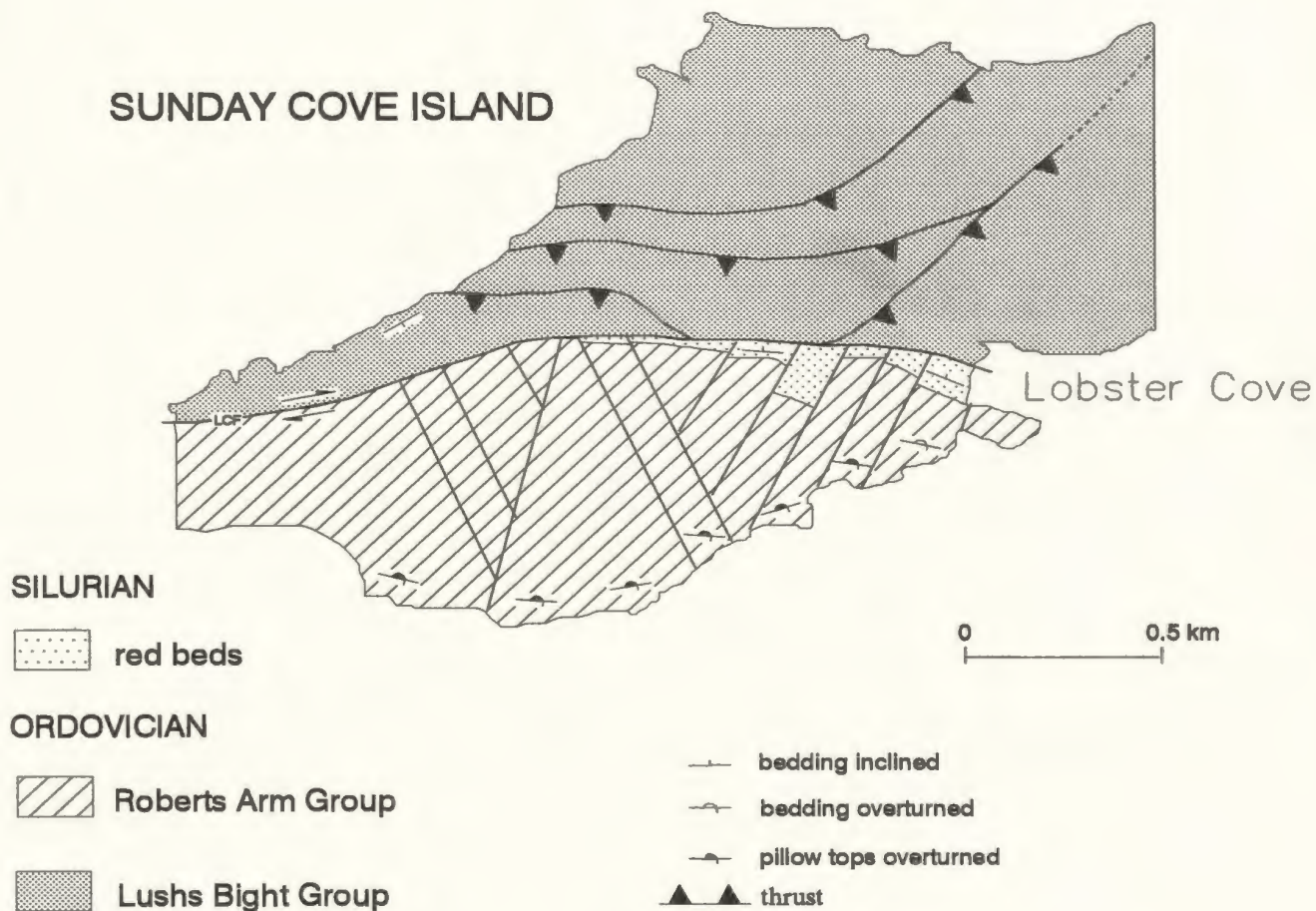


Figure 6.25. Mylonitic pillow lava of the Lushs Bight Group and cherts and tuffs of the Skeleton Pond Formation north of the Lobster Cove Fault, juxtaposed with red sandstones and underlying mafic rocks of the Roberts Arm Group south of the fault, Lobster Cove, Sunday Cove Island.

Rocks along the southern margin of the Lobster Cove Fault form an imbricate stack consisting of red beds and rocks of the Roberts Arm Group arranged in northeast- to northwest-trending domino-type horses. Deformation features within the red bed sequence (east-verging and north-plunging asymmetric folds and "drag" folds on faulted contacts between horses) suggest that the Lushs Bight Group rocks have moved east with respect to rocks of the Roberts Arm Group.

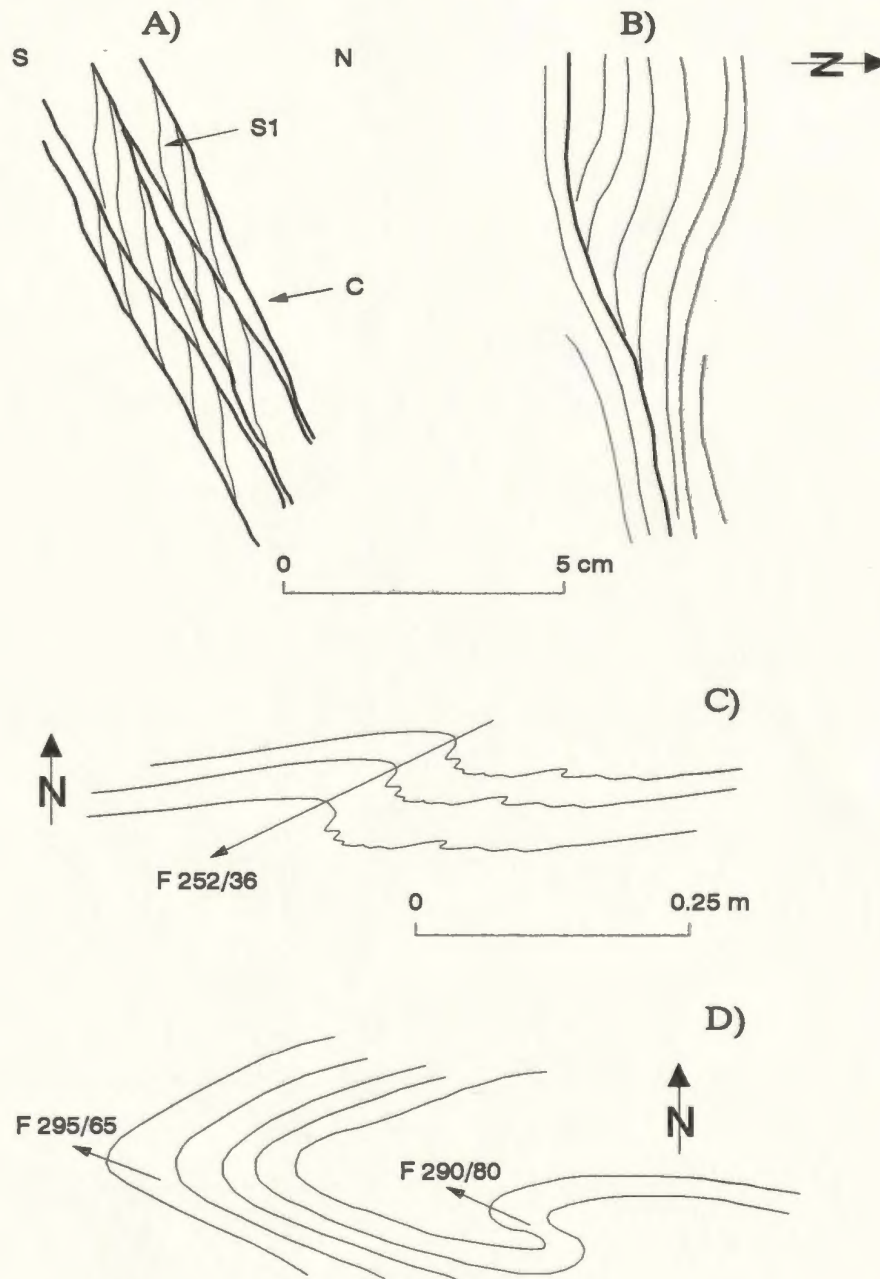


Figure 6.26. Well developed mylonitic S1 foliation is present within tuffaceous and cherty sediments on Sunday Cove Island in the area immediately north of the Lobster Cove Fault. The mylonitic foliation is cut and crenulated by discrete shear bands (A and B) indicating an oblique southwesterly directed thrusting (D1 - D2?). Two generations of post-mylonitic, intrafolial folds (C and D) present in cherts indicate easterly directed movement related to D3 nappe emplacement.

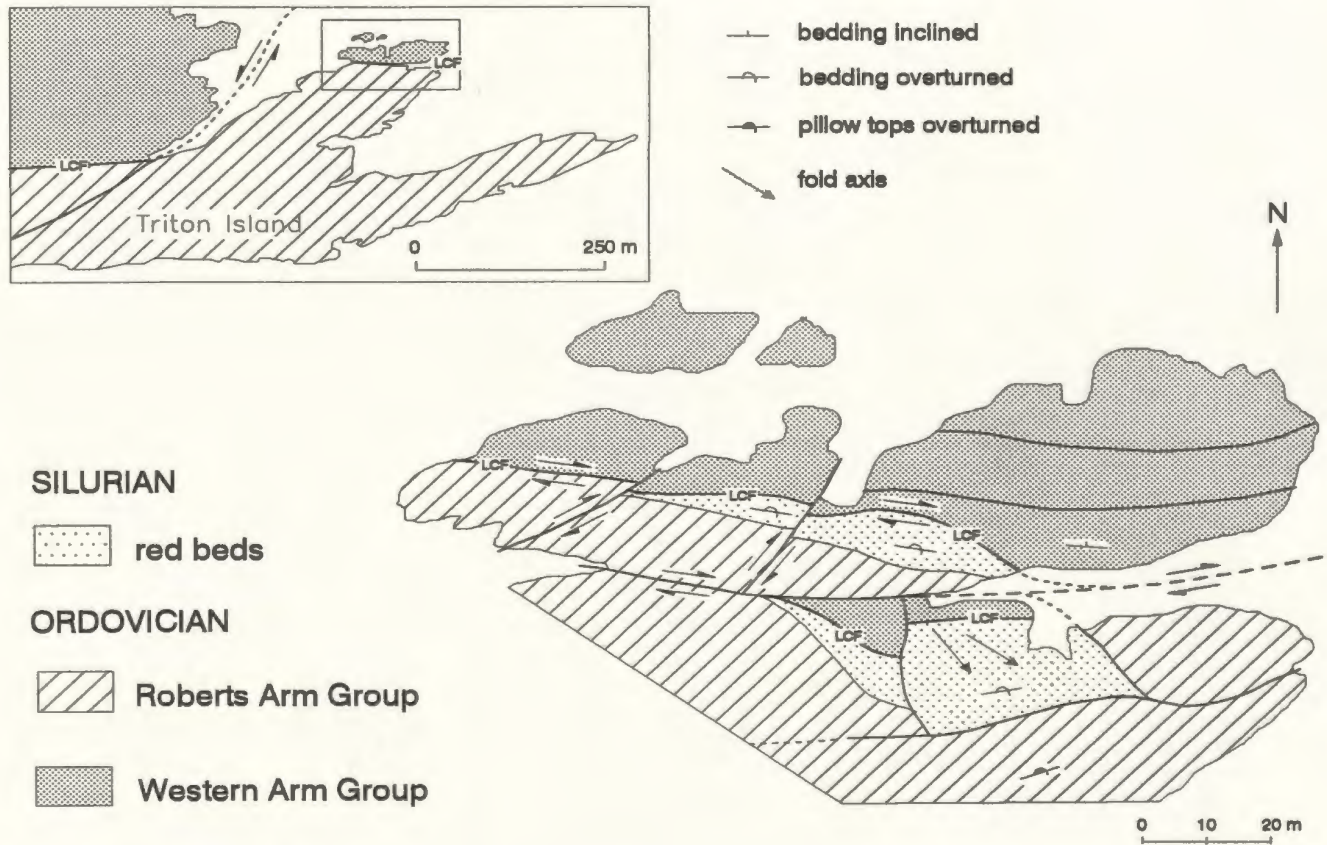


Figure 6.27. Lobster Cove Fault in the Grand Dismal Cove area, eastern Triton Island. The Lobster Cove Fault is offset approximately 1.3 km along a northeasterly trending, sinistral strike-slip fault (Fig.6.27, inset). East of the offset, units juxtaposed along the Lobster Cove Fault form a map scale duplex. The duplex involves repetition of the red bed sequence, volcanic rocks of the Roberts Arm Group and cherty to tuffaceous sedimentary rocks of the Western Arm Group, as well as the Lobster Cove Fault itself. Well developed folds in the red bed sequence are reclined, verge westerly and plunge southeasterly (Fig.6.28). The overall sense of movement on the Lobster Cove Fault, as deduced from kinematic indicators in this area, is apparently dextral.



Figure 6.28. Reclined F-3 syncline in red beds on the Lobster Cove Fault, Grand Dismal Cove, Triton Island. Viewed looking south, the fold is verging westward and is indicative of an apparently dextral strike-slip on the Lobster Cove Fault. The axis of this fold plunges steeply in a southwest direction. The field of view is about 5m.

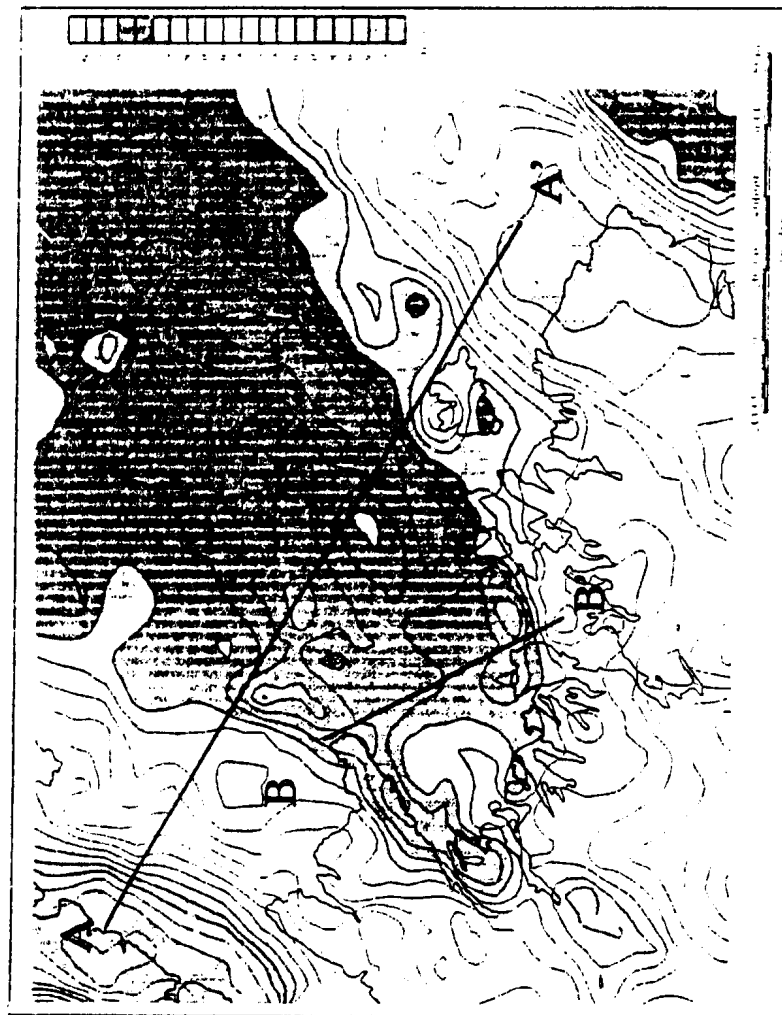


Figure 6.29. Bouguer gravity anomaly map for the area from the coast of Notre Dame Bay to the north and northeast (modified by Ron Wiseman from Haworth and Miller, 1982). Contours in milligal intervals. Line A-A' and B-B' show location of transects (Fig.6.30). North is to the left.

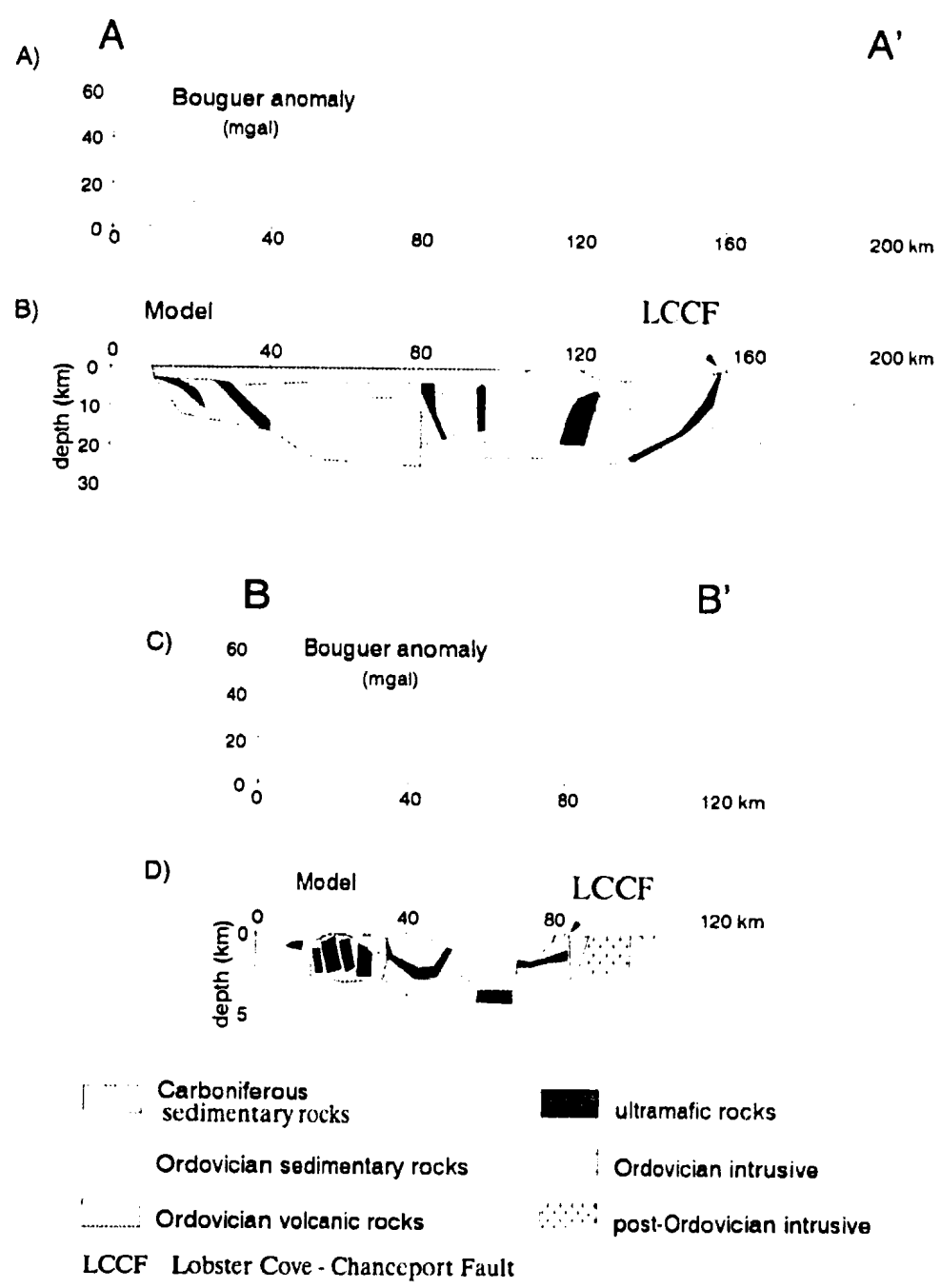


Figure 6.30. Geological models of gravity and magnetic data across Notre Dame Bay from Haworth and Miller (1982) and Miller (1990).

CHAPTER 7 - TOWARDS AN INTEGRATED MODEL

7.1 Introduction

The aim of this chapter is to integrate the stratigraphy, geochemistry and structural observations to produce a model which describes the geological and tectonic evolution of the western Notre Dame Bay area. To do this, the first section of this chapter will briefly review the major results from Chapters 3-6. Following this, a model for the geological and tectonic history of the study area will be presented and discussed. Conclusions and recommendations for further study will end the chapter.

7.2 Summary Of Major Results

7.2.1 STRATIGRAPHY

A major result of this study has been the redefinition of the lithostratigraphy in western Notre Dame Bay. In particular, field mapping, geochronology and micropaleontology show that the geology of the area can be described in terms of two principal geological successions, one older than ~500 Ma and one spanning the time interval from ca 485 to ca 465 Ma. These sequences record events that are significantly separated in time and have disparate geological histories that clearly represent contrasting tectonic environments. Their internal stratigraphies are illustrated in Figures 3.4 and 5.1.

7.2.1.1 The Pre-500 Ma Sequence

Lithostratigraphic units included in the pre-500 Ma sequence are spatially associated with each other, and assigned to the Lushs Bight Group (Indian Beach Complex, Little Bay Basalt), and the lower and middle parts of the Western Arm Group (Sugar Loaves Basalt, Skeleton Pond Formation and Big Hill Basalt). The Stag Formation may represent equivalent to this sequence.

The lowermost part of the sequence is represented by sheeted dykes of fine to medium grained diabase and minor gabbro intrusions assigned to the Indian Beach Complex. Clasts of similar rocks types are found in breccia of the Stag Formation, although locally (on League Rock), pegmatitic gabbro and trondhjemitic fragments are more abundant. The main body of the pre-500 Ma sequence is dominated by pillowed

and lesser massive flows which, in the lower section, are typically intruded by numerous diabase sills and dykes. The part of this lava pile that is included in the Lushs Bight Group (the Little Bay Basalt) is characterized by widespread, locally extensive epidote and chlorite alteration which gradually diminishes towards the stratigraphic top of the group. Interpillow material, where present, has pale colours similar to the lavas. Typically, pillowed flows of the Lushs Bight Group are characterized by a conspicuous chloritic foliation, particularly well developed in pillow margins, and locally by very strong flattening. In contrast, flows assigned to the Western Arm Group are little altered, blackish to dark green in appearance, commonly magnetic, and usually with red and green interpillow chert. The Western Arm Group flows lack the well developed cleavage and strong flattening typical of the Lushs Bight Group pillow lavas. In addition to mafic lavas, the upper part of the pre-500 Ma sequence (Skeleton Pond Formation) contains horizons of mafic pyroxene-phyric tuff and polymictic tuff breccia, with common beds of red to green chert and lesser shale, that are interbedded with massive to pillowed mafic flows.

All of the formations of the pre-500 Ma sequence, as well as the Stag Formation, are intruded by probably co-magmatic intrusive rocks as well as a younger, post-kinematic dykes, that have historically been referred to as "lanprophyric". These dykes are particularly common in the area of the Whalesback and Little Bay mines, where they form swarms that intrude the chloritic shear zones associated with the massive sulphide deposits. Many of these dykes contain large hornblendes and clinopyroxenes, as well as xenocrysts and/or clustered phenocryst assemblages, which locally exceed 50% of the rock. Hornblendes from several dykes were dated by the $^{40}\text{Ar}/^{39}\text{Ar}$ method at ~509 to 488 Ma. A chemically identical dyke intrudes breccia of the Stag Formation. In addition, the Stag Formation is intruded by minor bodies of gabbro, and hornblende from one such intrusion yielded a $^{40}\text{Ar}/^{39}\text{Ar}$ age of ~506 Ma. There are no reliable faunal indicators of the age of this older sequence.

The dykes are of critical importance in understanding the geological history of the western Notre Dame Bay area as their age provides the first clear evidence of the presence of pre-500 Ma stratified rocks in this area. As will be seen below, they also

provide an important constraint on the tectonic environments which the pre-500 Ma rocks encountered during their early Ordovician, post-depositional history.

7.2.1.2. The 485 - 465 Ma Sequence

This younger sequence is much more heterogeneous than the pre-500 Ma sequence. It includes the upper portion of the Western Arm Group (Welsh Cove and Western Head Formations). The Welsh Cove Formation, although mainly volcanoclastic and characterized by massive, thinly laminated and convolutedly folded felsic tuff (probably ignimbritic), also contains pillow lava and polymictic tuff breccia, felsic tuff and monomictic tuff breccia, and minor felsic flows and intrusions. In the Springdale area this sequence includes, as well, a single bed of fossiliferous limestone which has yielded an early to middle Arenig conodont fauna. A porphyritic tuff from this same unit yielded a U-Pb zircon age of ~480 Ma, early to middle Arenig according to Cooper's (1992) scale. The Welsh Cove Formation is intruded by numerous diabase and gabbro sills and dykes, that in the type section form over 50% of the bulk exposure, but in other sections are of limited volume.

The Western Head Formation is stratigraphically above the Welsh Cove Formation and normally contains a relatively homogenous tuff breccia, typically with pyroxene-phyric mafic clasts. Less voluminous hornblende-phyric tuff occurs at or near the exposed top of the unit. A comparable tuff breccia characterized by pyroxene-phyric mafic fragments associated with mineralogically and texturally similar pillow lava is present in the lowermost exposed part of the Cutwell Group on Little Bay Island. In both locations basalts contain abundant, large vesicles, indicating an originally high volatile content. However, clinopyroxenes in the tuff breccia differ; in the Western Head Formation tuff breccia they are diopside, whereas flows and clasts in tuff breccia on Little Bay Island contain augite. Samples of hornblende-phyric tuff from two separate localities in the Western Head Formation yielded $^{40}\text{Ar}/^{39}\text{Ar}$ (hornblende) ages as old as ~465 Ma.

A possible equivalent to this sequence in the northeastern part of the study area is the outlying Cutwell Group. The Cutwell Group, separated from the Western Arm Group by a fault, is divided into four formations, which represent a time span that

overlaps the deposition of the upper two formations of the Western Arm Group. The lowermost Pigeon Head Formation is a southwest dipping and facing unit, which contains cherty shale interbedded with tuffaceous sandstones, and overlain by a polymictic tuff breccia. It is intruded by a distinctive suite of black aphanitic diabase and fine- to medium-grained gabbro sills and dykes, that are mineralogically and texturally similar to flows in the lower formations of the Western Arm Group. There is no direct evidence as to its age of formation.

The Long Tickle Formation consists of a reworked tuff, chert and cherty shale, polymictic lapilli tuff and tuff breccia, and locally tuffaceous, bioclastic limestone interbedded with red argillite. These tuff and lapilli tuff/tuff breccia lithofacies interfinger with the flow lithofacies represented by pillowed and brecciated mafic flows, which form the main part of the exposure in the eastern and southern sections of Long Island. Siliceous shale in lower portion of the Long Tickle Formation has yielded late Arenig graptolites, and a similar age is indicated by conodont fauna from blocks in a limestone debris flow, also in the lower part of this formation. The uppermost horizon of the tuff-breccia included in the formation contains limestone clasts with a conodont fauna, the youngest of which indicate an early Llanvirn age.

The Parson's Point Formation contains interbedded welded mafic tuff, greywacke, shale, peperite, limestone and limestone breccia. These rocks interfinger with and are conformably overlain by felsic pyroclastic rocks of the Seal Cove Complex. The conodont fauna from limestone debris flows reveals a significant diversity in age. The lower part of the formation ranges from uppermost Arenig to early Llanvirn, whereas the upper horizon of the limestone breccia yields a younger fauna, representing a time span from the early/middle Llanvirn to the late Llanvirn, and possibly to the base of the Llandeilo (Ordovician time scale of Tucker et al., 1990). The graptolite assemblage obtained from the Parson's Point Formation indicates most likely an early Llanvirn age for the shale, that is cut by younger limestone debris flows.

Felsic volcanic rocks in the Seal Cove Complex include common plagioclase-phyric tuffs and tuff breccias, and rare felsic flows which in places are difficult to distinguish from co-magmatic intrusive phases. Columnar jointed, banded flows and monomictic

felsic tuff breccia are associated with a partially emergent felsic cryptodome in the eastern part of Long Island, immediately overlying mafic pillow lavas, tuff breccia and hematitic tuff of the Long Tickle Formation. The extrusive rocks are commonly silicified, sericitized and locally carbonatized.

The Cutwell Group is intruded by a variety of dykes, sills, plugs and small plutons which range from diabase and gabbro to quartz-feldspar porphyry and granite. Some types of intrusive rocks (such as those intrusive into the Pigeon Head Formation) are associated only with particular units. The majority of rocks intrusive into the Cutwell Group are co-magmatic; however some larger granodioritic bodies and dykes are post-kinematic with respect to main deformational events.

7.2.2 GEOCHEMISTRY

The geochemical results will be summarized in terms of the two geological sequences defined in the area. The results for the 509 - 488 Ma high-Mg dykes are dealt with separately, because they provide crucial time and tectonic constraints.

7.2.2.1 Geochemistry Of The Pre-500 Ma Sequence

Within the pre-500 Ma sequence, the Lushs Bight Group, appears to be geochemically relatively homogeneous when compared to the other units (cf. Kean et al, 1994). It is dominated by strongly depleted and refractory arc lavas of A-1 (boninitic) and A-2a,b (island arc tholeiite) types. The A-1 type (boninites) is cut by SA-1 type dykes (also boninites). The relationship between the A-1 and A-2a,b groups is unclear; however, Kean et al. (1994) report that an A-2 type dyke cuts an A-1 lava suggesting that locally at least, the A-1 rocks may be slightly older.

The Western Arm Group contains rocks that belong to NA-2 (T-MORB type tholeiites), TR (arc/non-arc transitional flows) and A (arc) geochemical types. The NA lavas are found in the Sugar Loaves Basalt, the lowermost Skeleton Pond Formation, and the Big Hill Basalt. TR type flows commonly interfinger with the NA type lavas in the Big Hill Basalt. Lavas with a well developed arc signature of A-2d subtype are present in the lower part of the Skeleton Pond Formation.

The Stag Formation consists dominantly of A and NA type lavas, which are cut by A type dykes. The arc lavas are flat to LREE - depleted island arc tholeiites. The

non-arc lavas are E-MORB type lavas, unlike any other non-arc volcanic rocks in the area. Among the arc dykes which cut this formation are the LREE-enriched, 509-488 Ma high-Mg dykes (type SA-3A).

The distribution of geochemical types between the Lushs Bight and Western Arm Groups suggests that, at least across the presently defined contacts, there is no substantial change in the chemistry of pillow lavas. Lavas with geochemical features similar to Lushs Bight Group flows are found as high as the Skeleton Pond Formation in the Western Arm Group. In the Stag Formation, such lavas are found within the Breccia Member and Upper Basalt Member, separated by E-MORB-type flows. Taken together the geochemical evolution of these groups supports a very gradational or transitional change between the tectonic setting represented by the Lushs Bight and Western Arm groups. The dominantly arc setting of the Lushs Bight Group gives way upward to a setting dominated by magmatic rocks which lack the arc signature interbedded with minor arc-related flows. Comparison with modern environments indicates that the close association of arc and non-arc lavas is most commonly encountered in back-arc basins and thus the geochemical evolution of the pre-500 Ma sequence is interpreted to reflect a tectonic evolution from island arc to back-arc basin.

The position of the Stag Formation may be further elucidated by using geochemical evidence. Clasts in the Breccia Member show similarity in geochemistry to the most depleted sheeted dykes and lavas of the Lushs Bight Group. However, diabase and gabbro intruding the breccia, and some of the lavas interfingering with the breccia have a close affinity to the less depleted generation of dykes and lavas of the Lushs Bight Group. Therefore, pointing to the possibility of derivation of the breccia clasts from units identical to or of the Lushs Bight Group itself. A close similarity is also revealed between arc type flows from the basalt members overlying the breccia, to lavas of the Skeleton Pond Formation, and the non-arc lavas of the Lower Basalt Member are also comparable in most aspects of their chemistry to those of the Big Hill Basalt. Therefore it is suggested that the Stag Formation consists of rock units that are correlatives of both the Lushs Bight and Western Arm Group.

7.2.2.2 Geochemistry Of The 509 - 488 Ma Dykes

The 509-488 Ma dykes include three subtypes: SA-2c, SA-2d, and SA-3a which reflect, respectively, increasing strength of the arc signature and steepening of the slope of the REE patterns. Dykes of all three types seem to be associated spatially with each other and intrude pillow lavas of the Little Bay Basalt, Skeleton Pond Formation, Big Hill Basalt, and the Stag Formation.

The dykes are of calc-alkalic affinity, according to most discrimination diagrams, and members of a medium- to high-K suite. The SA-2d, and SA-3a subtypes are characterized by relatively high Mg number (~64-68). An affinity to within plate volcanism for the SA-2d subtype is implied by Zr-Ti-Y and Zr-Nb-Y diagrams, but formation in a continental arc setting is suggested by Zr-Zr/Y and Nb/Yb-Th/Yb relationships.

7.2.2.3 Geochemistry Of The 485 - 465 Ma Sequence

The Welsh Cove and Western Head Formations contain only A type flows and tuffs, representing the A-2e, A-2e(t), and A-2f subtypes. There is very little difference between flows of the Welsh Cove Formation assigned to the A-2e subtype and tuffs collected from both of those formations and assigned to the A-2e(t) subtype. Members of both subtypes are calc-alkalic and belong to a medium-K suite characterized by noticeable LREE enrichment. Discrimination diagrams imply their formation in a setting transitional between intraoceanic and continental arc. The Welsh Cove Formation also contains extensive felsic volcanic rocks of CA arc affinity that are members of a medium-K suite, and are assigned to the F-1 type. Samples of the A-2f type occur in the Western Head Formation (one is from a flow or sill from the section assigned to the Welsh Cove Formation) and are calc-alkalic and of medium- to high-K suite. Discrimination diagrams imply an affinity to continental arc. Extended REE patterns show a striking similarity between the A-2f subtype and the SA-2d subtype ~500 Ma dykes suggesting, perhaps, similar sources and tectonic setting.

In contrast to the arc related volcanic rocks that form both uppermost formations of the Western Arm Group, subvolcanic rocks which occur as locally voluminous sills

intruding the Welsh Cove Formation are of non-arc (SNA) and transitional (STR-1, STR-2) affinity. Most of the sills of the Welsh Cove Formation lack a strongly developed negative Nb anomaly (STR-1); even when they exhibit a weak island arc geochemical signature in Nb, other aspects of their chemistry (e.g. Ti/Zr, Ti/V ratios) indicate some non-arc affinity (STR-2).

Of particular interest is the fact that the lowermost lithostratigraphic unit of the Cutwell Group, the Pigeon Head Formation, dominated by epiclastic and volcanoclastic rocks, is also intruded by STR-1 and STR-2 type sills and dykes that are geochemically identical to those intruding the Welsh Cove Formation. The age of these intrusions has not been established by age dating; however, because they only intrude two approximately coeval units (the Welsh Cove Formation is dated at ~ 480 Ma and contains a limestone bed with an early to middle Arenig fauna; the Pigeon Head Formation is pre-~470 Ma and predates shale of the Long Tickle Formation that contains upper Arenig graptolites) and are not found in the overlying Pigeon Head Formation, nor in the Western Head Formation that overlies the Welsh Cove Formation, they are interpreted to be Ordovician in age.

Other units of the Cutwell Group are characterized exclusively by arc related volcanism. The Long Tickle Formation is dominated by LREE enriched, transitional TH/CA lavas of the A-4 type and intruded by a geochemically similar suite of CA dykes assigned to the SA-3 type which, however, are of somewhat higher-K affinity. The Seal Cove Complex consists of voluminous felsic tuffs and tuff breccias, dykes and minor flows that are combined in the F-2 type, and are characterized by of CA, high-K arc affinity.

7.2.3. PALEOTECTONIC IMPLICATIONS

7.2.3.1 The Pre-500 Ma Sequence

The Little Bay Basalt includes two types of volcanic rocks, boninites and LREE depleted arc tholeiites. In terms of geochemical characteristics, the Lushs Bight Group boninites reveal REE patterns that are typical of boninites from the type area in the Bonin Islands. Although it has recently been shown that rocks with boninitic affinities can be found at various stages of arc evolution (e.g. type locality in the Izu-Bonin

forearc), and rocks with some geochemical features of boninites have also been recovered from actively spreading back-arc basins (e.g. the Lau Basin), boninites *sensu stricto* are thought to be associated exclusively with intraoceanic arc settings and their genesis is widely considered to be linked to the onset of subduction. In boninites, the enrichment in Th, LREE and Zr with respect to other REE and HFSE is interpreted to reflect the addition of a subduction-related component to a strongly refractory source region. It has recently been suggested that the concave-upward shape of the boninite REE pattern reflects the role of amphibole in that subduction-related component.

The LREE depleted tholeiites of the Little Bay Basalt in the A-2a to A-2c subtypes are similar to rocks which are commonly associated with the early stages of arc evolution. Only a few occurrences of such rocks have been reported from modern island arcs. The closest in terms of REE profiles to the most depleted samples (A-2a type) are rocks from the East Halmahera Ophiolite (Eastern Indonesia) and strongly depleted arc tholeiites recovered from the trench wall at the intersection between the Mariana and Yap trenches. Modern analogues for the A-2b and A-2c subtype are found in the Kermadec island arc, considered to be at a more primitive stage of arc evolution, than its northern extension, the Tonga Arc. Similar rocks occur in the Tonga and Mariana island arcs, where they are found in the trench wall and in the older part of the arc, respectively. In the Kermadec arc, a variably depleted MORB-like mantle wedge was postulated to be source of these lavas, and in all cases, this type of flow is interpreted to be associated with an early stage of arc evolution.

Volcanic rocks with REE and chemical characteristics similar to the Skeleton Pond Formation A-2d subtype tholeiites are somewhat more common in modern arc/back-arc settings. Good analogues have been reported from back-arc spreading centres of the Tonga, Mariana and Izu-Ogasawara back-arc basins.

REE profiles and most chemical features of the A-3 type tholeiites from the Stag Formation are similar to lavas from the Tonga and Kermadec arcs, but are also somewhat like lavas of the Valu Fa Ridge, Lau Basin, in which a well defined Nb anomaly indicates the presence of a slab-derived component in the back-arc basin mantle source. REE patterns of the A-3 samples are subparallel to those of the Valu Fa Ridge

samples, although they are less fractionated than their modern counterparts and differ from them in the lower Ti, Zr and Zr/Y, and higher V.

The arc lavas of the Skeleton Pond and Stag formations are spatially associated with the NA-2 and TR type, and NA-1 type flows, respectively. These show affinities to flows erupted from "anomalous" segments of ridges associated presently and in the past with mantle plumes/hot spots. Good analogues to various flows of the NA and TR type include lavas from the southern MAR segment associated with the Tristan da Cunha mantle plume, lavas from the Galapagos hot-spot spreading center, and the Tamayo Fracture Zone near the mouth of Gulf of California. Mauna Loa (Hawaii) tholeiites, thought to represent uncontaminated partial melts of a plume source, also display extended REE plots broadly similar to some of the NA-2 samples. However, the NA-2 and TR samples particularly closely resemble sills in the Yamato Basin, Sea of Japan. The Japan Sea is a marginal basin formed by crustal thinning and rifting of a continental volcanic arc (proto-Japan arc) in the mid-Tertiary, and the Yamato Basin in the southern part of the Sea is founded on extended continental crust. These sills, cored in ODP holes #794 and #797, intrude sediments on both sides of the Yamato spreading center (Yamato Basin), and although found to be broadly similar to rocks from other marginal basins, they are interpreted by some to be related to "continental initial rifting".

Some of the NA-2 rocks also have adequate analogues in rocks erupted from the spreading ridge in the Guaymas Basin, Gulf of California. The mantle underlying the Guaymas Basin and central part of the Gulf of California is thought to be metasomatized and to contain a minor sub-continental (calc-alkalic) component inherited from prolonged arc volcanism in that region. This has resulted in the eruption of transitional rift tholeiites with La/Yb and Zr/Ti ratios higher than those from the mouth of the Gulf of California, where there is no history of arc volcanism, or of those from its southern intraoceanic segment, the East Pacific Rise.

Among modern back-arc basins, lavas of the Ogasawara Trough - a nascent back-arc behind the Izu-Ogasawara arc, serve as close analogues for some of the TR samples, in terms of extended REE patterns, Sm/Nd ratios and Nb abundances. The Ogasawara Trough rocks are characterized by REE patterns that show affinity to

E-MORB, but their relatively low Ti/V, Nb, Ti and Zr are characteristic of island arc tholeiites. They are thought to result from variable mixing of E-type MORB, which may be generated at rift initiation, and depleted IAT magmas.

In summary, the NA and TR type lavas show a strong affinity to MORB, particularly to that erupted from "anomalous" segments of spreading ridges. Many of these rocks display, as well, a close similarity to the products of within plate volcanism. Although the NA type rocks have geochemical analogues in a considerable variety of intraoceanic and intracontinental rifts, their TR type counterparts have better analogues in flows from back-arc basins, particularly those in an incipient or immature stage of evolution (e.g. Ogasawara Trough, Mariana Trough, Lau Basin), as well as in flows from young and more mature marginal basins (e.g. Gulf of California and Japan Sea, respectively). Marginal basin environments, such as Sea of Japan or Gulf of California, both of which are considered to be related to mantle plumes, are one environment where the association of NA and TR type rocks might be expected in close association with arc lavas and are considered to be the likely setting for the formation of both NA and TR type rocks.

7.2.3.2 The 509 - 488 Ma Dykes

The high-Mg dykes (the SA-2c, SA-2d, and SA-3a types) are geochemically very similar to high-Mg andesites termed "sanukitoids" that occur in southwest Japan, which are considered to form in tectonic settings similar to that of boninite formation, i.e. near the trench and during the subduction of a hot and young lithosphere. In Japan, the short-lived high-Mg magmatism apparently occurred immediately after initial back-arc opening. Some of the high-Mg dykes have geochemical analogues in some modern high-Mg andesitic rocks termed "bajaites", the sporadic occurrence of which (Baja California, S. Chile, Aleutians) is linked to the termination of subduction resulting from a ridge-trench collision. Extended REE patterns of the SA-2d type dykes display a particularly good correspondence with some samples from the Baja California region.

7.2.3.3 The 485 - 465 Ma Sequence

Flows with chemical features similar to the A-2 type rocks of the Welsh Cove and Western Arm formations are reported from the intraoceanic island arcs of Fiji and the

Marianas, but rocks with analogous geochemical characteristics are also found in the Andes. These shoshonitic to calc-alkalic flows from Fiji, are linked to a volcanic activity arising from rifting of the extinct Vitiaz arc. Corresponding flows from the central part of the Mariana arc show a very good correspondence in extended REE patterns with those of the A-2 type; these lavas are typical of the mature central part of the Mariana arc but are unlike the enriched shoshonites of the northern, submarine part of the arc.

REE patterns of A-2 type samples from the Welsh Cove Formation are also rather similar to lavas erupted in the southern volcanic zone of the Andes. In particular, these A-2 rocks display a similarity to basaltic lavas from volcanoes located on thinner continental crust. Geochemical characteristics of the Andean lavas are typically explained by variable mixing of a component derived from subducted crust (characterized by high ratios of Th and LFSE to REE and HFSE), and enriched mantle similar to OIB source or subcontinental lithosphere. An important contribution to these magmas may also be made by mid- and upper-crustal melts and intracrustal assimilation and fractional crystallization (AFC).

Felsic volcanic and volcanoclastic rocks characterized by concave-upward REE patterns, such as those in the Welsh Cove Formation are presently found primarily within intraoceanic island arcs, for example the tonalite - trondhjemite Tholo suite of Fiji and rhyolites from the Bismarck Arc. However, equivalents to these felsites are also found in the regions underlain by young or subcontinental type crust (e.g. Taiwan, Japan).

There is reason to believe that the SNA and STR type sills and dykes that intrude the Welsh Cove and Pigeon Head Formations are contemporary with the arc volcanism and perhaps were intruded within a relatively short period of time, coeval with deposition of these formations. If that is the case, then they may together with their host be similar to sill-sediment complexes such as the one in Guaymas Basin, Gulf of California, or Yamato Basin, Sea of Japan. This may indicate the existence of a younger (than Sugar Loaves-Big Hill Basalt) back-arc or marginal basin, not well

represented in the exposed sections of the Western Arm and Cutwell Groups, or at least an (aborted?) rifting event.

The basal part of the Long Tickle Formation (Cutwell Group) contains flows and tuff breccias that are mineralogically, texturally and geochemically akin to the Western Head Formation tuff breccia, but also display a geochemical similarity to tuffs and flows of the Welsh Cove Formation. Ankaramitic flows from that lower part of the Cutwell Group, included in the A-4a subtype, have only a few modern analogues in little fractionated, medium- to high-Mg lavas, that are considered to represent parental or primitive magmas, and are rarely exposed in island arcs. In general, a genesis and setting analogous to that in which are thought to form sanukitoids and bajaites was invoked for these rare rocks.

In contrast to these, samples of the A-4b subtype have a wide range of modern analogues, that are associated with both intraoceanic and continental arc settings, including the Aleutians, Sunda arc, and the Southern Volcanic Zone of the Chilean Andes, i.e. mature continental arcs attached or adjacent to a continent. Other analogues for the A-4b samples are shoshonitic, rift related lavas of Fiji, and shoshonitic lavas from the northern Mariana arc, that are thought to be derived from a source which is similar to that of OIB. The A-4b type lavas resemble the wide range of ankaramites, alkali basalts and basanitoids from the islands of Grenada and Martinique and the Lesser Antilles, displaying similar REE patterns and similar trace element ratios. Rocks of the Martinique and Grenada suites are interpreted to be derived from alkalic magmas that assimilated continentally-derived sediment. The possibility of a continental crustal contaminant in magmas parental to the Cutwell Group is further emphasized by their similarity to flows of the Bushe Formation, Deccan., which are interpreted to be strongly contaminated by upper continental crust.

Dacitic and rhyolitic tephra with concave REE patterns similar to those of the F-2 type samples are present in the central Aleutians.

7.2.3.3 Sources For The Notre Dame Bay Magmas

A detailed consideration of possible sources for the western Notre Dame Bay magmas, using various combinations of trace elements that behave in diverse manners

during different petrogenetic processes, permits not only an interpretation of the nature of the magma sources and some insight into the petrogenetic processes that formed the magmas, but more importantly, further strengthens constraints on the tectonic environments in which the magmatism occurred. It is inferred that at least four types of sources contributed to western Notre Dame Bay magmatic rocks: 1) normal depleted mantle like that commonly invoked as the source for N-MORB - type lavas; 2) enriched mantle similar to that commonly proposed to generate E-MORB and OIB lavas; 3) metasomatic fluids probably derived from the subducting slab; and 4) a continentally derived component (continental lithosphere, continentally derived sediment or continental crust *sensu stricto*).

The influence of these sources on magma composition varies considerably from one unit to another, and in addition significant intraformational changes in the chemistry of lavas are present. Input from N-MORB and E-MORB sources is dominant in the NA and TR types. Most importantly, the TR type lavas show the slight but nonetheless clear influence of a metasomatic, slab-derived component, which is interpreted to cause the characteristic Th inflection in these rocks. Little or no crustal component in the parental magmas of the NA and TR type lavas is indicated.

Addition of continental crustal material to source(s) of the suite of high-Mg "sanukitoid/bajaite" dykes, that intrude the lower pre-500 Ma sequence is clearly reflected by the Sm/Nd-Nd relationship. This is an important relationship because it implies that the pre-500 Ma intraoceanic sequence was emplaced upon continental crust by the time these dykes were intruded. Similar geochemical evidence indicates that the petrogenesis of both mafic and felsic lavas of the 485-465 Ma volcanic sequence involved a continental crustal component and that hornblende played a major role in their petrogenesis. This raises the possibility that this younger island arc was built upon continental lithosphere.

7.2.3 STRUCTURE

In past studies of the western Notre Dame Bay area, minimal effort was taken to integrate geochemical and structural observations. In this study, the care was taken to

constrain the structural setting of all samples. There are four major results of the structural studies in this area, each of which is discussed in a separate section.

7.2.3.1 Faults Defining The Boundary Of The Study Area

The Green Bay and Lobster Cove Faults are two faults of regional extent within the Notre Dame Subzone, that form the western and the southern boundaries of the study area. The Green Bay Fault connects to the Cabot/ Long Range Fault system, a major fault system extending from White Bay to the area north of Cape Ray in southwestern part of Newfoundland. Along its course, the Green Bay Fault truncates the southern end of the Baie Verte-Brompton Line. The Green Bay Fault is poorly exposed and the precise kinematic history of the fault is poorly constrained. This fault's kinematic history may include formation and movement during first stages of Taconic Orogeny; however, the first documented movement is post-lower Silurian, and the latest established movement on the fault took place during or in the post-Carboniferous.

The NE-SW to E-W trending Lobster Cove Fault is interpreted as east-directed thrust with an apparent strike-slip displacement, bringing rocks of the Lushs Bight and Western Arm groups over volcanic rocks of the Roberts Arm and Springdale groups. The red bed sequence overlying the Roberts Arm and Springdale groups immediately south of the Lobster Cove Fault is the youngest stratigraphic unit affected by movements along the fault. The Lobster Cove fault is correlated with the Chanceport Fault in the eastern part of the Notre Dame Bay.

On Sunday Cove, Pilley's and Triton Islands, the strike of the Lobster Cove Fault is nearly parallel to bedding in the vertical to overturned and north-younging red bed sequence. The fault appears to be also parallel to the trend of volcanic and sedimentary rocks in the Robert's Arm Group. In most outcrops, the generally more deformed rocks of the Lushs Bight and Western Arm groups face into the Lobster Cove Fault.

Deformation within the fault zone involved the red bed sequence, the Silurian and Ordovician volcanic rocks, and the fault itself, and the fault zone is characterized by a series of imbricate structures. In current orientation the duplexes appear as contractional structures formed in a dextral strike-slip fault system.

7.2.3.2 Pre-500 Ma Deformation

The oldest recognized deformational event, D1, is reflected in the presence of high strain chlorite shear zones in the Lushs Bight Group, some of which are hosts to the sulphide mineralization. Similarly to all rocks of the pre-500 Ma sequence, these shear zones are intruded by apparently undeformed sanukitoid/bajaite dykes. The dykes are especially common within or near D1 chloritic shear zones which are intruded by dykes mostly in en-echelon manner. Although most of the dykes are planar, some exhibit buckling related to anticlockwise rotation a slight bend at their terminations, what supports the possibility of a late-kinematic emplacement of at least some of the dykes.

7.2.3.3 Pre-Silurian Deformation

The second event (D2) is a regionally penetrative event that produced closed to tight major upright folds and an associated axial planar cleavage, which can be recognized throughout the Notre Dame Subzone. The maximum age of this event is provided by the U-Pb (zircon) age of ~465 Ma on the Coopers Cove Pluton, which similarly to its volcanic/volcaniclastic host rock displays a well developed S2 foliation. This event predates deposition of the Springdale Group, and may be related to emplacement of the Notre Dame Subzone onto the Laurentian margin during the Ordovician Taconic orogeny.

7.2.3.3 Notre Dame Bay Nappe

The third deformational event (D3) is a major regional event manifested by the emplacement of a previously assembled regional scale F2 recumbent fold, consisting of the Cambrian-Ordovician rocks (Lushs Bight and Western Arm groups), upon the Lower Silurian Springdale Group and the underlying Lower Ordovician Robert's Arm Group. Sedimentary red beds of post-Lower Silurian age that overlie both the Springdale and Robert's Arm groups mark the sole thrust fault to the nappe throughout the study area, the Lobster Cove Fault, and are interpreted to be dynamically related to the nappe, having been deposited in the foreland basin forming in front of the advancing nappe.

7.2.3.3 Southeasterly Verging Fold And Thrust Belt

The D3 deformation or a separate, latter phase of this deformation, is primarily responsible for the present distribution of lithostratigraphic and structural units within the Notre Dame Bay area. A large scale imbrication took place during this event, both within the nappe and underlying rocks of the Springdale Group, and most of the major, NE striking and southeasterly verging thrust faults, and associated folds, were generated at this time.

The style of the D3 deformation was characterized by the development of numerous brittle-plastic shear zones (the Davis Pond Fault is good example) and associated, dominantly brittle, imbricate thrust systems in the Ordovician hangingwall rocks and in the Silurian footwall rocks. A foreland dipping duplex south of the Catchers Brook Fault involving rocks of the Springdale Group is one of the best examples of the latter structural style.

7.2.3.4 Post-Emplacement Disruption Of The Notre Dame Bay Nappe

The effects of the D4 deformation are mainly visible in the Eastern and Northern Domains. It is reflected in an apparent rotation of the Lobster Cove Fault, and folding and thrusting in rock units north and south of the fault. This deformation seems to be associated with a generation of a large regional, northerly plunging antiform, that has a hinge zone located in the southern part of the Halls Bay Head Peninsula, and a similar northerly plunging syncline with the hinge zone in the Springdale area.

The D5 deformation produced a northwest verging, NE-SW trending fold and thrust belt, that is predominantly manifested by variably sized folds in the Eastern and Northern Domains, but mainly by high-angle reverse faults in the Western Domain. The D5 folds form a wide variety of styles, and exhibit major differences in their shapes, interlimb angles and profile geometry. Bedding, and to some extent pre-existing cleavage, still have a strong mechanical control on folding, but at this stage major differences are controlled mainly by the shape of early fold profiles (e.g. Watkinson, 1981).

The F5 fold system forms a well defined pattern on a regional scale and produces a relatively complex fold interference pattern, which varies from the "crescent and

mushroom" (type 2), to more complex "double zigzag" (type 3) patterns. The simple "dome and basin" (type 1) pattern is less common and mostly observed in the Northern Domain, probably because of the fact that well developed early F2 folds were mainly isoclinal. This is consistent with the observations of Skjernaa (1975), who noted, that the type 1 interference pattern forms only when early folds are open, and it disappears when early folds are isoclinal (see also Watkinson, 1981).

A large, NE-SW trending and SW plunging regional F5 anticline dominates the southern part of Long Island and forms a large domal culmination off-shore within Wild Bight, as a result of interference with an early NW-SE trending fold. Parasitic D5 folds were observed in several exposures along the shore of Wild Bight, but it was not possible to follow any of them for any distance, because of the complexity of interference pattern, and the dense system of high angle reverse faults associated with those folds. The F5 faults are slightly overturned towards the northwest; whereas, the associated axial planar cleavage and high angle reverse faults dip steeply towards SE. There, the resulting interference pattern is of the type 1 and the dominant fold trend changes from panel to panel. The overall large scale interference pattern for whole island is 1(->2).

7.3 Geological And Tectonic History Of The Western Notre Dame Bay Area

Integrating stratigraphic, geochemical and structural evidence allows us to erect a detailed geological history for the area. This history is presented in chronological order, starting with the oldest event.

7.3.1 PRE-500 Ma

The oldest rocks in the western Notre Dame Bay area are contained within the Lushs Bight Group and represented by sheeted dykes and voluminous pillow lavas. Both rock types are geochemically identified as boninites (predominantly pillow lava and lesser dykes) and low-Ti tholeiites (pillow lavas and sheeted dykes). Both, the boninites and tholeiites exist in structurally bounded units and no convincing crosscutting relationship were documented. The presence of pillow lavas and sheeted dykes indicates formation in marine, extensional environment; whereas, paleotectonic affinity indicated by their

geochemistry and correlations with the rocks from modern tectonic environments suggest formation in supra-subduction zone. Boninites are known to erupt typically during the onset of subduction, whereas the strongly LREE depleted tholeiites are commonly found, locally associated with boninites, in primitive island arcs in early stages of their evolution. Thus, in the pre-500 Ma period, from the geological record preserved in the Lushs Bight Group, one can invoke with some confidence the beginning and early evolution of the supra-subduction zone and emergence of a nascent island arc. An intraoceanic setting, probably removed from any input of a continent, is assumed for the arc and subduction zone. Polarity of this subduction zone and the geometry of an arc with respect to the continental margins that bounded that oceanic realm remains unknown.

By the end of the pre-500 Ma period, a different tectonic setting was superimposed upon the early arc. The depleted arc tholeiites are interleaved with lavas of non-arc, MORB affinity and IAT-like flows (Skeleton Pond Formation) typically found in young back-arc basins. This change in the tectonic environment is probably best evidenced in the geological record preserved in the Stag Formation, where crude breccia was formed consisting of angular blocks of lithological/geochemical types common for the Lushs Bight Group prior to the eruption of first non-arc lavas. Formation of that breccia was associated with ongoing, but diminishing and eventually ceasing, depleted arc volcanism, and was probably derived by block faulting of the "Lushs Bight" arc related to the rifting event.

If the Stag Formation can be used as a model section, then the early stages of volcanism associated with the incipient back-arc built upon the faulted arc basement were tapping almost pristine E-MORB like source, but at once giving a way to arc-like island arc tholeiites only slightly different (less depleted in trace elements) from those erupting in the pre-existing arc. The interleaving of non-arc and arc lavas provides evidence that the presence of non-arc lavas does not reflect an entirely new tectonic setting, but normal evolution expected of the regions overlying a subduction zone and formation of a back-arc basin.

Apparently not everywhere in this back-arc setting first non-arc lavas were as enriched as in the case of the "Stag" segment of the spreading ridge, and the lowermost

non-arc flows at the base of the Western Arm Group were almost identical with N-MORB. Following the record preserved in the Skeleton Pond Formation, it is evident that arc-like volcanism within the basin persisted for some period of time resulting in IAT-like lavas, like those commonly erupting from spreading ridges of young modern back-arc basins like the Lau Basin or Mariana Trough. Eventually, as manifested by rocks of the Big Hill Basalt, the more non-arc volcanism prevailed, but some enrichment of these non-arc lavas in Th and LREE suggests addition of a slab component and/or contamination by arc crust, leading to formation of lavas with transitional arc/non-arc characteristics. At that stage, the non-arc and transitional lavas were more typical of basins evolved near or on continental margins, such as Sea of Japan or Baja California and associated with mantle plumes.

7.3.2 FIRST DEFORMATION EVENT

Pillow lavas of the Lushs Bight Group show effects of deformation that is not or is poorly recorded in the rocks of the lower part of the Western Arm Group. This deformation is evinced in the presence of locally extensive high strain chloritic shear zones developed within and subparallel to bedding of pillow lavas of the Lushs Bight, implying that the first deformation was associated with the thrusting. It is possible that this deformational event coincided with the block faulting and rifting postulated for the onset of the back-arc formation. Alternatively, since the cleavage defined mainly by chlorite is also present, but not widespread in rocks of the Western Arm Group, it is possible that extensive seafloor alteration of the Lushs Bight Group pillow lavas made them much more prone to the deformation that otherwise involved rocks of both groups. The timing of this deformation is constrained by the age of ~500 Ma of high-Mg dykes that intrude rocks of both of these groups. Field observations suggesting that some of these dykes are probably late-kinematic supports deformational event that postdates back-arc stage and the deposition of non-arc rocks and of the Western Arm Group.

7.3.3 INTRUSION OF HIGH-MG DYKES

Intrusion of high-Mg dykes into strongly depleted arc rocks of the Lushs Bight and non-arc and IAT lavas of the Western Arm Group mark yet another stage in the tectonic development of the western Notre Dame Bay area. All models for intrusion of such

dykes involve tectonic (preferably extensional) setting which will let a very hot magma, probably from an asthenospheric source, to erupt in an otherwise convergent environment. Intrusions of such unusual dykes are locally linked to various tectonic events in an arc evolution, which in the two best studied settings were identified as initial stages of back-arc opening (Japan), and the termination of subduction resulting from a ridge-trench collision (Baja California). Taking under the consideration that at the time of the dykes intrusion, the back-arc basin was already well established and well beyond the initial stage, the Baja California model may be considered here, but since it is not unique, some modifications may be required

The high-Mg dykes in the western Notre Dame Bay are typified by geochemistry that indicates contamination of their magmas by a continental component. This component was not identified before, at least not very convincingly, in lavas of the Lushs Bight and Western Arm Groups. By piecing together this aspect of the dykes geochemistry with their possible late-kinematic emplacement, the arc - Laurentian continent collision and probable termination of subduction is invoked here for the "Lushs Bight" arc/"Western Arm" back-arc pair. Although there are few constraints on a polarity of subduction until approximately 500 Ma, the "Lushs Bight" arc must have been separated from the continent by at least a spreading ridge (of the "Western Arm" back-arc"?) not allowing a continental component into source regions of the arc magmas. Such geometry favours subduction beneath the continental lithosphere. Clearly, by ~500 Ma ophiolitic rocks of the Lushs Bight Group were emplaced upon the continental crust, as evinced by presence of the "crustal" signature in high-Mg dykes.

7.3.4 DEPOSITION IN THE INTERVAL 485-465 Ma

Intrusion of ~500 Ma old high-Mg dykes marks also a beginning of the era, ~10-20 Ma long, from which there is no or little stratigraphic record preserved in the study area until about 485 Ma. The post-485 Ma period in the evolution of the western Notre Dame Bay was characterized by predominantly calc-alkalic volcanism, including voluminous felsic products that include ignimbrites (but locally also mafic pillow lava) which are typical of the Welsh Cove Formation. The felsic rocks show evidence for contamination by continental crust implying that the tectonic environment of their

formation was in close spatial association with the continent. On the other hand, field observations suggest that volcanism was almost exclusively submarine and there is no evidence for subaerial volcanism in the area. This precludes the possibility of an Andean-type subduction zone and for the evolution of the upper Western Arm Group in a continental arc setting. Numerous mafic sills and dykes of non-arc and transitional arc/non-arc affinity intrude solely the Welsh Cove Formation and the Pigeon Head Formation of the Cutwell Group, and are not found in units underlying or overlying these two. An intimate association of the sills with these two units implies that both are coeval, and that perhaps the sills (of non-arc to transitional affinity) and large amounts of felsic volcanic rocks (crustal melts?) are related to an (aborted?) rifting attempt. This event is followed by arc-like volcanism in the rocks of the Western Head Formation and units of the Cutwell Group overlying the Pigeon Head Formation. Based on isotopic and faunal constraints it appears that this period of volcanism continued and achieved its maximum at ~465 Ma resulting in voluminous felsic rocks of the Seal Cove Complex and contemporary magmatism reflected in intrusion of the Colchester-Coopers Cove pluton. It is not known if the magmatic activity during this period was associated at all with ongoing subduction, and if there was subduction we do not know what the geometry of it would be. Geochemical data and inherited zircon of Archean age found in the felsic tuff of the Cutwell Group (G.Dunning, pers.com.) indicate that close spatial association of the Western Arm/Cutwell tectonic environment with the continental crust/lithosphere continued throughout this period. It is quite possible, however, that the last pulse of pre-Silurian magmatism recorded in the western Notre Dame Bay area (Seal Cove Complex and Colchester-Coopers Cove intrusion) was associated with a major collisional event. There is evidence to suggest that emplacement of the Colchester-Coopers Cove intrusion was syn- to late-kinematic and coeval with the initial structural collapse of the Buchans-Roberts Arm Volcanic Belt in the footwall of the Hungry Mountain Complex.

Various stages of tectonic evolution of the western Notre Dame Bay area can be recognized in and compared to several modern tectonic environments including the Sea of Japan (rifting of old continental arc, formation of a marginal basin upon foundering fragments of thinned continental crust and ongoing active arc volcanism), Baja California

(ridge-trench collision and resulting emplacement of bajaites, followed by arc-like post-subduction volcanism, and rifting leading to formation of a marginal basin), or Papua New Guinea. In the latter, where there is an apparently "intraoceanic" setting, remote from the continent setting, arc-continent collision is driving slivers of continental crust into structural interleaving with ophiolitic and arc rocks, resulting in a geochemical imprint of post-subduction volcanism.

7.3.5 BETWEEN 465 Ma AND SILURIAN

The second period for which there is no geological record in the western Notre Dame Bay, took place after volcanism ceased in late Llanvirn/early Llandeilo, and ended with the early Silurian (lower Llandovery) magmatic event represented by the intrusion of the earliest phase of the episodic Silurian plutonism and volcanism of the Topsail Igneous Complex and the Springdale Group. The earliest components of this event have calc-alkaline, continental arc geochemical signatures, but an active subduction zone need not be invoked to explain this.

7.3.6 SILURIAN DEPOSITION

Volcanic and volcanoclastic rocks of Silurian age were deposited in the Springdale area and thought to be erupted in a large epicontinental-type caldera (Coyle and Strong, 1987; Coyle, 1990). The U-Pb zircon ages presented by various workers indicated that the group evolved from 432.4 ± 1.7 - 1.4 Ma to 425 ± 3 Ma (Chandler et al., 1987; Whalen et al., 1987; Coyle, 1990). Volcanic rocks of the Springdale are overlain by the red bed sequence, the later of which is considered to represent "caldera fill".

7.3.7 NAPPE EMPLACEMENT

The post-lower Silurian major regional event was manifested by the emplacement of an alpine style nappe consisting of the Cambrian-Ordovician rocks (Lushs Bight and Western Arm Groups) upon the Lower Silurian Springdale Group and the underlying Lower Ordovician Robert's Arm Group, and possibly the Stag Formation/Cutwell Group assemblage. Sedimentary red beds of post-Lower Silurian age that overlie both the Springdale and Robert's Arm groups mark the sole thrust fault to the nappe throughout the study area, the Lobster Cove Fault, and are interpreted to be dynamically related to

the nappe, having been deposited in the foreland basin forming in front of the advancing nappe. A large scale imbrication took place during this event, both within the nappe and underlying rocks of the Springdale Group, and most of the major, NE striking and southeasterly verging thrust faults were generated at this time. The D3 deformation is primarily responsible for the present distribution of lithostratigraphic and structural units within the Notre Dame Bay area.

7.3.8 POST-EMPLACEMENT DEFORMATION

The post-emplacment deformation is reflected best in folding and rotation of the sole thrust to the nappe, the Lobster Cove Fault, which is subhorizontal in the Springdale area, nearly north-dipping and vertical on Sunday Cove Island, and overturned and south dipping on Pilley's Island and Triton Island.

Post-emplacment deformation produced within the nappe and in its immediate footwall, a northwest verging, NE-SW trending fold and thrust belt, that is manifested mainly by high-angle reverse faults. The main structures in the western part of the Notre Dame Bay are hinterland-dipping duplexes, such as map scale duplex within units of the Western Arm Group in the Western Arm area. Rocks of the Lushs Bight Group are thrust over the red beds of the probable Carboniferous age in the King's Point area. As a result of the thrusting, red beds are folded and possibly provide the lower bracket for the age of the D5 event..

7.4 Conclusions And Recommendations

This study has highlighted the structural, tectonic and geochemical complexity within the Western Notre Dame Bay area, and there remain a number of outstanding problems which could be addressed by further dating, structural and isotopic studies. The latter would be particularly useful in addressing the full role that continental contamination has played in the petrogenesis of the medium - and high-K calc-alkalic rocks. Nonetheless, significant breakthroughs have been made in understanding the evolution of this area, and many of these have far broader tectonic and geologic implications than have been addressed in this thesis.

In a regional context, one of the most important results of this thesis has been the recognition of a pre-500 Ma intraoceanic terrane which was deformed and emplaced upon

continental lithosphere by ~495 Ma. The occurrence of the sanukitoid/bajaite dykes at 495 Ma with a geochemical signature showing strong interaction with continental material, implies that oceanic arc - Laurentian continental collision (Taconic Orogeny?) and ophiolite obduction (?) took place earlier in the Notre Dame Subzone, then had previously been suggested/implied. The subsequent history of volcanism in the area, while appearing to be consistent with an "intraoceanic" setting, also shows evidence of a strong continental influence. Together, with data from inheritance observed in U/Pb geochronology studies and Nd isotopic studies, the picture which is emerging for the late Ordovician evolution of the Notre Dame Subzone is one of either a continental margin arc or construction of arcs on foundered continental lithosphere. Either way the Laurentian continent is very close by and making its presence felt in the petrogenesis of the volcanics and their ore deposits.

The recognition of the Notre Dame Bay Nappe is another major finding from this thesis. Post-lower Silurian nappe emplacement and synchronous imbrication of the nappe into a southeasterly verging and propagating fold and thrust belt, and subsequent post-lower Carboniferous overprinting by northwesterly directed high-angle reverse faulting and imbrication make it very difficult to reconstruct the original stratigraphic order in this area. Recognition of the nappe provides a reasonable explanation for the often noted similarity in lithology, fauna, ages and geochemistry seen between the Cutwell and Robert's Arm groups, i.e. the Cutwell Group is exposed in a tectonic window from beneath the overlying Notre Dame Bay Nappe.

This thesis demonstrates the value of doing regional geological studies in which use is made of a wide variety of tools. The structural studies are crucial for understanding the distribution and relationship between rock units, and place stringent constraints on interpretation of geochemical and other data (for example, paleomagnetic studies). The geochronologic data are crucial for establishing not only the stratigraphic record, but also the history of deformation and thermal events. The geochemical data can help in establishing relationships between units, evaluating between different paleotectonic settings, and indicating when major changes in sources have occurred. The process by which the breakthroughs presented in this thesis were made, was largely an iterative (and time

consuming!) one, during which data from structural, geochronological and geochemical methods were continually used to test and constrain the development of models.

REFERENCES

- Agar, S.M. (1988). Shearing of partially consolidated sediment in a lower trench slope setting, Shimanto Belt, SW Japan. *Journal of Structural Geology*, v.10, No.1, pp.21-32.
- Al, T.A. (1990). The character and setting of gold mineralization associated with the Betts Cove Complex. M.Sc. thesis, Memorial University, 151p.
- Allan, F.J. and Gorton, M.P. (1992). Geochemistry of igneous rocks from legs 127 and 128, Sea of Japan. *in* Tamaki, K., Suyehiro, K., Allan, J., McWilliams, et al., *Proceedings of the Ocean Drilling Program, Scientific Results*, v.127/128, pp.905-929.
- Allegre, C.J. and Lewin, E. (1989). Chemical structure and history of the Earth: evidence from global non-linear inversion of isotopic data in a three-box model. *Earth and Planetary Science Letters*, v.96, pp.61-88.
- Allegre, C.J. and Minster, J.F. (1978). Quantitative models of trace element behaviour in magmatic processes. *Earth and Planetary Science Letters*, v.38, pp.1-25.
- Anderson, A.T., Jr. (1980). Significance of hornblende in calc-alkaline andesites and basalts. *American Mineralogist*, v.65, pp.837-851.
- Arculus, R.J. (1976). Geology and geochemistry of the alkali basalt-andesite association of Grenada, Lesser Antilles island arc. *Geological Society of America Bulletin*, v.87, pp.612-624.
- Arculus, R.J. and Johnson, R.W. (1981). Island arc magma sources: a geochemical assessment of the roles of slab-derived components and crustal contamination. *Geochemical Journal*, v.15, pp.109-133.
- Arculus, R.J. and Powell, R. (1986). Source component mixing in the regions of arc magma generation. *Journal of Geophysical Research*, v.91, pp.5913-5926.

- Arculus, R.J. and Wills, K.J.A. (1980). The petrology of plutonic blocks and inclusions from the Lesser Antilles island arc. *Journal of Petrology*, v. 21, pp. 743-799
- Arnott, R.J., McKerrow, W.S. and Cocks, L.R.M. (1985). The tectonics and depositional history of the Ordovician and Silurian rocks of Notre Dame Bay, Newfoundland. *Canadian Journal of Earth Sciences*, v. 22, pp. 607-618.
- Arth, J.G. (1979). Some trace elements in trondhjemites - their implications to magma genesis and paleotectonic setting. *in* *Trondhjemites, dacites, and related rocks*, edited by F. Barker, Elsevier, New York, pp. 123-132.
- Ballantyne P. (1991). Petrological constraints upon the provenance and genesis of the East Halmahera Ophiolite. *Journal of Southeast Asian Earth Sciences*, v. 6, pp. 259-269.
- Barnes, C.R., Norford, B.S., and Skevington, D. (1981). The Ordovician system in Canada: correlation chart and explanatory notes. *International Union of Geological Sciences, Publication No. 8*, 27p.
- Barsdell, M. and Berry, R.F. (1990). Origin and evolution of primitive island arc ankaramites from Western Epi, Vanuatu. *Journal of Petrology*, v. 31, pp. 747-777
- Basaltic Volcanism Study Project (1981). *Basaltic volcanism on the terrestrial planets*. New York: Pergamon Press, 1286p.
- Bates, R.L. and Jackson, J.A. (1980). *Glossary of Geology*, Second edition, American Geological Institute, Falls Church, Virginia, 751p.
- Bau, M. (1991). Rare elements mobility during hydrothermal and metamorphic fluid-rock interaction and the significance of the oxidation state of europium. *Chemical Geology*, v. 93, pp. 219-230.
- Beccaluva, L. and Serri, G. (1988). Boninitic and low-Ti subduction-related lavas from intraoceanic arc-backarc systems and low-Ti ophiolites: a reappraisal of their petrogenesis and original tectonic setting. *Tectonophysics*, v. 146, pp. 291-315

- Beccaluva, L., Bonatti, E., Dupuy, C., Ferrara, G., Innocenti, F., Lucchini, F., Macera, P., Petrini, R., Rossi, P.L., Serri, G., Seyler, M. and Siena, F. (1990).
Geochemistry and mineralogy of volcanic rocks from ODP sites 650, 651, 655,
and 654 in the Tyrrhenian Sea. *in* Kastens, K.A., Mascle, J., et al. (1990).
Proceedings of the Ocean Drilling Program, Scientific Results, v.107, pp.49-72.
- Bender, J.F., Langmuir, C.H. and Hanson, G.N. (1984). Petrogenesis of basalt glasses
from the Tamayo Region, East Pacific Rise. *Journal of Petrology*, v.25,
pp.213-254.
- Bergstrom, S.M., Riva, J. and Kay, K. (1974). Significance of conodonts, graptolites
and shelly faunas from the Ordovician of western and north-central Newfoundland.
Canadian Journal of Earth Sciences, v.11, pp.1625-1660.
- Berry, W.B.N. and Boucot, A.J. (1970). Correlation of the North American Silurian
rocks. Geological Society of America, Special Paper 102, 289p.
- Best, M.G. (1982). *Igneous and metamorphic petrology*. W.H. Freeman and Company,
New York, 630p.
- Bienvenu, P., Bougault, H., Joron, J.L., Treuil, M. and Dmitriev, L. (1990). MORB
alteration: Rare-earth element/non-rare-earth hygromagmaphile element
fractionation. *Chemical Geology*, v.82, pp.1-14.
- Bird, J.M. and Dewey, J.F. (1970). Lithosphere plate - continental marginal tectonics
and the evolution of the Appalachian Orogen. *Geological Society of America
Bulletin*, v.81, pp.1031-1060.
- Blackwood, R.F. (1985). *Geology of the Facheux Bay map area (11P/9), Newfoundland*.
Newfoundland Department of Mines and Energy, Mineral Development Division,
Report 85-4, 56 p.
- Blewett, R.S. (1989). The chronology and kinematics of deformation in the Lower
Paleozoic of north-central Newfoundland. Ph.D. thesis, University of Leicester.

- Bloomer, S.H. and Hawkins, J.W. (1987). Petrology and geochemistry of boninite series volcanic rocks from the Mariana trench. *Contributions to Mineralogy and Petrology*, v.97, pp.361-377.
- Bloomer, S.H., Stern, R.J., Fisk, E. and Geschwind, C.H. (1989). Shoshonitic volcanism in the Northern Mariana Arc I. Mineralogic and major and trace element characteristics. *Journal of Geophysical Research*, v.94, pp.4469-4496.
- Borradaile, G.J. (1982). Tectonically deformed pillow lava as an indicator of bedding and way-up. *Journal of Structural Geology*, v.4, pp.469-479.
- Borradaile, G.J. and Poulsen, K.H. (1981). Tectonic deformation of pillow lava. *Tectonophysics*, v.79, pp.17-26.
- Bostock, H.H. (1988). Geology and petrochemistry of the Ordovician volcano-plutonic Robert's Arm Group, Notre Dame Bay, Newfoundland. *Geological Survey of Canada, Bulletin 369*, 84p.
- Boucot, A.J. (1973). The Lower Ordovician brachiopod *Syntrophia* sp., cf. *S. arethusa* (Billings 1862) from South Catcher Pond, Northeastern Newfoundland. *Canadian Journal of Earth Sciences*, v.10, pp.427-430.
- Boyer, S.E. and Elliot, D. (1982). Thrust systems. *American Association of Petroleum Geologists Bulletin*, v.66, pp.1196-1230.
- Briqueu, L., Bougault, H. and Joron, J.L. (1984). Quantification of Nb, Ta, Ti and V anomalies in magmas associated with subduction zones: petrogenetic implications. *Earth and Planetary Science Letters*, v.68, pp.287-308.
- Brophy, J.G. and Marsh, B.D. (1986). On the origin of hi-alumina arc basalts and the mechanics of melt extraction. *Journal of Petrology*, v.27, pp.763-790.
- Brown, A.V. and Jenner, G.A. (1991). Geological setting, petrology and chemistry of Cambrian boninite and low-Ti tholeiite lavas in western Tasmania. // *Boninites*, edited by A.J. Crawford, Unwin Hyman, London, pp.233-263.

- Brown, L., Klein, J., Middleton, R., Sacks, I.S. and Tera, F. (1982). ^{10}Be in island-arc volcanoes and implications for subduction. *Nature*, v.299, pp.718-720.
- Busby-Spera, C.J. (1988). Evolution of a Middle Jurassic back-arc basin, Cedros Island, Baja California: evidence from a marine volcanoclastic apron. *Geological Society of America Bulletin*, v.100, pp.218-233.
- Calon, T.J. and Green, F.K. (1987). Preliminary results of a detailed structural analysis of Buchans Mine area. *in* Kirkham, R.V. (editor), *Buchans Geology, Newfoundland; Geological Survey of Canada, Paper 86-24*, pp.273-288.
- Calon, T.J. and Szybinski, Z.A. (1988). Lobster Cove Fault: dextral strike slip fault system. *in* Program with Abstracts, Joint Annual Meeting GAC, MAC, CSPG, p.A17.
- Cameron, W.E., Nisbet, E.G. and Dietrich, V.J. (1979). Boninites, komatiites and ophiolitic basalts. *Nature*, v.280, pp.550-553.
- Casey, J.F. and Kidd, W.S.F. (1981). A parallochthonous group of sedimentary rocks unconformably overlying the Bay of Islands ophiolite complex, North Arm Mountain, Newfoundland. *Canadian Journal of Earth Sciences*, v.18, pp.1035-1050.
- Cawood, P.A. and van Gool, J.A.M. (1993). Stratigraphic and structural relations within the western Dunnage Zone, Glover Island region, western Newfoundland. *in* *Current Research, Part D, Geological Survey of Canada, Paper 93-1D*, pp.29-37
- Cawthorn, R.G., Curran, E.B. and Arculus, R.J. (1973). A petrogenetic model for origin of the calc-alkaline suite of Grenada, Lesser Antilles. *Journal of Petrology*, v.14, pp.327-337.
- Cawthorn, R.G. and O'Hara, M.J. (1976). Amphibole fractionation in calc - alkaline magma genesis. *American Journal of Science*, v.276, pp.309-329.

- Chandler, F.W., Sullivan, R.W. and Currie, K.L., 1987. The age of the Springdale Group, western Newfoundland, and correlative rocks - evidence for a Llandoverly overlap assemblage in the Canadian Appalachians. *Transactions of Royal Society of Edinburgh: Earth Sciences*, 78: 17-28.
- Church, W.R. (1965). Structural evolution of northeast Newfoundland - comparison with that of the British Caledonides. *Maritime Sediments*, v.1, pp.10-14.
- Church, W.R. and Stevens, R.K. (1971). Early Palaeozoic ophiolite complexes of the Newfoundland Appalachians as mantle-oceanic crust sequences. *Journal of Geophysical Research*, v.76, pp.1460-1466.
- Clague, D.A. (1987). Hawaiian xenolith populations, magma supply rates, and development of magma chambers. *Bulletin of Volcanology*, v.49, pp.577-587
- Coish, R.A. (1977). Ocean floor metamorphism in the Betts Cove Ophiolite, Newfoundland. *Contributions to Mineralogy and Petrology*, v.60, pp.255-270.
- Coish, R.A., Hickey, R. and Frey, F.A. (1982). Rare earth element geochemistry of the Betts Cove ophiolite, Newfoundland: complexities in ophiolite formation. *Geochimica et Cosmochimica Acta*, v.46, pp.2117-2134.
- Colman-Sadd, S.P. (1980). Geology of south-central Newfoundland and evolution of the eastern margin of Iapetus. *American Journal of Science*, v.280, pp.991-1017.
- Colman-Sadd, S.P. and Swinden, H.S. (1982). Geology and mineral potential of south-central Newfoundland. Newfoundland Department of Mines and Energy, Mineral Development Division, Report 82-8, 102p.
- Colman-Sadd, S.P. and Swinden, H.S. (1984). A tectonic window in Central Newfoundland? Geological evidence that the Appalachian Dunnage Zone may be allochthonous. *Canadian Journal of Earth Sciences*, v.21, pp.1349-1367

- Colman-Sadd, S.P., Dunning, G.R., and Dec, T. (1992). Dunnage-Gander relationships and Ordovician orogeny in central Newfoundland: a sediment provenance and U/Pb age study. *American Journal of Science*, v.292, pp.317-355.
- Colman-Sadd, S.P., Stone, P., Swinden, H.S. and Barnes, R.P. (1992). Parallel geological development in the Dunnage Zone of Newfoundland and the Lower Paleozoic terranes of southern Scotland: an assesment. *Transactions of the Royal Society of Edinburgh: Earth Sciences*, v.83, pp.571-594.
- Conrad, W.K. and Kay, R.W. (1984). Ultramafic and mafic inclusions from Adak Island: Crystallization history, and implications for the nature of primary magmas and crustal evolution in the Aleutian Arc. *Journal of Petrology*, v.25, pp.88-125.
- Cooper, R.A. (1992). A relative timescale for the Early Ordovician derived from depositional rates of graptolite shales. *in* Webby, B.D. and Laurie, J.R., *Global Perspectives on Ordovician Geology, Proceedings of the Sixth International Symposium on the Ordovician System*, pp.3-21.
- Coulon, C. and Thorpe, R.S. (1981). Role of continental crust in petrogenesis of orogenic volcanic associations. *Tectonophysics*, v.77, pp.79-93.
- Cox, K.G. (1980). A model for flood basalt vulcanism. *Journal of Petrology*, v.21, pp.629-650.
- Cox, K.G., Bell, J.D. and Pankhurst, R.J. (1979). *The interpretation of igneous rocks*. Allen & Unwin, London, 450pp.
- Coyle, M.L., 1990. *Geology, geochemistry and geochronology of the Springdale Group, an early Silurian caldera in central Newfoundland*. Unpubl. PhD thesis, Memorial University of Newfoundland, 282pp.
- Coyle, M.L. and Strong, D.F. (1986a). *Geology of the southern and northern margins of the Springdale Caldera, Newfoundland*. Geological Survey of Canada, Current Research, Part A, Paper 86-1A, pp.499-506.

- Coyle, M.L. and Strong, D.F. (1986b). The Springdale Caldera. A field guide for the Annual Field Meeting of the Geological Association of Canada, Newfoundland Branch, 21p.
- Coyle, M.L. and Strong, D.F. (1987). Geology of the Springdale Group: a newly recognized Silurian epicontinental-type caldera in Newfoundland. Canadian Journal of Earth Sciences, v.24, pp.1135-1148.
- Crawford, A.J., Beccaluva, L., Serri, G. and Dostal, J. (1986). Petrology, geochemistry and tectonic implications of volcanics dredged from the intersection of the Yap and Mariana trenches. Earth and Planetary Science Letters, v.80, pp.265-280.
- Crawford, A.J., Faloon, T.J and Eggins, S. (1987). The origin of island-arc high-alumina basalts. Contributions to Mineralogy and Petrology, v.97, pp.417-430.
- Crawford, A.J., Faloon, T.J and Green, D.H. (1989). Classification, petrogenesis and tectonic setting of boninites. // Boninites and related rocks, edited by A J. Crawford, Unwin Hyman, London, pp.1-49.
- Dallmeyer, R.D. and Williams, H. (1975). $^{40}\text{Ar}/^{39}\text{Ar}$ ages for the Bay of Islands metamorphic aureole: their bearing on the timing of Ordovician ophiolite obduction. Canadian Journal of Earth Sciences, v.12, pp.1685-1690.
- Davidson, J.P. (1986). Isotopic and trace element constraints on the petrogenesis of subduction-related lavas from Martinique, Lesser Antilles. Journal of Geophysical Research, v.91, pp.5943-5962.
- Davidson, J.P., Dungan, M.A., Ferguson, K.M. and Colucci, M.T. (1987). Crust-magma interactions and the evolution of arc magmas: the San Pedro - Pellado volcanic complex, southern Chilean Andes. Geology, v.15, pp.443-446.
- Dean, P.L. (1977). A report on the geology and metallogeny of the Notre Dame Bay area. Newfoundland Department of Mines and Energy, Open File Report 77-10, 17 p.

- Dean, P.L. (1978) The volcanogenic stratigraphy and metallogeny of Notre Dame Bay, Newfoundland. Memorial University of Newfoundland, Geology Report 7, 205 p.
- Dean, P.L. and Strong, D.F. (1977). Folded thrust folds in Notre Dame Bay, central Newfoundland. American Journal of Science, v.277, pp.97-108.
- Dean, W.T. (1970) Lower Ordovician trilobites from the vicinity of South Catcher Pond, northeastern Newfoundland. Geological Survey of Canada, Paper 70-44, 15p
- Dec, T. and Colman-Sadd, S. (1990) Timing of ophiolite emplacement onto the Gander Zone: evidence from provenance studies in the Mount Cormack Subzone. *in* Current Research, Newfoundland Department of Mines and Energy, Geological Survey Branch, Report 90-1, pp.289-303.
- Dec, T. and Swinden, H.S. (1994). Lithostratigraphic model, geochemistry and sedimentology of the Cottrells Cove Group, Buchans-Roberts Arm Volcanic Belt, Notre Dame Subzone. *in* Current Research, Newfoundland Department of Mines and Energy, Geological Survey Branch, Report 94-1, pp.77-100.
- Dec, T., Swinden, H.S. and Dunning, G.R. (in press). Sedimentology, geochemistry and stratigraphy of the Cottrells Cove Group (Buchans-Roberts Arm Belt), eastern Notre Dame Bay, Newfoundland Appalachians.
- Defant, M.J., Maury, R.C., Ripley, E.M., Feigenson, M.D., and Jacques, D. (1991). An example of island-arc petrogenesis: geochemistry and petrology of the southern Luzon Arc, Philippines. Journal of Petrology, v.32, pp.455-500.
- Defant, M.J., Richerson, P.M., De Boer, J.Z., Stewart, R.H., Maury, R.C., Bellon, H., Drummond, M.S., Feigenson, M.D. and Jackson, T.E. (1991). Dacite genesis via both slab melting and differentiation: petrogenesis of La Yeguada Volcanic Complex, Panama. Journal of Petrology, v.32, pp.1101-1142.

- DeGrace, J.R. (1971). Structural and stratigraphic setting of sulphide deposits in Ordovician volcanics south of King's Point, Newfoundland. M.Sc. thesis, Memorial University.
- DeGrace, J.R., Kean, B.F., Hsu, E. and Green, T. (1976). Geology of the Nippers Harbour map area (2E/13), Newfoundland. Newfoundland Department of Mines and Energy, Mineral Development Division Report 76-3, 73 p.
- DeLong, S.E., Hodges, F.N. and Arculus, R.J. (1975). Ultramafic and mafic inclusions, Kanaga Island, Alaska, and the occurrence of alkaline rocks in island arcs. *Journal of Geology*, v.83, pp.721-736.
- DePaolo, D.J. (1981). Trace element and isotopic effects of combined wallrock assimilation and fractional crystallisation. *Earth and Planetary Science Letters*, v.53, pp.189-202.
- Dewey, J.F. and Bird, J. (1971). Origin and emplacement of the ophiolite suite Appalachian ophiolites in Newfoundland. *Journal of Geophysical Research*, v.76, pp.3179-3206.
- Dewey, J.F., Hempton, M.R., Kidd, W.S.F., Saroglu, F. and Sengor, A.M.C. (1986). In Coward, M.P. and Ries, A.C., *Collision Tectonics*, Geological Society Special Publication, No. 19, pp.3-36.
- De Wit, M.J., Hart, R. A. and Hart, R.J. (1987). The Jamestown Ophiolite Complex, Barberton mountain belt: a section through 3.5 Ga oceanic crust. *Journal of African Earth Science*, v.6, pp.681-730.
- Donohoe, H.V.Jr. (1968). The structure and stratigraphy of the Halls Bay Head area, Notre Dame Bay, Newfoundland. Final Report for British Newfoundland Exploration and Department of Geological Sciences, Lehigh University, 84p.
- Dostal, J. (1989). Geochemistry of Ordovician volcanic rocks of the Tetagouche Group of southwestern New Brunswick. *Atlantic Geology*, v.25, pp.199-209.

- Dube, B., Lauziere, K., and Gaboury, D. (1992). Preliminary report on the structural control of the Rendell-Jackaman gold deposit, Springdale Peninsula, Newfoundland. *in* Current Research, Geological Survey of Canada, Paper 92-1D, pp. 1-10.
- Duncan, A.R. (1987). The Karoo Igneous Province - a problem area for inferring tectonic setting from basalt geochemistry. *Journal of Volcanology and Geothermal Research*, v.32, pp.13-34.
- Dunning, G.R. (1987). Geology of the Annieopsquotch Complex, southwest Newfoundland. *Canadian Journal of Earth Sciences*, v.24, pp.1162-1174.
- Dunning, G.R. and Chorlton, L.B. (1985). The Annieopsquotch ophiolite belt of southwest Newfoundland: geology and tectonic significance. *Geological Society of America Bulletin*, v.96, pp.1466-1476.
- Dunning, G.R., Kean, B.F., Thurlow, J.G. and Swinden, H.S. (1987). Geochronology of the Buchans, Roberts Arm and Victoria Lake Groups and Mansfield Cove Complex, Newfoundland. *Canadian Journal of Earth Sciences*, v.24, pp.1175-1184.
- Dunning, G.R. and Krogh, T.E. (1985). Geochronology of ophiolites of the Newfoundland Appalachians. *Canadian Journal of Earth Sciences*, v.22, pp.1659-1670.
- Dunning, G.R. and Krogh, T.E. (1989). Stratigraphic correlation of the Appalachian Ordovician using advanced U-Pb zircon geochronology techniques. *in* Advances in Ordovician Geology, edited by C.R. Barnes and S.H. Williams, Geological Survey of Canada, Paper 90-9, pp.85-92.
- Dunning, G.R. and Krogh, T.E. (1988). Advanced techniques in U/Pb zircon geochronology applied to stratigraphic correlation: examples from the Ordovician of the Appalachians. *in* Program and Abstracts, Fifth International Symposium on the Ordovician System, p.68.

- Dunning, G.R. and Krogh, T.E. (1991). Stratigraphic correlation of the Appalachian Ordovician using advanced U-Pb zircon geochronology techniques. *in* Barnes, C.R. and Williams, S.H. (editors), Geological Survey of Canada, Paper 90-9, p.85-92.
- Dunning, G.R., Krogh, T.E., Kean, B.F., O'Brien, S.J. and Swinden, H.S. (1986) U/Pb zircon ages of volcanic groups from the Central Mobile Belt, Newfoundland (Abstract). Geological Association of Canada, Programs with Abstracts, v.11, p 66.
- Dunning, G.R., O'Brien, S.J., Colman-Sadd, S.P., Blackwood, R.F., Dickson, W.L., O'Neill, P.P., and Krogh, T.E. (1990). Silurian orogeny in the Newfoundland Appalachians. *Journal of Geology*, v.98, pp.895-913.
- Dunning, G.R., Swinden, H.S., Kean, B.F., Evans, D.T. and Jenner, G.A. (1991). A Cambrian island arc in Iapetus: geochronology and geochemistry of the Lake Ambrose volcanic belt, Newfoundland Appalachians. *Geological Magazine*, v.128, pp.1-17.
- Edwards, C., Menzies, M. and Thirlwall, M. (1991). Evidence from Muriah, Indonesia, for the interplay of supra-subduction zone and intraplate processes in the genesis of potassic alkaline magmas. *Journal of Petrology*, v.32, pp.555-592.
- Eastler, T.E. (1969). Silurian geology of Change Islands and eastern Notre Dame Bay, Newfoundland. *in* North Atlantic geology and continental drift, edited by M.Kay, American Association of Petroleum Geologists, Memoire 12, pp.425-432.
- Ellam, R.M. and Hawkesworth, C.J. (1988). Elemental and isotopic variations in subduction related basalts: evidence for a three component model. *Contributions to Mineralogy and Petrology*, v.98, pp.72-80.
- Ellam, R.M., Menzies, M.A., Hawkesworth, C.J., Leeman, W.P., Rosi, M. and Serri, G. (1988). The transition from calc-alkaline to potassic orogenic magmatism in the Aeolian Islands, Southern Italy. *Bulletin of Volcanology*, v.50, pp.386-398.

- Elliott, C G., Dunning, G R. and Williams, P. (1991). New U/Pb zircon age constraints on the timing of deformation in north-central Newfoundland and implications for early Paleozoic Appalachian orogenesis. *Geological Society of America Bulletin*, v 103, pp 125-135.
- Elliott, C G. and Williams, P.F. (1988). Sediment slump structures: a review of diagnostic criteria and application to an example from Newfoundland. *Journal of Structural Geology*, v 10, pp.171-182.
- Elthon, D. (1981). Geochemical evidence for formation of the Bay of Islands ophiolite above a subduction zone. *Nature*, v.354, pp.140-143.
- Epstein, A.G., Epstein, J.B., and Harris, L. (1977). Conodont color alteration - an index to organic metamorphism. *United States Geological Survey Professional Paper* 995, pp 1-27.
- Espenshade, G H. (1937). *Geology and mineral deposits of the Pilley's Island area*. Department of Natural Resources, Bulletin No.6, 52p.
- Evans, D T W., Kean, B.F. and Dunning, G.R. (1990). Geological studies, Victoria Lake Group, central Newfoundland. *in Current Research, Newfoundland Department of Mines and Energy, Geological Survey Branch, Report 90-1*, pp.131-144.
- Ewart, A. (1979). A review of the mineralogy and chemistry of Tertiary-Recent dacitic, latitic, rhyolitic, and related salic volcanic rocks. *in Trondhjemites, dacites, and related rocks*, edited by F.Barker, Elsevier, New York, pp.13-121.
- Ewart, A. and Hawkesworth, C.J. (1987). The Pleistocene-Recent Tonga-Kermadec arc lavas: interpretation of new isotopic and rare earth data in terms of a depleted mantle source model. *Journal of Petrology*, v.28, pp.495-530.
- Falloon, T.J. and Crawford, A.J. (1991). The petrogenesis of high-calcium boninite lavas dredged from the northern Tonga ridge. *Earth and Planetary Science Letters*, v.102, pp.375-394.

- Falloon, T.J., Green, D.H. and Crawford, A.J. (1987). Dredged igneous rocks from the northern termination of the Tofua magmatic arc, Tonga and adjacent Lau Basin. *Australian Journal of Earth Sciences*, v.34, pp.487-506.
- Falloon, T.J., Malahoff, A., Zonenshain, L.P. and Bogdanov, Y. (1992). Petrology and geochemistry of back-arc basin basalts from Lau Basin spreading ridges at 15, 18 and 19° S. *Mineralogy and Petrology*, v.47, pp 1-35.
- Ferguson, K.M., Dungan, M.A., Davidson, J.P. and Colucci, M.T. (1992) The Tatara - San Pedro Volcano, 36°S, Chile: a chemically variable, dominantly mafic magmatic system. *Journal of Petrology*, v.33, pp.1-43.
- Fisher, R.V. and Schmincke, H.-U. (1984). *Pyroclastic rocks*. Springer-Verlag, Berlin Heidelberg, 472p.
- Fleming, J.M. (1970). Petrology of the volcanic rocks of the Whalesback area, Springdale peninsula, Newfoundland. M.Sc. thesis, Memorial University.
- Foden, J.D. (1983). The petrology of the calcalkaline lavas of Rindjani volcano, East Sunda Arc: a model for island arc petrogenesis. *Journal of Petrology*, v.24, pp.98-130.
- Foden, J.D. and Green, D.H. (1992). Possible role of amphibole in the origin of andesite: some experimental and natural evidence. *Contributions to Mineralogy and Petrology*, v.109, pp.479-493.
- Foley, S.F. and Wheller, G.E. (1990). Parallels in the origin of the geochemical signatures of island arc volcanics and continental potassic igneous rocks: the role of residual titanates. *Chemical Geology*, v.85, pp.1-18.
- Francis, E.H. (1983). Magma and sediment - II; Problems of interpreting paleovolcanics buried in the stratigraphic column. *Journal of Geological Society of London*, v.140, pp.165-183.

- Fryer, P., Taylor, B., Langmuir, C.H. and Hochstaedter, A.G. (1990). Petrology and geochemistry of lavas from the Sumisu and Torishima backarc rifts. *Earth and Planetary Science Letters*, v.100, pp.161-178.
- Geological Time Table (1983). compiled by F.W.B. van Eysinga, F.W.B., 3rd edition, Elsevier Scientific Publishing Company, Amsterdam, The Netherlands.
- Gill, J.B. (1976). Composition and age of Lau Basin and Ridge volcanic rocks: implications for evolution of an interarc basin and remnant arc. *Geological Society of America Bulletin*, v.87, pp.1384-1395.
- Gill, J.B. (1981). Orogenic andesites and plate tectonics. Heidelberg, Springer - Verlag.
- Gill, J.B. (1982). Mountain building and volcanism. *in* Mountain Building Processes, edited by K.J. Hsu, Academic Press, pp.13-17.
- Gill, J.B. (1984). Sr-Pb-Nd isotopic evidence that both MORB and OIB sources contribute to oceanic island arc magmas in Fiji. *Earth and Planetary Science Letters*, v.68, pp.443-458.
- Gill, J.B. (1987). Early geochemical evolution of an oceanic island arc and backarc: Fiji and the South Fiji Basin. *Journal of Geology*, v.95, pp.589-615.
- Gill, J.B. and Stork, A.L. (1978). Miocene low-K dacites and trondhjemites of Fiji. *in* Trondhjemites, dacites and related rocks, edited by F.Barker, Elsevier, Amsterdam, pp.629-649.
- Gill, J. and Whelan, P. (1989). Early rifting of an oceanic island arc (Fiji) produced shoshonitic to tholeiitic basalts. *Journal of Geophysical Research*, v.94, pp.4561-4578.
- Gill, J. and Whelan, P. (1989). Postsubduction ocean island alkali basalts in Fiji. *Journal of Geophysical Research*, v.94, pp.4579-4588.
- Goodwin, L.B. and O'Neill, P.P., 1991: The structural evolution of the northern segment of the Dunnage Zone-Gander Zone Boundary, Newfoundland. *In* Current

- Research, Newfoundland Department of Mines and Energy, Geological Survey Branch, Report 91-1, pages 97-107.
- Green, D.H. (1969). The origin of basaltic and nephelinitic magmas in the earth's mantle *Tectonophysics*, v.7, pp.409-422.
- Green, T.H. (1980). Island arc and continent-building magmatism - a review of petrogenetic models based on experimental petrology and geochemistry. *Tectonophysics*, v.63, pp.367-385.
- Green, T.H. (1982). Anatexis of mafic crust and high pressure crystallization of andesite *in Andesites*, edited by R.S. Thorpe, Wiley, New York, pp.465-487.
- Green, T.H. and Pearson, N.J. (1986) An experimental study of Nb and Ta partitioning between Ti-rich minerals and silicate liquids at high pressure and temperature *Geochimica et Cosmochimica Acta*, v.51, pp.55-62.
- Green, T.H. and Watson, E.B. (1982). Crystallization of apatite in natural magmas under high pressure, hydrous conditions, with particular reference to "orogenic" rock series. *Contributions to Mineralogy and Petrology*, v.79, pp.96-105.
- Grenne, T. (1987). Marginal basin type metavolcanites of the Hersjo Formation, eastern Trondheim District, Central Norwegian Caledonides. *Nor. geol. unders. Bull.*, v.412, pp.29-42.
- Grenne, T. (1989). Magmatic evolution of the Lokken SSZ ophiolite, Norwegian Caledonides: relationships between anomalous lavas and high-level intrusions. *Geological Journal*, v.24, pp.251-274.
- Gromet, L.P. and Silver, L.T. (1987). REE variations across the Peninsular Ranges Batholith: implications for batholithic petrogenesis and crustal growth in magmatic arcs. *Journal of Petrology*, v.28, pp.75-125.
- Grove, T.L. and Baker, M.B. (1984). Phase equilibrium controls on the tholeiitic versus calc-alkaline differentiation trends. *Journal of Geophysical Research*, v. 89, pp.3253-3274.

- Grove, T.L. and Donnelly-Nolan, J.M. (1986). The evolution of young silicic lavas at Medicine Lak Volcano, California: Implications for the origin of compositional gaps in calc-alkaline series lavas. *Contributions to Mineralogy and Petrology*, v.92, pp.281-302.
- Gust, D.A. and Johnson, R.W. (1981). Amphibole-bearing inclusions from Boisa Island, Papua New Guinea: Evaluation of the role of fractional crystallization in an andesitic volcano. *Journal of Geology*, v.89, pp.219-232.
- Gust, D.A. and Perfit, M.R. (1987). Phase relations of a high-Mg basalt from the Aleutian Island Arc: Implications for primary island arc basalts and high-Al basalts. *Contributions to Mineralogy and Petrology*, v.97, pp.7-18.
- Harland, W.B. and Gayer, R.A. (1972). The Arctic Caledonides and earlier oceans. *Geological Magazine*, v.109, pp.289-314.
- Hanmer, S. (1981). Tectonic significance of the northeastern Gander Zone, Newfoundland: an Acadian ductile shear zone. *Canadian Journal of Earth Sciences*, v.18, pp.120-135.
- Hanmer, S. and Passchier, C. (1991). Shear-sense indicators: a review. *Geological Survey of Canada, Paper 90-17*, 72 pages.
- Hanson, G.N. (1980). Rare earth elements in petrogenetic studies of igneous rocks. *Annual Reviews of Earth and Planetary Science*, v.8, pp.371-406.
- Hawkesworth, C.J., Gallagher, K., Hergt, J.M. and McDermott, F. (1993). Trace element fractionation processes in the generation of island arc basalts. *Philosophical Transactions of Royal Society of London*, v.A342, pp.179-191.
- Hawkesworth, C.J., Hergt, J.M., Ellam, R.M. and McDermott, F. (1991a). Element fluxes associated with subduction related magmatism. *Philosophical Transactions of Royal Society of London*, v.A335, pp.393-405.

- Hawkesworth, C.J., Hergt, J.M., McDermott, F. and Ellam, R.M. (1991b). Destructive margin magmatism and the contributions from the mantle wedge and subducted crust. *Australian Journal of Earth Sciences*, v.38, pp.577-594.
- Hawkesworth, C.J., O'Nions, R.K., Pankhurst, R.J., Hamilton, P.J. and Evensen, N.M. (1977). A geochemical study of island-arc and back-arc tholeiites from the Scotia Sea. *Earth and Planetary Science Letters*, v.36, pp.253-262.
- Hawkins, J.W. and Melchior, J.T. (1985). Petrology of Mariana Trough and Lau Basin Basalts. *Journal of Geophysical Research*, v.90, pp.11,431-11,468.
- Hawkins, J.W., Lonsdale, P.F., Macdougall, J.D. and Volpe, A.M. (1990). Petrology of the axial ridge of the Mariana Trough backarc spreading center. *Earth and Planetary Science Letters*, v.100, pp.226-250.
- Haworth, R.T. and Miller, H.G. (1982). The structure of Paleozoic oceanic rocks beneath Notre Dame Bay, Newfoundland. *in* St-Julien, P. and Beland, J. (editors), Major structural zones and faults of the Northern Appalachians, Geological Association of Canada Special Paper 24, pp.149-173.
- Hekinian, R. and Walker, D. (1987). Diversity and spatial zonation of volcanic rocks from East Pacific Rise near 21°N. *Contributions to Mineralogy and Petrology*, v.96, pp.265-280.
- Hellman, P.L., Smith, R.E. and Henderson, P. (1979). The mobility of the rare earth elements: evidence and implications from selected terrains affected by burial metamorphism. *Contributions to Mineralogy and Petrology*, v.71, pp.23-44.
- Helz, R.T. (1973). Phase relations of basalts in the melting range at $P_{1120} = 5$ kb as a function of oxygen fugacity. *Journal of Petrology*, v.14, pp.249-302.
- Hess, P.C. (1989). *Origins of igneous rocks*. Harvard University Press, 336p.
- Hibbard, J. (1983). *Geology of the Baie Verte Peninsula, Newfoundland*. Department of Mines and Energy, Mineral Development Division, Memoir 2, 279p.

- Hickey, R.L. and Frey, F.A. (1982). Geochemical characteristics of boninite series volcanics: implications for their source. *Geochimica et Cosmochimica Acta*, v.46, pp.2099-2115.
- Hickey, R.L., Frey, F.A., Gerlach, D.C. (1986). Multiple sources for basaltic rocks from the southern volcanic zone of the Andes (34°-41°S): trace element and isotopic evidence for contributions from subducted oceanic mantle and continental crust. *Journal of Geophysical Research*, v.91, pp.5943-5962.
- Hildreth, W. and Moorbath, S. (1988). Crustal contributions to arc magmatism in the Andes of Central Chile. *Contributions to Mineralogy and Petrology*, v.98, pp.455-489.
- Hinton, R.W. and Upton, B.G.J. (1991). The chemistry of zircon: variations within and between large crystals from syenite and alkali basalt xenoliths. *Geochimica et Cosmochimica Acta*, v.55, pp.3287-3302.
- Hochstaedter, A.G., Gill, J.B., Kusakabe, M., Newman, S., Pringle, M., Taylor, B. and Fryer, P. (1990a). Volcanism in the Sumisu Rift, I. Major element, volatile, and stable isotope geochemistry. *Earth and Planetary Science Letters*, v.100, pp.179-194.
- Hochstaedter, A.G., Gill, J.B. and Morris, J.D. (1990b). Volcanism in the Sumisu Rift, II. Subduction and non-subduction related components. *Earth and Planetary Science Letters*, v.100, pp.195-209.
- Hofmann, A.W. (1988). Chemical differentiation of the Earth: the relationship between mantle, continental crust and oceanic crust. *Earth and Planetary Science Letters*, v.90, pp.297-314.
- Hole, M.J. (1990). Geochemical evolution of Pliocene-Recent post-subduction alkalic basalts from Seal Nunataks, Antarctic Peninsula. *Journal of Volcanology and Geothermal Research*, v.40, pp.149-167.

- Hole, M.J., Rogers, G., Saunders, A.D. and Storey, M. (1991). Relation between alkalic volcanism and slab-window formation. *Geology*, v.19, pp 657-660.
- Hole, M.J., Saunders, A.D., Marriner, G.F. and Tarney, J. (1984). Subduction of pelagic sediments: implications for the origin of Ce-anomalous basalts from the Mariana Islands. *Journal of geological Society of London*, v.141, pp 453-472.
- Horn, G.S. and Helwig, J.A. (1969). Ordovician stratigraphy of Notre Dame Bay, Newfoundland. *in* Kay, M. (editor), North Atlantic - Geology and Continental Drift, American Association of Petroleum Geologists, Memoir 12, pp 308-407.
- Humphris, S.E. and Thompson, G. (1983). Geochemistry of rare earths element in basalts from the Walvis Ridge: implications for its origin and evolution. *Earth and Planetary Science Letters*, v.66, pp.223-242.
- Humphris, S.E., Thompson, G., Schilling, J.-G. and Kingsley, R.H. (1985). Petrological and geochemical variations along the Mid-Atlantic Ridge between 46°S and 32°S: influence of the Tristan da Cunha mantle plume. *Geochimica et Cosmochimica Acta*, v.49, pp.1445-1464.
- Hussey, E.M. (1974). Geological and petrochemical data on the Brighton Complex, Notre Dame Bay, Newfoundland. B.Sc. thesis, Memorial University of Newfoundland, 66p.
- Hutton, D.H.W. (1988). Granite emplacement mechanism and tectonic controls: inferences from deformation studies. *Transactions of the Royal Society of Edinburgh, Earth Sciences*, v.79, pp.245-255.
- Hynes, A. (1980). Carbonatization and mobility of Ti, Y, and Zr in Ascot Formation metabasalts, SE Quebec. *Contributions to Mineralogy and Petrology*, v.75, pp.79-87.
- Ikeda, Y. and Yuasa, M. (1989). Volcanism in nascent back-arc basins behind the Shichito Ridge and adjacent areas in the Izu-Ogasawara arc, northwest Pacific:

evidence for mixing between E-type MORB and island arc magmas at the initiation of back-arc rifting. *Contribution to Mineralogy and Petrology*, v.101, pp.377-393.

Irvine, T.N. and Barager, W.R.A. (1971). A guide to the chemical classification of the common rocks. *Canadian Journal of Earth Science*, v.8, pp.523-548.

Irving, A.J. and Frey, F.A. (1984). Trace element abundances in megacrysts and their host basalts: constraints on partition coefficients and megacryst genesis. *Geochimica et Cosmochimica Acta*, v.48, pp.1201-1221.

James, J.E.S. (1967). Geology of the Buckshe Brook area, Springdale, Halls Bay, Nfld. B.Sc. thesis, Memorial University of Newfoundland.

Jenner, G.A. (1981). Geochemistry of high-Mg andesites from Cape Vogel, Papua New Guinea. *Chemical Geology*, v.33, pp.307-332.

Jenner, G.A., Cawood, P.A., Rautenschlein, M. and White, W.M. (1987). Composition of back-arc basin volcanics, Valu Fa Ridge, Lau Basin: evidence for a slab-derived component in their mantle source. *Journal of Volcanology and Geothermal Research*, v.32, pp.209-222.

Jenner, G.A., Dunning, G.R., Malpas, J., Brown, M. and Brace, T. (1991). Bay of Islands and Little Port complexes, revisited: age, geochemical and isotopic evidence confirm suprasubduction-zone origin. *Canadian Journal of Earth Sciences*, v.28, pp.1635-1652.

Jenner, G.A., Evans, D. and Kean, B.F. (1988). Lushs Bight Group revisited: new trace element and Sm/Nd isotopic evidence for its tectonic environment of formation (Abstract). *in* Program with Abstracts, GAC, MAC, CSPG Joint Annual Meeting, p.A61

Jenner, G.A. and Fryer, B.J. (1980). Geochemistry of the upper Snooks Arm Group basalts, Burlington Peninsula, Newfoundland: evidence against formation in an island arc. *Canadian Journal of Earth Sciences*, v.17, pp.888-900.

- Jenner, G. and Hertogen, J. (1986). Constraints on processes affecting the origin of oceanic crust: geochemical evidence from the 0-35 m.y. age basalts, between 30°N and 40°N, MAR. *Journal of Geodynamics* v.5, pp.49-78.
- Jenner, G.A., Longerich, H.P., Jackson, S.E. and Fryer, B.J. (1990). ICP-MS - a powerful tool for high-precision trace-element analysis in Earth sciences: evidence from analysis of selected U.S.G.S. reference samples. *Chemical Geology*, v.83, pp.133-148.
- Jenner, G.A. and Swinden, H.S. (1989). Trace element and isotope geochemistry of the Pipestone Pond Complex, Newfoundland: complex magmatism in an eastern Dunnage Zone ophiolite. *Geological Association of Canada, Program with Abstracts*, v. 14, p.A96.
- Jenner, G.A. and Swinden, H.S. (1993). The Pipestone Pond Complex, central Newfoundland: complex magmatism in an eastern Dunnage Zone ophiolite. *Canadian Journal of Earth Sciences*, v.30, pp.434-448.
- Jenner, G.A. and Szybinski, Z.A. (1987). Geology, geochemistry and metallogeny of the Catchers Pond Group and geochemistry of the Western Arm Group, Newfoundland. *Geological Survey of Canada, Unpublished report*, 116 p.
- Johnson, R.W. (1982). Papua New Guinea. *in: R.S. Thorpe (Editor) Andesites*. Wiley, London, pp.225-244.
- Johnson, R.W., Jaques, A.L., Hickey, R.L., McKee, C.O. and Chappell, B.W. (1985). Manam Island, Papua New Guinea: petrology and geochemistry of a low-TiO₂ basaltic island-arc volcano. *Journal of Petrology*, v.26, pp.283-323.
- Johnson, R.W., Perfit, M.R., Chappell, B.W., Jaques, A.L., Shuster, R.D., and Ridley, W.I. (1988). Volcanism in the New Ireland Basin and Manus Island region: notes on the geochemistry and petrology of some dredged volcanic rocks from a rifted-arc region. *in: M.S. Marlow, S.V. Dadisman and N.F. Exon (editors), Geology and offshore resources of Pacific island arcs - New Ireland and Manus*

region, Papua New Guinea; Circum-Pacific Council for Energy and Mineral Resources Earth Science Series, v.9, pp.113-10.

- Johnston, A. D. (1986). Anhydrous P-T phase relations of near-primary high-alumina basalt from the South Sandwich Islands: implications for the origin of island arc and the tonalite-trondhjemite series rocks. *Contribution to Mineralogy and Petrology*, v.92, pp.369-382.
- Jochum, K.-P., Seufert, H.M. and Thirlwall, M.F. (1990). High-sensitivity Nb analysis by spark-source mass spectrometry (SSMS) and calibration of XRF Nb and Zr. *Chemical Geology*, v.81, pp. 1-16.
- Kalliokoski, J. (1953). Preliminary map, Springdale, Newfoundland. Geological Survey of Canada, Paper 53-5.
- Karlstrom, K. E. (1983). Reinterpretation of Newfoundland gravity data and arguments for an allochthonous Dunnage Zone. *Geology*, v. 11, pp.263-266.
- Kay, M. (1967). Stratigraphy and structure of northeastern Newfoundland and bearing on drift in the North Atlantic. *American Association of Petroleum Geologists Bulletin*, v. 51, pp.579-600.
- Kay, R. W. (1984). Elemental abundances relevant to identification of magma sources. *Philosophical Transactions of Royal Society of London*, v.310, pp.353-547. *Contribution to Mineralogy and Petrology*, v.90, pp.276-290.
- Kay, S.M. and Kay, R. W. (1985). Aleutian tholeiitic and calc-alkaline magma series I: The mafic phenocrysts. *Contributions to Mineralogy and Petrology*, v.90, pp.276-290.
- Kay, S.M., Kay, R.W. and Citron, G.P. (1982). Tectonic controls of Aleutian tholeiitic and calc-alkaline magmatism. *Journal of Geophysical Research*, v.87, pp.4051-4072.

- Kean, B.F. (1973). Stratigraphy, Petrology and Geochemistry of Volcanic Rocks of Long Island, Newfoundland. M.Sc. thesis, Memorial University of Newfoundland, 155 p.
- Kean, B.F. (1983). Geology and mineral deposits of the Lushs Bight Group in the Little Bay Head - Halls Bay Head area. *in* Current Research, Newfoundland Department of Mines and Energy, Report 83-1, pp.157-174.
- Kean, B.F. (1984). Geology and mineral deposits of the Lushs Bight Group, Notre Dame Bay, Newfoundland. *in* Current Research, Newfoundland Department of Mines and Energy, Report 84-1, pp.141-155.
- Kean, B.F., Dean, P.L. and Strong, D.F. (1981). Regional geology of the Central Volcanic Belt of Newfoundland. *in* Swanson, E.A., Strong, D.F. and Thurlow, J.G. (editors), Geological Association of Canada Special Paper, No 22, pp.65-78
- Kean, B.F. and Evans, D.T.W. (1987a). Map 87-06: King's Point. Newfoundland Department of Mines, Open File 1987.
- Kean, B.F. and Evans, D.T.W. (1987b). Map 87-07: Little Bay Island. Newfoundland Department of Mines, Open File 1987.
- Kean, B.F. and Evans, D.T.W. (1990). Geology of the Whalesback mine *in* Metallogenic framework of base and precious metal deposits, central and western Newfoundland, edited by H.S.Swinden, D.T.W. Evans and B.F.Kean, Geological Survey of Canada Open File 2156, pp.137-140.
- Kean, B.F., Evans, D.T.W. and Jenner, G.A. (1995). Geology and mineralization of the Lushs Bight Group. *in press*, Newfoundland Department of Natural Resources, Geological Survey, Report 95-2.
- Kean, B.F. and Jayasinghe, N.R. (1980). Geology of the Lake Ambrose (12A/10) - Noel Paul's Brook (12A/9) map areas, central Newfoundland. Newfoundland Department of Mines and Energy, Mineral Development Division, Report 80-2, 29p.

- Kean, B.F. and Strong, D.F. (1975). Geochemical evolution of an Ordovician island arc of the Central Newfoundland Appalachians. *American Journal of Science*, v.275, pp.97-118.
- Kelemen, P.B. (1990). Reaction between ultramafic rock and fractionating basaltic magma I. Phase relations, the origin of calc-alkaline magma series, and the formation of discordant dunite. *Journal of Petrology*, v.31, pp.51-98.
- Kelemen, P.B., Joyce, D.B., Webster, J.D. and Holloway, J.R. (1990a). Reaction between ultramafic rock and fractionating basaltic magma II. Experimental investigation of reaction between olivine tholeiite and harzburgite at 1150-1050°C and 5 kb. *Journal of Petrology*, v.31, pp.99-134.
- Kelemen, P.B., Johnson, K.T.M., Kinzler, R.J. and Irving, A.J. (1990b). High-field-strength element depletions in arc basalts due to mantle-magma interaction. *Nature*, v.345, pp.521-524.
- Keen, C.E., Keen, M.J., Nichols, B., Reid, I., Stockmal, G.S., Colman-Sadd, S.P., O'Brien, S.J., Miller, H., Quinlan, G., Williams, H., Wright, J. (1986). Deep seismic reflection profile across the northern Appalachians; *Geology*, v.14, pp.141-145.
- Kennedy, M.J. and DeGrace, J.R. (1972). Structural sequence and its relationship to sulphide mineralization in the Ordovician Lush's Bight Group of western Notre Dame Bay, Newfoundland. *CIM Transactions*, v.LXXV, pp.300-308.
- Kennedy, M.B. and McGonigal, M.H., 1972: The Gander Lake and Davidsville groups of northeastern Newfoundland: new data and geotectonic implications *Canadian Journal of Earth Sciences*, Volume 9, pages 452-459.
- King, A.F. (1988). Geology of the Avalon Peninsula, Newfoundland (parts of 1K, 1L, 1M, 1N and 2C). Newfoundland Department of Mines, Mineral Development Division, Map 88-01.

- Knight, I. (1983). Geology of the Carboniferous Bay St. George Subbasin, western Newfoundland. Newfoundland Department of Mines and Energy Mineral Development Division Memoir 1, 358p.
- Kontak, D.J. and Strong, D.F. (1986). The King's Point volcano-plutonic complex, Newfoundland. *in* Current Research, Geological Survey of Canada, Paper 86-1A, pp.465-470.
- Kostopoulos, D.K. and Murton, B.J. (1993). Origin and distribution of components in boninite genesis: significance of the OIB component. *in* Parson, I. M., Murton, B.J. and Browning, P. (editors), Ophiolites and their modern oceanic analogues, Geological Society Special Publication No.60, pp.133-154.
- Kuno, H. (1950). Petrology of Hakone volcano and the adjacent areas, Japan. Geological Society of America Bulletin, v.61, pp 957-1020.
- Kuno, H. (1960). High-alumina basalt. Journal of Petrology, v.1, pp.121-145
- Kuroda, N., Shiraki, K. and Urano, H. (1978). Boninite as possible calc-alkalic primary magma. Bulletin of Volcanology, v.41, pp.563-575.
- LaFrance, B. (1989). Structural evolution of a transpression zone in north central Newfoundland. Journal of Structural Geology, v.11, pp 705-716
- LaFrance, B. and Williams, P.F. (1992). Silurian deformation in eastern Notre Dame Bay, Newfoundland. Canadian Journal of Earth Sciences, v.29, pp.1899-1914
- Langmuir, C.H. (1989). Geochemical consequences of *in situ* crystallization. Nature, v.340, pp.199-205.
- Leake, B.E. (1978). Nomenclature of amphiboles. The Canadian Mineralogist, v.16, pp.501-520.
- Leat, P.T. and Thorpe, R.S. (1989). Snowdon basalts and the cessation of Caledonian subduction by the Longvillian. Journal of the Geological Society, London, v.146, pp.965-970.

- Le Roex, A.P. (1987). Source regions of Mid-Ocean Ridge Basalts: evidence for enrichment processes. *in* M.A. Menzies and C.J. Hawkesworth (editors), *Mantle Metasomatism*, Academic Press, London, pp.389-422.
- LeMaitre, R.W. (editor)(1989). *A classification of igneous rocks and glossary of terms*. Blackwell, Oxford, 193p.
- Leybourne, M.I. and Van Wagoner, N.A. (1991). Heck and Heckle seamounts, Northeast Pacific Ocean: high extrusion rates of primitive and highly depleted mid-ocean ridge basalt on off-ridge seamounts. *Journal of Geophysical Research*, v.96, pp.16,275-16,293.
- Lightfoot, P. and Hawkesworth, C. (1988). Origin of Deccan Trap lavas: evidence from combined trace element and Sr-, Nd- and Pb-isotope studies. *Earth and Planetary Science Letters*, v.91, pp.89-104.
- Lightfoot, P.C., Hawkesworth, C.J., Devey, C.W., Rogers, N.W. and van Calsteren, P.W.C. (1990). Source and differentiation of Deccan Trap lavas: implications of geochemical and mineral chemical variations. *Journal of Petrology*, v.31, pp.1165-1200.
- Lin, P.-N., Stern, R.J. and Bloomer, S.H. (1989). Shoshonitic volcanism in the northern Mariana arc 2 Large-ion lithophile and rare earth element abundances: evidence for the source of incompatible element enrichments in intraoceanic arcs. *Journal of Geophysical Research*, v.94, pp.4497-4514.
- Lin, P.-N., Stern, R.J., Morris, J. and Bloomer, S.H. (1990). Nd- and Sr-isotopic compositions of lavas from the northern Mariana and southern Volcano arcs: implications for the origin of island arc melts. *Contributions to Mineralogy and Petrology*, v 105, pp.381-392.
- Lisle, R.J., Styles, P. and Freeth, S.J. (1990). Fold interference structures: the influence of layer competence contrast. *Tectonophysics*, v.172, pp.197-200.

- Lloyd, F.E., Arima, M. and Edgar, A.D. (1985). Partial melting of phlogopite-clinopyroxenite nodule from south-west Uganda: an experimental study bearing on the origin of highly potassic continental rift volcanics. *Contributions to Mineralogy and Petrology*, v.91, pp.321-329.
- Lofgren, G.E. and Donaldson, C.H. (1975). Curved branching crystals and differentiation in comb-layered rocks. *Contributions to Mineralogy and Petrology*, v.49, pp.309-319.
- Ludden, J.N. and Thompson, G. (1979). An evaluation of the behaviour of the rare earth elements during the weathering of sea-floor basalt. *Earth and Planetary Science Letters*, v.43, pp.85-92.
- Luhr, J.F., Allan, J.F., Carmichael, I.S.E., Nelson, S.A., and Hasenaka, T. (1989). Primitive calc-alkaline and alkaline rock types from the western Mexican volcanic belt. *Journal of Geophysical Research*, v.94, pp.4515-4530.
- Luhr, J. and Carmichael, I.S.E. (1981). The Colima Volcanic Complex, Mexico: Part II. Late-Quaternary cinder cones. *Contributions to Mineralogy and Petrology*, v.76, pp.127-147.
- Luhr, J. and Carmichael, I.S.E. (1986). Contemporaneous alkaline and calc-alkaline magmas from the volcanic front of the Mexican Volcanic Belt. *EOS*, v.67, p.1280.
- Macdonald, G.A. and Katsura, T. (1964). Chemical composition of Hawaiian lavas. *Journal of Petrology*, v.5, pp.82-133.
- MacLean, H.J. (1947). Geology and mineral deposits of the Little Bay area. *Bulletin No.22, Newfoundland Geological Survey*, 43p.
- Mahoney, J.J. (1988). Deccan Traps. *in* J.D. Macdougall (editor), *Continental Flood Basalts*, Kluwer Academic Publishers, pp.151-194.
- Marsh, J.S. (1991). REE fractionation and Ce anomalies in weathered Karoo dolerite. *Chemical Geology*, v.90, pp.189-194.

- Marten, B. E. (1971a). The geology of the Western Arm Group, Green Bay, Newfoundland. M.Sc. thesis, Memorial University of Newfoundland, 72 p.
- Marten, B. E. (1971b). Stratigraphy of volcanic rocks in the Western Arm area of the Central Newfoundland Appalachians. The Geological Association of Canada, Proceedings, v.24, pp.73-84.
- Masuda, Y. and Aoki, K.-I. (1979). Trace element variations in the volcanic rocks from the Nasu zone, northeast Japan. Earth and Planetary Science Letters, v.44, pp. 139-149.
- Mattinson, J.M. (1975). Early Paleozoic ophiolite complexes of Newfoundland: isotopic ages of zircons. Geology, v.3, pp.181-183.
- McBirney, A. R. (1984). Igneous Petrology. Freeman, Cooper & Company, San Francisco, 504p.
- McCulloch, M.T. and Gamble, J.A. (1991). Geochemical and geodynamical constraints on subduction zone magmatism. Earth and Planetary Science Letters, v.102, pp.358-374.
- McClay, K. R. (1992). Glossary of thrust tectonics terms. *in* McClay, K.R. (editor), Thrust Tectonics, Chapman & Hall, London, pp.419-433.
- McClay, K. R. and Buchanan, P.G. (1992). Thrust faults in inverted extensional basins. *in* McClay, K. R. (editor), Thrust Tectonics, Chapman & Hall, London, pp.93-104.
- McDermott, F. and Hawkesworth, C. (1991). Th, Pb, and Sr isotope variations in young island arc volcanics and oceanic sediments. Earth and Planetary Science Letters, v. 104, pp. 1-15.
- McGonigal, M.H. (1970). Geology of the Springdale Group west of the Little Bay Road, northwest central Newfoundland. B.Sc. thesis, Memorial University of Newfoundland, 37p.

- McKenzie, D. (1985). The extraction of magma from the crust and mantle. *Earth and Planetary Science Letters*, v.74, pp.81-91.
- McKenzie, D. and O'Nions, R.K. (1991). Partial melt distributions from inversion of rare earth elements concentrations. *Journal of Petrology*, v.32, pp.1021-1091.
- McLennan, S.M. (1992). Continental Crust. *in Encyclopedia of Earth System Science*, v. 1, Academic Press, pp.581-592.
- Mercer, B., Strong, D.F., Wilton, D.H.C. and Gibbons, D. (1985). The King's Point volcano-plutonic complex, western Newfoundland. *in Current Research, Geological Survey of Canada*, paper 85-1A, pp.737-741.
- Meschede, M. (1986). A method of discriminating between different types of mid-ocean ridge basalts and continental tholeiites with the Nb-Zr-Y diagram. *Chemical Geology*, v.56, pp.207-218.
- Meyer, J.R., Dean, P.L. and Barnes, C.R. (1988). Conodont ages for three carbonate samples from Middle Ordovician cherts and shales in central Newfoundland. *in Current Research, Newfoundland Department of Mines, Mineral Development Division*, Report 88-1, pp.189-192.
- Middlemost, E.A.K. (1975). The basalt clan. *Earth Science Reviews*, v. 11, pp.337-364.
- Miller, D.M., Langmuir, C.H., Goldstein, S.L. and Franks, A.L. (1992). The importance of parental magma composition to calc-alkaline and tholeiitic evolution: evidence from Umnak island in the Aleutians. *Journal of Geophysical Research*, v.97, pp.321-343.
- Miller, H.G. (1990). A synthesis of the geophysical characteristics of terranes in eastern Canada. *Tectonophysics*, v.177, pp.171-191.
- Minster, J.F. and Allegre, C.J. (1978). Systematic use of trace elements in igneous processes, Part III. *Contribution to Mineralogy and Petrology*, v.68, pp.37-52

- Miyashiro, A. (1974). Volcanic arc series in island arcs and active continental margins. *American Journal of Science*, v.274, pp.321-355.
- Miyashiro, A. (1978). Nature of alkalic volcanic rock series. *Contribution to Mineralogy and Petrology*, v.66, pp.91-104.
- Miyashiro, A. and Shido, F. (1975). Tholeiitic and calc-alkalic series in relation to the behaviors of titanium, vanadium, chromium, and nickel. *American Journal of Science*, v.275, pp.265-277.
- Moore, R.C. (1965). *Treatise in Invertebrate paleontology. Part H: Brachiopoda*, v.1. The Geological Society of America and the University of Kansas Press.
- Morris, J.D. and Hart, S.R. (1983). Isotopic and incompatible element constraints on the genesis of island arc volcanics from Cold Bay and Amak Island, Aleutians and implications for mantle structure. *Geochimica et Cosmochimica Acta*, v.47, pp.2015-2030.
- Morris, J.D., Leeman, W.P., and Tera, F. (1990). The subducted component in island arc lavas: constraints from Be isotopes and B-Be systematics. *Nature*, v.334, pp.31-36.
- Muggridge, M.G. (1989). Felsic volcanism and mineralisation in Ordovician Cutwell Group, Notre Dame Bay: geology and geochemistry. B.Sc. (Honours) thesis, Memorial University, 59 p.
- Mulchrone, K.F. (1991). The interpretation of fold axial data from regions of polyphase folding. *Journal of Structural Geology*, v.13, pp.275-280.
- Mullen, E.D. (1983). MnO/TiO₂/P₂O₅: a minor element discriminant for basaltic rocks of oceanic environments and its implications for petrogenesis. *Earth and Planetary science Letters*, v.62, pp.53-62.

- Murphy, J.B. and Hynes, A.J. (1986). Contrasting secondary mobility of Ti, P, Zr, Nb, and Y in two metabasaltic suites in the Appalachians. *Canadian Journal of Earth Sciences*, v.23, pp.1138-1144.
- Murray, A.H. and Howley, J.P., 1881: *Geological Survey of Newfoundland* Edward Stanford, London, 536 pages.
- Murray, A.H. and Howley, J.P., 1918: *Reports of the Geological Survey from 1881-1909. Geological Survey of Newfoundland.*
- Murton, B.J., Peate, D.W., Arculus, R.J., Pearce, J.A., and van der Laan, S (1992) Trace element geochemistry of volcanic rocks from site 786: the Izu-Bonin forearc. *in* Fryer, P., Pearce, J.A., Stokking, L.B. et al., *Proceedings of the Ocean Drilling Program, Scientific Results*, v. 125, pp.211-235.
- Myers, J.D. (1988). Possible petrogenetic relations between low- and high-MgO Aleutian basalts. *GSA Bulletin*, v.100, pp.1040-1053.
- Myers, J.D., Marsh, B.D. and Sinha, A.K. (1985). Strontium isotopic and selected trace element variations between two Aleutian volcanic centers (Adak and Atka): implications for the development of arc volcanic plumbing systems. *Contributions to Mineralogy and Petrology*, v.91, pp.221-234.
- Navon, O. and Stolper, E. (1987). Geochemical consequences of melt percolation: the upper mantle as chromatographic column. *The Journal of Geology*, v.95, pp.285-307.
- Neale, E.R.W. and Kennedy, M.J. (1967). Relationships of the Fleur de Lys Group to younger groups of the Burlington Peninsula, Newfoundland. *Geological Association of Canada Special Paper 4*, pp.139-169.
- Neale, E.R.W. and Nash, W.A. (1963). Sandy Lake (east half), Newfoundland. *Geological Survey of Canada, Paper 62-28.*

- Neale, E. R. W., Kean, B. F. and Upadhyay, H. D. (1975). Post-ophiolite unconformity, Tilt Cove - Betts Cove area, Newfoundland. *Canadian Journal of Earth Sciences*, v. 12, pp. 880-886.
- Nelson, K. D. and Casey, J. F. (1979). Ophiolitic detritus in the Upper Ordovician flysch of Notre Dame Bay and its bearing on tectonic evolution of western Newfoundland. *Geology*, v. 7, pp. 21-31.
- Neuman, R. B. (1984). Geology and paleobiology of islands in the Ordovician Iapetus Ocean: review and implications. *Geological Society of America Bulletin*, v. 95, pp. 1188-1201.
- Nohda, S., Tatsumi, Y., Otofujii, Y.-I., Matsuda, T. and Ishizaka, K. (1988). Asthenospheric injection and back-arc opening: isotopic evidence from northeast Japan. *Chemical Geology*, v. 68, pp. 317-327.
- North American Stratigraphic Code (1983). *The American Association of Petroleum Geologists Bulletin*, v. 67, No. 5, pp. 841-875.
- Nowlan, G. S. and Thurlow, J. G. (1984). Middle Ordovician conodonts from the Buchans Group, Central Newfoundland, and their significance for regional stratigraphy of the Central Volcanic Belt. *Canadian Journal of Earth Sciences*, v. 21, pp. 284-296.
- Nye, C. J. and Reid, M. R. (1986). Geochemistry of primary and least fractionated lavas from Okmok Volcano, Central Aleutians: implications for arc magmatogenesis. *Journal of Geophysical Research*, v. 91, pp. 10271-10286.
- O'Brien, B. H., O'Brien, S. J., and Dunning, G. R. (1991). Silurian cover, Late Precambrian - Early Ordovician basement, and the chronology of Silurian orogenesis in the Hermitage Flexure (Newfoundland Appalachians). *American Journal of Science*, v. 291, pp. 760-799.
- O'Brien, F. H. C. and Szybinski, Z. A. (1988). Lower-Middle Ordovician fauna from the Cutwell Group (Central Newfoundland): its implications on stratigraphy and

structure. *in* Program and Abstracts, Fifth International Symposium on the Ordovician System, p.69.

O'Brien, F.H.C. and Szybinski, Z.A. (1989). Conodont faunas from the Catchers Pond and Cutwell Groups, central Newfoundland. *in* Current Research, Newfoundland Department of Mines, Geological Survey of Newfoundland, Report 89-1, pp.121-125.

O'Brien, S.J. (1975). The stratigraphy, petrology and geochemistry of the extrusive and intrusive rocks of Little Bay Island, Newfoundland. B.Sc. thesis, Memorial University of Newfoundland, 70p.

O'Brien, S.J., Tucker, R.D., Dunning, G.R. and O'Driscoll, C.F. (1992). Four-fold subdivision of the Late Precambrian magmatic record of the Avalon Zone type area (east Newfoundland): nature and significance. Geological Association of Canada, Program with Abstracts v.17, p.A85.

O'Hara, M.J. (1968). The bearing of phase equilibria studies in synthetic and natural systems and the origin and evolution of basic and ultrabasic rocks. *Earth and Planetary Science Letters*, v.4, pp.69-133.

O'Hara, M.J. and Mathews, R.E. (1981). Geochemical evolution in an advancing, periodically tapped, continuously fractionated magma chamber. *Journal of Geological Society of London*, v.138, pp.237-277.

Oldow, J.S., Channell, J.E.T., Catalano, R., and D'Argenio, B. (1990). Contemporaneous thrusting and large-scale rotations in the western Sicilian fold and thrust belt. *Tectonics*, v.9, pp.661-681.

O'Reilly, S.Y., Griffin, W.L., Ryan, C.G. (1991). Residence of trace elements in metasomatized spinel lherzolite xenoliths: a proton-microprobe study *Contributions to Mineralogy and Petrology*, v.109, pp.98-113

- Othman, D.B., White, W.M., and Patchett, J. (1989). The geochemistry of marine sediments, island arc magma genesis, and crust-mantle recycling. *Earth and Planetary Science Letters*, v.94, pp.1-21.
- Pankhurst, R.J. (1977). Open system crystal fractionation and incompatible element variation in basalts. *Nature*, v.268, pp.36-38.
- Passchier, C.W. and Simpson, C. (1986). Porphyroclast systems as kinematic indicators. *Journal of Structural Geology*, v.8, pp.831-843.
- Paterson, S.R., Brudos, T., Fowler, K., Carlson, C., Bishop, K. (1991). Papoose Flat pluton: forceful expansion or postemplacement deformation? *Geology*, v.19., pp.324-327.
- Paterson, S.R. and Tobisch, O.T. (1988). Using pluton ages to date regional deformations: problems with commonly used criteria. *Geology*, v.16, pp.1108-1111.
- Payne, J.G. and Strong, D.F. (1979). Origin of the Twillingate trondhjemite, north-central Newfoundland: partial melting in the roots of an island arc. *in* Barker, F. (editor), *Trondhjemites, dacites and related rocks*, New York, Elsevier, pp.489-516.
- Pearce, J.A. (1982). Trace element characteristics of lavas from destructive plate boundaries. *in* *Andesites*; edited by R.S. Thorpe, Wiley & Sons, pp.525-548.
- Pearce, J.A. (1983). Role of the sub-continental lithosphere in magma genesis at active continental margins. *in* *Continental basalts and and mantle xenoliths*; edited by C.J. Hawkesworth and M.J. Norry, Nantwich, Shiva, pp.230-249.
- Pearce, J.A., Bender, J.F., De Long, S.E., Kidd, W.S.F., Low, P.J., Guner, Y., Saroglu, F., Yilmaz, Y., Moorbath, S. and Mitchell, J.G. (1990). Genesis of collision volcanism in Eastern Anatolia, Turkey. *Journal of Volcanology and Geothermal Research*, v.44, pp.189-229.

- Pearce, J.A. and Cann, J.R. (1973). Tectonic setting of basic volcanic rocks determined using trace element analyses. *Earth and Planetary Science Letters*, v. 19, pp.290-300.
- Pearce, J.A. and Flower, M.F.J. (1977). The relative importance of petrogenetic variables in magma genesis at accreting plate margins: a preliminary investigation *Journal of Geological Society of London*, v.134, pp.103-127
- Pearce, J.A, Harris , N.B.W. and Tindle, A.G. (1984). Trace element discrimination diagrams for the tectonic interpretation of granitic rocks. *Journal of Petrology*, v.25, pp.956-983.
- Pearce, J.A. and Norry, M.J. (1979). Petrogenetic implications of Ti, Zr, Y, and Nb variations in volcanic rocks. *Contributions to Mineralogy and Petrology*, v 69, pp.33-47.
- Pearce, J.A., van der Laan, S.R., Arculus, R.J., Murton, B.J., Ishii, T., Peate, D W , and Parkinson, i.J. (1992). Boninite and harzburgite from Leg 125 (Bonin-Mariana forearc): a case study of magma genesis during the initial stages of subduction // Fryer, P., Pearce, J.A., Stokking, L.B. et al., *Proceedings of the Ocean Drilling Program, Scientific Results*, v. 125, pp.623-659.
- Pearcy, L.G., DeBari, S.M. and Sleep, N.H. (1990) Mass balance calculations for two sections of island arc crust and implications for the formation of continents. *Earth and Planetary Science Letters*, v.96, 427-442.
- Pedersen, R.B. and Hertogen, J. (1990). Magmatic evolution of the Karmoy Ophiolite Complex, SW Norway: relationships between MORB - IAT - boninitic - calc - alkaline and alkaline magmatism. *Contributions to Mineralogy and Petrology*, v.104, pp.277-293.
- Penney, R. (1969). Springdale (East 1/2). B.Sc. thesis, Memorial University of Newfoundland.

- Perfit, M.R. and Gust, D.A. (1981). Petrochemistry and experimental crystallization of basalts from Aleutian Islands, Alaska. IAVCEI Symposium on Arc Volcanism, Tokyo, pp.288-289.
- Perfit, M.R. and Kay, R.W. (1986). Comment on "Isotopic and incompatible element constraints on the genesis of island arc volcanics from Cold Bay and Amak Island, Aleutians, and implications for mantle structure" by J.D. Morris and S.R. Hart *Geochimica et Cosmochimica Acta*, v.50, pp.477-481.
- Perfit, M.R., Brueckner, H., Lawrence, J.R. and Kay, R.W. (1980b). Trace element and isotopic variations in a zoned pluton and associated volcanic rocks, Unalaska Island, Alaska: a model for fractionation in the Aleutian calc-alkaline suite. *Contribution to Mineralogy and Petrology*, v.73, pp.69-87.
- Perfit, M.R., Gust, D.A., Bence, A.E., Arculus, R.J. and Taylor, S.R. (1980a). Chemical characteristics of island-arc basalts: implications for mantle sources. *Chemical Geology*, v.30, pp.227-256.
- Penney, R. (1969). Springdale (East 1/2). B.Sc. thesis, Memorial University of Newfoundland.
- Peters, R. (1970). Geology of the Nickey's Nose - Harry's Harbour area, Lushs Bight Group. B.Sc. thesis, Memorial University of Newfoundland, 20p.
- Piasecki, M.A.J., 1988: A major ductile shear zone in the Bay d'Espoir area, Gander Terrane, southeastern Newfoundland. In *Current Research, Newfoundland Department of Mines, Mineral Development Division, Report 88-1*, pages 135-144.
- Plank, T. and Langmuir, C.H. (1988). An evaluation of global variations in the major element chemistry of arc basalts. *Earth and Planetary Science Letters*, v 90, pp.349-370.
- Platt, J.P. (1984). Secondary cleavages in ductile shear zones. *Journal of Structural Geology*, v.6, pp.439-442.

- Platt, J.P. and Leggett, J.K. (1986). Stratal extension in thrust footwalls, Makran accretionary prism: implications for thrust tectonics. *The American Association of Petroleum Geologists Bulletin*, v. 70, pp.191-203.
- Pope, J.A. and Calon, T.J. (1990). A stratigraphic and structural analysis of the Gullbridge property, Central Newfoundland. Report for the Rio Algom Exploration Inc. by the Centre for Earth Resources Research, Department of Earth Sciences, Memorial University of Newfoundland.
- Pope, A.J., Calon, T.J. and Swinden, H.S., 1990. Stratigraphy, structural geology and mineralization in the Gullbridge area, central Newfoundland. In: H.S. Swinden, D.T.W. Evans and B.F. Kean (Editors), *Metallogenic framework of base and precious metal deposits, central and western Newfoundland, Field trip guidebook*, pp. 93-100.
- Poucllet, A. and Bellon, H. (1992). Geochemistry and isotopic composition of volcanic rocks from the Yamato Basin: hole 794D, Sea of Japan. *in* Tamaki, K., Suyehiro, K., Allan, J., McWilliams, et al., *Proceedings of the Ocean Drilling Program, Scientific Results*, v.127/128, pp.779-789.
- Prestvik, T. and Goles, G.G. (1985). Comments on petrogeneses and the tectonic setting of Columbia River basalts. *Earth and Planetary Science Letters*, v.72, pp.65-73.
- Price, R.C., Gray, C.M., Wilson, R.E., Frey, F.A. and Taylor, S.R. (1991). The effects of weathering on rare-earth element, Y and Ba abundances in Tertiary basalts from southeastern Australia. *Chemical Geology*, v.93, pp.245-265.
- Price, R.C., Johnson, L.E. and Crawford, A.J. (1990). Basalts of the North Fiji Basin: the generation of back arc basin magmas by mixing of depleted and enriched mantle sources. *Contributions to Mineralogy and Petrology*, v. 105, pp.106-121.
- Ramsay, J.G. (1967). *Folding and fracturing of rocks*. McGraw-Hill, New York.

- Ramsay, J.G. (1981). Tectonics of the Helvetic Nappes. *in* McClay, K.R. & Price, N.J. (editors), Thrust and Nappe Tectonics, Geological Society of London Special Publication, No.9, pp.293-310.
- Ramsay, W.R.H., Crawford, A.J. and Foden, J.D. (1984). Field setting, mineralogy, chemistry, and genesis of arc picrites, New Georgia, Solomon Islands. *Contributions to Mineralogy and Petrology*, v.88, pp.386-402.
- Rapp, R.P., Watson, E.B. and Miller, C.F. (1991). Partial melting of amphibolite/eclogite and the origin of Archean trondhjemites and tonalites. *Precambrian Research*, v.51, pp.1-25.
- Rejebian, V.A., Harris, A.G. and Huebner, J.S. (1987). Conodont color and textural alteration: an index to regional metamorphism, contact metamorphism, and hydrothermal alteration. *Geological Society of America Bulletin*, v.99, pp.471-479.
- Richards, J.P., Chappell, B.W. and McCulloch, M.T. (1990). Intraplate-type magmatism in a continent-island-arc collision zone: Porgera intrusive complex, Papua New Guinea. *Geology*, v.18, pp.958-961.
- Ritcey, D.H. (1993). Geology, U-Pb geochronology, and stable isotope geochemistry of the Hammer Down gold prospect, Green Bay District, Newfoundland. Unpublished M.Sc. thesis, Memorial University of Newfoundland.
- Roberts, J.L. (1970). The intrusion of magma into brittle rocks. *in* Mechanism of Igneous Intrusion; edited by G. Newall and N. Rast, Gallery Press, Liverpool, pp.287-335.
- Rodgers, J. and Neale, E.R.W. (1969). Possible "Taconic" klippen in western Newfoundland. *American Journal of Science*, v.261, pp.713-730.
- Rogers, G. and Saunders, A.D. (1989). Magnesian andesites from Mexico, Chile and the Aleutian Islands: implications for magmatism associated with ridge - trench

collision. *in* Boninites; edited by A.J. Crawford, Unwin Hyman, London, pp.416-445.

Romick, J.D., Kay, S.M. and Kay, R.W. (1992). The influence of amphibole fractionation on the the evolution of calc-alkaline andesite and dacite tephra from the central Aleutians, Alaska. *Contributions to Mineralogy and Petrology*, v.112, pp.101-118.

Ryerson, F.J. and Watson, E.B. (1987). Rutile saturation in magmas: implications for Ti-Nb-Ta depletion in island-arc basalts. *Earth and Planetary Science Letters*, v.86, pp.225-239.

Sakuyama, M. and Nesbitt, R.W. (1986). Geochemistry of the Quaternary volcanic rocks of the northeast Japan arc. *Journal of Volcanology and Geothermal Research*, v.29, pp.413-450.

Salters, V.J.M. and Shimizu, N. (1988). World-wide occurrence of HFSE-depleted mantle. *Geochimica et Cosmochimica Acta*, v.52, pp.2177-2182.

Sawlan, M.G. (1991). Magmatic evolution of the Gulf of California Rift. *in* Dauphin, J.P. and Simoneit, B.R.T., *The Gulf and Peninsular Province of the Californias*, American Association of Petroleum Geologists, Memoir 47, pp.301-369.

Saunders, A.D., and Tarney, J. (1979). The geochemistry of basalts from a back-arc spreading centre in the East Scotia Sea. *Geochimica et Cosmochimica Acta*, v.43, pp.555-572.

Saunders, A.D., and Tarney, J. (1984). Geochemical characteristics of basaltic volcanism within back-arc basins. *in* *Marginal basin geology: volcanic and associated sedimentary and tectonic processes in modern and ancient marginal basins*; edited by B.P. Kokelaar and M.F. Howells, Geological Society of London Special Publication, v.16, pp.56-76.

Saunders, A.D., Fornari, D.J. and Morrison, M.A. (1982). The composition and emplacement of basaltic magmas produced during the development of

continental-margin basin: the Gulf of California, Mexico. *Journal of Geological Society of London*, v.139, pp.335-346.

- Saunders, A.D., Norry, M.J. and Tarney, J. (1988). Origin of MORB and chemically-depleted mantle reservoirs: trace element constraints. *Journal of Petrology, Special Lithosphere Issue*, pp.415-445.
- Saunders, A.D., Norry, M.J. and Tarney, J. (1991). Fluid influence on the trace element compositions of subduction zone magmas. *Philosophical Transactions of Royal Society of London*, v.A335, pp.377-392.
- Saunders, A.D., Rogers, G., Marriner, G.F., Terrell, D.J., and Verma, S.P. (1987). Geochemistry of Cenozoic volcanic rocks, Baja California, Mexico: implications for the petrogenesis of post-subduction magmas. *Journal of Volcanology and Geothermal Research*, v.32, pp.223-245.
- Saunders, A.D., Tarney, J., Marsh, N.G. and Wood, D.A. (1980a). Ophiolites as ocean crust or marginal basin crust: a geochemical approach. *in* Proceedings of International Ophiolite Conference, Nicosia, Cyprus; edited by A. Panayiotou.
- Saunders, A.D., Tarney, J. and Weaver, S.D. (1980b). Transversal geochemical variations across the Antarctic Peninsula: implication for the genesis of calc-alkaline magmas. *Earth and Planetary Science Letters*, v.46, pp.344-360.
- Saunders, A.D., Storey, M., Kent, R.W. and Norry, M.J. (1992). Consequences of plume-lithosphere interactions. *in* Storey, B.C., Alabaster, T. and Pankhurst, R.J. (editors), *Magmatism and the Causes of Continental Break-up*, Geological Society Special Publication No.68, pp.41-60.
- Sayed, U.A. (1970). The tectonic setting of the Colchester Plutons, Southwest Arm, Green Bay, Newfoundland. Unpublished M.Sc. thesis, Memorial University, Newfoundland, 76p.

- Schilling, J-G., Kingsley, R.H. and Devine, J.D. (1982). Galapagos hot spot-spreading center system I. Spatial petrological and geochemical variations (83°W-101°W). *Journal of Geophysical Research*, v.87, pp.5593-5610.
- Schilling, J-G., Zajac, M., Evans, R., Johnston, T., White, V., Devine, J.D., and Kingsley, R. (1983). Petrologic and geochemical variations along the Mid-Atlantic Ridge from 29°N to 73°N. *American Journal of Science*, v.283, pp.510-586.
- Searle, M.P. and Stevens, R.K. (1984). Obduction processes in ancient, modern and future ophiolites. *in* Gass, I.G., Lippard, S.J., and Shelton, A.W., *Ophiolites and oceanic lithosphere*, Geological Society Special Publication, London, No.13, pp.303-319.
- Shervais, J.W. (1982). Ti-V plots and the petrogenesis of modern and ophiolitic lavas. *Earth and Planetary Science Letters*, v.59, pp.101-118.
- Shimizu, N. (1987). Trace element abundance patterns of pyroxenes in spinel nodules from Salt Lake Crater, Oahu. *EOS Transactions American Geophysical Union*, v.68, p.446.
- Shimizu, N. and Arculus, R.J. (1975). Rare earth element concentrations in a suite of basanitoids and alkali olivine basalts from Grenada, Lesser Antilles. *Contribution to Mineralogy and Petrology*, v.50, pp.231-240.
- Shimizu, H., Sawatari, H., Kawata, Y., Dunkley, P.N., and Masuda, A. (1992). Ce and Nd isotope geochemistry on island arc volcanic rocks with negative Ce anomaly: existence of sources with concave REE patterns in the mantle beneath the Solomon and Bonin island arcs. *Contributions to Mineralogy and Petrology*, v.110, pp.242-252.
- Schneider, M.E. and Egger, D.H. (1986). Fluids in equilibrium with peridotite minerals: implications from mantle metasomatism. *Geochimica et Cosmochimica Acta*, v.50, pp.711-724.

- Simpson, C. (1986). Determination of movement sense in mylonites. *Journal of Geological Education*, v.34, pp.246-261.
- Sinton, J.M. and Fryer, P. (1987). Mariana Trough lavas from 18°N: implications for the origin of back arc basin basalts. *Journal of Geophysical Research*, v.92, pp.12,782-12,802.
- Simpson, C. (1986). Determination of movement sense in mylonites. *Journal of Geological Education*, 1986, v.34, pp.246-261.
- Skjerna, L. (1975). Experiments on superimposed buckle folding. *Tectonophysics*, v.27, pp.255-270.
- Smith, I.E.M. and Johnson, R.W. (1981). Contrasting rhyolite suites in the late Cenozoic of Papua New Guinea. *Journal of Geophysical Research*, v.86, pp.10257-10272.
- Smitheringale, W.G. (1972). Low-potash Lushs Bight tholeiites: Ancient oceanic crust in Newfoundland?. *Canadian Journal of Earth Sciences*, v.9, pp.574-588.
- Sorensen, S.S. and Grossman, J.N. (1989). Enrichment of trace elements in garnet amphibolites from a paleo-subduction zone: Catalina Schist, Southern California. *Geochimica et Cosmochimica Acta*, v.53, pp.3155-3177.
- Stander, E. (1984). The stratigraphy and structural geology of the Twillingate region unpublished M.Sc. thesis, Memorial University of Newfoundland.
- Stauffer, M.R., Mukherjee, A.C. and Koo, J. (1975). The Amisk Group: An Aphebian(?) island arc deposit. *Canadian Journal of Earth Sciences*, v.12, pp.2021-2035.
- Stern, R.J. (1981). A common mantle source for Western Pacific island arc and "Hot-Spot" magmas - implications for layering in the upper mantle. *Carnegie Institut of Washington Yearbook*, v.80, pp.455-462.
- Stern, R.J. and Bibee, L.D. (1984). Esmeralda Bank: Geochemistry of an active submarine volcano in the Mariana Island Arc. *Contribution to Mineralogy and Petrology*, v.86, pp.159-169.

- Stern, R.J., Bloomer, S.H., Lin, P.-N. and Smoot, N.C. (1989). Submarine arc volcanism in the southern Mariana Arc as an ophiolite analogue. *Tectonophysics*, v. 168, pp 151-170.
- Stern, R.J., Lin, P.-N., Morris, J.D., Jackson, M.C., Fryer, P., Bloomer, S.H. and Ito, E. (1990). Enriched back-arc basin basalts from the northern Mariana Trough: implications for the magmatic evolution of back-arc basins. *Earth and Planetary Science Letters*, v. 100, pp.210-225.
- Stern, R.J., Morris, J., Bloomer, H.S., and Hawkins, J.W. Jr. (1991). The source of the subduction component in convergent margin magmas: Trace element and radiogenic isotope evidence from Eocene boninites, Mariana forearc. *Geochimica et Cosmochimica Acta*, v.55, pp.1467-1481.
- Stevens, R.K. (1970). Cambro-Ordovician flysch sedimentation and tectonics in west Newfoundland and their possible bearing on a proto-Atlantic ocean. *in* Lajoie, J. (editor), *Flysch Sedimentology in North America*, Geological Association of Canada Special Paper 7, pp.165-177.
- Stöpler, E. and Walker, D. (1980). Melt density and the average composition of basalt. *Contribution to Mineralogy and Petrology*, v.74, pp.13-27.
- Stouge, S. (1980). Lower and Middle Ordovician conodonts from Central Newfoundland and their correlatives in Western Newfoundland. *in* Current Research, Newfoundland Department of Mines and Energy, Mineral Development Division, Report 80-1, pp.134-143.
- Strong, D.F. (1973). Lushs Bight and Robert's Arm Groups, central Newfoundland: possible juxtaposed oceanic and island arc volcanic suites. *Geological Society of America Bulletin*, v.84, pp.3917-3928.
- Strong, D.F. (1977). Volcanic regimes of the Newfoundland Appalachians. *in* Volcanic regimes in Canada; Edited by W.R.A. Baragar, L.C. Coleman and J.M. Hall, Geological Association of Canada, Special Paper 16, pp.61-90

- Strong, D.F. and Kean, B.F. (1972). New fossil localities in the Lush's Bight Terrane of Central Newfoundland. *Canadian Journal of Earth Sciences*, v.9, pp.1572-1576.
- Strong, D.F., O'Brien, S.J., Taylor, S.W., Strong, P.G. and Wilton, D.H. (1978). Aborted Proterozoic rifting in eastern Newfoundland. *Canadian Journal of Earth Sciences*, v.15, pp.117-131.
- Stukas, V. and Reynolds, P.H. (1974). $^{40}\text{Ar}/^{39}\text{Ar}$ Dating of the Brighton Gabbro Complex, Lush's Bight Terrane, Newfoundland. *Canadian Journal of Earth Sciences*, v.11, pp.1485-1488.
- Sturchio, N.C., Muehlenbachs K. and Seitz, M.G. (1986). Element redistribution during hydrothermal alteration of rhyolite in an active geothermal system: Yellowstone drill cores Y-7 and Y-8. *Geochimica et Cosmochimica Acta*, v.50, pp.1619-1631.
- Sun, S.-S. (1980). Lead isotopic study of young volcanic rocks from mid-ocean ridges, ocean islands and island arcs. *Philosophical Transactions of Royal Society, London*, v.A297, pp.409-445.
- Sun, S.-S. and McDonough, W.F. (1989). Chemical and isotopic systematics of oceanic basalts: implications for mantle composition and processes. *in* *Magmatism in the ocean basins*; edited by A.D. Saunders and M.J. Norry, Geological Society Special Publication, n.42, pp.313-345.
- Sun, S.-S. and Nesbitt, R.W. (1978). Geochemical regularities and genetic significance of ophiolitic basalts. *Geology*, v.6, pp.689-693.
- Sun, S.-S., Nesbitt, R.W. and Sharaskin, A.Y. (1979). Geochemical characteristics of mid-ocean ridge basalts. *Earth and Planetary Science Letters*, v.44, pp.119-138.
- Swinden, H.S. (1987). Ordovician volcanism and mineralization in the Wild Bight Group, Central Newfoundland: a geological, petrological, geochemical and isotopic study. Unpubl. PhD thesis, Memorial University of Newfoundland

- Swinden, H.S. (1988). Geology and economic potential of the Pipestone Pond area (12A/1 NE; 12A/8 E), central Newfoundland. Newfoundland Department of Mines, Geological Survey Branch Report 88-2.
- Swinden, H.S. (1992). Bipartite massive sulphide metallogeny in the Buchans-Robert's Arm belt, central Newfoundland, as indicated by volcanic whole rock geochemistry. Geological Association of Canada, Program with Abstracts, v.17, p.A108.
- Swinden, H.S. and Kean, B.F. - editors (1988). The Volcanogenic Sulphide Districts of Central Newfoundland. Geological Association of Canada, Mineral Development Division, 250p.
- Swinden, H.S., Jenner, G.A., Fryer, B.J., Hertogen, J. and Roddick (1990). Petrogenesis and paleotectonic history of the Wild Bight Group, an Ordovician rifted island arc in Central Newfoundland. Contributions to Mineralogy and Petrology, v.105, pp.219-241.
- Swinden, H.S., Jenner, G.A., Kean, B.F. and Evans, D.T.W. (1989). Volcanic rock geochemistry as a guide for massive sulphide exploration in central Newfoundland. *in* Current Research, Newfoundland Department of Mines, Report 89-1, pp.201-219.
- Swinden, H.S. and Thorpe, R.I. (1984). Variations in style of volcanism and massive sulfide deposition in island arc sequences of the Newfoundland Central Mobile Belt. Economic Geology, v.79, pp.1596-1619.
- Swinden, H.S., Kean, B.F., and Dunning, G.R. (1988). Geological and paleotectonic settings of volcanogenic sulphide mineralization in central Newfoundland. *in* Swinden, H.S. and Kean, B.F. (editors), The Volcanogenic Sulphide Districts of Central Newfoundland, Geological Association of Canada, Mineral Deposit Section Guidebook, pp.5-30.

- Szybinski, Z.A. (1988). New interpretation of the structural and stratigraphic setting of the Cutwell Group, Notre Dame Bay, Newfoundland. *in* Current Research, Part B, GSC, Paper 88-1B, pp.263-270.
- Takahashi, E. (1986). Genesis of calc-alkali andesite magma in a hydrous mantle - crust boundary: petrology of Iherzolite xenoliths from the Ichinomegata crater, Oga Peninsula, northeast Japan, Part II. *Journal of Volcanology and Geothermal Research*, v.29, pp.355-395.
- Tamaki, K., Pisciotto, K., Allan, J. et al. (1990). Proceedings of the Ocean Drilling Program, Initial Reports, v.127.
- Tamaki, K., Suyehiro, K., Allan, J., Ingle, J.C., and Pisciotto, K.A. (1992). Tectonic synthesis and implications of Japan Sea ODP drilling. *in* Tamaki, K., Suyehiro, K., Allan, J., McWilliams, et al., Proceedings of the Ocean Drilling Program, Scientific Results, v.127/128, pp.1333-1348.
- Tatsumi, Y., Hamilton, D.L. and Nesbitt, R.W. (1986) Chemical characteristics of fluid phase released from a subducted lithosphere and origin of arc magmas: evidence from high-pressure experiments and natural rocks. *Journal of Volcanology and Geothermal Research*, v.29, pp.293-309.
- Tatsumi, Y. and Ishizaka, K. (1981). Existence of andesitic primary magma: an example from southwest Japan. *Earth and Planetary Science Letters*, v.53, pp.124-130.
- Tatsumi, Y. and Ishizaka, K. (1982). Origin of high-magnesian andesites in the Setouchi volcanic belt, southwest Japan, I. Petrographical and chemical characteristics. *Earth and Planetary Science Letters*, v.60, pp.293-304.
- Tatsumi, Y. and Maruyama, S. (1989). Boninites and high-Mg andesites: tectonics and petrogenesis. *in* Boninites; edited by A.J. Crawford, Unwin Hyman, London, pp.50-71.

- Tatsumi, Y., Otofujii, Y.-I., Matsuda, T. and Nohda, S. (1989). Opening of the Sea of Japan back-arc basin by asthenospheric injection. *Tectonophysics*, v.166, pp.317-329.
- Taylor, S.R. and McLennan, S.M. (1981). The composition and evolution of continental crust: rare earth evidence from sedimentary rocks. *Philosophical Transactions of Royal Society of London*, v.A301, pp.185-197.
- Taylor, S.R. and McLennan, S.M. (1985). *The continental crust: its composition and evolution*. Blackwell Scientific Publications, Oxford, 1985.
- Tera, F., Brown, L., Morris J., Sacks, I.S., Klein, J. and Middleton, R. (1986). Sediment incorporation in island-arc magmas: inferences from ^{10}Be . *Geochimica et Cosmochimica Acta*, v.50, 535-550.
- Thirlwall, M.F. (1982). Systematic variation in chemistry and Nd-Sr isotopes across a Caledonian calc-alkaline volcanic arc: implications for source materials. *Earth and Planetary Science Letters*, v.58, pp.27-50.
- Thirlwall, M.F. and Graham, A.M. (1984). Evolution of high-Ca, high-Sr C-series basalts from Grenada, Lesser Antilles: the effects of intra-crustal contamination. *Journal of Geological Society of London*, v.141, pp.427-445.
- Thirlwall, M.F. and Jones, N.W. (1983). Isotope geochemistry and contamination mechanics of Tertiary lavas from Skye, Northwest Scotland. *in* *Continental basalts and mantle xenoliths*; edited by C.J. Hawkesworth and M.J. Norry, Shiva Publishing Limited, pp.158-185.
- Thiessen, R. (1986). Two-dimensional re-fold interference patterns. *Journal of Structural Geology*, v.8, pp.563-573.
- Thiessen, R.L. and Means, W.D. (1980). Classification of fold interference patterns: a reexamination. *Journal of Structural Geology*, v.2, pp.311-316.

- Thompson, G. (1973). A geochemical study of the low-temperature interaction of sea-water and oceanic igneous rocks. *Transactions of American Geophysical Union*, v.54, pp.1015-1019.
- Thompson, R.N. and Morrison, M.A. (1988). Asthenospheric and lower-lithospheric mantle contributions to continental extensional magmatism: an example from the British Tertiary Province. *Chemical Geology*, v.68, pp.1-15.
- Thompson, R.N., Morrison, M.A., Dickin, A.P. and Hendry, G.L. (1983) Continental flood basalts... arachnids rule OK? *in* Continental basalts and mantle xenoliths, edited by C.J. Hawkesworth and M.J. Norry, Shiva Publishing Limited, pp.158-185.
- Thompson, R.N., Morrison, M.A., Hendry, G.L. and Parry, S.J. (1984). An assessment of relative roles of crust and mantle in magma genesis: an elemental approach. *Philosophical Transactions of Royal Society, London*, v.A310, pp.549-590
- Thompson, R.N., Morrison, M.A., Matthey, D.P., Dickin, A.P. and Moorbath, S. (1980). An assessment of the Th-Hf-Ta diagram as a discriminant for tectonomagmatic classifications and in the detection of crustal contamination of magmas. *Earth and Planetary Science Letters*, v.50, pp.1-10.
- Thurlow, J.G. (1981). The Buchans Group: its stratigraphic and structural setting. *in* Swanson, E.A., Strong, D.F. and Thurlow, J.G. (editors), *The Buchans Orebodies*, The Geological Association of Canada Special Paper 22, pp.79-90.
- Thurlow, J.G. and Swanson, E.A. (1987). Stratigraphy and structure of the Buchans Group. *in* Kirkham, R.V. (editor), *Buchans Geology, Newfoundland*, Geological Survey of Canada, Paper 86-24, pp.35-46.
- Thurlow, J.G., Spencer, C.P., Boerner, D.E., Reed, L.E. and Wright, J.A. (1992). Geological interpretation of a high resolution reflection seismic survey at the Buchans mine, Newfoundland. *Canadian Journal of Earth Sciences*, v.29, pp.2022-2037.

- Tucker, R.D., Krogh, T.E., Ross, R.J.Jr. and Williams, S.H. (1990). Time-scale calibration by high-precision U-Pb zircon dating of interstratified volcanic ashes in the Ordovician and Lower Silurian stratotypes of Britain. *Earth and Planetary Science Letters*, v. 100, pp 51-58.
- Upadhyay, H.D. (1973) The Betts Cove Ophiolite and related rocks of the Snooks Arm Group, Newfoundland. Unpublished Ph.D. thesis, Memorial University of Newfoundland
- Upadhyay, H.D., Dewey, J.F. and Neale, E.R.W. (1971). The Betts Cove Ophiolite Complex, Newfoundland: Appalachian oceanic crust and mantle. *Proceedings of the Geological Association of Canada*, v.24, pp.27-34.
- Upadhyay, H.D. and Neale, E.R.W. (1976). The Betts Cove - Tilt Cove ophiolite and associated rocks, Newfoundland. *Geological Society of America, Abstracts and Programs, Northeastern Section*, 8, p.290.
- Upadhyay, H.D. and Neale, E.R.W. (1979). On the tectonic regimes of ophiolite genesis. *Earth and Planetary Science Letters*, v.43, pp.93-102.
- Uzuakpunwa, A.B., 1973. Structural studies of the Gander and Davidsville groups in the Carmanville - Ladle Cove areas, Newfoundland. Unpublished M.Sc. Thesis, Memorial University of Newfoundland, St. John's, 140 pages.
- Vallier, T.L., Jenner, G.A., Frey, F.A., Gill, J.B., Davis, A.S., Volpe, A.M., Hawkins, J.W., Morris, J.D., Morton, J.L., Sholl, D.W., Rautenschlein, M., White, W.M., Williams, R.W., Stevenson, A.J. and White, L.D. (1991). Subalkaline andesite from Valu Fa Ridge, a back-arc spreading center in southern Lau Basin: petrogenesis, comparative chemistry, and tectonic implications. *Chemical Geology*, v.91, pp.227-256.
- Vallier, T.L., Stevenson, A.J. and Scholl, D.W. (1985). Petrology of igneous rocks from Ata Island, Kingdom of Tonga. *in* *Geology and offshore resources of Pacific*

- Island Arcs - Tonga region, edited by D.Scholl and T.Vallier, Circum-Pacific Council for Energy and Mineral Resources, Earth Science Series, v.2, pp.301-316.
- van der Plujim, B.A. (1986). Geology of eastern New World Island, Newfoundland an accretionary terrane in the northeastern Appalachians. Geological Society of America Bulletin, v.97, pp.932-945.
- van der Plujim, B.A., Karlstrom, K.E. and Williams, P. (1987) Fossil evidence for fault-derived stratigraphic repetition in the northeastern Newfoundland Appalachians. Canadian Journal of Earth Sciences, v.24, pp.2337-2350
- van Staal, C.R. and de Roo, J.A. (1993). Post-Ordovician structural history of the Central Mobile Belt of the northern Appalachians: Silurian collision, Salinic uplift, Early Devonian extensional collapse and the Acadian Orogeny. *in press*
- Verma, S.P. (1992). Seawater alteration effects on REE, K, Rb, Cs, Sr, U, Th, Pb and Sr-Nd-Pb isotope systematics of Mid-Ocean Ridge Basalt. Geochemical Journal, v.26, pp.159-177.
- Vocke, R.D., Hanson, G.N., and Grunefelder, M. (1987). Rare earth element mobility in the Rofna Gneiss, Switzerland. Contributions to Mineralogy and Petrology, v.95, pp.145-154.
- Voggenreiter, W., Hotzl, H. and Mechie, J. (1988). Low-angle detachment origin for the Red Sea Rift System? Tectonophysics, v.150, pp.51-75
- Volpe, A.M., Macdougall, J.D. and Hawkins, J.W. (1988). Lau Basin basalts (LBB): trace element and Sr-Nd isotope evidence for heterogeneity in back arc basin mantle. Earth and Planetary Science Letters, v 90, pp 174-186
- Vukadinovic, D. and Nicholls, I. A. (1989). The petrogenesis of island arc basalts from Gunung Slamet volcano, Indonesia: trace element and $87\text{Sr} / 86\text{Sr}$ constraints. Geochimica et Cosmochimica Acta, v.53, pp.2349-2363.

- Wang, P. and Glover III, L. (1992). A tectonic test of the most commonly used geochemical discriminant diagrams and patterns. *Earth-Science Reviews*, v.33, pp 111-131
- Watkinson, A J (1981). Patterns of fold interference: influence of early fold shapes. *Journal of Structural Geology*, v.3, pp.19-23.
- Watson, B.E. and Zindler, A. (1987). Preliminary results on the metasomatic transport potential of fluids produced by devolatilization of metabasalts. *EOS*, v.68, p.1543.
- Weaver, S.D., Saunders, A.D., Pankhurst, R.J. and Tarney, J. (1979). A geochemical study of magmatism associated with the initial stages of back-arc spreading. *Contribution to Mineralogy and Petrology*, v.68, pp.151-169.
- Weaver, B.L. and Tarney, J. (1981). Lewisian gneiss geochemistry and Archean crustal development models. *Earth and Planetary Science Letters*, v.55, pp.171-180.
- Wessel, J.M. (1975). Sedimentary petrology of the Springdale and Botwood formations, Central Mobile Belt, Newfoundland, Canada. Unpublished Ph.D. thesis, University of Massachusetts, 216p.
- Whalen, J.B. (1986). Geochemistry of the mafic and volcanic components of the Topsails igneous suite, western Newfoundland. *in* Current Research, Geological Survey of Canada, Paper 86-1B, pp.121-130.
- Whalen, J.B. (1989). The Topsails igneous suite, western Newfoundland: an Early Silurian subduction-related magmatic suite?. *Canadian Journal of Earth Sciences*, v.26, pp.2421-2434.
- Whalen, J.B., Currie, K.L. and van Breemen, O. (1987). Episodic Ordovician-Silurian plutonism in the Topsails igneous terrane, western Newfoundland. *Transactions of the Royal Society of Edinburgh*, v.78, pp.17-28.
- Williams, H. (1962) Botwood Map Area (west half). Geological Survey of Canada, Paper 62-9.

- Williams, H. (1964). The Appalachians in Newfoundland - a two-sided symmetrical system. *American Journal of Science*, v.262, pp.1137-1158.
- Williams, H. (1979). Appalachian Orogen in Canada. *Canadian Journal of Earth Sciences*, v.16, pp.792-807.
- Williams, H., Dallmayer, R.D. and Wanless, R.D. (1976). Geochronology of the Twillingate Granite and Herring Neck Group, Notre Dame Bay, Newfoundland. *Canadian Journal of Earth Sciences*, v.13, pp.1591-1601.=
- Williams, H., Colman-Sadd, S.P. and Swinden, H.S. (1988) Tectonic-stratigraphic subdivisions of Central Newfoundland. *in* Current Research, Part B, Geological Survey of Canada, Paper 88-1B, pp.91-98.
- Williams, H. and Hiscott, R.N. (1987). Definition of Iapetus rift-drift transition in western Newfoundland. *Geology*, v.15, pp.1044-1047.
- Williams, H. and St.-Julien, P. (1982). The Baie Verte - Brompton Line early Paleozoic continental ocean interface in the Canadian Appalachians. *in* St-Julien, P. and Beland, J. (editors), Major structural zones and faults of the northern Appalachians, Geological Association of Canada, Special Paper 24, pp.177-207
- Williams, H. and Stevens, R.K. (1974). The ancient continental margin of Eastern North America. *in* Burk, C.A. and Drake, C.L. (editors), The geology of continental margins, Springer-Verlag, New York, pp.781-796.
- Williams, S.H. (1988). Middle Ordovician graptolites from Central Newfoundland. *in* Current Research, Newfoundland Department of Mines, Mineral Development Division, Report 88-1, pp.183-188.
- Williams, S.H. (1989). New graptolite discoveries from the Ordovician of central Newfoundland. *in* Current Research, Newfoundland Department of Mines, Geological Survey of Newfoundland, Report 89-1, pp.149-157.

- Williams, S.H. (1989). Stratigraphy and graptolites of the Upper Ordovician Point Leamington Formation, central Newfoundland. *Canadian Journal of Earth Sciences*, v.28, pp.581-600.
- Williams, S.H. (1992). Lower Ordovician (Arenig-Lanvirn) graptolites from the Notre Dame Subzone, central Newfoundland. *Canadian Journal of Earth Sciences*, v.29, pp.1717-1733.
- Williams, S.H., Colman-Sadd, S., O'Brien, B.H. and Boyce, W.D. (1991). New discoveries of Ordovician (Arenig) and Silurian (Llandovery) graptolites from central Newfoundland, and their paleogeographic implications. *Geological Association of Canada, Program with Abstracts*, v.16, p.A132.
- Williams, S.H. and Stevens, R.K. (1988). Early Ordovician (Arenig) graptolites of the Cow Head Group, western Newfoundland, Canada. *Palaeontograph Can* 5.
- Williams, P.F., Elliot, C.G. and Lafrance, B. (1988). Structural geology and meinges of eastern Notre Dame Bay, Newfoundland - field trip guidbook. *Geological Association of Canada - Mineralogical Association of Canada - Canadian Society of Petroleum Geologists*, 60p.
- Wilson, J.T. (1966). Did the Atlantic close and then re-open?. *Nature*, v.211, pp.676-681.
- Wilson, M. (1989). *Igneous Petrogenesis*. Unwin Hyman, London, 466 p.
- Winchester, J.A. and Floyd, P.A. (1976). Geochemical magma type discrimination: application to altered and metamorphosed basic igneous rocks. *Earth and Planetary Science Letters*, v.28, pp.459-469.
- Winchester, J.A. and Floyd, P.A. (1977). Geochemical discrimination of different magma series and their differentiation products using immobile elements. *Chemical Geology*, v.20, pp.325-343.

- Wood, D.A. (1978). Major and trace element variations in the Tertiary lavas of Eastern Iceland and their significance with respect to the Iceland Geochemical Anomaly. *Journal of Petrology*, v. 19, pp.393-436.
- Wood, D.A. (1980). The application of a Th-Hf-Ta diagram to problems of tectonomagmatic classification and to establishing the nature of crustal contamination of basaltic lavas of the British Tertiary volcanic province. *Earth and Planetary Science Letters*, v.50, pp. 11-30.
- Wood, D.A., Joron, J.-L. and Treuil, M. (1979a). A re-appraisal of the use of trace elements to classify and discriminate between magma series erupted in different tectonic settings. *Earth and Planetary Science Letters*, v.45, pp.326-336.
- Wood, D.A., Joron, J.-L., Treuil, M., Norry, M. and Tarney, J. (1979b). Elemental and Sr isotope variations in basic lavas from Iceland and the surrounding ocean floor. The nature of mantle source heterogeneities. *Contribution to Mineralogy and Petrology*, v.70, pp.319-339.
- Woodcock, N.H. and Fischer, M. (1986). Strike-slip duplexes. *Journal of Structural Geology*, v.8, pp.725-735.
- Woodhead, J.D. (1988). The origin of geochemical variations in Mariana lavas: a general model for petrogenesis in intra-oceanic island arcs? *Journal of Petrology*, v. 29, pp.805-830.
- Woodhead, J.D. (1989). Geochemistry of the Mariana arc (western Pacific): source composition and processes. *Chemical Geology*, v 76, pp 1-24

APPENDIX A

Conodont Fauna From Locations On Long Island, Cutwell Group

CL-13-04: polymictic debris flow in North Beaumont; Upper Arenig - Upper Llanvirn.

Parapaltodus flexuosus (Barnes and Poplawski)

Walliserodus nakholmensis (Hamar)

Drepanoistodus sp.

Parapanderodus arcuatus Stouge

Periodon aculeatus Hadding

Protoprioniodus cf. *P. simplissimus* (McTavish)

Inarticulate brachiopods

CL-19-09g: lenses/clasts of limestone in cherty shale - Lower Llanvirn graptolites found by Henry Williams (1988, 1989); Upper Arenig-Llandeilo.

Periodon aculeatus Hadding

CL-13-19: limestone breccia in the ditch, south of the Lushes Bight-Beaumont road, and jct. to the picnic area; E. suecicus zone - Upper Llanvirn.

Ansella jemtlandica (Lofgren)

Histiodella kristinae Stouge

Periodon aculeatus Hadding

Protopanderodus costatus n. sp.

CL-13-22 (a, b): quarries south of the Lushes Bight-Beaumont road; Upper Arenig - Lower E. Suecicus Zone (Llanvirn).

Ansella jemtlandica (Lofgren)

Ansella sinuosa Stouge

Baltoniodus? prevarabilis medius (Dzik)

Cordyloclus? horridus Barnes and Poplawski

Drepanoistodus? cf. *D. venustus* (Stauffer)
Drepanoistodus tablepointensis Stouge
Histiodella holodentata Ethington and Clark
Histiodella kristinae Stouge
Periodon aculeatus Hadding
Protopanderodus cf. *P. varicostatus* (Sweet and Bergstrom)
Parapaltodus flexuosus (Barnes and Poplawski)
Polonodus n. sp.
Spinodus cf. *S. spinatus* (Hadding)
Walliserodus ethingtoni (Fahraeus)
Inarticulate brachiopods

CL-13-24: bioclastic limestone across the road from the CL-13-22 (quarry); Upper Arenig-Llandeilo

Ansella nevadensis (Ethington and Schumacher)
Cahabagnathus friendsvillensis Bergstrom
Cordylodus? *horridus* Barnes and Poplawski
Drepanoistodus cf. *D. bellburnensis* Stouge
Periodon aculeatus Hadding
Protoprioniodus sp.
Protopanderodus costatus n. sp.
Protopanderodus cutwellensis n. sp.
Ptiloncodon simplex Harris
Spinodus cf. *S. spinatus* (Hadding)

CI-13-24a: Llanvirn - E. suecicus Zone., northern bed of the limestone breccia, in Lushes Bight, near point CI-13-24d.

Ansella sinuosus Stouge
Baltoniodus? *prevariabilis medius* (Dzik)
?Coleodus sp. Barnes and Poplawski

Drepanoistodus tablepointensis Stouge

P.? *tablepointensis* Stouge

Periodon aculeatus Hadding

Polonodus? *clivus* (Viira)

Protoprioniodus tablepointensis (Stouge)

CL-13-24d: limestone clasts in reworked mafic, plagioclase-phyric tuff; Llanvirn

Eoplacognathus suecicus Bergstrom

Periodon aculeatus Hadding

Protopanderodus spp.

Protoprioniodus cf. *P. simplissimus* (McTavish)

CL-13-24g: lens of crinoid-rich bioclastic limestone, east of Lushes Bight; Upper Llanvirn

Ansella nevadensis (Ethington and Schumacher)

Periodon aculeatus Hadding

Protopanderodus costatus n. sp.

Protopanderodus cf. *P. giganteus* (Sweet and Bergstrom)

Protoprioniodus tablepointensis (Stouge)

Polonodus sp.

CL-13-25: road cut on the ferry road, just south of Lushes Bight, limestone breccia overlying cherty shale and graptolite shale. Middle Arenig-Llanvirn

Ansella jemtlandica (Lofgren)

?*Coleodus* sp. Barnes and Poplawski

Cordylodus? *horridus* Barnes and Poplawski

Juanognathus serpaglii Stouge

Fahraeusodus marathonensis (Bradshaw) - Arenig

Parapanderodus arcuatus Stouge

Polonodus? *clivus* (Viira)

Protopanderodus cf. *P. varicostatus* (Sweet and Bergstrom)

Protoprioniodus simplissimus McTavish - Arenig

Ptiloncodus simplex Harris

Spinodus cf *S. spinatus* (Hadding)

Sample Locations:

CI-13-04	5497075N	594950E
CI-13-09g	5495975N	591975E
CI-13-19	5494600N	594125E
CI-13-22(a,b)	5494175N	593255E
CI-13-24	5494350N	593175E
CI-13-24a	5494200N	592675E
CI-13-24d	5494025N	592600E
CI-13-24g	5493725N	593100E
CI-13-25	5493400N	592800E

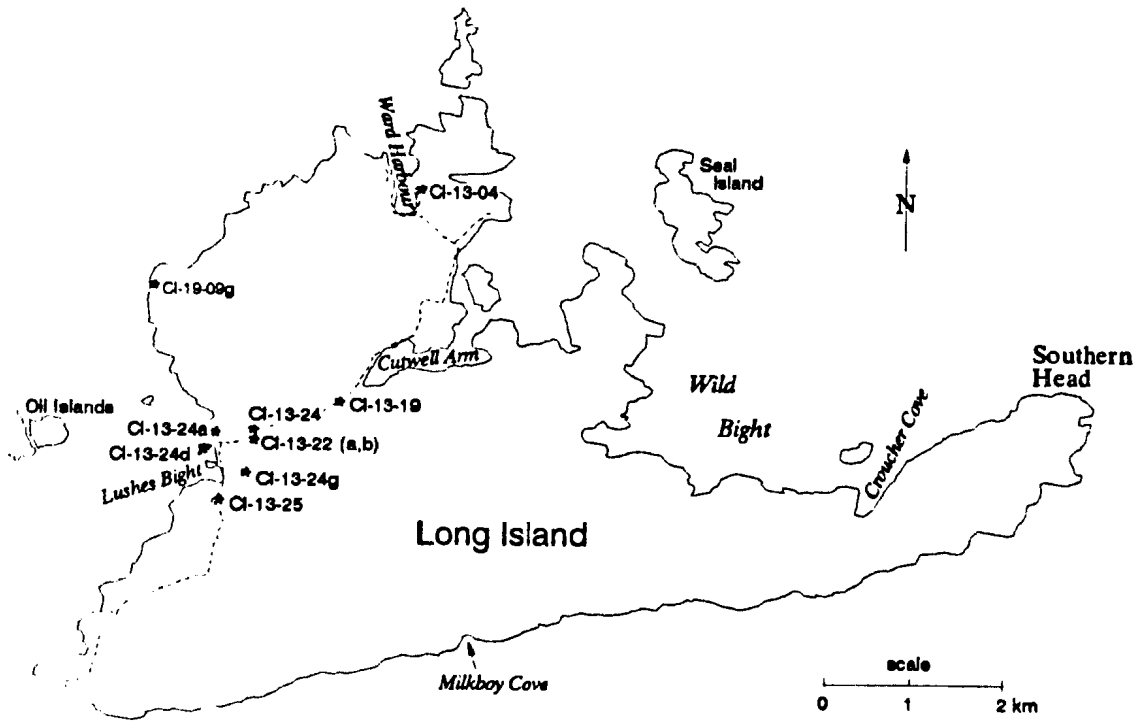


Figure A-i. Location of faunal occurrences.

APPENDIX B - Geochronology

Table 1 - Argon Data

TEMP	36AR	37AR	38AR	39AR	40AR	% Atmos	APPARENT AGE	39AR	
(°C)	(x10-9 cc STP)						40Ar	+/- 2s	(%)

88-PIG (202) (78.73 mg)(wt.% K2O = 0.081) AGE (total) = 477.2 +/- 7.14 Ma

700	.124	3.729	.111	.131	42.17	87.0	460.9	48.4	5.1
800	.061	3.136	.044	.067	22.05	82.2	614.9	188.4	2.6
1000	.061	44.829	2.086	.808	52.15	34.4	463.0	5.2	31.6
1030	.010	21.123	1.103	.258	14.06	20.9	470.3	9.0	10.1
1060	.004	8.193	.342	.115	6.24	20.0	473.2	12.2	4.5
1100	.004	5.839	.222	.091	5.12	20.4	486.7	20.3	3.6
1175	.007	11.051	.434	.157	8.97	22.0	483.8	18.0	6.1
1300	.019	37.476	1.342	.596	32.27	17.0	487.8	6.8	23.3
1550	.030	31.089	.926	.336	23.54	38.3	471.7	11.8	13.1
Total	.32	6.61	166.47	2.56	206.6	45.7	477.2	7.1	
(CC/g)	4.1	2114.39	83.96	32.49	2623.7				

88-LR-CLT (203) (90.4 mg)(wt.% K2O = 0.058) AGE (total) = 495 +/- 12 Ma

700	.043	4.021	.080	.029	14.29	88.0	626.4	666.3	1.4
800	.014	2.896	.023	.016	5.02	83.4	556.3	363.9	.8
1000	.033	36.897	.959	.421	28.14	35.1	479.6	7.7	19.8
1060	.013	49.278	1.445	.561	29.56	13.4	500.6	6.3	26.4
1080	.004	9.211	.259	.113	5.92	17.9	474.0	23.1	5.3
1100	.013	4.882	.136	.062	6.51	60.1	464.2	55.9	2.9
1175	.004	12.243	.340	.156	7.78	13.4	476.2	19.1	7.4
1300	.005	33.788	.987	.392	20.32	7.7	521.1	5.4	18.5
1550	.009	31.857	.929	.371	19.00	14.6	482.2	22.6	17.5
Total	.14	5.16	185.07	2.12	136.5	30.0	495.0	11.7	
(CC/g)	1.5	2047.26	57.06	23.47	1510.2				

85-AC-80-D223 (207) (92.32 mg)(wt.% K2O = 0.161) AGE (total) = 502 +/- 7.6 Ma

700	.041	.497	.140	.024	22.82	53.0	2541.8	405.2	.4
800	.015	.391	.037	.013	7.91	56.9	1918.4	912.0	.2
1000	.013	14.726	1.906	.436	25.67	15.1	540.9	8.2	7.2
1060	.016	74.767	10.480	2.503	113.94	4.2	480.5	1.0	41.3
1100	.005	19.515	2.558	.592	26.65	5.8	469.1	4.0	9.8
1175	.007	18.076	2.561	.623	28.59	7.7	468.1	12.3	10.3
1300	.007	43.720	6.017	1.449	65.01	3.1	479.3	1.3	23.9
1550	.005	14.734	1.704	.416	19.47	7.3	478.1	13.2	6.9
Total	.11	25.40	186.43	6.06	310.1	10.5	502.0	7.6	
(CC/g)	1.2	2019.36	275.16	65.60	3358.5				

RAL-88-1 (208) (87.82 mg)(wt.% K2O = 0.840) AGE (total) = 475 +/- 2.6 Ma

800	.110	2.379	.127	.158	38.13	84.9	409.4	79.2	.5
1000	.026	10.30	.109	.303	20.13	38.4	453.9	6.5	1.0
1080	.015	22.928	1.267	3.710	164.90	2.6	477.4	1.2	12.3
1100	.012	28.500	1.647	4.949	215.61	1.6	473.3	.6	16.5
1110	.010	29.545	1.676	5.150	224.28	1.3	474.5	.5	17.1
1120	.005	23.620	1.309	4.108	178.56	.9	475.5	1.1	13.7
1140	.004	21.632	1.155	3.629	158.01	.8	476.6	1.4	12.1
1210	.011	24.237	1.289	3.814	167.81	1.9	476.3	1.2	12.7
1300	.007	12.107	.645	1.916	85.09	2.6	477.3	.6	6.4
1550	.018	14.380	.778	2.310	105.10	5.1	476.3	.6	7.7
Total	.22	10.00	189.63	30.05	1357.6	4.7	475.1	2.6	
(CC/g)	2.5	2159.27	113.89	342.17	15459.1				

88-CL16-2b (210) (79.33 mg)(wt.% K2O = 0.215) AGE (total) = 507 +/- 3.5 Ma

700	.084	2.592	.175	.154	35.82	69.6	728.1	51.8	2.2
800	.048	1.478	.102	.117	22.17	63.7	712.0	36.7	1.7
1000	.042	6.731	.272	.588	39.66	31.4	506.6	6.8	8.4
1030	.002	2.747	.101	.135	7.01	9.5	512.9	52.2	1.9
1060	.003	3.800	.122	.166	8.25	12.0	483.2	10.6	2.4
1080	.002	5.107	.131	.211	10.32	5.7	506.2	10.4	3.0
1100	.004	5.329	.132	.215	10.92	11.8	492.9	14.2	3.1
1130	.035	45.512	1.075	1.813	92.58	11.2	497.8	2.0	26.0
1175	.011	20.845	.479	.827	39.61	8.5	483.4	4.3	11.9
1300	.042	60.349	1.524	2.417	122.79	10.2	500.4	2.2	34.7
1550	.016	8.198	.205	.324	19.30	24.3	495.4	14.6	4.7
Total	.29	4.32	162.69	6.97	408.4	21.0	506.9	3.5	
(CC/g)	3.7	2050.80	54.45	87.81	5148.				

88-LR-INT (211) (73.6 mg)(wt.% K₂O = 0.059) AGE (total) = 535 +/- 23 Ma

700	.094	1.431	.074	.031	29.51	93.7	628.5	1133.1	1.8
800	.025	.747	.020	.022	9.33	78.2	895.1	493.7	1.3
1000	.045	22.261	.569	.268	27.97	47.8	578.9	17.6	15.3
1030	.012	22.933	.771	.274	16.78	21.3	521.9	10.0	15.6
1060	.004	13.721	.483	.147	8.39	14.2	528.1	23.6	8.4
1100	.005	11.140	.432	.121	7.44	20.4	528.9	15.3	6.9
1175	.005	10.616	.372	.127	7.21	18.6	503.4	19.9	7.2
1300	.008	22.408	.815	.251	14.37	15.9	520.3	18.4	14.4
1550	.022	45.371	1.654	.510	30.78	21.3	515.0	8.3	29.1
Total	.22	5.19	150.63	1.75	151.8	42.7	535.3	23.2	
(CC/g)	3.0	2046.57	70.51	23.78	2062.3				

RAL-88-2 (55.57 mg)(wt. % K₂O = 0.98) AGE (total) = 473 +/- 2.2 Ma

700	.011	1.039	.057	.077	4.70	69.4	377.2	52.2	.2
800	.004	.41	.024	.041	2.74	47.0	657.1	97.9	.1
900	.007	.530	.019	.072	2.91	68.9	262.1	113.9	.2
950	.002	.335	.006	.047	2.55	46.7	360.7	171.5	.1
1000	.002	.848	.017	.061	2.30	28.8	525.6	71.0	.2
1020	.003	1.381	.050	.196	5.44	14.0	469.7	15.0	.5
1030	.002	2.394	.107	.407	10.9	4.9	496.8	10.0	1.0
1040	.000	2.094	.096	.360	9.24	1.1	496.2	8.8	.9
1050	.001	1.792	.084	.337	8.60	3.9	481.9	12.6	.9
1060	.000	2.004	.093	.364	9.06	0.0	488.7	15.1	.9
1070	.003	2.249	.099	.396	10.40	9.1	471.3	6.6	1.0
1080	.001	3.068	.135	.550	13.49	2.4	471.9	5.5	1.4
1090	.002	4.390	.189	.796	19.44	3.3	466.5	4.3	2.0
1100	.001	8.945	.386	1.616	39.46	1.0	476.2	9.7	4.1
1110	.002	11.774	.499	2.128	51.63	1.2	472.4	1.4	5.4
1120	.005	21.010	.864	3.816	92.98	1.7	472.1	1.3	9.7
1130	.003	22.529	.903	4.091	99.07	1.0	472.4	1.0	10.4
1140	.005	30.156	1.186	5.492	132.7	1.1	471.0	.8	13.9
1150	.004	26.817	1.038	4.899	118.1	1.1	470.5	.8	12.4
1160	.000	12.480	.479	2.281	55.14	.1	475.8	3.8	5.8
1170	.002	6.730	.274	1.225	29.86	2.5	468.9	6.5	3.1
1210	.005	19.121	.786	3.460	84.39	1.7	472.5	1.0	8.8
1250	.004	13.420	.567	2.439	59.28	1.8	470.7	1.4	6.2
1300	.002	7.145	.287	1.299	31.99	1.5	477.2	4.6	3.3
1350	.002	7.244	.295	1.313	32.29	2.1	474.4	1.6	3.3
1450	.014	7.718	.316	1.394	37.52	11.2	471.4	3.0	3.5
1550	.022	1.200	.050	.223	12.50	52.8	515.7	18.8	.6
Total	.1	8.90	218.83	39.38	977.7	3.4	472.7	2.2	
(CC/g)	2.0	3937.90	160.24	708.68	17593.2				

RAI-88-3 (51.99 mg)(wt. % K₂O = 0.76) AGE (total) = 473 +/- 2.4 Ma

700	029	3.837	.131	.150	9.72	89.3	149.1	103.3	.5
800	014	2.734	.069	.067	4.69	89.7	155.5	115.9	.2
900	006	2.895	.030	.047	2.25	82.0	131.9	80.5	.2
1000	004	3.464	.065	.123	4.06	27.6	468.2	45.2	.4
1020	002	1.863	.055	.105	3.25	18.8	489.5	40.9	.4
1040	003	2.639	.132	.286	8.43	11.5	505.2	14.4	1.0
1060	004	5.536	.309	.667	17.54	6.9	478.3	11.9	2.3
1080	002	7.768	.456	.982	24.54	3.0	474.2	2.7	3.4
1100	001	17.666	1.092	2.502	61.41	.5	477.4	5.3	8.8
1110	001	10.699	.681	1.702	41.70	.6	476.0	8.2	6.0
1120	002	12.748	.825	2.117	52.29	1.3	476.6	2.6	7.4
1130	001	13.312	.856	2.264	55.19	.6	473.9	2.9	7.9
1140	002	16.065	1.013	2.731	66.35	1.0	470.9	2.0	9.6
1150	000	14.275	.896	2.423	58.93	.2	474.8	2.9	8.5
1160	000	8.960	.559	1.475	36.03	.4	475.6	2.2	5.2
1170	001	5.453	.340	.859	21.04	1.1	473.7	3.6	3.0
1190	001	8.568	.538	1.340	32.9	1.1	475.8	11.1	4.7
1210	001	9.256	.587	1.462	36.29	.5	481.8	3.6	5.1
1250	003	15.464	.998	2.536	62.08	1.5	472.1	1.4	8.9
1300	003	15.263	.971	2.427	59.54	1.5	472.7	1.6	8.5
1350	001	7.207	.451	1.154	28.41	.5	478.1	3.4	4.1
1450	001	5.245	.334	.865	20.92	1.3	468.1	8.0	3.0
1550	002	1.207	.074	.207	5.88	8.2	505.4	24.0	.7
Total	.09	11.46	192.13	28.49	713.5	.6	472.6	2.4	
(C/C/g)	1.6	3695.43	220.5	548.03	13723.8				

89-ASWB-1(272)(wt. % K₂O = 0.388) AGE (total) = 475 +/- 5 Ma

700	.087	2.325	.122	.556		48.7	505.9	7.4	3.8
800	.042	.933	.106	.752		25.3	507.4	2.3	9.0
900	014	1.495	.039	1.294		6.5	470.1	2.2	17.9
1000	015	10.89	.191	1.427		6.8	437.9	4.0	27.7
1040	010	9.76	.242	.671		8.95	451.6	3.6	32.3
1080	013	23.14	.517	1.477		5.4	468.6	1.1	42.4
1080	003	.077	.003	.005		93.98	468.6	2272	42.5
1100	006	14.31	.257	.907		4.05	475.0	2.5	48.7
1120	006	18.14	.298	1.168		3.14	472.2	1.6	56.7
1140	004	8.85	.190	.554		4.63	474.5	2.3	60.5
1160	008	16.81	.365	1.054		4.46	482.2	2.0	67.8
1190	012	19.21	.418	1.23		5.83	479.8	1.5	76.2
1240	005	6.85	.150	.440		6.66	482.2	4.5	79.3
1300	016	22.83	.499	1.481		6.53	483.3	1.4	89.4
1550	029	23.73	.509	1.537		10.71	485.1	1.4	100.0
Total	.27	179.35	3.91	14.55			474.9	4.5	
(C/C/g)	2.76	1853	40.35	150.36					

89-ASWB-2 (274) (wt.% K2O = 0.395) AGE (total) = 497 +/- 6 Ma

700	.083	2.578	.220	.215	58.59	778.2	23.8	1.5
800	.070	1.629	.227	.477	41.94	611.3	9.2	4.7
900	.020	2.234	.065	1.127	10.08	491.9	1.2	12.4
1000	.025	18.677	.359	1.399	10.49	467.7	5.0	21.9
1040	.006	9.338	.262	.649	5.54	483.7	3.0	26.3
1080	.011	22.731	.601	1.730	3.88	484.6	1.2	38.1
1100	.007	16.706	.375	1.324	3.20	484.8	1.7	47.1
1120	.001	7.413	.166	.553	1.64	488.2	4.7	50.9
1140	.004	6.295	.158	.434	5.04	490.7	4.7	53.9
1140	.048	.089	.001	.007	97.56	533.6	7500	53.9
1160	.005	5.216	.131	.374	7.53	492.8	5.5	56.5
1190	.002	3.609	.095	.268	4.22	490.5	8.6	58.3
1240	.003	5.592	.158	.423	4.57	489.6	5.7	61.2
1300	.023	37.184	1.028	2.865	4.78	492.5	.7	80.7
1550	.048	36.775	.986	2.837	9.61	493.6	2.3	100
Total	.36	176.07	4.83	14.68		496.6	5.7	
(CC/g)	3.72	1838.6	50.46	153.34				

88-LR-INT (271) (wt.% K2O = 0.058) AGE (total) = 512 +/- 5 Ma

800	.060	4.552	.139	.081	76.35	675.3	75.6	3.0
1020	.044	84.859	2.632	.978	21.33	506.0	2.1	38.6
1100	.015	42.591	1.596	.445	17.22	504.9	1.6	54.9
1300	.027	68.255	2.440	.773	17.24	507.4	2.4	83.0
1550	.035	39.843	1.437	.465	31.45	506.1	4.1	100.0
Total	.18	240.1	8.24	2.74		511.5	5.2	
(CC/g)	1.50	1980.7	68.01	22.62				

88-CL-16-2b (273) (wt.% K2O = 0.207) AGE (total) = 504 +/- 5 Ma

700	.047	2.547	.214	.132	51.05	931.6	27.8	1.8
1000	.038	9.224	.412	.644	24.92	543.5	8.0	10.4
1100	.037	100.6	2.582	3.904	5.62	495.8	0.6	62.7
1115	.005	15.45	.326	.623	4.98	477.4	2.1	71.7
1130	.002	3.239	.080	.126	8.75	469.1	14.4	72.8
1175	.004	9.218	.229	.353	6.41	488.1	5.6	77.5
1225	.003	10.91	.256	.426	4.40	482.4	4.4	83.2
1275	.004	9.18	.215	.359	6.07	477.9	6.4	88.0
1350	.004	11.52	.273	.448	4.96	484.7	5.7	94.0
1550	.052	11.35	.273	.445	41.77	501.3	7.6	100.0
Total	.20	183.23	4.86	7.46		504.4	4.6	
(CC/g)	2.10	1969.6	52.24	80.20				

Western Head Fm. Nickey's Nose Tuff (wt.% K2O = 0.200) AGE (total) = 447 +/- 5 Ma

800	.059	4.018	.198	1.442	23.67	436.0	2.5	24.2
1020	.043	37.557	.730	2.163	12.87	443.5	1.8	60.6
1100	.012	36.107	.624	.949	8.81	451.2	6.5	76.5
1300	.025	57.396	1.105	1.267	12.41	462.2	2.7	97.8
1550	.068	8.654	.111	.133	79.36	443.7	66.1	100.0
Total	.21	143.53	2.77	5.95		446.9	4.5	
(CC/g)	2.86	1976.8	38.11	81.99				

Western Head Fm. (WA-44) (tuff) (wt.% K2O = 0.299) AGE (total) = 453 +/- 4 Ma

700	.023	2.721	.127	.266	39.63	444.1	31.9	2.5
800	.024	1.786	.075	.293	36.81	458.9	25.4	5.2
900	.008	7.115	.430	.763	7.71	418.9	4.9	12.3
1000	.014	54.20	3.837	2.542	3.88	441.8	2.0	36.0
1050	.015	15.31	1.055	.886	10.77	452.6	6.2	44.2
1100	.008	26.02	1.277	1.648	3.19	458.2	2.2	59.6
1300	.023	78.02	4.160	4.214	3.66	464.6	1.0	98.8
1550	.092	1.909	.124	.127	83.66	464.2	106	100.0
Total	.21	187.07	11.09	10.74		453.3	4.4	
(CC/g)	2.34	2134.3	126.47	122.52				

(WA-45) DOLLAND HEAD DIORITE (wt.% K2O = 0.159) AGE (total) = 481 +/- 7 Ma

800	.046	4.753	.148	.096	75.31	512.6	165.7	2.2
900	.004	2.759	.132	.080	24.66	497.6	22.3	4.0
1000	.010	25.343	2.951	.866	7.22	481.7	2.3	23.6
1100	.014	60.135	9.337	2.269	4.17	477.4	4.3	75.1
1150	.004	15.341	1.983	.508	5.26	472.3	5.8	86.7
1200	.002	8.287	.820	.215	6.93	474.7	21.0	91.5
1300	.005	15.897	.983	.256	12.79	474.0	12.6	97.4
1550	.097	6.816	.431	.117	82.34	568.0	119.1	100.0
Total	.18	137.33	16.78	4.41		480.9	7.1	
(CC/g)	2.71	2028.81	247.96	65.10				

TABLE 2 - U/Pb DATA

Brighton Intrusive Complex

Fraction	Wt. (mg) U (ppm) Pb* (ppm)			206Pb/204Pb	Pb (pg)	204Pb (%)	206Pb/238U	207Pb/235U	207Pb/206Pb	Apparent Age (Ma)		
	a	a	a							206/238	207/206	
<i>Zircon</i>												
Br 7-1a	0.019	142	12	1826	7	17.5	0.07673 +/- .09%	0.5978 +/- .15%	0.05651 +/- .11%	476.6	472.3 +/- 4.8	
Br 7-2a	0.021	502	43	2588	20	18.7	0.07574 +/- .09%	0.5923 +/- .12%	0.05672 +/- .07%	470.6	480.6 +/- 3.2	
Br 7-3	0.053	514	43	1749	70	22.1	0.07077 +/- .09%	0.5509 +/- .11%	0.05646 +/- .06%	440.8	470.3 +/- 2.4	
4	0.017	265	22	1326	16	55.9	0.07694 +/- .42%	0.6045 +/- .40%	0.05698 +/- .35%	477.8	490.7 +/- 15.6	
AA	0.009	313	28	1212	11	56.8	0.07640 +/- .23%	0.5971 +/- .27%	0.05668 +/- .13%	474.6	479.2 +/- 5.9	
<i>Titanite</i>												
1T	0.117	47	7	110	284	55.9	0.07633 +/- .58%	0.6012 +/- .83%	0.05712 +/- .72%	474.2	496.2 +/- 32	
2T	0.154	50	8	64	797	56.8	0.07461 +/- 1.3%	0.5968 +/- 1.3%	0.05801 +/- 1.2%	463.9	530.3 +/- 50	
3T	0.245	61	11	45	2686	59.4	0.07722 +/- 2.3%	0.6224 +/- 2.2%	0.05846 +/- 1.9%	479.5	546.9 +/- 83	
4T	0.051	56	9	44	531	55.1	0.07718 +/- 2.1%	0.6073 +/- 2.7%	0.05706 +/- 2.4%	479.3	494.0 +/- 105	

Catchers Pond Tuff 90-1-CTP

<i>Zircon</i>												
A	0.023	267	21	325	96	11.7	0.07680 +/- .15%	0.6021 +/- .49%	0.05686 +/- .40%	477.0	486.1 +/- 17.7	
B	0.042	281	22	2485	23	10.5	0.07632 +/- .13%	0.5964 +/- .19%	0.05668 +/- .14%	474.1	479.0 +/- 6.2	
C	0.028	259	20	1883	18	10.7	0.07626 +/- .09%	0.5960 +/- .16%	0.05668 +/- .12%	473.8	479.1 +/- 5.3	
D	0.015	242	19	832	21	11.6	0.07624 +/- .10%	0.5953 +/- .30%	0.05663 +/- .25%	473.6	477.2 +/- 11.1	

Colchester-Coopers Cove Plutonics 90-2-C

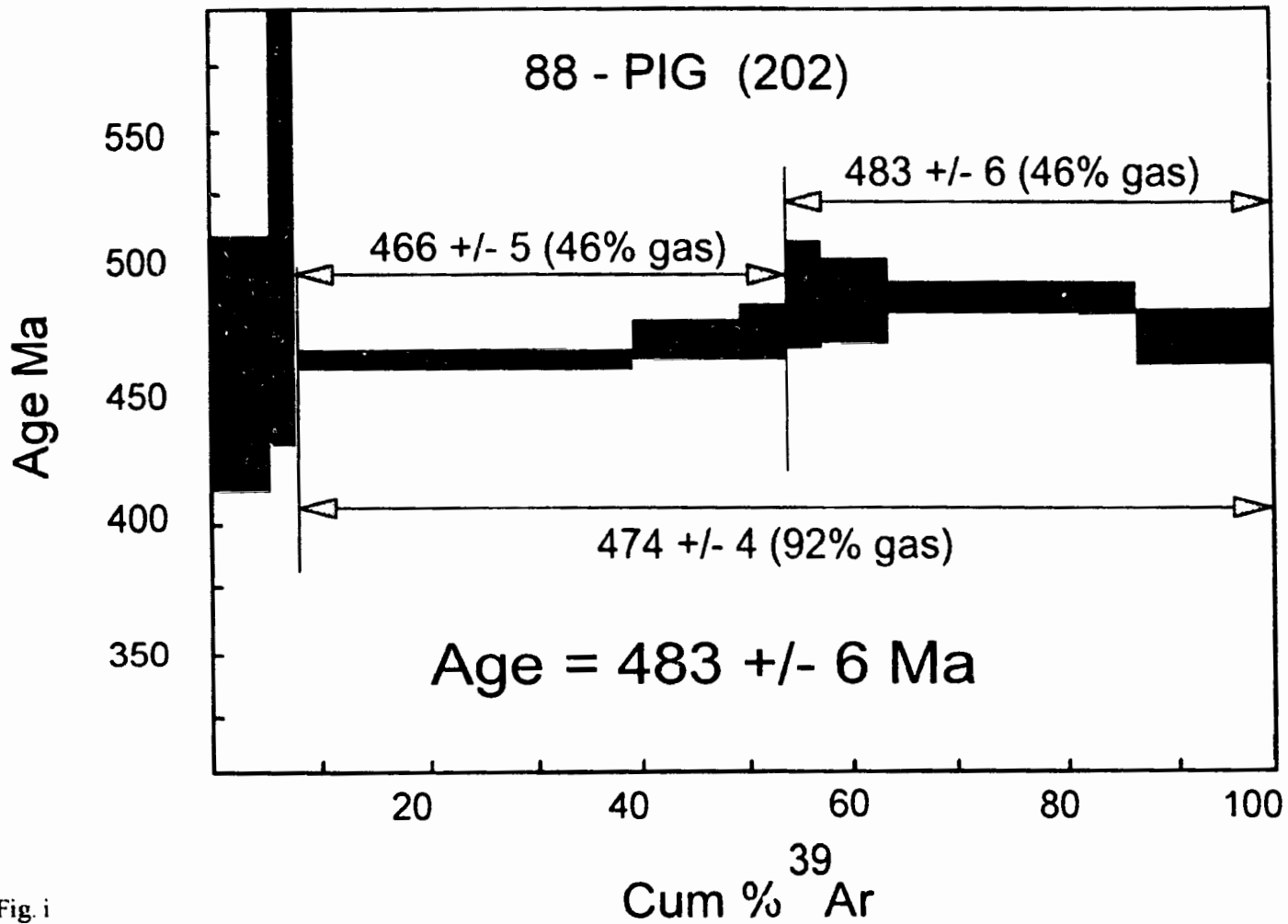
<i>Zircon</i>												
A	0.001	1416	116	552	17	17.6	0.07447 +/- .11%	0.5789 +/- .40%	0.05638 +/- .34%	463.0	467.5 +/- 15.1	
B	0.006	653	54	429	44	18.4	0.07357 +/- .14%	0.5715 +/- .43%	0.05635 +/- .36%	457.6	466.0 +/- 16.0	
C	0.008	702	57	1263	21	16.2	0.07436 +/- .10%	0.5770 +/- .21%	0.05628 +/- .16%	462.4	463.3 +/- 7.1	
D	0.026	620	50	3438	22	15.8	0.07420 +/- .09%	0.5764 +/- .12%	0.05634 +/- .06%	461.4	465.8 +/- 2.8	

Errors are 1 std. error of mean in % except 207/206 age errors which are 2 std. errors in Ma

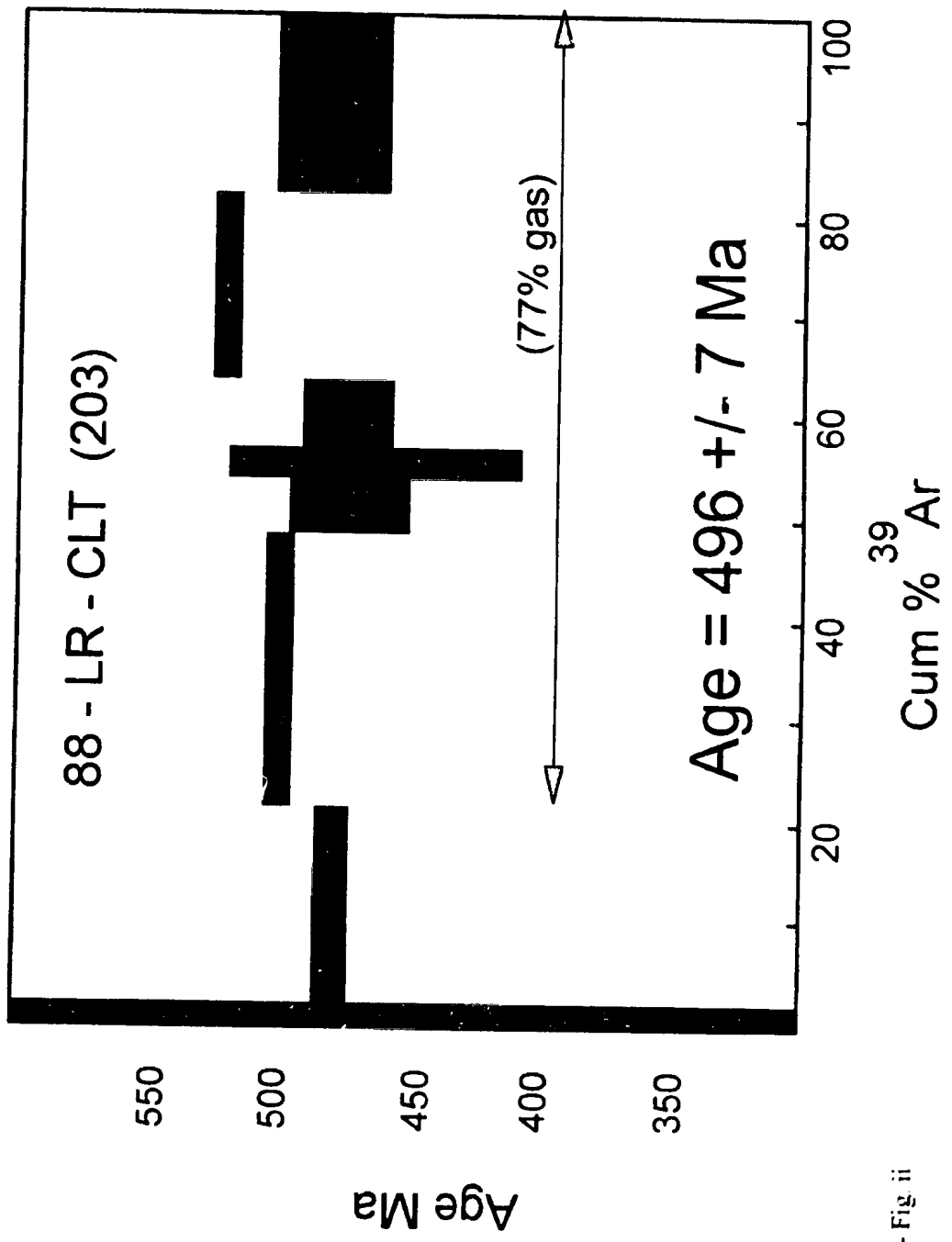
* = Radiogenic Pb

a = include sample weight error of +/- 0.001 mg in concentration uncertainty

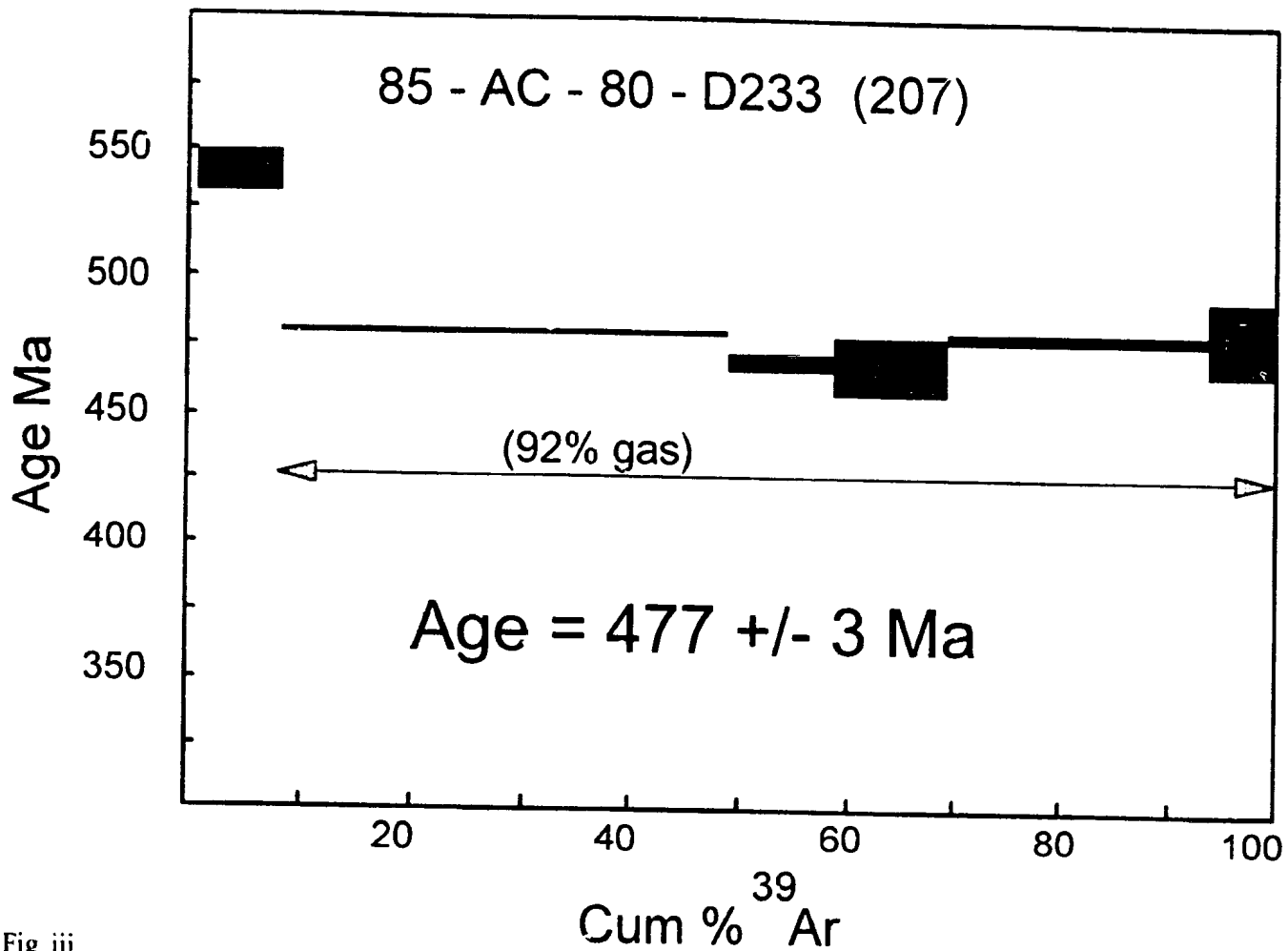
c = total common Pb in analysis



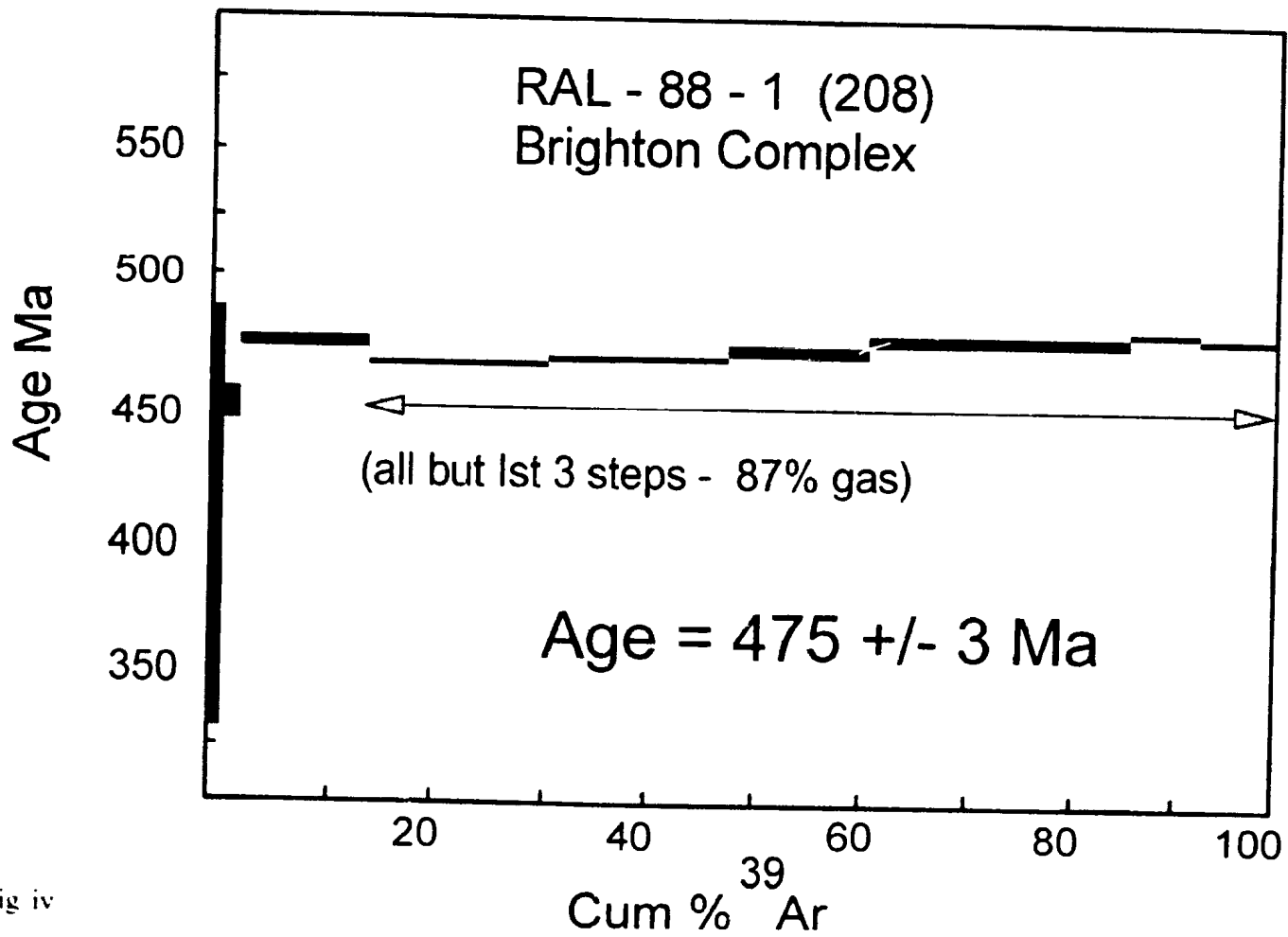
B - Fig. i



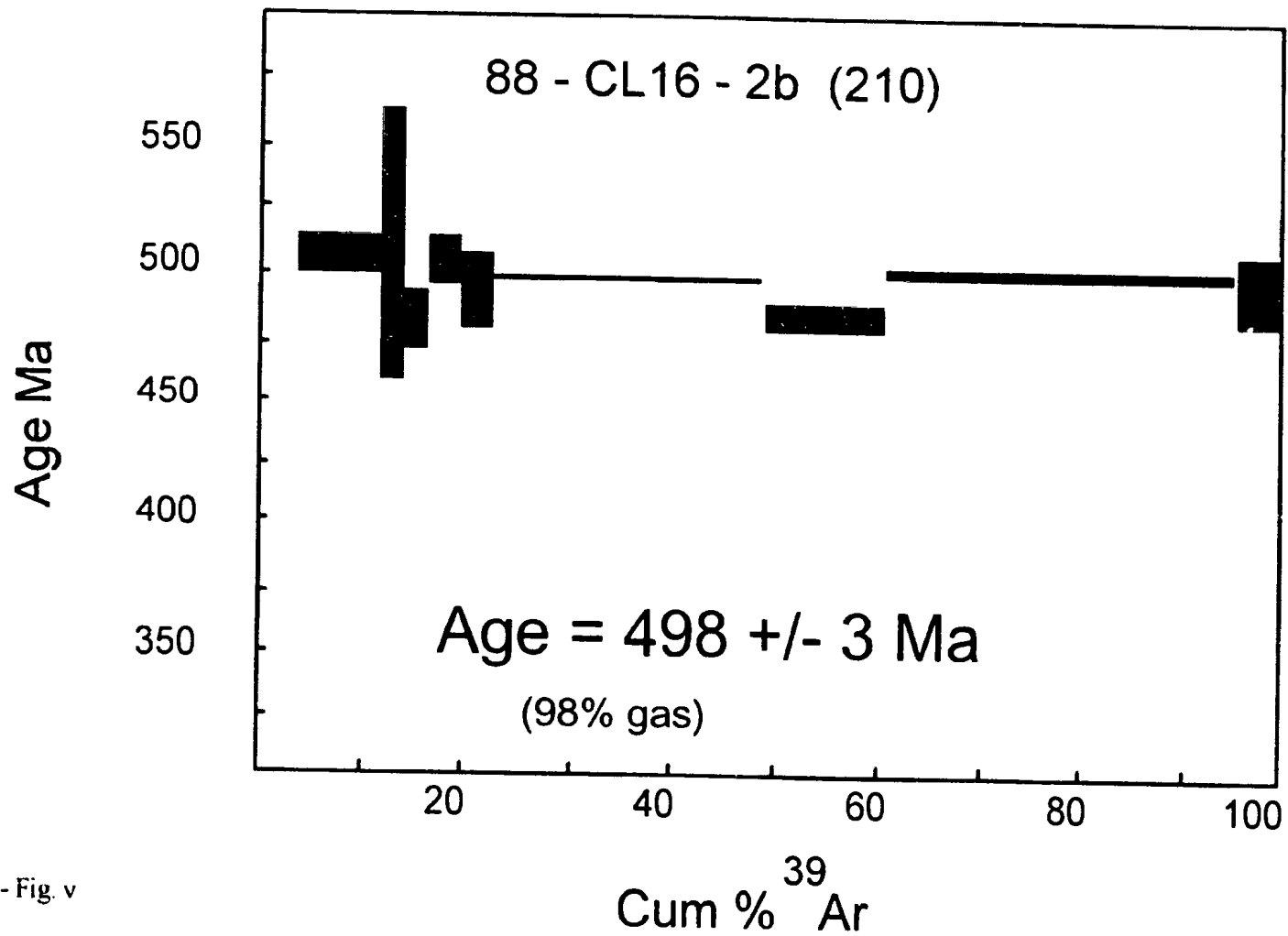
B - Fig. ii



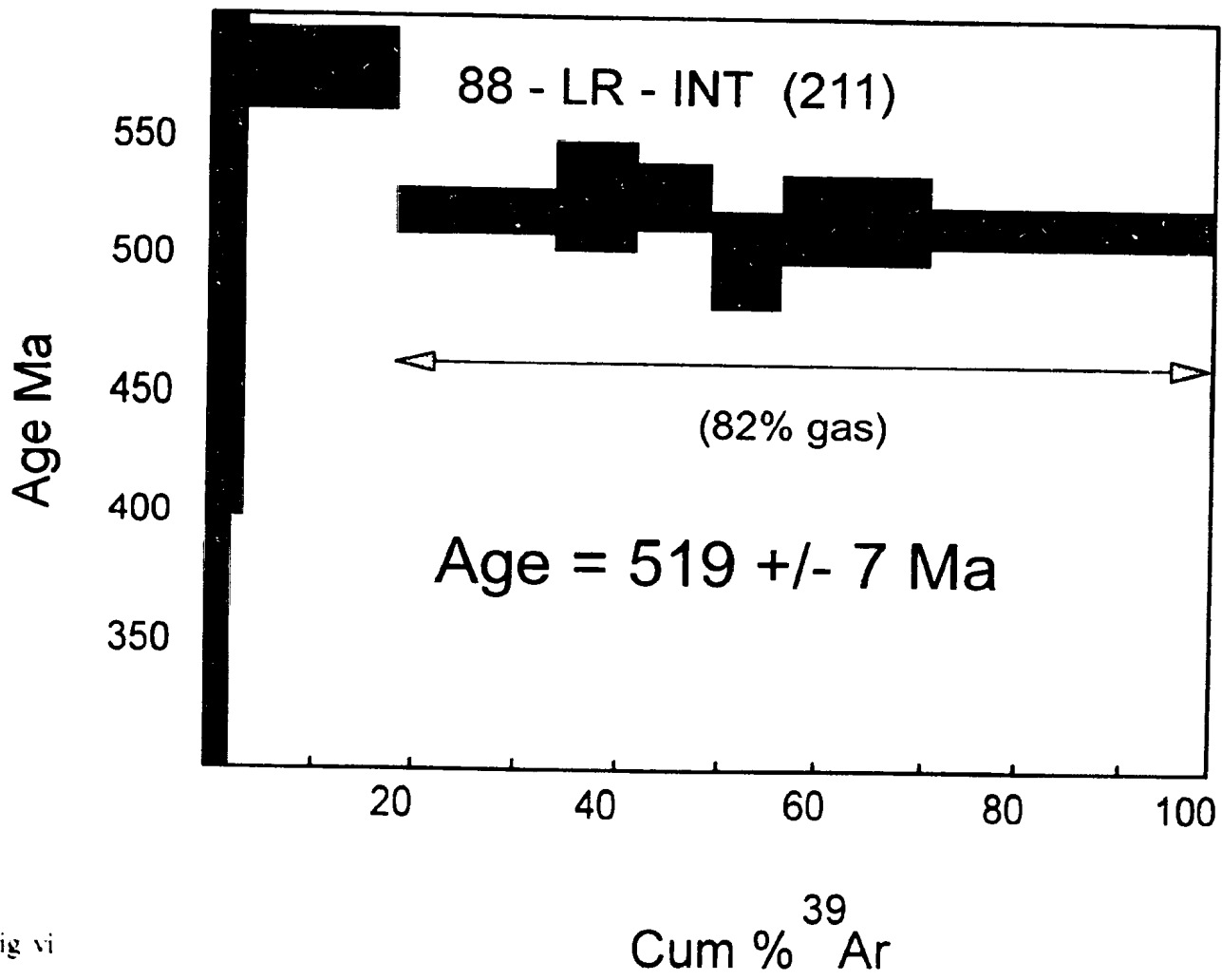
B - Fig. iii



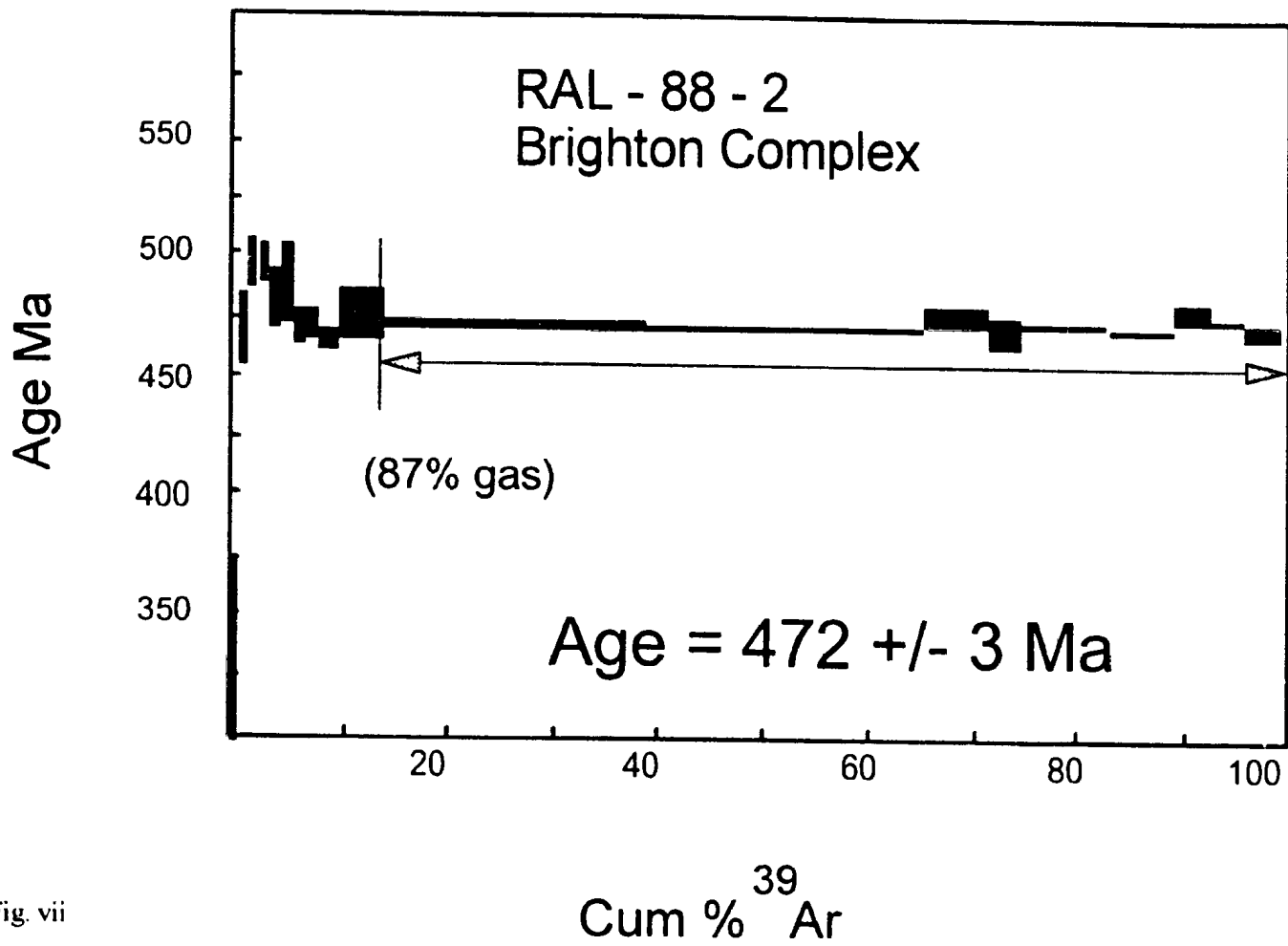
B - Fig iv



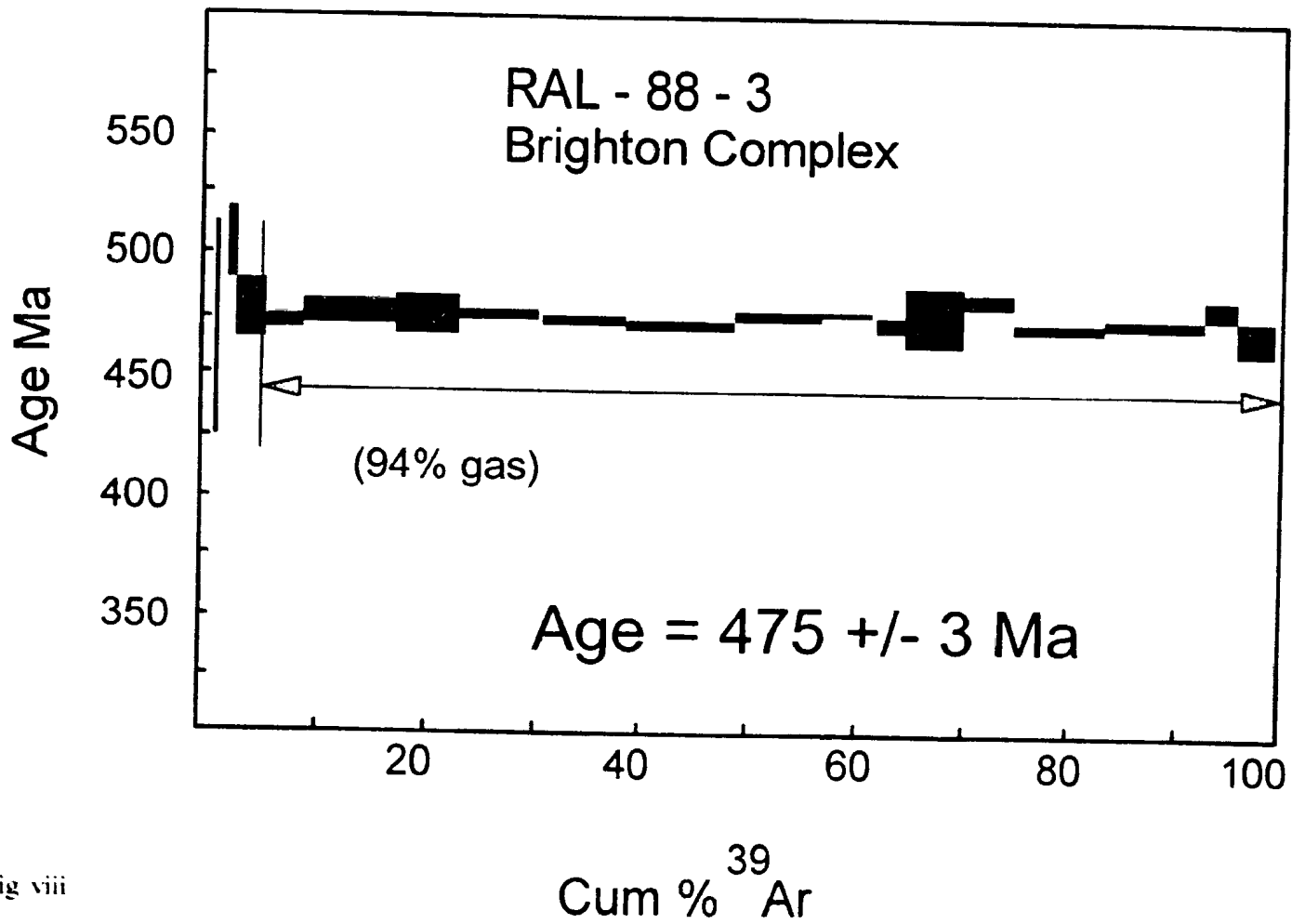
B - Fig. v



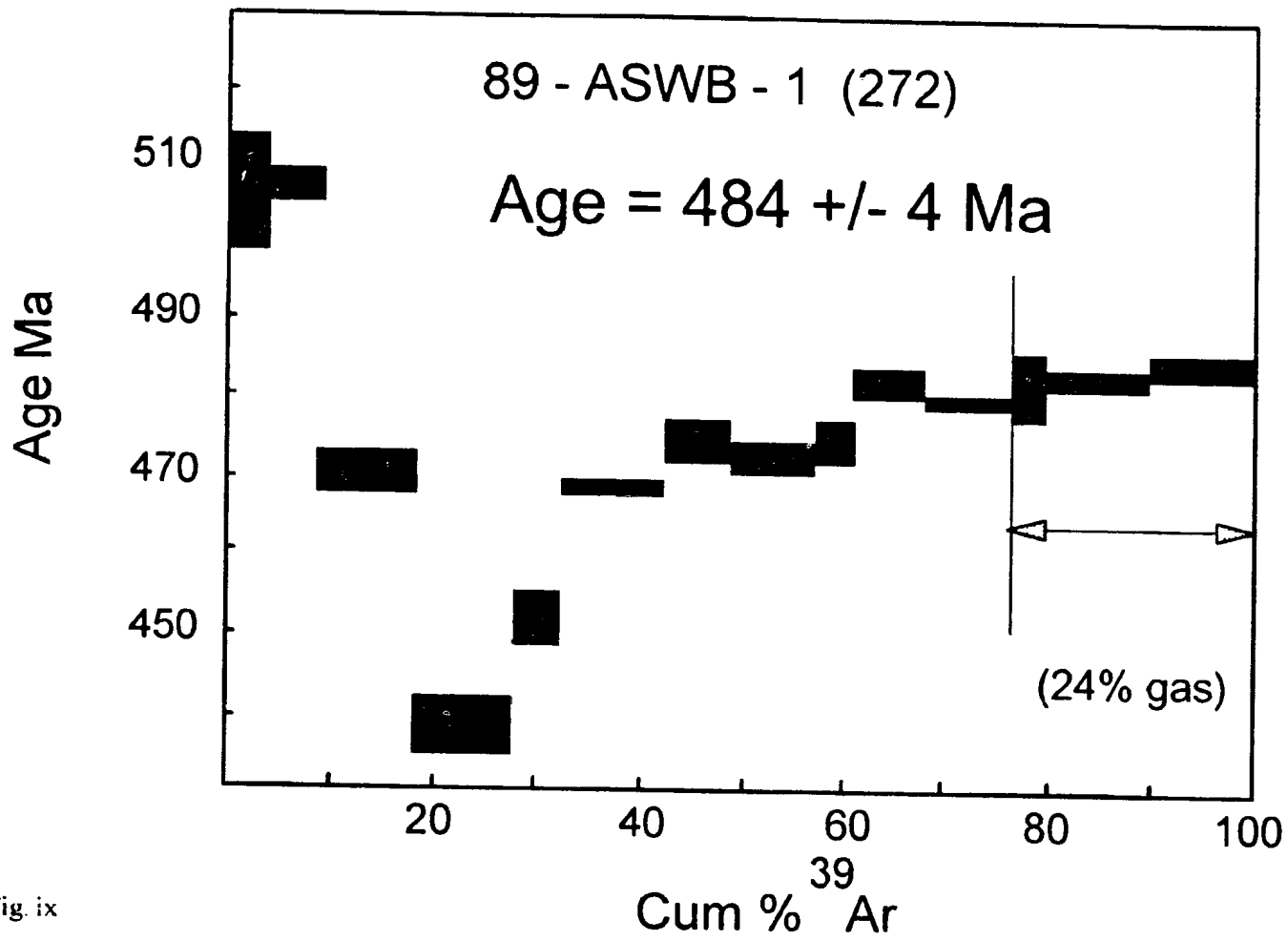
B - Fig vi



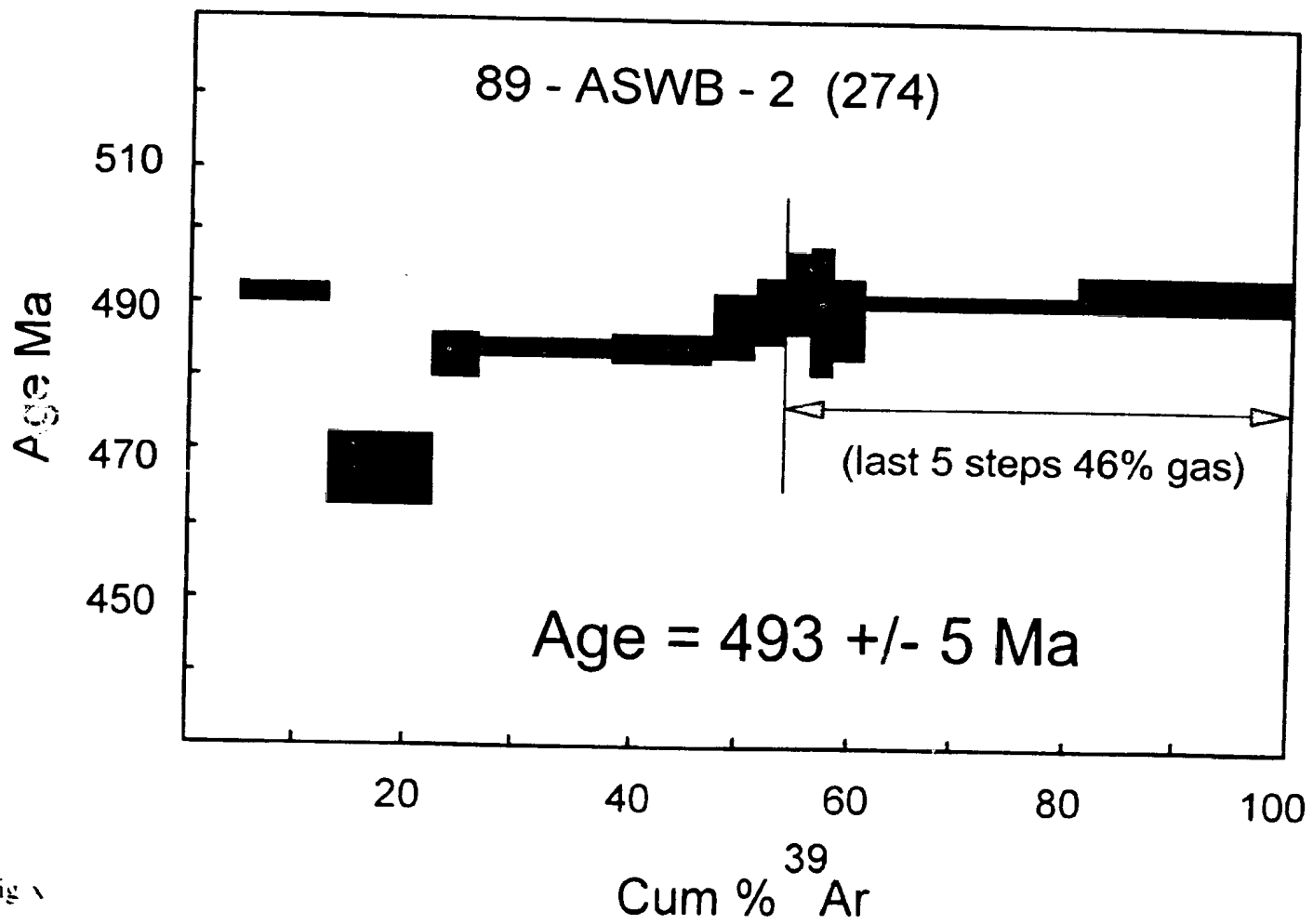
B - Fig. vii



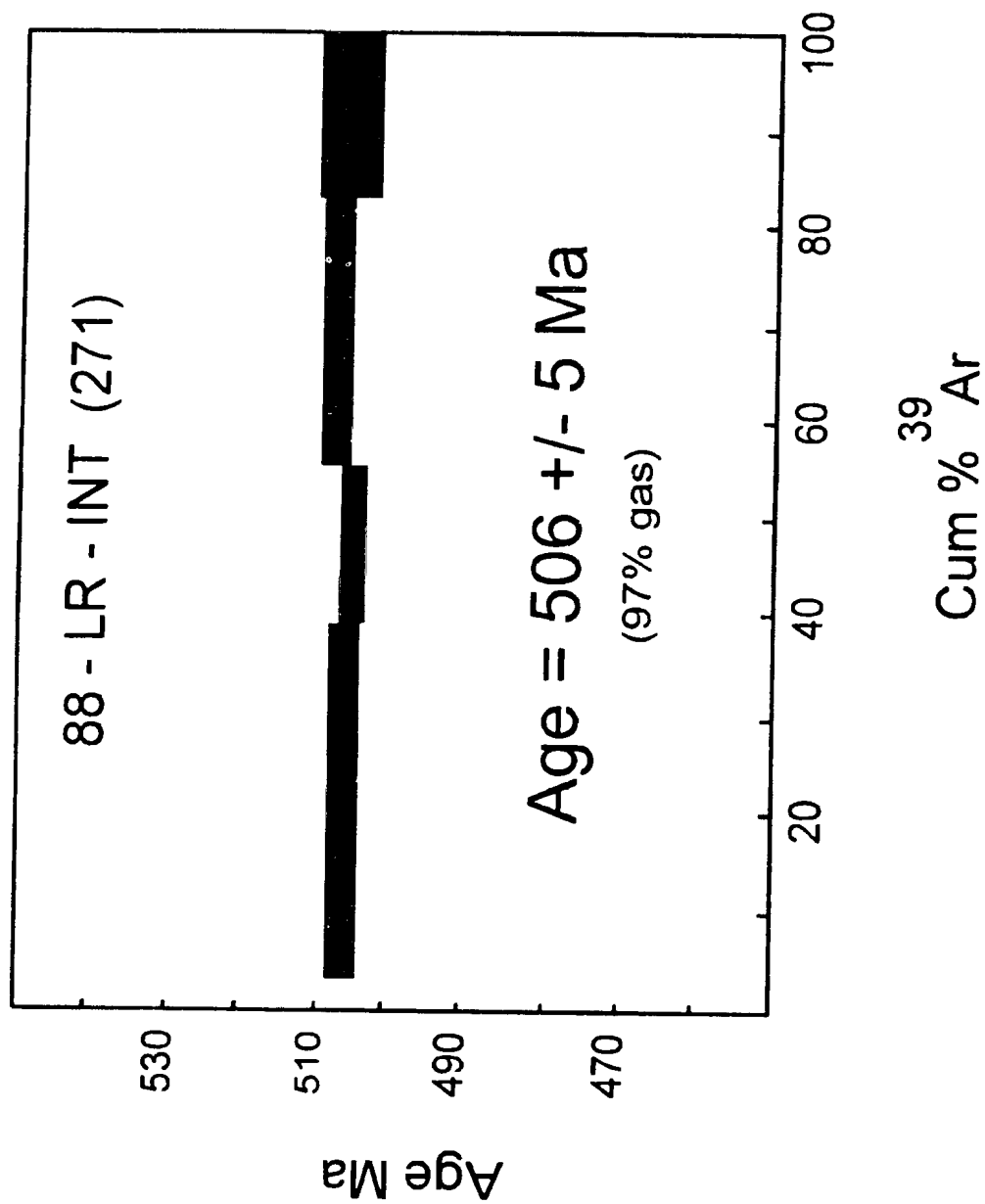
B - Fig viii



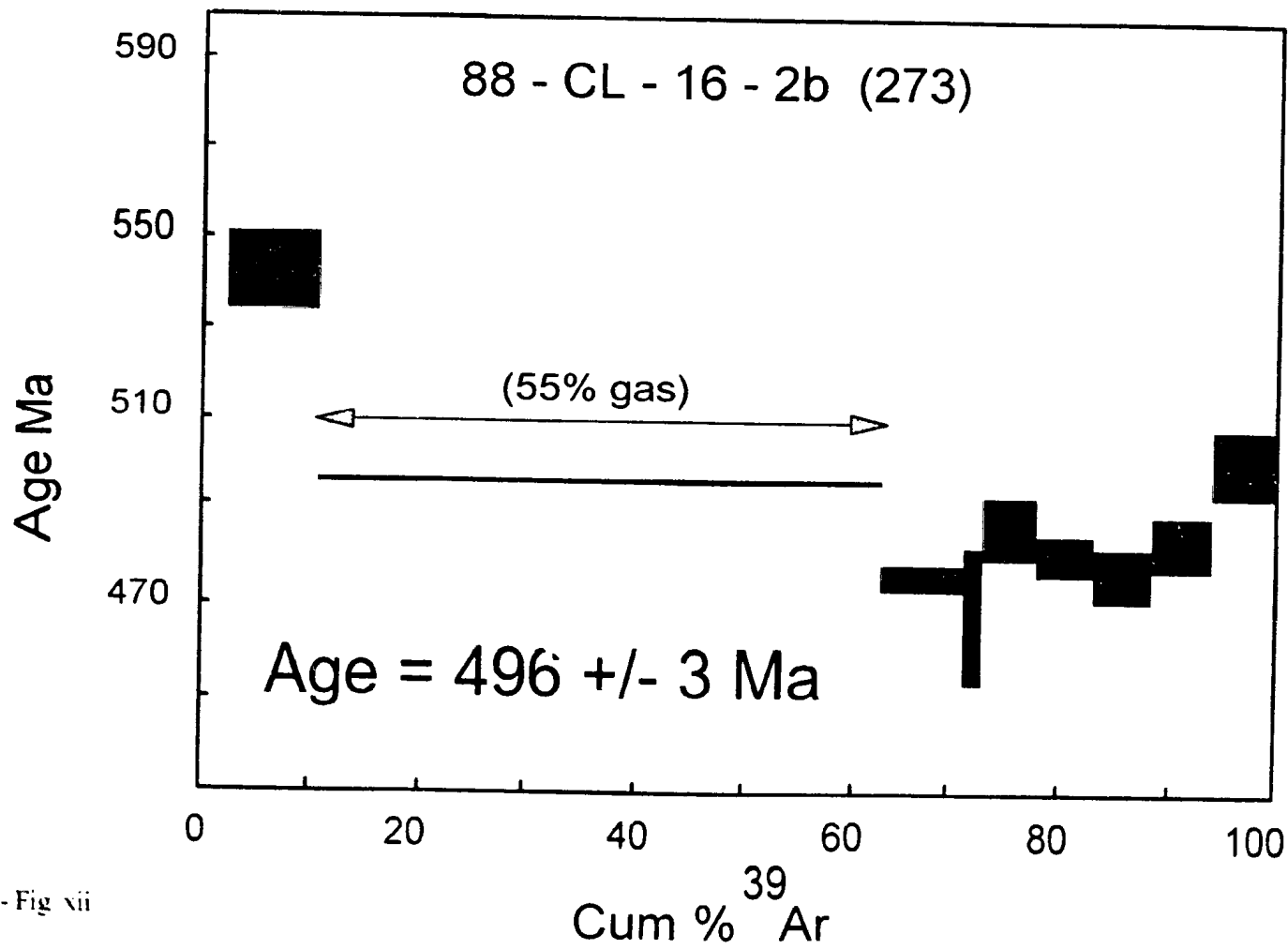
B - Fig. ix



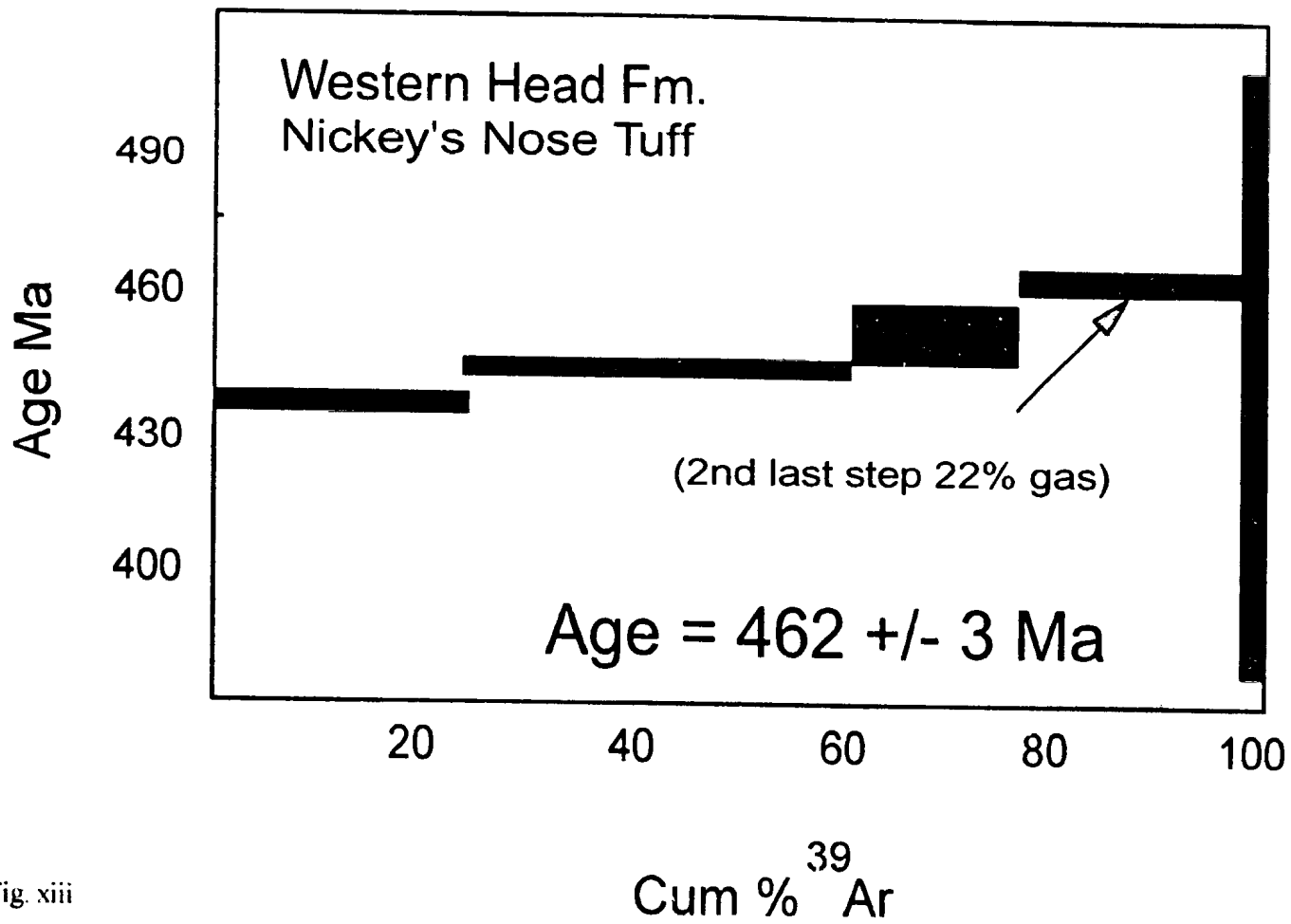
B - fig 1



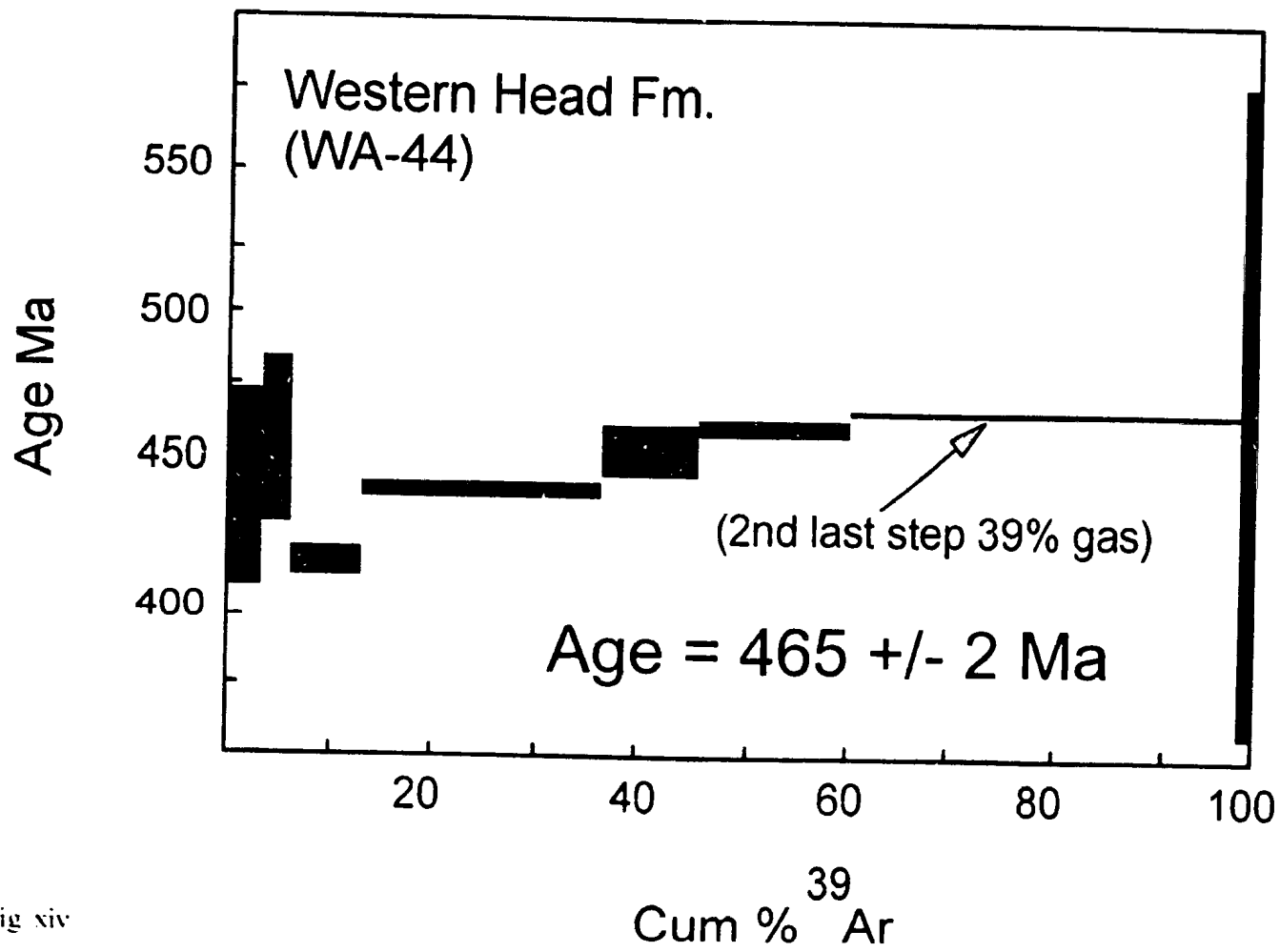
B - Fig. xi



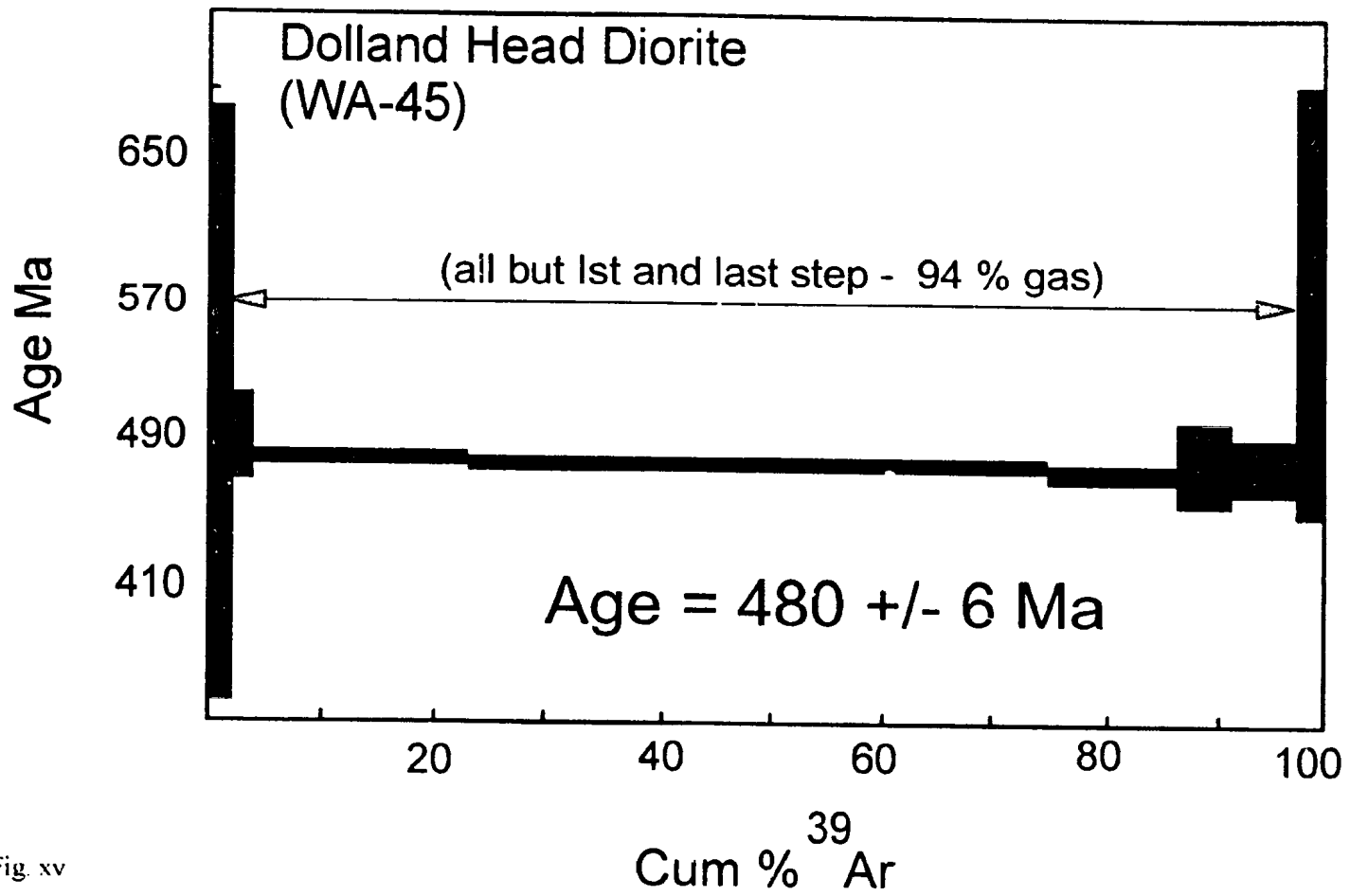
B - Fig xii



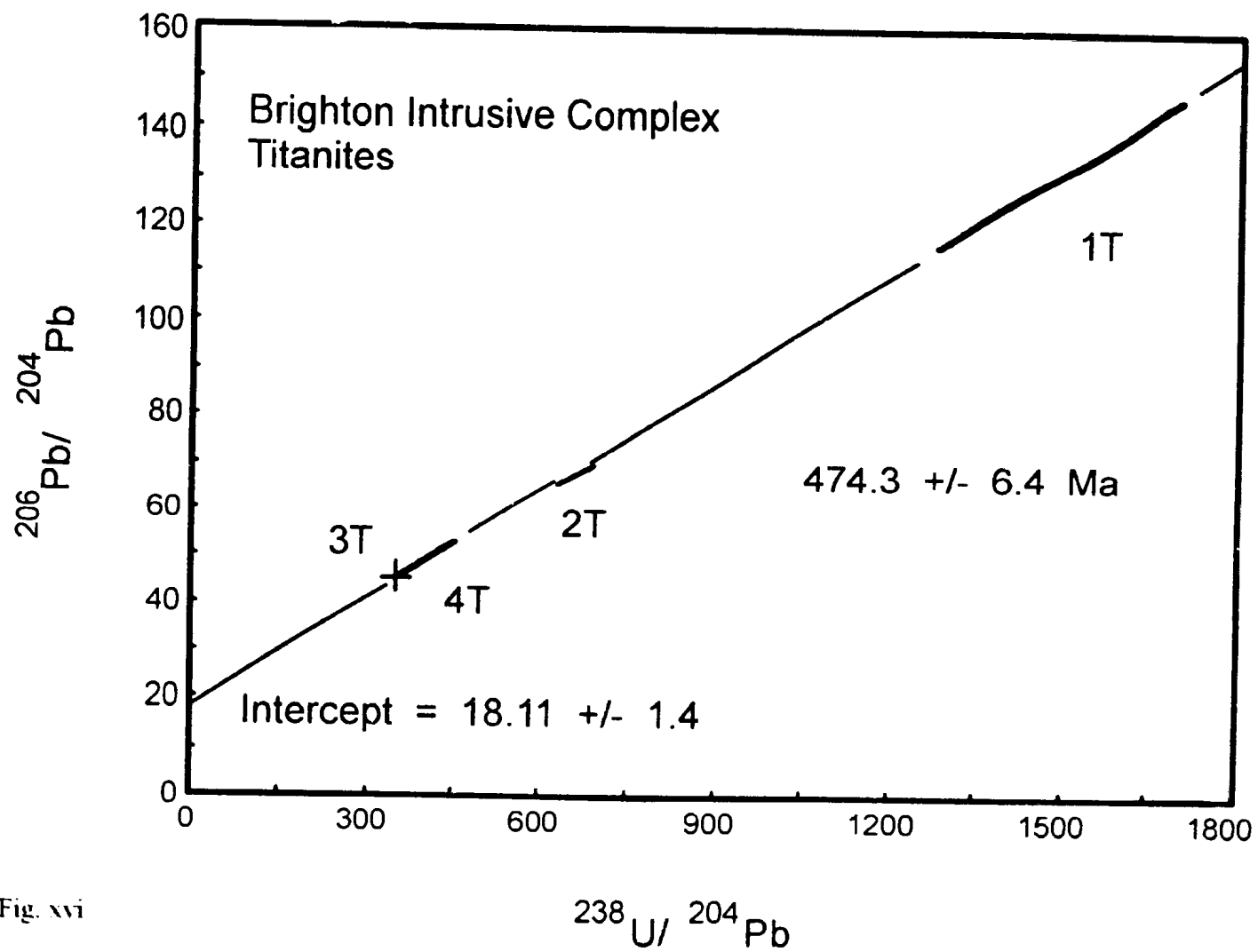
B - Fig. xiii



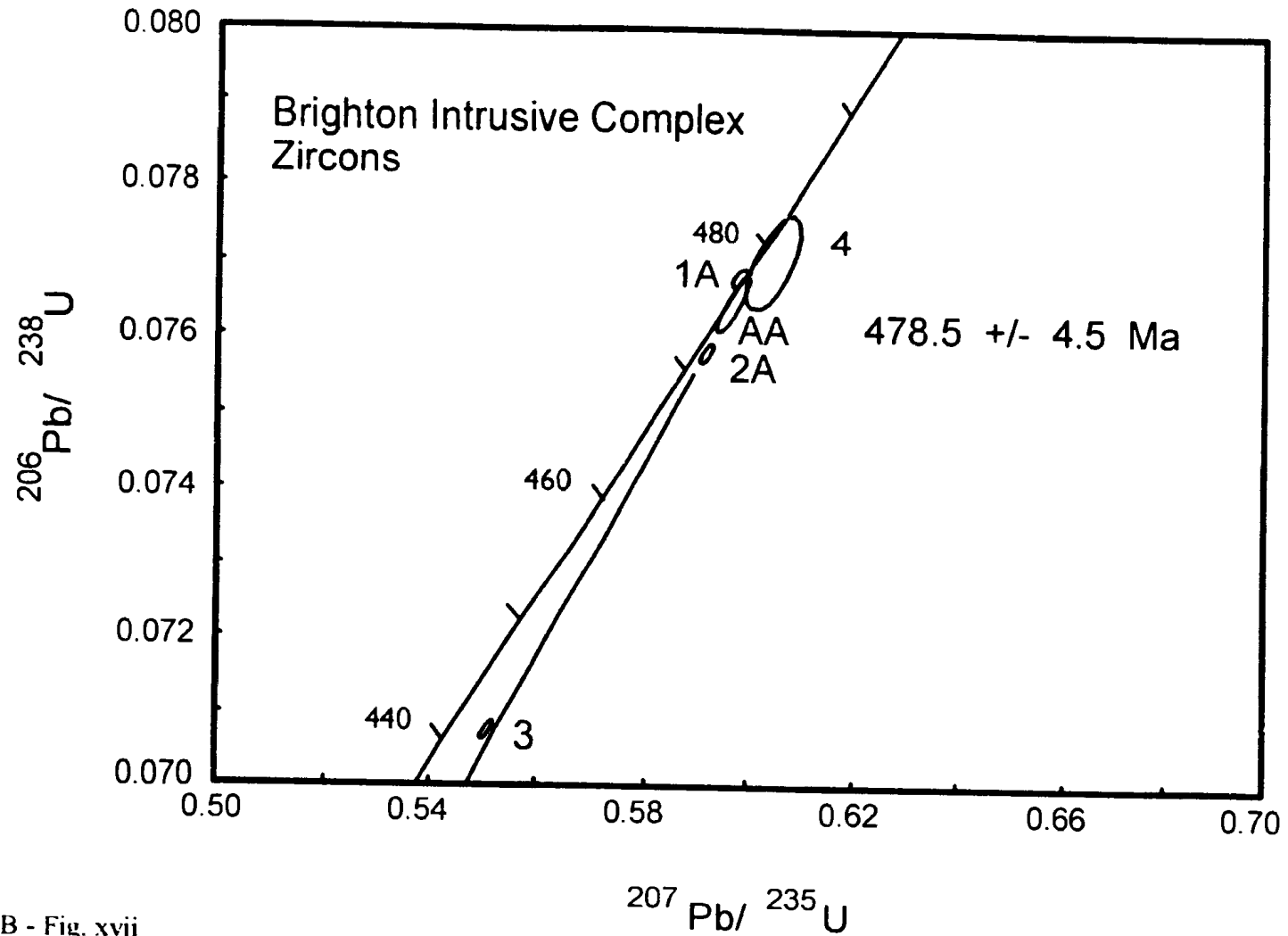
B - Fig xiv



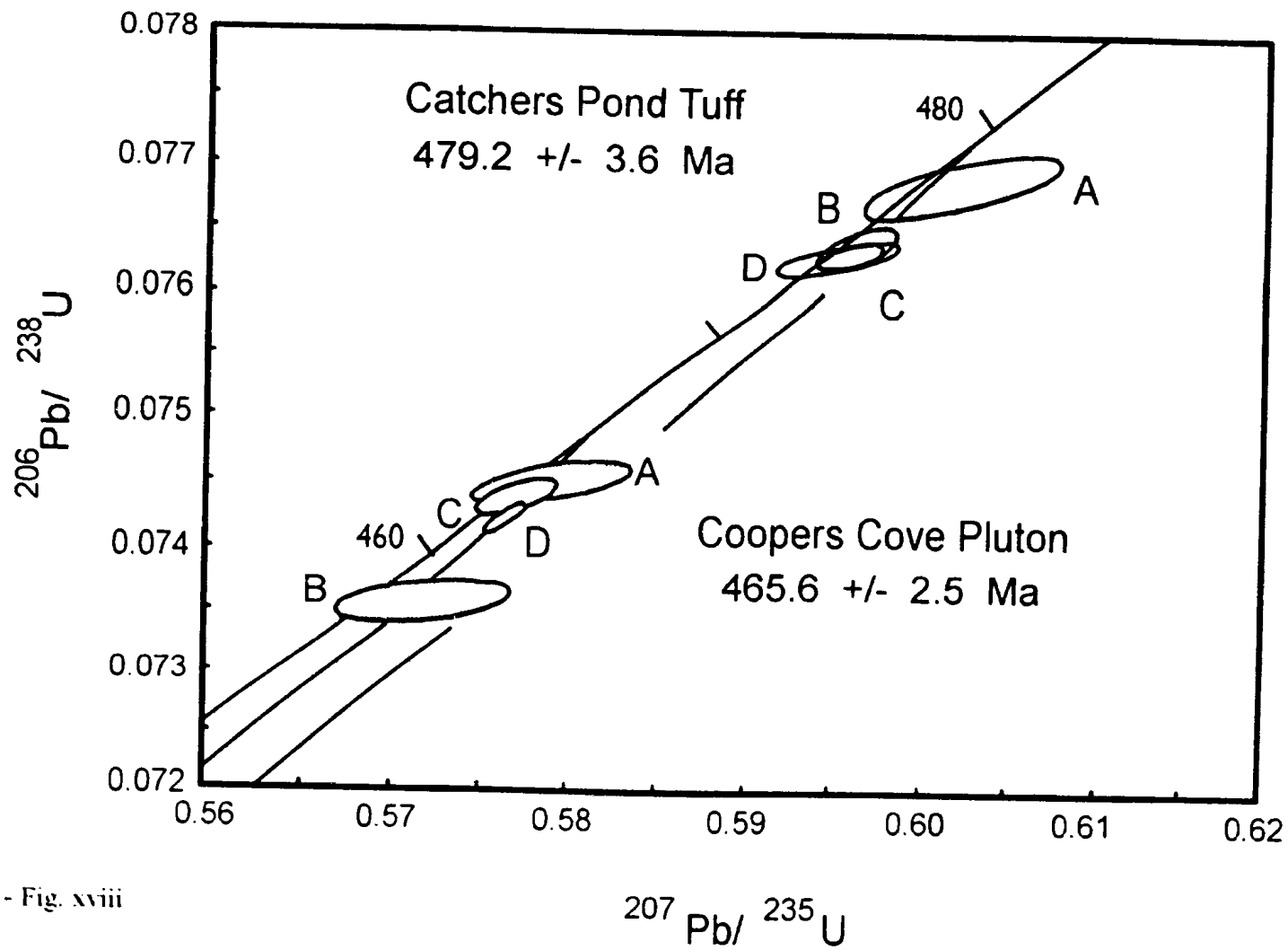
B - Fig. xv



B - Fig. xvi



B - Fig. xvii



B - Fig. xviii

APPENDIX C - ANALYTICAL TECHNIQUES

PART 1 - Geochemistry

Analytical Techniques

Major Elements

Analyses were performed at Memorial University of Newfoundland or at the Department of Mines and Energy, Newfoundland. Majors were determined by atomic absorption spectrometry. Details of the techniques can be found in Wagenbauer et al. (1983) and Langmyhr and Paus (1968). Precision and accuracy for these techniques is the same as that reported in Swinden (1988), Rautenschlein (1987) and Kean et al. (1994).

Trace Elements

A standard suite of trace elements (Cr, Ni, V, Sc, Rb, Sr, Y, Nb, Zr, Ba) were determined at Memorial University of Newfoundland using X-ray fluorescence (XRF) techniques. Details of the accuracy and precision of these methods is given in Swinden (1988). The only element of real concern in this suite is that of Nb. Nb was determined using the so-called "REPEAT" XRF method (along with Sr, Rb, Y and Zr), as described in Swinden (1988) and as discussed fully in Kean et al. (1994). Some data was also collected on the new ARL XRF at Memorial University using the techniques described by Longerich (1992, 1994). Since there is no fundamental differences in the standard values or detection limits between the "REPEAT" method and the new MUN ARL methods, data from the two techniques are not distinguished.

Rare Earth Elements

Rare earth elements (REE) were determined by inductively coupled plasma - mass spectrometry (ICP-MS) using the acid dissolution technique described in Jenner et al. (1990) and Longerich et al. (1990). Precision and accuracy for these elements are as reported in those papers, and the more recent paper of Jochum and Jenner (1994).

ICP-MS and XRF - which one for which elements

The routine ICP-MS acid - dissolution package also produces data for a number of trace elements routinely analysed for by XRF, i.e. Rb, Sr, Y, Zr, Nb, Ba (sometimes V

and Sc). In general, it is our policy to cross-check the XRF and ICP-MS results to verify complete sample dissolution and/or solution stability in the ICP-MS analyses. Failure to match data sets results in re-analysis of the sample (usually by both techniques). In reporting the data (Appendix D), we have taken XRF data for all trace elements, excluding Th, Nb and the REE. For Th, Nb and the REE, ICP-MS is the preferred technique.

PART 2 - Geochronology

Analytical Techniques

$^{40}\text{Ar}/^{39}\text{Ar}$

Analyses were performed at the Geochronology Laboratory of the Geological Survey of Canada. Amphibole (hornblende) mineral separates were obtained by standard magnetic and heavy-liquid techniques followed by hand-picking to obtain near 100% purity. Their K concentrations, determined from the $^{40}\text{Ar}/^{39}\text{Ar}$ analyses, range from 0.07 to 0.99%. Analytical data for the hornblendes is given in Table 1. Spectra for the results are illustrated in B - Figures i to xv. Figures are in the same order as the data in Table 1, reflecting both sequence of analyses and ease of getting the Table organized.

The hornblendes were weighed (see table) and wrapped in aluminum foil packets for neutron irradiation. The packets were loaded in an aluminum can, 40mm long by 19 mm in diameter, along with 9-12 packets of the MMI1b-1 hornblende $^{40}\text{Ar}/^{39}\text{Ar}$ flux monitor with an assumed age of 518.9 Ma (Roddick, 1983). Samples were irradiated in position 5C of the enriched uranium research reactor at McMaster University, Hamilton, Ontario on three separate occasions. For samples RAL-88-2 and RAI-88-3 irradiation was for 1.25 days (equivalent to an approximate fast neutron fluence of 1.1×10^{18} neutrons/cm²). All other samples were irradiated for 2 days. Flux variation over the irradiation can had a range of 2.0% along the axis of the can, in both irradiations. This results in an uncertainty of J for individual samples of about 0.3% (1 sigma). The errors quoted on the integrated ages take account of this J uncertainty, though the individual step ages in the data table and spectra diagrams do not. Decay constants recommended by Steiger and Jager (1977) have been used. Complete procedures for the $^{40}\text{Ar}/^{39}\text{Ar}$ analyses are detailed in Roddick (1990).

U/Pb

Zircon and titanite were concentrated from about 25 kg of each rock sample. Individual zircon populations were separated initially on the basis of grain size and magnetic susceptibility and subsequently by crystal habit, clarity, and absence of inclusions and fractures (see below). Most zircon fractions were abraded to remove potentially altered outer parts of the grains (Krogh, 1982). The very fine grained zircons (fraction 3) in sample BR-2 were not abraded.

Procedures for dissolution, separation and purification of Pb and U employing a $^{206}\text{Pb}/^{233-235}\text{U}$ spike are detailed in Parrish et al. (1987). Total procedural blanks for Pb ranged from 5 to 25 pg for zircon analyses and about 50 pg for titanites. U blanks averaged 1 pg. Isotopic analyses were carried out on a Finnigan MAT 261 solid-source mass spectrometer equipped with multiple collectors, secondary electron multiplier, and operating software designed for simultaneous measurement of all five Pb isotopes (Parrish et al., 1987; Roddick et al., 1987). Error estimates of U/Pb and $^{207}\text{Pb}/^{206}\text{Pb}$, and correlation coefficients, are derived from numerical propagation of measured errors (Roddick, 1987). Assumed common Pb compositions were derived from a Pb isotopic evolution curve (Stacey and Kramers, 1975) at the $^{207}\text{Pb}/^{206}\text{Pb}$ age of each zircon fraction, except for the Brighton Intrusive Complex for which compositions were derived from the titanite analyses (B - Fig. xvi). Linear regressions of data on concordia diagrams utilize a York (1969) error treatment (modified as suggested by Parrish et al., 1987) with errors as indicated in Table 2 for the U-Pb ratios. Correlation coefficients between the U-Pb ratios were calculated to be 0.6 to 0.95 (and >0.9 for titanite) using error propagation calculations. Uncertainties in ages are stated at the 2 sigma level. Constants used in U-Pb calculations are those recommended by Steiger and Jager (1977).

Comparison of U/Pb zircon and $^{40}\text{Ar}/^{39}\text{Ar}$ hornblende ages

It can be difficult/impossible to obtain U/Pb zircon ages on high field strength element depleted island arc volcanics/plutonics, and for this reason we choose, where applicable, to apply the $^{40}\text{Ar}/^{39}\text{Ar}$ technique. To facilitate comparison between U/Pb and $^{40}\text{Ar}/^{39}\text{Ar}$ ages on "ophiolitic" samples we obtained a sample of hornblende from a

pegmatitic trondjemite in the Annieopsquotch Complex, which had previously been dated by Dunning and Krogh (1985). The amphibole obtained is low in K (0.14%) and yielded an age of 477 ± 3 (92% of the gas) (B - Fig. iii). This result is in excellent agreement with the published U/Pb age of $477.5 \pm 2.6/2.0$ (see their Figure 8, Dunning and Krogh, 1985).

Brief Sample Discussion

Brighton Intrusive Complex (CI-BR-7)

Five zircon fractions (4 abraded, 1 unabraded) were analysed and the data are presented in Figure B - xvii. Regression using all 5 fractions gives an age of $479.8 \pm 9.9/6.2$ Ma with a lower intercept of 115 Ma ± 100 and an MSWD of 4.5. This result seems to be an overestimate of the error when consideration is given to the fact that 2 fractions overlap concordia and the $^{207}\text{Pb}/^{206}\text{Pb}$ ages of the near concordant fractions (AA & 2A) are 479-481 Ma. Our preferred age, 478.5 ± 4.5 Ma, is based on rejecting the most discordant fraction (3), which was not abraded, and forcing the regression through the origin.

Several titanite fractions were picked and the result of these analyses are illustrated in Figure B - xvi. The titanites yielded a $^{238}\text{U} - ^{206}\text{Pb}$ isochron age of 474.3 ± 6.4 , and (not illustrated) a $^{235}\text{U} - ^{207}\text{Pb}$ age of 471 ± 12 Ma. Note that the error on titanite fraction 3T is too small to be represented by an error ellipse on Figure B - xvi.

Three hornblende fractions from two separate localities from within the Brighton Intrusive Complex were used to determine $^{40}\text{Ar}/^{39}\text{Ar}$ ages and these are presented in Figures B - iv, vii, viii. Sample RAL-88-1 yielded a total fusion age of 475 ± 3 Ma and a preferred age of 475 ± 3 Ma based on 87% of the gas. Sample RAL-88-2 yielded a total fusion age of 473 ± 2 Ma and a preferred age of 472 ± 3 Ma based on 87% of the gas. A third hornblende sample - RAL-88-3, from a separate locality, yielded a total fusion age of 473 ± 3 Ma and a preferred age of 475 ± 3 Ma based on 94% of the gas.

There is excellent agreement between the titanite and hornblende ages which indicates an age for the BIC of about 475 Ma. It is possible that the zircons indicate a slightly older age, but the quality of the data is not ideal. Taking into account all 3

systems, it seems reasonable to constrain the origin of the BIC to between 475 and 480 Ma

Catchers Pond Tuff (CP-28-15, Skeleton Pond Formation)

Three zircon fractions (A, B, D) and a duplicate zircon fraction (C=B), all abraded, were analysed. The data are illustrated in Figure B - xviii as open ellipses. These data yield an age of 479.2 +/- 3.6 Ma, based on a York regression through the origin. No solution was found when we applied the regression method of Davis (1982). There was no evidence of inheritance in any of the analysed fractions, and we interpret the data to give the primary igneous age.

Colchester - Coopers Cove Plutonics (90-2CC, Coopers Cove Pluton)

Three abraded zircon fractions (A, B, C) and a duplicate zircon fraction (D=C) were analysed. The data are illustrated in Figure B - xviii as hatched ellipses. The data yield an age of 465.6 +/- 2.5 Ma, based on a York regression through the origin. No solution was found when we applied the regression method of Davis (1982), because of their close proximity on the concordia diagram. We interpret this age to be the primary igneous age of the intrusion. There was some evidence of inheritance and overgrowths in this sample, but care was taken not to include any of these materials in the analysed fractions.

Halls Bay Head Dyke (CL-16-02b)

The first hornblende separate from sample 88-CL 16-2b (Fig. B - v) yielded a total fusion age of 507 +/- 4 Ma and an age of 498 +/- 3 Ma based on 98% of the gas. The preferred age is 499 +/- 3 Ma based on 72% of the gas (i.e. the fraction between ~18-50% and ~60-100%). This sample was redone at a later date and the results are illustrated in Figure B - xii. The preferred age is 496 +/- 3 Ma based on 55% of the gas.

League Rock Gabbro (CL-LR-1a)

Sample 88-LR-INT yielded a K-poor hornblende (0.05%), which resulted in a rather noisy spectrum (Fig. B - vi). The total fusion age is 535 +/- 23 Ma, while the preferred age is 519 +/- 7 Ma based on 82% of the gas. Since this result was somewhat unsatisfactory, we repeated the analysis of this sample and obtained the result illustrated

in Figure B - xi. We have significantly improved on the result and our preferred age is 506 +/- 5 Ma.

Pilleys Cove Gabbro (CL-06-05)

Sample 88-PIG yielded a K-poor hornblende (0.07%) and a complex spectrum (Fig B - i). The simplest interpretation of the spectrum would yield an age of 474 +/- 4 Ma with 92% of the gas. This age would coincide with that of the BIC, however neither the chemistry nor mineralogy of the Pilleys Cove Gabbro suggest any relationship to the BIC. Within the spectrum for 88-PIG there is some indication of two plateaus (1) from approximately 8 to 54% (Fig. B - i) yielding an age of 466 +/- 5 Ma; and (2) from 55 to 100%, yielding an age of 483 +/- 6 Ma. Both of these ages are reasonable in the context of the regional geology, with the youngest age consistent with a collisional event (i.e. resetting) and the older age representing a minimum age of intrusion.

Whalesback Dyke (WB-1 and WB-2)

Two samples from the vicinity of the Whalesback Mine were taken, these are 89-ASWB-1 (Fig. B - ix) and 89-ASWB-2 (Fig. B - x). WB-1 cuts the shear zone (D1), but is modified (boudinaged) by subsequent deformational events. WB-2 was taken south of the shear zone, where it cuts apparently undeformed pillow lavas. We interpret the original age of intrusion of these dykes to be represented by our preferred age in WB-2, i.e. 493 +/- 5 Ma. This is consistent with the age of the dyke cutting Big Hill Basalt at Halls Bay Head (CL-16-02b). The spectra from WB-1 is quite screwed up by later deformation events.

Western Head Formation (WA-NN-1, WA-44)

Two samples were taken for analysis, these are: WA-NN-1 (from Nickey's Nose area); and WA-44 (from Western Arm). Spectra for these samples are illustrated in Figures B - xiii and xiv, respectively. Both spectra are very disturbed, probably during a Silurian reheating event. We interpret the oldest ages (from the 2nd last step) (465 Ma), to represent the original age of formation of these tuffs. This makes these samples essentially coeval with the Colchester - Coopers Cove Pluton.

Dolland Head Diorite (WA-45)

One sample was taken from the diorite intrusion at Dolland Head (see Fig. B - xv), a few hundred metres east of WA-44. This sample yielded a simple spectra, with a preferred age of 480 +/- 6 Ma, based on 94% of the gas.

Description of fractions used in U/Pb analyses.Brighton Intrusive Complex.*Zircons*

1A - +105 microns, abraded 0.5 hours

- equant, euhedral, multifaceted, sharp terminations
- light brown colour, nor cores or fractures
- clear, small number of inclusions, no zoning

AA - 100 microns, abraded 4.5 hours

- euhedral, equant, multifaceted
- no cores, no zoning, minor fractures
- pale, pinkish brown, clear, minor inclusions

2A - +105 microns, abraded 1 hour

- dominantly equant, occasionally grains 3:1
- cracked and fractured, few inclusions
- no cores, no zoning

3 - 50 microns, no abrasion

- equant, some grains with minor elongation (3:1)
- generally clear

4 - 50-100 microns, same as 1A

Titanites

Clear to light yellow with minor inclusions. Euhedral to subhedral, sharp faceted. No abrasion 1T - 105 to 125 microns; 2T 75 to 125 microns; 3T 100 to 200 microns; 4T < 105 microns.

Catchers Pond Tuff

A - 64-105 microns,

- sharp terminations, multifaceted, euhedral, prismatic
- inclusions and bubbles present,
- no cores or zoning present
- clear to very pale yellow

B and C - split fraction - ~100 microns

- broken tips only, well terminated
- inclusion and crack free

D - 64-105 microns

- euhedral, prismatic (3:1) longer than A but otherwise similar
- some inclusions, bubbles and fractures

Colchester - Coopers Cove Pluton

A - +74 microns, 1 hour abrasion

- equant to subequant, multifaceted, zoned
- no fractures, colourless

B - +74 microns, 7 hours abrasion

- elongated, length to width ratio 3:1 to 7:1
- zoned, trace inclusions/bubbles
- well faceted sharp terminations
- no cores or overgrowths

C and D - split fraction - +74 to 125 microns, 1 hour abrasion

- zoned, more cloudy or inclusion-rich but otherwise the same as B.

There was some evidence of cores and overgrowths in this sample, however these were not picked for chemistry.

Acknowledgements

The geochronology research presented in this section was supported by funding made available from: the Geological Survey of Canada (Roddick); NSERC Operating Grants to Jenner; Lithoprobe Grants to Jenner and Fryer; and the Newfoundland/Canada Mineral Development Agreement (Jenner and Szybinski). It should also be noted that the geochronology research was primarily carried out by Drs. Jenner and Roddick. The staff of the Geochronology Laboratory of the Geological Survey of Canada are thanked for their support and assistance in the generation of the data used in this paper. We wish to thank in particular Debra Lemkow for her skillful preparation of some of the U/Pb fractions and Tony LeCheminant. Geochemical analyses were facilitated by C. Collins, P. Horan, D. Clarke, P. King, S. Jackson, B. Chapman and G. Andrews.

Analytical Technique References

- Davis, D.W. 1982. Optimum linear regression and error estimation applied to U-Pb data. *Canadian Journal of Earth Sciences*, **26**: 1747-1763.
- Jenner, G.A., Longerich, H.P., Jackson, S.E. and Fryer, B.J. 1990. ICP-MS - a powerful tool for high precision trace-element analysis in Earth sciences: evidence from analysis of selected U.S.G.S. reference samples. *Chemical Geology*, **83**: 133-148.
- Jochum, K.P. and Jenner, G.A. 1994. Trace element analysis of Geological Survey of Japan silicate reference materials: comparison of SSMS with ICP-MS data and a critical discussion of compiled values. *Fresenius' Journal of Analytical Chemistry* (in press).
- Kean, B., Evans, D. and Jenner, G. 1994. Metallogeny of the Lushs Bight Group, Central Newfoundland. Memoir, Department of Mines and Energy, Newfoundland and Labrador, Geological Survey Branch (in press).
- Krogh, T.E. 1982. Improved accuracy of U-Pb zircon ages by the creation of more concordant systems using an air abrasion technique. *Geochimica et Cosmochimica Acta*, **46**: 485-494.
- Langmyhr, F.J. and Paus, P.E. 1968. Analysis of silicate rocks. *Analytical Chemica Acta*, **43**: 397-408.
- Longerich, H.P. 1992. Application of a new treated LiF200 crystal to x-ray fluorescence analysis of geological samples. *X-ray Spectrometry*, **22**: 114-118.

- Longerich, H.P. 1994. The analysis of pressed powder pellets of geological samples using wavelength dispersive x-ray fluorescence spectrometry. *X-ray Spectrometry* (in press)
- Longerich, H.P., Jenner, G.A., Fryer, B.J. and Jackson, S.E. 1990. Inductively coupled plasma - mass spectrometric analysis of geological samples: a critical evaluation based on case studies. *Chemical Geology*, **83**: 105-118.
- Parrish, R.R., Roddick, J.C., Loveridge, W.D., and Sullivan, R.W. 1987. Uranium-lead analytical techniques at the geochronology laboratory, Geological Survey of Canada. // *Radiogenic age and isotopic studies: Report 1. Geological Survey of Canada, Paper 87-2*, pp. 3-7.
- Rautenschlein, M. 1987. Geology and geochemistry of Akaki volcanics, Cyprus. Ph D thesis, Bochum University, 222 pages.
- Roddick, J.C. 1983. High precision intercalibration of ^{40}Ar - ^{39}Ar standards. *Geochimica et Cosmochimica Acta*, **47**: 887-898.
- ___ 1987. Generalized numerical error analysis with application to geochronology and thermodynamics. *Geochimica et Cosmochimica Acta*, **51**: 2129-2135.
- ___ 1990. $^{40}\text{Ar}/^{39}\text{Ar}$ evidence for the age of the New Quebec Crater, northern Quebec. // *Radiogenic age and isotopic studies: Report 3. Geological Survey of Canada, Paper 89-2*, pp. 7-16.
- Roddick, J.C., Loveridge, W.D., and Parrish, R.R. 1987. Precise U/Pb dating of zircon at the sub-nanogram level. *Chemical Geology (Isotope Geoscience Section)*, **66**: 111-121
- Stacey, J.S., and Kramers, J.D. 1975. Approximation of terrestrial lead isotope evolution by a two-stage model. *Earth and Planetary Science Letters*, **26**: 207-221.
- Steiger, R.H., and Jager, E. 1977. Subcommittee on geochronology: convention on the use of decay constants in geo- and cosmo-chronology. *Earth and Planetary Science Letters*, **36**: 359-362.
- Swinden, S. 1988. Ordovician volcanism and mineralization in the the Wild Bight Group, central Newfoundland: a geochemical, petrological, geochemical and isotopic study. Ph. D. thesis, Memorial University of Newfoundland, St. John's, 452 pages.

- Wagenbauer, H.A., Riley, C.A. and Dawe, G. 1983. Geochemical laboratory. *In* Current Research, Newfoundland Department of Mines and Energy, Mineral Development Division Report 83-1, pages 133-137.
- York, D. 1969. Least squares fitting of a straight line with correlated errors. *Earth and Planetary Science Letters*, 5: 320-324.

APPENDIX D - Tables of Analytical Data

The analytical data presented in the figures in this thesis is presented here in tables. The data has been recalculated volatile-free and totalled to 100%. Major elements are in weight percent oxide, with total iron as FeO (FeO*). Trace elements are in parts per million (ppm).

To simplify presentation of the data, it has been divided into 7 groups: arc volcanics; CL and CP (oddball samples); non-arc volcanics; transitional volcanics; arc intrusives; transitional & non-arc intrusives; and felsic rocks. In essence, this is a simplification of the scheme outlined in Figure 4.2 (page 4-53).

Complete sets of raw data will be available upon request from the author.

APPENDIX D - TABLE 1 - ARC VOLCANICS

Sample	CP-24-20	JLB-01	JLB-03	cl-92-11	CL-01-03	CL-SCI-1	CL-16-15a	CP-05-08	JLB-10	JLB-SC1	CL-15-04
SiO2	64.05	60.55	59.39	51.22	52.99	55.98	53.73	55.58	52.95	58.14	59.34
TiO2	0.30	0.10	0.15	0.15	0.30	0.50	0.84	0.67	0.83	0.62	1.23
Al2O3	16.58	13.96	14.27	10.26	15.99	15.46	15.46	14.44	14.61	14.45	14.80
FeO*	6.88	8.23	8.12	10.00	8.40	7.90	9.79	8.03	10.72	8.54	11.39
MnO	0.14	0.15	0.17	0.19	0.14	0.13	0.16	0.14	0.18	0.13	0.16
MgO	6.67	6.68	6.76	16.87	7.00	6.75	7.06	8.51	6.50	5.93	4.83
CaO	0.32	8.05	8.61	9.62	11.70	9.02	8.90	8.00	11.28	9.79	4.45
Na2O	4.41	2.25	2.46	0.90	2.41	4.04	3.80	4.29	2.82	2.36	4.66
K2O	0.53	0.02	0.04	0.79	0.05	0.18	0.23	0.28	0.05	0.00	0.04
P2O5	0.11	0.01	0.03	0.00	0.03	0.04	0.04	0.06	0.06	0.03	0.10
LOI	4.9	4.2	2.0		3.0	3.5	2.8	3.3	1.9	7.5	4.5
Mg #	63.4	59.1	59.7	75.0	59.7	60.4	56.2	65.4	51.9	55.3	43.0
Cr		252	265	751	38	124	147	94	81	148	
Ni		72	64	138	45	52	49	26	36	40	
Sc	40	45	46	46	39	37	44	46	35	47	44
V		353	309	251	298	244	297	266	324	372	432
Rb	12	3	4	12		1	2	3	1		
Ba	40	41	32	79				37	3	14	
Sr	44	136	119	154	47	56	70	108	79	57	52
Nb	0.7	0.9	1.3	0.9	0.4	0.4	0.6	0.7	0.6	0.6	1.2
Zr	28	22	24	16	16	17	39	37	41	32	67
Y	3	4	4	4	12	12	23	17	22	22	29
Th	0.20	0.44	0.45	0.35	0.15	0.14	0.13	0.10	0.10	0.16	0.21
La	1.57	2.35	1.55	1.35	0.69	0.81	1.09	1.14	1.28	1.38	2.31
Ce	4.01	4.90	3.67	2.87	1.69	2.27	3.58	3.82	4.14	3.92	6.70
Pr	0.54	0.54	0.41	0.33	0.26	0.48	0.70	0.68	0.72	0.65	1.19
Nd	2.56	2.03	1.61	1.30	1.36	2.50	4.04	4.05	4.15	3.58	6.46
Sm	0.67	0.42	0.38	0.32	0.54	1.16	1.82	1.47	1.64	1.53	2.49
Eu	0.18	0.13	0.13	0.14	0.28	0.53	0.67	0.68	0.65	0.67	0.84
Gd	0.67	0.31	0.30	0.42	0.97	1.91	2.81	2.16	2.09	2.16	3.34
Tb	0.08	0.05	0.06	0.08	0.20	0.39	0.55	0.43	0.41	0.42	0.69
Dy	0.62	0.50	0.56	0.59	1.59	2.84	3.81	2.90	3.08	3.12	4.68
Ho	0.13	0.12	0.15	0.14	0.39	0.65	0.87	0.59	0.70	0.68	1.02
Er	0.38	0.48	0.49	0.46	1.25	2.04	2.49	1.87	2.06	2.02	3.09
Tm	0.06	0.08	0.09	0.00	0.19	0.30	0.35	0.25	0.30	0.31	0.45
Yb	0.49	0.67	0.69	0.58	1.33	2.06	2.48	1.77	1.96	1.91	2.84
Lu	0.09	0.11	0.12	0.09	0.22	0.29	0.34	0.24	0.31	0.31	0.38

Sample	CL-19-22	CL-19-23	WA-08	WA-15	WB-5	cl-92-14	CL-02-03	CL-03-05a	CL-09-02	CL-12-04	CP-24-10
SiO2	56.63	53.57	54.10	53.25	56.11	47.94	51.06	55.06	64.96	53.82	57.54
TiO2	1.20	1.08	1.22	1.24	1.05	1.20	1.62	1.43	1.09	1.27	0.86
Al2O3	16.76	14.88	16.00	15.76	16.47	10.93	18.91	16.50	14.93	17.52	16.19
FeO*	9.75	10.62	11.01	11.41	10.84	13.92	11.18	12.09	7.71	12.52	8.37
MnO	0.12	0.19	0.15	0.20	0.16	0.25	0.17	0.22	0.15	0.15	0.15
MgO	4.60	5.32	6.02	6.71	5.11	10.61	5.98	3.90	1.81	6.54	4.72
CaO	4.94	9.68	5.58	6.37	4.78	11.58	5.34	4.08	2.59	2.95	5.14
Na2O	4.70	4.51	5.21	4.86	5.21	3.08	5.32	6.35	6.51	5.03	6.87
K2O	1.25	0.06	0.55	0.14	0.17	0.41	0.28	0.29	0.11	0.07	0.03
P2O5	0.05	0.09	0.17	0.06	0.10	0.06	0.14	0.08	0.16	0.13	0.12
LOI	4.1	5.5	2.9	3.8	3.3		4.7	2.0	3.1	4.2	5.8
Mg #	45.7	47.2	49.4	51.2	45.6	57.6	48.8	36.5	29.5	48.2	50.1
Cr				16		176	153				
Ni		8		17		50	29				
Sc	41	38	38	37	37	41	46	37	38	48	35
V	472	400	358	427	359	351	314	354	57	436	273
Rb	21	1	6	1		2	4	4	2		
Ba			42	10	20	58					
Sr	132	68	104	42	66	171	172	170	96	217	86
Nb	1.0	1.1	1.3	0.8	1.1	1.0	2.3	3.3	2.2	2.6	1.8
Zr	62	60	55	86		71	80	69	75	91	50
Y	21	30	26	29	25	28	23	26	30	26	18
Th	0.26	0.20	0.27	0.15	0.22	0.31	0.65	0.73	0.71	0.82	0.42
La	1.72	2.76	2.35	1.76	1.79	2.75	5.20	5.58	3.72	5.16	2.54
Ce	5.71	7.59	7.28	6.08	6.51	8.59	12.99	15.46	9.90	13.89	7.32
Pr	1.01	1.37	1.22	1.11	1.21	1.51	2.00	2.31	1.57	2.10	1.16
Nd	5.73	7.11	7.03	6.80	6.94	8.01	9.59	11.49	7.75	9.75	5.67
Sm	2.15	2.66	2.50	2.68	2.76	2.85	3.03	3.52	2.71	3.15	1.94
Eu	0.72	0.86	1.06	0.94	1.12	1.18	1.07	1.47	0.95	1.05	0.77
Gd	3.04	3.77	3.57	3.75	3.94	4.05	3.48	4.55	3.26	3.63	2.68
Tb	0.53	0.66	0.67	0.75	0.73	0.67	0.63	0.75	0.65	0.71	0.46
Dy	3.60	4.49	4.83	5.24	5.15	5.19	4.23	5.09	4.66	4.51	3.14
Ho	0.76	0.99	1.07	1.25	1.12	1.07	0.89	1.10	0.99	1.00	0.66
Er	2.25	3.29	2.93	3.44	3.35	3.15	2.77	3.03	3.30	2.90	1.93
Tm	0.33	0.50	0.43	0.49	0.48	0.00	0.38	0.45	0.46	0.40	0.28
Yb	2.11	3.19	2.69	3.17	3.26	3.18	2.49	2.83	3.26	2.72	1.85
Lu	0.31	0.49	0.40	0.46	0.44	0.48	0.36	0.39	0.47	0.41	0.27

Sample	WA-13	WA-14	WA-19	WA-22	WA-23	WA-24	cl-01-07	wa-30	wa-nn-1	wa-44	CP-03-03
SiO2	55.77	54.36	49.55	56.40	55.37	54.60	48.38	52.28	49.09	54.21	54.41
TiO2	1.30	1.17	1.60	1.05	1.09	1.24	0.78	0.62	0.62	0.55	1.28
Al2O3	15.51	16.86	15.99	16.21	16.11	15.51	12.86	15.48	13.22	15.38	16.00
FeO*	11.29	10.83	15.94	10.05	10.85	12.00	12.36	10.85	10.17	9.02	12.11
MnO	0.20	0.18	0.25	0.20	0.23	0.23	0.43	0.20	0.20	0.14	0.23
MgO	4.72	5.18	6.04	4.91	5.01	4.86	11.79	9.09	14.52	8.27	5.53
CaO	5.14	7.00	6.23	4.46	5.37	6.02	10.36	7.39	8.01	8.26	7.32
Na2O	5.77	3.80	4.23	6.43	5.64	5.22	2.43	3.59	3.35	2.94	2.16
K2O	0.16	0.45	0.04	0.11	0.17	0.12	0.55	0.48	0.79	1.20	0.74
P2O5	0.16	0.16	0.14	0.18	0.16	0.20	0.06	0.03	0.03	0.04	0.18
LOI	1.9	2.6	2.9	2.0	2.3	2.1					2.0
Mg #	42.7	46.0	40.3	46.6	45.1	41.9	63.0	59.9	71.8	62.0	44.9
Cr							303	84	518	124	
Ni							37	25	171	27	
Sc	40	38	47	36	37	39	44	25	43	35	50
V	471	361	568	331	381	462	335	267	271	293	468
Rb	1	6	1	1	2	1	7	7	17	27	11
Ba	39	96	8	33	59	27	131	130	465	343	119
Sr	96	219	114	91	132	88	158	250	203	273	253
Nb	3.2	2.6	3.4	2.2	2.5	3.1	2.0	1.1	1.9	1.4	2.9
Zr	73	71	77	67	76	73	37	45	41	36	84
Y	26	23	27	22	23	25	16	13	13	12	20
Th	0.69	0.59	0.73	0.63	0.64	0.66	0.85	0.84	1.26	1.96	1.17
La	4.50	4.43	4.46	4.27	4.53	4.77	4.65	4.24	4.48	7.95	6.54
Ce	12.57	12.32	12.75	11.70	11.97	12.91	11.24	9.66	10.54	15.67	15.38
Pr	1.80	1.72	1.98	1.78	1.81	1.80	1.54	1.32	1.36	1.92	2.18
Nd	9.44	8.83	10.05	8.75	8.94	8.99	7.46	5.81	6.03	7.94	10.26
Sm	2.84	2.65	3.23	2.78	2.78	2.70	2.12	1.65	1.68	1.93	2.91
Eu	1.11	1.05	1.14	1.07	1.01	1.06	0.69	0.57	0.54	0.62	1.02
Gd	3.58	3.30	3.76	3.42	3.53	3.45	2.73	2.03	2.03	2.02	3.39
Tb	0.66	0.60	0.72	0.62	0.62	0.64	0.40	0.32	0.32	0.29	0.57
Dy	4.48	3.99	4.87	3.98	4.15	4.19	3.00	2.41	2.39	2.21	3.78
Ho	1.00	0.88	1.07	0.87	0.91	0.95	0.63	0.48	0.49	0.47	0.82
Er	2.67	2.46	2.96	2.36	2.34	2.61	1.89	1.59	1.41	1.46	2.42
Tm	0.39	0.34	0.42	0.35	0.32	0.36	0.00	0.00	0.00	0.00	0.35
Yb	2.56	2.33	2.92	2.24	2.22	2.47	1.76	1.52	1.39	1.46	2.31
Lu	0.39	0.32	0.41	0.33	0.33	0.37	0.28	0.24	0.22	0.23	0.36

Sample	CP-12-03	CP-16-04	CP-18-06a	CP-29-06	CP-31-16	CP-32-11	CL-LR-2	cl-92-15	CL-14-06	CL-22-10	MM-01-01
SiO2	53.13	49.67	63.64	50.60	59.57	51.91	53.06	50.28	45.62	50.15	51.62
TiO2	1.03	1.19	0.97	0.93	0.78	0.63	1.23	1.19	0.55	0.69	0.81
Al2O3	17.75	17.91	16.38	17.57	14.92	16.99	16.45	12.95	16.77	14.03	16.75
FeO*	11.95	13.27	6.19	10.96	9.28	10.64	12.77	15.30	7.63	11.53	9.66
MnO	0.19	0.17	0.16	0.16	0.14	0.18	0.16	0.42	0.18	0.17	0.18
MgO	3.86	6.13	2.34	6.65	3.47	6.85	6.07	8.13	4.75	9.73	5.98
CaO	9.88	7.91	5.40	8.79	4.28	10.23	4.48	8.48	22.36	11.27	10.32
Na2O	2.04	3.38	4.39	4.22	6.50	2.21	5.62	2.73	2.01	2.32	3.82
K2O	0.03	0.18	0.30	0.03	1.05	0.25	0.07	0.47	0.05	0.07	0.70
P2O5	0.14	0.19	0.24	0.10	0.01	0.12	0.08	0.05	0.09	0.04	0.16
LOI	3.1	3.2	2.6	1.7	1.1	3.0	4.5		11.4	4.3	4.1
Mg #	36.5	45.1	40.3	52.0	40.0	53.4	45.9	48.6	52.6	60.1	52.5
Cr					21			33	86	214	
Ni								24	19	92	
Sc	45	56	29	46	44	43	45	40	34	44	
V	450	425	60	333	402	342	565	425	227	339	239
Rb	1	2	3		8	4		7		1	14
Ba	22	57	111	56	238	74		50			
Sr	374	330	263	889	198	279	64	136	296	255	269
Nb	2.2	4.0	3.0	1.8	3.2	2.3	0.8	0.3	0.6	0.5	1.3
Zr	22	102	120	44	56	41	50	43	38	37	63
Y	20	25	30	15	12	16	29	23	12	15	22
Th	1.15	1.60	1.79	0.79	1.71	0.73	0.98	0.51	0.93	0.95	2.20
La	6.35	8.24	11.21	4.46	6.95	4.36	4.47	2.54	3.62	4.67	7.69
Ce	15.08	20.09	26.18	10.93	15.22	10.70	11.50	7.29	7.80	8.99	16.77
Pr	2.01	2.66	3.61	1.48	1.92	1.48	1.74	1.17	1.10	1.34	2.30
Nd	9.32	12.20	16.45	7.37	8.29	6.97	8.40	6.09	4.81	5.71	10.48
Sm	2.67	3.40	4.55	2.03	2.15	2.08	2.97	2.24	1.48	1.62	2.77
Eu	0.96	1.28	1.47	0.86	0.62	0.85	0.98	0.79	0.54	0.54	1.07
Gd	3.45	4.02	5.12	2.47	3.01	2.53	4.00	3.11	1.80	1.97	3.54
Tb	0.57	0.72	0.87	0.41	0.40	0.44	0.80	0.55	0.30	0.33	0.59
Dy	3.75	4.53	5.68	2.75	2.66	2.83	5.22	4.39	1.99	2.28	3.86
Ho	0.79	0.88	1.22	0.55	0.57	0.55	1.15	0.90	0.46	0.48	0.85
Er	2.36	2.61	3.67	1.73	1.69	1.69	3.49	2.73	1.30	1.45	2.18
Tm	0.33	0.36	0.53	0.24	0.25	0.25	0.50	0.00	0.18	0.20	0.30
Yb	2.16	2.23	3.43	1.65	1.68	1.61	3.20	2.52	1.31	1.39	2.17
Lu	0.29	0.29	0.54	0.25	0.25	0.24	0.49	0.39	0.19	0.21	0.30

Sample	cl-22-10h	CL-13-10	CL-19-14	CL-20-05	CL-20-08	CL-24-06/8	CL-24-10d	CL-24-17a	CL-19-03	CL-20-06	CL-21-01
SiO2	45.40	48.10	50.83	49.70	54.03	52.16	52.90	49.98	51.47	53.46	50.82
TiO2	0.67	0.76	0.86	0.86	1.00	0.76	0.69	0.83	1.18	0.71	0.86
Al2O3	13.45	20.39	21.36	19.36	18.27	18.99	19.72	20.56	20.21	17.53	20.52
FeO*	13.12	8.99	8.49	10.21	10.47	9.13	7.64	9.94	11.21	8.72	9.50
MnO	0.23	0.17	0.14	0.17	0.14	0.17	0.13	0.14	0.17	0.15	0.17
MgO	9.45	3.55	3.71	5.10	3.24	3.69	2.98	4.19	3.12	4.92	3.10
CaO	16.50	13.70	9.24	9.70	8.33	10.99	11.83	8.05	8.09	11.97	11.83
Na2O	1.10	3.31	3.35	2.95	3.62	2.38	2.72	4.76	3.22	2.26	2.51
K2O	0.07	0.87	1.84	1.70	0.67	1.55	1.22	1.33	1.12	0.14	0.46
P2O5	0.01	0.16	0.18	0.25	0.23	0.18	0.17	0.22	0.21	0.14	0.18
LOI		5.5	2.3	5.2	6.2	9.7	6.9	7.9	3.4	6.6	4.7
Mg #	56.2	41.3	43.8	47.1	35.5	41.9	41.0	42.9	33.2	50.1	36.8
Cr	187	13	37	90	9	12	26			47	
Ni	58	5	13	32						7	
Sc	39	34	32	37	27						
V	351	304	327	301	192	347	266	345	39	35	32
Rb	1	22	61	34	12	41	25	27	362	256	277
Ba	51								38	2	7
Sr	522	324	413	271	335	256	269	320	528	343	471
Nb	0.7	1.0	1.1	1.2	1.6	1.0	0.8	1.2	3.2	1.7	1.4
Zr	19	56	65	65	72	55	46	61	104	91	81
Y	11	17	28	24	22	19	15	19	32	22	23
Th	0.89	2.55	3.11	3.69	3.76	2.87	2.46	3.43	6.20	2.93	3.92
La	4.11	9.25	11.00	12.85	12.31	7.92	8.47	11.31	21.48	10.78	14.33
Ce	8.53	17.88	22.65	27.14	25.96	16.42	17.41	23.99	43.98	21.38	28.99
Pr	1.16	2.46	2.88	3.44	3.36	2.16	2.29	3.01	5.81	2.85	3.79
Nd	5.39	10.38	12.73	14.60	14.33	9.23	9.59	12.77	24.18	11.53	15.21
Sm	1.54	2.65	3.11	3.64	3.62	2.45	2.51	3.28	5.67	3.06	3.90
Eu	0.53	0.70	0.94	0.87	1.16	0.78	0.75	1.18	1.34	0.76	1.09
Gd	1.81	3.30	3.64	4.34	4.32	3.03	2.68	3.99	4.67	3.02	4.02
Tb	0.27	0.51	0.50	0.62	0.61	0.49	0.40	0.56	0.77	0.52	0.61
Dy	2.07	3.07	3.27	3.77	3.87	3.17	2.61	3.48	4.84	3.30	3.80
Ho	0.45	0.66	0.67	0.88	0.87	0.70	0.54	0.74	1.00	0.71	0.78
Er	1.32	2.11	2.05	2.22	2.36	1.87	1.60	1.95	3.27	2.18	2.41
Tm	0.00	0.27	0.29	0.31	0.33	0.28	0.22	0.31	0.44	0.31	0.34
Yb	1.16	1.86	2.03	2.04	2.34	2.01	1.44	1.96	2.89	2.11	2.26
Lu	0.18	0.30	0.31	0.31	0.32	0.28	0.22	0.28	0.44	0.30	0.33

Sample	CL-21-06a	CL-22-07	CL-24-06/1	CL-24-06/5	CL-24-13a	CL-19-03	CL-20-06	CL-21-01	CL-21-06a	CL-22-07	CL-24-06/1
SiO2	60.54	55.55	63.36	59.89	56.40	51.47	53.46	50.82	60.54	55.55	63.36
TiO2	0.88	0.94	0.95	0.97	0.94	1.18	0.71	0.86	0.88	0.94	0.95
Al2O3	15.97	19.88	15.41	14.03	18.45	20.21	17.53	20.52	15.97	19.88	15.41
FeO*	10.37	6.67	7.11	10.76	8.93	11.21	8.72	9.50	10.37	6.67	7.11
MnO	0.14	0.13	0.29	0.25	0.47	0.17	0.15	0.17	0.14	0.13	0.29
MgO	3.48	2.54	2.49	2.33	2.57	3.12	4.92	3.10	3.48	2.54	2.49
CaO	4.05	9.49	4.66	7.18	6.46	8.09	11.97	11.88	4.05	9.49	4.66
Na2O	4.26	3.85	4.12	3.64	4.04	3.22	2.26	2.51	4.26	3.85	4.12
K2O	0.08	0.75	1.22	0.53	1.48	1.12	0.14	0.46	0.08	0.75	1.22
P2O5	0.24	0.20	0.39	0.42	0.26	0.21	0.14	0.18	0.24	0.20	0.39
LOI	2.6	1.8	4.7	6.6	4.3	3.4	6.6	4.7	2.6	1.8	4.7
Mg #	37.4	40.4	38.4	27.8	33.9	33.2	50.1	36.8	37.4	40.4	38.4
Cr							47				
Ni							7				
Sc	37	28				39	35	32	37	28	
V	110	231	397	256		362	256	277	110	231	397
Rb	2	19	44	18		38	2	7	2	19	44
Ba											
Sr	209	428	133	128		528	343	471	209	428	133
Nb	2.1	2.7	1.5	1.5	1.6	3.2	1.7	1.4	2.1	2.7	1.5
Zr	91	97	86	99	52	104	91	81	91	97	86
Y	33	26	32	38	22	32	22	23	33	26	32
Th	4.77	4.12	5.14	5.03	3.77	6.20	2.93	3.92	4.77	4.12	5.14
La	15.02	15.83	15.26	16.98	17.63	21.48	10.78	14.33	15.02	15.83	15.26
Ce	34.81	31.63	32.72	36.42	36.73	43.98	21.38	28.99	34.81	31.63	32.72
Pr	4.61	4.20	4.24	4.67	4.51	5.81	2.85	3.79	4.61	4.20	4.24
Nd	19.57	16.82	18.59	20.18	17.69	24.18	11.53	15.21	19.57	16.82	18.59
Sm	4.82	4.11	4.62	5.26	4.28	5.67	3.06	3.90	4.82	4.11	4.62
Eu	1.49	0.91	1.35	1.34	1.64	1.34	0.76	1.09	1.49	0.91	1.35
Gd	4.82	3.71	5.67	5.68	4.12	4.67	3.02	4.02	4.82	3.71	5.67
Tb	0.79	0.61	0.90	0.94	0.64	0.77	0.52	0.61	0.79	0.61	0.90
Dy	5.34	3.76	5.33	6.05	4.08	4.84	3.30	3.80	5.34	3.76	5.33
Ho	1.15	0.77	1.16	1.33	0.91	1.00	0.71	0.78	1.15	0.77	1.16
Er	3.00	2.49	3.33	3.91	2.50	3.27	2.18	2.41	3.00	2.49	3.33
Tm	0.44	0.34	0.47	0.52	0.39	0.44	0.31	0.34	0.44	0.34	0.47
Yb	2.97	2.33	3.14	3.56	2.38	2.89	2.11	2.26	2.97	2.33	3.14
Lu	0.41	0.35	0.49	0.50	0.36	0.44	0.30	0.33	0.41	0.35	0.49

Sample	CL-24-06/5	CL-16-12	cl-06-08	CL-11-11a
SiO2	59.89	51.13	49.55	50.42
TiO2	0.97	0.61	1.01	0.91
Al2O3	14.03	15.54	16.81	12.86
FeO*	10.76	7.72	9.36	11.61
MnO	0.25	0.26	0.17	0.20
MgO	2.33	6.60	5.63	10.81
CaO	7.18	14.67	11.79	10.26
Na2O	3.64	3.14	3.50	1.46
K2O	0.53	0.24	2.07	1.22
P2O5	0.42	0.09	0.11	0.25
LOI	6.6	7.4		10.0
Mg #	27.8	60.4	51.7	62.4
Cr		82	27	368
Ni		63	19	112
Sc		32	25	53
V	256	261	408	552
Rb	18	3	32	34
Ba			182	
Sr	128	367	339	225
Nb	1.5	3.0	2.8	2.8
Zr	99	50	71	72
Y	38	11	15	19
Th	5.03	1.42	2.54	4.19
La	16.98	7.26	10.81	13.45
Ce	36.42	14.99	25.54	30.09
Pr	4.67	1.84	3.22	3.98
Nd	20.18	7.56	13.88	17.30
Sm	5.26	1.75	3.54	4.04
Eu	1.34	0.55	1.02	1.28
Gd	5.68	2.12	3.36	4.47
Tb	0.94	0.29	0.49	0.60
Dy	6.05	2.02	3.16	3.22
Ho	1.33	0.44	0.59	0.65
Er	3.91	1.28	1.66	1.65
Tm	0.52	0.16	0.00	0.23
Yb	3.56	1.19	1.60	1.60
Lu	0.50	0.18	0.22	0.22

APPENDIX D - TABLE 2 - CL AND CP SAMPLES

Sample	CL-01-14	CL-01-14a	CL-16-01	CL-16-08a	CL-04-08a	CL-LR-1a	CL-19-20b/1CP-22-14	CP-30-07	CP-33-05	
SiO2	52.17	57.38	53.65	52.07	51.64	55.98	46.49	52.11	57.69	58.43
TiO2	2.29	1.25	1.59	1.79	1.63	0.21	1.16	1.98	0.62	0.83
Al2O3	16.77	17.93	17.02	14.15	14.40	9.62	10.74	12.74	15.60	15.04
FeO*	11.64	6.40	10.78	11.67	12.70	8.38	9.06	11.89	10.73	11.48
MnO	0.11	0.11	0.20	0.21	0.22	0.17	0.16	0.27	0.24	0.15
MgO	3.85	3.69	4.50	5.29	6.24	12.31	14.02	8.10	11.14	4.61
CaO	6.49	4.87	6.48	12.40	8.53	10.22	14.37	8.97	0.68	4.32
Na2O	5.91	7.61	5.58	2.13	3.46	2.84	0.19	3.60	3.18	4.97
K2O	0.15	0.32	0.08	0.03	0.90	0.27	2.62	0.16	0.02	0.03
P2O5	0.62	0.45	0.12	0.26	0.29	0.01	1.19	0.17	0.10	0.14
LOI	5.6		4.3	2.4	1.9	1.8	7.6	1.9	5.4	5.7
Mg #	37.1	50.7	42.7	44.7	46.7	72.4	73.4	54.8	64.9	41.7
Cr		14				271	688			
Ni		9		9	9	120	304			
Sc	45	13	42	41	58	70	26	45	36	33
V	537	89	396	384	431	216	297		526	429
Rb	3	3		2	18	1	38	1		1
Ba		153						27	12	13
Sr	371	435	76	364	319	53	440	149	22	92
Nb	15.3	14.5	1.5	10.0	4.7	0.4	8.4	4.0	5.2	3.2
Zr	182	232	84	178	138	20	289	103	101	79
Y	49	16	34	37	35	6	34	38	13	16
Th	3.12	5.39	0.20	1.39	0.76	0.10	13.15	0.27	0.66	0.60
La	28.46	26.10	2.56	13.63	8.50	0.85	74.25	9.16	7.59	4.89
Ce	60.20	59.18	8.08	32.18	22.07	2.57	182.69	22.21	19.95	12.90
Pr	7.43	7.23	1.35	4.38	3.40	0.41	23.37	3.11	2.66	1.89
Nd	32.06	28.90	7.72	18.92	15.38	2.03	96.55	15.22	12.57	9.72
Sm	7.49	5.48	2.75	5.18	4.66	0.70	19.19	4.68	3.02	2.80
Eu	2.32	1.69	1.10	1.96	1.97	0.22	5.10	1.37	0.89	0.92
Gd	7.84	4.48	4.32	6.21	6.20	0.76	14.45	6.43	2.58	2.94
Tb	1.24	0.60	0.77	1.00	1.04	0.14	1.64	0.98	0.34	0.49
Dy	7.99	3.24	5.00	6.56	6.89	0.97	7.40	7.14	1.95	3.08
Ho	1.65	0.59	1.15	1.39	1.44	0.23	1.14	1.44	0.45	0.65
Er	4.88	1.61	3.16	3.47	3.76	0.65	2.39	4.28	1.39	1.88
Tm	0.69	0.22	0.43	0.46	0.50	0.09	0.28	0.59	0.23	0.27
Yb	4.52	1.38	2.97	2.90	3.58	0.69	1.59	3.88	1.70	2.05
Lu	0.67	0.20	0.40	0.38	0.46	0.12	0.23	0.55	0.31	0.30

APPENDIX D - TABLE 3 - NON-ARC VOLCANICS

Sample	CL-19-20	CL-19-29	CL-19-30	CL-19-24	CL-01-14	CP-33-19	JLB-07	WA-3344	CL-04-15	CL-08-06	CL-10-04	CL-10-12b
SiO2	54.98	47.67	52.63	52.12	52.17	51.22	49.76	50.88	49.10	51.01	51.04	45.57
TiO2	1.22	0.79	1.15	1.93	2.29	1.74	1.33	1.48	1.09	1.33	1.40	1.25
Al2O3	16.30	19.04	15.80	15.34	16.77	14.59	15.15	15.44	20.19	15.90	15.88	15.51
FeO*	12.04	7.17	8.84	11.23	11.64	10.89	10.01	10.21	7.60	9.75	9.86	18.37
MnO	0.14	0.13	0.16	0.13	0.11	0.22	0.15	0.21	0.13	0.17	0.17	0.16
MgO	5.52	6.14	6.60	4.35	3.85	6.62	6.35	6.62	6.54	7.27	6.98	7.54
CeO	4.82	14.73	10.21	9.77	6.49	10.86	12.41	11.28	11.98	11.72	10.99	7.49
Na2O	4.61	3.71	4.21	4.04	5.91	3.54	2.31	3.59	2.88	2.55	3.43	3.66
K2O	0.10	0.52	0.27	0.88	0.15	0.17	2.44	0.15	0.41	0.21	0.12	0.35
P2O5	0.27	0.10	0.14	0.20	0.62	0.16	0.08	0.14	0.08	0.10	0.13	0.10
LOI	6.4	7.1	4.3	1.9	5.6	1.7	3.4	3.4	2.8	2.0	3.0	4.4
Mg #	45.0	60.4	57.1	40.8	37.1	52.0	53.1	53.6	60.5	57.1	55.8	42.2
Cr	161	280	255	34		222	367	96	202	74	191	211
Ni	86	63	85	25		29	69	30	64	16	35	71
Sc	49	25	34	44	45	56	47		39	42	47	48
V	343	186	289	372	537	357	310	311	197	273	299	278
Rb	2	10	7	25	3	2	5	3	7	5	1	6
Ba						27	24					
Sr	137	246	150	199	371	256	175	232	344	265	244	311
Nb	7.2	4.3	7.0	7.3	15.3	2.9	2.0	3.2	1.6	3.1	2.3	1.9
Zr	81	55	70	177	182	114	87	114	85	104	102	103
Y	32	17	24	47	49	34	28	36	18	25	26	22
Th	0.57	0.33	0.46	0.45	3.12	0.19	0.14	0.35	0.16	0.23	0.26	0.17
La	7.00	4.34	5.31	6.05	28.46	4.09	2.90	4.22	3.43	4.61	4.51	3.58
Ce	15.00	9.26	12.63	16.62	60.20	12.96	9.43	12.52	9.58	12.32	12.47	10.85
Pr	2.28	1.42	1.75	2.75	7.43	2.14	1.55	2.08	1.65	2.14	2.15	1.74
Nd	10.87	6.14	8.34	13.56	32.06	11.84	8.03	10.82	8.04	10.42	10.76	8.40
Sm	3.28	1.86	2.54	4.53	7.49	3.93	2.77	3.72	2.48	3.19	3.58	2.58
Eu	1.11	0.68	0.89	1.78	2.32	1.57	1.09	1.44	0.98	1.13	1.31	1.10
Gd	3.82	2.23	3.31	6.42	7.84	5.28	3.13	4.78	2.78	3.95	4.03	3.36
Tb	0.73	0.41	0.59	1.15	1.24	0.98	0.62	0.95	0.54	0.74	0.77	0.62
Dy	4.68	2.77	4.03	7.64	7.99	6.28	4.31	6.18	3.57	4.52	4.93	3.90
Ho	1.00	0.57	0.90	1.69	1.65	1.22	0.93	1.38	0.74	0.95	1.03	0.80
Er	2.93	1.86	2.51	4.21	4.88	3.74	2.60	3.87	2.23	2.79	3.03	2.12
Tm	0.41	0.25	0.36	0.55	0.69	0.51	0.39	0.56	0.30	0.36	0.41	0.27
Yb	2.69	1.59	2.30	3.77	4.52	3.32	2.35	3.53	1.98	2.40	2.55	1.86
Lu	0.40	0.24	0.30	0.49	0.67	0.47	0.36	0.56	0.26	0.33	0.39	0.24

Sample	WA-21	CL-01-06a	CL-01-10	CL-10-09	CL-16-05a	1CL-07-11	CL-09-06	CL-12-01	CP-01-08a	WA-01	WA-16	CL-07-11
SiO2	48.18	51.81	56.39	56.73	49.56	49.16	50.57	50.53	48.84	50.63	49.51	49.16
TiO2	1.43	2.19	2.18	2.49	1.74	1.70	2.12	1.98	1.74	2.26	1.55	1.70
Al2O3	16.41	14.53	12.79	13.63	14.86	17.56	15.05	14.21	15.41	13.86	16.33	17.56
FeO*	10.74	12.44	12.47	12.53	11.27	10.42	11.37	11.95	10.22	13.53	10.23	10.42
MnO	0.19	0.23	0.22	0.19	0.20	0.17	0.19	0.21	0.18	0.21	0.19	0.17
MgO	7.93	5.39	4.33	4.52	6.67	5.43	7.29	6.79	7.30	6.96	7.60	5.43
CaO	12.45	8.15	7.00	5.09	11.29	12.37	9.65	10.72	12.07	7.61	10.93	12.37
Na2O	2.02	4.72	4.19	4.37	4.12	2.68	3.41	2.72	3.94	4.51	3.17	2.68
K2O	0.49	0.16	0.18	0.12	0.11	0.32	0.07	0.69	0.10	0.07	0.36	0.32
P2O5	0.16	0.38	0.24	0.33	0.19	0.19	0.27	0.20	0.20	0.35	0.15	0.19
LOI	2.5	1.7	2.4	2.4	3.2	2.0	3.6	2.7	2.9	2.8	2.3	2.0
Mg #	56.8	43.6	38.2	39.1	51.4	48.1	53.3	50.3	56.0	47.8	57.0	48.1
Cr	218				55	117	143	55	214		182	117
Ni	84				10	33	35	23	36	7	50	33
Sc	49	51	44	40	49	38	41	45	49	43	41	38
V	320	372	490	454	334	322	393	405	326	427	309	322
Rb	12			2		6	1	10		1	6	6
Ba	51								48	20	155	
Sr	238	209	183	238	170	288	234	273	255	152	347	288
Nb	2.7	5.4	5.8	8.3	4.6	5.5	11.4	7.4	5.9	11.1	5.5	5.5
Zr	98	167	174	222	130	116	141	141	119	158	104	116
Y	25	41	42	53	31	29	26	32	30	41	27	29
Th	0.28	0.41	0.68	0.92	0.43	0.48	1.03	0.60	0.49	1.27	0.56	0.48
La	4.61	7.47	8.85	11.51	6.71	7.94	12.22	8.90	7.01	13.15	6.99	7.94
Ce	13.25	21.21	23.77	31.30	18.70	19.42	29.32	22.67	20.26	33.47	19.34	19.42
Pr	2.15	3.30	3.76	4.89	2.86	2.98	4.05	3.31	3.00	4.47	2.74	2.98
Nd	11.23	15.97	18.36	23.26	14.56	13.72	17.92	14.99	15.03	21.41	14.01	13.72
Sm	3.38	4.98	5.69	6.99	4.17	4.18	4.82	4.23	4.38	5.83	3.88	4.18
Eu	1.33	2.00	1.80	2.03	1.74	1.48	1.56	1.75	1.69	2.12	1.48	1.48
Gd	4.14	6.83	5.88	7.83	5.67	4.51	4.46	5.42	5.05	6.79	4.51	4.51
Tb	0.77	1.13	1.14	1.10	0.95	0.82	0.74	0.92	0.89	1.16	0.78	0.82
Dy	4.81	7.18	7.31	9.28	5.88	5.05	4.53	5.52	5.77	7.50	5.02	5.05
Ho	1.07	1.57	1.52	1.91	1.29	1.03	0.89	1.15	1.18	1.61	1.09	1.03
Er	2.69	4.19	4.86	5.89	3.30	3.01	2.80	2.97	3.15	4.08	2.92	3.01
Tm	0.38	0.55	0.68	0.86	0.42	0.42	0.36	0.40	0.41	0.56	0.41	0.42
Yb	2.37	3.50	4.23	5.37	2.75	2.60	2.32	2.47	2.72	3.54	2.58	2.60
Lu	0.34	0.51	0.59	0.82	0.36	0.39	0.34	0.34	0.37	0.50	0.39	0.39

APPENDIX D - TABLE 4 - TRANSITIONAL VOLCANICS

Sample	CL-01-14	CL-16-01	CL-16-08a	CL-10-11a	CL-16-02	CP-09-01	WA-12	WA-10	CL-11-12a	CL-04-04a	CP-HD-01
SiO ₂	52.17	53.65	52.07	55.64	49.16	52.25	49.60	53.54	46.52	55.70	54.43
TiO ₂	2.29	1.59	1.79	1.30	1.26	1.55	1.56	1.69	1.31	1.42	1.71
Al ₂ O ₃	16.77	17.02	14.15	14.62	17.48	13.61	15.62	14.47	19.35	16.12	16.02
FeO*	11.64	10.78	11.67	9.73	8.71	9.54	11.36	10.87	9.68	9.10	9.38
MnO	0.11	0.20	0.21	0.16	0.20	0.20	0.20	0.17	0.18	0.16	0.14
MgO	3.85	4.50	5.29	6.58	10.46	6.75	7.10	5.82	9.27	4.76	4.01
CaO	6.49	6.48	12.40	8.96	9.12	11.18	11.02	8.07	10.47	8.15	7.64
Na ₂ O	5.91	5.58	2.13	2.63	3.24	4.46	3.25	4.82	2.95	3.58	6.21
K ₂ O	0.15	0.08	0.03	0.25	0.24	0.25	0.12	0.34	0.14	0.84	0.23
P ₂ O ₅	0.62	0.12	0.26	0.12	0.13	0.20	0.18	0.22	0.14	0.17	0.23
LOI	5.6	4.3	2.4	3.2	3.8	2.3	2.7	2.7	3.5	2.5	5.6
Mg #	37.1	42.7	44.7	54.7	68.2	55.8	52.7	48.8	63.1	48.3	43.3
Cr				22	46	128	199	16	340	42	
Ni			9	13	24	41	47	11	174	12	
Sc	45	42	41	46	37	52	49	44	43	39	32
V	537	396	384	284	275	334	354	392	240	300	235
Rb	3		2	3	26	2	1	3	2	13	
Ba					145	50	45	46	15	249	51
Sr	371	76	364	226	267	141	200	159	264	287	149
Nb	15.3	1.5	10.0	3.1	3.5	4.3	4.6	5.9	2.1	7.3	6.6
Zr	182	84	178	121	105	112	111	142	104	148	128
Y	49	34	37	29	23	28	29	36	21	37	31
Th	3.12	0.20	1.39	0.47	0.67	0.79	0.64	1.09	0.36	1.97	2.07
La	28.46	2.56	13.63	5.89	6.03	6.74	7.36	10.23	3.88	11.87	12.29
Ce	60.20	8.08	32.18	16.14	16.68	17.70	19.81	26.32	11.97	29.05	30.96
Pr	7.43	1.35	4.38	2.60	2.54	2.65	2.93	3.78	1.92	3.90	4.21
Nd	32.06	7.72	18.92	13.46	12.08	13.29	14.48	17.71	9.28	18.11	18.57
Sm	7.49	2.75	5.18	3.89	3.42	3.87	4.15	4.97	2.97	4.94	5.10
Eu	2.32	1.10	1.96	1.29	1.40	1.22	1.45	1.75	1.21	1.69	1.83
Gd	7.84	4.32	6.21	4.26	4.28	4.71	4.88	5.93	4.26	5.91	6.01
Tb	1.24	0.77	1.00	0.83	0.72	0.78	0.79	1.01	0.70	0.96	0.95
Dy	7.99	5.00	6.56	5.09	4.62	5.20	5.24	6.46	4.57	6.22	6.03
Ho	1.65	1.15	1.39	1.04	0.91	1.08	1.12	1.34	0.96	1.37	1.23
Er	4.88	3.16	3.47	3.15	2.67	3.06	3.16	3.88	2.54	3.58	3.65
Tm	0.69	0.43	0.46	0.42	0.39	0.45	0.45	0.55	0.33	0.49	0.50
Yb	4.52	2.97	2.90	2.80	2.44	2.87	2.86	3.45	2.14	3.48	3.13
Lu	0.67	0.40	0.38	0.42	0.35	0.41	0.42	0.53	0.28	0.51	0.41

Sample WA-03

SiO2	57.02
TiO2	1.20
Al2O3	15.16
FeO*	7.92
MnO	0.14
MgO	5.78
CaO	9.14
Na2O	2.77
K2O	0.70
P2O5	0.17
LOI	1.9
Mg #	56.5
Cr	140
Ni	50
Sc	32
V	211
Rb	10
Ba	202
Sr	227
Nb	6.8
Zr	142
Y	33
Th	2.07
La	11.11
Ce	26.50
Pr	3.66
Nd	17.03
Sm	4.59
Eu	1.42
Gd	4.96
Tb	0.96
Dy	5.72
Ho	1.27
Er	3.38
Tm	0.49
Yb	3.28
Lu	0.49

APPENDIX D - TABLE 5 - ARC INTRUSIVES

Sample	JLB-02	JLB-04	JLB-02	JLB-04	CL-01-01a	CL-06-06a	CL-19-27	CL-06-05	CL-19-27a	CL-07-03	CL-16-02b
SiO2	47.42	61.85	47.42	61.85	58.30	52.63	50.06	53.54	56.23	57.36	52.85
TiO2	0.11	0.17	0.11	0.17	0.77	0.61	0.25	0.34	0.77	1.00	1.46
Al2O3	11.55	11.09	11.55	11.09	14.79	16.52	14.08	16.79	14.14	15.48	18.03
FeO*	12.34	9.12	12.34	9.12	10.34	9.21	5.27	6.92	11.77	11.56	9.28
MnO	0.28	0.17	0.28	0.17	0.13	0.10	0.13	0.23	0.24	0.09	0.17
MgO	19.51	8.07	19.51	8.07	4.35	7.75	13.02	9.91	4.82	4.04	6.52
CaO	8.44	7.52	8.44	7.52	11.21	8.32	14.75	7.65	9.97	5.44	8.94
Na2O	0.18	0.97	0.18	0.97	0.06	4.35	1.24	4.04	1.98	3.97	2.35
K2O	0.17	1.03	0.17	1.03	0.01	0.44	1.21	0.54	0.04	1.03	1.34
P2O5	0.01	0.01	0.01	0.01	0.04	0.06	0.00	0.04	0.05	0.14	0.06
LOI	8.1	2.6	8.1	2.6	3.8	1.7	3.2	3.3	5.8	2.6	2.5
Mg #	73.8	61.2	73.8	61.2	42.9	60.0	81.5	71.8	42.2	36.4	55.6
Cr	1726	289	1726	289		52	205	176			46
Ni	516	74	516	74	6	6	108	84			24
Sc	57	46	57	46	28	55	55	41	43	45	36
V	297	286	297	286	361	338	177	253	371	361	272
Rb		1		1	1	4	17	7	2	23	26
Ba	8		8								
Sr	6	103	6	103	100	216	164	177	113	250	265
Nb	0.7	1.2	0.7	1.2	0.7	0.3	0.1	0.3	0.9	2.6	1.3
Zr	14	23	14	23	41	32	12	30	61	80	34
Y	3	4	3	4	20	14	7	9	30	20	12
Th	0.30	0.36	0.30	0.36	0.21	0.15	0.02	0.24	0.68	0.71	0.50
La	0.94	1.28	0.94	1.28	1.66	1.07	0.44	1.35	3.37	5.64	3.03
Ce	2.29	2.90	2.29	2.90	4.21	2.68	0.87	3.23	9.57	15.54	7.06
Pr	0.28	0.35	0.28	0.35	0.72	0.44	0.21	0.46	1.42	2.14	1.05
Nd	1.20	1.47	1.20	1.47	3.77	2.43	0.99	2.29	7.50	10.62	4.41
Sm	0.32	0.37	0.32	0.37	1.54	0.98	0.47	0.88	2.64	3.13	1.36
Eu	0.08	0.10	0.08	0.10	0.56	0.47	0.26	0.36	0.92	1.21	0.59
Gd	0.29	0.31	0.29	0.31	2.34	1.73	0.72	1.35	3.44	4.29	1.96
Tb	0.05	0.06	0.05	0.06	0.46	0.33	0.15	0.24	0.66	0.69	0.31
Dy	0.44	0.52	0.44	0.52	3.43	2.32	1.10	1.80	4.86	4.79	2.19
Ho	0.12	0.13	0.12	0.13	0.83	0.55	0.25	0.40	1.06	0.98	0.46
Er	0.39	0.45	0.39	0.45	2.28	1.56	0.69	1.26	3.09	2.85	1.25
Tm	0.07	0.08	0.07	0.08	0.35	0.22	0.09	0.20	0.45	0.39	0.19
Yb	0.50	0.60	0.50	0.60	2.50	1.56	0.62	1.32	2.83	2.54	1.23
Lu	0.09	0.10	0.09	0.10	0.36	0.24	0.09	0.19	0.37	0.34	0.18

Sample	A112b	BS-5	JLB-08	WB-1	CL-LR-1a	CL-01-01a	CL-06-06a	CL-19-27	CL-06-05	CL-19-27a	CL-24-16c/2
SiO2	55.64	52.21	61.48	57.91	55.98	58.30	52.63	50.06	53.54	56.23	62.71
TiO2	1.02	1.06	0.75	0.59	0.21	0.77	0.61	0.25	0.34	0.77	0.64
Al2O3	15.87	15.63	15.76	17.62	9.62	14.79	16.52	14.08	16.79	14.14	16.43
FeO*	7.01	6.78	5.65	6.82	8.38	10.34	9.21	5.27	6.92	11.77	4.60
MnO	0.12	0.17	0.11	0.10	0.17	0.13	0.10	0.13	0.23	0.24	0.09
MgO	8.18	8.85	5.88	5.61	12.31	4.35	7.75	13.02	9.91	4.82	4.55
CaO	5.54	10.62	5.75	7.41	10.22	11.21	8.32	14.75	7.65	9.97	4.04
N2O	5.16	4.01	4.19	3.49	2.84	0.06	4.35	1.24	4.04	1.98	4.57
K2O	1.25	0.32	0.11	0.38	0.27	0.01	0.44	1.21	0.54	0.04	2.19
P2O5	0.22	0.35	0.32	0.06	0.01	0.04	0.06	0.00	0.04	0.05	0.18
LOI	3.4	9.9	5.2	2.8	1.8	3.8	1.7	3.2	3.3	5.8	5.3
Mg #	67.5	69.9	65.0	59.4	72.4	42.9	60.0	81.5	71.8	42.2	63.8
Cr	495		317	170	271		52	205	176		181
Ni	179		160	89	120	6	6	108	84		84
Sc	21		20	23	70	28	55	55	41	43	18
V	202	185	143	262	216	361	338	177	253	371	125
Rb	23	4	59	6	1	1	4	17	7	2	43
Ba	323	270	487	122							
Sr	391	1605	270	319	53	100	216	164	177	113	306
Nb	6.8	6.8	6.2	2.7	0.4	0.7	0.3	0.1	0.3	0.9	2.0
Zr	114	127	139	77	20	41	32	12	30	61	124
Y	19	16	18	11	6	20	14	7	9	30	12
Th	2.90	4.56	4.99	1.89	0.10	0.21	0.15	0.02	0.24	0.68	4.68
La	18.48	24.01	26.03	7.85	0.85	1.66	1.07	0.44	1.35	3.37	13.51
Ce	39.83	53.42	57.09	17.55	2.57	4.21	2.68	0.87	3.23	9.57	29.46
Pr	4.88	6.51	6.64	2.28	0.41	0.73	0.44	0.21	0.46	1.42	3.52
Nd	20.43	25.37	24.73	9.38	2.03	3.77	2.43	0.99	2.29	7.50	14.06
Sm	4.15	5.06	4.42	2.15	0.70	1.54	0.98	0.47	0.88	2.64	2.90
Eu	1.17	1.51	1.07	0.61	0.22	0.56	0.47	0.26	0.36	0.92	0.84
Gd	4.06	4.93	2.59	2.23	0.76	2.34	1.73	0.72	1.35	3.44	2.85
Tb	0.54	0.58	0.38	0.30	0.14	0.46	0.33	0.15	0.24	0.65	0.35
Dy	3.59	3.34	2.85	2.26	0.97	3.43	2.32	1.10	1.80	4.86	2.02
Ho	0.69	0.65	0.57	0.41	0.23	0.53	0.55	0.25	0.40	1.06	0.38
Er	2.15	1.71	1.59	1.28	0.65	2.28	1.56	0.69	1.26	3.09	1.11
Tm	0.31	0.24	0.23	0.15	0.09	0.35	0.22	0.09	0.20	0.45	0.16
Yb	2.02	1.64	1.46	1.28	0.69	2.50	1.56	0.62	1.32	2.83	0.99
Lu	0.32	0.23	0.22	0.20	0.12	0.36	0.24	0.09	0.19	0.37	0.16

Sample	CL-LIP-1	BS-01	CL-19-20c	CP-33-21a	LBM-1	WB-3	CL-22-10b/2	MM-04-07 6	CL-24-13b	CL-24-17b	CL-24-13c
SiO2	60.12	51.03	51.01	54.96	49.79	48.53	54.34	52.41	57.19	54.99	60.73
TiO2	0.95	0.39	0.60	0.69	0.48	0.43	0.93	1.08	0.98	0.85	0.48
Al2O3	16.70	13.51	14.14	18.43	17.93	8.33	20.34	20.54	19.24	18.76	16.91
FeO*	5.50	10.19	9.23	14.00	9.03	9.39	8.50	8.20	8.41	9.92	6.80
MnO	0.10	0.18	0.16	0.20	0.16	0.17	0.10	0.26	0.21	0.21	0.32
MgO	4.33	9.64	10.97	7.04	8.06	18.52	3.11	2.13	3.47	4.41	4.07
CaO	6.85	12.10	11.06	0.35	11.32	14.21	5.55	8.30	3.64	6.05	5.25
Na2O	4.13	1.81	2.49	4.00	2.91	0.18	6.19	1.62	5.66	2.44	2.58
K2O	1.24	1.08	0.20	0.25	0.22	0.19	0.82	5.25	0.99	2.20	2.69
P2O5	0.08	0.07	0.13	0.09	0.09	0.04	0.12	0.21	0.32	0.17	0.16
LOI	1.4	2.6	12.0		3.1	3.6	3.9	9.0	3.5	5.3	6.7
Mg #	58.4	62.8	67.9	47.2	61.4	77.8	39.5	31.6	42.4	44.2	51.6
Cr	78		609			1237					35
Ni	23		160			368					
Sc	22	48	53	39	40	62	30	32		25	
V	164	318	307		289	279	371	314	290	309	232
Rb	29	21	2	5	3	5	15	166	25	44	68
Ba				60	51	52					
Sr	544	175	133	39	244	54	391	218	274	354	123
Nb	3.3	0.7	1.1	1.4	0.9	0.4	1.0	2.1	3.0	1.2	2.7
Zr	176	22	42	30	20	13	58	79	86	69	108
Y	17	9	14	12	12	8	16	22	26	22	22
Th	4.06	0.90	0.80	1.52	1.78	0.96	1.58	3.99	5.22	3.59	8.01
La	11.83	3.84	7.86	4.77	7.36	3.83	6.48	13.21	16.72	12.16	18.30
Ce	26.64	8.44	16.82	10.89	15.05	8.16	14.11	28.06	37.88	25.56	39.19
Pr	3.36	1.10	2.14	1.45	1.79	1.14	1.85	3.63	4.99	3.31	4.77
Nd	13.28	4.96	9.30	6.48	7.63	5.23	8.44	14.44	20.89	14.36	18.62
Sm	3.04	1.41	2.15	1.68	1.80	1.50	2.35	3.35	4.69	3.52	3.79
Eu	1.12	0.50	0.63	0.54	0.65	0.45	0.82	1.00	1.29	1.07	1.13
Gd	3.30	1.91	2.32	2.26	2.31	1.61	2.50	3.27	4.39	4.24	3.61
Tb	0.51	0.27	0.32	0.33	0.32	0.22	0.44	0.51	0.69	0.58	0.53
Dy	3.07	1.87	2.00	2.41	2.20	1.45	2.87	3.17	4.27	3.69	3.37
Ho	0.62	0.40	0.39	0.51	0.43	0.31	0.60	0.67	0.93	0.79	0.73
Er	1.70	1.29	1.16	1.60	1.33	0.92	1.73	1.83	2.60	2.30	2.09
Tm	0.22	0.19	0.16	0.20	0.21	0.12	0.24	0.26	0.39	0.32	0.29
Yb	1.63	1.24	1.10	1.38	1.26	0.82	1.71	1.89	2.46	2.18	2.01
Lu	0.23	0.20	0.16	0.21	0.20	0.12	0.23	0.27	0.38	0.32	0.30

Sample CL-24-15b

SiO2	61.67
TiO2	0.56
Al2O3	16.58
FeO*	7.38
MnO	0.17
MgO	2.62
CaO	3.85
Na2O	4.00
K2O	2.81
P2O5	0.36

LOI	4.8
Mg #	38.7

Cr	
Ni	
Sc	
V	83

Rb	70
Ba	
Sr	143
Nb	4.2
Zr	149
Y	29
Th	9.05

La	28.37
Ce	61.25
Pr	7.76
Nd	30.30
Sm	6.69
Eu	2.00
Gd	6.22
Tb	0.91
Dy	5.68
Ho	1.20
Er	3.47
Tm	0.47
Yb	3.46
Lu	0.53

APPENDIX D - TABLE 6 - TRANSITIONAL AND NON-ARC (cp-92-53) INTRUSIVES

Sample	CL-13-01a	CL-19-19	wa-33	CL-24-18b/1	CP-23-19	CL-04-08a	CL-01-14a	NON-ARC cp-92-53
SiO2	50.88	49.56	51.03	53.34	56.30	51.64	57.38	45.42
TiO2	2.50	1.44	1.75	2.19	1.75	1.63	1.25	2.12
Al2O3	15.22	15.73	14.77	15.54	15.09	14.40	17.93	15.68
FeO*	12.69	9.90	11.06	11.37	8.99	12.70	6.40	14.18
MnO	0.20	0.17	0.17	0.12	0.16	0.22	0.11	0.22
MgO	5.26	7.88	6.67	6.92	5.88	6.24	3.69	9.61
CeO	8.68	12.63	9.89	6.11	6.81	8.53	4.87	8.66
Na2O	3.33	2.04	3.70	2.49	3.33	3.46	7.61	2.32
K2O	0.83	0.53	0.77	1.67	1.30	0.90	0.32	1.52
P2O5	0.41	0.12	0.19	0.25	0.40	0.29	0.45	0.26
LOI	2.2	1.2		8.1	2.6	1.9		
Mg #	42.5	58.6	51.8	52.0	53.8	46.7	50.7	54.7
Cr	20		145	58	189		14	211
Ni	8	11	47	29	86	9	9	105
Sc		31	37	46	26	58	13	38
V	307	301	323	494	229	431	89	303
Rb	12	85	11	28	36	18	3	26
Ba		506	170		271		153	206
Sr	358	299	313	170	321	319	435	200
Nb	10.9	5.2	7.8	5.3	7.0	4.7	14.5	5.8
Zr	222	71	120	138	152	138	232	127
Y	37	21	25	26	21	35	16	22
Th	1.81	0.82	1.43	1.96	4.56	0.76	5.39	0.61
La	15.40	8.25	10.71	13.63	16.42	8.50	26.10	10.55
Ce	39.21	19.91	25.40	31.18	36.48	22.07	59.18	25.78
Pr	5.38	2.78	3.48	4.17	4.69	3.40	7.23	3.74
Nd	23.77	13.01	15.78	18.39	19.81	15.38	28.90	16.20
Sm	5.97	3.55	4.18	4.75	4.79	4.66	5.48	4.31
Eu	2.22	1.25	1.35	1.64	1.75	1.97	1.69	1.47
Gd	6.64	4.13	4.70	5.41	4.75	6.20	4.48	4.55
Tb	1.10	0.66	0.68	0.89	0.73	1.04	0.60	0.67
Dy	6.88	3.98	4.79	5.36	4.38	6.89	3.24	4.74
Ho	1.44	0.79	0.93	1.15	0.89	1.44	0.59	0.90
Er	3.78	2.25	2.72	2.95	2.44	3.76	1.61	2.51
Tm	0.50	0.32		0.39	0.35	0.50	0.22	
Yb	3.58	2.05	2.34	2.60	2.14	3.58	1.38	2.30
Lu	0.50	0.29	0.37	0.37	0.32	0.46	0.20	0.33

APPENDIX D - TABLE 7 - FELSIC ROCKS

Sample	CP-03-02b	CP-05-05	CP-20-07j	CP-25-08	CP-28-15a	JLB-09	CP-28-15p	CL-11-09	CP-09-06	CL-8R-7	CL-18-00
SiO2	75.58	77.96	76.63	77.09	66.04	73.75	77.22	66.39	78.13	66.17	72.86
TiO2	0.21	0.08	0.25	0.04	0.33	0.08	0.16	0.59	0.08	0.29	0.29
Al2O3	13.05	11.26	12.27	11.77	17.03	12.14	12.09	16.73	12.85	16.95	14.45
FeO*	2.53	3.73	2.95	3.71	4.89	6.19	1.38	3.35	0.68	2.07	2.73
MnO	0.04	0.10	0.14	0.04	0.04	0.11	0.03	0.12	0.02	0.04	0.08
MgO	1.25	2.13	0.73	2.74	2.46	1.37	0.38	0.85	1.55	1.92	1.50
CaO	1.00	0.25	1.38	0.06	0.19	1.08	1.33	1.49	0.21	3.00	1.84
Na2O	2.61	4.14	4.00	3.75	6.50	5.20	5.46	5.99	6.03	6.17	3.78
K2O	3.64	0.22	1.60	0.73	2.48	0.04	1.94	4.34	0.35	3.32	2.43
P2O5	0.08	0.14	0.04	0.06	0.05	0.04	0.01	0.15	0.09	0.08	0.05
LOI	2.7	2.0	3.8	2.1	1.9	2.4	1.3	3.0	1.1	0.8	2.2
Mg #	46.9	50.4	30.7	56.8	47.2	28.3	32.8	31.1	80.3	62.3	49.5
Cr							26				
Sc	13	10	21	9	10	27	5	12	10	6	5
V	24	8		51	50	43	25	7	41		15
Rb	38	4	27	13	36	1	19	95	7	47	76
Ba	441	63	58	349	265	53	399	76	688		
Sr	69	91	82	56	105	63	99	173	92	670	322
Nb	4.0	0.8	5.6	2.1	3.4	1.6	1.5	9.0	3.0	4.1	8.0
Zr	199	141	160	104	88	55	58	208	107	52	188
Y	37	10	23	12	14	11	10	40	14	3	23
Th	4.34	2.66	2.98	2.99	6.37	0.73	4.36	14.00	4.12	3.88	16.87
La	16.47	5.86	11.09	5.19	13.02	2.58	9.02	37.05	18.52	17.02	24.11
Ce	35.34	14.16	26.59	9.88	25.74	5.92	18.41	82.57	29.43	35.63	48.41
Pr	4.28	1.81	3.33	1.13	2.76	0.73	2.04	10.45	3.74	4.41	5.88
Nd	17.39	8.41	15.77	3.96	10.63	3.17	7.69	41.14	13.62	17.63	20.83
Sm	4.11	2.00	4.04	0.91	2.32	0.86	1.44	8.09	2.68	3.31	3.86
Eu	0.75	0.50	1.07	0.20	0.60	0.26	0.38	2.18	0.46	0.77	0.23
Gd	4.08	1.91	3.52	1.04	2.52	0.92	1.74	7.55	2.56	2.22	3.62
Tb	0.68	0.26	0.60	0.21	0.37	0.16	0.26	1.07	0.41	0.18	0.45
Dy	4.66	1.54	3.87	1.44	2.47	1.27	1.62	6.37	2.60	0.76	2.89
Ho	0.96	0.40	0.30	0.34	0.56	0.29	0.42	1.29	0.57	0.11	0.61
Er	3.01	1.41	2.65	1.03	1.85	0.97	1.25	3.48	1.76	0.27	2.02
Tm	0.44	0.24	0.42	0.15	0.31	0.16	0.22	0.51	0.29	0.03	0.33
Yb	3.11	1.96	3.11	1.11	2.03	1.11	1.53	3.71	1.98	0.21	2.32
Lu	0.49	0.36	0.51	0.18	0.34	0.19	0.26	0.56	0.32	0.03	0.40

Sample	CL-19-11a	CL-24-03	CL-24-03/2	CL-24-12a	MM-03-03b	CL-19-06a	CL-19-11b	CL-24-01b	CL-SAP-1	90-2CC	1543324
SiO2	77.06	72.32	70.84	68.56	73.13	70.28	69.84	69.25	68.74	69.66	77.39
TiO2	0.00	0.00	0.29	0.34	0.08	0.46	0.34	0.29	0.50	0.33	0.10
Al2O3	13.27	14.83	17.79	15.63	14.22	16.27	16.02	15.84	15.94	15.13	12.14
FeO*	0.44	2.25	1.28	3.37	2.81	2.36	2.53	2.38	2.54	3.13	2.49
MnO	0.01	0.10	0.04	0.12	0.11	0.03	0.05	0.06	0.03	0.08	0.02
MgO	0.16	0.23	1.01	1.30	1.53	1.12	1.94	1.62	1.68	1.25	0.97
CaO	0.49	1.08	3.47	2.44	3.10	2.06	1.86	2.69	3.27	3.68	1.52
Na2O	4.79	3.98	2.74	2.77	0.09	5.31	5.06	5.97	5.00	3.10	4.90
K2O	3.79	5.22	2.48	5.36	4.91	2.03	2.27	1.79	2.22	3.54	0.44
P2O5	0.00	0.00	0.05	0.12	0.02	0.08	0.08	0.10	0.09	0.10	0.04
LOI	0.8	1.2	3.7	4.3	5.2	3.0	2.8	3.6	2.7	1.7	1.2
Mg #	39.3	15.4	58.4	40.7	49.2	45.7	57.7	54.8	54.1	41.5	40.9
Cr			6	5	4		6	27	8	30	
Sc						8	4	6	7	8	10
V		4	38	48	1		52	57	52	55	22
Rb	48	181	61	124	144	51	87	64	71	108	3
Ba				936		424		229		1382	53
Sr	430	130	266	94	63	408	107	352	786	457	113
Nb	2.1	4.6	1.9	3.7	7.2	2.8	0.6	1.4	1.4	10.5	3.5
Zr	114	153	122	166	167	62	96	123	158	118	90
Y	7	28	13	21	25	6	6	9	9	16	8
Th	21.68	14.31	10.32	13.18	11.95	4.72	4.26	5.91	5.22	14.50	4.14
La	32.42	36.99	22.99	25.91	34.15	13.11	9.53	13.65	16.69	35.15	8.53
Ce	52.87	76.32	36.55	50.31	70.59	27.83	21.55	28.63	34.08	66.75	17.42
Pr	5.13	8.90	3.22	5.57	8.19	3.30	2.44	3.26	3.99	7.09	1.94
Nd	15.39	30.60	9.75	18.98	29.00	12.96	9.53	12.29	14.54	24.06	7.14
Sm	2.39	5.60	1.68	3.60	4.91	2.48	1.85	2.22	2.83	4.04	1.53
Eu		1.05	0.43	0.87	1.01	0.67	0.66	0.67	0.87	0.41	0.43
Gd	2.13	5.19	1.82	3.09	4.58	2.32	1.87	1.89	2.28	2.25	1.17
Tb	0.21	0.71	0.27	0.45	0.62	0.22	0.25	0.24	0.32	0.34	0.20
Dy	1.26	4.27	1.88	2.86	3.69	1.43	1.23	1.31	1.78	2.61	1.40
Ho	0.26	0.90	0.43	0.61	0.76	0.25	0.26	0.25	0.32	0.51	
Er	0.96	2.70	1.22	1.73	2.38	0.64	0.63	0.69	0.84	1.59	0.90
Tm	0.16	0.41	0.18	0.27	0.37	0.08	0.07	0.08	0.11	0.24	
Yb	1.19	3.18	1.34	1.98	2.73	0.64	0.59	0.60	0.77	1.58	1.20
Lu	0.21	0.52	0.22	0.33	0.41	0.09	0.08	0.08	0.11	0.25	0.19

APPENDIX E

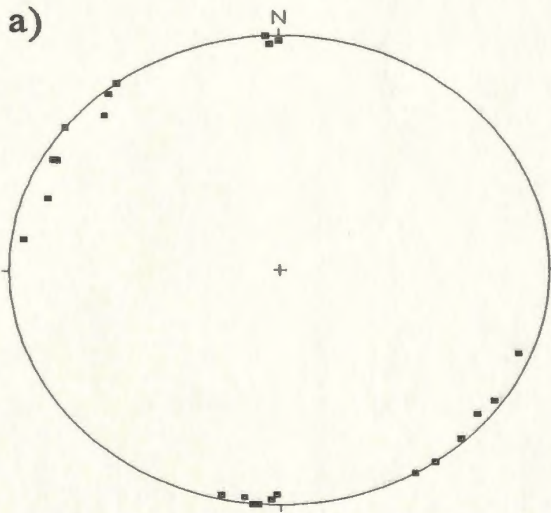
Structural Orientation Data

The data presented in this Appendix are referred to in Chapter 6. The collected and compiled data are plotted on equal-area projection and lower hemisphere stereo plots using a computer program Quickplot by D van Everdingen and J van Gool. Orientations of planar and linear structural elements used in this thesis are presented in form of: dip->dip direction (azimuth) (e.g. 30-~180). Both bedding and foliations data are plotted as poles to planes.

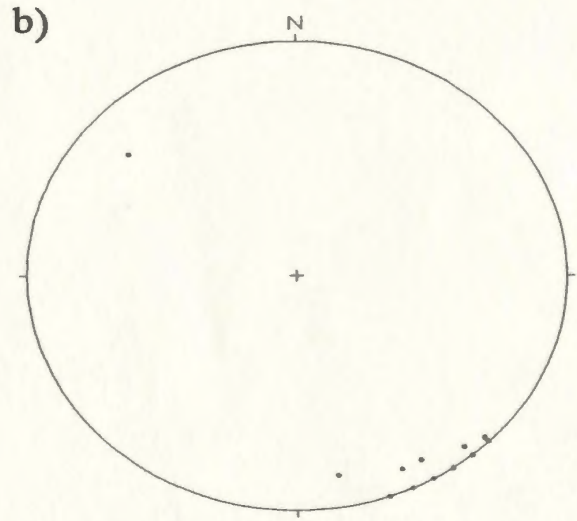
The structural observations for this study were carried out at mesoscopic and macroscopic scale. Structural data collected during the course of this study have been augmented by data from Maclean (1947), Donohoe (1968), Sayeed (1970), Fleming (1970), Marten (1971), DeGrace (1971), and Kean and Evans (1987). Structural orientation data are generally compiled for relatively large areas, that encompass many geological structures that vary considerably in style and size. This has resulted in some cases in poorly defined, locally nondescript clusters on some stereograms. The data sets taken from the previous work mostly did not distinguish between different generations of foliations, and are here presented as S2. For plotting, the dip angles of the orientation data from the published sources, which are commonly rounded to multiples of five, were increased or decreased by a random number between +2 and -2, in order to prevent formation of biased maxima.

WESTERN DOMAIN

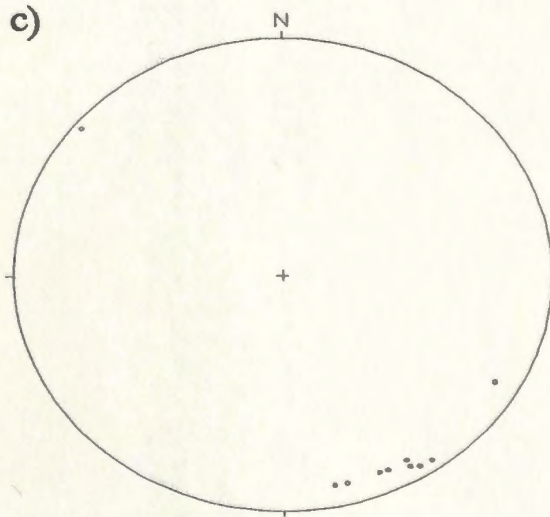
WHALESBACK MINE



poles to dykes N=23



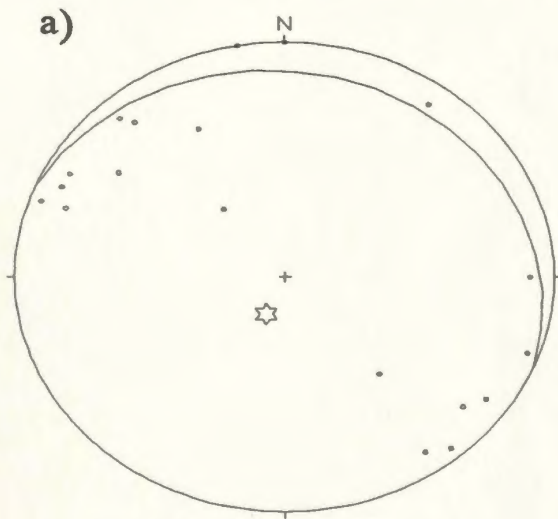
poles to S2 cleavage N=16
mean: 89- > 326



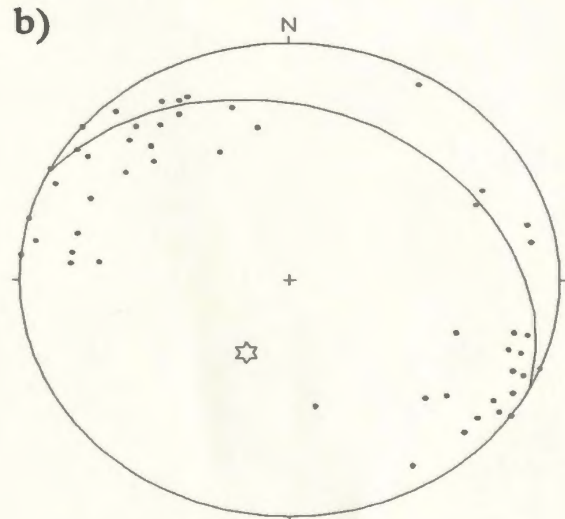
poles to bedding N=10
mean: 82- > 329

Figure E-i

**WESTERN DOMAIN
CATCHERS POND PANEL - NW**

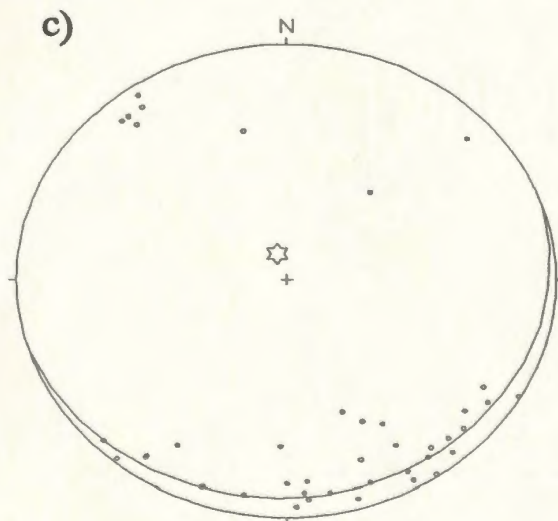


poles to bedding N=19
axis: 76->203

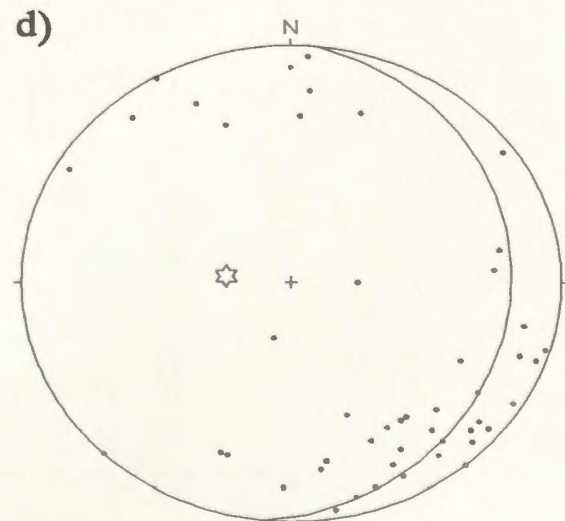


poles to S2/S3 cleavage N=53
axis: 61->207

**WESTERN DOMAIN
CATCHERS POND PANEL - SE**



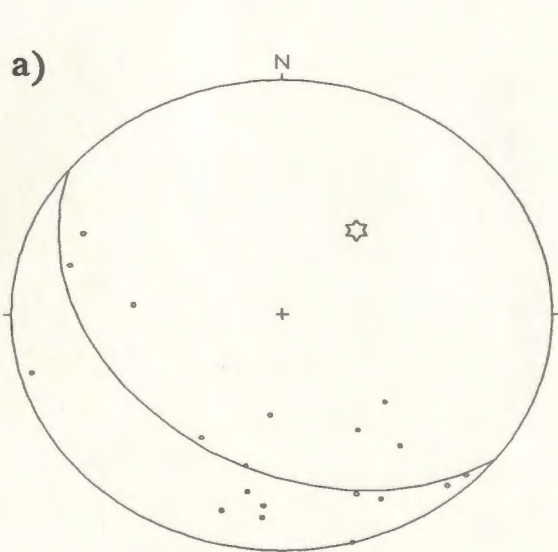
poles to bedding N=41
axis: 81->341



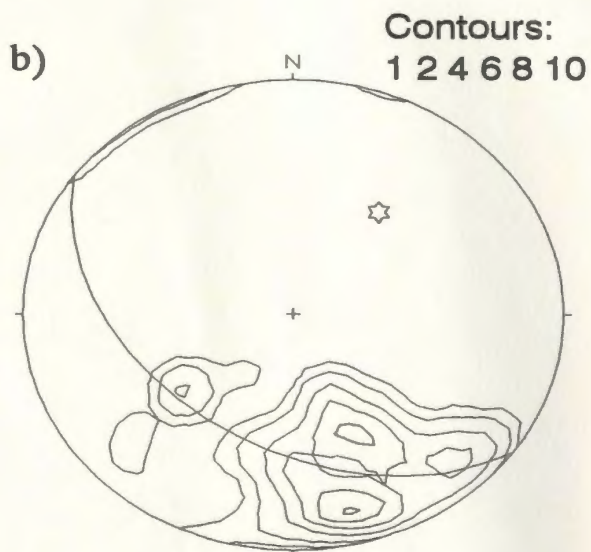
poles to S2/S3 cleavage N=48
axis: 70->276

Figure E-ii

**WESTERN DOMAIN
MISTAKEN POND PANEL
SW PART**

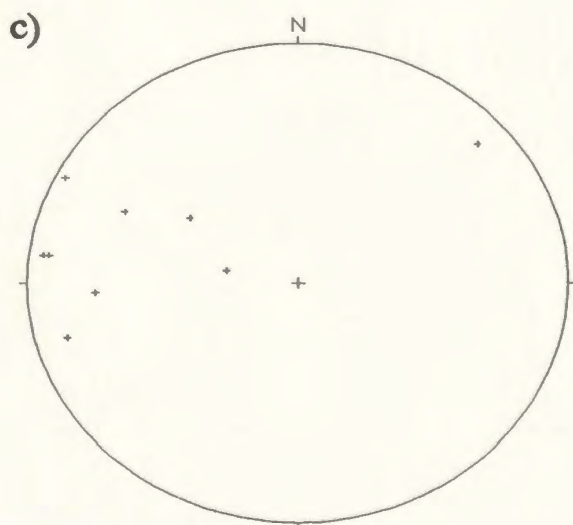


poles to bedding N=19
axis: 53->038

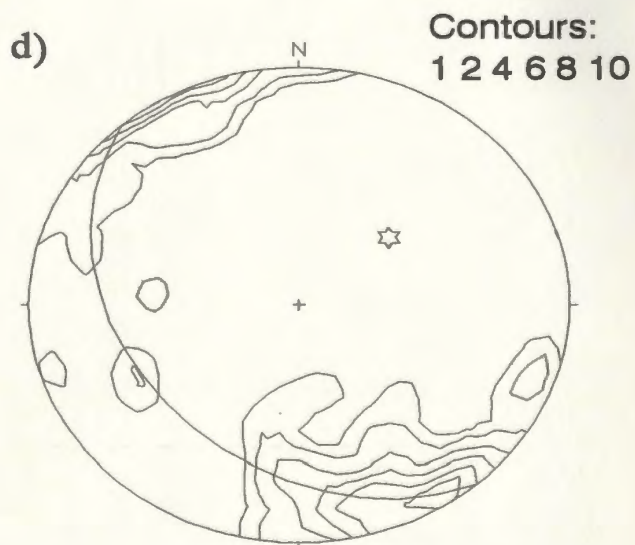


poles to S2 cleavage N=72
axis: 46->036

WHOLE PANEL



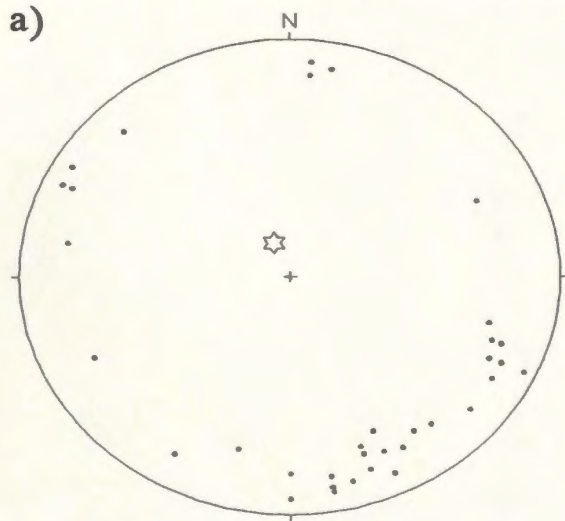
S0/S2 x lineations N=9



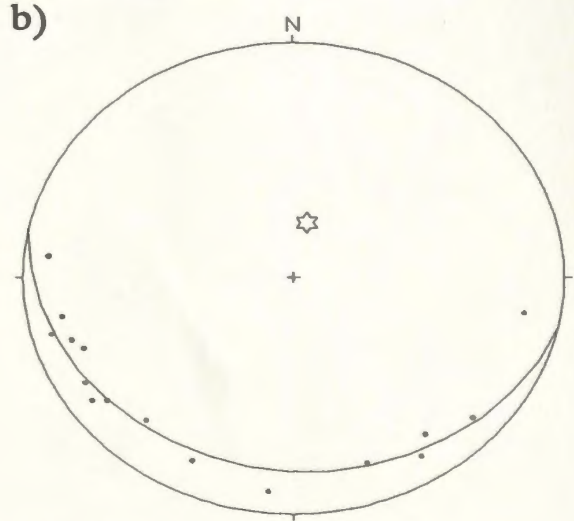
poles to S0&S2 cleavage N=64
axis: 54->049

Figure E-iii

WESTERN DOMAIN SOUTHWEST ARM PANEL COOPER'S COVE AREA

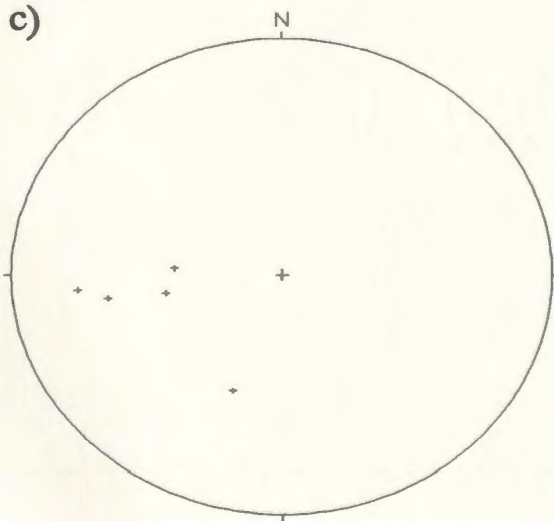


poles to S2 cleavage N=35
axis: 77->336
volcanic host

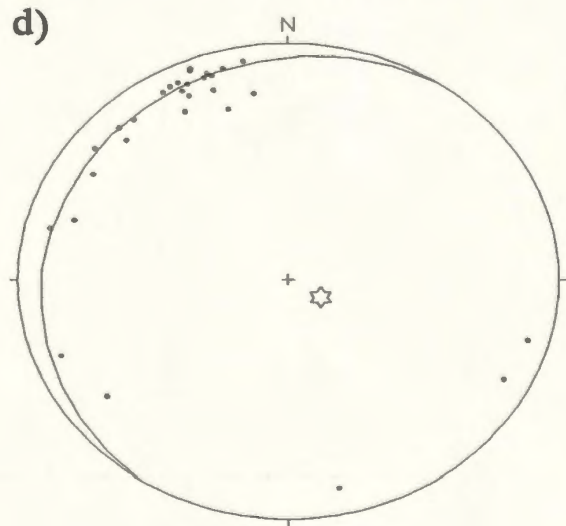


poles to S2 cleavage N=16
axis: 70->012
sill

COLCHESTER AREA



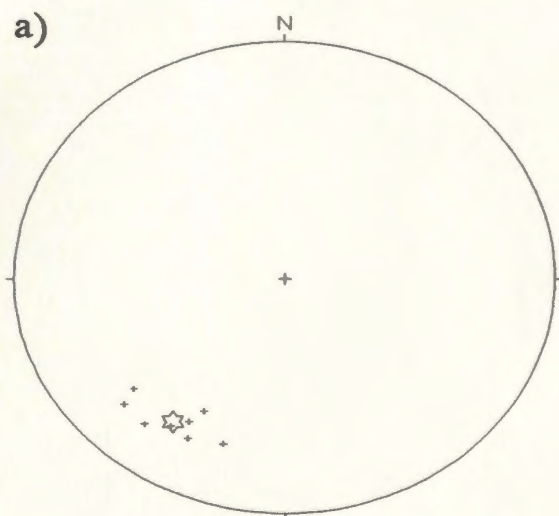
S2/S3 x lineations N=5
volcanic host



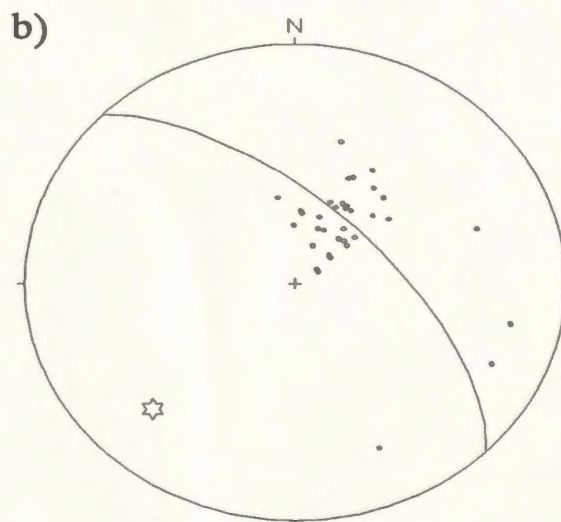
poles to S2 cleavage N=29
axis: 78->122

Figure E-iv

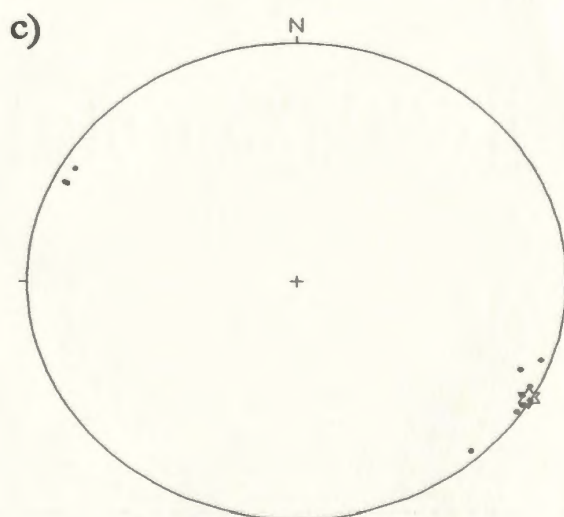
**WESTERN DOMAIN
SOUTHWEST ARM PANEL
CARBONIFEROUS(?) COVER ROCKS**



**F5(?) fold axes N=9
axis: 27-→214**



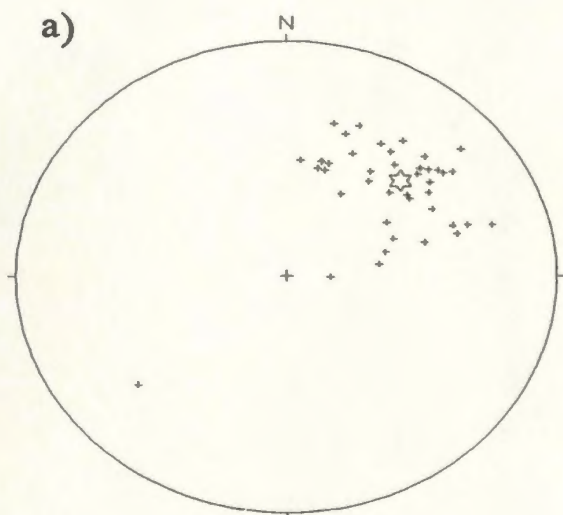
**poles to bedding N=36
axis: 26-→224**



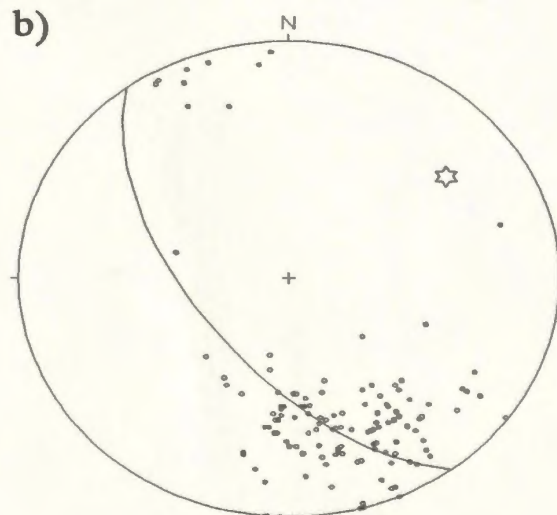
**poles to S5(?) cleavage N=11
mean: 89-→300**

Figure E-v

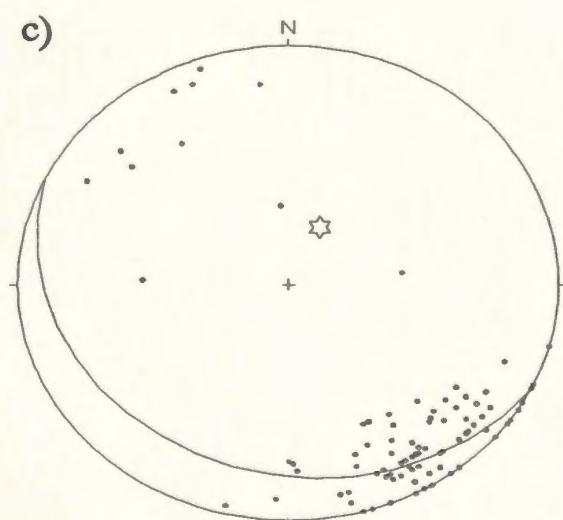
WESTERN DOMAIN SUGAR LOAVES PANEL



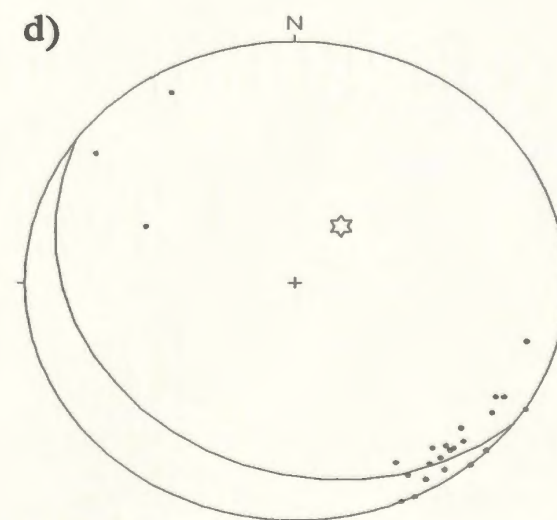
S0/S2 lineations N=41
axis: 41->046



poles to bedding N=128
axis: 29->053



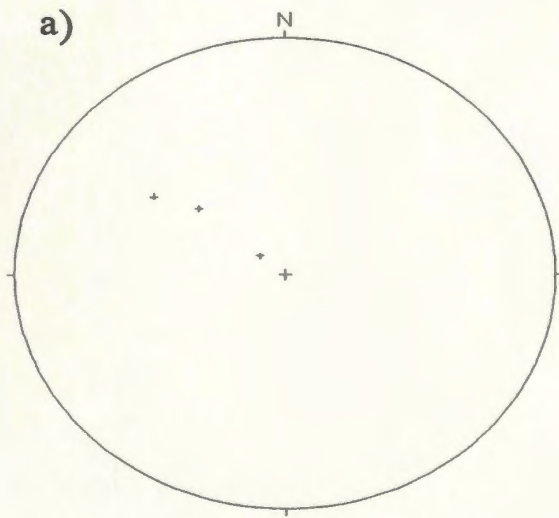
poles to S2&S3 cleavage N=95
axis: 68->026



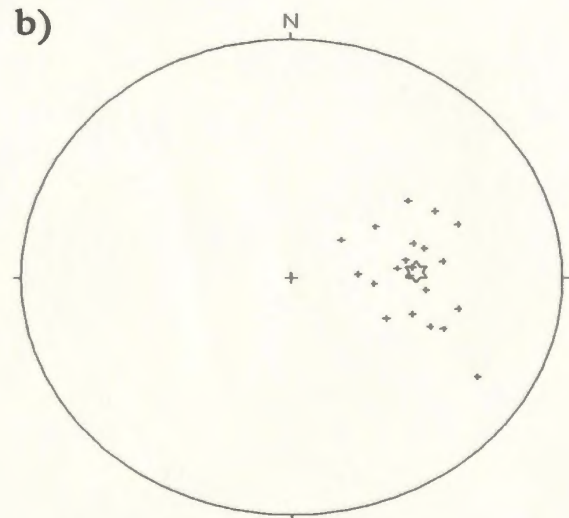
poles to S2&S3 cleavage N=28
axis: 68->026

Figure E-vi

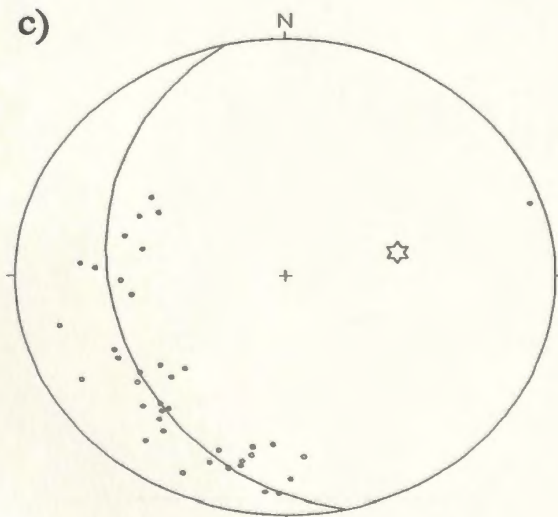
**WESTERN DOMAIN
SUGAR LOAVES PANEL
HARRY'S HARBOUR SECTION**



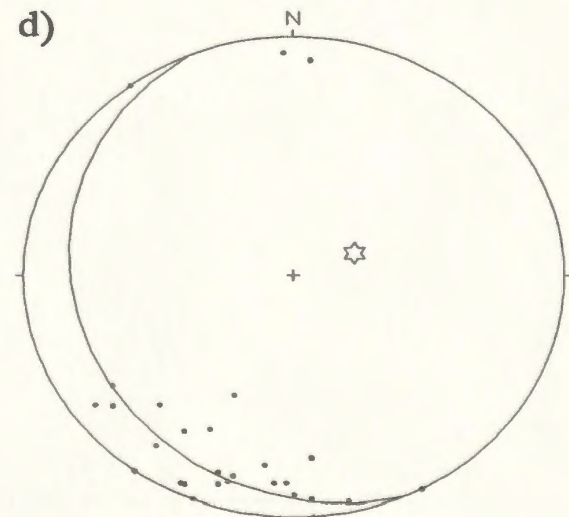
F3(?) fold axes N=3



**S0/S2 lineations N=21
axis: 52->087**



**poles to bedding N=39
axis: 55->077**

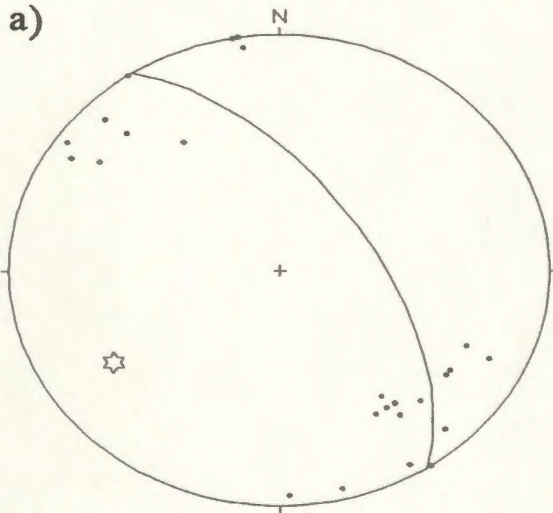


**poles to cleavage N=28
axis: 70->067**

Figure E-vii

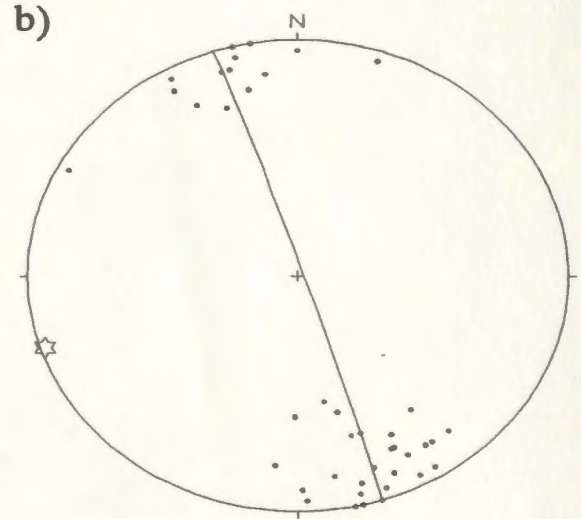
WESTERN DOMAIN

LITTLE BAY PANEL



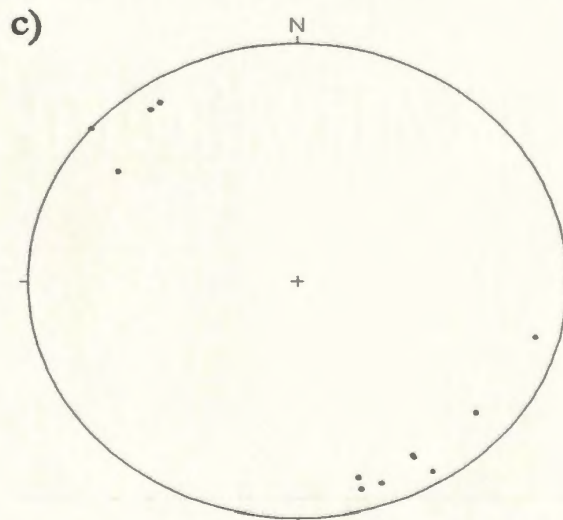
poles to cleavage N=25
axis: 28->237

GULL POND PANEL



poles to cleavage N=41
axis: 02->251

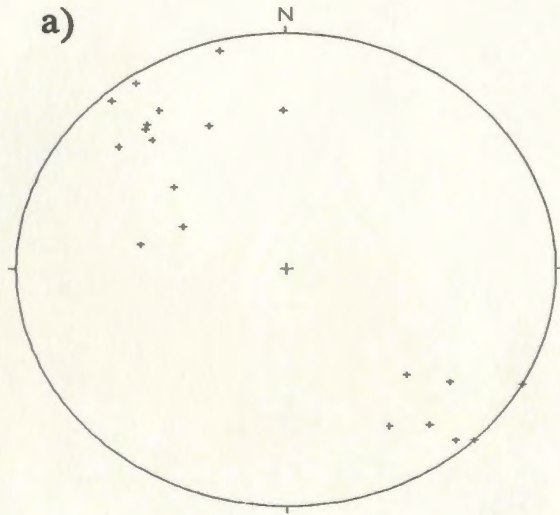
LINE POND PANEL



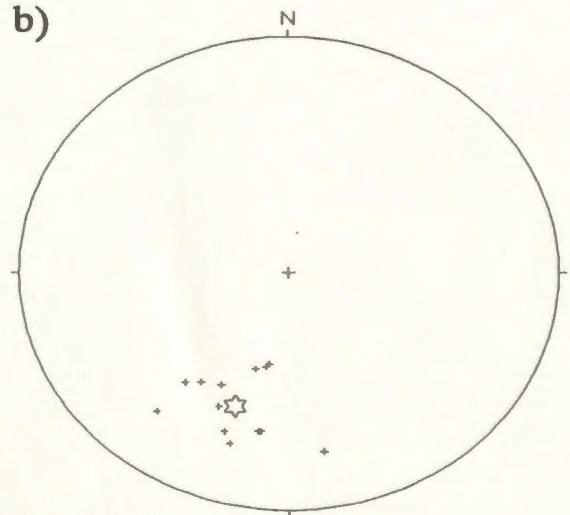
poles to S0 and cleavage N=12

Figure E-viii

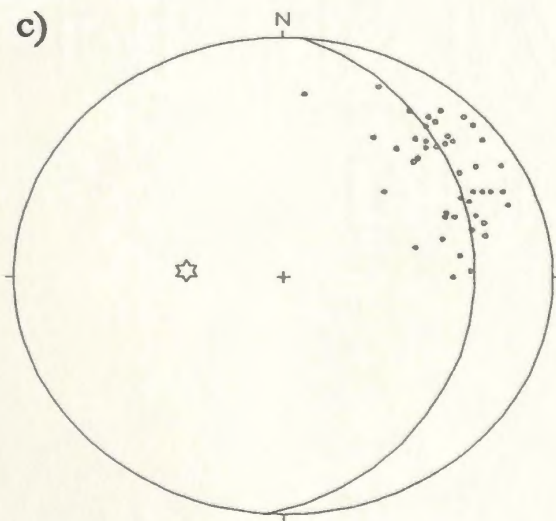
EASTERN DOMAIN LITTLE BAY PANEL



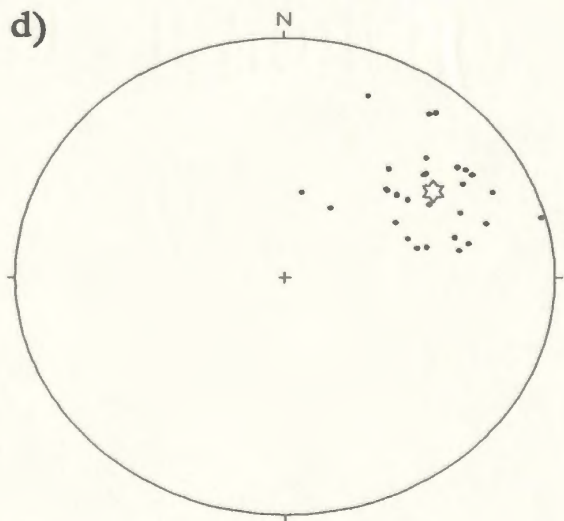
fold axes N=23



fold axes N=13
axis: 40- > 200



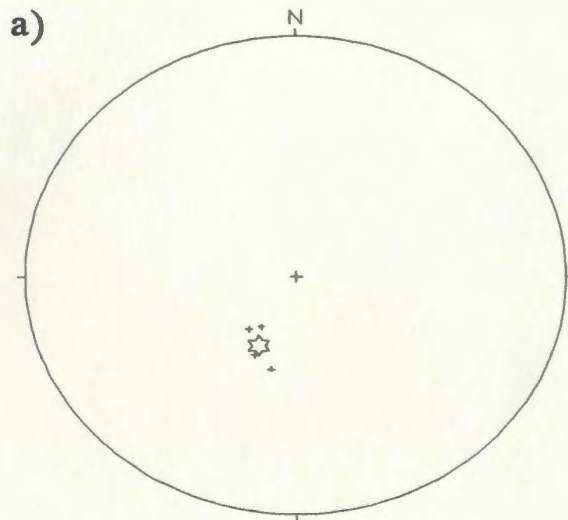
poles to bedding N=45
axis: 60- > 274



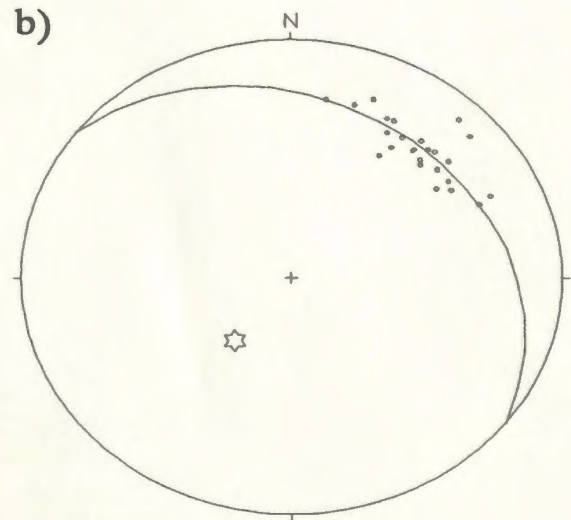
poles to cleavage N=29
mean: 55- > 236

Figure E-ix

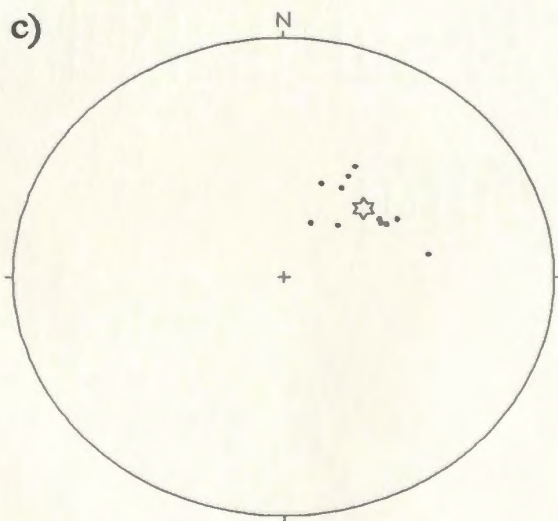
EASTERN DOMAIN SHAG CLIFF PANEL - FOX NECK



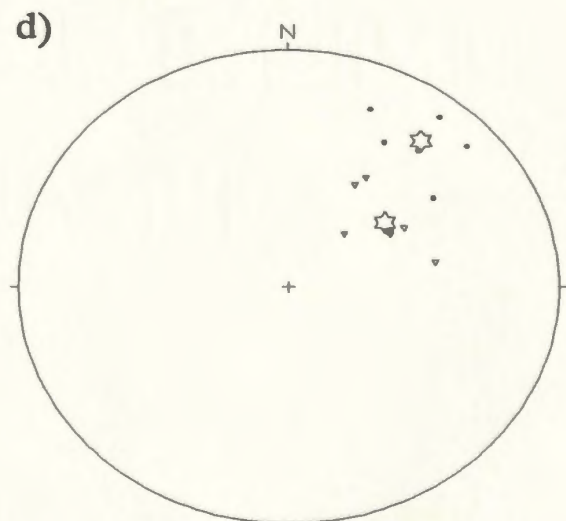
axes of 4 minor folds
mean: 64- \rightarrow 205



poles to bedding N=25
axis: 62- \rightarrow 218



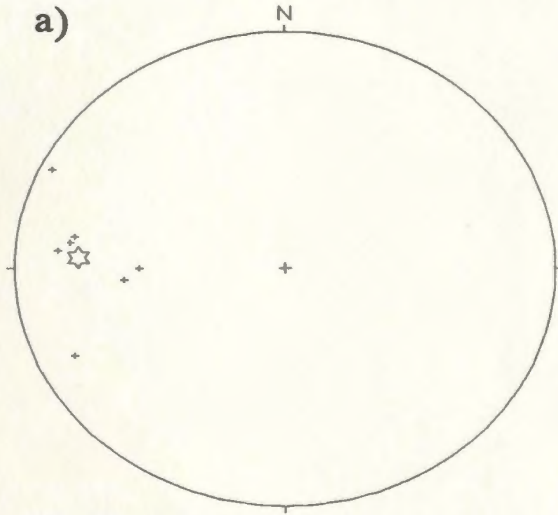
poles to cleavage N=11
mean: 34- \rightarrow 226



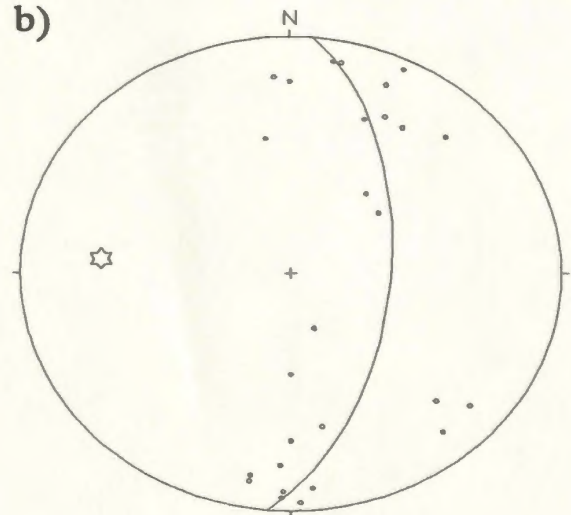
• poles to S2 cleavage N=6
mean: 68- \rightarrow 219
▽ poles to shear bands N=8
mean: 36- \rightarrow 233

Figure E-x

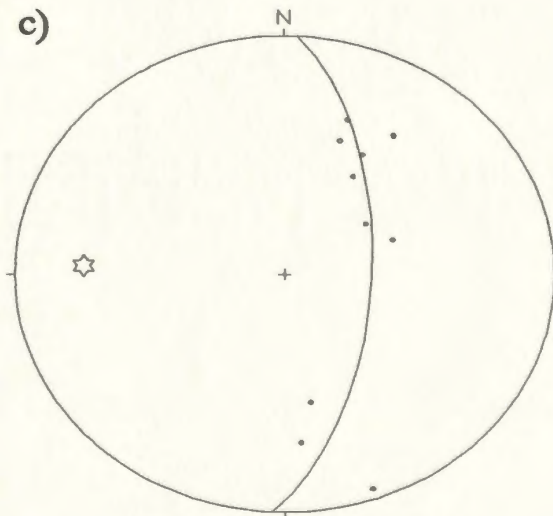
EASTERN DOMAIN SHAG CLIFF PANEL - HALLS BAY HEAD



fold axes N=7
mean: 24- \rightarrow 273



poles to bedding N=27
axis: 30- \rightarrow 274



poles to cleavage N=10
axis: 26- \rightarrow 272

Figure E-xi

EASTERN DOMAIN

NOGOOD ISL. PANEL - PILLEY'S ISL.

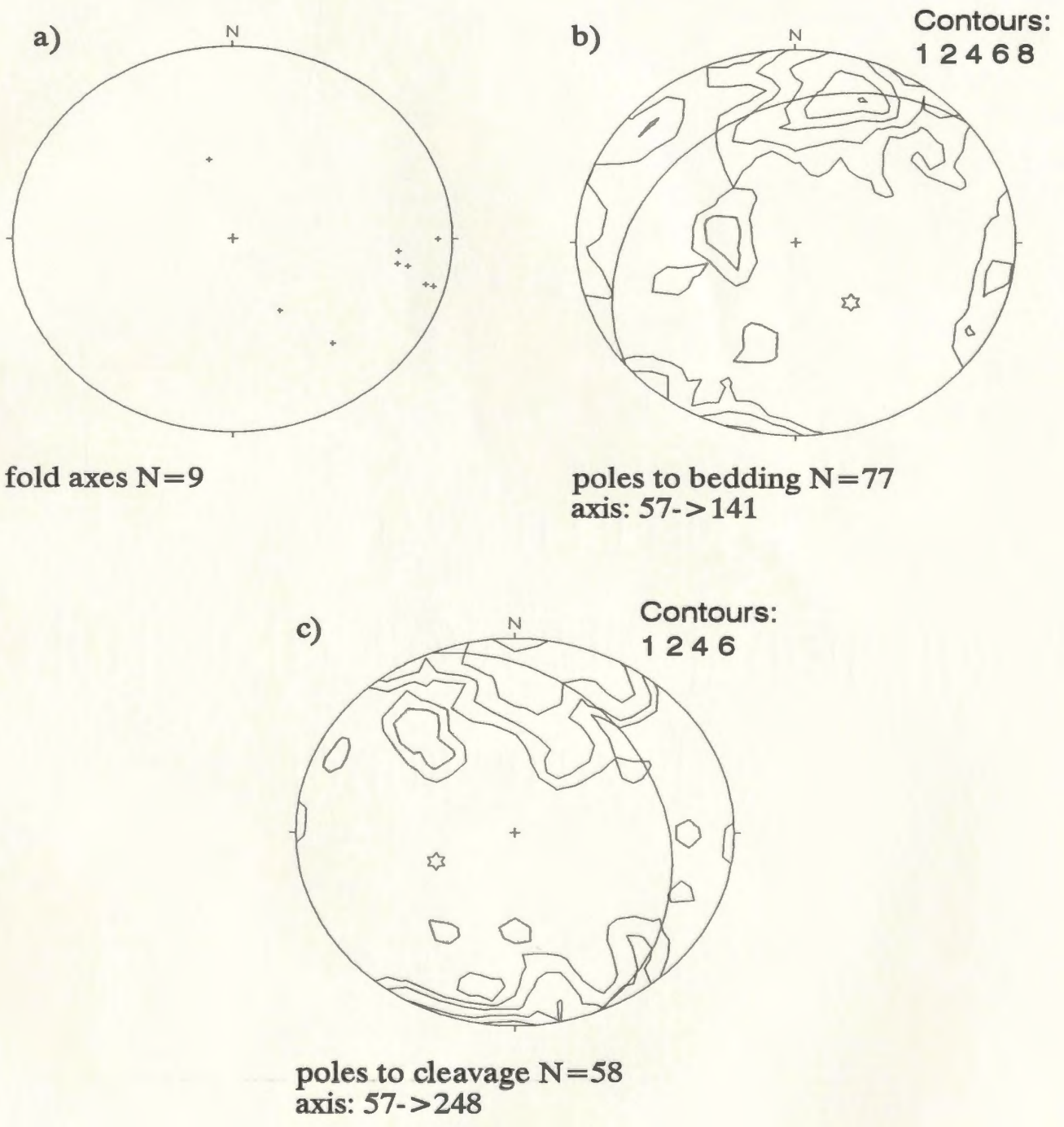
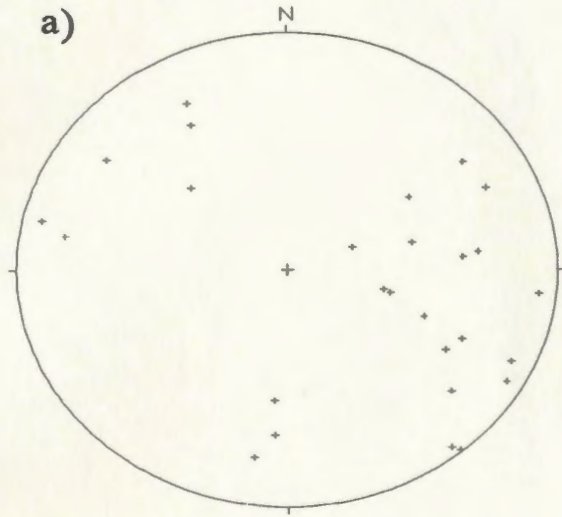
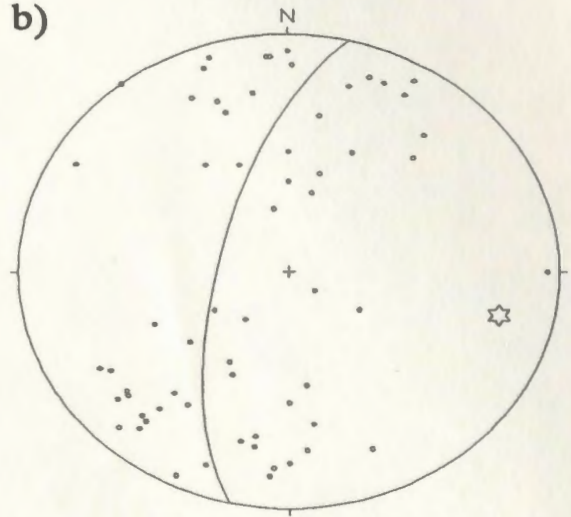


Figure E-xii

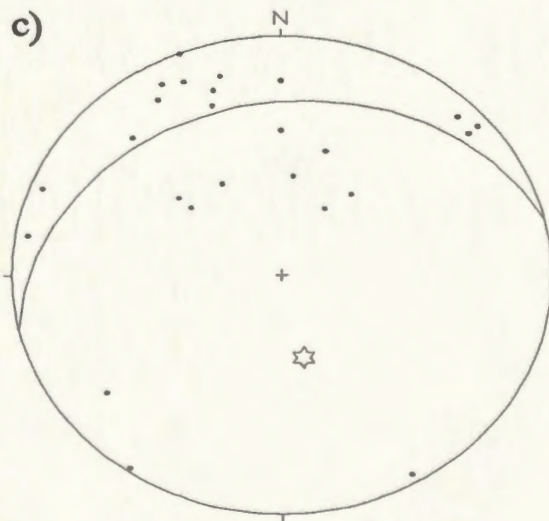
EASTERN DOMAIN
NOGOOD ISL. PANEL - NW TRITON ISL.



fold axes N=27



poles to bedding N=62
axis: 21- > 103

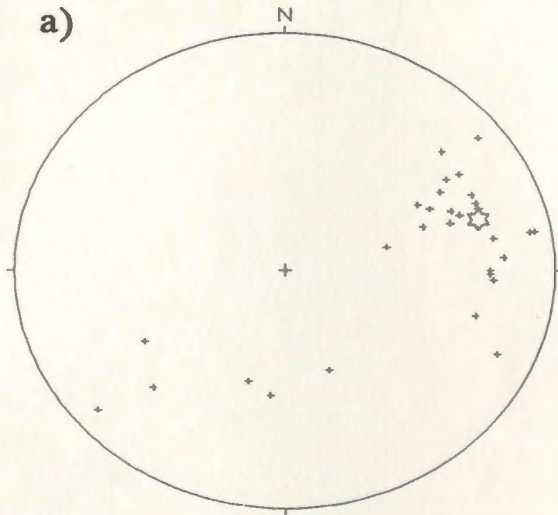


poles to cleavage N=25
axis: 61- > 167

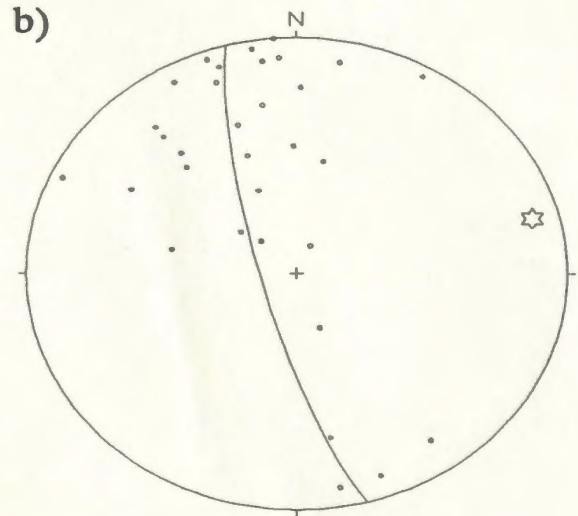
Figure E-xiii

EASTERN DOMAIN

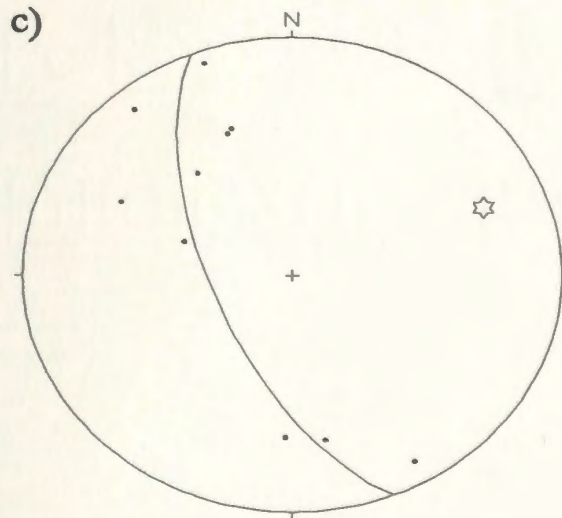
NOGOOD ISL. PANEL - E TRITON ISL.



fold axes N=30
axis: 26->73



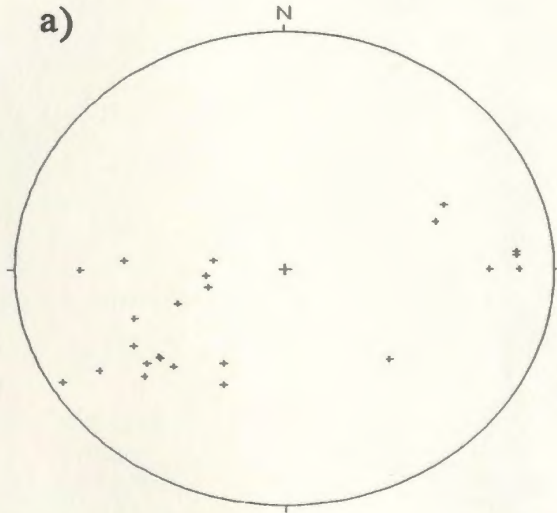
poles to bedding N=32
axis: 11->75



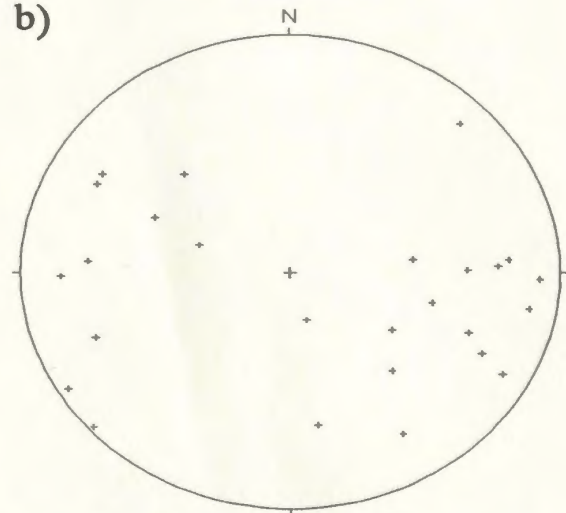
poles to cleavage N=10
axis: 24->68

Figure E-xiv

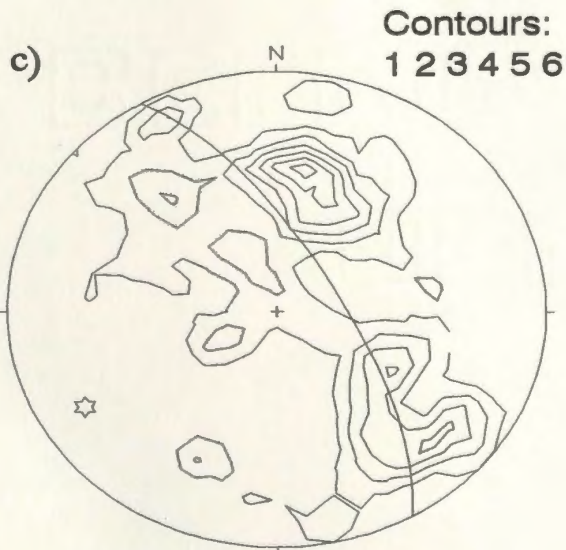
LONG ISLAND SUB-DOMAIN SOUTHERN HEAD PANEL



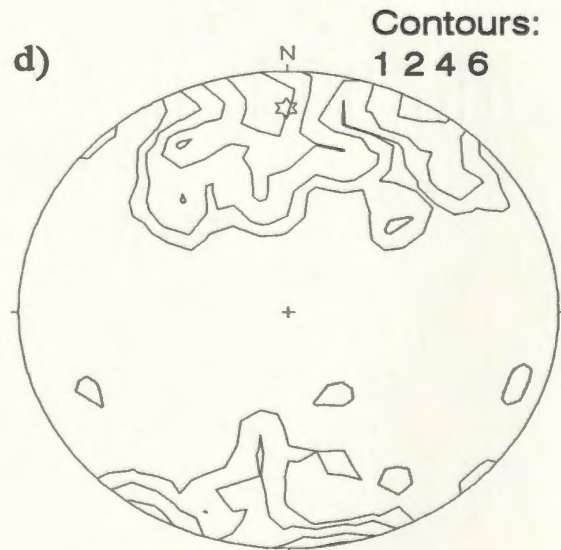
fold axes N=24



S0/S2 and S3 lineations N=25



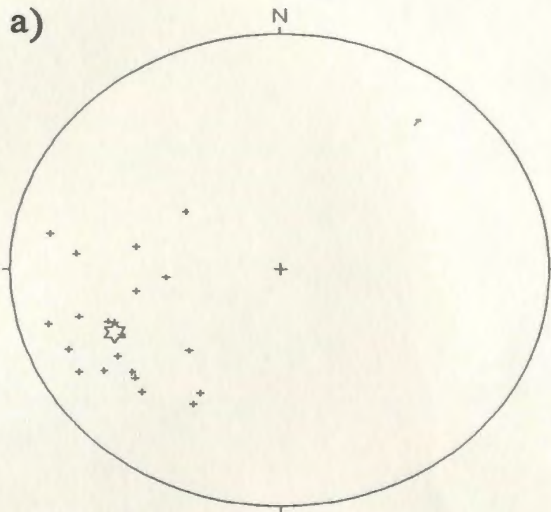
poles to bedding N=78
axis: 20->240



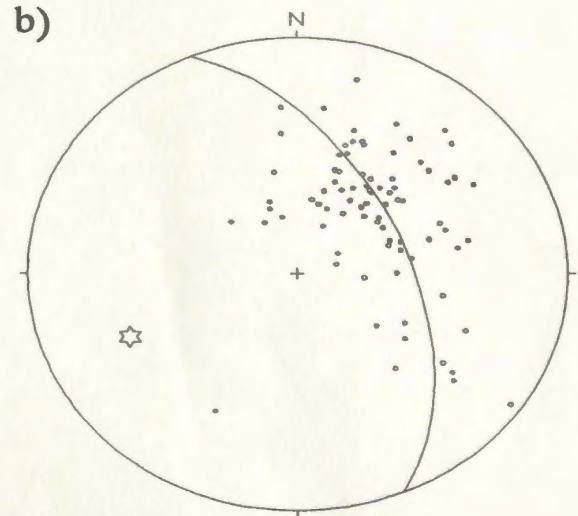
poles to cleavage N=60
mean: 73->180

Figure E-xv

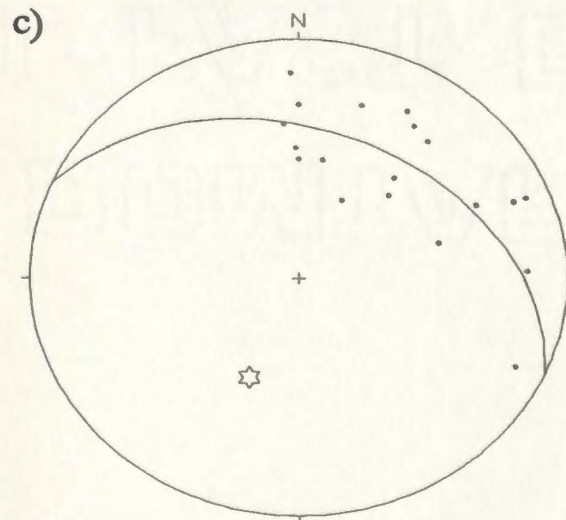
LONG ISLAND SUB-DOMAIN CUTWELL ARM PANEL



fold axes N=21
axis: 34- \rightarrow 246



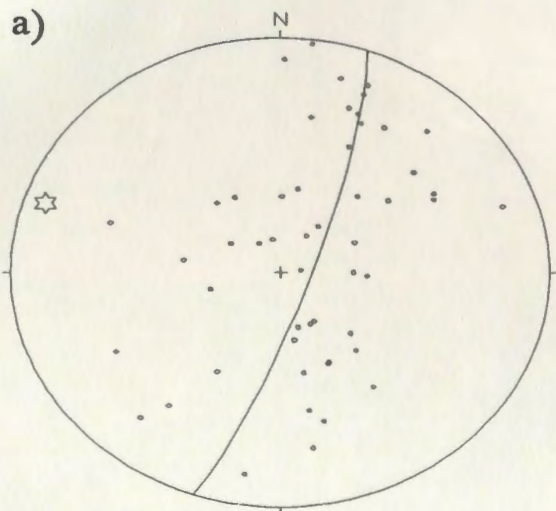
poles to bedding N=85
axis: 33- \rightarrow 246



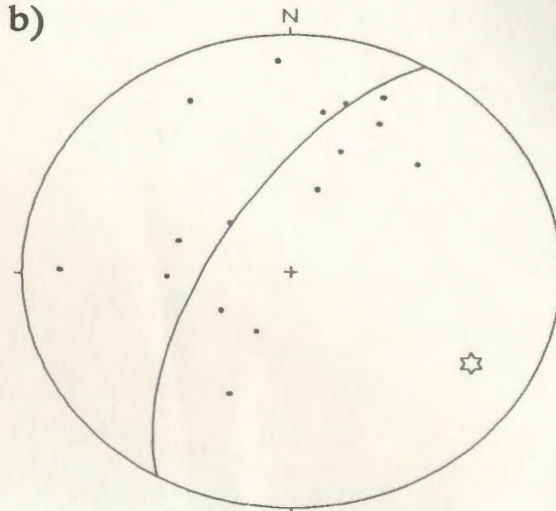
poles to cleavage N=20
axis: 52- \rightarrow 204

Figure E-xvi

LONG ISLAND SUB-DOMAIN ASPEN COVE PANEL

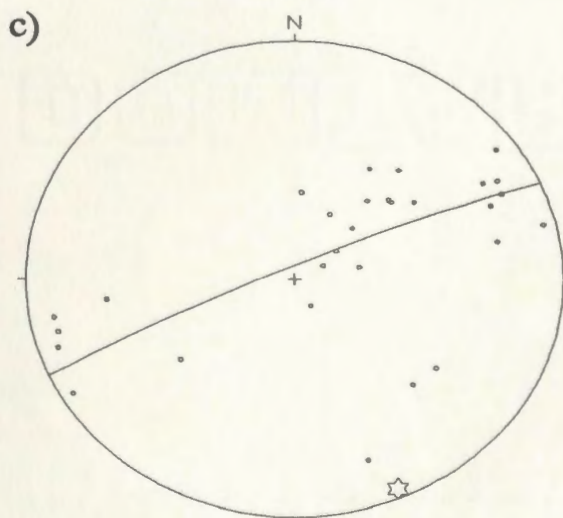


poles to bedding N=52
axis: 09->289



poles to cleavage N=16
axis: 24->120

STAG ISLAND SUB-DOMAIN



poles to bedding N=29
axis: 05->156

Figure E-xvii

